Sobri Harun
Ilya Khairanis Othman
Mohamad Hidayat Jamal   *Editors*

Proceedings of the 5th International Conference on Water Resources (ICWR) – Volume 1

Current Research in Water Resources, Coastal and Environment

Springer

Lecture Notes in Civil Engineering

Volume 293

Lecture Notes in Civil Engineering (LNCE) publishes the latest developments in Civil Engineering—quickly, informally and in top quality. Though original research reported in proceedings and post-proceedings represents the core of LNCE, edited volumes of exceptionally high quality and interest may also be considered for publication. Volumes published in LNCE embrace all aspects and subfields of, as well as new challenges in, Civil Engineering. Topics in the series include:

- Construction and Structural Mechanics
- Building Materials
- Concrete, Steel and Timber Structures
- Geotechnical Engineering
- Earthquake Engineering
- Coastal Engineering
- Ocean and Offshore Engineering; Ships and Floating Structures
- Hydraulics, Hydrology and Water Resources Engineering
- Environmental Engineering and Sustainability
- Structural Health and Monitoring
- Surveying and Geographical Information Systems
- Indoor Environments
- Transportation and Traffic
- Risk Analysis
- Safety and Security

To submit a proposal or request further information, please contact the appropriate Springer Editor:

- Pierpaolo Riva at pierpaolo.riva@springer.com (Europe and Americas);
- Swati Meherishi at swati.meherishi@springer.com (Asia—except China, and Australia, New Zealand);
- Wayne Hu at wayne.hu@springer.com (China).

All books in the series now indexed by Scopus and EI Compendex database!

Sobri Harun · Ilya Khairanis Othman ·
Mohamad Hidayat Jamal
Editors

Proceedings of the 5th International Conference on Water Resources (ICWR) – Volume 1

Current Research in Water Resources, Coastal and Environment

🐴 Springer

Editors
Sobri Harun
School of Civil Engineering
Universiti Teknologi Malaysia
Johor, Malaysia

Ilya Khairanis Othman
School of Civil Engineering
Universiti Teknologi Malaysia
Johor, Malaysia

Mohamad Hidayat Jamal
School of Civil Engineering
Universiti Teknologi Malaysia
Johor, Malaysia

Acknowledgment

Contents

Hydro-Environment

About the Editors

Dr. Sobri Harun is a professor in water resources engineering at Universiti Teknologi Malaysia (UTM). He received BSc in Civil Engineering from the University of Salford, a Master's degree from Imperial College London, and a PhD from UTM. His lectures concern hydrology, hydraulics, hydraulic structures, water resources, and urban stormwater management for undergraduate and postgraduate. His research and publication mostly related to modelling in hydrology, river engineering, water resources, and climate changes. His research works were published in various indexed journals. He is a panel member of the Malaysian Quality Assurance Agency, visiting professor of Universiti Tun Hussein Onn Malaysia, member of IAHR & IAHS, guest editor to Journal of Water and Climate Change, and editorial board to Malaysian Construction Research Journal. He was chairman of the International Conference on Water Resources, which received support from UNESCO Jakarta and the Department of Drainage and Irrigation Malaysia.

Dr. Mohamad Hidayat Jamal is an Associate Professor at Universiti Teknologi Malaysia (UTM). He obtained his PhD in coastal engineering in 2011 from the University of Plymouth, UK. His bachelor's degree is in Civil Engineering, and his master's degree is in Hydraulics and Hydrology from UTM. He has experience in academics for nearly 20 years. He serves the Department of Water and Environmental Engineering, School of Civil Engineering, Faculty of Engineering, UTM. He is also a member of the Center for Coastal and River Engineering (CRCE), Research Institute for Sustainable Environment (RISE), UTM. He is also a Professional Engineer, Board of Engineer Malaysia (BEM), a Chartered Marine Engineer, the Institute of Marine Engineering, Science & Technology, UK (IMarEST), a Chartered Engineer of Engineering Council, UK (EC, UK), a Certified Professional in Erosion and Sediment Control (CPESC), and a professional Technologist, Malaysia Board of Technologist (MBOT).

Dr. Ilya Khairanis Othman is a Senior Lecturer at the Department of Water and Environmental Engineering, School of Civil Engineering, Faculty of Engineering, UTM Universiti Teknologi Malaysia (UTM). She completed her bachelor's degree in Civil Engineering from UTM in 2007 and joined UTM after completing her MSc at the University of Plymouth, UK, in 2008/9. She obtained her PhD from the University of Queensland, Australia, in 2014 in the field of coastal engineering. Her teaching and research evolve around fluid and coastal hydraulics and have led to several national research grants. She is currently serving as deputy director for Coastal and River Engineering (CRCE), Research Institute for Sustainable Environment (RISE), UTM. She is a lifetime member of the International Association of Coastal Reservoir Research (IACRR), a professional member of the American Society of Civil Engineers (ASCE), and a registered engineer with the Board of Engineer Malaysia (BEM).

List of Figures

Reducing Uncertainties in Infiltration Model Using SCS-CN for Mixed Land Use Catchment

A Review on Heavy Duty Mobile Flood Wall Barrier: Way Forward for Malaysia

Investigating SWAT Model Efficiency to Determine Water Balance Components (Case Study: Sungai Muda Watershed)

Development of the National Water Balance Management System (NAWABS) for the Perak, Kurau and Kerian River Basins

Managing Disputes in Water Management Contracts: The DID Perspective

The Influence of Vegetated Alternate Bar on Flow Resistance in an Alluvial Straight Channel

A Mathematical Study of the Relation Between Discharges, Froude Number, Bed Width in Dividing Open Channel Flows

Laboratory Investigations on Porous Concrete Drainage Systems Performance

**Permeability and Mechanical Properties of Pervious Concrete
Curb with Different Aggregate Sizes**

**Application of Building Information Modelling (BIM) Technology
in Drainage System Using Autodesk InfraWorks 360 Software**

**Comparison of Drag Models in Shallow Flow for Spherical Particle
Trajectory**

Numerical Analysis of Flow Characteristics for Idealised Y-Shaped Channels

Modelling of an Embankment Failure Using Flow-3D

Water Distribution System Modelling in Pasir Gudang, Johor with EPANET

Sentiment Analysis and Topic Modeling for Identifying Key Public Concerns of Water Quality/Issues

Islamic Institutional Arrangements of the Aflaj Systems Maintenance in Sultanate of Oman: Operation of the Different *Aflaj* Type Case Study

Salinity Behavior and Intrusion in Kelantan River Estuary

Physical and Chemical Variability of Mangrove Island: A Case Study of Pulau Kukup, Johor

Potential Development of Coastal Reservoir in Malaysia

Numerical Study of Wave Groups in Wind-Swell Seas

Numerical Simulations of Wave Diffraction Around a Low-Crested Semicircular Breakwater

Modelling of Wave Runup and Overtopping Over Accropode II Breakwater

Marine Debris Assessment and Clean Coast Index of Pantai Navy Labuan, Wilayah Persekutuan Labuan, Malaysia

List of Tables

**Bibliometric Analysis of Global Research on Probable Maximum
Precipitation Estimation Using Scopus Database**

**Multivariate Statistical Analysis of Morphometric Parameters
in Watersheds of Peru**

**Hydrological Drought Evaluation on Streamflow Drought Index
(SDI) in Upstream and Downstream Area of Lampao Reservoir,
Northeast of Thailand**

**Characteristic of Stormwater Quality Using BIOECODS in JKR
Pilot Projects**

Prediction of Flow Structure in Axial Flow Submersible Pumps During Intake by Numerical Simulation

Numerical Analysis of Flow Characteristics for Idealised Y-Shaped Channels

Modelling of an Embankment Failure Using Flow-3D

Water Distribution System Modelling in Pasir Gudang, Johor with EPANET

Removal of Ammoniacal Nitrogen from Aqueous Solution Using Clinoptilolite as Adsorbent

Determination of the Relationship Between River Ecosystems and Benthic Macroinvertebrate Ecological Indices as a Basis for River Health Assessment

Integrated River Basin Management

The Integrated River Basin Management (IRBM) chapter presents papers related to precipitation or rainfall analysis, watershed morphology, water availability under climate change, drought index analysis, stormwater quality, flood modelling and infrastructure, water balance and management issues beneficial to practising engineers and researchers. The hydrometeorological data represent the selected catchment or watershed is utilised. These issues were investigated using multiple types of software and statistical method. The first few papers dealt with design rainfall analysis based on statistical methods. Papers on rainfall analysis in various areas in Malaysia present the trend results, depth-area-duration curves, fitting gamma and normal distribution and probable maximum precipitation. The multivariate analysis of morphometric parameters in the watershed of Peru is also presented. The following paper is the hydrological drought evaluation on streamflow in Thailand's upstream and downstream reservoir areas and the terrestrial research on water availability under climate change in the Amu River basin. The stormwater quality aspect is presented using Bio-Ecological Drainage System (BIOECOD) in JKR Malaysia pilot projects. Papers on the flood issues discuss the uncertainties in the infiltration model and heavy-duty mobile flood wall infrastructure. The last three papers address water balance management and water disputes in Malaysia.

Statistical and Trend Analysis of Annual Maximum Daily Rainfall (AMDR) for Kuching City, Sarawak, Malaysia

C. H. J. Bong, S. C. Liew, M. Neging, E. Matthew Ruji, and D. Gabda

Abstract Kuching city and its surrounding urban areas frequently experience extreme high annual maximum daily rainfall (AMDR), resulting in flash floods. This study aims to carry out statistical and trend analysis of extreme AMDR events for Kuching Airport rainfall station from 1975 to 2017. From the analysis, the AMDR records a high variability with a value of 36.9% while January has the highest occurrence of AMDR with 53.5% of the total data. Findings from the linear regression plot have shown that the AMDR has a slight decreasing trend over the past four decades though the trend was insignificant. Based on the drainage design capacity of Kuching city, AMDR of magnitude 180 mm was identified as a threshold. The frequency analysis results showed that the return period of flooding events with daily rainfall exceeding 180 mm was 2.69 years. The occurrence probability of the flood event at least once in 1, 2, 3, 4 and 5 years was 0.37, 0.60, 0.75, 0.84 and 0.90, respectively. This study contributed to understanding the magnitude and frequency of extreme high AMDR which could lead to flooding events in Kuching city.

Keywords Annual maximum daily rainfall · Climate change · Extreme events · Rainfall trend · Urban drainage

C. H. J. Bong (✉)
Faculty of Engineering, Universiti Malaysia Sarawak, Kota Samarahan, Malaysia
e-mail: bhjcharles@unimas.my

S. C. Liew
Faculty of Engineering, Computing and Science, Swinburne University of Technology Sarawak Campus, Kuching, Malaysia
e-mail: scliew@swinburne.edu.my

M. Neging
School of Civil Engineering, College of Engineering, Universiti Teknologi MARA Cawangan Sarawak, Kota Samarahan, Malaysia
e-mail: maureenneging@uitm.edu.my

E. Matthew Ruji
Department of Irrigation and Drainage Sarawak, Kuching, Malaysia
e-mail: ednamr@sarawak.gov.my

D. Gabda
Faculty of Science and Natural Resources, Universiti Malaysia Sabah, Kota Kinabalu, Malaysia
e-mail: darmesah@ums.edu.my

1   Introduction

High maximum daily rainfall events are among the causes of flood disasters that have disastrous consequences for human society. For example, recently in Henan, China, a rainfall of 622.7 mm within 24 h had caused casualties and more than 100,000 people evacuated [1]. Also, in the Rhine Basin, Germany, a record high of 154 mm of rain within 24 h had killed at least 58 people and tens of thousands of homes flooded [2]. Since severe rainfall is highly variable in time and space and rarely lasts more than one day [3], the critical parameter is the maximum daily rainfall. The annual maximum daily rainfall (AMDR) is defined as an extreme instance with critical duration for a watershed, region or state [4], or in other words, the highest maximum daily rainfall for the particular year.

Studies on the probability of occurrence of a particular level of AMDR has been done in various part of the world, for example, in Brazil [4] and Nelspruit, South Africa [5]. From these studies, the return period of flood disasters and the change of behaviour of extreme events can be determined. These extreme events are normally represented by Gumbel distribution [6, 7]. Besides probability of occurrence, other statistical analyses such as coefficient of variability (CV), linear regression analysis and seasonal variation [8] as well as the contribution of AMDR in annual totals [9] has been conducted on maximum daily rainfall. As for Malaysia, the rainfall pattern has begun to transform due to climate change [10]. This was evident as extreme floods have become more frequent and severe in several states in recent years. Several studies have been conducted using statistical methods such as Mann–Kendall and linear regression especially in Peninsular Malaysia to understand the extreme rainfall trend, [11, 12] including Sarawak [13]. A more localised study for Sarawak River Basin (where Kuching city is located) by [14] has shown an upward trend in the annual rainfall, temperature and evaporation for the past 3 to 4 decades. A study by [15] on historical rainfall data has shown high variability for Kuching city, with the monthly rainfall peaking at the end of the year 2009 and early 2010. On the other hand, a recent study on drought by [16] has shown an increase in the number of dry months in the recent decade for most of the rainfall stations in the Sarawak River Basin compared to the previous 30 to 40 years.

Since most of the existing studies, especially the one localised in the Sarawak River Basin were generally focused on the annual and monthly rainfall trend and drought, further study on extreme daily rainfall events is required. This is due to the limited study on maximum daily rainfall, especially on the frequency and magnitude of high AMDR events in Kuching city. Occurrences of floods in Kuching city due to extreme high AMDR events have become more frequent recently. In 2021 alone, Kuching city has experienced floods in most of its urban area caused by high daily rainfall, namely on 12 January 2021 due to 179.5 mm rainfall and on 18 February 2021 due to 231.0 mm of rainfall. Both these rainfalls were recorded at the Kuching Airport rainfall station. According to [17], Kuching city's drainage system was designed for a maximum of 180 mm of rain and most of the flooding events were caused by the drainage system unable to cope with the high daily rainfall. Hence, the current

study aims to carry out statistical and trend analysis for extreme AMDR events for Kuching city and the identification of occurrence probability of flood events due to high AMDR, which could lead to flooding events.

2 Study Area

Kuching city is the capital of the state of Sarawak and is located in Sarawak River Basin as shown in Fig. 1. The main river passing through Kuching city is Sg. Sarawak river with a flow length of 120 km and Sarawak River Basin has a catchment area of 2456.04 km^2. Kuching city experiences two main monsoon seasons, namely northeast monsoon (November–March) when the wet season is recorded and the southwest monsoon (June–September) when the dry season is recorded. The basin has a high annual rainfall with an average of 4163.8 mm as shown in Table 1 for the rainfall data from Kuching Airport station (Station ID: 1403001) for the past four decades. The Kuching Airport rainfall station was chosen for this study due to the consistent and reliable data (less than 10% missing data) and located within the city.
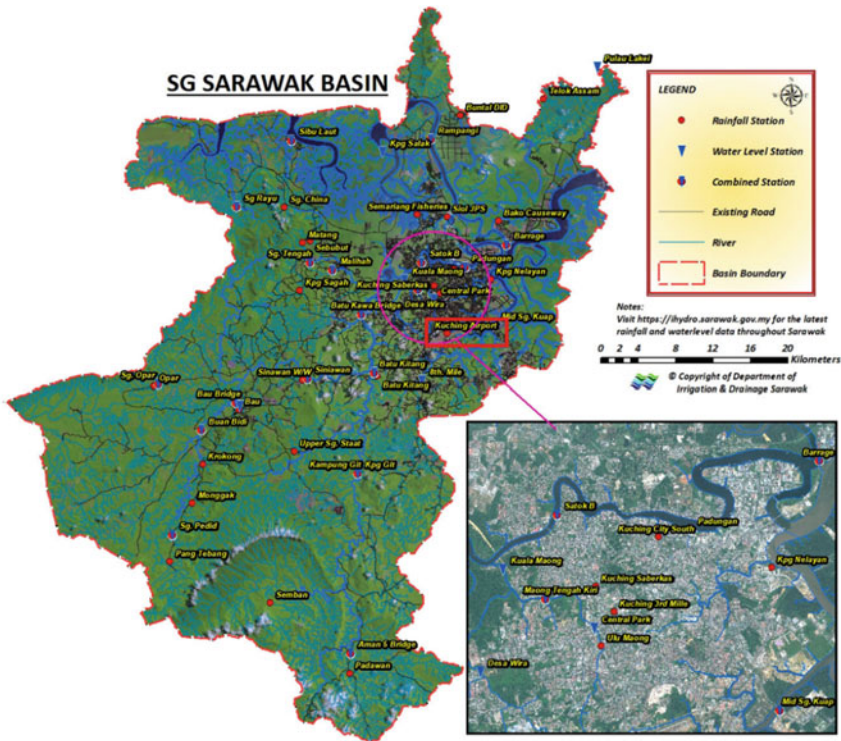
Fig. 1 Sarawak River Basin and location of Kuching Airport rainfall station (in red box) [18]

Table 1 Annual maximum daily rainfall (AMDR) events for Kuching Airport rainfall station (1975–2017) with month of occurrence, the total annual rainfall and percentage of AMDR to the total annual rainfall

Year	AMDR (mm)	Month of occurrence	Total annual rainfall (mm)	% of AMDR to total annual rainfall
1975	282.5	Dec	4467.0	6.3
1976	222.3	Jan	3749.0	5.9
1977	260.1	Jan	5287.0	4.9
1978	210.1	Jan	4228.0	5.0
1979	131.8	Mar	4357.0	3.0
1980	290.0	Jan	4649.0	6.2
1981	134.9	Dec	3861.0	3.5
1982	102.0	Feb	3158.0	3.2
1983	141.9	Jan	4142.0	3.4
1984	208.2	Jan	4529.0	4.6
1985	137.5	Jan	3844.0	3.6
1986	222.6	Jan	4285.0	5.2
1987	158.4	Jan	3859.0	4.1
1988	170.8	Dec	4305.0	4.0
1989	190.8	Dec	4700.0	4.1
1990	86.8	Jan	3466.0	2.5
1991	103.2	Apr	3814.0	2.7
1992	160.2	Dec	4265.0	3.8
1993	135.8	Aug	3742.0	3.6
1994	157.4	Jan	5129.0	3.1
1995	175.6	Feb	4549.0	3.9
1996	155.9	Jan	3836.0	4.1
1997	96.3	Apr	2815.0	3.4
1998	302.3	Jan	4404.0	6.9
1999	109.8	Feb	4111.0	2.7
2000	284.6	Jan	4299.0	6.6
2001	153.0	Jan	3785.0	4.0
2002	265.2	Jan	4599.0	5.8
2003	364.2	Feb	3785.0	6.9
2004	302.6	Jan	4860.0	6.2
2005	131.6	Jan	3843.0	3.4
2006	159.8	Feb	3813.0	4.2
2007	191.4	Oct	4654.0	4.1
2008	127.0	Aug	4075.0	3.1

Table 1 (continued)

Year	AMDR (mm)	Month of occurrence	Total annual rainfall (mm)	% of AMDR to total annual rainfall
2009	165.5	Jan	4456.0	3.7
2010	149.5	Jan	3507.5	4.3
2011	218.0	Jan	4238.0	5.1
2012	106.0	Jan	3680.0	2.9
2013	113.0	Mar	3932.5	2.9
2014	135.5	Feb	3523.5	3.8
2015	200.5	Jan	4223.0	4.7
2016	153.5	Feb	4974.0	3.1
2017	142.0	Dec	3782.5	3.8
Mean	**179.3**		**4163.8**	
SDev	**66.2**			
CV	**36.9**			

3   Methodology

The daily rainfall (mm) data for the years 1975 to 2017 for the Kuching Airport rainfall station was obtained from the Sarawak Department of Irrigation and Drainage (DID). From the daily rainfall data, the maximum daily rainfall for each year was extracted. The extracted annual maximum daily rainfall formed the AMDR events. Table 1 shows the AMDR events for the period 1975–2017. From the data compiled in Table 1, the month with the highest occurrence of AMDR and the percentage of AMDR with the total annual rainfall for the particular year can be determined. The mean, standard deviation (*SDev*) and coefficient of variation (*CV*) can also be obtained from the data in Table 1.

The coefficient of variation (*CV*) was used to assess the temporal variability of rainfall and is defined as:

$$CV = \frac{\sigma}{\mu} \times 100 \tag{1}$$

where σ is the standard deviation and μ is the mean rainfall for the chosen timescale. High values of *CV* indicate high variability of rainfall and vice versa. Asfaw et al. [19] define the degree of variability of rainfall events as low ($CV < 20$), moderate ($20 < CV < 30$) and high ($CV > 30$).

To further understand the AMDR trend, a linear regression plot was used. The slope from the linear regression plot indicates the average rate of change. A positive slope defines an increasing trend, while the negative one indicates a decreasing trend [9]. To further determine the trend significance, Mann–Kendall (MK) test was used. Mann Kendall [20, 21] test is a nonparametric statistical test widely used to assess the

trend in hydrological time series [10]. For the MK test in the current study, the null hypothesis was tested at a 95% confidence level ($\alpha = 0.05$). The null hypothesis H_0 assumes no trend in the rainfall data series while the alternative H_1 assumes there is a trend in the series. The probability value (p-value) from two-tailed tests was applied in this test. The Excel add-in, downloadable from real-statistics.com/free-download/ [22], was used to perform the MK test for the current study. For the Mann Kendall statistics, S is given by:

$$S = \sum_{k=1}^{n-1} \left[\sum_{j=k+1}^{n} sign(x_j - x_k) \right] \tag{2}$$

$$sign(x_j - x_k) = \begin{cases} 1, & x_j - x_k > 0 \\ 0, & x_j - x_k = 0 \\ -1, & x_j - x_k < 1 \end{cases} \tag{3}$$

where x_j and x_k are the sequential data values and n is the number of observations. For the number of observations (n) larger than 10, S statistics is approximately normally distributed with the mean equal to 0. A positive S value indicates an increasing trend, whereas a negative value indicates decreasing trend. The equation of variance for the S statistics is given by:

$$Var(S) = \frac{n(n-1)(2n+5)}{18} \tag{4}$$

The standardized Z statistic is calculated to measure the statistical significance of the trends. The equation of Z is given by:

$$Z = \begin{cases} \frac{S-1}{\sqrt{Var(S)}}, & if\, S > 0 \\ 0, & if\, S = 0 \\ \frac{S+1}{\sqrt{Var(S)}}, & if\, S < 0 \end{cases} \tag{5}$$

If the Z value is larger than the chosen significance level/confidence level, then the null hypothesis is rejected. The p-value approach is defined as the probability of rejecting the null hypothesis. If the p-value is larger than α, the null hypothesis is failed to be rejected.

The probability of exceedances (p) of the AMDR events was determined using the rank-order method. This method involved ordering from the largest to the smallest event. Rank 1 was assigned to the largest event and rank 43 to the smallest event since the sample size for this study was 43. The Weibull formula was applied to obtain the ρ of each event:

$$\rho = \frac{i}{n} + 1 \tag{6}$$

where ρ is the exceedance probability for an event with rank i and n is the sample size. The return period for each event was then defined as the inverse of its exceedance probability:

$$T = 1/\rho \tag{7}$$

To perform the flood risk analysis, the AMDR events ≥ 180 mm were identified as the events that may result in flood disasters in Kuching city based on the capacity of the drainage system [17]. Hence AMDR event of magnitude 180 mm was adopted as the threshold. Eq. (8) was applied to determine the occurrence probability of flood disaster risk associated with AMDR events of magnitude ≥ 180 mm at least once in 1, 2, 3, 4 and 5 years.

$$P(X \geq x_T \text{ at least once in } N \text{ years}) = 1 - \left(1 - \frac{1}{T}\right)^N \tag{8}$$

The Gumbel probability parameters were determined for the AMDR in the current study. These parameters will be useful for comparison with the AMDR of other cities from other existing studies. The Gumbel distribution was represented by the following Probability Distribution Function (PDF):

$$f(x) = \frac{1}{\beta} e^{\left[\frac{x-\alpha}{\beta} - e^{\frac{x-\alpha}{\beta}}\right]} \tag{9}$$

where, α and β is the location and scale parameters of the distribution respectively, while x is the random variable [23]. For the current study, the Gumbel distribution parameters were calculated using online Distribution Calculators available at https://agrimetsoft.com/distributions-calculator/gumbel-distribution-calculator [24].

4　Results and Discussion

From Table 1, most of the AMDR occurred in the month of January (53.5% of the total data), which is during the northeast monsoon season. The AMDR ranged between 86.8 and 364.2 mm, which was between 2.5 and 6.9% of the total annual rainfall of the respective years. The AMDR also has high variability with a coefficient of variation (CV) value of 36.9. Figure 2 shows the linear regression plot between the AMDR and year. From the plot, the AMDR was observed to have a slight downward trend (slope $= -0.7369$) throughout the decades. This was confirmed by the Pearson correlation analysis performed on the data, which showed a very weak negative correlation between the year and AMDR ($r = -0.14$, p-value $= 0.372$). Mann–Kendall (MK) test was performed to determine the significance of the trend. Results from the MK test showed that the S value was -89 (confirming a downward trend); however, with
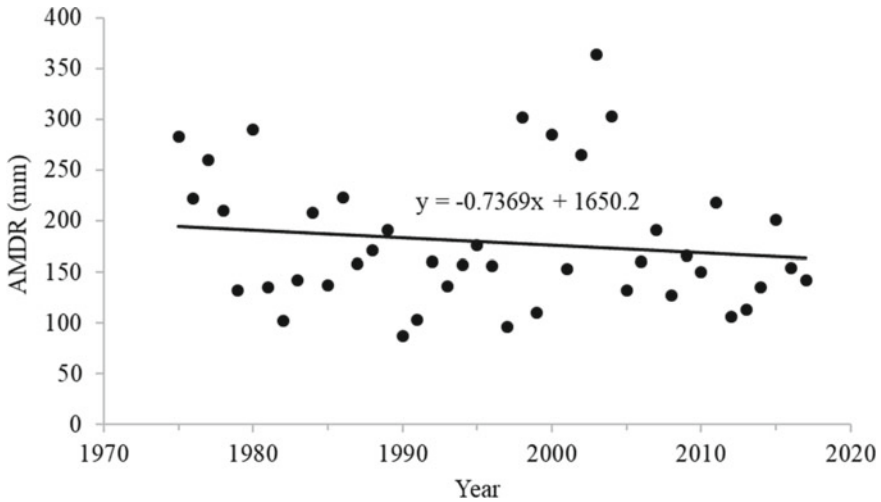
Fig. 2 Linear regression plot of AMDR for the period 1975–2017

the p-value of 0.357 (which is more than $\alpha = 0.05$); meaning the null hypothesis H_0 of no trend cannot be rejected.

As for the plotting positions and return period, Eqs. (6) and (7) were used for the calculation and were presented in Table 2. For this study, the AMDR event of magnitude 180 mm was taken as threshold (x_T) as mentioned in the previous section. AMDR events equal to or greater than x_T were considered as flood events for Kuching city. From Table 2, the number of occurrence of events $x_T \geq 180$ mm was 16 and the number of intervals was 15. Therefore, the empirical return period of the event X_T was 2.69 years (43/15 = 2.69 years) with exceedance probability $\rho = 0.37$. The exceedance probability of flood disaster event (AMDR event: $X \geq 180$ mm) at least once in 1, 2, 3, 4 and 5 years calculated using Eq. (8) was presented in Table 3. The exceedance probability of a flood event (≥ 180 mm) occurring at least once in 5 years is 0.90. This result is important for decision-making on the acceptable level of risk in designing specific infrastructure for flood reduction in Kuching city.

The result of fitting Gumbel distribution to the analysis of AMDR for Kuching city was plotted in Fig. 3. The Gumbel distribution parameters were observed to have values of $\alpha = 209.116$ and $\beta = 51.647$. Figure 3 can be used to determine the magnitude of AMDR events for frequency analysis.

Table 2 Plotting positions and return periods

Rank	X (mm)	P_i	T (years)
1	364.2	0.02	44.00
2	302.6	0.05	22.00
3	302.3	0.07	14.67
4	290.0	0.09	11.00
5	284.6	0.11	8.80
6	282.5	0.14	7.33
7	265.2	0.16	6.29
8	260.1	0.18	5.50
9	222.6	0.20	4.89
10	222.3	0.23	4.40
11	218.0	0.25	4.00
12	210.1	0.27	3.67
13	208.2	0.30	3.38
14	200.5	0.32	3.14
15	191.4	0.34	2.93
16	190.8	0.36	2.75
17	175.6	0.39	2.59
18	170.8	0.41	2.44
19	165.5	0.43	2.32
20	160.2	0.45	2.20
21	159.8	0.48	2.10
22	158.4	0.50	2.00
23	157.4	0.52	1.91
24	155.9	0.55	1.83
25	153.5	0.57	1.76
26	153.0	0.59	1.69
27	149.5	0.61	1.63
28	142.0	0.64	1.57
29	141.9	0.66	1.52
30	137.5	0.68	1.47
31	135.8	0.70	1.42
32	135.5	0.73	1.38
33	134.9	0.75	1.33
34	131.8	0.77	1.38
35	131.6	0.80	1.26
36	127.0	0.82	1.22
37	113.0	0.84	1.19

Table 2 (continued)

Rank	X (mm)	P_i	T (years)
38	109.8	0.86	1.16
39	106.0	0.89	1.13
40	103.2	0.91	1.10
41	102.0	0.93	1.07
42	96.3	0.95	1.05
43	86.8	0.98	1.02

Table 3 Exceedance probability of flood event ($X \geq 180$ mm)

Year	1	2	3	4	5
P (> 180)	0.37	0.60	0.75	0.84	0.90
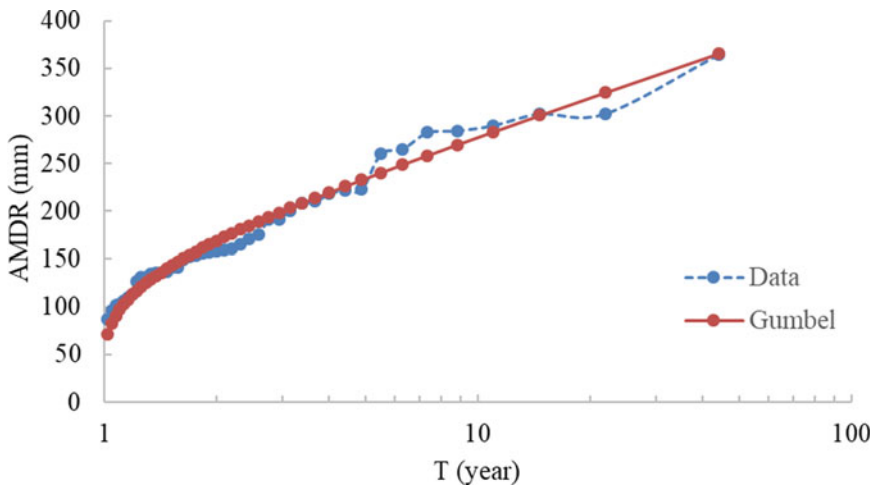
Fig. 3 Frequency curve for AMDR for Kuching city for period 1975–2017

5 Conclusion

This study presented the annual maximum daily rainfall (AMDR) trend for Kuching city for the years 1975 to 2017. High variability of AMDR was observed, with the month of January (during northeast monsoon) having the most occurrence of AMDR. It was also observed a slight downtrend of AMDR through the decades, but the trend was insignificant. From the study, the occurrence probability of AMDR events of magnitude 180 mm or more was 2.69 years. A frequency curve for AMDR was also developed in the current study for Kuching city. These results can be applied in planning for flood infrastructure for Kuching city.

References

1. Davies R (2021, July 21) China—massive floods hit Henan province after 600 mm of rain in 24 hours. Floodlist. https://floodlist.com/asia/china-floods-henan-zhengzhou-july-2021
2. Watts J (2021, July 16) Climate scientists shocked by scale of floods in Germany. The Guardian. https://www.theguardian.com/environment/2021/jul/16/climate-scientists-shocked-by-scale-of-floods-in-germany
3. Haktanir T, Bajabaa S, Masoud M (2013) Stochastic analyses of maximum daily rainfall series recorded at two stations across the Mediterranean Sea. Arab J Geosci 6(10):3943–3958
4. Porto de Carvalho JR, Assad ED, de Oliveira AF, Silveira Pinto H (2014) Annual maximum daily rainfall trends in the midwest, southeast and southern Brazil in the last 71 years. Weather Clim Extremes 5(1):7–15
5. Masereka EM, Ochieng GM, Snyman J (2018) Statistical analysis of annual maximum daily rainfall for Nelspruit and its environs. Jàmbá 10(1):a449
6. Vivekanandan V (2017) Assessment of extreme rainfall using Gumbel distribution for estimation of peak flood discharge for ungauged catchments. Int J Res Innov Social Sci 1(6):1–5
7. Zamir F, Hanif F, Naz S (2021) Extreme rainfall frequency analysis for Balakot, Pakistan, using Gumbel's distribution. Arab J Geosci 14:1283
8. Hasan GMJ, Chowdhury MAI, Ahmed S (2014) Analysis of the statistical behaviour of daily maximum and monthly average rainfall along with rainy days variation in Sylhet, Bangladesh. J Eng Sci Technol 9(5):559–578
9. Ghenim AN, Megnounif A (2016) Variability and trend of annual maximum daily rainfall in Northern Algeria. Int J Geophys. 2016:6820397
10. Othman MA, Zakaria NA, Ab. Ghani A, Chang CK, Chan NW (2015) Analysis of trends of extreme rainfall events using Mann-Kendall test: a case study in Pahang and Kelantan river basin. Jurnal Teknologi (Sci Eng) 72(1):1–6
11. Suhaila J, Deni SM, Zin WW, Jemain AA (2010) Trends in Peninsular Malaysia rainfall data during the southwest monsoon and northeast monsoon seasons: 1975–2004. Sains Malaysiana 39(4):533–542
12. Syafrina AH, Zalina MD, Juneng L (2015) Historical trend of hourly extreme rainfall in Peninsular Malaysia. Theoret Appl Climatol 120(1–2):259–285
13. Sa'adi Z, Shahid S, Ismail T, Chung E-S, Wang X-J (2019) Trends analysis of rainfall and rainfall extremes in Sarawak, Malaysia using modified Mann-Kendall test. Meteorol Atmos Phys 131:263–277
14. Bong CHJ, Ting SY, Bustami, RA, Putuhena FJ (2009) Impact of climate change and its variability on the rainfall pattern in Sarawak River Basin. Proceedings of International Conference on Water Resources (ICWR2009), Langkawi, Kedah, Malaysia
15. Tang KHD (2019) Climate change in Malaysia: trends, contributors, impacts, mitigation and adaptations. Sci Total Environ 650(2):1858–1871
16. Bong CHJ, Richard J (2020) Drought and climate change assessment using standardized precipitation index (SPI) for Sarawak River Basin. J Water Clim Change 11(4):956–965
17. Davies R (2016, February 29) Malaysia—flash floods in Kuching, Sarawak, after 300 mm of rain in 24 hours. Floodlist. https://floodlist.com/asia/malaysia-flash-floods-kuching-sarawak-300mm-rain

18. DID (2021) Resource centre—hydrology stations at Sg Sarawak Basin. Department of Irrigation & Drainage Sarawak. https://did.sarawak.gov.my/modules/web/pages.php?mod=webpage&sub=page&id=317
19. Asfaw A, Simane B, Hassen A, Bantider A (2018) Variability and time series trend analysis of rainfall and temperature in northcentral Ethiopia: a case study in Woleka sub-basin. Weather Clim Extremes 19:29–41
20. Kendall MG (1975) Rank correlation methods, 4th edn. Charles Griffin, London, UK
21. Mann HB (1945) Nonparametric tests against trend. Econometrica 13:163–171
22. Zaiontz C (2022). Real statistics using Excel. http://real-statistics.com/free-download/
23. Gumbel EJ (1960) Statistics of extremes, 2nd edn. Columbia University Press, New York
24. AgriMetSoft (2019) Distribution Calculators. https://agrimetsoft.com/distributions-calculator/gumbel-distribution-calculator

Development of Depth-Area-Duration (DAD) Curves for Kuantan River Basin

Norasman Othman, Nurul Farhana Abu Manshor, and Shairul Rohaziawati Samat

Abstract Depth-Area-Duration (DAD) analysis is a procedure to determine the maximum amount of rainfall of different durations over a range of areas. DAD analysis, also referred to as DAD curves, forms an important aspect of the hydrological study. In this study, the DAD curves for the Kuantan River Basin (KRB) were developed for durations of 1, 2 and 3-day. The rainfall data from the Department of Irrigation and Drainage Malaysia (DID) were collected for eight stations in KRB to determine maximum daily rainfall. The selected maximum rainfall data for each rainfall duration were extracted afterwards. The analysis was performed using isohyetal maps initially generated by the Inverse Distance Weighting (IDW) method to calculate the average of maximum rainfall depths for each rainfall duration. Since the maximum rainfall was required, the initial DAD curves for each duration were combined to produce a final DAD curve, which is mainly the maximum depth-area curve for the corresponding duration. This step was repeated for all durations, resulting in three final DAD curves for each time duration. By using this procedure, the average maximum rainfall for the basin area up to 1700 km^2 can be estimated.

Keywords Rainfall · Depth-Area-Duration curves · Isohyetal map · Kuantan River Basin

1 Introduction

In a hydrological study, a depth-area relationship is the areal distribution characteristics of a storm over a period of time. There are some interrelated aspects, including the depth, area, and duration of the storm. Depth-Area-Duration (DAD) analysis is a

N. Othman (✉) · S. R. Samat
Faculty of Civil Engineering Technology, Universiti Malaysia Pahang, Gambang, Malaysia
e-mail: norasman@ump.edu.my

S. R. Samat
e-mail: shairul@ump.edu.my

N. F. A. Manshor
College of Engineering, Universiti Malaysia Pahang, Gambang, Malaysia

procedure to determine the maximum amount of rainfall of different durations over a range of areas [1]. The DAD analysis is an important aspect of hydro-meteorological study in the development of the relationship between maximum depth-area-duration for an area. The maximum depth-area plot for the different duration is prepared by assuming the area distribution of rainfall. It is also referred to as DAD curves. The preparation of the DAD curve involves considerable computational effort and requires meteorological and regional topographical information. Detailed data on the most severe storms in the past is needed [2]. The analysis is commonly used for the development process in designing rainfall based on extreme rainfall events. Others, the preparation of the DAD curves is intended to determine the maximum rainfall depth for the study areas selected in different rainfall durations. Rainfall stations will record the amount of rain in each place. However, the average amount of maximum rainfall is often not recorded by the station. The study aims to develop DAD curves for different rainfall durations of 1-, 2-, and 3-day depending on the historical daily rainfall data of the Kuantan River Basin (KRB) from the year 2008 until 2019. The outcomes from this study could offer more information about maximum rainfall depth under various rainfall durations for hydrological design purposes in the KRB.

In recent decades, the radar-based system has been made available to detect and observe rainfall. According to Durrans et al. in 2002, a geographically fixed depth-area curve connects an average point rainfall depth derived from is pluvial maps for a fixed duration and return period to an average areal rainfall depth obtained from the same maps for the same duration and return period [3]. As a result, geographically fixed depth-area relationships are commonly employed in conjunction with data from precipitation-frequency studies. In this study, analysis of depth-area relationships by using NEXRAD radar-rainfall data for Arkansas-Red Basin River Forecast Center (ABRFC). Solaimani et al. [4] prepared the DAD curves of rainfalls in a semi-arid and arid region at Sirjan Kafeh Namak Watershed using the geostatistical method. The isohyets maps of 1 to 3 days duration were drawn by using the Kriging method, and DAD curves were constructed. It showed that the ratio of the amount of rainfall at the centre over the amount of rainfall at an area of 20,000 km^2 is 1.98, 1.74 and 1.48 for durations of 1-, 2- and 3-day, respectively. In 2009, Mohammadi et al. obtained the DAD curves in the Kurdistan Province for time durations of 24-, 48-, 72- and 96-h. The calculations of the Moving Average method have been used to develop isohyetal maps. It was found that rainfall with a duration of two or more days indicates stable climatic systems. Such stable climatic systems always produce more rainfall.

Parzybok et al. [5] have used data sources from precipitation radar algorithms to develop precipitation depth-area relationships. It summarizes the utility of DAD for monitoring storms that have occurred, are occurring or the forecasted to occur over a specific region, watershed, or catchment. The information contained in near real-time DAD curves could be used for activating emergency action plans (EAPS) and initiating flood warnings. Kim et al. [6] summarize the DAD analysis provides a basis for analysing drought events when storm depth is replaced by an appropriate measure of drought severity which is called the drought severity–effective area-drought duration (SAD) curves. Monthly rainfall data from 58 rainfall measuring sites under the Korean meteorological administration was used, and the SAD curves were

displayed with the variability of drought severity with respect to the effective drought area and drought duration. When the duration of a drought event was extended, or the effective area of a drought event was extended, the severity reduction rate in SAD curves was reduced. Meanwhile, Patrick et al. [7] developed the DAD of maximum rainfall relationships based on the rainfall event in January 2004 as a case study over Sungai Sarawak Basin. The study discovered that if a specific area within a certain duration increases, then the maximum areal average rainfall will decrease. Furthermore, when the time in a certain objective area increases, so does the maximum areal average rainfall in the DAD curves. They were also noticed that there is no major relevance or relationship between rainfall and elevation.

2 Methodology

2.1 Study Area

The study was focused on the whole Kuantan River Basin (KRB), which is located in Pahang Darul Makmur. KRB is the third largest basin in Pahang after Pahang River Basin and Rompin River Basin, with an area of approximately 1703.15 km^2. The length of the Kuantan River is 99.8 km with Sungai Keliu upstream, and it ends in the South China Sea at Tanjung Lumpur. Figure 1 shows the map of the Kuantan River Basin.

2.2 Data Collection

The rainfall in KRB is very much influenced by the monsoon season. In general, the northeast monsoon was known as the wet season in Malaysia, which carries more rainfall compared to the southwest monsoon or known as the dry season. The northeast monsoon has the greatest influence on rainfall in this area, especially those on the coastline. The wettest months usually happened in December and January. Meanwhile, the driest months occurred in February and April. The southwest monsoon also influences the rainfall but not to the same degree as the northeast monsoon.

For this study, all rainfall data are obtained from the Department of Irrigation and Drainage (DID) Malaysia from the year 2008 until 2019. The data were collected and extracted from eight stations in KRB into maximum daily rainfall for 1-, 2-, and 3-day. Table 1 shows the list of the rainfall stations in KRB.
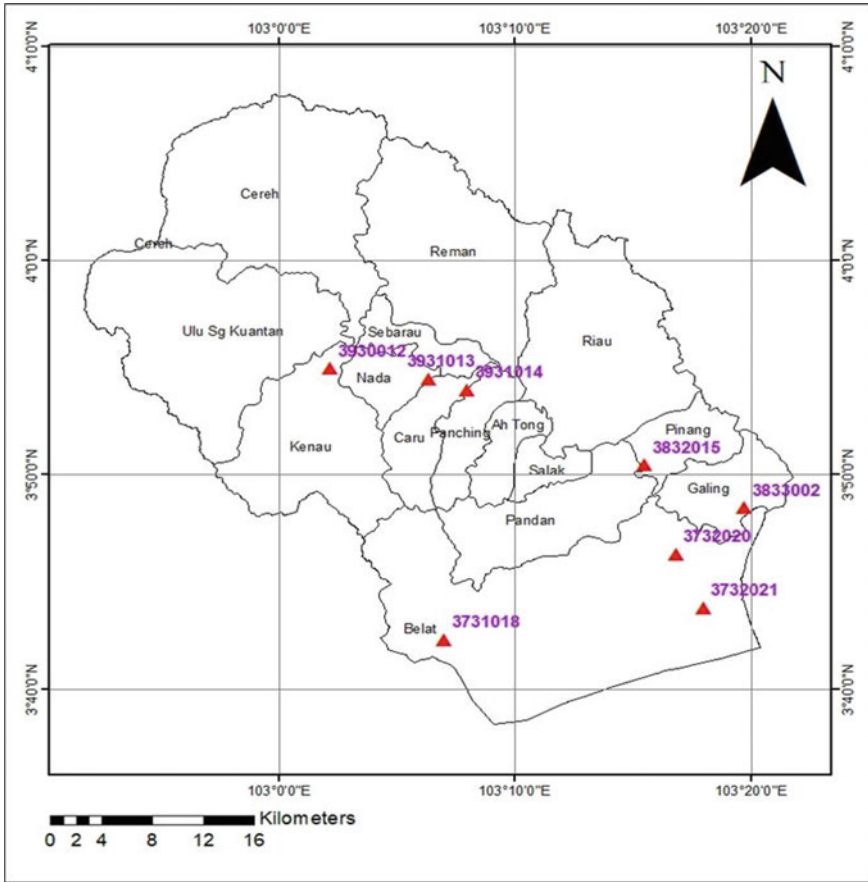
Fig. 1 Map of Kuantan River Basin

Table 1 List of rainfall stations in KRB

Station ID	Station name	Latitude	Longitude
3731018	JKR Gambang	03° 42′ 20″ N	103° 07′ 00″ E
3732020	Paya Besar di Kuantan	03° 46′ 20″ N	103° 16′ 50″ E
3732021	Kg. Sg. Soi	03° 43′ 50″ N	103° 18′ 00″ E
3832015	Rancangan Pam Paya Pinang	03° 50′ 30″ N	103° 15′ 30″ E
3833002	Pejabat JPS Negeri Pahang	03° 48′ 30″ N	103° 19′ 45″ E
3930012	Sg. Lembing P.C.C.L Mill	03° 55′ 00″ N	103° 02′ 10″ E
3931013	Ldg. Nada	03° 54′ 30″ N	103° 06′ 20″ E
3931014	Ldg. Kuala Reman	03° 54′ 00″ N	103° 08′ 00″ E

2.3   Selection of Rainfall Data

In this study, the daily data were chosen and extracted for the time durations of 1 day, 2 days and 3 days for 11 years. Next, the maximum rainfall for each duration was selected. About 19 rainfall events were identified and used to prepare the DAD curves. The selected events include six rainfalls of 1 day, seven rainfalls of 2 days, and six rainfalls of 3 days.

2.4   Drawing of Isohyetal Maps

The isohyetal lines of the KRB were prepared using the information of rainfall stations such as longitude, latitude and maximum rainfall depths of eight rainfall stations. The Inverse Distance Weighting (IDW) interpolation method was used to draw the isohyetal lines. This method assumes that objects that are close nearby are more similar than objects that are far apart. IDW estimates a value for an unmeasured area based on the measured values in the estimation area's surroundings. The closer the measured values are to the estimation location, the greater their effect on the estimated value [8].

2.5   Initial DAD Curves

For each rainfall event with 1-, 2-, and 3-day durations, calculations of cumulative area and average maximum rainfall were conducted, and the initial DAD curves were plotted. The cumulative area is plotted on the X-axis and the average of maximum rainfall on the Y-axis to draw the curves.

2.6   Final DAD Curves

The final DAD curves are the combination of the selected initial DAD curves of 1-, 2, and 3-day durations. After determination of the initial DAD curve for each rainfall, the maximum rainfall among all three different durations was selected. Then, the final DAD curves were developed. The X-axis represents the area of the KRB. The Y-axis represents the maximum value of rainfall with the same duration can be inferred from the initial DAD curves. For example, if six curves of 1-day rainfall are to be combined, the corresponding rainfall in mm (Y) of each particular area in km^2 (X) needs to be found, and then for each area, the maximum rainfall should be chosen. This procedure should be repeated for the seven 2-days rainfall initial DAD curves

and six 3-days rainfall initial DAD curves. Then to plot the final DAD curves, the values of the maximum rainfalls are plotted against their corresponding area.

3   Results and Discussion

Since 19 rainfall events were selected for three different durations, the isohyetal lines were developed using the IDW interpolation method. From the assessment, all those rainfall events occurred during the northeast monsoon, which contributed to the heavy rainfall in December and January. Then, analysis of isohyetal lines found that the amount of rainfall depths significantly increases from the upper (northwest) of the basin toward the lower (southeast) of the basin. All isohyetal lines from 19 rainfall events for 1-, 2- and 3-day duration have been analysed in Tables 2, 3 and 4, respectively, to select the maximum rainfall values for each area/km^2. Figure 2 shows an example for the isohyetal map of the 1-day rainfall on 1/1/2018 for every 10 mm rainfall depth in KRB using the IDW method and the distribution of studied rainfall stations.

After developing isohyetal lines, the analysis of the cumulative area and average maximum rainfall were calculated. The initial DAD curves were obtained for each rainfall event using the calculated parameter, and the maximum rainfall among all three different duration was selected. Table 5 represents the example of calculation of a 1-day rainfall event on 1/1/2018, and the initial DAD curves were plotted. Meanwhile, Fig. 3 illustrates the initial DAD curve for 1-day rainfall on 1/1/2018 in KRB.

Next, the final DAD curves are developed. The DAD curves for different rainfall with identical durations were combined. The combination of the selected initial DAD

Table 2 The amount of 1-day rainfall for different areas

Area/km^2	2/1/2009	3/1/2009	12/1/2012	24/12/2012	24/1/2017	1/1/2018	Maximum rainfall (mm)
10	193.35	206.67	233.43	311.75	393.82	245.29	393.82
20	188.68	204.65	228.70	304.75	388.27	242.69	388.27
50	179.72	198.62	221.20	289.10	378.03	235.63	378.03
100	168.49	192.02	213.91	264.65	367.87	226.41	367.87
200	156.34	188.30	208.91	242.06	351.44	215.07	351.44
400	147.93	180.87	200.97	218.97	325.03	204.52	325.03
600	141.81	175.84	197.34	202.34	304.96	200.03	304.96
800	138.77	172.13	194.78	190.43	288.81	195.54	288.81
1000	135.73	168.58	192.20	181.40	277.66	191.35	277.66
1350	130.99	163.24	188.42	169.30	261.55	187.58	261.55
1700	126.52	157.59	183.85	158.61	249.27	183.31	249.27

Table 3 The amount of 2-days rainfall for different areas

Area/km^2	23/1/2017	24/1/2017	2/1/2009	1/1/2018	23/12/2012	31/12/2017	11/1/2012	Maximum rainfall (mm)
10	473.84	455.40	398.14	336.39	472.03	317.28	280.25	473.84
20	464.87	445.44	391.75	334.16	466.98	315.00	275.78	466.98
50	451.63	426.59	378.09	327.93	458.74	308.24	268.51	458.74
100	438.81	409.47	358.78	321.26	449.69	298.12	263.78	449.69
200	419.53	389.01	339.30	315.07	434.52	286.31	258.27	434.52
400	389.99	359.30	321.41	307.90	399.35	274.91	253.39	399.35
600	367.64	336.15	310.88	303.08	366.07	269.54	248.52	367.64
800	348.93	317.59	304.63	298.88	341.84	264.17	246.68	348.93
1000	335.48	304.55	300.25	295.47	324.26	261.29	244.85	335.48
1350	316.87	286.29	292.58	289.76	302.03	256.34	241.64	316.87
1700	302.79	272.45	285.08	284.53	283.65	250.83	236.40	302.79

Table 4 The amount of 3-days rainfall for different areas

Area/km^2	1/1/2009	1/1/2018	31/12/2017	23/1/2017	23/12/2012	22/1/2017	Maximum rainfall (mm)
10	498.28	442.91	404.53	535.09	580.53	479.92	580.53
20	490.42	438.96	401.11	523.89	574.48	474.95	574.48
50	473.24	431.97	393.71	501.38	561.84	466.11	561.84
100	449.82	427.37	387.04	480.64	548.38	454.61	548.38
200	430.20	420.76	380.22	457.43	529.27	435.55	529.27
400	415.50	412.39	373.98	424.23	489.91	405.36	489.91
600	406.65	404.65	368.48	398.64	452.45	382.90	452.45
800	403.31	397.05	364.83	377.56	424.33	365.03	424.33
1000	399.97	390.37	362.02	362.23	404.48	351.75	404.48
1350	394.17	380.37	357.11	341.73	379.29	334.07	394.17
1700	386.74	372.17	352.28	325.87	357.98	320.48	386.74

curves of 1-, 2-, and 3-day durations is called the final DAD curves. Table 6 shows the maximum rainfall for different areas and durations, while Fig. 4 demonstrates the final DAD curves for KRB.

From the final DAD curves, the amount of rainfall in 10 km^2 areas of KRB increases with the different time durations. The maximum amount for 1 day, 2 days, and 3 days of rainfall are 393.82 mm, 473.84 mm and 580.53 mm, respectively. This means that by increasing the duration from 1-day to 3-day, the rainfall depths increase. There is a gap between 1-, 2- and 3-day duration rainfalls. The gap between 1 and 2 days gradually decreases around 1 mm to 2 mm for up to an area of 50 km^2. By increasing the area, the amounts of rainfall for 1 day and 2 days duration are closed to one another. For example, in the area of 600 km^2, the difference is 63 mm,
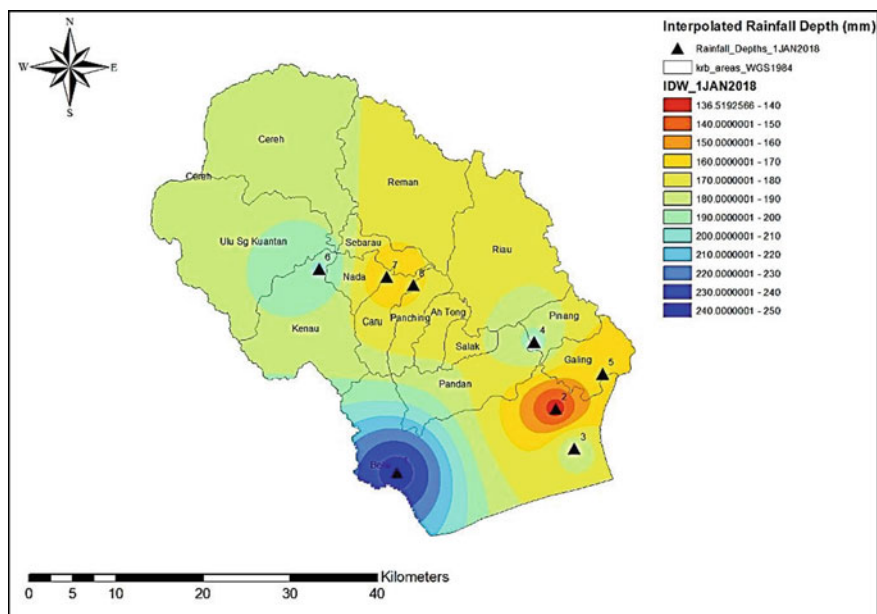
Fig. 2 The isohyetal map of the 1-day rainfall on 1/1/2018 in KRB using IDW

Table 5 Calculation of 1 day rainfall event on 1/1/2018

Limit of isohyetal lines	Average of isohyetal (mm)	Area (km^2)	Cumulative area (km^2)	Volume of the rainfall (mm·km^2)	Volume of the cumulative (mm·km^2)	Average of maximum rainfall (mm)
240.01–250	245.01	11.07	11.07	2,713.28	2,713.28	245.01
230.01–240	235.01	27.45	38.52	6,450.74	9,164.02	237.88
220.01–230	225.01	26.98	65.50	6,069.76	15,233.79	232.58
210.01–220	215.01	31.61	97.11	6,797.20	22,030.99	226.86
200.01–210	205.01	41.36	138.47	8,479.72	30,510.71	220.33
190.01–200	195.01	157.69	296.16	30,750.84	61,261.56	206.85
180.01–190	185.01	676.90	973.06	125,232.63	186,494.19	191.66
170.01–180	175.01	566.15	1,539.21	99,082.77	285,576.96	185.53
160.01–170	165.01	124.94	1,664.15	20,616.24	306,193.20	183.99
150.01–160	155.01	23.80	1,687.96	3,689.97	309,883.17	183.58
140.01–150	145.01	11.97	1,699.93	1,736.20	311,619.36	183.31
136.52–140	138.26	3.22	1,703.15	444.94	312,064.30	183.23
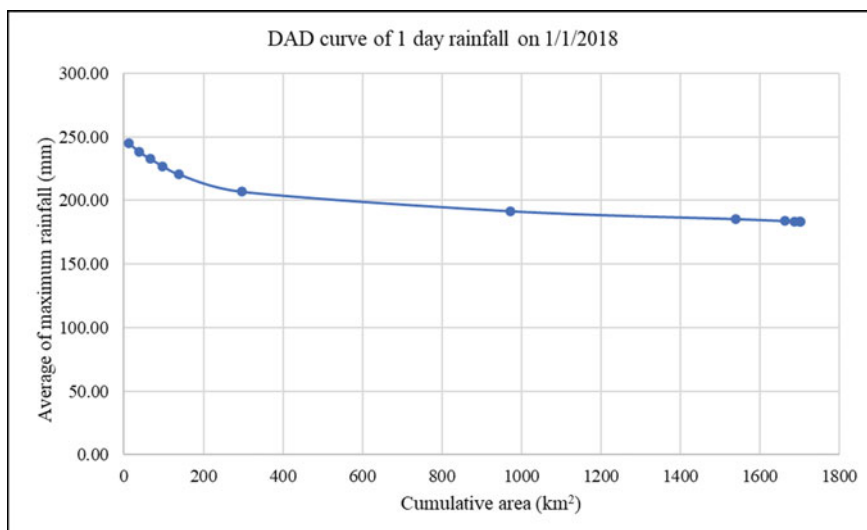
Fig. 3 DAD curve of 1 day rainfall on 1/1/2018

Table 6 The maximum rainfall (mm) for different areas and durations

Area/km^2	1 day	2 days	3 days
10	393.82	473.84	580.53
20	388.27	466.98	574.48
50	378.03	458.74	561.84
100	367.87	449.69	548.38
200	351.44	434.52	529.27
400	325.03	399.35	489.91
600	304.96	367.64	452.45
800	288.81	348.93	424.33
1000	277.66	335.48	404.48
1350	261.55	316.87	394.17
1700	249.27	302.79	386.74

and in an area of 1700 km^2, the difference is 54 mm. The differences between 2 and 3 days duration rainfalls are a decrease in the area of 50 km^2 and an increase in the area of 600 km^2.
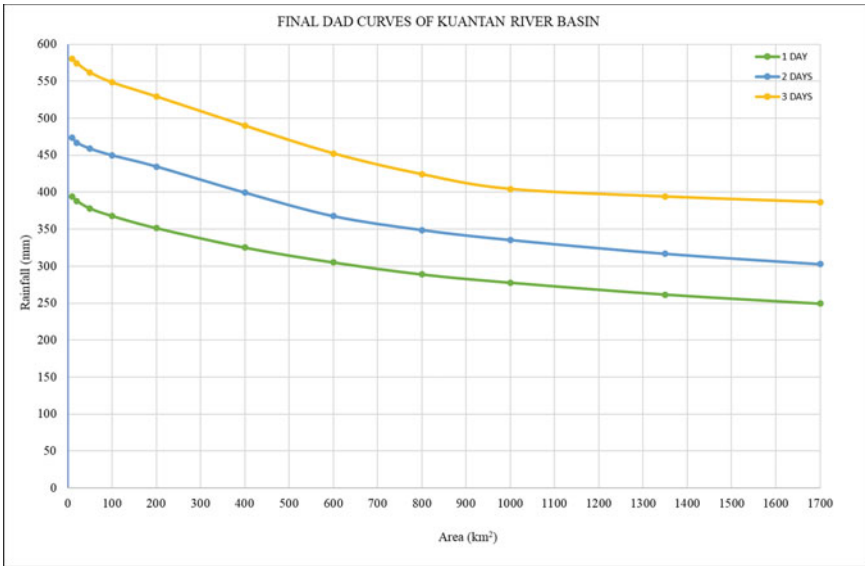
Fig. 4 Final DAD curves of Kuantan River Basin

4   Conclusions

In conclusion, all the objectives of this study were successfully achieved. The daily historical data of rainfall distribution within KRB have been analysed using the IDW interpolation method to generate the isohyet maps for maximum rainfall events of 1-, 2- and 3-day. After that, the DAD curves for 1-, 2- and 3-day rainfall duration of KRB have been developed. The average maximum rainfall depths for 1-, 2- and 3-day duration of KRB have been examined when the duration in a certain selected area increases, thus does the maximum areal average rainfall in the DAD curves.

The study also found that if a specific area within a certain duration increases, then the maximum areal average rainfall will be decreased. In order to enhance the limitation of KRB's DAD curves, we can use other rainfall durations such as 1 h, 6 h, 12 h, 4 days, 5 days, 6 days or 7 days. Since the DAD curves are produced based on real rainfall data for each specific area, the developed curves for one area cannot be used for the other area because the rainfall in KRB has its own specific characteristics. The plotted DAD curves can be further investigated to estimate the probable maximum precipitation (PMP) for hydraulic structure design needs, and the plotted DAD curves can be used as important for monitoring storms that have occurred, are occurring or are forecasted to occur in order to activate emergency action plans (EAPs) or initiating flood warnings. As a result, it can control and forecast the flood for the future.

References

1. Mohammadi SE, Mahdavi M (2009) Investigation of depth-area-duration curves for Kurdistan Province. World Appl Sci J 6(12):1705–1713
2. Subramanya K (2009) Engineering hydrology, 3rd edn. Tata McGraw-Hill
3. Durrans SR, Julian LT, Yekta M (2002) Estimation of depth-area relationships using radar-rainfall data. J Hydrol Eng 7(5):356–367. https://doi.org/10.1061/(asce)1084-0699(2002)7:5(356)
4. Solaimani K, Abkar A, Habibnejad M, Ahmadi MZ (2006) Analysis of depth-area-duration curves of rainfall in semi-arid and arid regions using geostatistical methods (case study: Sirjan Kafeh Namak Watershed). Pak J Biol Sci 9(9):1764–1768. https://doi.org/10.3923/pjbs.2006.1764.1768
5. Parzybok TW, Hultstrand DM, Tomlinson EM, Kappel B (2009) Real-time depth-area duration analysis for EAPs and flood warning systems. Association of State Dam Safety Officials Annual Conference 2009, Dam Safety 2009, 2, pp 680–685
6. Kim S, Kim B, Ahn TJ, Kim KHS (2011) Spatio-temporal characterization of Korean drought using severity-area-duration curve analysis. Water Environ J 25(1):22–30. https://doi.org/10.1111/j.1747-6593.2009.00184.x
7. Patrick M, Mah DYS, Putuhena FJ, Wang YC, Selaman OS (2019) Constructing depth-area-duration curves using public domain satellite-based precipitation data. Int J Hydrol Sci Technol 9(3):281–302. https://doi.org/10.1504/IJHST.2019.102317
8. Johnston K, Ver Hoef JM, Krivoruchko K, Lucas N (2013) Using ArcGIS geostatistical analyst using ArcGIS geostatistical analyst. Esri, USA

A Feasibility Study of Fitting the Normal Distribution and Gamma Distribution to Rainfall Data at Kuantan River Basin

Nadiatul Adilah Ahmad Abdul Ghani, Azlyna Senawi, and Roshan Subramaniam

Abstract Rainfall data can be very useful for decision makers in developing precautionary strategies to mitigate the impact of climate change in a variety of ways, such as forecasting floods. Prior to the data being utilised, it is critical to determine the best fit probability distribution of the data. Only after this has been done then it is possible to obtain reliable analysis and results. In this study, the feasibility of fitting the data with normal distribution was investigated. The investigation specifically used peak monthly values of rainfall data from ten hydrological stations of the Kuantan River Basin during the year 1975 to 2017. Four different test statistics were employed to assess the possibility of fitting the data to the normal and Gamma distributions: Skewness, excess kurtosis, Kolmogorov–Smirnov and Shapiro–Wilk. Results obtained show that normal distribution fits well with the annual daily maximum rainfall data for only two hydrological stations, but normal distribution is not a good fit for the seasonal daily maximum rainfall case for all stations involved. Gamma 1P distribution was found to be not an ideal fit for both annual and seasonal data for all stations, but Gamma 2P, on the contrary, was discovered to fit well for all stations except one station. The findings of the study are anticipated to improve rainfall forecasting in the future.

Keywords Rainfall · Kuantan river basin · Normal distribution · Gamma distribution · Kolmogorov–Smirnov · Skewness

N. A. A. A. Ghani (✉) · R. Subramaniam
Department of Civil Engineering, College Engineering, Universiti Malaysia Pahang, Lebuhraya Tun Razak, 26300 Kuantan, Pahang, Malaysia
e-mail: nadiatul@ump.edu.my

A. Senawi
Centre for Mathematical Sciences, College of Computing and Applied Sciences, Universiti Malaysia Pahang, Lebuhraya Tun Razak, 26300 Gambang, Kuantan, Pahang, Malaysia
e-mail: azlyna@ump.edu.my

Centre for Software Development & Integrated Computing, Universiti Malaysia Pahang, Lebuhraya Tun Razak, 26300 Gambang, Kuantan, Pahang, Malaysia

1 Introduction

The rainfall trend is changing on both the global and the regional scale due to global warming. The discrete nature of rainfall amount in time and space has always posed more unique problems if compared to more continuous climatic elements such as temperature and pressure. Rainfall data analysis heavily relies on its distribution pattern. Identifying the right probability distribution allows simulation or forecasting the rainfall amount accurately. The probability of occurrence of rainfall amount is varied during the whole year due to the seasonal rainfall in Malaysia as stated in [1].

Establishing a probability distribution that provides a good fit for rainfall data has been a topic of interest in numerous literature. Zalina [2] performed a comparative assessment of eight candidate distributions. Annual maximum rainfall series for a one-hour duration from 17 gauging stations located in Peninsular Malaysia were studied. The considered distributions were the Gamma, generalised normal, Generalised Pareto, Generalised Extreme Value (GEV), Gumbel, Log Pearson Type III, Pearson Type III and Wakeby. Nashwan et al. [3] assessed the nonstationary behaviour of extreme rainfall amounts in Peninsular Malaysia. The 20-h rainfall data with a minimum amount of missing values from twenty-two stations distributed over Peninsular Malaysia were fitted using GEV distributions. The results revealed a nonstationary character in maximum rainfall amounts of different rainfall durations at the majority of the stations in Peninsular Malaysia. In [4], the Gamma distribution was found as a good fit for the daily up to the ten-day cumulative rainfall data.

The main objective of this study is to assess the feasibility of fitting the normal distribution and gamma distribution to rainfall data from 10 stations at the Kuantan river basin. The skewness, excess kurtosis, Kolmogorov–Smirnov and Shapiro–Wilk were utilized as test statistics to investigate the feasibility of the considered distributions.

2 Datasets

This research is based on rainfall data obtained from 10 hydrological stations located around the Kuantan river basin for the year 1975 to 2017. Supervision and collection of the data were done by the Department of Irrigation and Drainage (JPS), Kuantan, Pahang. Table 1 lists the location details of the hydrological stations involved in the study.

The data were extracted from every hydrological station according to the maximum daily rainfall received on any one day of each year and each month of the monsoon season (November to March). Based on [5], monitoring and studying the pattern of weather in the surrounding is very important because changing trends in rainfall distribution also have an effect on hydrological analysis especially related to historical rainfall records.

Table 1 Location details of the 10 hydrological stations

Station	Station name	Latitude	Longitude
3631001	Kg. Pulau Manis	3.65	103.12
3731018	SK Gambang	3.72	103.14
3732020	Paya Besar, Kuantan	3.77	103.28
3732021	Ladang Kuala Reman	3.90	103.13
3832015	Rancangan Pam Paya Pinang	3.84	103.26
3833002	Kg. Sg. Soi	3.73	103.30
3930012	Ladang Nada	3.91	103.11
3931013	Sg. Lembing PCCL Mill	3.92	103.04
3931014	Pejabat JPS Negeri Pahang	3.81	103.33
3933003	Balok, Kuantan	3.94	103.38

Table 2 Probability distributions being considered

Distribution	Probability density function	Parameters
Normal	$f(x) = \frac{1}{\sigma\sqrt{2\pi}}\exp\left(-\frac{(x-\mu)^2}{2\sigma^2}\right)$ where $-\infty < x < \infty$	$\mu = \text{mean}$ $\sigma = \text{standard deviation}$
Gamma 1P	$f(x) = \frac{x^{\alpha-1}}{\Gamma(\alpha)}\exp(-x)$ where $x > 0, \alpha > 0$	$\alpha = \text{shape parameter}$ $\Gamma = \text{gamma function}$ $\beta = \text{inverse scale parameter}$
Gamma 2P	$f(x) = \frac{x^{\alpha-1}}{\beta^\alpha \Gamma(\alpha)}\exp(-\frac{x}{\beta})$ where $x > 0,\ \alpha > 0, \beta > 0$	

3 Fitting Data into Probability Distributions

Two different probability distributions are considered for this study: Normal and Gamma distributions. Two variants of Gamma distribution were tested: one-parameter-Gamma (Gamma 1P) and two-parameter-Gamma (Gamma 2P). The description of these probability distributions is given in Table 2.

Four different test statistics were employed: Skewness, excess kurtosis, Kolmogorov–Smirnov and Shapiro–Wilk. The XLSTAT, which is an add on package for Microsoft Excel was used to perform the analysis.

4 Skewness and Excess Kurtosis

Skewness provides a measure of the symmetry of data distribution. A dataset has symmetric distribution if it appears identical to the left and right of the distribution's centre point. A dataset whose distribution is symmetrical such as normal distribution

would have a skewness value of zero or near to zero. If the skewness value is positive, the distribution is positively skewed, of which heavier tail can be observed on the right side than the left side of the distribution. On the contrary, if the skewness value is negative, the data are negatively skewed. A general rule of thumb to determine the skewness level is suggested as follow [6]:

- If the skewness value is between -0.5 and 0.5, the distribution of the data is approximately symmetric.
- If the skewness value is either between -1 and -0.5 or between 0.5 and 1, the distribution of the data is slightly skewed.
- If the skewness value is less than -1 or larger than 1, the distribution of the data is heavily skewed.

Kurtosis is a numerical measure that quantifies the degree of the peak and the tails of a distribution. A higher value of kurtosis indicates a higher and sharper peak as well as the presence of a light-tailed distribution. Meanwhile, a lower value suggests a lower and less visible peak, with a heavy-tailed distribution. The values of kurtosis range from 1 to infinity, and a normal distribution has a kurtosis value of 3 [7]. Since associating the kurtosis to the normal distribution is of interest in this study, the excess kurtosis is used here for easier comparison. The excess kurtosis is calculated by subtracting kurtosis by 3. Therefore, a normal distribution would have a kurtosis of zero or near zero. Positive kurtosis indicates a heavy-tailed distribution is inherent, while negative kurtosis indicates a light-tailed distribution.

In this study, a series of analyses were conducted to find the values of excess kurtosis and skewness on each extracted dataset. The results of these measures are basically useful to understand where the majority of the data is concentrated.

Deciding on the normality of a dataset solely on the basis of its skewness and kurtosis scores is too risky [8]. Therefore, the results of the calculated skewness and kurtosis that seem to suggest normal distribution should be verified using a goodness-of-fit test.

5   Goodness-of-Fit Tests

A goodness-of-fit test is used to measure how well the data fit a hypothesized theoretical distribution. In particular, the following null and alternative hypotheses are tested in a goodness-of-fit test:

H_0 : The maximum daily rainfall data follow a specified distribution
H_1 : The maximum daily rainfall data do follow the specified distribution

In this study, a level of significance $\alpha = 0.05$ that acts as a reference point to identify whether significant probability distribution is fitted for the data was employed.

i. Kolmogorov–Smirnov Test

The Kolmogorov–Smirnov test statistic is calculated by comparing the maximum distance between the experimental cumulative distribution function (EDF) and the theoretical cumulative distribution function (CDF). The test statistic is defined by

$$D = \max_{1 \leq i \leq n} |F_n(X_i) - F(X_i)| \tag{1}$$

where n is the sample size, $F_n(X_i)$ represents the EDF and $F(X_i)$ denotes the CDF.

ii. Shapiro–Wilk Test

The Shapiro–Wilk test statistic is computed based on the correlation between the observed data and the corresponding normal scores. This statistic is recommended as numerical means of assessing normality when the sample size is less than 50 [9]. The test statistic is given by

$$W = \frac{\left(\sum_{i=1}^{n} a_i x_{(i)}\right)^2}{\sum_{i=1}^{n} (x_i - \overline{x})^2} \tag{2}$$

where n is the sample size, x_i are the sample values, $x_{(i)}$ are the i-th order sample values with $x_{(1)}$ is the smallest and $\overline{x}$ is the sample mean. The constants a_i are computed based on the means, variances and covariances of the ordered sample values which are independent and identically distributed random variables from a normal distribution. The value of W lies between zero and one. A small value of W indicates that the data are far from normality, whereas a value of one signifies normality of the data.

If the p-value of the test statistic is greater than α, the null hypothesis is not rejected. In other words, the considered data follows the specified distribution in the null hypothesis.

The Kolmogorov–Smirnov statistic was used to test the feasibility of fitting normal distribution and gamma distribution on each extracted dataset. However, when a normal distribution and the sample size is less than 50 (i.e. when the maximum daily rainfall of annual rainfall data) were considered, the Shapiro–Wilk test was used instead.

6   Results and Discussion

Table 3 presents the skewness, excess kurtosis and p-value of the Shapiro–Wilk test results for the annual daily maximum rainfall data. Note that the Shapiro–Wilk test was used for normality assessment because the sample size for each station involved is less than 50. It can be observed that based on the skewness values, rainfall data

Table 3 Skewness, excess kurtosis and *p*-value of the Shapiro–Wilk test for normal distribution fitting of the annual daily maximum rainfall data

Station name	Skewness	Excess kurtosis	Shapiro–Wilk (*p*-value)
Kg. Pulau Manis	1.29	1.37	0.0001
SK Gambang	1.34	1.81	0.0003
Paya Besar	**−0.25**	−1.22	0.0064
Ladang Kuala Reman	0.74	**0.01**	0.0071
Rancangan Pam Paya Pinang	1.43	2.91	0.0006
Kg. Sg. Soi	1.55	2.83	0.0001
Ladang Nada	**0.46**	**−0.29**	**0.1198**
Sg. Lembing PCCL Mill	0.96	0.75	0.0064
Pejabat JPS Negeri Pahang	0.60	**0.05**	**0.0901**
Balok	1.41	5.33	0.0025

from Paya Besar and Ladang Nada stations suggest normal distribution is a possible fit, provided that the $-0.5 <$ skewness < 0.5. However, from these two stations, only Ladang Nada data provides further evidence that normal distribution is a good fit as suggested by the excess kurtosis value which is close to 0. When the *p*-value of the Shapiro–Wilk test is compared with $\alpha = 0.05$, the Ladang Nada data is confirmed to fit the normal distribution. In the meantime, the annual daily maximum rainfall data collected from Pejabat JPS Negeri Pahang station also fit with the normal distribution as indicated by excess kurtosis and Shapiro–Wilk test results. Although its skewness statistic is greater than 0.5, the difference is not significant to deny the normal distribution is appropriate. Despite the fact that excess kurtosis of the Ladang Kuala Reman data is very close to 0, which indicates normal distribution is relevant, both of its skewness and Shapiro–Wilk test results state the opposite.

Referring to Table 4, none of the skewness, excess kurtosis and *p*-value of the Kolmogorov–Smirnov test suggests normal distribution is a good fit for the seasonal daily maximum rainfall data for all hydrological stations.

Since many of the considered cases of the rainfall data have right-skewed distribution (skewness > 0), Gamma distribution can be considered as one of the possible alternatives for fitting a more appropriate distribution. Two variants of Gamma distribution were tested: Gamma 1P and Gamma 2P. The same rainfall datasets as listed in Tables 3 and 4 were used again for this purpose.

The Kolmogorov–Smirnov test results in Table 5 show that the annual daily maximum rainfall data for all stations do not fit with the Gamma 1P distribution since all *p*-values are less than $\alpha = 0.05$. In contrast, the Gamma 2P distribution fits all stations.

Table 4 Skewness, excess kurtosis and *p*-value of the Kolmogorov–Smirnov test for normal distribution fitting of the seasonal daily maximum rainfall data

Station name	Skewness	Excess kurtosis	Kolmogorov–Smirnov (*p*-value)
Kg. Pulau Manis	2.09	5.69	0.00
SK Gambang	2.67	9.04	0.00
Paya Besar	1.22	0.61	0.00
Ladang Kuala Reman	1.74	3.04	0.00
Rancangan Pam Paya Pinang	2.68	9.98	0.00
Kg. Sg. Soi	2.02	5.83	0.00
Ladang Nada	1.60	2.60	0.00
Sg. Lembing PCCL Mill	1.59	3.63	0.00
Pejabat JPS Negeri Pahang	1.27	1.39	0.00
Balok	1.92	6.23	0.00

Table 5 Kolmogorov–Smirnov test results (*p*-values) for Gamma distribution fitting of the annual daily maximum rainfall data

Station name	Gamma 1P	Gamma 2P
Kg. Pulau Manis	<0.0001	**0.072**
SK Gambang	<0.0001	**0.403**
Paya Besar	<0.0001	**0.235**
Ladang Kuala Reman	<0.0001	**0.774**
Rancangan Pam Paya Pinang	<0.0001	**0.813**
Kg. Sg. Soi	<0.0001	**0.855**
Ladang Nada	<0.0001	**0.812**
Sg. Lembing PCCL Mill	<0.0001	**0.588**
Pejabat JPS Negeri Pahang	<0.0001	**0.880**
Balok	<0.0001	**0.311**

When seasonal daily maximum rainfall data are considered, all stations do not fit well with the Gamma 1P distribution as for the annual daily maximum rainfall data (Table 6). Conversely, all datasets exhibited a good fit with the Gamma 2P except for the SK Gambang station. A new distribution method can be introduced to improve the performance of all stations to overcome this problem.

Table 6 Kolmogorov–Smirnov test results for Gamma distribution fitting of the seasonal daily maximum rainfall data

Station name	Gamma 1P	Gamma 2P
Kg. Pulau Manis	<0.0001	**0.087**
SK Gambang	<0.0001	0.003
Paya Besar	<0.0001	**0.709**
Ladang Kuala Reman	<0.0001	**0.088**
Rancangan Pam Paya Pinang	<0.0001	**0.028**
Kg. Sg. Soi	<0.0001	**0.770**
Ladang Nada	<0.0001	**0.418**
Sg. Lembing PCCL Mill	<0.0001	**0.309**
Pejabat JPS Negeri Pahang	<0.0001	**0.490**
Balok	<0.0001	**0.563**

7 Conclusion

Normal distribution fits well with the annual daily maximum rainfall data for only two hydrological stations out of 10. On the other hand, when the seasonal daily maximum rainfall data are considered, the normal distribution is not an adequate fit. Further observations revealed that Gamma 1P distribution is not an ideal fit for both annual and seasonal data for all stations, but Gamma 2P, on the contrary, appeared to fit well for all stations except one station. Based on these findings, it proved that normal distribution is not really suitable for analyzing data for these areas, but results using Gama 2P distribution perform well and are suitable to be used for data collected in these areas.

References

1. Suhaila J, Jemain AA (2009) A comparison of the peninsular of the rainfall patterns between stations on the East and the West coasts of peninsular Malaysia using the smoothing model of rainfall amounts. Met Appl 16:391–401
2. Zalina MD, Desa MNM, Nguyen VTA, Kassim AHM (2002) Selecting a probability distribution for extreme rainfall series in Malaysia. Water Sci Technol 45(2):63–66
3. Nashwan MS, Tarmizi I, Kamal A (2019) Non-stationary analysis of extreme rainfall in peninsular Malaysia. J Sustain Sci Manage 14(3):17–34
4. Bermudez VAB, Abilgos ABB, Cuaresma DCN, Rabajante JF (2017) Probability distribution of Philippine daily rainfall data.

5. Nadiatul Adilah AAG, Mohamad Zarif M, Mohamad Idris A (2020) Rainfall trend analysis using box plot method: case study UMP Gambang and Pekan. IOP Conf Ser: Mater Sci Eng 712:012021
6. Awala SK, Hove K, Wanga MA, Valombola JS, Mwandemele OD (2019) Rainfall trend and variability in semi-arid northern Namibia: implications for small holder agricultural production. Welwitschia Int J Agric Sci 1:1–25
7. Cain MK, Zhang Z, Yuan KH (2017) Univariate and multivariate skewness and kurtosis for measuring nonnormality: prevalence, influence and estimation. Behav Res Methods 49(5):1716–1735
8. Orcan F (2020) Parametric or non-parametric: skewness to test normality for mean comparison. Int J Assess Tools Educ 7(2):255–265
9. Mishra P, Pandey CM, Singh U, Gupta A, Sahu C, Keshri A (2019) Descriptive statistics and normality tests for statistical data. Ann Card Anaesth 22(1):67

Bibliometric Analysis of Global Research on Probable Maximum Precipitation Estimation Using Scopus Database

Rasnavi Paramasivam, Nor Eliza Alias, Sitti Asmah Hassan, and Fara Aiza Md. Sanin

Abstract Climate change impact on the intensity of extreme precipitation is very significant nowadays. The impact of extreme rainfall events causes an increase in flood frequencies and the risk of dam failure. Therefore, the analysis of extreme events is required for future risk reduction assessment. Probable maximum precipitation (PMP) estimation has received positive attention among engineers in the design of water engineering. Therefore, understanding the methods that are most suitable for the estimation and broadening collaboration networks are important for advanced research development. In this bibliometric study, our aim was to evaluate the global research trends in PMP estimation based on publication outputs, co-authorships among authors and affiliated countries, and co-occurrences of author keywords. Two hundred thirty-four journal articles that were published between 1953 and 2020 were rectified using the Scopus database. From the analysis, it is found that after 2010, the publications of articles regarding PMP estimation had shown a significant increase, resulting in a steady increase in the cumulative total publications till present. Most of the total global publications were contributed by researchers from the United States, India, Canada, United Kingdom, China and other 30 countries. In conclusion, recent progress in the PMP estimation method includes the Hershfield method and the Hydrometeorological method.

R. Paramasivam (✉) · N. E. Alias · S. A. Hassan · F. A. Md. Sanin
School of Civil Engineering, Faculty of Engineering, Universiti Teknologi Malaysia, Johor Bahru, Malaysia
e-mail: rasnavi2@graduate.utm.my

N. E. Alias
e-mail: noreliza@utm.my

S. A. Hassan
e-mail: sasmah@utm.my

F. A. Md. Sanin
e-mail: faraaiza@graduate.utm.my

N. E. Alias
Centre for Environmental Sustainability and Water Security (IPASA), Research Institute for Sustainable Environment (RISE), Universiti Teknologi Malaysia, Johor Bahru, Malaysia

1   Introduction

Climate change is considered a global challenge, and it has been affecting every country on every continent. The risks resulting from unabated climate change having cumulative nature and which further leads to more violent weather such as extreme precipitation [1]. Intensive rainfall and heavy floods are among the most catastrophic natural hazards which have large social consequences for communities all over the world. In order to reduce the destructive effects of these phenomena, it is necessary to calculate the probable maximum precipitation (PMP) [2]. PMP has been defined as "the greatest depth of precipitation for a certain duration meteorologically possible for a given size storm area at a specific time of year" [3].

2   Problem Statement

Although there has been a growing interest in PMP estimation, very few studies were dedicated to measuring and analysing scientific publications from a global perspective. Bibliometric analysis is a cross-disciplinary science of qualitative information (e.g., research focus and potential future research) and quantitative analysis (e.g., contributing works by authors, institutions, journals, and cited articles) to assess research performance based on published articles [4–6]. Bibliometric analysis has become prominent for analysing scientific literature in various disciplines, including works from research collaborations in a particular journal (Journal of Productivity Analysis) [7], blockchain technology (bitcoin) [8], computer networking [9], and the industrial revolution (industry 4.0) [10].

3   Objectives

The objectives of this paper are to analyze temporal distribution patterns of PMP estimation journal articles, to interpret contributions of prolific authors, journals, countries, and academic institutions and to determine research topics and the methods used by the countries in the PMP estimation.
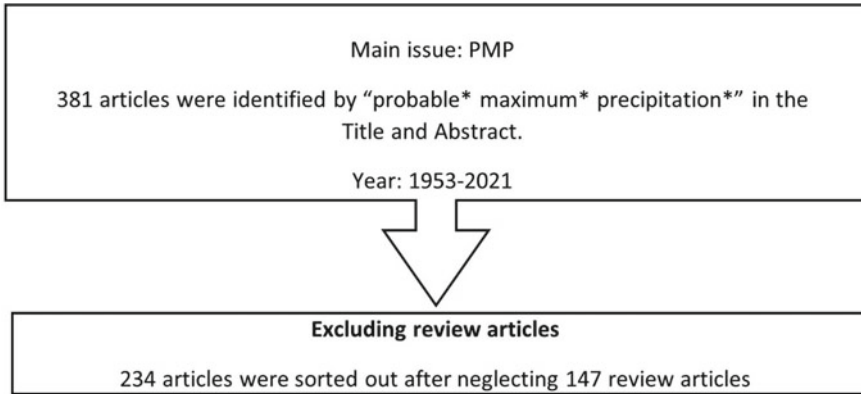
Fig. 1 Flowchart of gathering data from the Scopus database

4 Methodology

4.1 Data Collection

Data were collected to review the analysis of PMP estimation applications in the world using the Scopus database. The Scopus database is a comprehensive and reliable tool with various selection criteria [11, 12]. The central theme in this study was research articles containing "probable* maximum* precipitation*" in the title and abstract. The publication period ranges between 1953 and 2021. The query string that was used for the search was: (TITLE-ABS ("probable* maximum* precipitation*")) AND DOCTYPE (ar) AND (LIMIT-TO (SRCTYPE, "j")). A total of 381 documents were reviewed through this search. In the data screening, the review articles in the search were removed. There were 147 review articles from the query string search. The flow chart in Fig. 1 shows the steps in the data collection.

4.2 Bibliometric Maps

Numerous software tools are available to support bibliometric analysis (e.g., BibExcel, R, CitNetExplorer, VOSviewer, SciMAT, CiteSpace, and VantagePoint). VOSviewer (version 1.6.11) software was used to perform the bibliometric analysis in this study. This software allows for the creation, visualization, and exploration of maps based on bibliometric network data. The output results are displayed in clusters to allow for clear visualization of the existing connections among the bibliometric data [13].

Author keywords were conducted to create the network maps. There is a link or connection between the two things mentioned above. Each link has a strength,

represented by a positive numerical value. The higher this value, the stronger the link. The total link strength represents the total strength of a certain country's co-authorship linkages with other nations, whereas the link strength between countries indicates the number of articles that two affiliated countries have co-authored. Similarly, in co-occurrence analysis, the strength of the link between author keywords represents the number of publications in which two keywords occur together. The number of clusters visualized in the network maps is determined by the resolution parameter. The higher its value, the higher the level of details. This value can be set to visualize an appropriate number of clusters in the maps [14]. The resolution for the analyses is one which is the minimum value. This is to avoid the formation of small clusters, which will affect the analyses. When the resolution increases, the number of clusters also increases.

5 Publication Pattern

Two hundred thirty-four research articles were identified to be published from 1953 to 2020, as shown in Fig. 2. The oldest publication on PMP started on the year 1953. From the Emergency Events Database (EM-DAT), the frequency of disasters that occurred from 1953 to 2020 is shown in Fig. 3. It shows that natural disasters, especially flood and storm, increase yearly and parallelly causes damages and economic losses. In 2020, the estimated economic loss of natural disasters worldwide was 268 billion U.S. dollars, while the estimated insured loss amounted to 97 billion U.S. dollars. In order to reduce the impact of floods and storms, the estimation of the highest precipitation is required. It will be very useful for the water engineers to design the hydraulic structures such as dams and drainage that occur clutter the unexpected rainfall due to climate change. Therefore, PMP estimation is the tool used by researchers to compute the greatest precipitation from past rainfall events. It is also the reason for the urge to publish the PMP estimation recently. The analyses of the publication pattern on authors, journals, countries and institutions will be discussed further.

5.1 Authors Analysis

The results show that a total of 154 authors participated in PMP estimation research. However, only two of the authors published more than ten articles during the period between 1953 and 2021. Table 1 shows the top ten most prolific authors in PMP. The most productive author in the research of PMP throughout the world is from Asian countries, which is Rakhecha Pukhraj from India with 15 publications (6.4%). According to the statistics, 68% of India's land is prone to drought, 60% to earthquakes, 12% to floods and 8% to cyclones making India one of the most disaster-prone countries in the world, affecting overall 85% of Indian land and more than
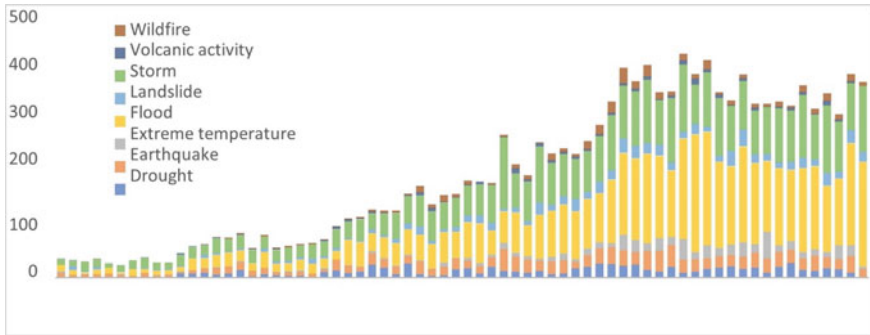
Fig. 2 The frequency of natural disasters from 1953 to 2020
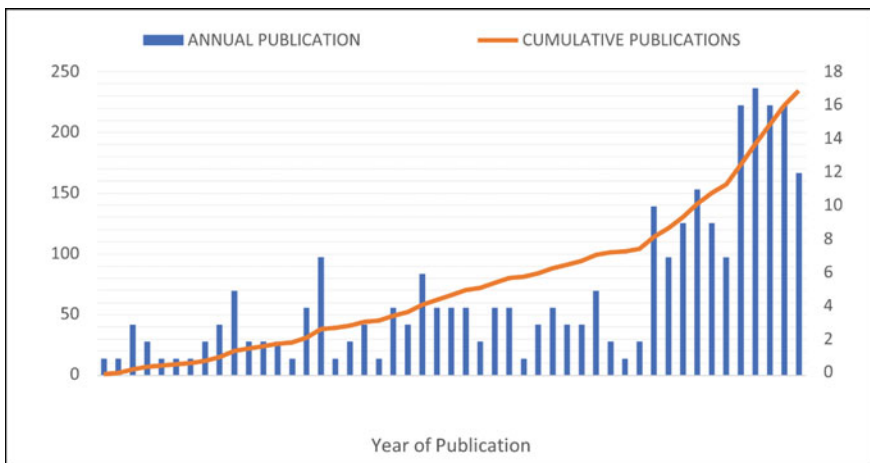
Fig. 3 The annual and cumulative numbers of research articles publication Authors Analysis

50 million people. This causes India researchers to be more active on PMP estimation to reduce the impact of floods and storms. Looking at the top 1% of rainfall events, as measured by the amount of rain that fell within a 24-h period, the amount of precipitation falling in these heavy events has increased substantially across the United States of America (USA) since the 1950s (Wuebbles et al. 2017). Flooding is the result of many factors, including the amount of precipitation falling during a particular time interval and the kinds of surfaces on which it falls. Therefore, the estimation of the greatest depth of precipitation is very important for researchers in the USA. Indeed, Hossain Faisal from the USA had published ten articles (4.3%) which made him be the second most impactful author in this PMP research. Then, the third and fourth productive authors are Dhar O.N. (India), with seven publications (3%), and Clark Colin (United Kingdom) had published six publications (2.6%), respectively. Another six authors from India, USA and Switzerland, had contributed

Table 1 The top ten most prolific authors in PMP research

Rank	Author	Current affiliation	Country	Scopus author ID	Year of 1st publication	Total publication	h-index	Total citation
1.	Rakhecha Pukharj	Indian Institute of Tropical Meteorology	India	6701699491	1981	15	9	243
2.	Hossain Faisal	University of Washington	United States	7003510377	2012	10	7	180
3.	Dhar O.N.	Indian Institute of Tropical Meteorology	India	7003918912	1973	7	4	35
4.	Clark Colin	Charldon Hill Research Station	United Kingdom	57213539181	1995	6	4	79
5.	Deshpande Nayana R.	Indian Institute of Tropical Meteorology	India	36762296500	1992	6	3	49
6.	Mandal B.N.	Indian Institute of Tropical Meteorology	India	7102080773	1981	6	4	36
7.	Riedel John T.	National Weather Service	United States	7005695498	1970	6	3	25
8.	Chan Xiaodong	University of Washington	United States	57110980000	2016	4	4	44
9.	England John F.	Risk Management Canter, U.S. Army Corps of Engineers	United States	7103114146	2007	4	3	47
10.	Felder Guido	University of Bern	Switzerland	56344961400	2017	4	4	55

four to six articles. Next, the leading total citation authors were Rakhecha Pukhraj (TC = 243, h-index of 9), Hossain Faisal (TC = 180, h-index of 7), Clark Colin (TC = 79, h-index of4), Felder Guido (TC = 55, h-index of 4) and Deshpande Nayana R. (TC = 49, h-index of 6).

5.2 Journal Analysis

Table 2 represents the top ten most influential journals. A total of 234 articles were published by 108 journals with a minimum of one publication, respectively. Journal of Hydrology (9.8%), Journal of Hydrologic Engineering (6.8%), Water Resources Research (5.1%), Theoretical and Applied Climatology (4.3%) and International Journal of Climatology (2.6%) with 23, 16, 12, 10 and 6 articles respectively were ranked as the top five most productive journals in the research of PMP. The percentage

Table 2 The top 10 most productive journals on MFC research with their most cited article

Rank	Journal	No. of publications	No. of citations	Citescore 2020	The most cited article	Times cited	Publisher
1.	Journal of Hydrology	23 (9.8%)	417	7.3	Flood risk assessment using an integrated hydrological and hydraulic modelling approach: a case study	56	Elsevier
2.	Journal of Hydrologic Engineering	16 (6.8%)	165	3.5	Physically based estimation of maximum precipitation over American River Watershed, California	66	ASCE
3.	Water Resources Research	12 (5.1%)	389	7.5	A probabilistic view of Hershfield's method for estimating probable maximum precipitation	60	AGU
4.	Theoretical and Applied Climatology	10 (4.3%)	126	5.1	Estimation of probable maximum precipitation for dams in the Hongru River catchment, China	32	SpringerLink
5.	International Journal of Climatology	6 (2.6%)	116	7.8	Estimation of the probable maximum precipitation in Barcelona (Spain)	47	RMetS
6.	Journal of Hydrometeorology	6 (2.6%)	101	6.9	Probable maximum precipitation estimation using multifractals: Application in the eastern United States	76	AMS
7.	Meteorological Applications	6 (2.6%)	79	2.9	Revised estimates of one-day probable maximum precipitation (PMP) for India	29	Elsevier
8.	Water (Switzerland)	5 (2.1%)	23	3.7	Estimation of probable maximum precipitation in Korea using a regional climate model	14	MDPI
9.	Hydrological Sciences Journal	5 (2.1%)	31	4.7	PMP and PMF estimations in sparsely-gauged Andean basins and climate change projections	12	Elsevier
10.	Journal of Hydraulic Engineering	5 (2.1%)	47	4.1	Estimating probabilities of extreme rainfalls	31	ASCE

ASCE: American Society of Civil Engineers; AGU: American Geophysical Union; RMetS: Royal Meteorological Society; AMS: America Meteorological Society; MDPI: Multidisciplinary Digital Publishing Institute

of publications in the journals is low, indicating a wide range of chances with a broad interest in this field's study. The most influential journals were published by Elsevier, American Society of Civil Engineers (ASCE), American Geophysical Union (AGU), SpringerLink, Royal Meteorological Society (RMetS), American Meteorological Society (AMS) and Multidisciplinary Digital Publishing Institute (MDPI).

CiteScore is one of the criteria that researchers look through to find the most suitable journal to publish their study. According to the CiteScore 2016 report, the journals should have a CiteScore of between two and eight. Journal of Hydrology and International Journal of Climatology have the highest CiteScore, which is 7.8 and Meteorological Applications has the lowest CiteScore of 2.9. The lowest total citation is belonged to Water Journal (Switzerland), with only 23 citations compared to the other journals. This is because the journal is still new, as it had the first publication only in 2016. However, all the journals have a potential influence on the research of PMP estimation.

5.3   Country and Institution Analysis

Among all the 234 articles, 50% of the publications were contributed by USA, India, Canada, and United Kingdom. Figure 4 represents the 15 most productive countries and the respective institutions that contribute to the development of PMP research worldwide. This shows that these countries are very active in the PMP research in the world. The USA had 60 articles published, which covers 26% of the total articles and makes it the productive county in this research field. In the United States, many federal and state agencies use the PMP and PMF for evaluating the adequacy and safety of major hydraulic structures. According to the Federal Guidelines for Inundation Mapping of Flood Risks Associated with Dam Incidents and Failures (2021), federal agencies and private dam owners have commissioned site-specific PMP studies throughout the United States. High-hazard potential dams are typically evaluated using a full PMF, and significant- or low-hazard potential dams are evaluated on a percentage of a PMF or some more frequent storm event. Therefore, research on PMP estimation in the USA plays a major role in dam safety in that country. The institution that is most productive in the USA is the University of Washington.

Next, the second most influential country belong to India with 29 publication (12%). SASTRA Deemed University is an institution in India that are productively working toward PMP research. PMP estimation is very important in water engineering. This is to clutter the extreme rainfall events that may occur due to climate change which causes deaths and losses in the economic sector. For instance, tropical cyclones that affected India in 1977 killed 14,204 people; in 1999, killing 9,843 people and in 1971, killing 9,658 people figure in the top ten list in terms of deaths. India's 2014 floods figure in the list of costliest disasters with a loss of approximately 16.90 billion USD (Nandi 2021). Therefore, India had shown more interest in the PMP estimation as a mitigation measure to reduce the impact of natural disasters.

Rank	Country	TPc	SCP (%)	The most productive academic institution	Tpi	Rank	Country	TPc	SCP (%)	The most productive academic institution	Tpi
1	United States	60	77	University of Washington	6	9	Switzerland	7	71	University of Bern	3
2	India	29	93	SASTRA Deemed University	1	10	Japan	5	40	Kyoto University	2
3	Canada	16	69	Université de Sherbrooke	4	11	Saudi Arabia	5	60	King Abdulaziz University	3
4	United Kingdom	13	85	University of Salford	2	12	South Korea	5	100	Pukyong National University	3
5	China	12	67	Hohai University	3	13	France	4	75	Coyne et Bellier	1
6	Iran	8	88	Islamic Azad University	2	14	Germany	4	25	Karlsruhe Institude of Technology, Campus South	1
7	Australia	7	43	Bureau of Meteorology Australia	1	15	Greece	3	75	National Technical University of Athens	3
8	Malaysia	7	71	Universiti Tunku Abdul Rahman	2						

TPc: total publications of a given country; TPi: total publications of a given academic institution; SCP: single country publications

Fig. 4 The top 15 most productive countries and academic institutions in MFC publications

Furthermore, most of the countries had more than 50% single-country publications (SCP). The countries have solid intra-country collaboration, which shows that the research on PMP is actively broadening within the countries. The country that has the lowest SCP is Germany, with only 25%. This shows that the country had a more international collaboration for the publication. International collaboration is very important in this era where we can exchange our ideas, knowledge, and network for the development of research.

6 Bibliometric Analysis

The bibliometric analysis proposed a qualitative and quantitative way to manage numerous studies in academic research. The visualization tools in bibliometric analysis, such as network analysis, focused on the relationships and dominant players in the studies. This technique can provide comprehensive information because of its adaptability, as it can manage all the literature.

6.1 Co-occurrence Network Analysis

Useful information, such as goals, methods, and perspectives, can be obtained from keywords in publications [15]. Therefore, keyword frequency analysis is useful for identifying focal areas and development related to a given field [16]. The analysis of the co-occurrence of keywords from 234 articles presents 407 keywords. For the analysis in VOSviewer, the minimum number of co-occurrences of a keyword was set to be two. A total of 48 keywords were analysed and Fig. 5 shows the bibliometric network map of co-occurrence keywords in PMP research. The results show that "probable maximum precipitation (PMP)" was the commonly used keyword with 90 occurrences and a total link strength of 137. The "probable maximum flood (PMF)" was the second frequently applied keyword by the authors, with co-occurrence of 28 and total link strength of 61. PMP is used for the calculation of PMF, which is then used for the design of hydraulic structures, such as large dams and spillways, flood control works, levees, and nuclear power plants. PMF is used to size the hydraulic structures such that the risk of their failure is minimized [17]. Therefore, PMP and PMF are interrelated to each other.

The other top keywords in this PMP research were "extreme precipitation", "climate change", "dam", "Hershfield method", and "floods". Intensification of the hydrological cycle is one of the major consequences of climate change [18, 19]. Such intensification leads to higher intensity and frequency of precipitation events
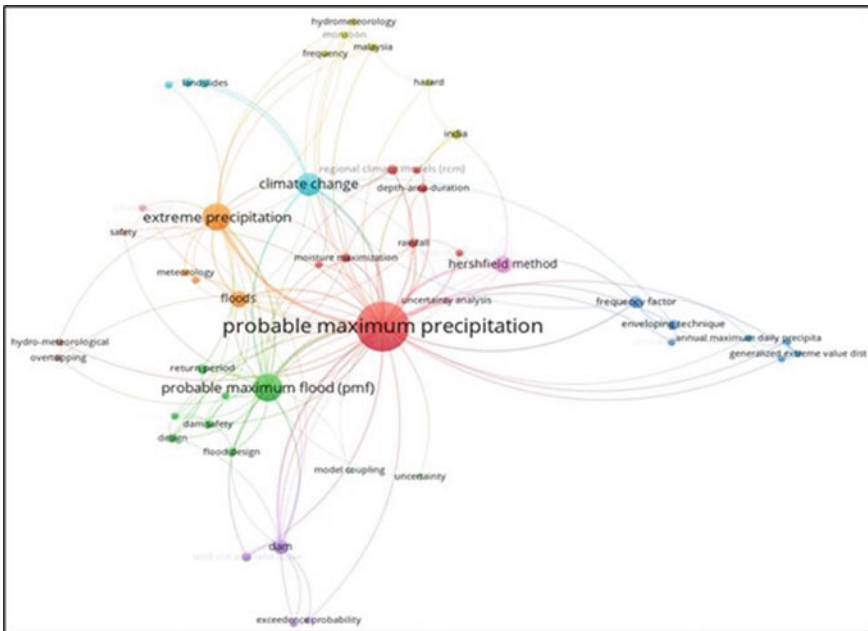
Fig. 5 The bibliometric network map of co-occurrence keywords in PMP research
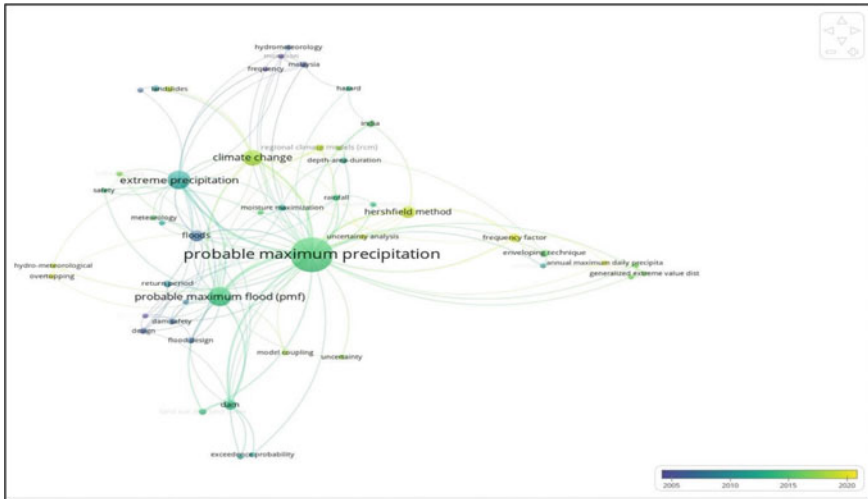
Fig. 6 The overlay visualization of the bibliometric network map of co-occurrence keywords in PMP research

at a global and local scale (Trenberth et al. 2003; Giorgi et al. 2011). An increase in extreme precipitation is being reported in many studies [20–22]. As a result, PMP estimation is required by the engineers for designing hydraulic structures such as dams to decrease the impact of the disasters (floods and storms) that will be caused by extreme precipitation. Thus, the keywords are on the top list for this topic of interest. In WMO [23], there are two PMP estimation methods which are hydro-meteorological method using moisture maximization and storm transposition and a statistical method using only annual maximum time series of rainfall data. The statistical method is usually referred to as Hershfield's method (Hershfield 1961) [17], which is based on the general frequency equation proposed by [24]. Thus, the keywords are on the top list for this topic of interest.

From the bibliometric network map, the size of their nodes represents the total link strength which indicates that these keywords frequently occur in the literature. Moreover, the proximity of the nodes represents the strength of the relationship between the research topics. From the map, the frequently used method in PMP estimation by the researchers is the Hershfield method as it has a bigger size of node than the hydro-meteorological method. In the Hershfield method, the keys are the frequency factor which refers to the value of K that will establish after analyzing many historical data of storm annual daily maximums so that an upper bound of K was determined, which was bigger than all values of K obtained from the historical sample or by using the enveloping technique to obtain a significant value of K. In the hydrometeorological method, the key concepts involved include depth-area duration analysis of large storms, storm maximization, storm transposition, and envelopment. The methods based on storm models use physical parameters such as dew point

temperature, storm depth, and inflow and outflow fluxes depending on the storm type [25].

Figure 6 shows the overlay visualization of the bibliometric network map of co-occurrence keywords. This network map shows the average publication year, the number of occurrences and link strength of the keywords. The colour of a keyword denotes the average year of publication of the papers in which it appears.

7 Conclusion

An overview of PMP research trends based on the 234 publications was retrieved from the Scopus database. The number of publications has shown an increase in the last ten years and will gradually have a growth. USA and India had given the highest number of publications in this field of interest. However, there are researchers from other countries who have been working in this field recently. The bibliometric analysis also shows that PMP estimation is correlated with PMF. This is because engineers use PMF for analyzing dams and power plants. PMF is determined through the PMP estimation, and this causes an urge in interest in this research among the researchers. PMP estimation is very important because the rate of natural disasters increases due to extreme precipitation. There are more record-breaking rainfalls have been recorded recently because of climate change. The most common method that is used by researchers in PMP estimation is the Hershfield method. From the analyses, we can conclude that PMP estimation research is getting more attention among researchers.

References

1. Chanapathi T, Thatikonda S, Raghavan S (2018) Analysis of rainfall extremes and water yield of Krishna river basin under future climate scenarios. J Hydrol Reg Stud. 19:287–306
2. Afzali-Gorouh Z, Bakhtiari B, Qaderi K (2018) Probable maximum precipitation estimation in a humid climate. Nat Hazard 18(11):3109–3119
3. World Meteorological Organization (2009) Manual on estimation of probable maximum precipitation (PMP), 3rd edn. WMO, no. 1045. World Meteorological Organization, Geneva, xxxii, 259
4. Ellegaard O, Wallin JA (2015) The bibliometric analysis of scholarly production: how great is the impact? Scientometrics 105(3):1809–1831
5. Osareh F (1996) Bibliometrics, citation analysis and co-citation analysis: a review of literature I. Libri. https://doi.org/10.1515/libr.1996.46.3.149
6. Xu S, Zhang X, Feng L, Yang W (2020) Disruption risks in supply chain management: a literature review based on bibliometric analysis. Int J Prod Res 58(11):3508–3526

7. Choi HD, Oh DH (2020) The importance of research teams with diverse backgrounds: research collaboration in the Journal of Productivity Analysis. J Prod Anal 53(1):5–19
8. Merediz-Solà I, Bariviera AF (2019) A bibliometric analysis of bitcoin scientific production. Res Int Bus Financ 50:294–305
9. Iqbal W, Qadir J, Tyson G, Mian AN, Hassan SU, Crowcroft J (2019) A bibliometric analysis of publications in computer networking research. Scientometrics 119(2):1121–1155
10. Muhuri PK, Shukla AK, Abraham A (2019) Industry 4.0: a bibliometric analysis and detailed overview. Eng Appl Artif Intell 78:218–235
11. Gao C, Sun M, Geng Y, Wu R, Chen W (2016) A bibliometric analysis based review on wind power price. Appl Energy 182:602–612
12. Solvoll S, Alsos GA, Bulanova O (2015) Tourism entrepreneurship–review and future directions. Scand J Hosp Tour 15(sup1):120–137
13. Pauna VH, Buonocore E, Renzi M, Russo GF, Franzese PP (2019) The issue of microplastics in marine ecosystems: a bibliometric network analysis. Mar Pollut Bull 149:110612
14. Van Eck NJ, Waltman L (2018) VOSviewer Manual 1.6. 11. Manual (Version 1.6.9)
15. Tian X, Geng Y, Sarkis J, Zhong S (2018) Trends and features of embodied flows associated with international trade based on bibliometric analysis. Resour Conserv Recycl 131:148–157
16. Wang Z, Zhao Y, Wang B (2018) A bibliometric analysis of climate change adaptation based on massive research literature data. J Clean Prod 199:1072–1082
17. Hershfield DM (1965) Method for estimating probable maximum rainfall. J Am Water Works Ass 57(8):965–972
18. Allen MR, Ingram WJ (2002) Constraints on future changes in climate and the hydrologic cycle. Nature 419(6903):228–232
19. Jacob D, Hagemann S (2007) Intensification of the hydrological cycle: an important signal of climate change. In: Global change: enough water for all? (pp 170–173). Wissenschaftliche Auswertungen
20. Madakumbura GD, Kim H, Utsumi N, Shiogama H, Fischer EM, Seland Ø, Scinocca JF, Mitchell DM, Hirabayashi Y, Oki T (2019) Event-to-event intensification of the hydrologic cycle from 1.5 C to a 2 C warmer world. Sci Rep 9(1):1–7
21. O'Gorman PA (2015) Precipitation extremes under climate change. Curr Clim change Rep 1(2):49–59
22. Utsumi N, Seto S, Kanae S, Maeda EE, Oki T (2011) Does higher surface temperature intensify extreme precipitation? Geophys Res Lett 38(16)
23. World Meteorological Organization (1986) Manual for estimation of probable maximum precipitation, 2nd edn. Operational Hydrology Report No. 1, WMO No. 332. World Meteorological Organization, Geneva, Switzerland
24. Chow VT (1951) A general formula for hydrologic frequency analysis. EOS Trans Am Geophys Union 32(2):231–237
25. Collier CG, Hardaker PJ (1996) Estimating probable maximum precipitation using a storm model approach. J Hydrol 183(3–4):277–306
26. Wuebbles DJ, Fahey DW, Hibbard KA (2017) Climate science special report: fourth national climate assessment, volume I. Trenberth KE, Dai A, Rasmussen RM, Parsons DB (2003). The changing character of precipitation. Bull Am Meteorol Soc 84(9):1205-1218
27. Giorgi F, Im ES, Coppola E, Diffenbaugh NS, Gao XJ, Mariotti L, Shi Y (2011) Higher hydroclimatic intensity with global warming. J Clim 24(20):5309–5324
28. Hershfield DM (1961) Estimating the probable maximum precipitation. J Hydraulics Div 87(5):99–116
29. Nandi S, Sarkis J, Hervani AA, Helms MM (2021) Redesigning supply chains using blockchain-enabled circular economy and COVID-19 experiences. Sustainable Prod Consum 27:10–22

Multivariate Statistical Analysis of Morphometric Parameters in Watersheds of Peru

M. López-Silva, D. Carmenates-Hernandez, I. Sao-Cancio, A. Valderrama-Romero, and P. Huamaní-Navarrete

Abstract Peru is a country recognized for its natural resources, but it is the third most vulnerable country, different research projects have predicted natural. The objective of the research was to hold out the Multivariate Statistical Analysis to 91 watersheds of Peru to get homogeneous water characteristics in different regions. Twenty morphometric parameters were determined to characterize the watersheds in qualitative and quantitative terms. The principal component analysis was applied, including Factor analysis, Hierarchical Cluster analysis in R and Ward's method. It had been obtained that 75.52% of the watershed studied are favoured by morphometric parameters that contribute to a high frequency of streams, which allows adequate use of water resources. The steep slopes are vulnerable watersheds product to their immediate hydrological response and water erosion, which means a greater need for hydraulic works. Six main components were defined that specify 94.58% of the entire variance denominated as geometric, shape, drainage, and relief factors. The results of the Cluster Analysis showed that 35% of the watersheds have homogeneous zones within the geometric and shape factor, while 65% within the drainage and relief factor.

Keywords Climate change · Cluster analysis · Factor analysis · Principal component · River

M. López-Silva (✉) · D. Carmenates-Hernandez · P. Huamaní-Navarrete
Ricardo Palma University/Engineering Faculty, Lima, Peru
e-mail: maiquel.lopez@urp.edu.pe

D. Carmenates-Hernandez
e-mail: dayma.carmenates@urp.edu.pe

P. Huamaní-Navarrete
e-mail: phuamani@urp.edu.pe

I. Sao-Cancio
MEDELHI/Natural Sciences Area, Quito, Ecuador

A. Valderrama-Romero
National University of Cañete/Soil and Water Laboratory, Lima, Peru
e-mail: avalderrama@undc.edu.pe

1 Introduction

Peru, globally, is one among the countries most affected by variability and global climate change [24], impacting the spatial distribution of water resources in Peru's Andes, a fundamental source of water supply for the population, agriculture, and energy production [26].

The sustainable development of natural resources and watersheds in Peru is managed through optimal processes of integrated water resource management, which promotes the multisectoral use of water and soil. The north–south Andean Mountain range divides Peru into three main drainage watersheds: the Pacific watershed, the Atlantic watershed, and the Titicaca watershed [13]. The heterogeneity of precipitation, runoff, and soil loss regimes is strong in Peru's three main watersheds on seasonal and interannual time scales, accentuated by the extreme events of El Niño and La Niña in the Pacific Ocean. As a result, natural environments, floods, water quality, and availability, as well as droughts and soil losses between 38 and 54% in areas with natural infrastructure and untreated croplands, respectively, are affected [23]. In particular, the Pacific slope is of utmost importance because it is home to more than 50% of the country's population and the main economic zone of the country [17]. In this regard, both national and international authorities consider it essential to plan actions aimed at ensuring water security in appropriate quantity and quality to preserve health and the environment. Therefore, it is important to identify the watersheds with the greatest and least water resources for planning activities and decision making. The analysis of drainage watershed management begins with the morphometric parameters and land cover of the watershed, while its management depends on the interrelationship between geomorphology, lithology, geology, and soil [1]. In this context, there is a requirement for sustainable watershed management ranging from an efficient morphometric characterization [6] with new scientific tools to enable adaptation to variability and global climate change with attention on prediction until the solution of problems [11].

There is a great deal of recent research on the watershed characterization, classification, and prioritization, using geospatial, geophysical, land use patterns, land cover, hybrid and statistical models [3, 14, 19, 27]. Statistical models are based on the Principal Component Analysis (PCA) method allows the various morphometric variables to explain the most significant part of the variance of the data to identify cause-effect relationships, zones with homogeneous climate or similar hydrological characteristics [8]. This analytical approach groups similar data while identifying relationships between variables [7]. There are significant contributions in the literature on the use of the PCA by [4, 14, 18, 22] to determine the most important morphometric parameters of the watershed, these involving Factor Analysis (FA), Cluster Analysis (CA), and Regression Analysis. However, watershed studies using PCA have been limited to a few watersheds, low climatic diversity, as well as mountainous areas such as the Andes of Peru. All of which influences an optimal multivariate statistical result. New methods are essential that allow better management of watersheds in Peru due to its climatic diversity and fragile ecosystems. Therefore, the objective of

the research is to carry out a multivariate statistical analysis of the morphometric parameters in watersheds of Peru to classify potential areas with more benefits from water resources.

2 Materials and Methods

Fourteen regions with different hydrographic, hydrological, geological, and ecological conditions were selected as the study area for the 91 watersheds. Figure 1 shows the geographic location of each of the watersheds. These watersheds are located in two of the country's largest main drainages, the Pacific and the Atlantic. The Pacific slope drains towards the Pacific Ocean, and the Atlantic slope drains towards the Amazon watershed.
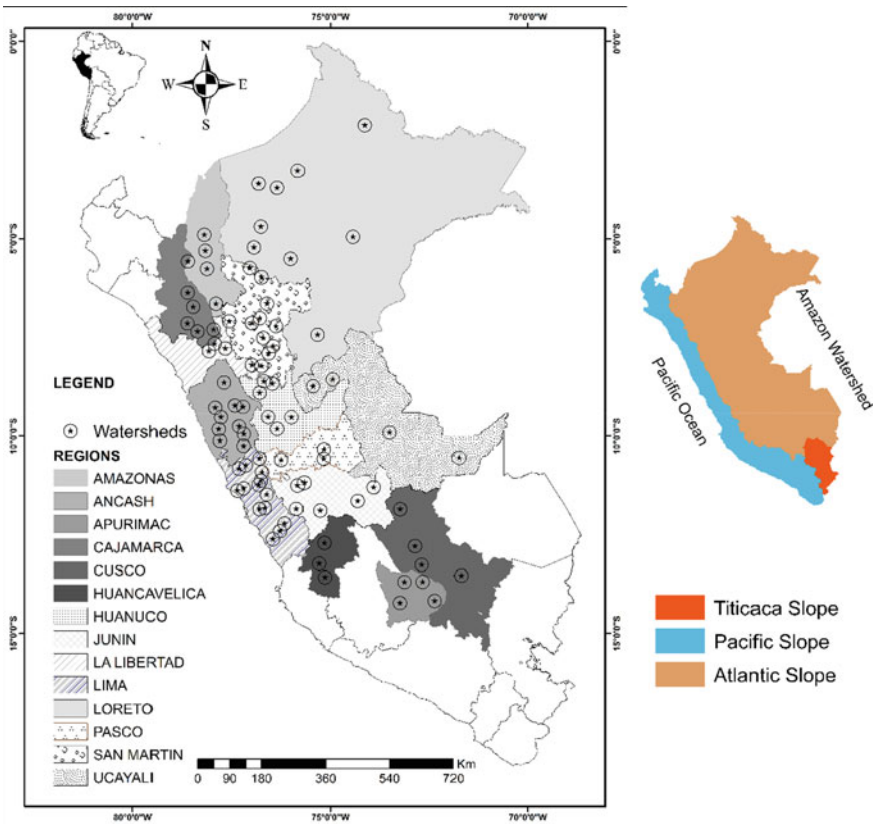
Fig. 1 The study watersheds

Table 1 Formulas of the morphometric parameters of the watersheds

Morphometric Parameters	Formula	References
Maximum altitude (Z_{max}) (m)	Module of ArcGIS	–
Minimum altitude (Z_{min}) (m)	Module of ArcGIS	–
Altimetric amplitude (H_m) (m)	Module of ArcGIS	–
Watershed area (A) (km^2)	Module of ArcGIS	–
Watershed perimeter (P) (km)	Module of ArcGIS	–
Watershed length (L_c) (km)	Module of ArcGIS	–
Stream length (L_r) (km)	Module of ArcGIS	–
Watershed amplitude (W) (km)	$W = AL_c^{-1}$	[9]
Slope of the watershed (S_c) (%)	$S_c = e \sum l_i A^{-1}$	[29]
Gravelius coefficient (K_c)	$K_c = 0,282PA^{-0,5}$	[29]
Form factor (F_f)	$F_f = AL_c^{-2}$	[9]
Shape index (S_w)	$S_w = L^2 A^{-1}$	[10]
Elongation ratio (R_e)	$R_e = 1,1284A^{0,5}L^{-1}$	[21]
Circularity ratio (R_c)	$R_c = 4\pi AP^{-2}$	[15]
Relief ratio (R_a)	$R_a = H_m L_c^{-1}$	[21]
Mean stream slope (S_r) (%)	$S_r = \Delta H L_r^{-1}$	[29]
Drainage density (D_d) (km/km^2)	$D_d = L_r A^{-1}$	[10]
Length of overland flow (L_f) (km^2/km)	$L_f = 0,5D_d^{-1}$	[10]
Constant of channel maintenance (C) (km^2/km)	$C = D_d^{-1}$	[21]
Roughness coefficient (C_r)	$C_r = D_d S_r$	

The digitized watersheds were processed in the module of ArcGIS Pro, and based on the formulas in Table 1, the morphometric parameters of the watersheds can be calculated. The characterization of the watersheds will be carried out in qualitative and quantitative terms that are grouped into geometric, shape, drainage, and relief parameters.

2.1 Principal Component Analysis

It is a complicated process to classify potential areas with more benefits from water resources in 91 watersheds. The aim of Principal Component Analysis (PCA) is to explain the variance–covariance structure in multiple data sets using a few linear combinations of the original variables, according to [12]. The PCA is a technique for summarizing a complex set of data, distinguishing quantitative dependent and independent variables, as well as identifying closely related variables. The variance–covariance matrix X is represented using Eqs. 1 and 2. In practice is estimated by the sample covariance matrix S:

$$S = \frac{X^T X}{(n-1)} = \begin{bmatrix} s_{11} & s_{12} & . & s_{1p} \\ s_{21} & s_{22} & . & s_{2p} \\ . & . & . & . \\ s_{p1} & s_{p2} & . & s_{pp} \end{bmatrix} \tag{1}$$

$$s_{ij} = \frac{1}{(n-1)} \sum_{k=1}^{n} X_{kj} \cdot X_{ki} \tag{2}$$

where S becomes the sample correlation matrix, X^T is the transpose of the standardized X variables, and s_{ij} is the value of each element of the covariance.

In the PCA, the variance of the Principal Component (PC) is maximized, which is mainly related to the eigenvalues of the sample covariance or correlation matrix [12, 14]. The correlation r between the X_{ij} of the PC is obtained by the ratio of the covariance of the X matrix and the variance of Z_j of the PCs using Eq. 3.

$$r(x_i; z_j) = \frac{Cov(x_i; z_j)}{\sqrt{Var(z_j)}} \tag{3}$$

where r is the correlation coefficient; Cov (x_i, z_j) is the covariance of X variables in the ith row and the jth row of the PCs; and Var (z_j) is the variance of jth PCs. Value of r greater than 0.90 indicates a strong correlation, r between 0.75 and 0.90 indicates a good correlation, and r between 0.60 and 0.75 indicates moderate correlation [20].

2.2 Factor Analysis

Factor Analysis (FA) is a procedure similar to principal components analysis to identify physically significant variables and reduce morphometric parameters. Therefore, the correlation between the variables is related to the factor loadings. Considering correspondence between the factor score matrix and the Zs in the PCs, the orthogonal in the rotation has an impact on the PCs and the corresponding factors are equivalent. Therefore, a comparison with the unrotated components is possible, while the rotation should be such that meaningful physical interpretations are possible from the resulting components obtained.

2.3 Cluster Analysis

The hierarchical Cluster Analysis (CA) technique was applied to classify the homogeneous groups called clusters. The method applied for data agglomeration was in R mode and Ward's criterion [25], one of the most widely used in hydrology and

meteorology [2], to achieve similarity between watersheds based on morphometric parameters with a focus on water resource use. The study used the SPSS 26.0 statistical package and STATISTICA 12 as the computational tool for the PCA.

3   Results and Discussion

The PCA was started by obtaining the matrix of the simple linear Pearson correlation coefficient (r). There is a strong correlation (r > 0.9) between the morphometric parameters of 1) watershed area with watershed perimeter, watershed length, stream length, and watershed amplitude; 2) watershed perimeter with watershed length, Stream length, and watershed amplitude; 3) watershed length with stream length and watershed amplitude; 4) stream length and watershed amplitude; 5) Gravelius coefficient and circularity ratio; 6) form factor with shape index and elongation ratio; 7) shape index and elongation ratio; 8) drainage density with a length of overland flow and constant of channel maintenance; 9) length of overland flow and constant of channel maintenance. While there is a good correlation (0.75 < r < 0.9) between 1) altimetric amplitude and relief ratio; 2) mean stream slope and roughness coefficient. In addition, there is moderately acceptable Pearson correlation coefficients (0, 60 < r < 0.75) at 1) maximum altitude with minimum altitude and relief ratio; 2) watershed perimeter with Gravelius coefficient and circularity ratio; 3) watershed amplitude with form factor, shape index, and elongation ratio. The parameters of the slope of the watershed and mean stream slope did not show a relationship with the rest to the other variables that explain their effect, except for the roughness coefficient. Similar results achieved [28] in watersheds of the Western Arabian Peninsula and [16] in watersheds of Iran fundamentally in the parameters of watershed area, watershed length, elongation ratio, form factor, circularity ratio, and drainage density with strong correlation. While, with a certain approximation by those of [14] strongly correlated to the length of overland flow, form factor, circularity ratio, Gravelius coefficient, elongation ratio and differs with drainage density in Indian watersheds. Based on the significant correlations, no drainage correlations are observed with the geometric variables, which are in agreement with those reached by [20]. Other authors, such as [5], demonstrated that watershed area and stream length influence the maximum flow and the unit hydrograph at its peak time with a correlation coefficient of 0.98, an aspect that could be related to the current research.

The application of the FA to the twenty morphometric parameters in the first iteration, six PCs were defined with eigenvalues greater than one, and that represents around 88.26% of the total variance. However, the morphometric parameters with weak loads slope of the watershed and mean stream slope were extracted to improve the FA. Under these conditions, the same factor load was reached with 6 PC but explained 94.58% of the total variance. The Varimax rotation showed improvement in the loads, Table 2, which is because the matrix of the rotated PC was considered. It is for this reason that they are reduced to 18 morphometric parameters relevant to PCs.

Table 2 Factor loading matrix of reduced morphometric variables

Parameters	Principal components					
	PC1	PC2	PC3	PC4	PC5	PC6
Z_{max}	0.15	0.09	− 0.10	0.75	− 0.03	0.63
Z_{min}	–0.01	0.04	− 0.13	–0.05	− 0.07	0.98
H_m	0.18	0.08	− 0.01	0.97	0.02	–0.05
A	0.93	0.26	− 0.03	0.01	0.21	0.01
P	0.83	0.32	− 0.02	0.02	0.43	–0.01
L_c	0.94	0.18	− 0.03	0.01	0.21	0.01
L_r	0.93	0.27	− 0.04	0.01	0.20	–0.01
W	0.83	0.52	0.01	0.02	0.17	0.01
K_c	0.32	0.01	− 0.05	–0.01	0.93	–0.06
F_f	0.28	0.94	0.06	0.03	0.01	0.02
S_w	–0.26	–0.93	− 0.05	–0.06	− 0.01	–0.05
R_e	0.29	0.95	0.06	0.03	0.01	0.02
R_c	–0.28	0.01	0.04	0.07	− 0.93	0.03
R_a	–0.28	–0.02	0.03	0.93	− 0.09	–0.04
D_d	0.02	–0.08	− 0.97	–0.01	0.08	0.07
L_f	0.01	0.04	0.99	–0.03	− 0.01	–0.05
C	–0.01	0.03	0.99	–0.03	− 0.01	–0.05
C_r	–0.50	0.04	− 0.15	0.34	0.28	–0.14

In Table 2, the factor load of PC1 constitutes 26.56% of the total variance in the rotated matrix, the second PC2 17.87%, and the third PC3 explains 16.82% of the total variance, having these first three components a strong charge of 60.95%; while, from PC4 to PC6, factor loadings only explain 33.63% of the total variance.

The factor load of PC1 in Table 2 is strongly correlated with the factor loadings of watershed area, watershed perimeter, watershed length, stream length, and watershed amplitude, which could be called geometric factors that explain 26.56% of the total variance of the 18 parameters analyzed. The second PC2 has a strong correlation with the variables of form factor, shape index, and elongation ratio, which is why it is called the form factor of the watershed that explains 17.87% of the total variance; while the PC3 load factor, its strong correlation is with the drainage density, length of overland flow and Constant of channel maintenance called drainage factor that explains 16.52% of the total variance. The fourth-factor load of PC4 has a strong correlation with the variables of maximum altitude and altimetric amplitude, which is why it is called the relief factor of the watershed, which explains 13.82% of the total variance. The first four components account for 74.77% of the total variance, which explains the most important morphometric parameters and the most significant physical factors. Being very useful, the PCA defines the most relevant variables. [28] achieved results similar to the current ones, in 36 watersheds in which three

CPs explained 73% of the total variance that strongly reflected the dimensions and geometric of the watershed, as well as the drainage texture. In the same sense, [20] three PCs defined drainage, slope, and shape,later, with similar results, it was by [14] with a strong correlation in shape and drainage parameters.

Figure 2 shows the dendrogram obtained from the cluster analysis in R mode. All parameters of the watershed are presented with the exclusion of light loads, the slope of the watershed and mean stream slope. It is observed that there are two main clusters (A and B), and each one is subdivided into two main clusters. Cluster A is subdivided into cluster A(I) with two watershed parameters form factor and elongation ratio, and cluster A (II) includes six parameters watershed area, stream length, watershed length, watershed perimeter, watershed amplitude, and Gravelius coefficient; while cluster B is subdivided into cluster B (III) that includes two parameters length of overland flow and constant of channel maintenance, and cluster B(IV) that contains eight parameters maximum altitude, minimum altitude, altimetric amplitude, circularity Ratio, relief ratio, shape index, drainage density and roughness coefficient, the latter, with the lowest correlation and highest Euclidean linkage distance.

The dendrogram obtained by the CA of Fig. 2 indicates on its ordinate axis the similarity of the different groups of clusters; the smaller the linkage distance, the
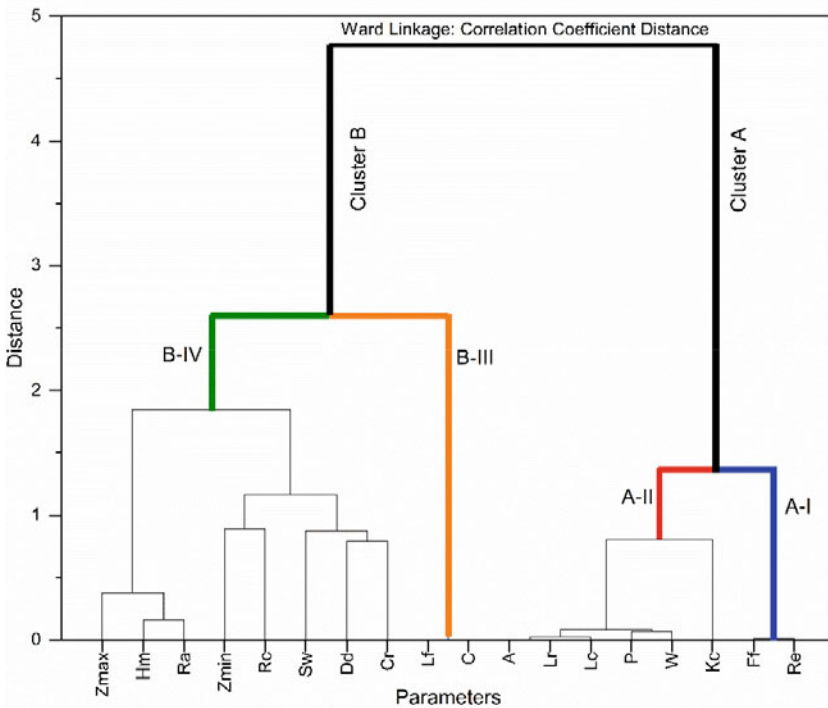
Fig. 2 Dendrogram of cluster analysis results in R-mode

greater the similarity of the analysis parameter. In this sense, cluster A presents a better correlation and less Euclidean linkage distance below 0.2 with respect to cluster B. Consequently, it is shown that eight parameters favour the existence of homogeneous or similar watersheds in Cluster A. On the other hand, there are ten parameters in Cluster B that cause dissimilarity between watersheds. According to [3], although FA is not a grouping method, there are similarities between main Cluster A (I and II) and CP (1 and 2), as well as B (I and II) and CP (3, 4, 5 and 6).

Figure 3 shows the result of the dendrogram obtained by the CA for the 91 watersheds in Peru, numbered in the abscissa axis. It is observed that there are two main Clusters, C and D. Cluster C, with 32 watersheds, is subdivided into C-I and C-II with 19 and 13 watersheds, respectively. The Cluster D with 59 watersheds was also subdivided into Cluster D-III and D-IV in watersheds 11 and 48, respectively. The Euclidean linkage distance of less than 20 in Cluster C concerning Cluster D in Fig. 3 reflects that there are tendencies to be homogeneous 32 watersheds representing 35% of the total. The degree of similarity is a product of morphometric parameters such as the geometric and shape factor that encompasses the watershed area, Stream length, watershed length watershed perimeter, watershed amplitude, Gravelius coefficient, form factor, and elongation ratio as defined in Fig. 2. When this characteristic is classified by main watersheds, 72% belong to the Atlantic slope and 28% to the Pacific slope. These factors favour the likelihood of higher rainfall catchments, abundant rivers, and consequently accessible water resources.

However, Cluster D in Fig. 3 has 65% of the set of watersheds with the greatest differences in the drainage and relief factor parameters. Regarding the parameter of drainage density and altitude, the differences accentuate the differences of watersheds in the regions of Loreto, San Martin, Ucayali, and Cajamarca, which have favourable characteristics for large sources of water resources. Although the watersheds are located on the Atlantic slope and on the Amazon, plains have a higher drainage
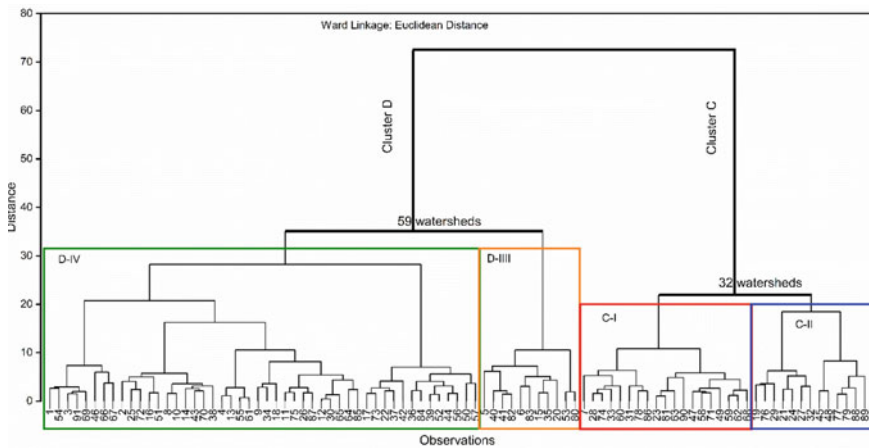
Fig. 3 Dendrogram obtained by CA

density than the Pacific slope. However, the northern area of Peru, due to the El Niño Southern Oscillation (ENSO) phenomenon, is favoured by the heavy rains, giving rise to greater floods in the rivers, in relation to the southern area where they are scarcer. In summary, the regions of Lima, Huancavelica, and Apurimac have the highest priority in watershed management for water security due to the unfavourable morphometric parameters of the watersheds and their geographical location. Previous studies by [3, 22] have obtained in the CA a similarity of the watersheds in the geometric variables, a factor that coincides with the result of the research.

The procedure of morphometric analysis of the watersheds using the PCA makes it possible to classify the similar zones according to the morphometric parameters and consequently the hydric homogeneity. In addition, it allows the identification of watersheds susceptible to erosion and flooding, thus improving the decision-making process.

4   Conclusion

The research illustrated the procedure for the quantification of morphometric parameters and therefore, the use of the principal components to define regions with homogeneous hydrological characteristics. In this sense, an excellent water potential has been identified with its respective need for hydraulic works for the utilization, protection, and sustainable management of natural resources. The PCA has been satisfactory because it allowed identifying the correlation in an optimal way, the parameters, and similarities between watersheds. The matrix reflected strong correlations (r > 0.9) with 65% of the variables, while the factor load matrix reveals six CPs that specify 94.58% of the total variance of the morphometric parameters of the watersheds, named geometric, shape, drainage, and relief factors. The dendrogram by Ward's method explains that only 35% of the watersheds are homogeneous based on geometric parameters and in shape, with dissimilarities in sources of water resources. The study provides information and useful tools for the development of integrated river watershed management projects at the national level. Also, it provides a series of important data for the implementation of hydraulic works for the capture, use, protection, and control of streams in specific regions. Future research could include geological, hydrological, environmental, ecological, and socioeconomic aspects to enrich the statistical series, improve the model and optimize decision-making at all levels of management, planning, use, and conservation of natural resources.

References

1. Bhattacharya RK, Chatterjee ND, Das K (2019) Multi-criteria-based sub-basin prioritization and its risk assessment of erosion susceptibility in Kansai-Kumari catchment area. Appl Water Sci 9(76):1–30

2. Cupak A, Walega A, Bogusław M (2017) Cluster analysis in determination of hydrologically homogeneous regions with low flow. Formatio Circumiectus 16:53–63

3. Eltahan HA, Elhamid AM, Abdelaziz SM (2021) Multivariate statistical analysis of geomorphological parameters for Sinai Peninsula. Alex Eng J 60:1389–1402

4. Gajbhiye MS, Sharma SK (2017) Prioritization of watershed through morphometric parameters: a PCA-based approach. Appl Water Sci 7:1505–1519

5. Gede TI, Anwar N, Lasminto U (2017) Analysis of main morphometry characteristic of watershed and it's effect to the hydrograph parameters I. Maejo Int J Sci Technol 28:30–36

6. Ghosh M, Gope D (2021) Hydro-morphometric characterization and prioritization of sub-watersheds for land and water resource management using fuzzy analytical hierarchical process (FAHP): a case study of upper Rihand watershed of Chhattisgarh State. Appl Water Sci 11:1–20

7. Gorgoglione A, Gioia A, Iacobellis VA (2019) Framework for assessing modeling performance and effects of rainfall-catchment-drainage characteristics on nutrient urban runoff in poorly gauged watersheds. Sustainability 11:1–16

8. Helness H, Damman S, Sivertsen E, Ugarelli R (2019) Principal component analysis for decision support in integrated water management. Water Supply 19:2256–2262

9. Horton RE (1932) Drainage basin characteristics. Trans Am Geophys Union 13:350–361

10. Horton RE (1945) Erosional development of streams and their drainage basins: hydrological approach to quantitative morphology. Bull Geol Soc America 56:275–370

11. Jacobs LK, Brian SR (2020) The next generation of climate services. Climate Services 20:1–7

12. Kottegoda NT, Rosso R (2008) Applied statistics for civil and environmental engineers, 2nd edn. Blackwell Publishing Ltd., Oxford, UK, pp 326–394

13. Lavado Casimiro WS, Ronchail J, Labat D, Espinoza JC, Guyot JL (2012) Basin-scale analysis of rainfall and runoff in Peru (1969–2004): Pacific, Titicaca and Amazonas watersheds. Hydrol Sci J 57(4):625–642

14. Malik A, Kumar A, Kushwaha D, Kisi O, Salih S, AlAnsari N, Yaseen Z (2019) The implementation of a hybrid model for hilly sub-watershed prioritization using morphometric variables. Water 11:1–20

15. Miller VC (1953) A quantitative geomorphic study of drainage basin characteristics in the Clinch Mountain area, Varginia and Tennessee, Project NR 389042, Tech Rept 3. Columbia University Department of Geology, ONR, Geography Branch, New York

16. Mokarram M, Sathyamoorthy D (2015) Morphometric analysis of hydrological behavior of North Fars watershed. Eur J Geogr 6:88–106

17. Rau P, Bourrel L, Labat D, Melo P, Dewitte B, Frappart F, Lavado W, Felipe O (2016) Regionalization of rainfall over the Peruvian Pacific slope and coast. Int J Climatol 34(1):143–158

18. Raux J, Copard Y, Laignel B, Fournier M, Masseï N (2011) Classification of worldwide drainage basins through the multivariate analysis of variables controlling their hydrosedimentary response. Global Planet Change 76:117–127

19. Rojas BN, Barboza CE, Gamarra TO, Oliva M, Leiva TD, Barrena GM, Corroto F, Salas LR, Rascón J (2020) Morphometric prioritization, fluvial classification, and quality in high Andean livestock micro-watersheds in Northern Peru. ISPRS Int J Geo Inf 9(5):2–25

20. Sharma SK, Gajbhiye S, Tignath S (2015) Application of principal component analysis in grouping geomorphic parameters of a watershed for hydrological modelling. Appl Water Sci 5:89–96

21. Schumm SA (1956) Evolution of drainage systems and slopes in Badlands at Perth Amboy. New Jersey: Bull Geol Soc Am 67:597–646

22. Subyani AM, Qari MH, Matsah MI (2012) Digital elevation model and multivariate statistical analysis of morphometric parameters of some Wadis. Arab J Geosci 5:147–157

23. Vanacker V, Molina A, Rosas-Barturen M, Bonnesoeur V, Román-Dañobeytia F, Ochoa Tocachi BF, Buytaert W (2021) The effect of natural infrastructure on water erosion mitigation in the Andes. Soil 8:133–147

24. Vega JF, Lavado CW, Felipe OO (2018) Assessing hydrological changes in a regulated river system over the last 90 years in Rimac Basin (Peru). Theoret Appl Climatol 132:347–362

25. Ward JH (1963) Hierarchical grouping to optimize an objective function. J Am Stat Assoc 58:236–244
26. Wongchuig SC, Mello CR, Chou SC (2018) Projections of the impacts of climate change on the water deficit and on the precipitation erosive indexes in Mantaro River Basin. J Mt Sci 15:264–279
27. Yang W, Zhao Y, Wang D, Wu H, Lin A, He L (2020) Using principal components analysis and idw interpolation to determine spatial and temporal changes of surface water quality of Xin'anjiang River in Huangshan, China. Int J Environ Res Public Health 17(8):2–14.
28. Yunus AP, Oguchi T, Hayakawa YS (2014) Morphometric analysis of drainage basins in the Western Arabian Peninsula using multivariate statistics. Int J Geosci 5:527–539
29. Zavoianu I (1985) Morphometry of drainage basins, 1st edn., vol 20, Elsevier Science Publishers, Amsterdam, The Netherlands, p 1–237.

Hydrological Drought Evaluation on Streamflow Drought Index (SDI) in Upstream and Downstream Area of Lampao Reservoir, Northeast of Thailand

Kowit Boonrawd, Jirawat Supakosol, and Haris Prasanchum

Abstract Drought is a widespread natural phenomenon throughout the world. It occurs at a time when streamflow availability in the watershed shows a trend that is lower than the annual average, causing insufficient demand and affecting the reservoir's water resource management. The objective of this study was to determine the occurrence of hydrologic drought related to streamflow using the Streamflow Drought Index (SDI) of the Lampao Reservoir in Thailand. The SDI values were calculated over time periods of 3, 6, 9, and 12 months, comparing the upstream area above the reservoir and the downstream area of the reservoir with regulating over water allocation. The results of hydrological drought analysis using SDI in both areas showed trends in the same direction. At Stations E65 and E75, the number of months of drought-phenomena ranged between 40.2% and 48.1% of all months. The SDI values were mainly expressed in Mild Drought between 22.8% and 34.9%. In addition, the SDI at the upstream area illustrates a higher chance of drought than the downstream area due to reservoir management. The methodology and results obtained from this study are expected to be used as statistical data for decision-making in drought mitigation planning during the recurrence period in the watershed area.

Keywords Hydrological drought · Streamflow · Streamflow Drought Index · Lampao reservoir · Watershed management

K. Boonrawd (✉) · J. Supakosol
Department of Civil Engineering, Faculty of Industrial and Technology, Rajamangala University of Technology Isan, Sakonnakhon Campus, Sakonnakhon, Thailand
e-mail: kowit.bo@rmuti.ac.th

J. Supakosol
e-mail: jirawat.su@rmuti.ac.th

H. Prasanchum
Department of Civil Engineering, Faculty of Engineering, Rajamangala University of Technology Isan, Khon Kaen Campus, Khon Kaen, Thailand
e-mail: haris.pr@rmuti.ac.th

1 Introduction

Drought is a natural phenomenon reoccurring yearly in Thailand and it significantly has negative impacts on the management of surface water and groundwater. Drought also causes an economic loss by ruining crops as well as starting a conflict amongst the water consumers [1]. Particularly, drought seems to exist more often according to the climate change forecast in several contexts, including meteorology, agriculture, hydrology, and socioeconomics. After all, it will lead to water shortages. Generally, drought starts when the rainfall becomes very lower than the average or predicted amount during certain periods of time. When caused by rainfall, droughts are often referred to as meteorological droughts and develop into other droughts, for example, agricultural drought or hydrologic drought [10]. However, Streamflow Drought Index (SDI) uses monthly streamflow values and a historical time series for the streamflow gauge, both wet and dry periods can be investigated, as well as the severity of these occurrences. In this regard, SDI is granted as a simple and effective indexing method since it requires a small number of variables so that this SDI has been broadly implemented to define and examine the characteristics of hydrological drought as well as to properly assess the severity and occurrence rate of the drought in all levels of the area. SDI is used to monitor and identify drought events with reference to a particular gauge, which may or may not represent larger basins [7].

Several studies on metrological drought and hydrological drought in many regions around the world were conducted by implementing the SDI; for example, the SDI-based study on the hydrological drought in the upper Yangtze River Basin in China [4], Tigris Basin in Turkey [8] and Peninsular Malaysia [3]. In Thailand, the SDI was applied to estimate the drought from the future climate change [9] and in the river basins without gauge stations [6]. The advantage of SDI is that it is widely available and easy to use. Missing data are allowed, and the longer the streamflow record, the more accurate the results. As with SPI, various timescales can be examined, and the disadvantage of SDI is single input (streamflow) does not take into account management decisions, and periods of no flow can skew the results [7]. Still, there has previously been only fewer studies using this SDI to describe the relationship between the streamflow and the droughts in the watershed around the reservoir directly correlated to the streamflow in the upstream are that flow freely into the reservoir while the water in the downstream area is being drained properly from the reservoir for seasonal consumptions, especially the regional watersheds around the northeast of Thailand. Accordingly, the main purpose of this study was to implement the streamflow data from the observed station to develop the SDI in order to understand all related hydrological factors as the cause of the drought in both the upstream and downstream areas of Lampao Reservoir, one of the three major multi-purpose reservoirs in the northeast of Thailand. Exactly, it was expected that the study outcome would provide a clearer insight toward the hydrological factors, especially the streamflow that directly encourages the existence of drought so that all the stakeholders would join one another to make a good plan and suitably prepare themselves for the sustainable water resources management.

2 Study Area and Data Collection

Lampao Reservoir is the multi-purpose reservoir in the Chi River Basin in the northeast of Thailand, supplying water through the irrigation system to an area of 505 sq. km as well as preventing the flood in the middle area of the northeast region, as illustrated in Fig. 1. The reservoir consists of several structures, including the clay core with 7.8 km of length, 33 m of height, the regular storage of 1,980 MCM, and the annual inflow of 1,967 MCM. The residents around the reservoir earn their living from agriculture by growing rice, cassava, and sugarcane and usually encounter water problems, including water shortage, flood, and conflicts over the water resource and environment conservation. Physically, the major watershed on the upstream area is the Upper Lampao Basin, where Lampao River is the mainstream flowing into the reservoir; it is located with the observed Station E65 for the streamflow estimation. On the other hand, the Lower Lampao Basin is located in the downstream area with the observed Station E75. Specifically, the streamflow data used in this study were recorded monthly at those two stations during the period of 1984–2020 by the Hydrology Irrigation Center for Upper North-eastern Region (Royal Irrigation Department of Thailand). The hydrological data of the two basins are given in Table 1.
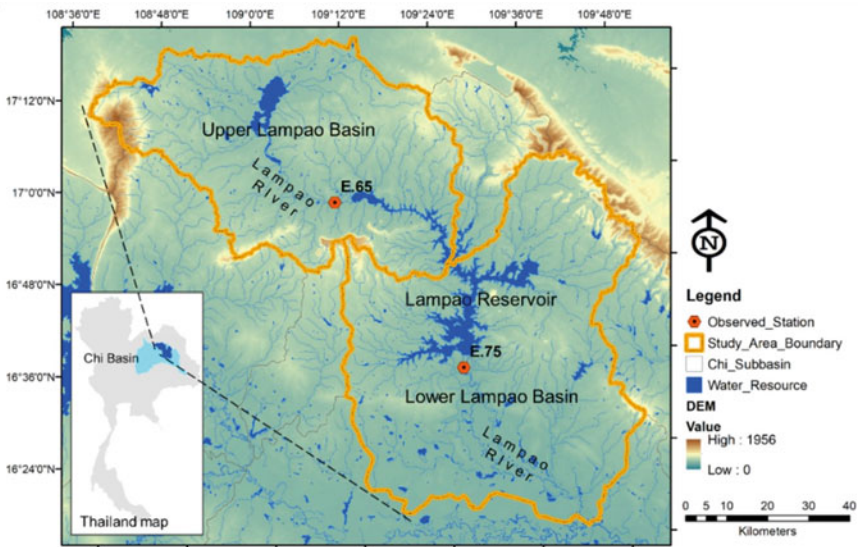
Fig. 1 Study area

Table 1 The hydrological conditions in the watershed area covering the Lampao Reservoir: http://hydro-3.rid.go.th/, Hydrology Irrigation Center for Upper North-eastern Region (Khon Kaen province, Thailand)

Data	Upper Lampao basin	Lower Lampao basin
Watershed area (sq. km)	3,283	4,202
Annual temperature (°C)	26.68	27.55
Annual rainfall (mm)	1,410.83	1,383.96
Annual streamflow (MCM)	365.8	791.7
Observed station	E65	E75
Time of record (years)	1984–2020	1987–2020

3 Standard Drought Index (SDI)

The concept of the SDI had been developed by [7] with an aim to identify the characteristics of hydrological drought. This SDI was a calculation method that uses the monthly streamflow [2] from the observed station as an input. Indeed, the SDI could be calculated from Streamflow Data V_i, k in each of Reference Range k of Hydrological Year i as described in Eq. (1) below

$$SDI_{i,k} = \frac{V_{i,k} = \bar{V}}{s_k} \, i = 1, 2, \ldots \quad k = 1, 2, 3, 4 \tag{1}$$

where V_k and s_k were the mean scores and the standard deviation of the total streamflow at Reference Period k. since these parameters were predicted in a long period of time. Particularly by this definition, the cut-down level was defined as V_k in spite of other available values. The negative results from the SDI represented the hydrological drought, and each level of the drought was presented with certain numbers from 0 (No Drought) to –4 (Extreme Drought), as shown in Table 2 [7]

Table 2 Drought classification for SDI

Description	Class
Non-drought	$SDI \leq 0.0$
Mild drought	$-1.0 \leq SDI < 0.0$
Moderate drought	$-1.5 \leq SDI < -1.0$
Severe drought	$-2.0 \leq SDI < -1.5$
Extreme drought	$SDI < -2.0$

4　Results and Discussion

4.1　Monthly Streamflow from Observed Stations

Use observed the monthly streamflow from Stations E65 and E75 (Hydrology Irrigation Center for Upper North-eastern Region in Khon Kaen province, Thailand). When considering the average annual streamflow from Station E65, it was presented in Fig. 2. It was 695 MCM (the total of 37-years data) that was lower than the average by 13 years (35.1%). Namely, the lowest average, 161.9 MCM (–76.8%), was found during 2019 to 2020, and the next lowest averages were found during 1992–1993, 1993 to 1994, and during 2012 to 2013, respectively. In the case of Station E75, the annual streamflow was 854.4 MCM (the total of 32-years data) which was far lower than the average by 19 years (59.4%), and the streamflow had been found lower than 60% for ten years in a row. The lowest streamflow, 64.1 MCM (92.5%), was found during 1993 to 1994, and the next was found during 2012–1013, 2013–2014, and 1988–1989 respectively. Surprisingly, we found a correlation in some periods of time when the streamflow from both stations was lower than the average; for example, a period of 1991–1994 and a period of 1997–2000. Nevertheless, during a period of 2012–2016, the streamflow at Station E75 was continually lower than the average due to the limited quantity of water supplied into the rivers following the decrease of the water quantity flowing into the reservoir. This had happened until a period of 2017–2018 and reoccurred in a period of 2018–2020.
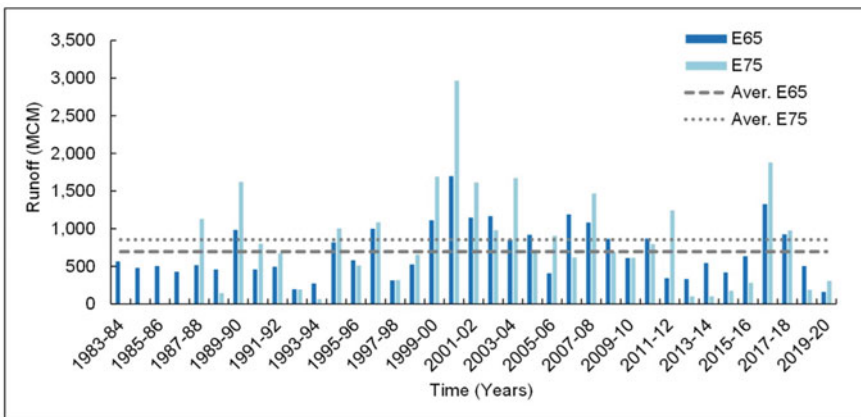
Fig. 2　The average annual streamflow data from observed stations E65 and E75

4.2   SDI Series

The SDI was calculated from the monthly streamflow from the observed stations starting from October to September (in the next year). The SDI calculation in this study was classified into four periods, including 1) 3-Month; 2) 6-Month; 3) 9-Month; and 4) 12-Month [5]. The time series distribution and the drought levels of the SDI from Station E65 are illustrated in Fig. 3. That is, the SDI at Station E65 suggested the results from those four periods were similar, which could be obviously seen that SDI (negative values) were distributed continually during a period of 1983–1998, and later these negative values were lightly found during a period of 1999–2011. Still, these negative values were increased in the period of 2012 to 2017. When evaluated by the 3-Month (Fig. 3(a)) and 6-Month Calculation Periods (Fig. 3(b), it was found that a case of Extreme Drought has been mostly found in a period of 2021–2014 from September to January (between –2.98 and –4.05. Remarkably, the 6-Month Calculation Period had indicated the drought levels from "Severe Drought to Extreme Drought" for 21 months in a row from July 2021–March 2014; meanwhile, the 9-Month Calculation Period (Fig. 3(c)) and the 12-Month Calculation Period (Fig. 3(d)) gradually described the phenomenon in a long period of time with the increasing SDI as seen in a period of 1991–1992 from the 9-month and 12-month periods when the phenomenon had been long occurring for 46 and 47 months with the mean score of –1.13 and –1.15 respectively; these were noticed as Moderate Drought. Those two periods of calculation also presented the Extreme Drought phenomena in 2021 that kept continuing to 2015 and 2016.

(a) SDI-3 at E65

(b) SDI-6 at E65

(c) SDI-9 at E65

(d) SDI-12 at E65
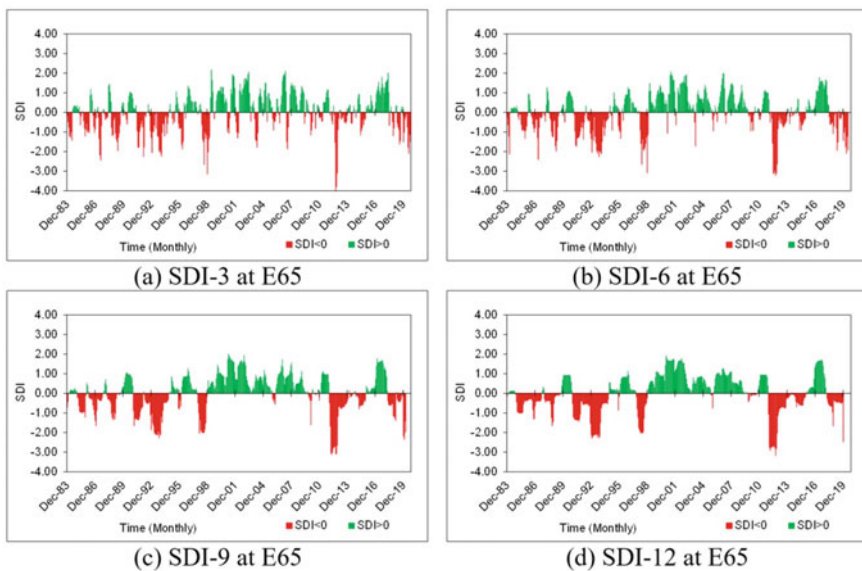
Fig. 3 Time series distribution and drought levels of SDI from station E65

The analysis of SDI at Station E75 is the observed point of streamflow in the Lampao River that has been controlled from the water discharge of the Lampao Reservoir. The results of the calculations for the four periods can be shown in Fig. 4. It can be seen that the SDI occur in groups of approximately four consecutive time periods, chronologically from 1988–1989, 1993–1994, 2012–2017 and 2019–2020. In the case of a 3-month series of calculations (Fig. 4(a)), the highest extreme drought SDI occurred during the mid-drought to early rainy season between February and August 1989 (SDI was −3.22 in April). The longest sustained drought events occurred between September 2012 and December 2016, for a total period of 49 months, with mean SDI in the mild drought level, and another Extreme Drought event occurred during the 2019 rainy season. Analysis results from a series of calculations 6, 9, and 12 months, as shown in Fig. 4(b), (c), and (d), respectively, indicate that there is a similar event period to the results calculated from the 3-month series. Only the Extreme Drought period 1989 and the long-term sequential period 2012–2017, which amounted to 54 to 56 months, while the SDI average represents a moderate drought threshold.

Tables 3 and 4 presented the total number of the months when the drought phenomena were detected at the two observed stations. According to the four calculation periods at Station E65 in the upstream area of Lampao Reservoir, it was found that the number of the months when the drought existed was in a range of 44.7% to 48.1% of all months. Most of the SDI was in a range of 30.3%–34.9% and noticed as Mild Drought while the SDI at the Extreme Drought level were often found when assessed by the 9-Month and 12-Month Calculation Period, and the results were 5.1% and 6.2%, respectively. In the meantime, the data analysis at Station E75, where the
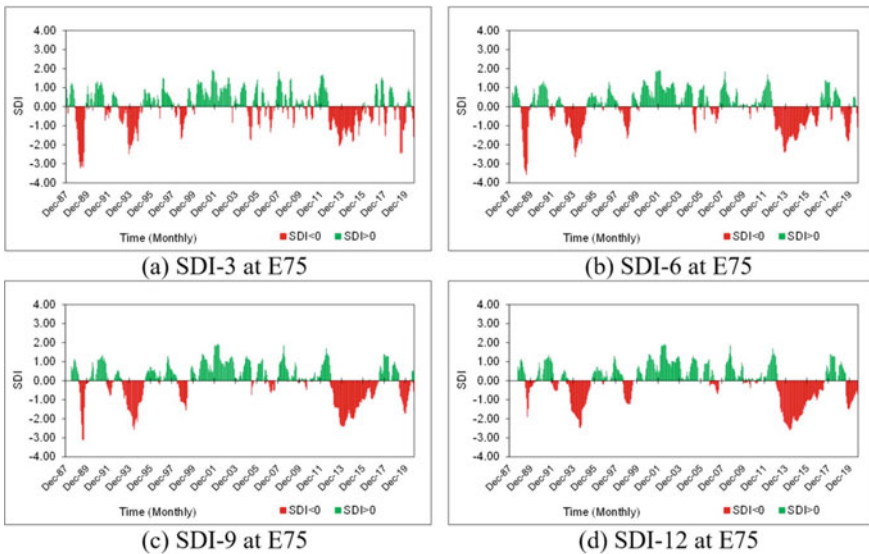
Fig. 4 Time series distribution and drought levels of SDI from station E75

Table 3 Number of months (M) in drought conditions at E65 station

SDI levels	SDI-3		SDI-6		SDI-9		SDI-12	
	M	%	M	%	M	%	M	%
Non drought	237	53.6	240	54.7	241	55.3	225	51.9
Mild drought	134	30.3	137	31.2	132	30.3	151	34.9
Moderate drought	42	9.5	27	6.2	27	6.19	22	5.1
Severe drought	15	3.3	19	4.3	14	3.21	8	1.9
Extreme drought	14	3.2	16	3.6	22	5.1	27	6.2
Total	442	100	439	100	436	100	433	100

Table 4 Number of months (M) in drought conditions at E75 station

SDI levels	SDI-3		SDI-6		SDI-9		SDI-12	
	M	%	M	%	M	%	M	%
Non drought	219	55.6	234	59.9	221	56.9	s	58.2
Mild drought	109	27.7	89	22.8	98	25.3	93	24.2
Moderate drought	33	8.4	30	7.7	30	7.7	28	7.3
Severe drought	18	4.6	25	6.4	22	5.7	20	5.2
Extreme drought	15	3.8	13	3.3	17	4.4	20	5.2
Total	394	100	391	100	388	100	385	100

streamflow was influenced by the water drainage from the reservoir, notably demonstrated a smaller number of the months when the drought existed compared to Station E65; the number of the drought months was in a range of 40.2%–44.4% of all months. The SDI at Mild Drought were the most often found ranged from 22.8% to 27.7% and followed by the SDI at the Moderate Drought level found in a range of 7.3%–8.4%. In the same vein, the frequency of the SDI at the Extreme Drought level could be detected in the 9-Month and 12-Month Calculation Period, and the results were 4.4% and 5.2%, respectively.

5   Conclusion

In conclusion, to conduct the study on the hydrological drought index, the streamflow data from Station E65 and Station E75 were developed as the Streamflow Drought Index (SDI) to analyze and assess the drought phenomena in both the upstream and downstream areas of Lampao Reservoir, one of the major multi-purpose reservoirs in the northeast of Thailand. In order to assess the data in deferent periods of time from past to present, the data was processed in four calculation periods together with the time series distribution, and the results suggested different levels of the drought. Particularly, the summary on the monthly assessment indicated that the time periods

when the drought existed was in a range of 40%–48% compared to the total number starting from the midst of drought season to the beginning of raining season. Most of the data were noticed as Mild Drought and Moderate Drought. On the contrary, the data at the Extreme Drought level were found in a range of 3%–6% of all months. Furthermore, the comparative study on the location of the observed station found that Station E65 demonstrated a longer period of drought months compared to the data from Station E75 since the streamflow at this station was dependently regulated by the water drainage from the reservoir in order to prevent the water shortage in the downstream area. On the other hand, the streamflow flowing into the rivers in the upstream area around the reservoirs was mainly influenced by the metrological changes within the local area. However, this study was encountered with the limited streamflow data that were taken from only two stations which could not completely represent all the streamflow data around the reservoir. Additionally, there are more effective factors that cause the drought, such as the land use or the demand for water for human activities that have not been discussed in this study. Still, it was expected that the research methodology implemented in this study would be a support for preparing an effective management plan for the water resource in the river basins around the reservoir in the future.

References

1. Acharya V, Halanaik B, Ramaprasad A, Kumara Swamy TR, Singai CB, Syn T (2020) Transboundary sharing of river water: informating the policies. River Res Appl 36(1):161–170
2. Aghelpour P, Bahrami-Pichaghchi H, Varshavian V (2021) Hydrological drought forecasting using multi-scalar streamflow drought index, stochastic models and machine learning approaches, in northern Iran. Stoch Env Res Risk Assess 35:1615–1635. https://doi.org/10.1007/s00477-020-01949-z
3. Hasan HH, Razali SFH, Muhammad NS, Ahmad, A (2021) Hydrological Drought across Peninsular Malaysia: implication of drought index. Nat Hazards Earth Syst 1–28. https://doi.org/10.5194/nhess-2021-176
4. Hong X, Guo S, Zhou Y, Xiong L (2015) Uncertainties in assessing hydrological drought using streamflow drought index for the upper Yangtze River Basin. Stoch Env Res Risk Assess 29(4):1235–1247
5. Jahangir MH, Yarahmadi Y (2020) Hydrological drought analyzing and monitoring by using Streamflow Drought Index (SDI) (case study: Lorestan, Iran). Arab J Geosci 13:110. https://doi.org/10.1007/s12517-020-5059-8
6. Lohpaisankrit W, Techamahasaranont J (2021) Analysis of precipitation and streamflow data for drought assessment in an unregulated watershed. Environ Nat Res J 19(2):112–121
7. Nalbantis I, Tsakiris G (2009) Assessment of hydrological drought revisited. Water Resour Manage 23(5):881–897
8. Ozkaya A, Zerberg Y (2019) A 40-year analysis of the hydrological drought index for the Tigris Basin, Turkey. Water 11(4):657. https://doi.org/10.3390/w11040657

9. Pandhumas T, Kuntiyawichai K, Jothityangkoon C, Suryadi FX (2020) Assessment of climate change impacts on drought severity using SPI and SDI over the Lower Nam Phong River Basin, Thailand. Eng Appl Sci Res 47(3):326–338
10. Pathak AA, Dodamani CBM (2016) Comparison of two hydrological drought indices. Persp Sci 8:626–628

Trend Analysis of Terrestrial Water Availability in the Amu River Basin Under Climate Change

Obaidullah Salehie, Tarmizi bin Ismail, and Shamsuddin Shahid

Abstract Amu River basin is one of Central Asia's largest international transboundary river basins, gradually experiencing more water stress due to increased human interventions and climate change. The objective of this study was to find trends in water availability in the Amu river basin. For this purpose, the Jet Propulsion Laboratory (JPL) data as one of the Gravity Recovery and Climate Experiment (GRACE) solutions with a high spatial resolution of 0.5° for the period 2002–2019 was used. The results of variability in Terrestrial Water Storage (TWS) showed higher variability ($\geq$30 cm) in the Tundra and warm-dry continental climate and gradually decreased towards the hot-summer Mediterranean climate zone. In contrast, the spatial variability is low towards the west and northwest of the basin, which means water resource reliability increases in the steppe and cold desert climate zone. The trend analysis results revealed a higher decrease in water availability in the Tundra and warm, dry continental climate zones and the delta region of the basin, with a negative value ranging from 0.04 to –0.08 cm/year. Therefore, the results indicate that GRACE could be applied successfully for a large-scale basin with a diverse climate condition.

Keywords Gravity recovery and climate experiment · Terrestrial water storage · Resiliency · Amu river basin

O. Salehie (✉) · T. bin Ismail · S. Shahid
Department of Water and Environmental Engineering, School of Civil Engineering,
Faculty of Engineering, Universiti Teknologi Malaysia (UTM), 81310 Skudai, Johor, Malaysia
e-mail: salehie1985@graduate.utm.my

T. bin Ismail
e-mail: tarmiziismail@utm.my

S. Shahid
e-mail: sshahid@utm.my

O. Salehie
Faculty of Environment, Kabul University, Kabul, Afghanistan

1 Introduction

Water is the key component of the earth that maintains the functions of ecosystems, environmental sustainability and human life [14]. Global water demand has increased at an annual rate of nearly 1.8% in the past century [46]. It is projected to increase by 55% in 2050 with population growth and economic development [7]. Arid and semi-arid regions are more prone to water stress due to lower precipitation, high evaporation and dry conditions [26, 27, 38]. Climate change has caused a decrease in precipitation and lessening water availability in many parts of the globe, especially in arid regions [22, 25, 38, 42]. Therefore, water availability must be well understood to meet water demands in various sectors [1, 5, 31, 33, 45]. Information on spatiotemporal water availability in a basin is required to track and monitor water availability [2, 23, 39]. Although sufficient hydrological observations are not available in many developing countries, making GRACE data has been widely used recently to track water availability and monitor spatiotemporal changes in TWS globally [28, 30, 42, 50]. GRACE provides an estimation of the total water stored above and below the ground, including surface water, ground water, soil moisture and snow water equivalent [3, 42].

GRACE satellite data measure the earth's gravitational field every 30 days with a spatial resolution of 400 km to 40,000 km. The GRACE helps track spatiotemporal changes in total water availability and the hydrological cycle at the global and regional levels. Anomalies of terrestrial water storage (TWS) from GRACE are usually used in hydrological studies at global and regional levels [10]. Due to its coarse spatial resolution not being suitable for local water resources studies, it is suitable for large basins only. There are three products of GRACE data, including Jet Propulsion Laboratory (JPL), Center for Space Research at University of Texas, Austin (CSR) and Geoforschungs Zentrum Potsdam (GFZ) [9].

Many researchers used GRACE to assess changes in groundwater, surface water and drought. For example, [47] used GRACE data to find changes in water storage in the Three Gorges Reservoir of China. Some researchers, for example [19, 24, 41], used GRACE and the Global Land Data Assimilation System (GLDAS) to evaluate changes in TWS over river basin. [19] used GRACE to evaluate groundwater storage variation in Australia's Murray-Darling Basin. Other researchers used it to assess and monitor hydrological drought [6, 8, 17, 43]. [42] used GRACE to project water availability and sustainability in Nigeria.

Numerous water availability indices have been developed to measure water stress and water sustainability [14, 20]. Statistical methods like correlations, regression analysis, and nonparametric tests like Mann–Kendall (MK) and Modified Mann–Kendall (MMK) have been widely used by researchers to detect trends in water resources and water quality [4, 12, 13, 15, 18, 29, 40, 49, 51]. Recently, the random forest model, a machine learning method, has been proposed to project future water storage change [42].

Few studies have assessed the impact of climate change on water resources in the Amu river basin [11, 16, 34–37, 48]. Therefore, this study was conducted to find

trends in water availability in the Amu river basin using a GRACE product for the period 2002–2019 and MMK trend analysis.

2 Study Area

The Amu river is the longest transboundary river in Central Asia, shared by five countries, including Kyrgyzstan, Tajikistan, Afghanistan, Turkmenistan and Uzbekistan [16], as shown in Fig. 1. The river is 2,540 km in length, with an average annual flow of about 79 km^3. The basin area covers 534,739 km^2 [32]. The basin's topography is complex, with 7500 m altitude in the upstream mountains in the east to about 200 m in the downstream northwest plains [37]. The basin can be classified into five main climatic zones, as presented in Fig. 1. The upstream of the basin receives about 2000 mm of rainfall in a year, while the downstream receive only 100 mm. The basin's climate is completely dry continental with a mean annual temperature of 13.0 °C [44].
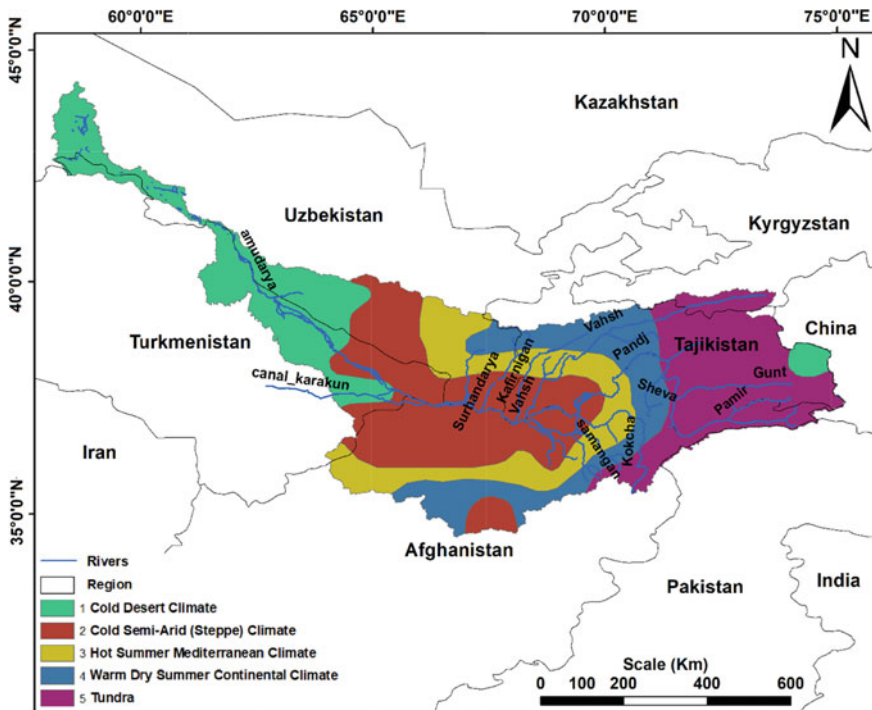
Fig. 1 The climate zones of Amu river basin

3   Methods

3.1   Trend Analysis of Water Availability

Sen's slope estimator was used to calculate the variation of TWS, and the MMK test was used to identify the significance of trends. Sen's slope is a nonparametric method commonly used to estimate the change in time series data. It is calculated as the median of the rate of change between two successive times Q_i as follows:

$$Q_i = \frac{x_i - x_k}{i - k} \text{for} N = 1, 2, 3, \ldots, n \tag{1}$$

where x_i and x_k estimated at the time, i and k. The Sen's estimator of the slope is the median of these n values of Q_i as follows:

$$Q_i = \begin{cases} \frac{Q_{N+1}}{2} & \text{if N is odd} \\ \frac{1}{2}\left(\frac{Q_N}{2} + \frac{Q_{N+2}}{2}\right) & \text{if N is even} \end{cases} \tag{2}$$

The MK test statistic (S) for a time series $x_1, x_2, x_3 \ldots$, and x_n can be calculated as follows:

$$S = \sum_{k=1}^{n-1} \sum_{i=k+1}^{n} \text{sign}(x_i - x_k) \tag{3}$$

$$\text{where sign}(x_i - x_k) = \begin{cases} +1 \text{ if sign}(x_i - x_k) > 0 \\ 0 \text{ if sign}(x_i - x_k) = 0 \\ -1 \text{ if sign}(x_i - x_k) < 0 \end{cases} \tag{4}$$

where n is the number of data points, x_k and x_i are sequential data, S is the sum of positive or negative signs. The Z statistic is then calculated from the variance of S to decide trend significance,

$$Z = \begin{cases} \frac{S-1}{\sqrt{\text{Var}(S)}} & \text{when } S > 0 \\ 0 & \text{when } S = 0 \\ \frac{S+1}{\sqrt{\text{Var}(S)}} & \text{when } S < 0 \end{cases} \tag{5}$$

The null hypothesis on no trend is rejected at a confidence interval of 95% if $|Z| > 1.96$. The MMK is applied when the null hypothesis of no trend is rejected. The procedure of MMK followed the analysis of trends using the MK test. If a significant trend is found in the time series, the MMK test de-trends the series and

ranks the data (R_i) to estimate its equivalent normal variants (Z_i), which can be estimated using the inverse standard normal distribution function ($\varnothing^{-1}$),

$$Z_i = \varnothing^{-1}\left(\frac{R_i}{n+1}\right) \text{for } i = 1:n \tag{6}$$

where $\varnothing^{-1}$ is the inverse standard normal distribution function. The Z is used to calculate the Hurst coefficient (H) via the maximum log-likelihood function [21].

$$\log L(H) = -\frac{1}{2}\log|C_n(H)| - \frac{z^{\tau}[C_n(H)]^{-1}Z}{2\gamma_0} \tag{7}$$

where $|C_n(H)|$ is the determinant of the correlation matrix of lag for a given H; z^{τ} indicates the transpose and variance of Z and H that yields the maximum value of log L(H) is counted to define the presence of long-term dependency in the time series. The significance of H can be obtained by using mean and standard deviation for H = 0.5. When H is found to be significant, the biased estimate of $Var(S)^{H'}$ can be expressed as follows:

$$Var(S)^{H'} = \sum_{i<j} \cdot \sum_{k<l} \frac{2}{\pi} \sin^{-1}\left(\frac{\rho|j-i| - \rho|i-1| - \rho|j-k| + \rho|i-k|}{\sqrt{(2-2\rho|i-j|)(2-2\rho|k-1|)}}\right) \tag{8}$$

where ρ_1 is the autocorrelation function for a given H.

4 Results

4.1 Geographical Variation in TWS

The geographical distribution in TWS availability was assessed using the standard deviation of JPL-GRACE to represent the basin's spatial variation of water availability, as presented in Fig. 2. The variability values in TWS range from (0.775 to 30.68 cm). The higher variability means the lower reliability of water resources and vice versa. The figure shows that the higher variability in TWS (≥ 30 cm) happened in the eastern and southeastern parts. This area covers the Tundra and warm-dry continental climate and slowly decreases towards the hot-summer Mediterranean climate zone. However, the variability amounts became less or close to zero towards the west and northwest of the basin. It shows that the reliability in TWS increases from hot-summer Mediterranean climate to steppe and even cold desert climate area.
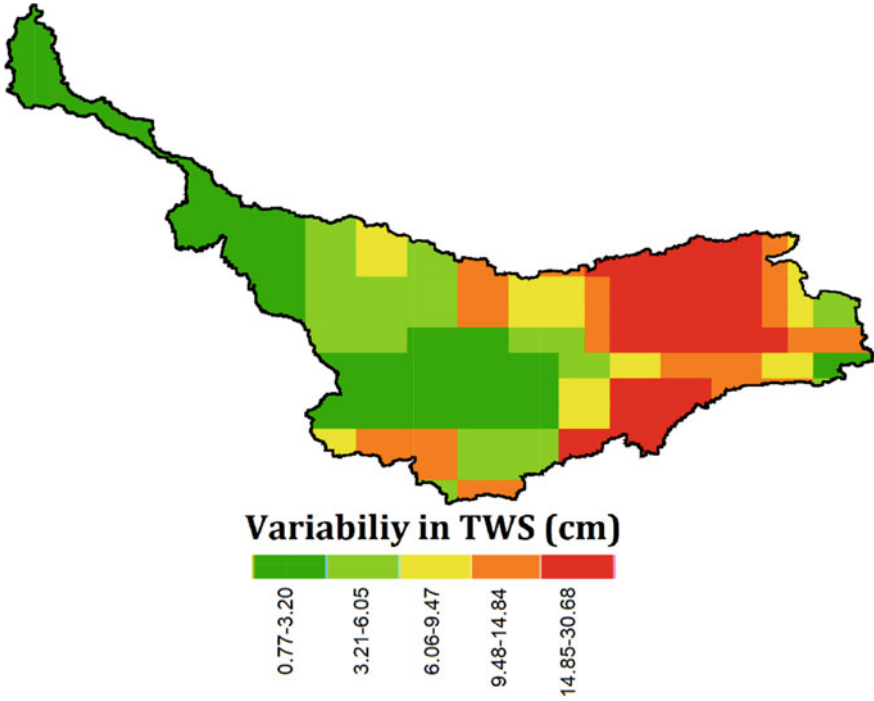
Fig. 2 Spatial variability of TWS (cm) in the Amu river basin for JPL product

4.2 Trend Analysis of TWS

The change in TWS over space was obtained using the JPL product and presented in Fig. 3. The rate of the changes was evaluated using Sen's slope estimator and visualized using colour ramps. MMK test was used to find whether the rate of the changes is significant or not, and the significant change showed as node symbols at each grid location in the figure. The confidence level was considered 95% based on the MMK trend test. The rate of the change in the five climate zones ranges from 0.08 to –0.12 cm/year. The results revealed negative changes in TWS in most parts in the northeast, the Tundra and warm-dry continental climate zones and small parts in the delta of the basin ending to the Aral Sea under the cold desert climate zone according to Sen's slope method. This reflects a potential decrease in water resources in those regions. However, most cold desert climates and cold semi-arid (steppe) climate zones showed relatively less change.
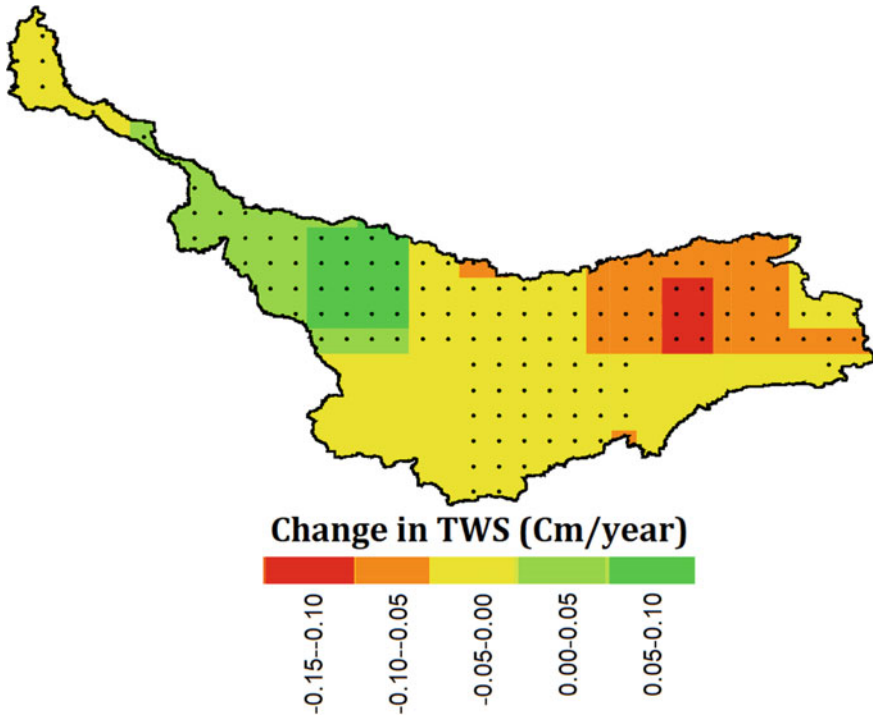
Fig. 3 The spatial patterns of change in TWS (cm/year) using the JPL dataset. The colour ramps show the rate of change obtained by applying Sen's slope, and the black dot inside each cell specifies the trend is significant at a 95% confidence interval obtained by MMK

5   Discussion

The spatial variability of TWS in the basin is presented in Fig. 2, showing that the higher value of variability ($\geq$30 cm) can be seen in the east and small patches in the central part of the study area. This is indicating water resources are less reliable in these areas. Spatial variability is less in the hot-summer Mediterranean climate and cold semi-arid (steppe) and clod desert climate regions. These areas are more reliable in terms of water reliability.

Results obtained from trend analysis is shown in Fig. 3, further supporting the results obtained by spatial variability analysis. Outcomes obtained from the trend analysis shows more decrease in water resources in the Tundra and a small part in warm-dry continental climate zones and the delta of the basin. In contrast, water resources in the Mediterranean climate, cold semi-arid (steppe), and most clod desert climate zones showed lower variabilities. In these regions, the trend analysis values were positive (0- 0.10 cm/ear).

Salehie et al. [37] assessed thermal bioclimate indicators in the Amu river catchment. They showed that the diurnal temperature range (TBI2) would considerably

increase in the eastern part of the basin. Moreover, Isothermality (TBI3) revealed a significant rise in temperature in cold months in the same parts of the basin. This change in the upstream climate could potentially cause glacier retreats and water unreliability in that region.

6 Conclusion

The objective of this study was to find out the spatial variability and trend in water availability in the Amu river watershed by using GRACE data and employing the MMK and Sen's slope method. The findings indicate that the variability is more in the basin's eastern part by (≥ 30 cm). The results further sufficed by trend analysis showing a potential decrease of water resources in most parts in the northeast of the basin, the Tundra and warm-dry continental climate zones and small parts in the delta of the basin under the cold desert climate zone. Overall, the results of water availability using GRACE data via applying trend analysis provided a better understanding of water resources availability of the basin.

References

1. Ahmed K, Shahid S, Bin Harun S, Ismail T, Nawaz N, Shamsudin S (2015) Assessment of groundwater potential zones in an arid region based on catastrophe theory. Earth Sci Inf 8(3):539–549
2. Ahmed K, Shahid S, Demirel MC, Nawaz N, Khan N (2019) The changing characteristics of groundwater sustainability in Pakistan from 2002 to 2016. Hydrogeol J 27(7):2485–2496
3. Al-Mohammdawi JA, Al-Abadi AM, Al-Ali AK, Shahid S, Fryar A, Wang X (2022) Assessing the spatial and temporal variations of terrestrial water storage of Iraq using GRACE satellite data and reliability–resiliency–vulnerability indicators. Arab J Geosci 15(4):1–13
4. Antonopoulos VZ, Papamichail DM, Mitsiou KA (2001) Statistical and trend analysis of water quality and quantity data for the Strymon River in Greece. Hydrol Earth Syst Sci 5(4):679–692
5. Barlow PM, Alley WM, Myers DN (2004) Hydrologic aspects of water sustainability and their relation to a national assessment of water availability and use. Water Reso (127):76–86
6. Boergens E, Güntner A, Dobslaw H, Dahle C (2020) Quantifying the Central European droughts in 2018 and 2019 with GRACE Follow-On. Geophys Res Lett 47(14):e2020GL087285
7. Boretti A, Rosa L (2019) Reassessing the projections of the world water development report. NPJ Clean Water 2(1):1–6
8. Cammalleri C, Barbosa P, Vogt JV (2019) Analysing the relationship between multiple-timescale SPI and GRACE terrestrial water storage in the framework of drought monitoring. Water 11(8):1672
9. Dai C, Shum C, Wang R, Wang L, Guo J, Shang K, Tapley B (2014) Improved constraints on seismic source parameters of the 2011 Tohoku earthquake from GRACE gravity and gravity gradient changes. Geophys Res Lett 41(6):1929–1936
10. Frappart F, Ramillien G (2018) Monitoring groundwater storage changes using the Gravity Recovery and Climate Experiment (GRACE) satellite mission: a review. Remote Sens 10(6):829
11. Glantz MH (2005) Water, climate, and development issues in the Amu Darya basin. Mitig Adapt Strat Glob Change 10(1):23–50

12. Hadi Pour S, Abd Wahab AK, Shahid S, Wang X (2019) Spatial pattern of the unidirectional trends in thermal bioclimatic indicators in Iran. Sustainability 11(8):2287

13. Hirsch RM, Slack JR, Smith RA (1982) Techniques of trend analysis for monthly water quality data. Water Resour Res 18(1):107–121

14. Huang S, Feng Q, Lu Z, Wen X, Deo RC (2017) Trend analysis of water poverty index for assessment of water stress and water management polices: a case study in the Hexi Corridor, China. Sustainability 9(5):756

15. Iqbal Z, Shahid S, Ahmed K, Ismail T, Nawaz N (2019) Spatial distribution of the trends in precipitation and precipitation extremes in the sub-Himalayan region of Pakistan. Theoret Appl Climatol 137(3):2755–2769

16. Jalilov S-M, Keskinen M, Varis O, Amer S, Ward FA (2016) Managing the water–energy–food nexus: gains and losses from new water development in Amu Darya river basin. J Hydrol 539:648–661

17. Jin S, Zhang T (2016) Terrestrial water storage anomalies associated with drought in southwestern USA from GPS observations. Surv Geophys 37(6):1139–1156

18. Khan N, Pour SH, Shahid S, Ismail T, Ahmed K, Chung ES, Wang X (2019) Spatial distribution of secular trends in rainfall indices of Peninsular Malaysia in the presence of long-term persistence. Meteorol Appl 26(4):655–670

19. Li T, Zhang Q, Zhao Y, Gao Y (2019) Detection of groundwater storage variability based on GRACE and CABLE model in the Murray-Darling basin. Paper presented at the E3S Web of Conferences

20. Maiolo M, Pantusa D (2019) Sustainable water management index, SWaM_Index. Cogent Eng 6(1):1603817

21. McLeod AI, Hipel KW (1978) Simulation procedures for Box-Jenkins models. Water Resour Res 14(5):969–975

22. Mehran A, AghaKouchak A, Nakhjiri N, Stewardson MJ, Peel MC, Phillips TJ, Ravalico JK (2017) Compounding impacts of human-induced water stress and climate change on water availability. Sci Rep 7(1):1–9

23. Mirrah A, Kusratmoko, E (2017) Application of GIS for assessment of water availability in the Cianten watershed, West Java. Paper presented at the IOP Conference Series: Earth and Environmental Science

24. Mo X, Wu J, Wang Q, Zhou H (2016) Variations in water storage in China over recent decades from GRACE observations and GLDAS. Nat Hazard 16(2):469–482

25. Mohammed R, Scholz M (2017) Adaptation strategy to mitigate the impact of climate change on water resources in arid and semi-arid regions: a case study. Water Resour Manage 31(11):3557–3573

26. Muhammad MKI, Nashwan MS, Shahid S, Tb I, Song YH, Chung E-S (2019) Evaluation of empirical reference evapotranspiration models using compromise programming: a case study of Peninsular Malaysia. Sustainability 11(16):4267

27. Nashwan MS, Shahid S, Dewan A, Ismail T, Alias N (2020) Performance of five high resolution satellite-based precipitation products in arid region of Egypt: an evaluation. Atmos Res 236:104809

28. Pang Y, Wu B, Cao Y, Jia X (2020) Spatiotemporal changes in terrestrial water storage in the Beijing-Tianjin sandstorm source region from GRACE satellites. Int Soil Water Conserv Res 8(3):295–307

29. Pour SH, Abd Wahab AK, Shahid S, Ismail ZB (2020) Changes in reference evapotranspiration and its driving factors in peninsular Malaysia. Atmos Res 246:105096

30. Prakash S, Gairola R, Papa F, Mitra A (2014) An assessment of terrestrial water storage, rainfall and river discharge over Northern India from satellite data. Curr Sci 1582–1586

31. Qutbudin I, Shiru MS, Sharafati A, Ahmed K, Al-Ansari N, Yaseen ZM, Wang X (2019) Seasonal drought pattern changes due to climate variability: case study in Afghanistan. Water 11(5):1096

32. Rakhmatullaev S, Huneau F, Kazbekov J, Le Coustumer P, Jumanov J, El Oifi B, Hrkal Z (2010) Groundwater resources use and management in the Amu Darya river basin (Central Asia). Environ Earth Sci 59(6):1183–1193

33. Rathnayaka K, Malano H, Arora M (2016) Assessment of sustainability of urban water supply and demand management options: a comprehensive approach. Water 8(12):595

34. Salehie O, Ismail T, Hamed MM, Shahid S, Muhammad MKI (2021a) Projection of hot and cold extremes in the Amu River basin of Central Asia using GCMs CMIP6

35. Salehie O, Ismail T, Shahid S, Ahmed K, Adarsh S, Asaduzzaman M, Dewan A (2021) Ranking of gridded precipitation datasets by merging compromise programming and global performance index: a case study of the Amu Darya basin. Theoret Appl Climatol 144(3):985–999

36. Salehie O, Tb I, Shahid S, Hamed MM, Chinnasamy P, Wang X (2022) Assessment of water resources availability in Amu Darya river basin using GRACE data. Water 14(4):533

37. Salehie O, Ismail Tb, Shahid S, Sammen SS, Malik A, Wang X (2022b) Selection of the gridded temperature dataset for assessment of thermal bioclimatic environmental changes in Amu Darya River basin. Stoch Environ Res Risk Assesshttps://doi.org/10.1007/s00477-022-02172-8

38. Salman SA, Shahid S, Afan HA, Shiru MS, Al-Ansari N, Yaseen ZM (2020) Changes in climatic water availability and crop water demand for Iraq region. Sustainability 12(8):3437

39. Sediqi MN, Shiru MS, Nashwan MS, Ali R, Abubaker S, Wang X, Manawi SMA (2019) Spatio-temporal pattern in the changes in availability and sustainability of water resources in Afghanistan. Sustainability 11(20):5836

40. Shalini TA, Pandey A, Nathawat M (2012) Groundwater level and rainfall variability trend analysis using GIS in parts of Jharkhand state (India) for sustainable management of water resources. Int Res J Environ Sci 1(4):24–31

41. Shamsudduha M, Taylor RG, Jones D, Longuevergne L, Owor M, Tindimugaya C (2017) Recent changes in terrestrial water storage in the Upper Nile Basin: an evaluation of commonly used gridded GRACE products. Hydrol Earth Syst Sci 21(9):4533–4549

42. Shiru MS, Shahid S, Park I (2021) Projection of water availability and sustainability in Nigeria due to climate change. Sustainability 13(11):6284

43. Singh A, Reager JT, Behrangi A (2021) Estimation of hydrological drought recovery based on precipitation and Gravity Recovery and Climate Experiment (GRACE) water storage deficit. Hydrol Earth Syst Sci 25(2):511–526

44. Sun J, Li Y, Suo C, Liu Y (2019) Impacts of irrigation efficiency on agricultural water-land nexus system management under multiple uncertainties – a case study in Amu Darya River basin, Central Asia. Agric Water Manag 216:76–88

45. Tariq MAUR, van de Giesen N, Janjua S, Shahid MLUR, Farooq R (2020) An engineering perspective of water sharing issues in Pakistan. Water 12(2):477

46. Wada Y, Flörke M, Hanasaki N, Eisner S, Fischer G, Tramberend S, Ringler C (2016) Modeling global water use for the 21st century: The Water Futures and Solutions (WFaS) initiative and its approaches. Geosci Model Dev 9(1):175–222

47. Wang X, de Linage C, Famiglietti J, Zender CS (2011) Gravity Recovery and Climate Experiment (GRACE) detection of water storage changes in the three gorges reservoir of China and comparison with in situ measurements. Water Resour Res 47(12)

48. White CJ, Tanton TW, Rycroft DW (2014) The impact of climate change on the water resources of the Amu Darya Basin in Central Asia. Water Resour Manage 28(15):5267–5281

49. Xie P, Chen G, Lei H (2009) The assessment method of water resources based on trend analysis of changing environments. J Hydroelectr Eng 28:14–19

50. Xie Y, Huang S, Liu S, Leng G, Peng J, Huang Q, Li P (2018) GRACE-based terrestrial water storage in northwest China: changes and causes. Remote Sens 10(7):1163

51. Zhang Y, Cabilio P, Nadeem K (2016) Improved seasonal Mann–kendall tests for trend analysis in water resources time series. Advances in time series methods and applications, Springer, p 215–229

Characteristic of Stormwater Quality Using BIOECODS in JKR Pilot Projects

Sanisah Sulaiman, Noor Ezlyn Othman, Atikah Abdul Hamid, Nor Azazi Zakaria, and Chun Kiat Chang

Abstract The effectiveness of Bio-Ecological Drainage System (BIOECODS) in terms of improving water quality is crucial as it denotes one of the key objectives of the sustainable drainage system. This research aimed to evaluate the performance of stormwater quality using BIOECODS as compared to the conventional drainage system. For this purpose, a pilot project was implemented at the District Police Headquarters at Pasir Mas, Kelantan (IPD Pasir Mas), Kelantan. Stormwater samples were collected at six sampling points identified within the study area since June 2020 upon project completion with a Certificate of Practical Completion obtained. The nine water quality parameters tested were Ammoniacal Nitrogen (AN), Biochemical Oxygen Demand (BOD_5), Chemical Oxygen Demand (COD), Dissolve Oxygen (DO), pH, Total Dissolve Solids (TDS), Total Suspended Solids (TSS), turbidity, and temperature. The result has proven the effectiveness of this system by a significant reduction in water quali parameters concentration, i.e. BOD_5, COD, TDS, AN, pH and temperature, as well as substantial increments for DO. Overall results have also demonstrated that all the parameters complied with Class IIA and Class IIB, National Water Quality Standard for Malaysia before the runoff is discharged via discharge point approved by the Local Authority.

S. Sulaiman · A. A. Hamid
Civil and Structural Branch, Public Works Department (JKR), Kuala Lumpur, Malaysia
e-mail: sanisah@jkr.gov.my

A. A. Hamid
e-mail: atikah@jkr.gov.my

N. E. Othman
Civil and Structural Design Section of Kedah Public Works Department, Public Works
Department of Malaysia, Kuala Lumpur, Malaysia
e-mail: noorezlyn@jkr.gov.my

N. A. Zakaria · C. K. Chang (✉)
River Engineering and Urban Drainage Research Centre (REDAC), Universiti Sains Malaysia,
Penang, Malaysia
e-mail: redac10@usm.my

N. A. Zakaria
e-mail: redac01@usm.my

1 Introduction

The adoption of green technology in infrastructure design has emerged as one of the crucial measures from Jabatan Kerja Raya (JKR) Malaysia, thus warranting that all the designers implement the green characteristics in their design works. JKR, as the most prominent technical agency in Malaysia, is moving towards embracing the sustainability concept, which was launched in 2013 by enforcing all the designers to adhere to JKR's Green Policy. Among the initiatives taken by the JKR is launching the JKR Malaysia Sustainable Development Policy Book (2016–2020), which is a continuation of the previous Edition (2013–2015). The book summarized the background, efforts, and strategies formulated by JKR to fulfil the country's commitment to sustainable development at the national and world levels.

A working committee, known as Jawatankuasa Induk Pembangunan Lestari (JKIPL), was established to coordinate the involvement and support from all JKR staff, especially Specialist Sector Branches in integrating, coordinating and outlining sustainable development initiatives in the implementation of JKR's projects. JKR Green Rating Scheme is formulated to ensure that buildings and infrastructure are constructed in a safe and environmentally friendly manner. The Green Rating Scheme covers six (6) key areas: construction site, energy, construction materials, indoor water quality, water and innovation. As a result, the design project team will work closely with the supervision team to achieve the intended Green Rating and comply with the requirements of Local Authorities and other government agencies in targeting sustainable development through this green building rating process. With the time and data from all over the country available in JKR, the Green Ratings can be adapted to meet the needs of green infrastructure and buildings at all levels, regardless of location. Hence JKR pH Scheme and continuous development by JKR can improve the sustainability of all government infrastructures in the future.

Implementing green technology in drainage systems calls upon the implementation of Bio-Ecological Drainage System (BIOECODS), which consists of an ecological swale, on-site detention (OSD), detention pond, constructed wetlands, dry pond and wet pond. Stormwater being conveyed in the ecological swale is able to increase the lag time in the surface runoff, reduce the volume as well as the rate of runoff through enhanced infiltration and promote storage before being accumulated in OSD or detention ponds. The ecological pond system is strategically placed at the downstream end of the BIOECODS to optimize and effectively attenuate and treat stormwater runoff generated from the development area before release to nearest discharge points allowed by the Local Authority. BIOECODS is an example of an innovative sustainable urban drainage system that will help restore the natural environment [4, 10]. It has been implemented in numerous JKR projects, such as health clinics, training centers, universities, etc. BIOECODS provides an alternative design in green, offering ease of maintenance and economical overall construction cost.

However, the study of the effectiveness of BIOECODS in water quality control [2, 3, 8, 10] utilizing local data is still minimal.

2 Study Area

The development at District Police Headquarters (IPD) Pasir Mas (Fig. 1) covered 4.5 hectares on medium soil type. The existing land use of the development area was a rubber plantation. More than 75% of the total area has been developed into an impervious area such as paved road, car park, playground and utilities other than the buildings. The proposed project development is on a new site in Lot 11901, Mukim Gua, Kuala Lemal, Pasir Mas District, Kelantan, with 4.31 hectares (10.65 acres). The overall project duration takes about 152 weeks which started in June 2016. The construction of BIOECODS began in early March 2019 and was completed in August 2019.

The development site is located along Jalan Rantau Panjang, heading to the West about 15 km and Jalan Kota Bahru heading to the East about 35 km. The original
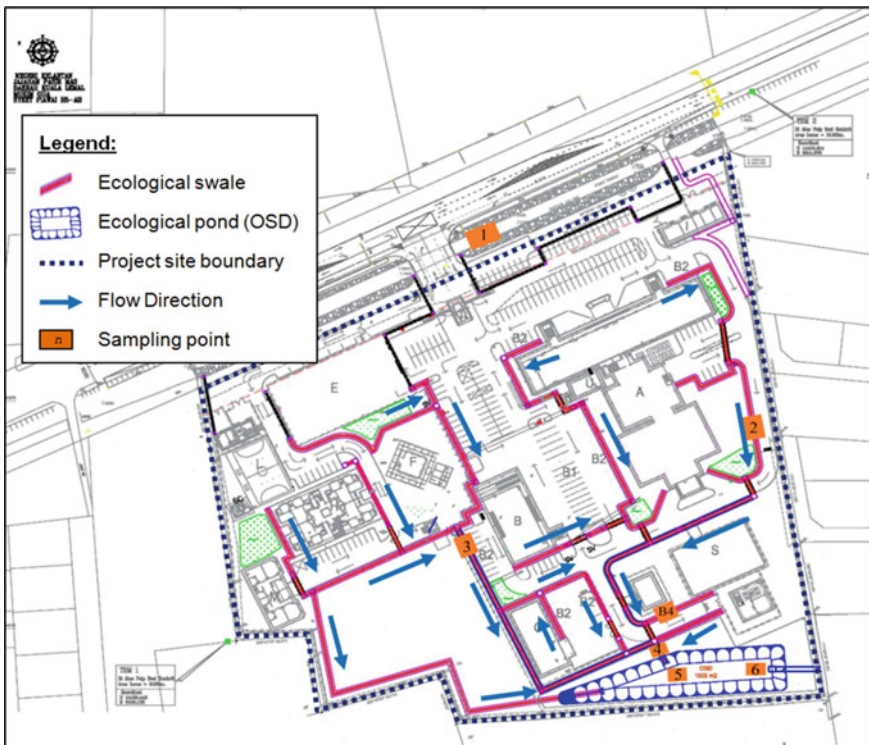
Fig. 1 Site layout of District Police Headquarters, Pasir Mas, Kelantan

ground level of this site ranges from +8.00 m to +9.50 m. The designed platform levels as per decided by the designers to be +10.80 m taking into account the sewerage system's design and ensuring the collected stormwater could be discharged to the final discharge without any obstruction. The final design showed that 3.43 hectares of the site would be an impervious area while the remaining. Based on the findings from Kelantan State's Department of Irrigation and Drainage, the site is located in a low lying area and easily inundated by the overflow water of Sungai Golok, especially during the flood season. It is, therefore, the proposed final discharge point for the development site at the roadside of Pasir Mas-Rantau Panjang highway and fully complies with the 2nd edition of Urban Stormwater Management Manual for Malaysia (MSMA 2nd Edition) [5].

3   Data Collection Process

The sampling process of stormwater in the ecological swale has been carried out from June 2020 (upon Certificate of Practical Completion (CPC) obtained) until April 2021. Three (3) sampling points (Fig. 1) at ecological swale were identified for sampling purposes. Besides that, sampling points (no.5 and no.6) have been identified at strategic locations that represented the OSD inlet and outlet to determine the effectiveness of the ecological pond in water quality control within site. Point no.1 is located at the conventional drain outside the study area. This location is chosen as a baseline which is to be compared with the results of the test of samples taken from the BIOECODS.

The samples were collected immediately after storm events from point no.1 to point no.6. Figure 2 shows the site locations of the sampling points. The water samples were collected and tested in the laboratory to determine the effectiveness of BIOE-CODS in enhancing water quality. Nine (9) parameters tested in the study, which include Ammoniacal Nitrogen (AN), Biochemical Oxygen Demand (BOD_5), Chemical Oxygen Demand (COD), Dissolve Oxygen (DO), pH, Total Dissolve Solids (TDS), Total Suspended Solids (TSS), turbidity, and temperature. In situ measurements were conducted for pH, DO, temperature, and turbidity. The measurements were carried out using a portable YSI Multi-parameter probe except for turbidity, measured using a turbidity meter. The collection of water samples was done according to the American Public Health Association (APHA) procedure for in situ measurement. The water samples were then transported back to the laboratory to perform COD, BOD, AN, and TSS analysis using the HACH method.

Sampling Point no.1	Sampling Point no.2	Sampling point no.3
Receiving waterway	Swale	Swale
Sampling Point no.4	Sampling Point no.5	Sampling Point no.6
Swale	OSD Inlet	OSD Outlet
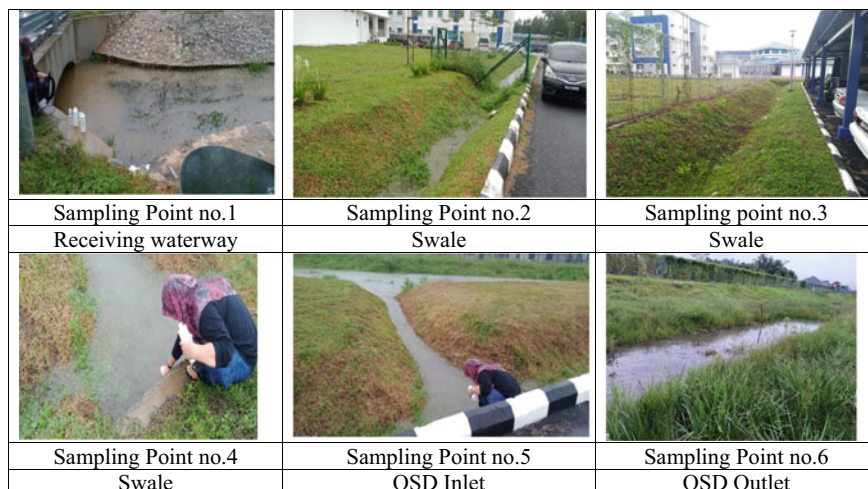
Fig. 2 Six sampling points

4 Results and Discussion

4.1 Ecological Swale

The results of water quality monitoring at the ecological swale from November 2020 to August 2021 are shown in Figs.3, 4, 5, 6, 7 and 8. Dissolved oxygen (DO) in water is vital as it determines whether the water can support aquatic microorganisms which are involved in water purification. Figure 3 shows the result for the individual parameter, i.e. DO for sampling taken. The DO concentration monitoring result at ecological swale showed an average of 6.00 mg/L for samples taken at points no. 2, no. 3 and no. 4. Meanwhile, it is also observed that the average value of DO concentration was higher, denoting the effectiveness of the BIOECODS in improving the water quality throughout the study period.

Figure 4 showed the water quality monitoring at ecological swale for parameter Biochemical Oxygen Demand (BOD_5) for sampling. From the result, it is observed that the BOD_5 at point no.3, which is the outlet of the swale, recorded an average of 2.68 mg/L, while for point no.4, the average was 2.22 mg/L. Both values comply with the limit (below 3.00 mg/L) for Class IIA and Class IIB of National Water Quality Standards for Malaysia.
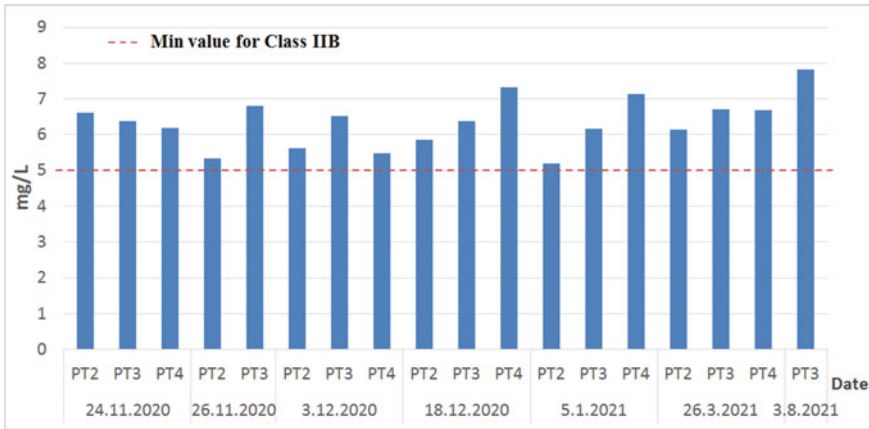
Fig. 3 Water quality monitoring at ecological swale (dissolve oxygen)
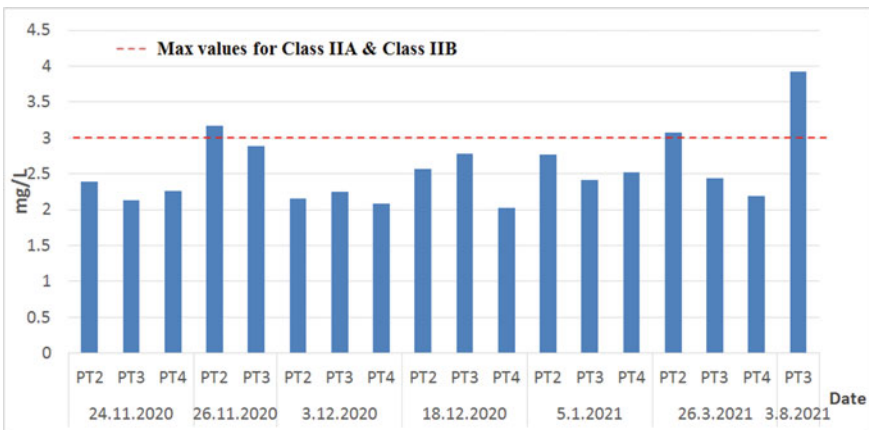
Fig. 4 Water quality monitoring at ecological swale (BOD$_5$)

Figures 5, 6 and 7 showed the parameters COD, Ammoniacal Nitrogen (AN), and pH for samples taken at points no.3 and no.4. The ecological swale has a range of COD between 4.00 mg/L and 27.0 mg/L, AN between 0.020 mg/L and 0.25 mg/L, pH between 5.90 and 8.95. Based on the water quality observed, the monitoring results fall under Class IIA and Class IIB standard classification limits indicating that the performance of swale is able to trap and remove pollutants and thus improve water quality.
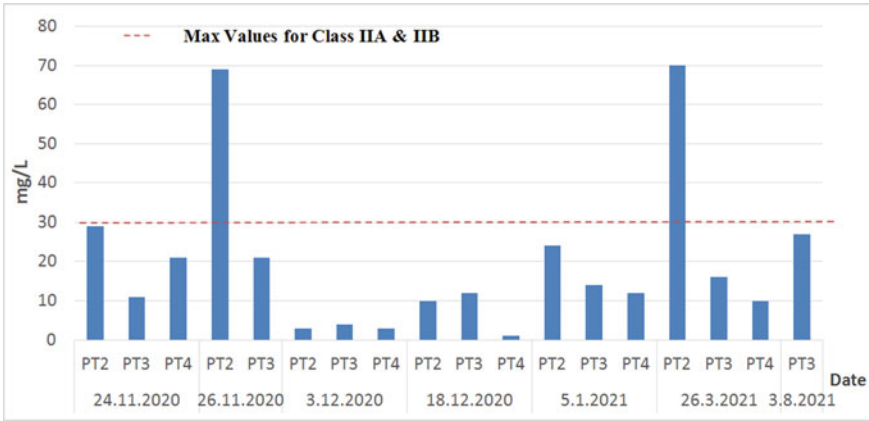
Fig. 5 Water quality monitoring at ecological swale (COD)
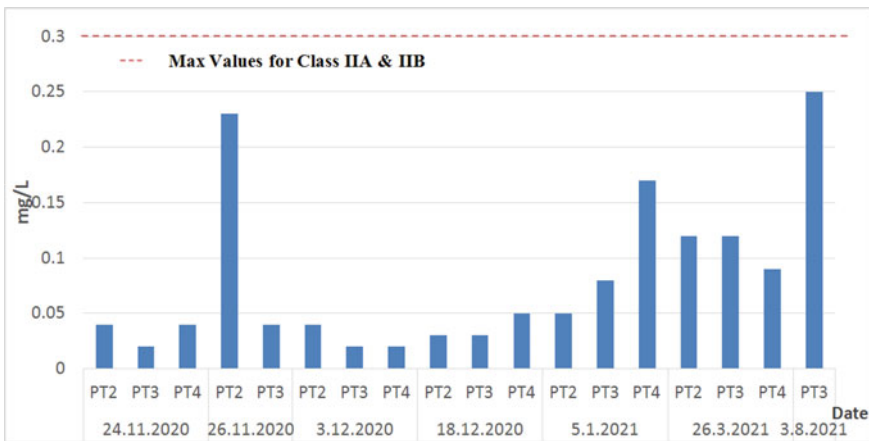
Fig. 6 Water quality monitoring at ecological swale (AN)

Figure 8 shows the water quality monitoring for TSS taken at ecological swale from November 2020 to August 2021. However, results show higher fine sediment concentration with heavy rainfall events causes higher TSS. This also might cause considerably more sediment flush during the heavy storm events within the study area.
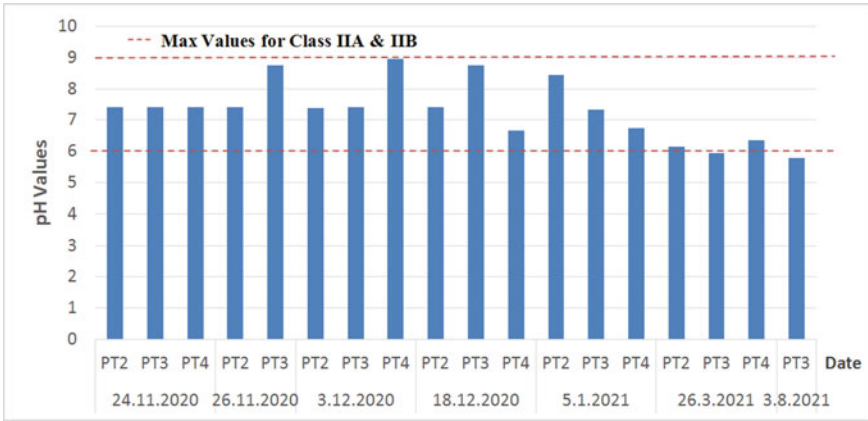
Fig. 7 Water quality monitoring at ecological swale (pH)
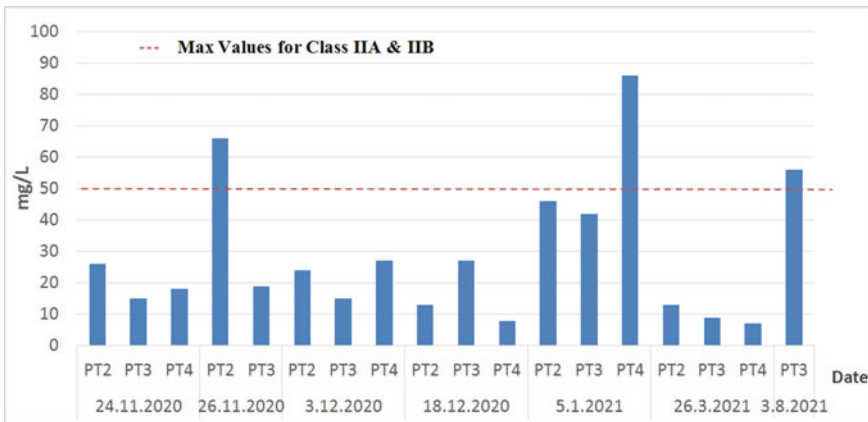
Fig. 8 Water quality monitoring at ecological swale (TSS)

4.2 Ecological Pond

Table 1 shows the result of preliminary water quality sampling conducted at an ecological pond on 15 June 2020. From the first sampling being kickoff at the study area, only three sampling points (no.1, no.5 and no.6) were available as the stormwater infiltrated from the surface of ecological swale into the sub-surface modules in a rapid manner. Except for TSS and turbidity, other parameters such as COD, TDS, AN, pH, and DO show similar results of good water quality at the ecological pond, which are under the limit for Class I and Class IIB Standard Classification by the Department of Environment (DOE) Malaysia. However, higher TSS and turbidity at point no.5 and point no.6 compared to the water quality result at point no.1 might be due to the

Table 1 Stormwater quality result (15 June 2020)

Parameter	Sampling point no. 1*	Sampling point no. 5	Sampling point no. 6
BOD_5 (mg/L)	10.9	5.89	6.34
COD (mg/L)	40	4.85	27
TSS (mg/L)	15	31	27
TDS (mg/L)	45.5	46.8	36.4
AN (mg/L)	0.09	0.05	0.04
Turbidity (NTU)	14.2	28.4	34
Temperature (°C)	29.7	28.9	28.8
pH	6.49	7.00	6.69
DO (mg/L)	8.46	4.85	3.57

*Note Sampling point at conventional drainage outside the study area

higher fine sediment concentration and considerably during heavy rainfall event on 15 June 2020. It is expected more sediment flushing to OSD after issuing CPC to the site contractor upon completion of construction.

Figures 9, 10, 11, 12, 13 and 14 show the water quality monitoring result at point no.5 and point no.6 in the ecological pond from August 2020 until August 2021. From the result, for January 2021 and August 2021, the majority results recorded that DO concentrations are within the limit for Class IIA and Class IIB of the National Water Quality Standards (5 mg/L to 7 mg/L). Besides that, results on August 2021 show that points no.5 and no.6 have a very high DO concentration; thus, the results of DO concentration comply with Class I, which is suitable for water supply without further treatment, conservation of the natural environment and fisheries for very sensitive aquatic species (DOE, 2021). The ecological pond has a range of BOD_5 between 2.01 mg/L and 4.02 mg/L, COD between 1.0 mg/L and 71.0 mg/L, AN between 0.01 mg/L and 0.30 mg/L, pH between 5.97 and 8.49, respectively. For BOD_5, COD, AN, pH and TSS, samples fall under the limit for Class IIA and Class IIB. The good water quality observed at the ecological pond gives an indication that some purification occurs within the storage system. The overall water quality results also show water quality improvement at the ecological pond when stormwater conveys from the ecological swale to the ecological pond.

BIOECODS is designed based on infiltration, delayed flow, storage and purification as stormwater pre-treatment. Based on the water quality result, Table 2 concludes that sampling points no.2, no.3, no.4 no.5 and no.6 have better water quality results than sampling point 1. The range of water quality parameters indicates that the ecological swale's performance in treating stormwater for the runoff during storm events generally falls under Class I to Class IIB Standard Classification by the Department of Environment (DOE) Malaysia.
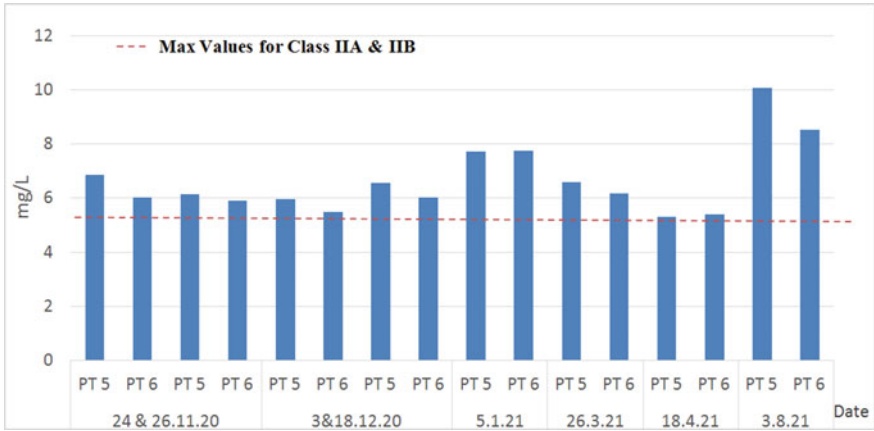
Fig. 9 Water quality monitoring at ecological pond (DO)
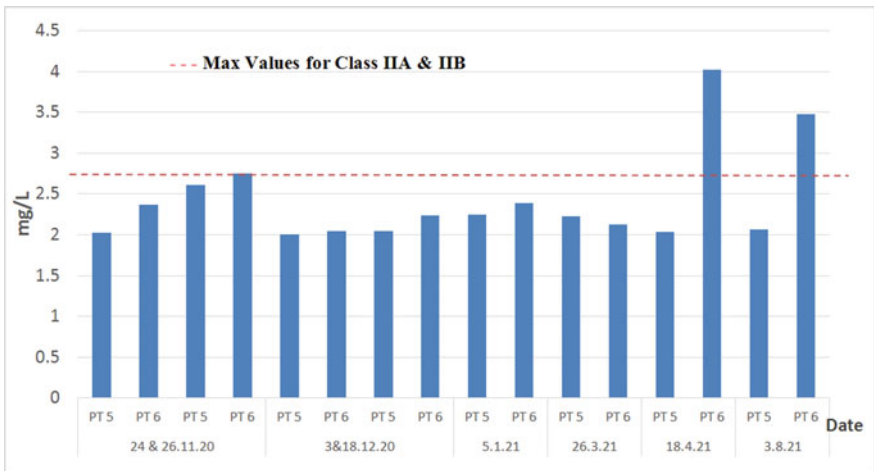
Fig. 10 Water quality monitoring at ecological pond (BOD$_5$)

Table 2 summarized the water quality result at ecological swale based on the 16 storm events from August 2020 until August 2021. Sampling point no.1 represents data taken from conventional drainage, while sampling points no. 2, no.3, and no. 4 represent data taken from the ecological swale. Generally, water quality data in the study area show better water quality than sampling point no.1. BOD analysis for sampling point no.1 (conventional drainage) was higher (3.91 mg/L to 6.94 mg/L) as compared to the result from samples taken at ecological swale (2.03 mg/L to 3.92 mg/L). Indeed, other parameters, such as COD, DO, AN, turbidity and pH, also showed a better water quality than point no.1.
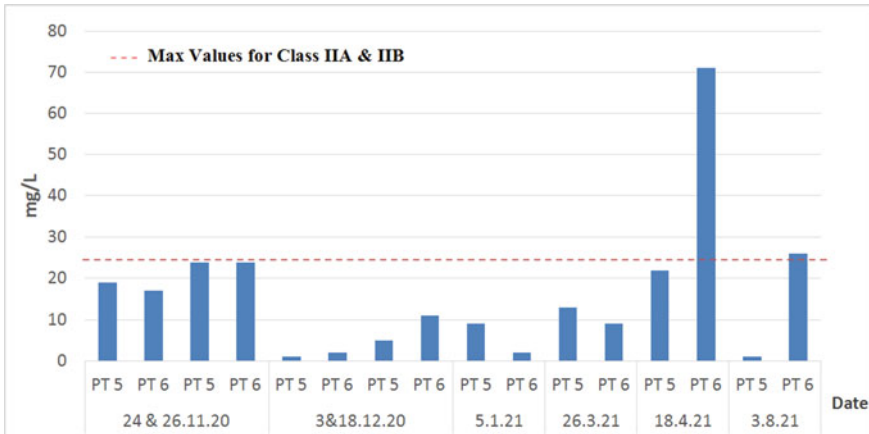
Fig. 11 Water quality monitoring at ecological pond (COD)
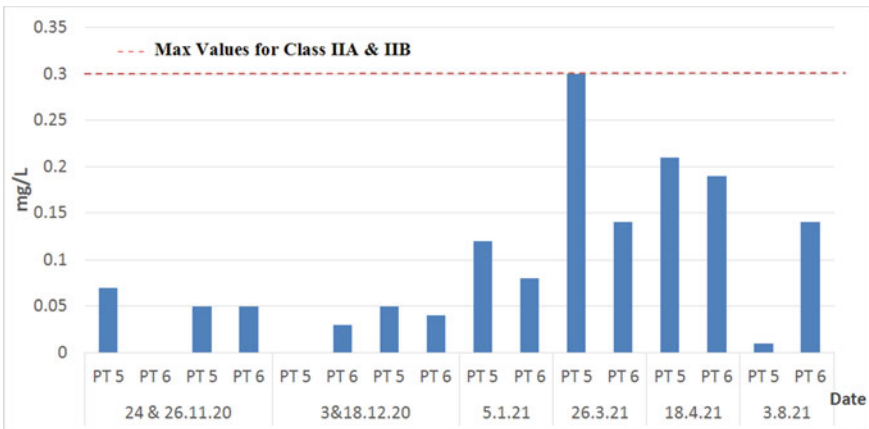
Fig. 12 Water quality monitoring at ecological pond (AN)

TSS and TDS showed a slightly higher range for samples taken from the ecological swale and conventional concrete. The results showed that there is a strong correlation between turbidity and TSS. Besides that, both turbidity and TSS was higher could be associated during wet seasons in the drain outside the project boundary and the ecological swale in the study area.
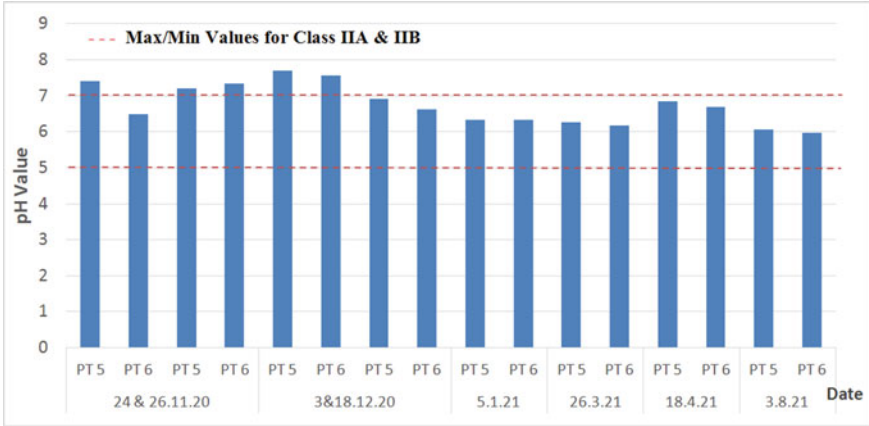
Fig. 13 Water quality monitoring at ecological pond (pH)
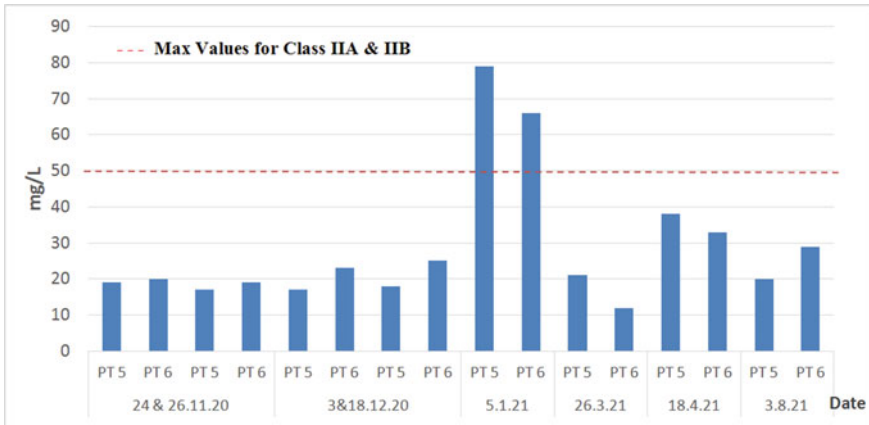
Fig. 14 Water quality monitoring at the ecological pond (TSS)

Table 2 Range of water quality for each parameter (August 2020–August 2021)

Parameter	Sampling point no. 1*	Sampling point no. 2	Sampling point no. 3	Sampling point no. 4
Total phosphorus (mg/L)	0.29–1.51	0.27–0.87	0.28–0.71	0.22–0.66
BOD_5 (mg/L)	3.39–6.94	2.16–3.17	2.13–3.92	2.03–2.52
COD (mg/L)	3.00–71.00	3.00–70.00	4.00–27.00	1.00–21.00
TSS (mg/L)	9.00–58.00	13.00–66.00	9.00–56.00	8.00–86.00
TDS (mg/L)	11.70–94.90	7.39–44.85	9.45–197.60	9.10–100.10
AN (mg/L)	0.06–5.70	0.03–0.23	0.02–0.25	0.02–0.17
Turbidity (NTU)	7.30–71.50	7.13–63.4	7.40–39.00	6.70–28.20
Temperature (°C)	24.70–28.30	23.30–28.50	23.50–26.50	23.40–27.20
pH	5.80–9.14	6.14–8.44	5.94–8.76	6.35–8.95
DO (mg/L)	0.60–6.55	5.34–6.61	6.16–7.81	6.48–7.13

*Note Sampling point at conventional drainage outside the study area

5 Conclusion

Performances of BIOECODS in treating most pollutants show that there is a reduction in their concentrations in the ecological swale and ecological pond during the study period (June 2020 until April 2021). Overall results also show that all the parameters complied within Class I and Class IIB, National Water Quality Standard for Malaysia before the runoff is discharged via discharge point at OSD outlet as per approved by Local Authority. Meanwhile, the current study has also proven that the later stage of water quality monitoring result obtained in 2021 shows a significant improvement in water quality throughout the study period.

References

1. Asmaliza MNN, Lariyah MS, Rozi A, Aminuddin, AG (2013, September) Performance of artificial wetland in removing contaminants from storm water under tropical climate. In 5th International Conference on Flood Management, ICFM 2011, p 208–216
2. Ayub KR, Mohd Sidek L, Ainan A, Zakaria NA, Ab Ghani A (2005) Storm water treatment using bio-ecological drainage system. Special Issue Rivers'04, Int J River Basin Manage IAHR & INBO 3(3):215–221
3. Beh CH, Ab Ghani A, Zakaria NA, Ayub KR (2011) Field evaluation of BMP performance in BIOECODS. In: 3rd International Conference on Managing Rivers in 21st Century: Sustainable Solutions for Global Crisis of Flooding, Pollution and Water Scarcity (Rivers 2011), Penang, Malaysia, p 252–257, 6–9 December 2011

4. Chang CK, Zakaria NA, Ab Ghani A, Goh HW (2018) Securing water for future generations through sustainable urban drainage design and management: Bioecological Drainage System (BIOECODS): Malaysian experiences. Mag Chin Inst Civ Hydraulic Eng 45(6)

5. Department of Irrigation and Drainage Malaysia or DID (2012) Urban stormwater management manual for Malaysia (Manual Saliran Mesra Alam), 2nd edn. Kuala Lumpur, Malaysia

6. Jabatan Kerja Raya Malaysia (2012) Manual Penarafan Hijau JKR, pH JKR, Kuala Lumpur

7. Ayub KR, Mohd Sidek L, Ainan A, Zakaria NA, Ab. Ghani A, Abdullah R (2004) Storm water treatment using bio-ecological drainage system. In: 1st International conference on managing rivers in the 21st century: issues & challenges. Penang, Malaysia, p 426–433, 21–23 September 2004

8. Mohd Sidek L, Ainan A, Zakaria NA, Ab Ghani A, Abdullah R, Ayub KR (2004) Stormwater purification capability of BIOECODS. In: 6th International Conference on Hydro-Science and Engineering (ICHE-2004), Brisebane, Australia, 31 May-3 June 2004

9. Shaharuddin S, Chan NW, Zakaria NA, Ab Ghani A, Chang CK, Roy R (2014) Constructed wetlands as a natural resource for water quality improvement in Malaysia. Nat Res 5:292–298

10. Zakaria NA, Ab Ghani A, Abdullah R, Mohd Sidek L, Ainan A (2003) Bio-Ecological Drainage System (BIOECODS) for water quantity and quality control. Int J River Basin Manage IAHR INBO 1(3):237–251

Reducing Uncertainties in Infiltration Model Using SCS-CN for Mixed Land Use Catchment

A. J. Hassan, S. Harun, T. Ismail, and H. Zulkarnain

Abstract Soil Conservation Services (SCS) is a quite popular method to estimate the infiltration of the catchment. The method has an advantage since it can be used for various land use and soil type using a single parameter of Curve Number (CN). However, the method may not suit catchment scaled due to land use heterogeneity. Averaging the CN value for the catchment of mixed land use may produce different runoff estimations compared to individual land-use calculations within the catchment. This situation will lead to higher uncertainty in the estimation of CN. This study investigates the effect of sub-catchment delineation to improve the CN estimation on catchment scaled. It shows that when the catchment is divided into smaller sub-catchment based on second level tributaries, the dominant land use of more than 80% in the basin increases to 50% of the whole catchment. This indicates that runoff computation shall improve by using the weighted CN as proposed in this study.

Keywords Rainfall runoff · Infiltration model · SCS-CN · Catchment delineation · Dominant land use

A. J. Hassan (✉) · S. Harun · T. Ismail
School of Civil Engineering, Faculty of Engineering, University Teknologi Malaysia,
81310 Johor Bahru, Johor, Malaysia
e-mail: abdjalil.hassan@gmail.com

S. Harun
e-mail: sobriharun@utm.my

A. J. Hassan
RiverNet Consulting Sdn. Bhd. No 3, Lot 2816, Jalan Sri Gambut, Syeksen 32, 40460 Shah Alam,
Selangor, Malaysia

H. Zulkarnain
Faculty of Civil Engineering Technology, Universiti Malaysia Perlis (UniMAP), Kompleks Pusat
Pengajian Jejawi 3, 02600 Arau, Perlis, Malaysia
e-mail: zulkarnainh@unimap.edu.my

1 Introduction

One of the components in rainfall runoff model is the infiltration or loss model which extract rainfall into the soil to produce excess rainfall. Infiltration model highly depends on the land use/cover, soil type and antecedent moisture condition [9]. Many hydrologists had developed method to compute the amount of rainwater infiltrate into the soil in order to determine the surface runoff. Among the popular infiltration model are Green-Ampt and Horton which were developed for rural area [4].

In Malaysia, Department of Irrigation and Drainage (DID) published various hydrological procedure (HP) such as HP11 and, HP27 to compute runoff mostly for rural catchment [6–8]. Rational Method provide coefficient for many types of land use but the method is only applicable for small catchment [5].

For many years, Malaysia is facing many monsoon and flash floods due to urbanisation but the appropriate tools to analyse the land use variation may not be suitable. One of the popular methods which is more flexible for different land use is Soil Conservation Services (SCS) method which was introduce in 1954 [3]. It provides Curve Number (CN) for wide range of soil type and land use. However, the SCS-CN method was developed from extensive small catchment and the CN is given for specific land use and cover.

Therefore, when the method is applied to large catchment which contains many types of land use, the weighted averaging approach is adopted to produce average CN [4]. However, since the infiltration of rainwater is not linear, possibly the average method may not be good as compared to the individual runoff computation for different land use or soil type. Bondelid et al. [3] reported that runoff estimated from SCS-CN has large error when applied to the low intensity rainfall and the error tend to reduce as the rainfall increased. [2] highlighted the issue of uncertainties due to catchment properties should be understand during the development of hydrologic model.

To verify the effect of land use variation, an experiment for large catchment was carried out on Sg Ketil with drainage area of 754 km^2. The catchment contains various type of land use including forest, agriculture and develop area.

2 Objectives of the Study

The main objectives of this paper are:

- To demonstrate the different of runoff between individual and weighted averaging CN
- To show the improvement on land use estimation parameter when catchment is break down into smaller subcatchment
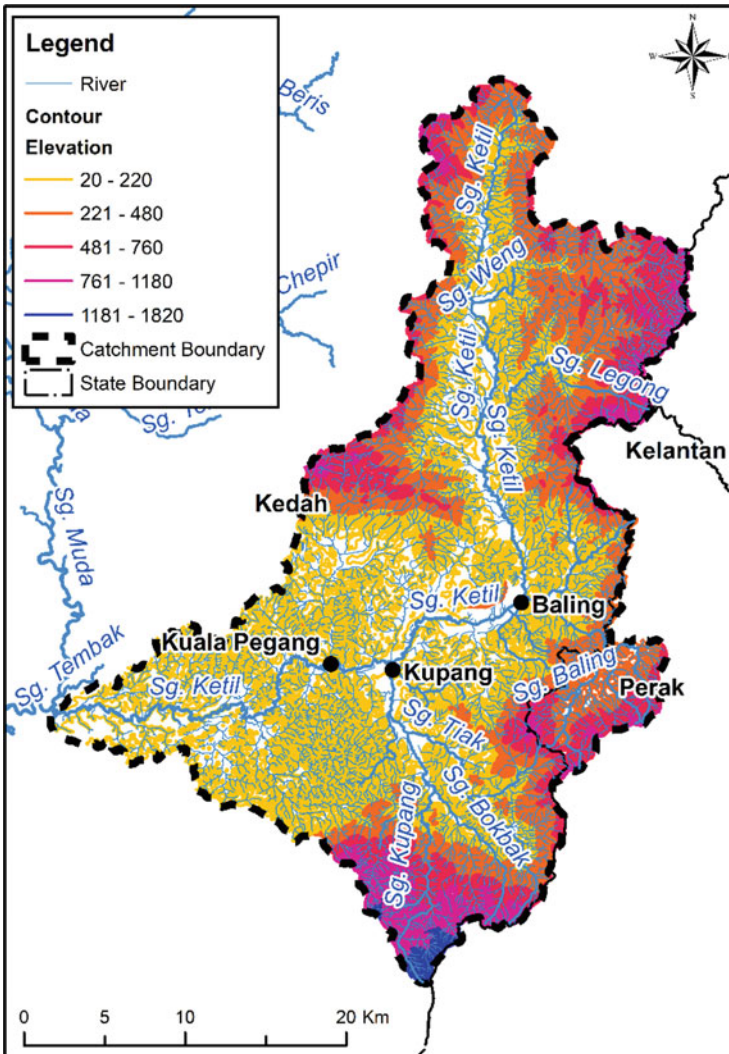
Fig. 1 Contour and river map of Sg Ketil catchment

3 Case Study Area

Sg Ketil is located at the north of Peninsular Malaysia was selected for the experiment (Figs. 1 and 2). It is one of the tributaries of Sg Muda basin with total catchment area about 754 km2 and the main river is about 60 km long. The river starts from elevation of 1100 m from mean sea level and ends at Kuala Pegang, the confluence of Sg Muda at elevation of about 20 m (MSL). The land-use of the catchment is

mainly covers with forest, agriculture, and some patches of urban and residential. Flood occurs very frequent along the river which affecting the town of Baling.
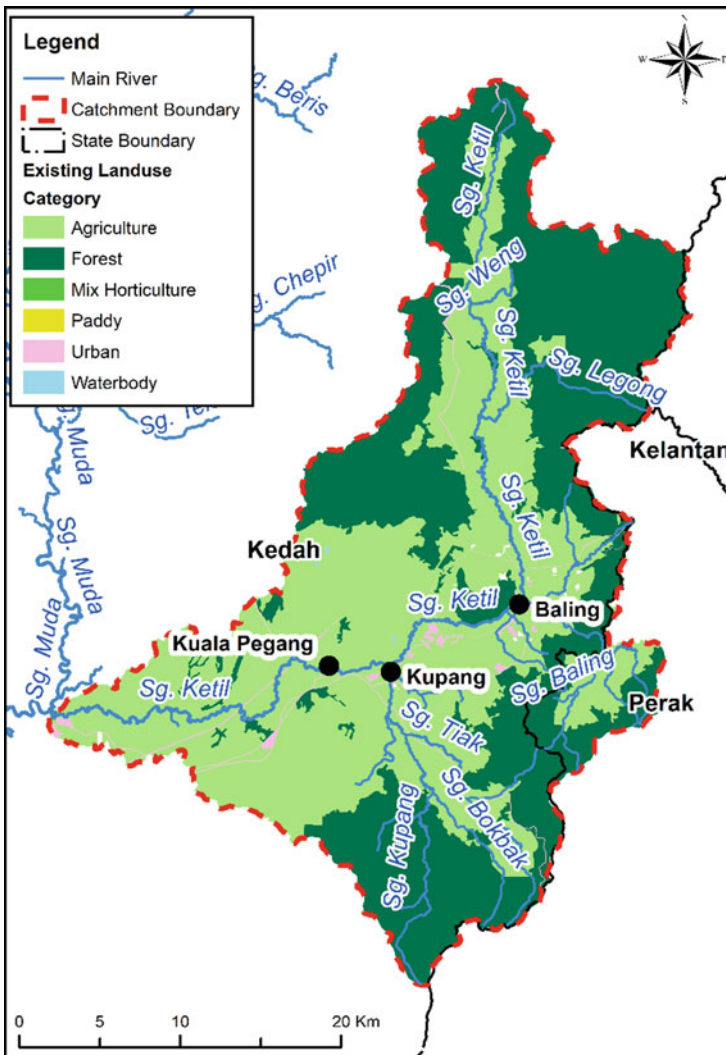
Fig. 2 Land use of Sg Ketil catchment

4 Methodology

Chow et al. [4] stated that the hypothesis of SCS method is "the ratio of the two actuals to the two potential quantities are equal". The equations below described the process to determine the runoff for any land use.

$$S = \frac{1000}{CN} - 10 \tag{1}$$

$$\frac{F_a}{S} = \frac{P_e}{P - I_a} \tag{2}$$

$$P = P_e + I_a + F_a \tag{3}$$

$$P_e = \frac{(P - I_a)^2}{P - I_a + S} \tag{4}$$

$$I_a = 0.2S \tag{5}$$

$$P_e = \frac{(P - 0.2S)^2}{P + 0.8S} \tag{6}$$

where:
  P = Precipitation (ins)
  Pe = Direct runoff (ins)
  Fa = Additional depth of water retained in the watershed
  S = Potential maximum retention (ins)
  Ia = Initial abstraction before ponding (ins)

Figure 3 shows the typical relationship between CN, S and Ia. The example of the curve line is evidence that the relationship is not linear. Therefore, the weighted averaging CN use to calculate runoff may not be accurate when comes to catchment with mixed land use.

   To determine the different between runoff computation using weighted averaging and individual CN for mixed land use catchment, the approach below is carry out.

 (i) Compute runoff using individual CN
 (ii) Compute runoff using weighted average CN_{avg}

   Since there are many types of land use/cover, only three type of land use were used in the experiment which are forest, agriculture and urban with CN equal to 55, 70 and 90 respectively. Firstly, one dominant land use is set ranging from 50 to 90% of the catchment area. Secondly, the other two land use are divided equally. For example, if urban is set as dominant land use covering 70% of the total catchment, then agriculture and forest is set at 15% each. For easy computation, the total area was set to 100 hectares.
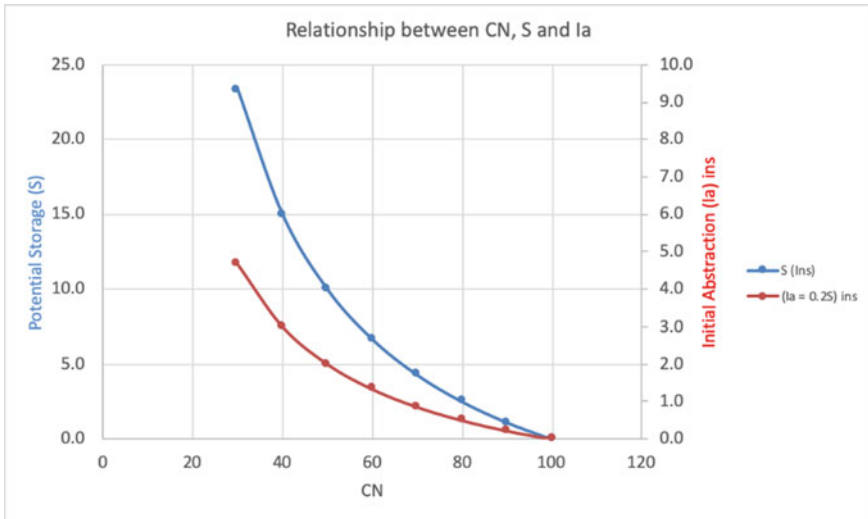
Fig. 3 Typical relationship between CN, S and I$_a$

Tables 1, 2 and 3 show example of the percentage land use distribution when a specific type of land use is set as dominant land use while the other two are divided equally. Experiments were conducted for three type of land use using different rainfall intensity ranging from 3 to 7 ins. (The imperial unit used in this paper is to maintain the same unit as in the reference.)

On the catchment scaled experiment, there level of catchment for Sg Ketil sub-basin was selected to evaluate the land use distribution. Catchment delineations were made for Level I for one single catchment, Level II which cover main tributaries and

Table 1 Land use distribution with urban as dominant land use

Dominant land use		Other land use	
	%		%
Urban	50	Agriculture	25
		Forest	25
	60	Agriculture	20
		Forest	20
	70	Agriculture	15
		Forest	15
	80	Agriculture	10
		Forest	10
	90	Agriculture	5
		Forest	5

Table 2 Land use distribution with Forest as dominant land use

Dominant land use		Other land use	
	%		%
Forest	50	Agriculture	25
		Urban	25
	60	Agriculture	20
		Urban	20
	70	Agriculture	15
		Urban	15
	80	Agriculture	10
		Urban	10
	90	Agriculture	5
		Urban	5

Table 3 Land use distribution with agriculture as dominant land use

Dominant land use		Other land use	
	%		%
Agriculture	50	Urban	25
		Forest	25
	60	Urban	20
		Forest	20
	70	Urban	15
		Forest	15
	80	Urban	10
		Forest	10
	90	Urban	5
		Forest	5

Level III which further extended to the second tributaries [1]. Land use percentage for each subcatchment were calculated to determine the dominant land use effect on subdivide the main catchment into smaller subcatchment.
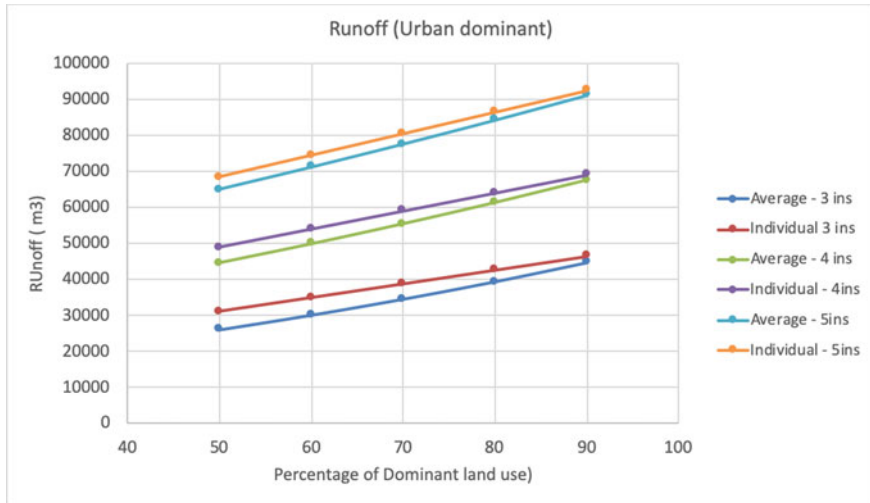
Fig. 4 Runoff between average and individual (Rainfall 3 in to 5 in)

5   Results and Discussion

5.1   Dominant Land Use

Runoff calculation was demonstrated for urban as dominant land use using different rainfall shown in Figs. 4 and 5. For the other two dominant land use i.e., forest and agriculture land use only the percentage different are shown in Figs. 6, 7 and 8.

Based on the results, the different of runoff between the two calculations method is reduce below 10% once the dominant land use exceed 80% except for the case of forest with rainfall at 3 inches. This experiment concludes that if any catchment does not have any specific dominant land use, the weighted average CN may not provide a good runoff estimation.

5.2   Catchment Scaled Experiment

Figures 9, 10 and 11 shown the land use distribution for three different level of catchment delineation in Sg Ketil. The colours indicate the percentage of dominant land use for each subcatchment. Tables 4, 5 and 6 tabulated the percentage of dominant land use for each level of catchment delineation.

For Level I, forest cover about 55% while agriculture and urban represent 45% and 2% respectively. Therefore, there is no specific land use exceed 80%. As for Level II, 26% of the catchment has dominant land use which is above 80%. However, for Level III, as the catchment is further breakdown to smaller area following the second
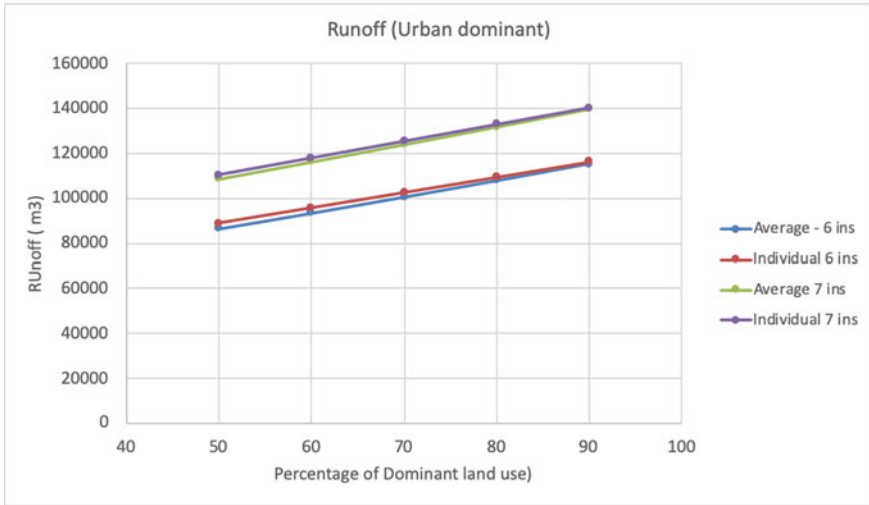
Fig. 5 Runoff between average and individual (Rainfall 6 in and 7 in)
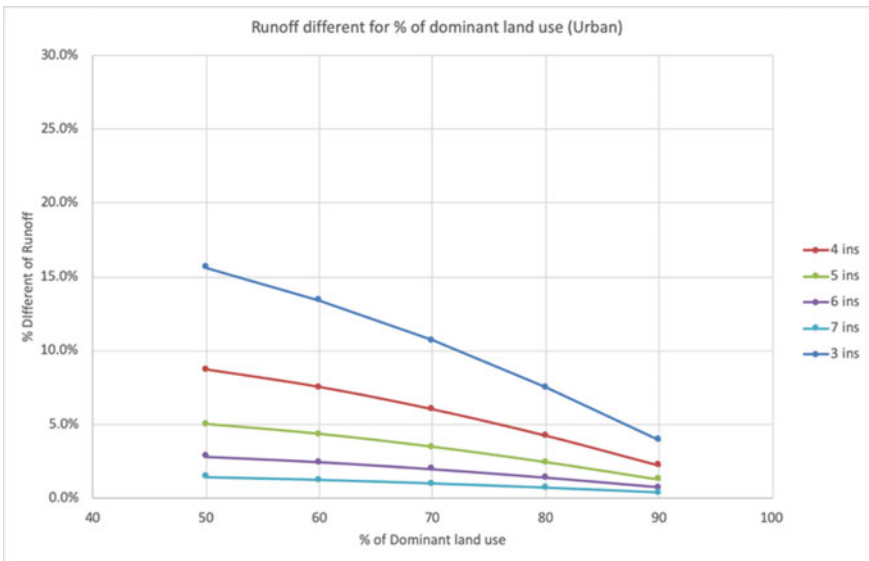
Fig. 6 Percentage runoff different (Dominant land use – Urban)

tributary, the dominant land use increased to 50% as shown in Table 4. It is important to note that, the type of land use which is dominant is not significant as being shown previously.
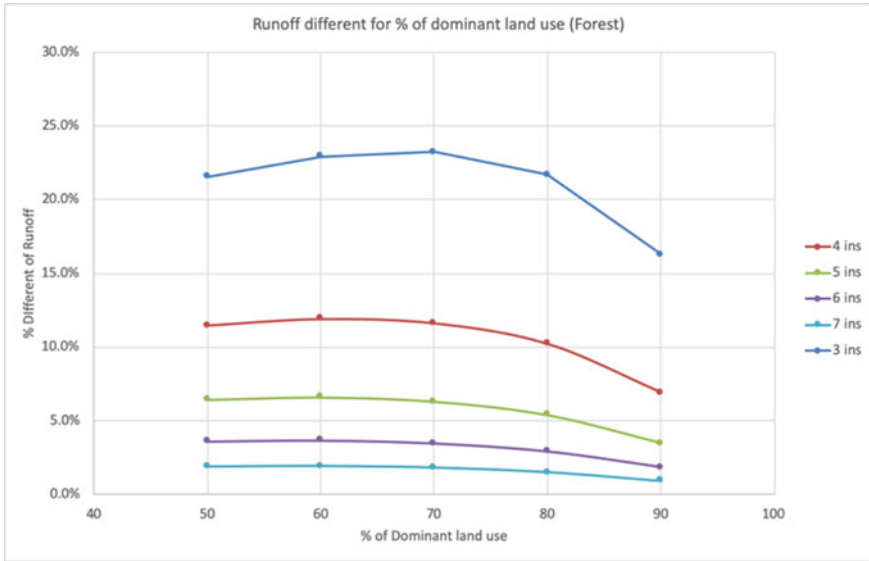
Fig. 7 Percentage runoff different (Dominant land use – Forest)
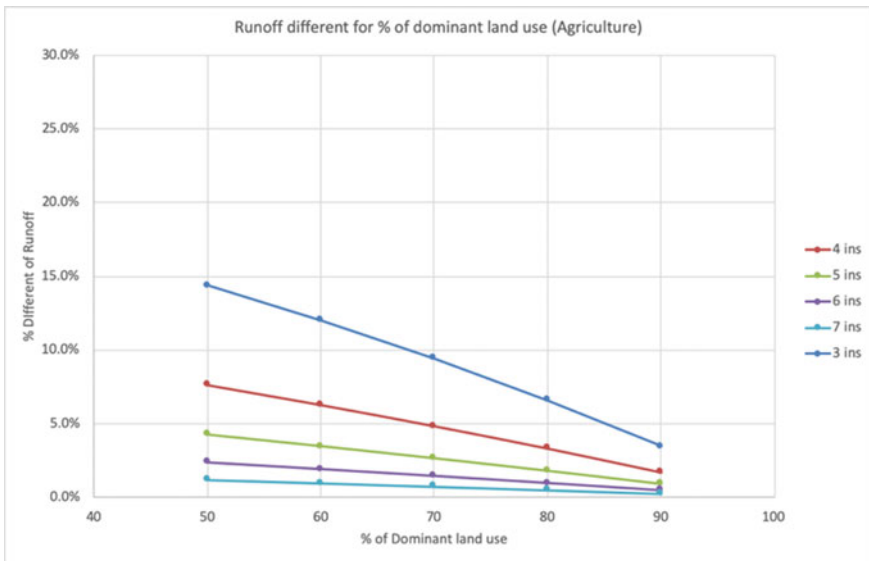
Fig. 8 Percentage runoff different (Dominant land use – Agriculture)
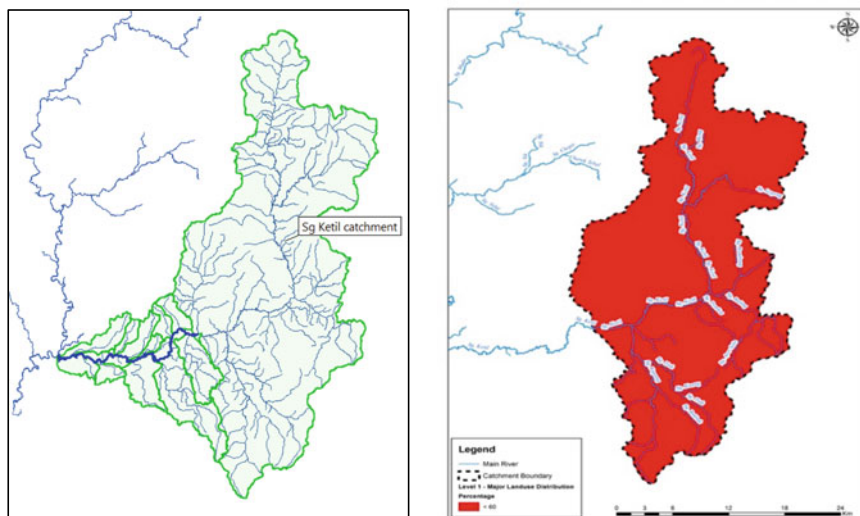
Fig. 9 Left: Subcatchment for level I; Right: Percentage of dominant land use
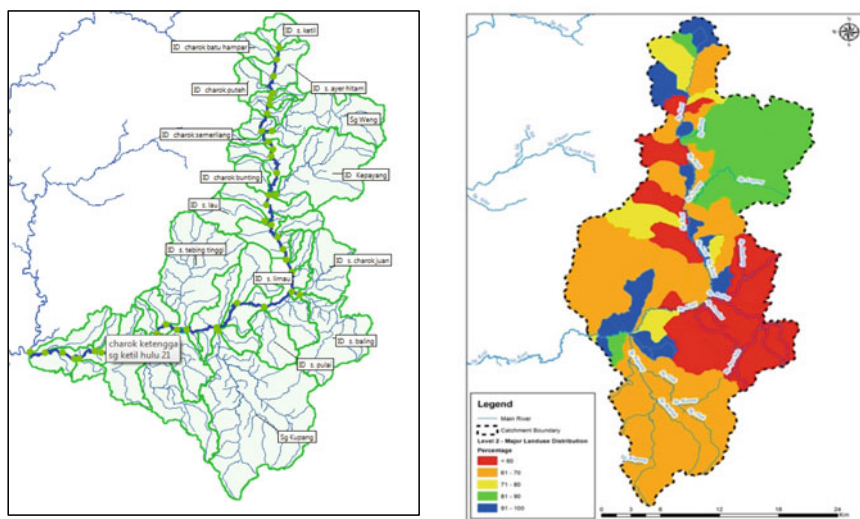
Fig. 10 Left: Subcatchment level II; Right: Percentage of dominant land use for subcatchment Level II
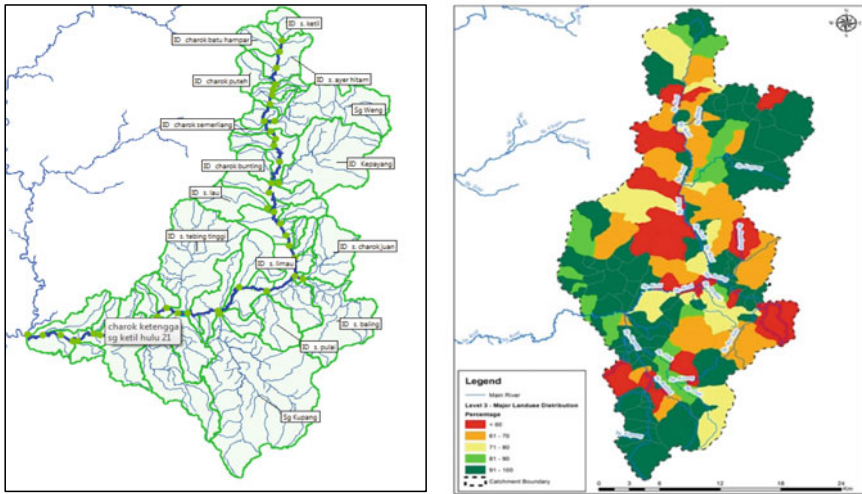
Fig. 11 Left: Subcatchment for level III; Right: Percentage of dominant land use for subcatchment Level III

Table 4 Summary of land use distribution for subcatchment (Level I); existing condition with all land use < 60% dominant land use

Land use	Area (ha)	Percentage (%)
Agriculture	31,889	42
Forest	41,501	55
Urban	1273	2
Waterbody	720	1
Total	75,384	100

Table 5 Summary of land use distribution for subcatchment (Level II); with only 23% dominant land use < 80% area

Dominant land use	Area (ha)	Percentage (%)
<60	17,573	23
61–70	33,000	44
71–80	5267	7
81–90	12,967	17
91–100	6577	9
Total	75,384	100

Table 6 Summary of land use distribution for subcatchment (Level III) with more dominant land use capture as 50% categorise as > 80% dominant land use

Dominant land use	Area (ha)	Percentage (%)
< 60	12,655	17
61–70	15,288	20
71–80	9477	13
81–90	6707	9
91–100	31,256	41
Total	75,384	100

6 Conclusion

Based on the experiments conducted, two conclusions can be derived. The first experiment was conducted to test the sensitivity of the SCS-CN computation for runoff using weighted average and individual CN. To reduce the different of runoff computed between the two methods, it is crucial to ensure that the catchment contain one dominant land use which contribute to more than 80% of overall area.

The second experiment on catchment scaled shows that as the catchment is breakdown into the tributaries, the dominant land use for each subcatchment will increased which will minimise the error of runoff computation regardless of the method applied. This approach should be given high attention or adopted during the development of rainfall runoff model in hydrologic model.

References

1. Abd Jalil H (August, 2017) Reducing calibration dependency in runoff estimation by systematic development of distributed hydrologic model in flood modelling. In 37th IAHR 2017 World Congress, Kuala Lumpur
2. Beven K (2012) Rainfall-runoff modelling. Wiley-Blackwell, Lancaster University, UK
3. Bondelid TR, McCuen RH, Jackson TJ (1982) Sensitivity of SCS models to curve number variation 1. JAWRA 18(1):111–116
4. Chow VT, Maidment DR, Mays LW, (1998) Applied hydrology. McGraw-Hill
5. DID (2000) Manual Saliran Mesra Alam. Department of Irrigation and Drainage, Malaysia
6. DID (2010) HP27. Department of Irrigation and Drainage, Malaysia
7. DID (2018) Hydrological procedure no. 11 (Design flood hydrograph estimation for rural catchments in Peninsular Malaysia), Revised and Updated. Department of Irrigation and Drainage Malaysia
8. JPS D (1994) Hydrological procedure no. 11 (Design flood hydrograph estimation for rural catchments in Peninsular Malaysia). Jabatan Pengairan Dan Saliran, Kuala Lumpur
9. Subramanya K (2009) Engineering hydrology, 3rd edn. McGraw Hill International Edition, Kanpur

A Review on Heavy Duty Mobile Flood Wall Barrier: Way Forward for Malaysia

Woon Yang Tan, Mohamad Nazif Daud, Norlida Mohd Dom, Cha Yao Tan, Xin Yi Chong, Chow Hock Lim, Chung Lim Law, and Fang Yenn Teo

Abstract Climate change have led to extreme weather events such as higher rainfall frequency that can cause severe flooding. In Malaysia, there is an increasing trend on extreme rainfall events and short temporal rainfall, particularly during the inter-monsoon season. In order to protect private properties and public premises from flooding, Mobile Flood Wall Barrier (MFWB) has been found to be more suitable as it is less costly, easier to deploy and does not require large space. Buildings such as factories and commercial shops that have larger entrances, they would require heavy-duty type of MFWB as compared to those for residential buildings. Heavy-duty MFWB has a better ability to withstand higher hydrostatic pressure from flood-water, hence suitable for public premises and buildings in industrial and commercial areas. In this paper, various types of heavy-duty MFWB and their application will be presented and discussed. The standards for testing MFWB products presented in this paper are summarised. Some existing testing requirements are also presented. Based on the review, the mobility characteristic indicated that the heavy MFWB can

W. Y. Tan (✉) · M. N. Daud · N. M. Dom
Department of Irrigation and Drainage, Humid Tropics Centre Kuala Lumpur, 50480 Kuala Lumpur, Malaysia
e-mail: wyang@water.gov.my

M. N. Daud
e-mail: nazif@water.gov.my

N. M. Dom
e-mail: norlidamd@water.gov.my

C. Y. Tan · X. Y. Chong · C. H. Lim · C. L. Law · F. Y. Teo (✉)
Faculty of Science and Engineering, University of Nottingham Malaysia, Semenyih 43500, Selangor, Malaysia
e-mail: fangyenn.teo@nottingham.edu.my

C. Y. Tan
e-mail: keey5tcy@nottingham.edu.my

X. Y. Chong
e-mail: khyy5cxy@nottingham.edu.my

C. H. Lim
e-mail: evxcl6@nottingham.edu.my

C. L. Law
e-mail: chung-lim.law@nottingham.edu.my

be installed temporarily to prevent flooding and be removed easily to ensure no interruption to the daily activities after flood events. There are many potential advantages for flood protection, in particular, it serves as the way forward for Malaysia.

Keywords Heavy duty · Mobile flood wall barrier · Flood protection system

1 Introduction

The average annual rainfall in Peninsular Malaysia is about 2420 mm [1]. This is above the 2000 mm minimum condition for the formation of a rainforest [7]. Malaysia is considered a great location as the home for rainforest biomass. Historical studies concluded that there is an increasing trend in high precipitation events and short temporal rainfall during the inter-monsoon season [11, 13]. However, high precipitation around the floodplain area has become a serious issue to many cities in this country [3]. Floods have massive impacts on people, properties, public facilities, and infrastructures, including vehicles on roads [12, 15, 18].

From 2001 to June 2016, Kuala Lumpur City Centre located in Klang Valley experienced more than 25 flash flood events, which led to high economic loss and massive traffic congestion [2]. As the population of Klang Valley increases and the region becomes more developed, the occurrence and frequency of floods are expected to increase in future [4]. In the longterm, the government may need to invest more in mega projects for flood protection, such as the SMART tunnel and Sri Johor flood detention pond. However, such mega projects are very costly, time-consuming and require relatively large space for construction. The government is looking into other alternative solutions. Therefore, the use of mobile flood protection system may be an appropriate and cost-effective alternative approach for the high-density area in the long term.

Flood protection system is an engineering approach to protect land, building and lives from the destructive power of flooding. There are two types of mobile flood protection systems, namely permanent and temporary flood protection systems [10]. A permanent flood protection system is a permanent solution for flood protection within high flood risk regions like river banks, floodplains, and grounds that are lower than sea level. Engineered structure such as a levee, dike, bund, floodwall, and flood retention basin are designed and built as protection from flooding during monsoon season. The permanent flood protection system is a more effective way for flood protection and it is able to cover a larger area compared to temporary systems. However, these engineered structures require a large amount of time and cost, and occupies more space. Subsequently, a permanent flood protection system is mostly large in size and designed to withstand high water levels; inappropriate design of engineered structures may lead to a catastrophic disaster.

A temporary flood protection system or mobile flood protection system is a flexible approach for flood protection with higher mobility. It can be hidden during normal days with no interruption to daily activities and can be assembled quickly
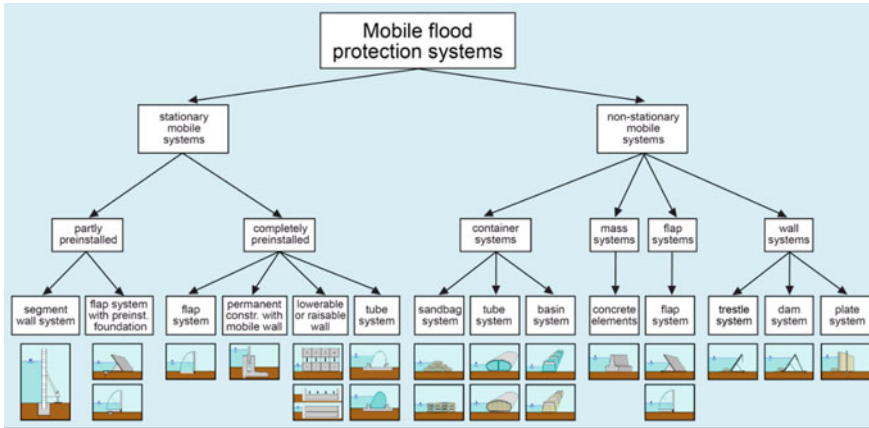
Fig. 1 Proposed classification of mobile flood protection system. (*Source* Koppe and Brinkmann [10])

in case of emergency for the region with or without a permanent protection system. However, any inappropriate design or use of mobile flood protection system could potentially lead to the failure of flood protection. Five general situations of mobile flood protection system failure were mentioned in [5], these include sliding or rolling, seepage, leakage, tilting, and collapse.

Koppe and Brinkmann [10] classified mobile flood protection systems into two categories, which are stationary, mobile systems and non-stationary mobile systems. Figure 1 shows the mobile flood protection system classification as proposed by Koppe and Brinkmann [10].

Mobile Flood Wall Barrier (MFWB) is a type of mobile flood protection system implemented to safeguard an area from flood hazards. It is different from permanent flood protection systems; it offers mobility and expedites installation in high traffic or cramped spaces. It can also be applied in case of emergency for an area of low protection against flood. MFWB can be categorised into two types, as heavy-duty and lightweight products, and also designed by two options, either as partly pre-installed stationary mobile system or completely mobile system [10].

The products of heavy-duty MFWB have been widely used in many developed countries for flood protection and resilience purposes. This paper will focus on various types of heavy-duty MFWB globally and their potential applications for flood protection in Malaysia. The objectives of this paper are: i) to identify the characteristics of the heavy-duty MFWB, ii) to explore available commercial products, iii) to explore different MFWB's working principles, and iv) to explore the advantages and disadvantages of their applications in particular, the way forward for Malaysia.

2   Methodology

In conducting the literature review on heavy-duty MFWB, the main source of information are from scholastic publications, commercial company products and technical guidelines. Articles, journal papers and conference papers form the bulk of the scholastic publications. With Google Search, product catalogues were easily obtained from various manufacturers' websites. All scholastic references in this paper are found through Google Scholar. One of the reference sources is a technical guideline, and it was sourced from various authorities and non-government organisations' websites.

3   Testing Requirements of MFWB

The Institution of Engineers, Malaysia has published a guideline in 2019 known as Guideline on Flood Abatement Equipment – Engineering Guide of Designation, Testing and Documentation. This guideline recommends four essential tests, which are: i) Required Mandatory Test, ii) Component Required Test, iii) Optional Test, and iv) Power Supply and Control for Automatic Equipment [17]. For the Required Mandatory Test, MFWB must be tested for hydrostatic leakage, wave leakage and current leakage. The Component Required Test is to assess the durability and reliability of each component of MFWB, and some special tests may carry out, such as salt spray for testing the MFWB under the condition of high salt concentration. Under the Optional Test, various optional tests may be performed, for example: overtopping, debris impact and outside load condition (vehicle). As for the Power Supply and Control Test for mobile flood wall barrier, which is operated automatically by electricity, the whole power supply system should be tested under the condition of flooding, ensuring the workability of the power supply system and preventing the risk of electric leakage.

[14] has published an article pertaining to the application and test requirement for mobile flood gates. There are six necessary tests in this article, which are Loading Test, Deployment Test, Vertical Water Pressure Test, Impact Test, Hydrostatic and Leaking Test, and End of Test. These six tests may not be suitable for all types of MFWB, hence, the production company should perform the tests with careful consideration. Loading Test is for investigating the ability of MFWB to withstand static and impact load from a vehicle under undeployed conditions. Deployment Test is for testing the smoothness of deploying process of MFWB. Vertical Water Pressure Test is for studying the impact of water wave pressure on the main body. Impact Test is for investigating the impact of floating wood and rubbish, which carried by the water wave. Hydrostatics and Leaking Test is for investigating the ability to prevent water leakage under certain water load and duration. The last test, known as End of Test, is to identify the smoothness of uninstalling process of MFWB and its structural stability after all the tests above.

Kadar [9] classified the type of load that should be considered during the design stage and for testing, which are dead load, live load and extra loads. Dead load refers to the self-weight of MFWB. Live load is any type of variable load that has a force impact on the MFWB, such as hydrostatic pressure and hydrodynamic pressure, where hydrodynamic pressure includes flow pressure, water elevation on the outer bank, wave pressure, impact load, wind load, and other live loads such as people and vehicle. Extra load that was mentioned in Kadar [9] were dry-side water pressure, screw loss, and overtopping effect.

4 Heavy Duty MFWB

In this paper, heavy-duty MFWB is defined as a higher floodwater load resistance compared to the lightweight MFWB. The main water blockage panel is usually made from lightweight metal such as aluminium or concrete materials since the plastic component may not have sufficient strength for a heavy load. Thus, heavy-duty MFWB is comparatively heavier than lightweight MFWB. Other than the main water blockage panel, for high water pressure resistance, it requires a better support system for load transfer.

Heavy-duty MFWB is summarised in Table 1 with more technical details. There are more examples for heavy-duty MFWB with a strong support system, such as Segment Wall System, Flap System with Preinstalled Foundation, Permanent Constructed with Mobile Wall and Lowerable or Raiseable Wall System. Another way to resist high water pressure is by self-stabilisation, which is Concrete Element System. Its self-weight provides high skid resistance between the MFWB and the contacted ground. Thus, it can withstand pressure from high floodwater levels.

Table 1 A Summary of Heavy Duty MFWB with Technical Details [6][8][16] (*Source* Delta Technology, The Flood Company, and JP Concrete)

Types	Materials/Characteristics	Mechanisms	Height, m	Drawbacks
Segment wall system (Partly preinstalled)	Aluminium or stainless steel for the waterproof panel	Multiple waterproof panels can be manually slotted	Varies	Relatively slow installation speed
Flap system with preinstalled foundation (Completely preinstalled)	Aluminium or stainless steel for the waterproof panel. If the application site is concrete or asphalt flooring, the surface can be concrete or asphalt	Hydraulic press machine pushes up the waterproof panel, which usually is hidden. The panel functions as an accessible surface	2.5	The deployment process requires site clearing to avoid accidents, or the panel could be damaged by nearby obstacles

(continued)

Table 1 (continued)

Types	Materials/Characteristics	Mechanisms	Height, m	Drawbacks
Permanent constructed with mobile wall system (Completely preinstalled)	Concrete tank as basin, aluminium frame for strength and composite materials for floatability	Floodwater will enter the basin underneath, the waterproof panel which hidden underground will be floated due to the presence of water	2.5	The basin may be blocked by dirt and sand, causing the floating system do not function properly during a flood event
Lowerable or raiseable wall system (Completely preinstalled)	Aluminium or stainless steel for waterproof panel	Drop-down, rolled down or swing down multiple waterproof panels as the barrier to block floodwater. Mostly automatic operate	3.0 to 5.0	The deployment process requires site clearing to avoid accident, or the panel could be damaged by nearby obstacles
Concrete element system (Mass system)	Reinforced concrete	Self-weight for stability to resist water pressure. Multiple stacking to achieve a higher height of protection	2.0	Require machinery and larger space for a higher water level of protection

4.1 Segment Wall System (Partly Preinstalled)

Manual Slot Flood Wall Barrier from Delta Technology is a segment wall system of heavy-duty MFWB (partly preinstalled), commonly implemented at the entrance of the factory, school, shops, malls, office buildings and condominiums. Channels are pre-installed on both sides of the entrance as the main support structure to secure barrier stability. It is designed as a modular system; multiple segment walls can be manually slotted in the channel as the main water blockage. Rubber is stuck between the segment wall and the preinstalled channel to provide water tightness. The segment wall withstands the hydrostatic pressure from floodwater, and the load is transferred to both end channels and supported by the wall. A lesser segment can be slotted into the channel when the water level is not obvious and high (Fig. 2).

Fig. 2 Manual slot flood wall barrier (*Source* Delta Technology [6])

Fig. 3 Auto-flip flood wall barrier (*Source* Delta Technology [6])

4.2 Flap System with Preinstalled Foundation (Completely Preinstalled)

Auto-Flip Flood Wall Barrier is a Flap System (Completely Preinstalled) of heavy-duty MFWB. It is commonly implemented at the entrance of road access like an underground car park and the entrance of the fenced area. It is hidden underground during normal days; it can be automatically flipped by powering the motor. The upper site of the Auto-Flip Flood Wall Barrier must be free of obstacles during activation. Else, it might damage the vehicle on top of it or injure the person bypassing it; reversely, the surface or structural element of the Auto-Flip Flood Wall Barrier may be damaged by any obstacles. The clearing stage after a flood must be carefully executed; any debris may permanently damage the Auto-Flip Flood Wall Barrier (Fig. 3).

4.3 Permanent Constructed with Mobile Wall System (Completely Preinstalled)

Self-Closing Flood Barrier is a Permanent Constructed with Mobile Wall System (Completely Preinstalled). It can be used at riverbanks, public spaces, commercial and private homes. A basin is preconstructed underground to allow floodwater to enter
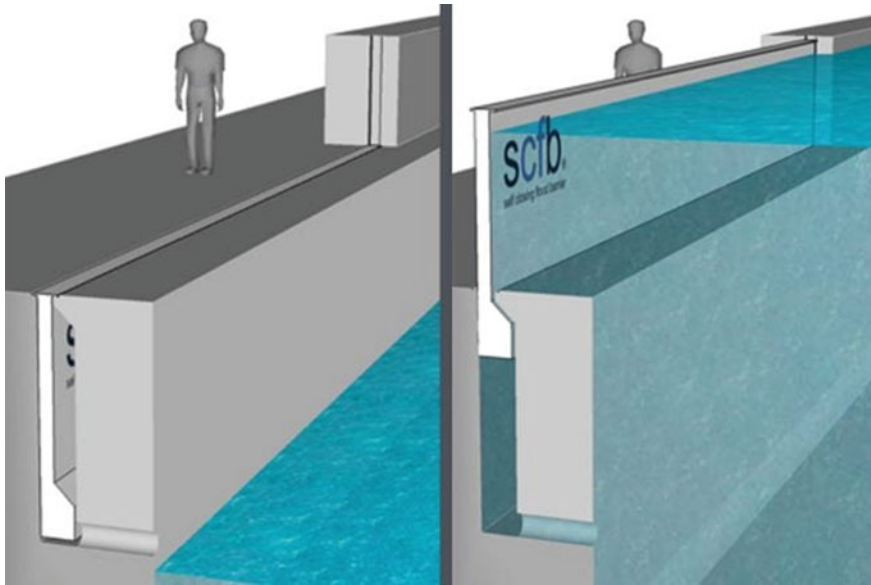
Fig. 4 Self-closing flood barrier (*Source* The Flood Company [16])

the basin during a flood event. When the floodwater enters the basin, the buoyant force causes the wall barrier of the Self-Closing Flood Barrier to be elevated without manpower and electricity. Before reaching the top position, the rubber seal is free to move to avoid wear of the seals; after reaching the top position, the angled support block will push the wall to the dry side and automatically lock the wall in position (Fig. 4).

4.4 Lowerable or Raiseable Wall System (Completely Preinstalled)

Lowerable or Raiseable Wall System (Completely Preinstalled) is commonly used at the entrance of buildings and gates of factories, schools, shops, malls, office buildings and condominiums. Delta Technology delivers different types of lowerable or raiseable wall systems of heavy-duty MFWB, such as Manual Swing Flood Wall Barrier and Auto-Stacking Flood Wall Barrier. Manual Swing Flood Wall Barrier behaves like a normal swing gate door, but the rubber seal is stuck around the edge and connected for water tightness to prevent water flow through the void. It is designed to withstand any outdoor weather conditions and floodwater up to 3 m. It can be further improved by connecting the power source to become an automated system (Figs. 5 and 6).

Fig. 5 Manual swing flood wall barrier (*Source* Delta Technology [6])

Fig. 6 Auto-stacking flood wall barrier (*Source* Delta Technology [6])

4.5 Concrete Element System (Mass System)

The Allegro® Interlocking Concrete Block (JP Concrete) is a Concrete Elements System (Mass System) of heavy-duty MFWB. It is commonly used on the riverside and open space. It is a precast concrete product with an interlocking system to connect multiple units together like a Lego block for floodwater blockage. It is precast by lightweight concrete. The overall density is 18 kN/m^3, and it is 21.7% lighter than a normal concrete block (23 kN/m^3). The rubber seal is placed in between each block to seal up the void. The advantage does not require extra support, and it is supported and stabilised by self-weight. The disadvantage is too heavy, and the installation procedure requires machinery for transporting and lifting with spherical head lifting clutches (Fig. 7).
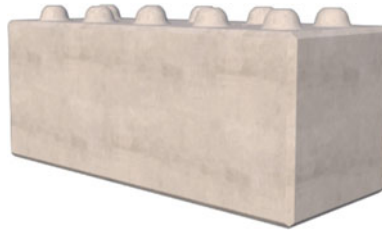
Fig. 7 The Allegro® interlocking concrete block (*Source* JP Concrete [8])

4.6 Other Available Commercial Products

The commercial products are summarised in Table 2. The table has provided the information on the classification, product name, maximum span, maximum height, operation system, and the testing standard. Most of the commercial products are automatic operation and able to withstand at least 2 m height of floodwater.

Table 2 A Summary of commercial products for the heavy duty MFWB [6][8][16] (*Source* Delta Technology, The Flood Company, and JP Concrete)

Classification	Product name	Company name	Maximum span, m	Maximum height, m	Operation system	Testing standard
Segment wall system (Partly Preinstalled)	Manual slot flood barrier	Delta Technology Pte Ltd	3.5/6.0	Varies	Manual	PAS 1188
Flap system with preinstalled foundation (Completely Preinstalled)	Auto-flip flood wall barrier	Delta Technology Pte Ltd	8.0	2.5	Automatic	PAS 1188
Permanent constructed with mobile wall system (Completely Preinstalled)	Self-closing flood barrier	The Flood Company	Unlimited	2.5	Automatic	Unknown
Lowerable or raiseable wall system (Completely preinstalled)	Auto-stacking flood barrier	Delta Technology Pte Ltd	8.0	5.0	Automatic	PAS 1188

(continued)

Table 2 (continued)

Classification	Product name	Company name	Maximum span, m	Maximum height, m	Operation system	Testing standard
Lowerable or raiseable wall system (Completely preinstalled)	Manual swing flood wall barrier	Delta Technology Pte Ltd	7.0/8.0	3.0	Automatic	PAS 1188
Concrete element system (Mass System)	Allegro® interlocking concrete block	JP Concrete Ltd	Unlimited	2.0	Manual	BS and EN

5 Conclusion

This paper has discussed a variety of heavy-duty MFWB with technical details and products available in the commercial market. Based on the review and further investigation, heavy-duty MFWB might be the appropriate solution for both emergency use and planned flood protection in Malaysia. Generally, it is useful for space-saving in densely populated areas to provide mobile flood protection with fast deployment. The products that are discussed in this paper are applicable for the heavy-duty MFWB, which can resist up to 2.0 m depth of floodwater with local conditions. It is proposed that it is necessary to further analyse the requirements and site conditions in every specific application. The heavy-duty MFWB possibly can be introduced as the best practice throughout the world, particularly the way forward for Malaysia.

References

1. Ahmad F, Ushiyama T, Sayama T (2017) Determination of Z-R relationship and inundation analysis for Kuantan River basin. Malaysian Meteorological Department, Petaling Jaya
2. Bhuiyan TR, Reza MIH, Choy EA, Pereira JJ (2018) Facts and trends of urban exposure to flash flood: a case of Kuala Lumpur city. Improv Flood Manage Pred Monitor Case Stud Asia 20:79–90
3. Caddis B, Nielsen C, Hong W, Tahir PA, Teo FY (2012) Guidelines for floodplain development – A Malaysian case study. Int J River Basin Manage 10:161–170
4. Cheah R, Billa L, Chan A, Teo FY, Pradhan B, Alamri AM (2019) Geospatial modelling of watershed peak flood discharge in Selangor, Malaysia. Water 11(12):2490
5. Chen S, Li H, Guo L, Wang L, Cao Y (2018) Testing the key performance of mobile flood protection system. Adv Civil Eng 2018:1–11
6. Delta Tech Group (n.d.) Flood barrier product [Online]. https://www.deltatech.com.sg/floodbarrier. Accessed 16 Jul 2021
7. Earth Observatory (n.d.) Rainforest [Online]. NASA's Earth Observing System Project Science, New York. https://earthobservatory.nasa.gov/biome/biorainforest.php. Accessed 22 Aug 2021
8. JP Conrete (n.d.) The Allegro® interlocking concrete block [Online]. https://www.jpconcrete.co.uk/1500mm-interlocking-concrete-blocks/. Accessed 12 Aug 2021
9. Kadar I (2015) Mobile flood protection walls. Int J Eng Inf Sci 10:133–142

10. Koppe B, Brinkmann B (2010) Opportunities and drawbacks of mobile flood protection systems. Coast Eng Proc Manage 1(32):24
11. Shah SMH, Mustaffa Z, Teo FY, Imam MAH, Yusof KW, Al-Qadami EHH (2020) A review of the flood hazard and risk management in the South Asian region, particularly Pakistan. Sci Afr 10:e00651
12. Shah SMH, Mustaffa Z, Khahro SH, Yusof KW, Ab Ghani A, Al-qadami EHH, Teo FY (2020) Froude number variance with respect to the hydrodynamic response of a non-static vehicle at a low-lying flooded roadway. IIUM Eng J 22(1):35–46
13. Syafrina AH, Zalina MD, Juneng L (2014) Historical trend of hourly extreme rainfall in Peninsular Malaysia. Theoret Appl Climatol 120:259–285
14. Taiwan Professional Civil Engineers Association (2010) Discuss on the application and test of flood gate [Online, Mandarin]. http://www.twce.org.tw/modules/freecontent/include.php?fname=twce/paper/687/3-1.htm. Accessed 16 Jul 2021
15. Teo FY, Xia J, Falconer RA, Lin B (2012) Experimental studies on the interaction between vehicles and floodplain flows. Int J River Basin Manage 10(2):149–160
16. The Flood Company (n.d.) Self-closing flood barrier [Online]. https://thefloodcompany.co.uk/products/self-closing-flood-barrier/. Accessed 22 Aug 2021
17. The Institution of Engineers, Malaysia (IEM) (2019) IEM guideline on flood abatement equipment – engineering guide of designation, testing and documentation, petaling Jaya, The Institution of Engineers, Malaysia
18. Xia J et al (2018) Hydrodynamic experiments on the impacts of vehicle blockages at bridges. J Flood Risk Manage 11(S1):S395–S402. https://doi.org/10.1111/jfr3.12228

Investigating SWAT Model Efficiency to Determine Water Balance Components (Case Study: Sungai Muda Watershed)

Mohd Syazwan Faisal bin Mohd, Mohamad Hidayat bin Jamal, Khairul Anuar bin Mohamad, and Liew Juneng

Abstract Sungai Muda watershed is one of the most important watersheds which serve as a source of water supply for the agriculture, domestic sector, fishery, and hydropower. In this study, water balance components were simulated using the SWAT hydrological model to investigate the model efficiency and its ability to use as a water balance simulator in the Sungai Muda Watershed. The SWAT model was calibrated for ten years (1981–1990) with a value of the coefficient of determination, $R^2 = 0.76$. Then, the model was validated for ten years (1997–2006) which gives $R^2 = 0.71$. Finally, the calibrated SWAT model was used to simulate the water balance components of the Sungai Muda watershed. The results showed that 42% of precipitation enters the atmosphere through evapotranspiration, and approximately 30% of it goes to the waterway as the surface runoff and lateral flow, while 28% of water enters the soil layers as the underground water. The results of this research showed the acceptable performance of the SWAT model to simulate the water balance in the Sungai Muda watershed, and the model can be used for water resources planning in this study area.

Keywords Sungai Muda · Watershed · Water balance · SWAT model

M. S. F. bin Mohd (✉) · K. A. bin Mohamad
National Water Research Institute of Malaysia, Seri Kembangan, Malaysia
e-mail: syazwan@nahrim.gov.my

K. A. bin Mohamad
e-mail: khairulanuar@nahrim.gov.m

M. H. bin Jamal
School of Civil Engineering, Faculty of Engineering, Universiti Teknologi Malaysia, Johor Bahru, Malaysia
e-mail: mhidayat@utm.my

L. Juneng
Faculty of Science and Technology, Universiti Kebangsaan Malaysia, Bangi, Malaysia
e-mail: juneng@ukm.edu.my

1 Introduction

Malaysia is located in the equatorial region and has a tropical rainforest climate. Malaysia's climate is categorized as tropical, being hot and humid throughout the year. The average temperature is 27 °C (80.6 °F). Malaysia experiences approximately 2900 mm of annual average rainfall, which is far surpassing the global average annual rainfall of 800 mm. However, the spatial and temporal disparity may occur from one region to another due to the typical hydrological system. The selected watershed for this study is the Sungai Muda watershed located in Kedah.

Sungai Muda basin is the largest river basin in Kedah and is located in the southeast part of the state. It originates from the mountainous area in the east of the adjoining state of Thailand, which is shaded in red colour (see Fig. 1). The watershed with a total catchment area of 4,150 km^2 comprises major tributaries of Sungai Ketil, Sungai Sedim, and Sungai Kerangan. The upper and middle part of the basin belongs to Kedah, whereas the downstream forms the boundary between the state of Kedah and Pulau Pinang. Sungai Muda at the northeast part of the watershed flows in a south-westerly direction and capture Sungai Ketil coming from the southeast near Jambatan Syed Omar. After capturing Sungai Sedim and Sungai Kerangan from the southeast, Sungai Muda changes its course towards the west and discharges into the Straits of Melaka. The total river length is approximately 180 km (see Fig. 1).

The water resources in Sungai Muda Basin have been developed for agriculture and potable water supply for the State of Kedah and Pulau Pinang. There are two dams, namely, Muda Dam and Beris Dam, located in Sungai Muda Basin for water supply purposes. Muda Dam, which is located upstream of Sungai Muda, stores water from its catchment of 984 km^2 and conveys it to the nearby Pedu reservoir via the Saiong Tunnel. The water is released from the Pedu reservoir to augment the natural flow in Sungai Padang Terap, where the Pelubang Barrage is located to divert the water to the MADA irrigation canals. Muda dam could also supply the domestic water for Sungai Muda region and Pulau Pinang. Beris Dam (catchment area of 116 km^2), which is located at Sungai Beris (a tributary of Sungai Muda), is used for irrigation of paddy downstream and also for domestic and industrial water supply [9].

The main objectives of this study:

- To develop and test the performance and feasibility of SWAT by inspecting the influence of topography, land use, soil and climatic condition on water balance components.
- To calibrate and validate the model output on a Monthly time step using SWATCUP-Sufi2 and perform the Sensitivity and Uncertainty Analyses.
- To assess and analyse the observed water balance/budget component in Sg. Muda Watershed.
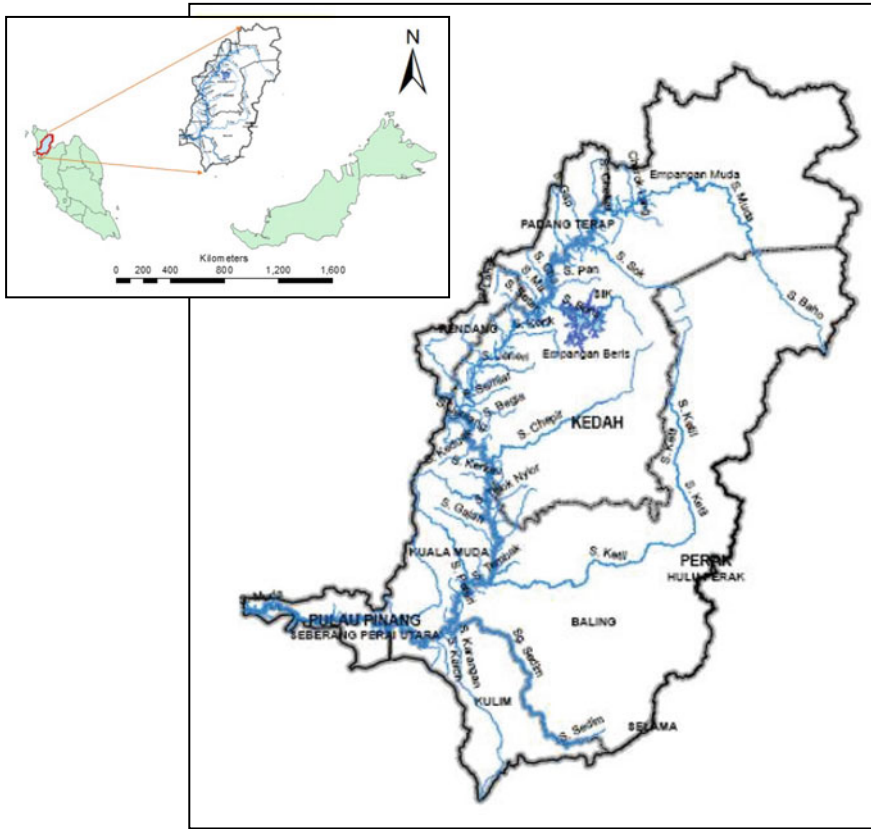
Fig. 1 Sungai Muda Watershed tributary (*Source* After NWRS [9])

2 Methodology

2.1 SWAT Model Development

Two types of datasets are required to run SWAT, which is comprised of spatial dataset and weather/climate dataset (see Table 1). The spatial data required to run the SWAT model are digital elevation model (DEM), land use map and soil map. The Digital Elevation Model was obtained from Shuttle Radar Topography Mission (SRTM), while the land use map was obtained from the Department of Agriculture of Malaysia (DOA), and the soil map was obtained from Food and Agriculture Organization (FAO). For the calibration and validation period, gridded daily hydro-meteorological dataset such as rainfall, mean temperature, wind speed and solar radiation for Peninsular Malaysia developed by Wong et al. [14] was used. This

dataset was developed purposely for the use of hydrologists and modelling practitioners in climate and hydrology research. However, this dataset was only available from 1976 until 2006. Streamflow data were obtained from the Department of Irrigation and Drainage of Malaysia (DID). The streamflow stations are located at Sungai Muda near Jambatan Syed Omar. A streamflow dataset of 20 years was used for this study. For model set up, five years' data from 1976 to 1980 were used for model warm-up. Data from 1981 to 1990 were used for model calibration, and data from 1997 to 2006 were used for model validation. For the period of 1991 to 1996, the streamflow data are not available partially and not used in calibration and validation processes.

After the simulation ends, SWAT output needs to be archived and saved. The important files output such as output.rch, output.sub and output.hru need to be imported to the output database. The output.rch contains detailed information about the reach, output.sub contains detail information about each sub-basin and output.hru contains detailed information about each hru in the entire watershed. After the simulation output is archived, then the current climate scenario analysis may be performed. Several key parameters or variables for water budget components such as surface runoff, water yield, potential evapotranspiration (PET), actual evapotranspiration

Table 1 Sources of spatial and weather dataset

No.	Variables/Dataset	Source	Resolution	Format
1	Spatial Dataset			
1(a)	Topography	SRTM DEM	90 m	Raster Grid
1(b)	LULC	Land-use from Department of Agriculture Malaysia (The year 2006)	1 km	Polygon Shapefile
1(c)	Soil and their Physical Properties	FAO Dataset	1 km	Polygon Shapefile
2	Climate and Hydrological Time Series Dataset			
2(a)	Air Temperature (maximum & minimum)	Berkeley Earth	Daily (Deg. Celcius)	Text
2(b)	Precipitation	Observed Gridded Dataset (Wong et al. [14])	Daily (in mm)	Text
2(c)	Wind Speed		Daily (ms^{-1})	Text
2(d)	Solar Radiation		Daily (MJ/sq m/day)	Text
2(e)	Relative Humidity		Daily (Fraction)	Text
2(f)	GCM Dataset	Precipitation	Daily	Text
2(g)	Discharge Data	Department of Irrigation and Drainage (DID) Malaysia	Monthly	Text

(AET), lateral soil flow, and groundwater recharge will be quantified. Below is the explanation about each water budget component:

a. Surface runoff: Surface runoff is water from rain, snowmelt, or other sources, that flows over the land surface and is a major component of the water cycle. Runoff that occurs on surfaces before reaching a channel is also called overland flow. A land area that produces runoff draining to a common point is called a watershed.

b. Water-yield: The total outflow from all or part of a drainage basin through surface channels or subsurface aquifers within a given time (e.g., one year).

c. Potential Evapo-Transpiration (PET): Potential evaporation or potential evapotranspiration is defined as the amount of evaporation that would occur if a sufficient water source were available.

d. Actual Evapo-Transpiration (AET): Actual evapotranspiration is the quantity of water that is removed from a surface due to the processes of evaporation and transpiration.

e. Lateral soil flows: Lateral flow is the movement of water under gravitational forces parallel to the slope of the land.

f. Groundwater recharge: Groundwater recharge or deep drainage or deep percolation is a hydrologic process where water moves downward from surface water to groundwater. Recharge is the primary method through which water enters an aquifer.

2.2 Climate Condition at Study Area

Based on the reported data by Wong et al. (2007), temperature and rainfall data were discussed. Figure 2 shows the mean temperature during 1976–2006 for the Sungai Muda watershed. The annual mean temperature ranges from 21.5 to 27 °C, which is the lowest temperature usually experienced at higher altitudes, especially in the mountainous area. The seasonal mean temperature, especially during December-January–February (DJF) and June-July–August (JJA) does not show differences very much and have an almost same range with annual mean temperature. Figure 3 shows the mean precipitation for the Sungai Muda watershed during 1976–2006. This watershed received a lot of rainfall every year in the range from 1900 to 2900 mm per year. Sungai Muda watershed, located on the western side of Peninsular Malaysia, is protected by the mountainous range, namely Banjaran Titiwangsa. During the winter monsoon in DJF, it received less rainfall compared to the JJA summer monsoon. During DJF season, the seasonal mean rainfall is around 200 to 360 mm/season, while during JJA the average amount is around 480 to 640 mm/season. The abundant source of rainfall in this watershed is the key element that promotes agriculture activities here.
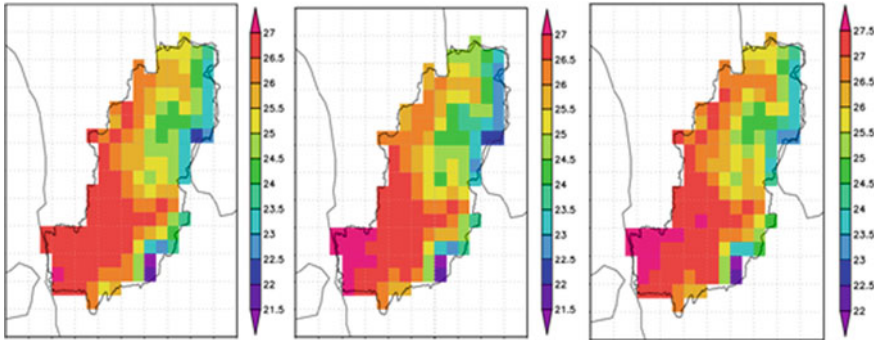
Fig. 2 Mean temperature: annual (left); DJF (middle); JJA (right) in 1976–2006 (°C) (*Source* Wong et al. 2007)
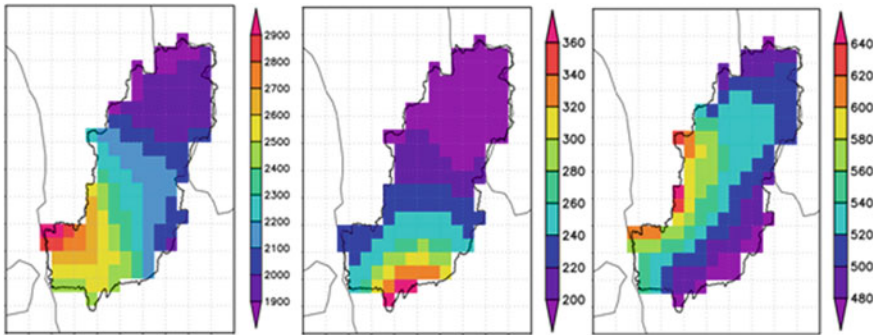
Fig. 3 Mean precipitation: annual (left); DJF (middle); JJA (right) in 1976–2006 (mm/year) (*Source* Wong et al. 2007)

3 Results and Discussion

3.1 SWAT Model Calibration and Validation

During the calibration period, several sensitive parameters that may influence the flow simulation results include the base flow alpha-factor (ALPHA_BF), groundwater delay (GW_DELAY), threshold water depth in the shallow aquifer for flow (GWQMN), groundwater "revap" coefficient (GW_REVAP), deep aquifer percolation fraction (RCHRG_DP) and effective hydraulic conductivity in main channel alluvium (CH_K2) were selected and then optimized using the SUFI2 algorithm.

3.2 Simulated Hydrograph and Correlation

The graphs shown below are the initial visualization of the outputs. The model achieves a good performance (Fig. 4) with a value of the coefficient of determination (R^2) of 0.76 (Fig. 5), and a validation value of R^2 is 0.71 (Fig. 6) [8]. The calibration procedure was carried out using the SWAT-CUP Sequential Uncertainty Fitting Procedure version 2 (SUFI2), which was developed by [1]. During this calibration period, the SWAT model performs well in capturing the higher peak flows and lower base flows (Fig. 4). Only four peak flows out of fourteen cannot be simulated well by the model. However, during the validation period (Fig. 6), the model failed to capture four major storm events recorded during 1997–2006 and resulting in lower R^2. According to the reviews of applications of some hydrological models by [3, 4], SWAT is reliable for yearly and monthly average or yield predictions but less for months with severe hydrological storms. Meanwhile, daily predictions from SWAT are less reliable, especially for the days that have an intense storm. Therefore, SWAT is not suited for analyzing severe storm events [3]. Lack of information regarding the watershed characteristics, hydrometeorological observed dataset, aquifer systems, both deep and shallow, also can impact the streamflow modelling processes [6].

3.3 Water Balance/Budget for the SWAT Model

Water balance is useful to understand the hydrologic behaviour of the study area. Water balance can be carried out for a small to a large area depending on the necessities. Table 2 summarize the water balance component for the Sungai Muda watershed
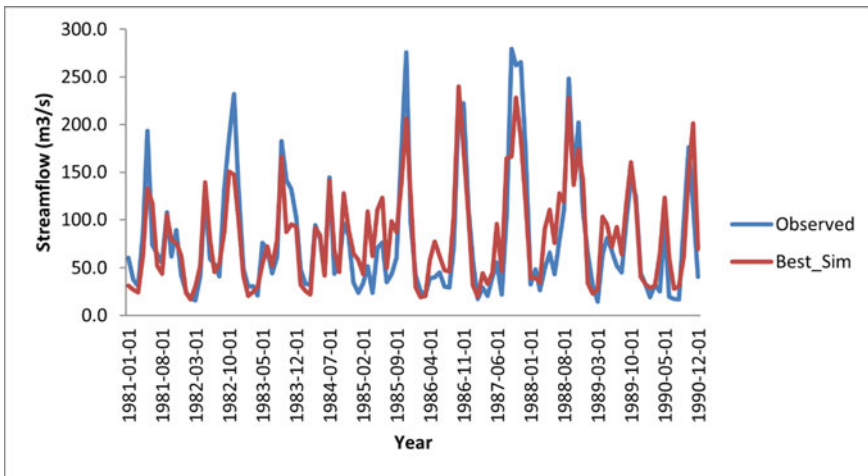
Fig. 4 Hydrograph of observed and simulated flow during calibration period (1981–1990)
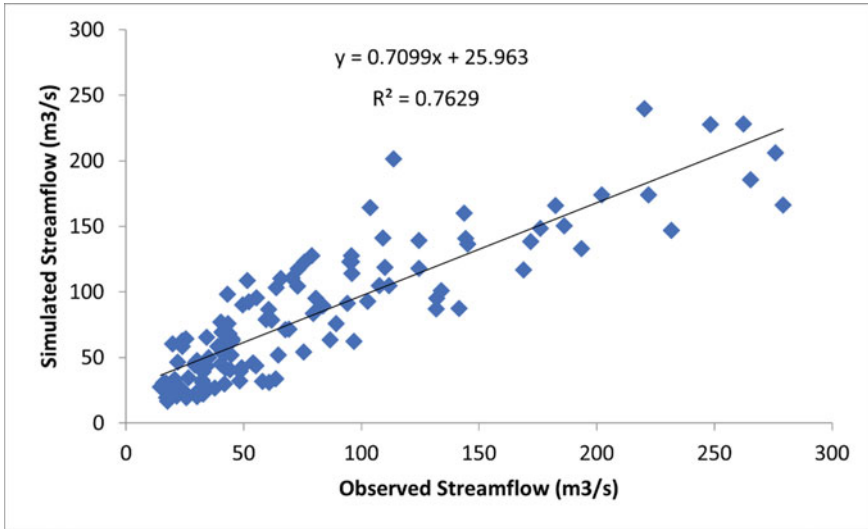
Fig. 5 Coefficient of determination (R2) value for calibration period
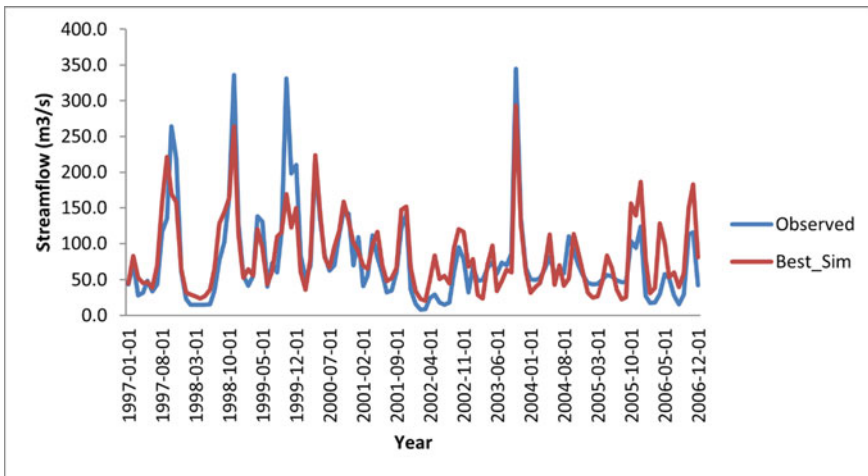
Fig. 6 Hydrograph of observed and simulated flow during validation period (1997–2006)
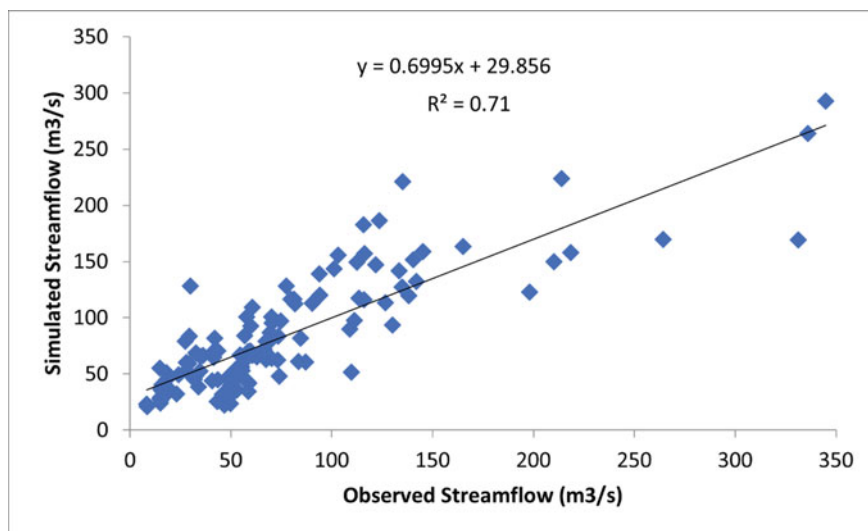
Fig. 7 Coefficient of determination (R2) value for the validation period

during the calibration and validation phase. We may conclude that the quantities of the water budget for each component are quite balanced during both periods. However, the values of the water component during validation is slightly higher than the calibration period. It seems that the validation period experienced a wetter condition compared to the calibration period. Table 2 showed that 42% of precipitation enters the atmosphere through evapotranspiration, and approximately 30% of it goes to the waterway as the surface runoff and lateral flow, while 28% of water enters the soil layers as the underground water.

Table 2 Annual water balance/budget component for basin

Annual basin	Calibration (mm)	Validation (mm)	Average (mm)
Precipitation	2,186	2,314	2,250
Surface runoff	595	643	619
Lateral soil runoff	60	63	61.5
Groundwater recharge	603	658	630.5
Evapotranspiration	928	950	939
Potential evapotranspiration	1,448	1,396	1,442
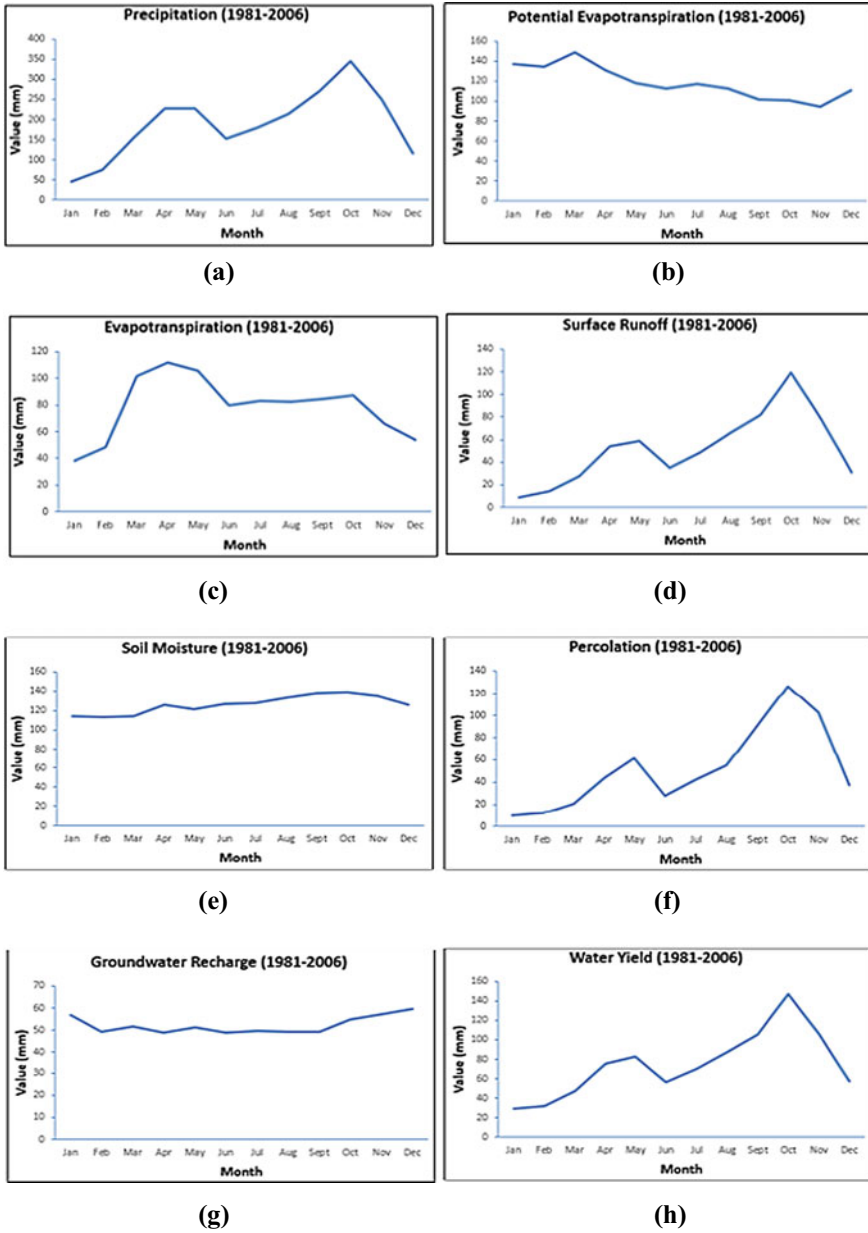
Fig. 8 a-h Different components of water balance showing the variation on the monthly basis for the year 1981–2006

4 Estimation of Water Balance

Water Balance is mainly the driving force behind all the processes in SWAT because of its impact on plant growth and the movement of sediments, nutrients, pesticides, etc., within the watershed area (SWAT Theoretical documentation 2009). The most important components of water balance in a basin consist of precipitation, surface runoff, lateral flow, base flow and evapotranspiration. The SWAT model was used to quantify the hydrological parameter occurring in the catchment area. Figure 8(a–h) shows the different components of water balance annual cycle variation on a monthly basis for the year 1981–2006. The amount of average rainfall received during this period was varied from 50 to 350 mm per month. PET value varied from 90 to 150 mm per month. AET value varied from 40 to 110 mm per month. The surface runoff value varied from 10 to 120 mm per month. The soil moisture shows almost uniform values throughout the annual cycle, around 115 to 140 mm per month. However, the percolation value and trend seem to follow the precipitation and surface runoff trend, which is the value was around 10 to 120 mm per month. The groundwater recharge value also shows an almost uniform trend which varied from 50 to 60 mm per month. Finally, the water yields varied from 30 to 140 mm per month, which seems to follow the precipitation, surface runoff, and percolation trend. Figure 9 shows the comparison of the element of water budget on a monthly basis for the year 1981–2006. We may conclude that precipitation is the main driving force for this watershed.
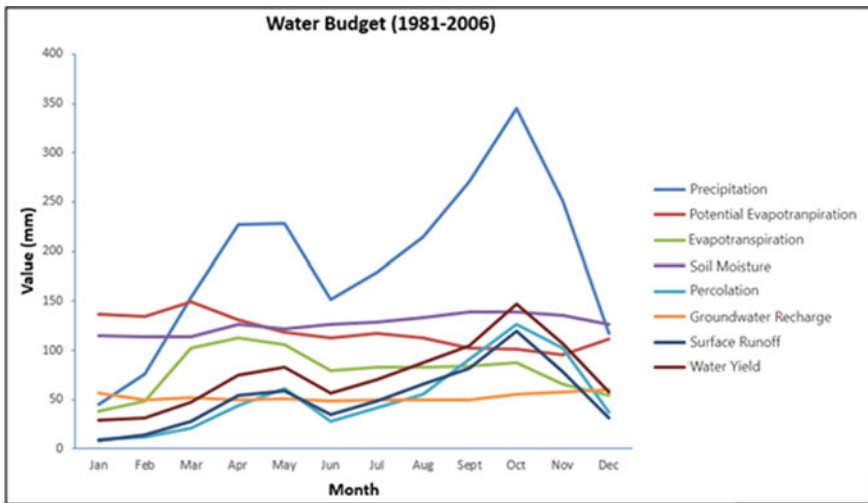
Fig. 9 Diagram showing the comparison of the element of water budget on a monthly basis for the year 1981–2006

5 Conclusion

Soil and Water Assessment Tool (SWAT) is used to model the streamflow of the Sungai Muda Watershed. The simulation results show very good performance for the calibration period and acceptable skill for the validation period, with R2 values of 0.76 and 0.71, respectively. The results showed that 42% of precipitation enters the atmosphere through evapotranspiration, and approximately 30% of it goes to the waterway as the surface runoff and lateral flow, while 28% of water enters the soil layers as the underground water. The results of this research showed the acceptable performance of the SWAT model to simulate the water balance in the Sungai Muda watershed and the model can be used for water resources planning in this study area.

References

1. Abbaspour KC, Johnson CA, van Genuchten MT (2004) Estimating uncertain flow and transport parameters using a sequential uncertainty fitting procedure. Vadose Zone J 3(4):1340–1352. https://doi.org/10.2136/vzj2004.1340
2. Arnold JG, Srinivasan R, Muttiah RS, Allen PM (1998) Large-area hydrologic modeling and assessment: part I. Model development. J Am Water Resources Assoc. 34(1):73–89
3. Borah DK, Arnold JG, Bera M, Krug EC, Liang XZ (2007) Storm event and continuous hydrologic modeling for comprehensive and efficient watershed simulations. J Hydrol Eng 12(6):605–616
4. Borah DK, Bera M (2004) Watershed scale hydrologic and nonpoint source pollution models: review of applications. Trans ASAE 47(3):789–803
5. Gupta HV, Sorooshian S, Yapo PO (1999) Status of automatic calibration for hydrologic models: comparison with multilevel expert calibration. J Hydrol Eng 4(2):135–143
6. Jajarmizadeh M, Harun S, Salarpour M (2013) An assessment on base and peak flows using a physically based model. Res J Environ Earth Sci 5(2):49–57
7. Jarvis A, Reuter HI, Nelson A, Guevara E (2008) Hole-filled SRTM for the globe Version 4, available from the CGIAR-CSI SRTM 90m Database. (http://srtm.csi.cgiar.org)
8. Moriasi DN, Arnold JG, Van Liew MW, Bingner RL, Harmel RD, Veith TL (2007) Model evaluation guidelines for systematic quantification of accuracy in watershed simulations. Trans ASABE 50(3):885–900
9. National Water Resource Study (2011) Department of Irrigation and Drainage Malaysia
10. Rahman NFA, Ali MF, Khalid K, Ariffin J, Mispan MR (2014) A frameworkfor integrated stream flow and sediment yield using SWAT in Langat watershed. J Appl Sci Agric 9(18):156–162
11. SWAT-CUP (2012) SWAT Calibration and Uncertainty Programs - A User Manual
12. White MJ, Storm DE, Busteed PR, Matlock MD, West RR (2011) Evaluating potential phosphorus management impacts in the Lake Eucha basin using SWAT. Trans ASABE 54(3):827–835
13. Wise M, Calvin K, Thomson A, Clarke L, Bond-Lamberty B, Sands R, Smith SJ, Janetos A, Edmonds J (2009) Implications of limiting CO2 concentrations for land use and energy. Science 324:1183–1186

14. Wong CL, Venneker R, Jamil ABM, Uhlenbrook S (2011) Development of a gridded daily hydrometeorological data set for Peninsular Malaysia. Hydrol Process 25(7):1009–1020
15. Wu K, Xu YJ (2006) Evaluation of the applicability of the swat model for coastal watersheds in Southeastern LOUISIANA1. J Am Water Resour Assoc 42(5):1247
16. Zahabiyoun B, Goodarzi MR, Bavani AR Azamathulla HM (2013) Assessment of climate change impact on the Gharesou River Basin using SWAT hydrological model. CLEAN–Soil Air Water 41(6):601–609

Development of the National Water Balance Management System (NAWABS) for the Perak, Kurau and Kerian River Basins

A. M. Ishak, A. Ahmad, N. A. Abdullah, U. A. Abdul Karim, M. M. Mohammad Husni, J. Lau, and N. G. Md. Nor

Abstract Water resources in Malaysia face significant challenges from changing climate, growing populations, increased water demands and pollution. In daily operations, river basin managers and stakeholders face difficult decisions in balancing the short and long term demands with the available and predicted supplies in the basin. This paper presents the background and development of the NAWABS Sungai Perak, Kurau and Kerian. The NAWABS system has been developed to study the overall water balance of the three catchments in an integrated manner. It considers satellite rainfall, climate predictions, surface, river and groundwater systems. It also considers the full-cycle water demand, including the demands of potable water, irrigation (padi and non-padi crop), livestock, fisheries and tourism. The issues of Water, Energy and Food (WEF), environmental flow requirements and land use planning is also considered.

Keywords Water balance model · Drought forecasting · Decision support system · Water management

1 Introduction

1.1 Background of NAWABS Perak, Kurau and Kerian

An overview of the NAWABS Perak, Kurau and Kerian study and system is presented in Fig. 1. As its core, the NAWABS system will look at the overall account of water for a system. One of the key elements in managing water resources is to provide a comprehensive management instrument that could provide multiple functions,

A. M. Ishak (✉) · A. Ahmad
Department of Irrigation and Drainage, Kuala Lumpur, Malaysia
e-mail: drasnor@water.gov.my

A. Ahmad
e-mail: asmadi_ahmad@water.gov.my

N. A. Abdullah · U. A. Abdul Karim · M. M. Mohammad Husni · J. Lau · N. G. Md. Nor
Megaconsult Sdn. Bhd., Kuala Lumpur, Malaysia

including accounting for water resources, providing real-time online information on water availability, an assessment tool to evaluate operation options for efficient water allocation and forecasting to assist in the decision management process.

The NAWABS system will investigate the complete water balance system and assess the water availability (volume and levels) and demands (multi demand). The water balance from the hydrological cycle perspective is defined as the amount of water entering and leaving a controlled space during a specific time period. It also accounts for major hydrological inputs, outputs and delayed components over a specific spatial and temporal scale. The main reason for the development of a water balance modelling which typically includes a modelling tool, is to provide a comprehensive solution to water resources management issues such as providing updated information on water availability, priority, allocation, quality, release and storage, environmental index (Water resources and drought and water auditing). By doing this, the NAWABS system will provide a decision management support system (DMSS) which will enable all users and vested stakeholders to better deal with the challenges of climate change/variability, increasing demand and sustainability of resources.

To ensure that the system is developed successfully, five different studies will be conducted to support the development of the NAWABS system. These are the Water Balance Study, Demand Management Study, Water Resources Conservation Plan, Environmental Flow Study and WEF and Water Footprint Study.
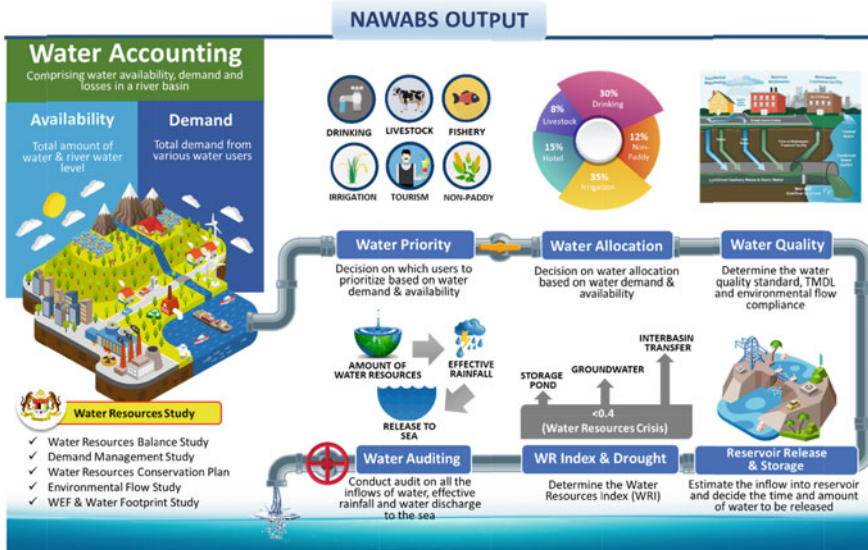
Fig. 1 Overview of NAWABS Perak, Kurau and Kerian (JPS 2021)

2 Background of the Study Area and Its Key Features

2.1 Sungai Perak

Sungai Perak, with a river length of approximately 427 km long, is the second longest river in Peninsular Malaysia after Sungai Pahang. Sungai Perak basin has a catchment area of 14,931 km^2, covering about 71% of the Perak State. Sungai Perak originates from the Titiwangsa range in the Perak-Kelantan-Thailand border at the Royal Belum Forest Reserve in the northern area of the state. From there, the river meanders southwardly and finally meets with the Straits of Melaka at Bagan Datuk.

Sungai Perak is subjected to tidal influence, which can reach up to the confluence with Sungai Kinta. Sungai Perak serves many purposes; besides hydropower generation and water supply, other important roles such as navigation, recreational and tourism activities are also included. Besides the above, the river basin also owns several prominent environmental and historical features such as the 117,500 ha Royal Belum State Park at the river upstream and Terrapin Conservation Centre in Bota Kanan, at the river downstream beside the Pasir Salak historical complex. The Sungai Perak estuary has been subjected to morphological changes brought on by inland sediments transported along the river as well as prolonged dynamic coastal processes. Such impacts have warranted the implementation of coastal protection works along the shoreline of the river mouth, which can be evidently seen.

The main tributaries of Sungai Perak include Sungai Rui, Sungai Belum, Sungai Temenggor, Sungai Piah, Sungai Pelus, Sungai Kinta and Sungai Bidor. Among these tributaries, Sungai Kinta flows through Ipoh, the State capital. There are several major towns located along the Sungai Perak which are Kuala Kangsar, Parit, Kampung Gajah, Teluk Intan and Bagan Datuk.

2.2 Sungai Kurau

Sg. Kurau, with a river length of about 94 km, drains a total catchment of 681 sq. km in the districts of Selama-Larut Matang and Kerian in Perak. It has two main tributaries—Sg. Ara that originates in the Bintang Range and Sg. Merah. Bukit Merah reservoir that serves as the main source of irrigation water to the Kerian Irrigation Scheme is located at the middle reach of the river. The river system generally flows easterly and discharges into the Straits of Melaka. The location plan of the project area is shown in Fig. 2. Sg. Kurau originates in the Bintang Range that runs from southern Thailand to the south of Perak and drains into the Straits of Melaka. There are two main tributaries—Sg. Ara and Sg. Merah—both of which also originate in Selama-Larut Matang district. Both drain into the Bukit Merah Reservoir that supplies water to the Kerian Irrigation Project for paddy cultivation. The upper reaches of Sg. Kurau and its tributaries are steep due to the mountainous terrain, whilst the lower reach
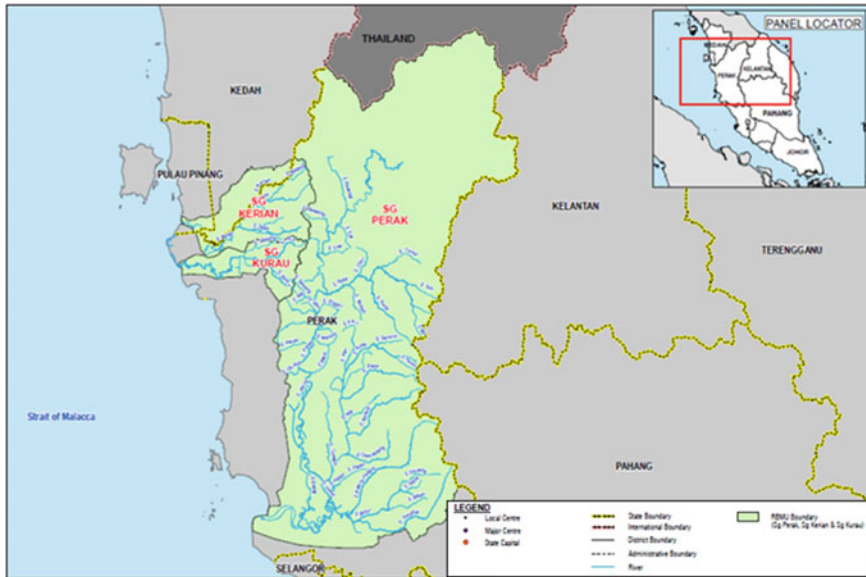
Fig. 2 Sungai Perak, Kurau and Kerian River Basin (JPS 2021)

near the coast is gentle and meandering. The Bukit Merah Dam is sited at a distance of 70 km upstream of the Sg. Kurau river mouth.

There are three major crossings on Sg. Kurau downstream of Bukit Merah Reservoir, viz. North–South Highway bridge about 730 m downstream of Bukit Merah spillway, Padang Lalang flume located at 7.1 km downstream of the highway bridge, and Gedong bridge (along Ipoh-Butterworth Road) that is about 18.6 km downstream of the flume. Sg. Kurau basin is largely agricultural in terms of land use. Oil palm and rubber are the principal tree crops in the upper and lower reaches of the river basin, and paddy is mainly cultivated in areas between Bagan Serai and Bukit Merah Dam and south of Batu Kurau. While Bagan Serai is the major town in the river basin, there are also many riverine villages from the middle to the lower reaches of the river. These villages have experienced frequent flooding due to Sg. Kurau overspills its banks during periods of heavy rainfall. Major flooding lasting as long as six days have been recorded in the past.

2.3 Sungai Kerian

The Kerian river basin of approximately 1,418 km^2 spreads into three states, viz. Perak, Kedah and Seberang Perai, Pulau Pinang. The river originates in the Bintang Range and flows westerly before discharging into the Straits of Malacca near Nibong Tebal Town. The middle and upper reaches of this river form the boundary of the

Kedah and Perak. The main tributaries of Sg Kerian include Sg Selama, Sg Ijok, Sg. Samagagah and Sg Ulu Mengkuang.

Rapid development in the Kerian river basin, particularly over the last decade, has led to changes in the river basin and flow regimes, raising serious concerns over issues related to flooding and the environment. Overspilling of flow at the middle reach of Kerian river is causing low lying areas near Parit Buntar, Bagan Serai and Bandar Baharu to experience persistent flooding during heavy downfall and monsoon season, while Seberang Perai Selatan, Pulau Pinang, which is located downstream of the river is experiencing frequent flooding due to the exposure to high tides, heavy downpour and surge of flows from upstream when the Kerian barrage is opened.

Sg Kerian has a steep and mountainous upper reach that is still covered with primary and secondary forests, while the terrain in the middle reach is undulating, separated by broad valleys of low gradients. The lower reaches of the river are almost entirely made up of flat coastal plains.

2.4 Challenges

The river basin forms the appropriate unit to manage the water resources for all development needs. In the future, results from the Study will be used for the development of a water balance model for the management and long-term sustainability of water resources.

Key considerations that justify the development of the modelling to manage water resources for the future include:

I. Multiple stakeholders who have different priorities;

    a. River basin managers—need short term operational and long-term seasonal planning tools to balance demand with supply management. The modelling system shall be capable of advising users of the abstraction value from the river and groundwater (from model auto-optimization).
    b. Water users—need access to up to date information on river flows and levels to better manage their own operations
    c. Policymakers—need to understand the long-term risks to supply to enable them to make informed economic investment decisions based on cost–benefit analysis from the study.

II. Change in land use and uncertain weather pattern warrants water resources management to be supported by a water balance model and decision support system. The water resource conservation plan shall be linked in the DMSS and Webpage;

III. Water resources available within the basin are now deemed to be limited, and the available resource and current and future demands of that resource need to be quantified, and an allocation mechanism under various conditions need to be established;

IV. Groundwater resource potential need to be explored, although information is limited;

V.   Within the Sg. Perak, Sg. Kurau and Sg. Kerian basin, there are various water demand points that are operated by different entities. Coordination of the management of water resources within the basin is important, including but not limited to the possibility of water transfer from Perak River to Bukit Merah Dam to Pulau Pinang and/or Perak River to Kerian River to Pulau Pinang can be explored;

VI. Lack of knowledge of the water availability and usage, and lack of analytical tools to optimally manage the resource in the short, medium and longer-term time scales. Maybe also a lack of coordination (or knowledge sharing platform) between different stakeholders.

3   Uniqueness of Nawabs Perak, Kurau and Kerian

3.1   Management of Three Integrated River Basins

The usage of water as a resource is already interlinked within the Sg. Kurau and Sg. Kerian basin, with the paddy irrigation canals by IADA in Kerian and Seberang Perak being connected whilst sourcing water from both Sg. Kurau (through Rumah Pam Padang Lalang) and Sg. Kerian (through Rumah Pam Sg. Bogak). With the water transfer proposals from Sg. Perak aims to utilize portions of the river network in Sg. Kurau and Sg. Kerian (either through Bukit Merah Dam as a balancing reservoir and subsequently to Sg. Kerian), it makes practical sense to analyse and systematically derive the management of the water resource in the three basins in an integrated manner. NAWABS aims to assist the water resource managers in this aspect in order for a holistic solution to be proposed and implemented via a common management platform.

3.2   Long Term Integration of Options (Water Transfers)

The long-term analysis of NAWABS Perak, Kurau and Kerian basins shall take into account the water transfer proposals to transfer water from Sg. Perak to Sg. Kerian to supply water to the state of Penang, details of which can be found in Water Transfer from Sg. Perak to Sg. Kerian and Pulau Pinang. As such, careful deliberation with relevant stakeholders from the states of Perak, Kedah and Penang shall be taken into account to ensure that a common solution that benefits all parties can be achieved, as water resources in the basin are heavily utilized to generate hydroelectricity, water treatment, irrigation and others. Main water users within all three states include, but are not limited to:

  i. Lembaga Air Perak (LAP)
  ii. Perbadanan Air Pulau Pinang (PBAPP)
 iii. Lembaga Sumber Air Negeri Kedah (LSANK)
 iv. Syarikat Air Darul Aman (SADA)
  v. Kawasan Pembangunan Pertanian Bersepadu (IADA)
 vi. Tenaga Nasional Berhad (TNB)
 vii. Jabatan Pengairan dan Saliran (JPS) Perak, Kedah and P. Pinang

3.3 Full Water-Energy-Food Nexus Inter-Relationship

This component of the study sets out to achieve the followings:

  i. Identify the governance context of demands for water, energy and food in the river basin.
  ii. Identify drivers or pressures on basin resources.
 iii. Analyse nexus linkage, mapping the interactions between sectors.
 iv. Develop a series of dialogues between actors that normally operate with divergent perspectives and at different levels and scales.
  v. Identify the benefits of adopting the nexus approach and options for reducing trade-offs and negative impacts between sectors or on the environment, economy and society.

The Sungai Perak, Sungai Kurau and Sungai Kerian river basins are socio-economically dynamic regions. Population growth, economic expansion, land use changes, increased urbanization, industrial development, new government policies and lifestyle changes are known drivers of change that exert significant influence on the WEF nexus. Figure 3 provides a general overview of these interacting forces among the resource base, WEF nexus and the drivers of change.

The success in maximizing the values of available resources depends critically on the management of the nexus by balancing the needs and interests of stakeholders that evolves with the drivers of change. For example, population growth (a driver of change) simultaneously increase the demand for water, energy and food. This additional demand for the three nexus components puts pressure on existing resources that must be managed in a holistic manner using the WEF nexus approach.

Of all the potential drivers indicated in Fig. 2, six key drivers have been identified as the most significant influencers of change that must be taken into consideration in the current and future management of resources in the Sungai Perak, Kurau and Kerian river basins. These drivers of change are:

- Population growth.
- Expansion in economic activities.
- Landuse change.
- Increased rate of urbanization.
- National food security policy.
- Changing lifestyle and expectations.
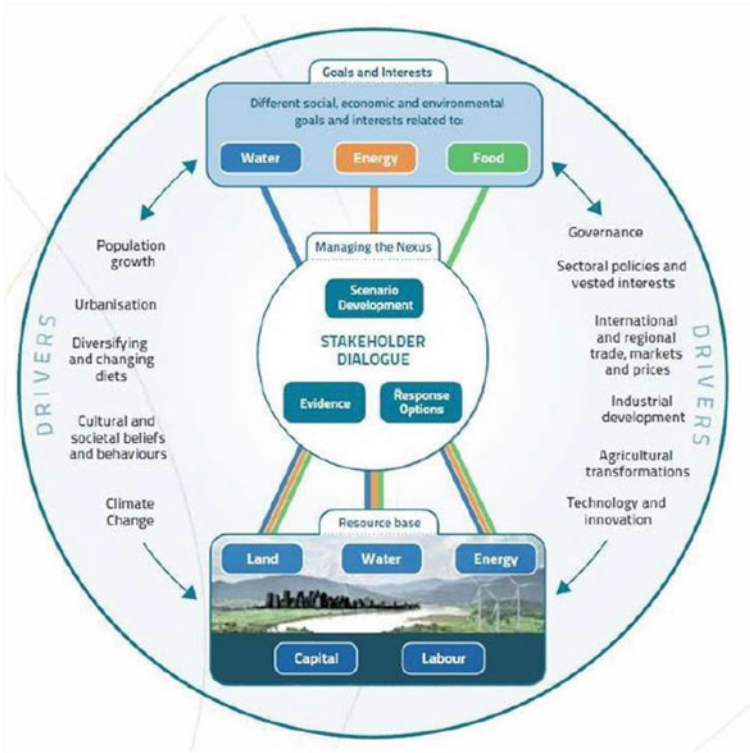
Fig. 3 Drivers of change in the context of competing stakeholders' interests and finite resource base [1]

In the next phase of this study, data will be gathered to build narratives of the drivers of change and their likely influence on the nexus components. These narratives will be used to provide context for the nexus analysis and to demonstrate the importance of taking the nexus approach in the management of available resources within the Sungai Perak, Sungai Kurau and Sungai Kerian River Basins.

3.4 Nexus Linkages and Mapping of Interactions Between Sectors

Considering the existing situation in Sungai Perak, Sungai Kurau and Sungai Kerian River Basins, the WEF linkages can be represented by Fig. 4. Water is used to produce both food (via agriculture activities) and energy (via electricity generation at hydropower plants). Simultaneously, energy is used to produce both food (to power agriculture activities) and water (to power water treatment plants and pumphouses

for potable water production and distribution, and to power pumphouses for irrigation). Food sub-sectors included in the analysis are paddy, non-paddy crops, poultry, livestock and fisheries/aquaculture.

The interlinkages of sectors can also be represented in table format. Table 1 shows such a mapping where it can later be expanded once the linkages are quantified in terms of values. The capital letters in the first column refer to the same letters in Fig. 3.
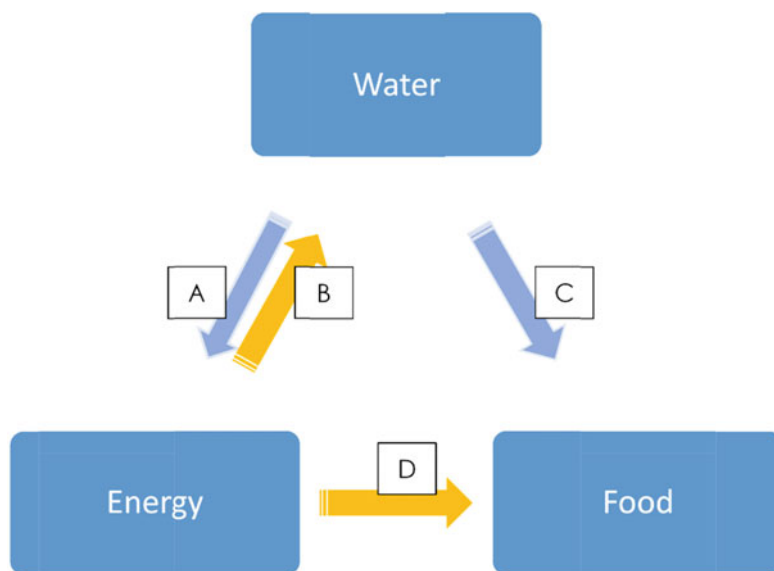
Fig. 4 Interlinkages between sectors (WEF Nexus)

Table 1 Interlinkages between sectors (with quantities/values)

	Nexus link	Description
A	Water for energy	Water use in hydro**electricity** production
B	Energy for water	To power water treatment plants and pumphouses for **potable water production and distribution**
		To power pumphouses for **irrigation**
C	Water for food	Water use in the production of: Paddy Non-paddy crops Poultry Livestock Fisheries/aquaculture
D	Energy for food	To power agricultural activities

4 Long Term Challenges

4.1 Water Transfer from Sg. Perak to Sg. Kerian and Pulau Pinang

Northwest Perak comprises the districts of Kerian, Larut Matang and Selama. For Northwest Perak, the water transfer system is not only to satisfy the projected additional potable water demand until 2050 but also the deficit in irrigation water supply for paddy cultivation. This area is planned to be developed as industrial and growth areas under the Perak Aman Jaya development plan and the Northern Corridor Economic Region (NCER) investment programmes. The completion of Sultan Abdul Halim Muadzam Shah Bridge (Penang Second Bridge) and the development of the West Coast Expressway are anticipated to boost the development rate and further increase the domestic and industrial water demand in this region, which is already increasing.

The projected water demand for Northern Perak will increase by more than 50% by the year 2050 as compared to the projected demand in 2015. It is believed that there will be a deficit in potable water supply for Kerian, Larut Matang and Selama until 2050 [3].

Under the current operating conditions, the existing reservoir is unable to sustain 100% cultivation whilst meeting the committed potable water demand as well as flood mitigation function. The issue can be critical with increasing potable water demand and increasing pressure to resolve flood issues. The issue is further complicated by the frequent requests from the LAP to release more water to achieve the required water level at its WTP intake.

As the present reservoir storage is insufficient to fulfil all the needs, the "Kajian Pemindahan Air Sg. Perak, 2016" has carried out reservoir simulations and come out with the solutions. The study proposed a total raw water transfer of 2,000 Mld from Sungai Perak. Four (4) options have been identified as follows:

a. Sg. Perak (downstream of Chenderoh Dam)—Sg. Kurau—Bukit Merah Dam (25.5 km);
b. Sg. Perak (upstream of Chenderoh Dam)—Sg. Kurau—Bukit Merah Dam (14 km);
c. Sg. Perak (downstream of Kenering Dam)—Sg. Kerian (36 km); and
d. Sg. Perak (upstream of Kenering Dam)—Sg. Kerian (28 km).

NAWABS Perak, Kurau and Kerian aim to replicate the options above in order to ensure that water as a resource is managed in an efficient manner, using simulation and modelling to come up with the impacts of the transfer proposals.

4.2 Water Quality

As water is a common and finite resource utilized by various agencies in the three basins, it is imperative that its quality is maintained at an acceptable level to ensure the demanding operating conditions are met. These are expected to worsen with the change in land use, further development and urbanization in the basin, and greater economic activities that are expected to increase within the basins.

As such, NAWABS Perak, Kurau and Kerian basins shall take into account the concerns by not only the water users but as well as regulating bodies to ensure the specific requirements are met and propose improvement measures. This includes the Department of Environment (DOE) and the Ministry of Health (MOH), amongst others. In the DMSS, the system is also expected to display the water quality measurements by the DOE for monitoring by relevant water users.

4.3 Water Allocations

As the water is being utilized by various agencies within the basins, appropriate water allocation analysis shall be conducted with close liaison with relevant agencies. This is highly imperative, especially in the dry seasons, where the water balance exercise could advise the water users to utilize the common resource in a common platform in a more efficient manner.

5 Key Features

5.1 Water Resource Schematic

The development of a water resource schematic is crucial to provide a detailed understanding of all water resource users and infrastructure in a basin whilst presenting the information in an informative manner through the use of infographics. Users will be able to capture important information pertaining to the usage of water in a single glance, as shown in Fig. 5. This information shall be updated accordingly throughout the course of the project. Currently, Kuran and Kerian basins are linked by the Terusan Besar canal. Sg Perak is not linked to Sg Kurau or Kerian. However, if the water transfer scheme goes ahead from Sg Perak to Penang (see section above), there will be significant interactions and potentially competing demands for water which require a detailed understanding of the dynamics.
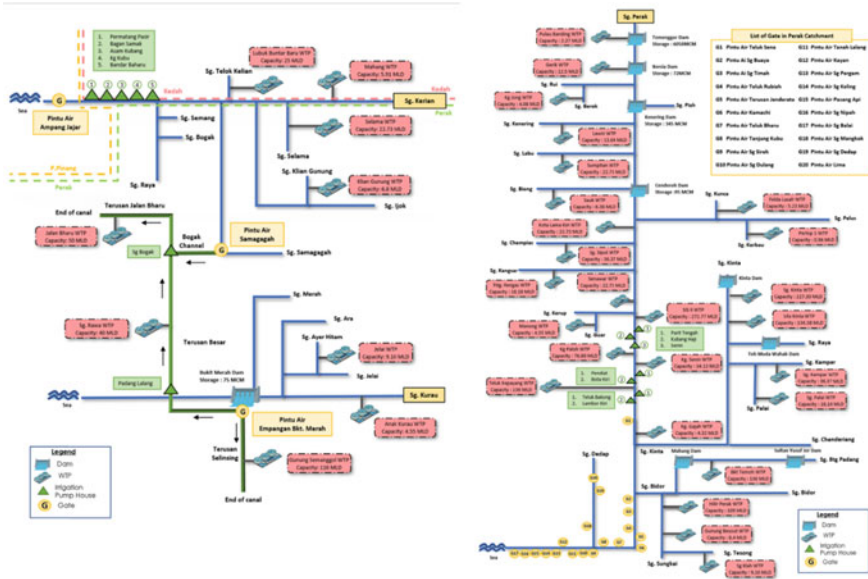
Fig. 5 Water resource schemating for the Perak, Kurau, and Kerian Basins

6 Conclusions

This paper has presented an overview of the ongoing development of the NAWABS Perak, Kurau and Kerian systems. It has also highlighted some of the key features, uniqueness and challenges. Currently, the project is at its study phase. The development of DMSS system will be developed following the completion of the study phase at the beginning of 2023.

References

1. Fao (2022) Water-energy-food nexus. http://www.fao.org/land-water/water/watergovernance/waterfoodenergynexus/en/
2. JPS Malaysia (2003) National register of river basins. Final report volume 2 updating of condition of flooding in Malaysia
3. JPS Malaysia (2011) Review of the national water resource study (2000–2050) and formulation of national water resources policy. Final report

Managing Disputes in Water Management Contracts: The DID Perspective

Sr Ruaidah binti Idris

Abstract Disputes are common problems in the construction industry and water management projects are no exception. In order to minimise the problem, it is imperative to identify the disputes and conflicts arising in the industry. Thus, the objective of this paper is to highlight the common disputes and issues between the Contractor and the Government. In the DID context, the common types of disputes often faced are temporary work and issues on unforeseeable hydrological conditions. Thus, to elaborate further on the disputes, sample cases and projects are identified and this paper further outlines steps or actions to overcome them. Therefore, it is very important to manage them for better and more efficient completion of the projects. This paper is expected to be of assistance in the management of conflict and disputes in upcoming DID projects.

Keywords Department of Irrigation and Drainage (DID) · Disputes · Managing disputes · Temporary Work · Unforeseeable hydrological conditions

1 Introduction

The construction industry is a significant sector of the economy that plays a major role in the economic development of a nation. Construction works are usually associated with works relating to the construction, extension, installation, repair, maintenance, renewal, removal, renovation, alteration, dismantling, or demolition of a building or structure. However, the nature of DID projects mainly involves works underwater or by water bodies that include, among others, excavation underwater, dredging, filling, rock revetment, beach nourishment works, et cetera. Therefore, it is different from normal construction works and it has unique features that need to be understood in order for it to be able to perform effectively and efficiently.

The complexity and competitive environment of the construction industry involve many participants working together, and it is inevitable for conflict to occur whenever

S. Ruaidah binti Idris (✉)
Quantity Surveying and Contract Management Division, Department of Irrigation and Drainage, Kuala Lumpur, Malaysia
e-mail: ruaidah@jkr.gov.my

differences in perceptions among the participants of the projects arise. Eventually, if conflicts are not well managed, they quickly turn into disputes, which is one of the main factors that prevent the successful completion of construction projects.

Hence, this paper focuses on the two main issues of disputes in DID contracts, namely Temporary Work and Unforeseeable Hydrological Conditions. This is an overview of how we manage such disputes so as to avoid losses to the Government.

Subsequently, it is important to be aware of the causes of disputes in order to complete the construction projects in the desired time, cost and quality. Failure to do so may cause delays in the schedule, which results in claims that need lawsuit measures to resolve them, loss of money and time.

2   Common Disputes in DID Contracts

2.1   Misinterpretation on Temporary Work

In the construction industry, temporary work (TW) is required in the erection of permanent works, and it is under the Contractor's responsibility. TW is defined as parts of the works that allow or enable the construction of, protect, support or provide access to the permanent works and which might or might not remain in place at the completion of the works [1].

According to Construction Industry Development Board Malaysia [3] in the Malaysian Civil Engineering Standard Method of Measurement (2nd Edition) (MyCESMM2), TW is defined as work that is temporary in nature but is necessary for the execution of the permanent works. TW is not expressly stated, which means the works are not shown in the drawings and also not stated in the specification. TW is categorized under **Class A: General Items**. TW items defined such as access roads, bridges, cofferdams, pumping, dewatering, river diversion, jetty, staging, compressed air, access scaffolding, support scaffolding, propping, piling, formwork, shafts, pits and hardstanding. However, MyCESMM2 allow the Contractor to insert additional TW items where necessary under Method-Related Charges (MRC).

This concept of TW as set out in MyCESMM2 can be called into question, as it creates potential ambiguities. Most engineers may choose not to itemise any TW under the 'specified' bill of quantities (BQ) because they leave such works for the Contractor to decide and itemise under MRC.

Fundamental principles in MyCESSM2 under Section 6: Method-Related Charges, MRC means the sum for an item inserted in the BQ by a tenderer. There are two types of MRC, **time-related charges**—a method-related charge for work, the cost of which is to be considered as proportional to the length of time taken to execute the work or **fixed charges**—a method-related charge which is not a time-related charge. A tenderer may insert in the BQ the MRC as he may decide to cover items of works relating to his intended method of executing the works, the cost of

which are not to be considered as proportional to the quantities of the other items and for which he has not allowed in the rates and prices for the other items.

The misunderstanding in principles of MRC will lead, either the Contractor pricing accordingly to the list of TW in the BQ, which then entitles him to receive payment for those TW on the same principles, OR, when an item in the TW list is found missing, the Contractor will claim for additional costs.

2.2 Unforeseeable Hydrological Conditions

The typical nature of work related to DID projects is works underwater or by water bodies that include, among others, excavation underwater, dredging, filling, rock revetment, beach nourishment works and et cetera. A common issue arising from this work is unreasonable, excessive quantities due to loss of materials. There are a number of reasons that contribute to this situation, namely settlement that may be caused by default in design, poor execution of construction methods or natural events such as being washed away by water current or waves, tidal or marine phenomena, flood, earth tremor and etc.

Disputes often arise on which party should bear the high additional costs due to the loss of materials. The fundamental aspect to look into in answering this is by establishing the root cause of the event and how the risks are allocated in the contract.

2.3 Conflict, Disputes and Claims

Construction of work is bedevilled with uncertainties. As the saying goes, we are not living in a perfect world. If it was, then all contract documents would be fault-free. Unfortunately, human beings are often known to err, and as a result, disputes are always apt to appear between the Government and the Contractor.

2.4 Common Disputes Pertaining to TW

It is a common occurrence for DID projects to be saddled with disputes in relation to TW once construction at the site has started. This is because the concepts of TW as set out in MyCESMM2 has created ambiguities. Below are three (3) BQ samples of TW in DID Contracts.

As shown in Fig. 1—BQ Sample for Project No. 1, **'the engineer'** (an appointed consultant who prepared the BQ) has itemised TW under the BQ for MRC. The Contractor has priced the TW deemed as accurate according to their own assumptions without submitting to the Government any detailed drawings, specifications and information. As a consequence, in practice, MRC was not effectively used and it is

conceded that the priced bill does not reflect the pricing accurately because it does not indicate the variables which may affect the costs.

In this situation, where MRC for this TW are not properly quantified, and the Contractor has priced too low, the Contractor will submit additional claims to the Government on the grounds that his method statement did not sufficiently account to execute the work. In cases where the Contractor had priced too high, the construction cost is unreasonably inflated, ineffective and not value for money to the Government.

Figures 2 and 3 shows the BQ Sample for Project No. 2; the engineer did not itemise any major TW under any 'specified' BQ because he left such works for the Contractor to decide and itemise under MRC. In this BQ, the Contractor was instructed to insert any other items/works as deemed necessary to be executed for the works at the site. Detail drawings, specifications and other information were not provided anywhere in the tender documents as a basis for the Contractor to price all the related works. This is unfair to the Contractor because he is not expected to know whether a major TW of any kind is to be constructed at the site. The BQ should serve as an accurate pricing tool for the Contractor to price the items accordingly. This may then result in the Contractor pricing unreasonably (too high/too low) for the item.

Although the BQ is successful in saving duplication of efforts while tendering and provides a basis for valuing works as the work proceeds, the main disadvantage in this situation is the difficulty to analyse MRC during the tender analysis stage due to different methods/approaches by different tenderers in their tenders.

During the construction stage and whenever there is a need for any TW to be constructed at the site, the Superintending Officer (S.O.) will issue an instruction to the Contractor to that effect without any additional costs since it has been deemed to be included in the rates inserted elsewhere such as in Preliminaries and General Items.

The Contractor may also dispute the Government's decision in this case on the grounds that the contract is based on the Conditions of Contract PWD203A (Rev. 2010) (PWD203A) whereby all items related to the works must be itemised and measured accordingly. Since the works are not properly itemised, the Contractor may form his own assumptions and may overprice them. Either way, this does not benefit the Government.

In BQ Sample for Project No. 3, as presented in Fig. 4, the engineer also did not itemise any major TW at any 'specified' BQ because it was intended for the Contractor to decide and itemise such works under MRC.

In this case, the Contractor submitted their claim to the Government with regards to the absence of TW itemised in the BQ for the execution of the L-Shape Retaining Wall for Bypass Channel (permanent work). The engineer refused this claim on the ground that it was the obligation of the Contractor to examine and investigate the nature of the site, which the Contractor had priced for MRC.

The matter was brought to arbitration, and the Contractor was awarded a sum in favour of their claimed amount because the BQ itemised for the work were substantially insufficient to suit the execution of the permanent work on site.

BILL OF QUANTITIES

O. 9 - METHOD - RELATED CHARGES

Code No.	Description	Units	Quantity	Rate (RM)	Amount (RM)
	Tenderer may insert in this Bill items for Method-Related Charges as he may decide so as to cover items of work relating to his intended method of executing the Works.				
	Each Item for a Method-Related Charge of the Work shall be fully described so as to define the extent of work covered and to identify the resources to be used whether of permanent or temporary work.				
	Items as described herein are not conclusive and Tenderer may add or omit items deem necessary				
A521.1	Construct temporary access roads to site; fixed charge	sum			15,000.00
A521.2	Removal upon completion temporary access roads to site; fixed charge	sum			10,000.00
A521.2	Maintain access road for the duration of contract period; time related charge	sum			10,000.00
A523.1	Construct cofferdams; diversion, planking and strutting of excavation and remove upon completion; fixed charge. Cofferdam to be 20 years ARI.	sum			100,000.00
A523.1	Remove upon completion, cofferdam; fixed charge				
A523.2	Maintain cofferdam; diversion, planking and strutting for duration of construction; time related charge	sum			20,000.00
A524.1	Install pumping and dewatering at site ; fixed charge	sum			10,000.00
A524.1	Remove upon completion; pumping and dewatering at site; fixed charge				
A524.2	Operation and maintenance of pumping and dewatering for duration of construction; time related charge	sum			5,000.00
	Total To Be Carried Forward To Summary				170,000.00

Fig. 1 BQ Sample for Project No. 1: Bill No. 9: Method-Related Charges Rancangan Tebatan Banjir Sungai Rampayan Lembangan Sunggai Menggatal, Kota Kinabalu, Sabah (Tawaran Semula)

KERJA MENCEGAH HAKISAN PANTAI MEK MAS, KOTA BHARU, KELANTAN (TAWARAN SEMULA)

TENDER NO : JPS/IP/PT/06/2019

GENERAL ITEMS

Code No.	Description	Unit	Qty	Rate (RM)	Amount (RM)
500	**CONTRACTOR'S REQUIREMENTS**				
	Facilities				
	Rate shall be deemed to include the provision of water supply, electricity sanitary facilities and their continuing operation and/or maintenance				
511.1	Set up offices and remove upon completion	sum			25,000.00
511.2	Maintenance of office for duration of contract period	sum			7,200.00
517.1	Set up workmen accomodation and remove upon completion	sum			15,000.00
517.2	Maintenance of workmen accomodation for duration of contract period	sum			5,000.00
	Site Management				
559	Site Management including site agent, site staff and site work coordination	sum			156,000.00
560	Allow for mobilisation of land base machineries, equipments, storage cabins and etc to project site as specified in the contract or as directed by the S.O.	sum			5,000.00
519.1	Allow for provision of all temporary works, provision of temporary crossing necessary and removal of all temporary works and reinstatement of site upon the completion of the works	sum			15,000.00 10,000.00
519.2	Maintain all temporary works for duration of contract period	sum			20,000.00
521.1	Allow for provision of temporary access roads and removal of all temporary works and reinstatement of site upon the completion of the works	sum			40,000.00
521.1	Maintain temporary access roads for duration of contract period	sum			10,000.00

IMANCO BINAAN SDN. BHD.
(301503-X)
No.8A-9A, Taman Mewah Jaya,
Batu 3 Tandop, 05400 Alor Setar,
Kedah Darul Aman.
Tel /Fax : 04-7720769

Total Carried To Collection Page ... 293,200.00 298,200.00

F2/1-3

Fig. 2 BQ Sample for Project No. 2 (a) Bill No. 1: General Items—Kerja Mencegah Hakisan Pantai Mek Mas, Kota Bharu, Kelantan (Tawaran Semula)

Fig. 3 BQ Sample for Project No. 2 (b): Bill No. 4: Method-Related Charges—Kerja Mencegah Hakisan Pantai Mek Mas, Kota Bharu, Kelantan (Tawaran Semula)

MEMBINA PINTASAN BANJIR, PINTU KAWALAN PASANG SURUT DAN KERJA-KERJA BERKAITAN

BAGI RANCANGAN TEBATAN BANJIR (RTB) LEMBANGAN SUNGAI KESANG.

Tender No: JPS/IP/PB/07/2014

BILL NO.1 - PRELIMINARIES AND GENERAL ITEMS

Item No.	Code No.	Description	Unit	Quantity	Rate (RM)	Amount (RM)
		CONTRACTOR'S REQUIREMENTS (cont'd)				
1.5.1.6	A517.1	Set up workmen accomodation and remove upon completion; fixed charge	sum			36,000-00
1.5.1.7	A517.2	Maintain workmen accomodation for duration of contract period; the related charge	mth	18	500-00	9,000-00
1.5.2		Temporary Works				
1.5.2.1	A521.1	Construct temporary access roads to site; fixed charge.	sum			8,000-00
1.5.2.2	A521.2	Maintain temporary access roads for duration of contract period; time-related charge.	mth	18	350-00	6,300-00
1.5.2.3	A529.1	Construct temporary drains and dewatering to site; fixed charge.	sum			6,000-00
1.5.2.4	A529.2	Maintain temporary drains and dewatering for duration of construction; time-related charge.	mth	18	190.00	3,420-00
1.5.3		Site Management				
1.5.3.1	A531	Site agent for the duration of contract period; time related charge	man-mth	18	4,000-00	72,000-00
1.5.3.2	A532	QA/QC officer for the duration of contract period	man-mth	18	2,500-00	45,000-00
1.5.3.3	A540	Mobilisation and demobilisation of plant and machineries	sum			12,000-00
1.6		**MISCELLANEOUS**				
1.6.1	H110	Contractor's Plant and Equipment Provide, erect, keep insured, maintain and remove on completion all plant and equipment as specified (excluding piling equipment) as specified in the Specifications.	sum			22,000-00
1.6.2		Method Related Charges (MRC) Please Specified each item				
		a)...............	sum			
		b)...............	sum			
		c)...............	sum			
		d)...............	sum			
		Total Carried To Summary Page				219,720-00

F2/1-4

Fig. 4 BQ Sample for Project No. 3: Bill No. 1: Preliminaries and General Items—Membina Pintasan Banjir, Pintu Kawalan Pasang Surut Dan Kerja-Kerja Berkaitan Bagi Rancangan Tebatan Banjir (RTB) Lembangan Sungai Kesang

3 Common Disputes Pertaining to Unreasonable Excessive Quantities

3.1 Project No. 1: Quantity of Sand

A formal contract dated 5th February 2016 was executed between the Government and the Contractor, in the Standard Form of Contract PWD203A; a contract with BQ in the sum of RM48,000,000.00. The contract stipulated the Date for Possession of Site as 1st December 2015 and the Date for Completion of the Works as 30th November 2017, which is a construction period of twenty-four (24) months. The construction period has been extended to 18th April 2019 since there were three (3) Extensions of Time (EOT) granted. The scope of dispute for this project is riverbank protection.

The original quantity in the contract for the sand filling is 180,000m^3. However, the quantity has been increased to 530,000 m^3 due to erosion. The Contractor has claimed RM23,000,000.00 for the additional work. The Contractor alleged that the settlement occurred for the whole stretch of the project from Zone A CH0- CH1700 (1700 m) and Zone B CH 2150-CH 2450 (300 m). This incident happened in 2017, and the Contractor has done the re-filling works to reach the final level due to the loss of materials. All the incidents have been recorded in the site diary, and the survey works have been done by the Contractor.

The S.O., on the other hand, opined that the Contractor did not perform the works in a proper manner and in accordance with good management practices and to the best advantage of the Government. This is stipulated in Clause 10.0 (b) of PWD 203A. The Contractor also failed to take the necessary steps to mitigate the loss of material.

Furthermore, the S.O. solely relies on the provision stated in the Specification, *"Method of Filling 5001 Weather, Tidal Risk and Precautions; (2) Without limiting his liabilities under the contract, the Contractor shall take all necessary precautions to protect permanent works, temporary works, plant and equipment against the effect of weather, tidal and marine conditions."* Therefore, the Contractor is not entitled to any claim.

The S.O. refuted the Contractor's claim that the cause for the additional quantity of sand filling was due to settlement. In order to establish the cause for settlement, soil investigation must be carried out in order to determine the characteristics of the soil which had not been taken into account by the engineer during the design stage.

The issue is whether the Contractor should be paid for the re-filling of the placed materials, which includes maintaining of levels during construction. The S.O. refuted the Contractor's claim on the grounds of the provision in the specification; *"Method of Filling 5022 Allowance for Settlement; Where approved by the S.O. or his representative, the Contractor may place additional material in advance to allow for such settlement all at no additional cost to the Government, provided that the S.O. or his representative is satisfied that this will not jeopardize stability. Notwithstanding any such approval, the Contractor shall remain solely responsible for any instability*

which might occur and bear for any additional cost incurred" and *"Method of filling 5023 Final Levels (2); The Contractor shall entirely be responsible for maintaining the lines and levels of the placed materials during construction and for making good any losses due to any cause whatsoever at his own expenses. This may include losses of lines and levels due to settlement of the underlying soil losses of materials placed*."

The Contractor challenged the S.O. by submitting their joint survey data as evidence for the re-filling works. The joint survey was done by the Contractor and the S.O.'s representative during settlement. The Contractor contended that due to the long waiting period for S.O.'s decision, the Contractor had to commence work in order to complete the work. The S.O. was adamant that the responsibility of re-filling materials until completion belonged to the Contractor based on the provision as stated in the Specification. As a result of this dispute, the Contractor refuses to sign the Final Account, and the case is still ongoing.

3.2   Project No. 2: Quantity of Armour Rock

A formal contract dated 24th March 2017 was executed between the Government and the Contractor, in the Standard Form of Contract PWD203A; a contract with BQ in the sum of RM200,000,000.00. The contract stipulated the Date for Possession of Site as 13th December 2016 and the Date for Completion of the Works as 12th December 2019, which is a construction period of thirty-six (36) months. The construction period has been extended to 20th September 2020 since there were three (3) Extensions of Time (EOT) granted. This project consists of the construction of breakwaters with revetment and training wall at the river mouth of Sungai Kemaman, Terengganu.

During the placement of armour rocks at the breakwaters, it was identified the quantity had exceeded the provisional quantities in the contract. The Contractor submitted a claim of additional quantities of armour rock due to settlement and design fault of the breakwater.

The Contractor then appointed soil investigation experts and specialist geotechnical consultants to support their claims. Based on the report findings and the survey data, the additional quantity of armour rock was estimated at $324,000 \, \text{m}^3$ with the cost incurred of RM37,000,000.00. This matter was prolonged due to the S.O.'s inability to make a decision. The Contractor also appealed for the works to be suspended and will only resume with the works until a decision has been made.

The S.O., however, disagreed with the Contractor's claims based on the calculations and report by the consultant engineer appointed by the Government. The S.O. refuted the Contractor's claim on the grounds of the provision in the specification;

"Quarry Armour Rocks: The Contractor shall include in his offer, the requirement of over height or extra volume of rock to cater loss due to settlement in the soft ground and all cost/rates deemed inclusive of the matter"; "Settlement: The rate in the Bill of Quantities shall include for all settlement as may arise, and payment

will be made based on the quantity computed from pre-filling and final post-filling surveys multiplied by the rates from the bills of quantities"; and "Topping Up Rocks: The Contractor is required to deliver the crest level of the breakwater as shown in the drawing until toward the end defect liability period. Any topping up of rocks required to maintain the level at the end of the defect liability period shall be solely the Contractor's responsibility. The topping up rocks shall be according to the size of the design as shown in the drawing."

However, the Contractor argued that this is a construct only contract whereby the design liability belongs to the Government. The Contractor has priced the tender for the works based on the drawing, BQ and specifications provided in the tender. Any changes to the abovesaid shall cause a variation to the contract based on the scope, time and price involved to be determined in accordance with the terms and conditions of the contract. This includes soil conditions. The Contractor was dissatisfied with the Government's decision and had referred this dispute to arbitration. This is stipulated in Clause 66.3 of PWD203A.

Based on the above two cases, we would like to compare with the provision in the FIDIC Form of Contract whereby action to be taken when encountering unforeseeable conditions are clearly outlined. Clause 4.12 of the FIDIC Form of Contract clearly defines the meaning of unforeseeable physical conditions. In the same clause, specified procedures are outlined in the event if the Contractor encounters physical conditions that the Contractor considers to have been unforeseeable and may have adverse effects on the progress and/or increase the cost of the execution of the works. Furthermore, clients are able to modify the general conditions and guidance provided to assist the drafter by giving options for various sub-clauses where appropriate. For instance, vis å vis Clause 4.12, alternative risks allocation is provided if the project involves significant sub-surface works or hydrological conditions.

Whereas the PWD203A, which is commonly used in DID projects, contains the provisions in dealing with unforeseeable conditions under Clause 10.0(f). However, the actions to be taken by both parties are outlined very generally, whereby the risks of unforeseeable conditions encountered at the site are explained in the specifications and preamble to the BQ. Contractors are cautioned to take necessary actions in protecting placed materials.

4 Root Causes and Consequences of Disputes

4.1 Additional Costs Incurred by the Government Due to Misinterpretation

The Government is always the losing party. Whenever the TW and MRC items are overpriced, the Contractor will demand full payment under the presumption that it is considered as a Lump Sum item, and therefore, full payment must be made regardless

if the work is executed or not. The provision in MyCESMM2 also clearly states that MRC items are not subjected to be measured.

If the items are under-priced, additional claims will also be submitted by the Contractor to the Government on the grounds of natural justice that all works properly done must be paid accordingly. In addition, the MRC is not in accordance with the requirements of PWD203A, where all works must be properly described in the BQ, supported by detailed design and specification.

4.2   Additional Costs by the Government Due to Unfair Risk Allocation

In a conventional contract whereby the client provides the design, the risk of default in design is borne by the client. In order to rectify this, variation orders can be issued under the terms provided in the contract. Often occurred, while remedial action can be taken, the lack of necessary mitigation works will contribute to the continuing loss of materials. Thus, it becomes the basis of additional costs claimed by the Contractor.

The main responsibility of the Contractor is to carry out the construction of the work that is required for the completion of a project. Obligations of the Contractor are outlined in Clause 10.0 (b) of PWD203A. Therefore, any additional costs incurred due to poor workmanship, which includes loss of materials, shall be borne by the Contractor.

Also, one of the common risks prevalent in construction projects is the effect of natural events, whether anticipated or beyond reasonable contemplation. Despite the measurement of severity of the effect, it will somehow incur extra costs to the construction inevitably. Due to this, it is common in construction contracts to transfer the risk to the Contractor. And it is not the exception for DID's contracts. Nonetheless, Contractors will find ways to claim if it involves substantial amounts of money at their ends.

5   Best Practice Resolutions

5.1   Temporary Work

TW is a crucial part of the construction process that will determine the construction operations at the site. As a major component in the contract, the execution of TW must be thoroughly identified and itemised in the BQ to avoid disputes during the construction stage. The common practice in DID that leaves the Contractor to decide and itemise TW under MRC has proven to be ineffective since it has caused millions of ringgit in terms of losses to the Government.

However, to get the best value for money to both parties and the best practice in itemising the TW, it is recommended that the engineer has to provide the basis for accurate pricing by inserting the following documents during the tender stage:

(i) Detailed drawings, specifications and information of the TW;
(ii) Soil Investigation (SI) Report; and
(iii) Properly itemising the TW in the BQ

The failure to provide the abovementioned documents is usually stemmed from arguments provided by the engineer. It is often pointed out by them that TW is an alternative method to execute the works thus should not be identified and itemised by the engineer who prepared the designs and BQ. Therefore, it is solely at the discretion of the Contractor to identify and suggest the most effective method for them.

In consideration of the arguments, it is then fair to ask the engineer why the designs and works must be identified and itemised by the Contractor since MRC are actually an alternative method to execute the work as per individual preference. It is unfair to transfer all of the engineer's liabilities and responsibilities towards the Contractor since the functions and expertise of the parties differ from one to another. The engineers are the designer, whereby the Contractor is the builder who constructs based on the design. Any switching of roles between the two parties must be agreed upon and reasonable within their respective expertise.

Also, reference to MyCESMM2 clearly states MRC as not mandatory. It is merely a pricing tool to represent the ability of the individual Contractor to propose different methods of executing the works but not the ability of the Contractor to identify, design and propose the job scope. Therefore, it is suggested to totally omit the item for MRC from the BQ.

Another way of resolving the issues would be to conduct tender interviews with the Contractors as a way to obtain further clarification from them regarding their construction methods and pricing. Since the current Government procedures do not allow for this option, the department may need to get the necessary approval from a higher authority, namely the Ministry of Finance (MOF) Malaysia, to introduce the interviewing of Contractors as part of our overall procurement method.

5.2 Unforeseeable Hydrological Conditions

It is an important consideration to allocate clear and sufficient provisions in carrying out the related works in the contract. In addition, it is best to specify actions to be taken by both parties in the event of encountering unforeseeable hydrological conditions. This is to eliminate ambiguities in determining causes of the events and appropriate interventions can be carried out to avoid prolonged issues which will eventually result in contractual disputes.

In PWD203A, provisions on how to deal with unforeseeable hydrological conditions are outlined generally in the conditions of contract. These risks are explained

in the specifications and preamble to the BQ. Contractors are cautioned to take necessary actions in protecting placed materials.

It is clearly specified above that the burden to ascertain uncertainties factors such as loss of material and other similar risks falls under Contractor. To be able to offer a competitive price, Contractors are prone to ignore pricing in the BQ. Hence, eventually finding any means to claim when they have to bear exorbitant additional costs.

Therefore, it is crucial for both Contractor and S.O. to take appropriate and necessary actions in the event of facing issues of unreasonable, excessive quantities due to settlement. Matters to be considered in order to mitigate the further loss which results from claims are:

(i)   Both Contractor and S.O. should adhere strictly to provisions in the specifications that is executing proper joint surveys, continuous monitoring, protections of placed materials which will help the S.O. in determining the cause of event when it arises. The Contractor should immediately inform S.O. of the occurrence of any factor or event which is likely to affect the works. Immediately after receiving such notification from the Contractor, S.O. should take necessary actions to determine the cause of event; possible site investigation, assessing information on weather, tidal and marine conditions and etc.;

(ii) Proper records of site activities during construction;

(iii) The S.O. must engage independent surveyors to evaluate survey data submitted by the Contractor;

(iv) Immediate mobilisation of particular experts, i.e. geotechnical, hydrological, forensic and etc. to carry out inspection and investigation upon receiving notification from the Contractor on the event;

(v)   Clear and sufficient procedure to be taken when encountering unforeseeable conditions should be provided in the conditions of the contract;

(vi) Pursuit of a fair and equitable distribution of risk in the cause of natural events or acts of God. Transferring the risks solely to the Contractor will eventually result in claims when the Contractor has to bear exorbitant additional costs. [2] states, "*proper risk identification and equitable distribution of risk is the essential ingredient to increasing the effective, timely and efficient design and construction of projects*". While Lane (2005) states, *"[a] contract which balances the risks fairly between a Contractor and an employer will generally, in the absence of bad faith, lead to a reasonable price, qualitative performance and the minimisation of disputes."* It is recommended to improve the conditions of the contract to consider 50–50 allocation risks when it comes to the effect of natural events or acts of God. In this case, adoption of the FIDIC Form of Contract on this matter can be a consideration; and

(vii) Establish engineering solutions to the open-ended scope of works such as continuous dredging work prior to practical completion and/or end of defect liability period due to sedimentation.

6   Conclusion

Managing disputes in water management contracts are indeed challenging, particularly from the DID perspective. Two common types of disputes often faced by DID has been discussed that is, temporary work and issues on unforeseeable hydrological conditions. This paper has suggested best practice resolutions that may facilitate improvements in managing each dispute.

In dealing with disputes relating to temporary works, three (3) suggested approaches that can be adopted are:

 (i)   providing sufficient documents as a basis for accurate pricing during the tender stage;
 (ii) omitting the item for MRC from the BQ; and
 (iii) conducting tender interviews with the Contractor for clarification on construction methods and pricing.

The second dispute that has been discussed is on unforeseeable hydrological conditions. For this reason, there are seven (7) suggested approaches in managing this dispute, which are:

 (i)   strict adherence by the Contractor and S.O. to the provisions in the specifications in relation to the execution of joints surveys, continuous monitoring and protection of placed materials,
 (ii) proper records of site activities during construction,
 (iii) engagement of independent surveyors by the S.O.,
 (iv) immediate mobilisation of particular experts by the S.O. to inspect and investigate upon receiving notification from the Contractor on the event,
 (v)   the provision in the Conditions of Contract a clear and sufficient procedure to be taken when encountering unforeseeable conditions;
 (vi) improving the existing Conditions of Contract by adopting the FIDIC Form of Contract for a 50–50 with risk allocation in the effect of natural event or act of God; and
 (vii) establish engineering solutions to the open-ended scope of works.

The issues highlighted in this paper serve as useful lessons for us to learn from and to avoid repeating them in our projects. Thus, by adopting some, if not all of the resolutions presented, we can move forward by charting a path for a better way to manage the disputes that will benefit both the department and the Contractor.

References

1. Board of Engineers Malaysia (2015) Guidelines No.: 001 - roles and responsibility of professional engineers for temporary works during construction stage, Kuala Lumpur: s.n.
2. Bryan Shapiro QC (2010) Transferring risks in construction contracts, p 17

3. Construction Industry Development Board Malaysia (2018) Malaysian civil engineering standard method of measurement (MyCESMM2), 2nd edn, Kuala Lumpur
4. Department of Irrigation and Drainage (DID) (2016) Section 6 - specifications for breakwater & coastal protection works, Kuala Lumpur
5. Federation Internationale des , Ingenieurs, -Conseils (FIDIC) (2017) Conditions of Contract for Construction, 2nd edn. FIDIC Publication, Geneva
6. Patrick Lane SC (2005) The apportionment of risk in construction contracts. Int Constr Law Rev 20:6. Part 1
7. Public Work Department Malaysia (2010) PWD Form 203A (Rev. 1/2010). Government of Malaysia, Kuala Lumpur

Hydro-Environment

The Hydro-Environment section presents papers related to various open channel hydraulics and environmental issues beneficial to practising engineers and researchers. These issues were investigated experimentally and simulated using multiple types of software. The first few papers dealt with flow resistance in open channel flow due to the interaction of vegetation and alternate bars from sediment deposition, the relationship between discharge, Froude number and bed width in the flow branches. The performance of porous concrete drainage systems and concrete curbs were also tested in a laboratory and presented in this section. Paper on environmental aspects presents a laboratory study to understand the influence factor of ammoniacal nitrogen removal. A case study on the relationship between river ecosystems and benthic macroinvertebrate ecological indices was presented as part of an indicator for river health. There are also papers related to numerical simulations using software such as Autodesk Infraworks 360, TELEMAC2D, Flow3D, The InfoWorks ICM and EPANET. These simulations cover problems ranging from drag coefficient in a sphere, pressure head in a partially submerged orifice, axial flow characteristics in a submersible pump, channel branches and dam breaching to the estimation of water demand. A proposal for a new dam safety and management is presented as Risk-Informed Decision-Making (RIDM). It is a program that integrates engineering, cybersecurity and socioeconomic elements to minimize the risks of dam failure. Research that extracts public sentiments and opinion on water-related issues in an unstructured text from Twitter are also presented. Finally, the historical method of institutional arrangements of water extraction in Oman using the *aflaj* (singular *falaj*) was revisited.

The Influence of Vegetated Alternate Bar on Flow Resistance in an Alluvial Straight Channel

M. Z. M. Salleh, Z. Ibrahim, R. Saari, M. E. Mohd Shariff, and M. Jumain

Abstract Alternate bars significantly affect river characteristics, especially bed roughness and flow resistance. Additionally, the presence of vegetation on the bar surface impacts river hydrodynamics and morphology significantly. However, the details on their impacts are insufficient for us to interpret. This study analyzes the interaction of vegetation and alternate bars with the flow resistance in an alluvial river. The study aims to investigate the bed roughness parameters of Darcy's friction factor and Manning's roughness coefficient that impacted from vegetated alternate bars. The study was based on experimental analysis. A straight flume channel 10 m long and 1 m wide was used with bed material of uniform sediment size 0.8 mm. The measurement was made based on the seven cross-sections created along the channel. The obtained results revealed that the friction factor and Manning's roughness coefficient were significantly increased on the vegetated alternate bar compared with the other areas in the channel. Thus, the resistance of flow increased around the vegetated alternate bar as the bed roughness increased.

Keywords Alternate bar · Vegetation · Flow resistance · Bed form · Straight channel

1 Introduction

The alternate bar is one of the bed features that are visible in an alluvial river. It normally occurs with macro size in a straight alluvial channel [24]. The alternate bar is defined as the deposition of sediment that is two times longer in size than the channel width [5, 7]. This bar is formed in a sequence in which each bar is attached to the bank with successive bars attached to opposite banks [19]. This type of bar is usually

M. Z. M. Salleh (✉)
School of Civil Engineering, College of Engineering, Universiti Teknologi MARA Pasir Gudang, Johor, Malaysia
e-mail: kayzul00@gmail.com

M. Z. M. Salleh · Z. Ibrahim · R. Saari · M. E. Mohd Shariff · M. Jumain
School of Civil Engineering, Faculty of Engineering, Universiti Teknologi Malaysia, 81310 UTM Johor Bahru, Johor, Malaysia

not stable and migrates downstream [8, 11]. The presence of an alternate bar has negative impacts on the river system as it alters the hydrodynamics and morphology of the river [6, 14]. The flow and roughness conditions are changed, followed by the presence of an alternate bar [1, 4]. The formation of an alternate bar is an initial development of the meandering channel [23]. The alternate bar also diverts the flow directly into the thalweg to produce significant erosion that is established from the increase in velocity at the area [27]. Duró et al. [13] had produced a formula for determining the behaviour of alternate bar formation in rivers based on the number of bar modes. The bar mode number (m), is the number of braid levels that form in each measured cross-section of the river. Single, double, and multiple rows of river bars are defined as mode 1 when m = 1, mode 2 as m = 2, and mode 3 of m > 2, respectively. Equation 1 is used to determine the bar modes.

$$\mathrm{m}^2 = 0.17\,\mathrm{g}\frac{(b-3)}{\sqrt{\Delta}D_{50}}\frac{B^3 S}{C Q_w}. \tag{1}$$

where m is the bar mode, b is the degree of nonlinearity in the relation between sediment transport rate and depth-averaged flow velocity, B is the channel width, S is the longitudinal channel gradient or bed slope, $\triangle$ is the relative submerged mass density of the sediment, D_{50} is the median grain size, C is the Chezy coefficient for hydraulic resistance, and Q_w is the water discharge.

In the natural alluvial river, the alternate bar is formed from the instability of flow and sediment [16]. The alternate bar may form in several conditions of non-vegetated and vegetated bars [17, 22]. The vegetated bar is formed when the vegetation grows on top of the bar surface. The vegetation may form as non-woody and woody based on the ages of the alternate bar [9]. The longer the bar stand gives more time for vegetation to grow. Many researchers have studied the formation, stability, and influences of alternate bars [3, 5, 10, 12, 20, 26, 29, 30]. Several findings were established related to the alternate bar. They discovered the dimensional and dimensionless behaviours of alternate bars. The dimensional parameters that are commonly considered are wavelength, height, and wavenumber of alternate bars [25, 28]. In addition, the dimensionless parameters involved are the bed shear stress and shield parameter. They also found that several factors could contribute to alternate bar formation, such as hydraulic conditions, sediment properties, cohesion and cohesionless sediment, bedload and suspended load, sediment supply, channel uniformity, channel slope, and vegetation conditions. Among those studies, most of the investigations focused on non-vegetated rather than vegetated alternate bars. Therefore, the present study initiates the analysis of the behaviour of woody vegetated alternate bars that focus on straight alluvial rivers. The purpose of the study is to analyze the impacts of the vegetated alternate bar on the flow resistance capacity in the river. The discussion of the study based on the bed roughness parameters includes Darcy's friction factor (f) and Manning's roughness (n) coefficient, as shown in Eqs. 2 and 3.

$$f = \frac{8gRS_0}{U^2} \tag{2}$$

where g is gravitational acceleration, R is the hydraulic radius, S_0 is the channel bed slope and U is the mean streamwise velocity.

$$n = \frac{R^{2/3} S_0{}^{1/2}}{U} \tag{3}$$

where R is the hydraulic radius, S_0 is the channel bed slope, and U is the mean streamwise velocity.

2 Methodology

The study was based on the experimental approach. A straight flume channel with a length of 10 m and a width of 1 m located in the hydraulic and hydrology laboratory of Universiti Teknologi Malaysia was utilized. The flume channel was filled with 15 cm high 0.8 mm sediment as bed material. The initial bed remained in a flat condition and the bed slope was set to 0.002 m/m. The experiment started when the water was flowing into the channel with a lower flow rate of 2 to 3 L/s to ensure that the bed material was naturally compacted. Then, the flow of water was increased gradually until the required flow was achieved and maintained until the experiment was completed. The flow depth and width of the channel are the main parameters in determining the width to depth ratio (β) [7, 21, 29]. In this study, we used two different flow rates of 15 L/s and 20 L/s with width to depth ratios of 21 and 17, respectively. These values were utilized as they were suitable for the formation of alternate bars, according to Kuang [18]. The water was recirculated until the experiment was stopped. The sediment catcher was created at the outlet of the flume channel used to monitor sediment transport. The experiment was stopped when the channel achieved an equilibrium condition in which there was no major change in bed condition and a minor sediment load trapped in the sediment catcher.

The experiment was monitored for bed and velocity changes. A digital camera was used to capture the bed changes and was later processed in a computer for the bed topography condition. For the velocity measurements, an electromagnetic current meter was used to determine the velocity along the channel.

The experiment was started and continued until the non-vegetated alternate bar (NV) was formed and the flow and bed changes were observed. After that, steel rods of 5 mm diameter with 5 cm spacing were installed in a fully covered bar area. These rods represent the vegetation stem grown on top of the bar surface [31]. The experiment was continued again until the equilibrium state was achieved. Again, the bed and flow conditions were observed with the condition of a fully vegetated alternate bar (FV). One cycle of the experiment with a required flow rate was completed after all two steps were applied. Figure 1 shows the final condition of bed topography for non and full vegetation cover after the experiment was completed.

Six experiments were tested with both conditions of alternate bars. Seven cross-sections were marked as measurement stations CH200, CH300, CH400, CH500,
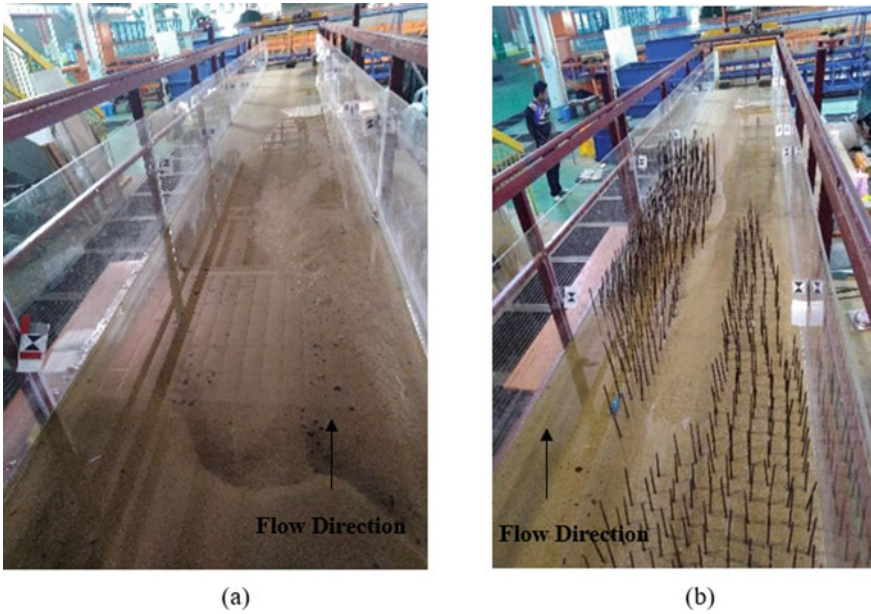
Fig. 1 Final condition of bed topography after the experiment was completed. **a** Non-vegetated bar, **b** full vegetation bar

CH600, CH700, and CH800. The first and last stations of CH200 and CH800 were located 2 m after and before the inlet and outlet, respectively to ensure that the area of observation was not affected by any non-uniform flow and bed changes such as backwater and channel boundary conditions. The other stations were located at 1 m intervals. Figure 2 shows the locations of the measurement stations used in the flume channel and the details of the experiment are shown in Table 1.
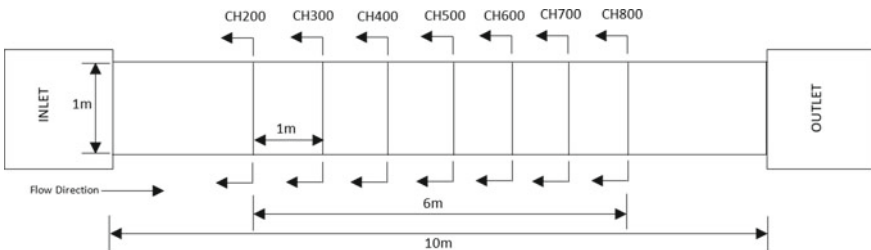
Fig. 2 Location of measurement stations along the flume channel

Table 1 Details of the parameters used in the experiment

Exp no	Q(1/S)	Sediment supply rate (g/s)	Vegetation cover	Fr	D_0(m)	Re	β	ds
1a	15.3	–	NV	0.41	0.047	17745	21	0.01
1b	15.17	–	FV	0.4	0.047	14841	21	0.01
2a	15.68	5	NV	0.39	0.047	9690	21	0.01
2b	15.68	5	FV	0.36	0.047	12750	21	0.01
3a	20.09	5	NV	0.36	0.069	21113	17	0.01
3b	20.23	5	FV	0.35	0.065	18809	17	0.01

3 Results and Discussion

The observation showed that the alternate bar formed in all experimental conditions proving that the width to depth ratio of 21 and 17 within the range of 10 to 50 could induce alternate bar formation—Experiment 1. A lower flow rate and without sediment feeding shows only one alternate bar formed in both conditions with and without vegetation. In experiment 2, with a similar flow rate but with sediment feeding, one bar formed under non-vegetation conditions and two bars formed under vegetation cover with larger wavelengths and heights. This could prove that the relationship of vegetation and sediment feeding that induced the sediment transport rate turned the bedform into an active mode to produce more bar formation. This was also agreed upon by Venditti et al. [32]. For experiment 3, with a higher flow rate and with sediment feeding, two bars formed in non and full vegetation. However, in the half-vegetation condition, Bar 2 vanished and a new bar formed downstream that was marked as BAR 3 as shown in Fig. 3(C). The erosion process occurred in the area of BAR 2, even though this bar has vegetation cover. Even though vegetation could reduce the flow capacity, it could not affect the higher flow rates. This finding was also in agreement with the bar mode analysis of Duró et al. [13] as the value of m = 1 for both experiments except for the condition of full and vegetation in experiment 3 where m = 2 to form central bar.

The bar formed in the area of CH200 to CH400 in experiment 1. In experiment 2, the bar formed in the area of CH200 to CH400 for BAR 1 and CH400 to CH700 for BAR 2. Experiment 3 formed in areas CH200 to CH600 for BAR 1, CH500 to CH700 for BAR 2, and CH500 to CH800 for BAR 3. This study focused on flow resistance analysis at these stations located in the area of alternate bar formation. It was found that the relationship of flow, sediment, and vegetation played an important role in controlling the formation and stability of the alternate bar. The change in bed topography could alter the bed roughness conditions.

The bedform and vegetation increased flow resistance in the channel. This result agreed with findings by many researchers [13, 22, 26, 33]. However, there were insufficient findings on the combined effects of vegetation and bedform on flow resistance. Therefore, this study focused on the impacts of bedform with vegetation on flow resistance. Darcy's friction factor and Manning's roughness coefficient
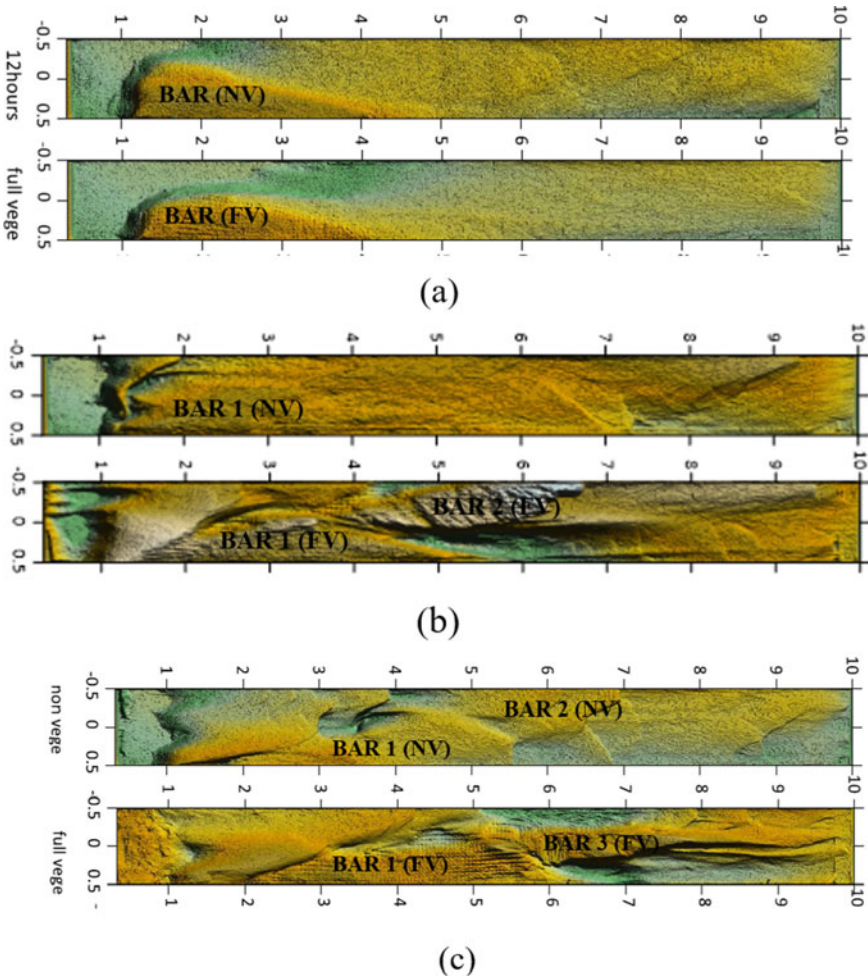
Fig. 3 Formation of an alternate bar in all experiments with and without vegetation, **a** experiment 1, **b** experiment 2, and **c** experiment 3

were used as indicators to measure the behaviour of bed roughness that affected the condition of flow resistance.

Figure 4 shows the normalized condition of the friction factor (f) at each station for both experiments with all conditions of vegetation cover. The friction factor for the NV condition was higher at CH200, CH300, and CH400, with values of 0.0006, 0.001, and 0.0006, respectively, as shown in Fig. 4(a) of experiment 1. CH200 to CH400 are the areas of alternate bar formation, as shown in Fig. 3(a). Thus, it could be seen that the alternate bar increased the friction factor and induced higher flow resistance. In addition, when the vegetation was installed in full cover (FV), the

(a)

(b)

(c)
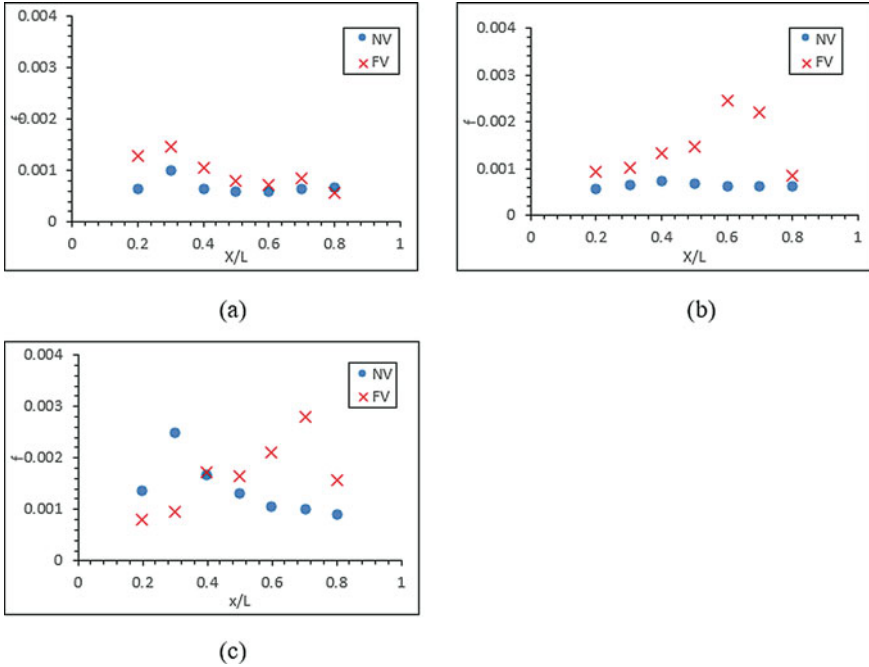
Fig. 4 The relationship of friction factor with alternate bar formation at each measured cross-section. **a** experiment 1, **b** experiment 2, **c** experiment 3

friction factor increased higher at similar locations by 0.0013, 0.0015, and 0.001, respectively.

A similar situation occurred in experiment 2, as shown in Fig. 4(b). The Friction Factor was almost constant along the NV channel. However, it changed after the vegetation was installed on the bar surface. The highest friction factor was at CH600, with a value of 0.0025. This station is also located in the area of bar formation (BAR 2). This explained why the vegetation increased bed roughness and thus reduced velocity.

In experiment 3, with a Q equal to 20 L/s, the friction factor was still higher at the area of bar formation. It was highest at CH300 at the location of BAR 1 for NV and CH700 at BAR 3 of FV, as shown in Fig. 4(c). The friction factor decreased at CH300 and increased at CH700 after the vegetation was applied. This situation occurred because Bar 3 formed in CH700, which is a new bar that occurred at the centre of the channel after BAR 2 vanished. The change of alternate bar to central bar followed by the change of bar mode from m = 1 to m = 2. The friction factor also changes in parallel with this condition. The increased value of the friction factor at the central bar proved that the vegetated central bar, normally known as the vegetated mid-channel bar, produced even more resistance of flow to reduce the friction factor in the other areas, including the area of BAR 2. This finding agreed
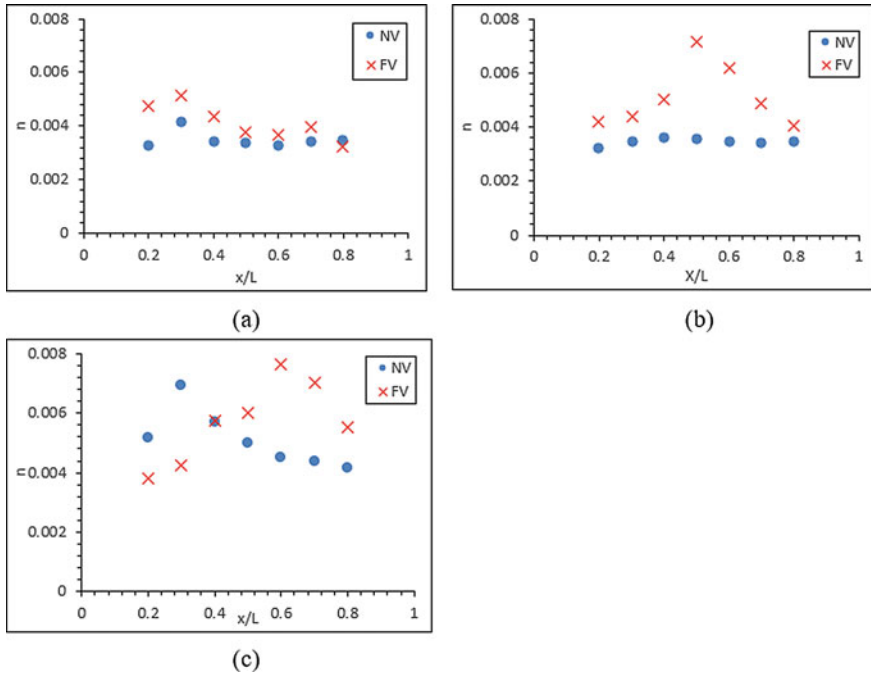
Fig. 5 The relationship of Manning's n with alternate bar formation at each measured cross-section. **a** experiment 1, **b** experiment 2, **c** experiment 3

with the previous investigation of Gurnell and Bertoldi [15]. Thus, BAR 2 vanished as the flow increased due to the reduction in bed roughness.

Furthermore, Figs. 4(a) to (c) show that the value of the friction factor at each station was higher in experiments 2 and 3 than in experiment 1, especially for the vegetation condition. This proves that the existence of sediment feeding could induce more flow resistance in the channel, as mentioned by Bankert [2], Venditti et al. [32].

Other than the analysis of the friction factor, the study also provides an analysis of Manning's n. This analysis was used to enhance the findings from the investigation of friction factors. In general, the n-value analysis was almost similar to the friction factor. The n-value was higher at the area of alternate bar formation, and it increased even higher when the vegetation was installed on the bar surface.

Figure 5(a) shows that the value of n for NV was higher at CH200, CH300 and CH400, with values of 0.0033, 0.0042, and 0.0034, respectively. Then, it increased higher with values of 0.0048, 0.0051, and 0.0043, respectively, at each station for FV after the vegetation was installed. The average increment was approximately 30.8% for all three stations. A similar situation occurred in experiment 2, as shown in Fig. 5(b). The value of n was almost constant at all stations in NV and increased to a maximum of 0.0072 at station CH500 within the area of bar formation. The n-value rapidly increased at this station after vegetation was installed with a percentage

increment of 99%. In experiment 3, as shown in Fig. 5(c), a similar condition occurred as the friction factor, where the formation of the mid-channel bar changed the value of n, where its highest value was at CH300 of 0.0069 in the NV condition. However, it dropped in the FV condition, and the highest location changed at CH600 with a value of 0.0076 due to the formation of a central bar.

4 Conclusion

This study is a collaborated research between Universiti Teknologi MARA Pasir Gudang Branch and Universiti Teknologi Malaysia. The research was funded by the Fundamental Research Grant Scheme (FRGS) No. 5F089. The authors would like to acknowledge those who were involved directly and indirectly in this project, in particular, UiTM Pasir Gudang and UTM, for providing research facilities and manpower.

References

1. Aliaga J, Flores E, Link O, Hellwig F, Jeldres F, Laborde A (2020) The impact of vegetation on sedimentation on alluvial bars along the Carampangue River, Chile. River Flow 2020:1589–1594. https://doi.org/10.1201/b22619-221
2. Bankert A (2016) Alternate bar dynamics in response to increases and decreases of sediment supply. Master thesis, Colorado State University
3. Calvani G, Francalanci S, Solari L (2018) Flume experiments on vegetated alternate bars. E3S Web Conf 40:1–6. 02034
4. Carlin M, Redolfi M, Tubino M (2020) Effect of flow unsteadiness on the long-term evolution of alternate bars. River Flow 2020, August, pp 539–547. https://doi.org/10.1201/b22619-76
5. Chang HH (1985) Formation of alternate bars. J Hydraul Eng 111(11):1412–1420
6. Claude N, Rodrigues S, Bustillo V, Bréhéret JG, Tassi P, Jugé P (2014) Interactions between flow structure and morphodynamic of bars in a channel expansion/contraction, Loire River, France. Water Resour Res 50(4):2850–2873
7. Colombini M, Tubino M (1991) Finite amplitude free-bars: a fully nonlinear spectral solution. Sand Transport in River, Estuaries and Sea
8. Cordier F, Tassi P, Claude N, Crosato A, Rodrigues S, Pham Van Bang D (2020) Bar pattern and sediment sorting in a channel contraction/expansion area: application to the Loire River at Bréhémont (France). Adv Water Resour 140:103580. https://doi.org/10.1016/j.advwatres.2020.103580
9. Crosato A (2019) River channel formation and response to variations in discharge, sediment and vegetation. The XXXVIII International School of Hydraulics, Łąck, Poland, pp 21–24

10. Crosato A, Desta FB, Cornelisse J, Schuurman F, Uijttewaal WSJ (2012) Experimental and numerical findings on the long-term evolution of migrating alternate bars in alluvial channels. Water Resour Res 48(6)
11. Crosato A, Getaneh AA, Desta FB, Uijttewaal WSJ, Le U (2010) Long-duration laboratory experiment of slow development of steady alternate bars. River Flow 2010:1035–1039
12. Defina A (2003) Numerical experiments on bar growth. Water Resour Res 39(4):1–12
13. Duró G, Crosato A, Tassi P (2016) Numerical study on river bar response to spatial variations of channel width. Adv Water Resour 93:21–38
14. Francalanci S, Solari L, Toffolon M, Parker G (2012) Do alternate bars affect sediment transport and flow resistance in gravel-bed rivers? Earth Surf Proc Land 37(8):866–875
15. Gurnell AM, Bertoldi W (2020) Extending the conceptual model of river island development to incorporate different tree species and environmental conditions. River Res Appl 36(8):1730–1747
16. Ikeda S (1984) Prediction of alternate bar wavelength. J Hydraul Eng 110(4):371–386
17. Jourdain C, Claude N, Antoine G, Tassi P (2018) Influence of flood regime on riparian vegetation dynamics in rivers with alternate bars 02025:1–8
18. Kuang H (2011) Physical and numerical modelling study of meandering in fluvial rivers. Ph.D. thesis, Cardiff University
19. Lanzoni S (2000) Experiments on bar formation in a straight flume 1. Uniform sediment. Water Resour Res 36(11):3337–3349
20. Lanzoni S, Tubino M (1999) Grain sorting and bar instability. J Fluid Mech 393:149–174
21. Lisle TE, Ikeda H, Iseya F (1991) Formation of stationary alternate bars in a steep channel with mixed-size sediment: a flume experiment. Earth Surf Proc Land 16(5):463–469
22. Mao L, Ravazzolo D, Bertoldi W (2020) The role of vegetation and large wood on the topographic characteristics of braided river systems. Geomorphology 367
23. Muramoto YF, Fujita Y (1985) Studies on the process of development of alternate bars 35(3):55–86
24. Redolfi M (2021) Free alternate bars in rivers: key physical mechanisms and simple formation criterion. Water Resour Res 57(12). https://doi.org/10.1029/2021wr030617
25. Redolfi M, Welber M, Carlin M, Tubino M, Bertoldi W (2020) Morphometric properties of alternate bars and water discharge: a laboratory investigation. Earth Surf Dyn 8(3):789–808. https://doi.org/10.5194/esurf-8-789-2020
26. Rominger JT, Asce SM, Lightbody AF, Asce AM, Nepf HM (2010) Effects of added vegetation on sand bar stability and stream hydrodynamics. J Hydraulic Eng 994–1002
27. Salleh MZM, Ibrahim Z, Jumain M, Saari R, Fathullah MFM, Ismail Z, Jamal MH (2020) Simulation of flow profile response to alternate bar formation in rivers. In: Lecture notes in civil engineering, vol 53, pp 1209–1218
28. Shimizu Y, Nelson J, Arnez Ferrel K, Asahi K, Giri S, Inoue T, Iwasaki T, Jang CL, Kang T, Kimura I, Kyuka T, Mishra J, Nabi M, Patsinghasanee S, Yamaguchi S (2020) Advances in computational morphodynamics using the International River Interface Cooperative (iRIC) software. Earth Surf Proc Land 45(1):11–37. https://doi.org/10.1002/esp.4653
29. Schielen BR (1993) On the nonlinear dynamics of free bars in straight channels. J Fluid Mech 252:325–356
30. Serlet A, Koch A, Zolezzi G (2018) Observations of morphological and vegetation dynamics in regulated rivers with alternate bars. In: 12th ISE 2018, Tokyo, Japan
31. Vargas-Luna A, Crosato A, Calvani G, Uijttewaal WSJ (2016) Representing plants as rigid cylinders in experiments and models. Adv Water Resour 93:205–222
32. Venditti JG, Nelson PA, Minear JT, Wooster J, Dietrich WE (2012) Alternate bar response to sediment supply termination. J Geophys Res Earth Surf 117(2):1–18
33. Wintenberger CL, Rodrigues S, Bréhéret JG, Villar M (2015) Fluvial islands: first stage of development from nonmigrating (forced) bars and woody-vegetation interactions. Geomorphology 246:305–320

A Mathematical Study of the Relation Between Discharges, Froude Number, Bed Width in Dividing Open Channel Flows

Puteri Nadia Shafiqah Harmizi, Iskandar Shah Mohd Zawawi, Mohd Ridza Mohd Haniffah, Taufiq Khairi Ahmad Khairudin, and Hazleen Aris

Abstract Open-channel with branches makes the channel flow more complex and difficult to analyse due to the complex variables and a large number of geometric properties related to the junction. The aim of this paper is to employ the mathematical model to investigate the relationship between discharge, Froude number and bed width in the dividing open-channel flow. Several assumptions have been made and input values are taken from the literature to solve the proposed model. Results indicated that the highest discharge ratio is obtained when the dividing angle at channel 2 is 30°. The discharge ratio slightly increases as the Froude number decreases for all angles. However, the Froude number of subcritical flows had a significant effect on the bed width ratio. For angles 30°, 45°, 60° and 75°, the discharge ratio decreases when the bed width ratio increases, but it remains unchanged when the angle is 90°. In conclusion, there is a linear relationship between discharges, Froude number and bed width ratio at certain dividing angles.

Keywords Open-channel · Dividing flow · Flowrate ratio · Froude number · Bed width

P. N. S. Harmizi · I. S. M. Zawawi (✉)
Faculty of Computer and Mathematical Sciences, Kompleks Al-Khawarizmi, Universiti Teknologi MARA, 40450 Shah Alam, Selangor, Malaysia
e-mail: iskandarshah@uitm.edu.my

P. N. S. Harmizi
e-mail: 2021575203@isiswa.uitm.edu.my

M. R. M. Haniffah
Department of Water and Environment Engineering, School of Civil Engineering, Faculty of Engineering, Universiti Teknologi Malaysia, 81310 Johor Bahru, Johor, Malaysia
e-mail: mridza@utm.my

T. K. A. Khairudin
Faculty of Science, Universiti Teknologi Malaysia, 81310 Johor Bahru, Johor, Malaysia
e-mail: taufiq@utm.my

H. Aris
Institute of Informatics and Computing in Energy, Universiti Tenaga Nasional, 43000 Kajang, Selangor, Malaysia
e-mail: hazleen@uniten.edu.my

1 Introduction

Grace and Priest [2] proposed an experimental approach to study the division of flow at different width ratios of the branch channel to the main channel based on subcritical Froude number.

Most of the earlier researchers, such as Ramamurthy et al. [8] and Barkdoll et al. [1], focused on dividing flow behaviour at the right angle channel or T-junction. Hsu et al. [4] introduced a theoretical model of branching flow at a right angle branch channel. Kesserwani et al. [6] proposed unsteady mathematical modelling on the right-angled open channel junction to predict the flow divisions. The predictions presented closely with the experimental data and results obtained by the theoretical predictions. Ghostine et al. [3] presented the one-dimensional (1D) and two-dimensional (2D) numerical simulation using second-order Runge–Kutta Discontinuous Galerkin (RKDG) to estimate the distribution flow at T-junction.

According to Yonesi et al. [13], constructing a branch channel to divert some part of the flow from the main channel causes some changes in hydraulic conditions of the flow in the main channel and channel after the junction. This leads to many consequences related to natural disasters such as sedimentation, erosion in the river bank and flood. In river management, the best design for the structure or side of the channel is important to prevent overflowing. Thus, Pandey and Mishra [7] proposed the general equation of dividing flow at rectangular and trapezoidal channel junctions based on momentum principle and continuity equation to investigate the relationship between depth ratio and complex flow features of combining and dividing flows. The results from Pandey and Mishra [7] proved that the flow depth ratio in rectangular and trapezoidal channels increases when the discharge ratio increases. Other types of cross-sectional channels, such as circular and triangular, will also influence the behaviour of open channel dividing flow [10].

Since the theory of bifurcation or dividing open channel flow is relatively new in the area of mathematical modelling, Zawawi et al. [14] have detailed the derivation of dividing the flow equation proposed by Pandey and Mishra [7] using algebraic manipulation and ratio principle. Further investigation has been made by Zawawi et al. [14] on the relationship between the bifurcation discharge with different angles of the branch channel in a trapezoidal cross-sectional. The results of the study revealed an appropriate bifurcation angle to avoid overflow, in which the amount of discharge after the junction is below the critical discharge. Recently, Shahari et al. [11] proposed the numerical approach for combining open channel flow for the types of trapezoidal and V-shaped cross-sectional channels. The general equation of combining flow was modified in the form of nonlinear polynomial equations of degree five and solved numerically to investigate the effects of the Froude number and discharge ratio in both types of channels. As the Froude number and discharge ratio increase, the value of flow depth in the trapezoidal channel is higher than the V-shaped channel.

However, the relationship between Froude number, bed width, and discharge ratio in dividing flow has limited data reported in the mathematical study. The aim of the study is to review the relevant mathematical model presented by Zawawi et al. [14]

in order to investigate the relationship of several important features in dividing open-channel flow. In this paper, the methodology section includes a brief description of the channel followed by the general equation of dividing flow. Subsequently, the proposed equation is solved using Maple software. Then the results of discharges ratio based on certain values of Froude number, bed width ratio and dividing angles are discussed. Some conclusions are made as well as the recommendation for future study.

2 Methodology

This section briefly reviews the description of the channel and mathematical modelling of dividing flow.

2.1 Review on Mathematical Model

The geometric and hydraulic properties of the channel, as well as the shape of the cross-sectional, are important to model the dividing open-channel flow. In this study, the main channel is divided into two branch channels, namely, channel 1 and channel 2 whereas the type of cross-sectional area of the channel is trapezoidal. The uniform discharge Q is taking place from the main channel to channel 1 and channel 2. The direction of the main channel with respect to the axis of channel 1 and channel 2 are θ_1 and θ_2.

Several assumptions have been made, such as the wall friction is neglected as compared to other forces, the depth of the flow in all channels is equal and bed width in the main channel and channel 1 is equal. The model of the channel is illustrated in Fig. 1. The subscript of 0 is the main channel, while 1 and 2 are channel 1 and channel 2, respectively.

The general equation for open channel dividing flow is given as follows:

$$
(1 + 2k_0)\left[\frac{1}{2}\left(1 - y_r^2 - Br_1 y_r^2 \cos\theta_1\right) + \frac{k_0}{3}\left(1 - y_r^3 - y_r^3 \cos\theta_1\right)\right]
$$
$$
= F_0^2 (1 + k_0)^2 \left[\frac{(1 + k_0)}{y_r}\left(\frac{(1 - q_r)^2}{(Br_2 + k_0 y_r)}\cos\theta_2 + \frac{q_r^2}{(Br_1 + k_0 y_r)}\cos\theta_1\right) - 1\right.
$$
$$
\left. + C((1 - q_r)\sin\theta_2 + q_r \sin\theta_1)\right], \tag{1}
$$

where $k_0 = \frac{z y_0}{b_0}$ and $C = \frac{5}{6} - \frac{F_0^2}{40} - \frac{k_0}{12 q_r}\left(\frac{1 + 2k_0}{(1 + k_0)^2}\right)$. In addition, the following notations are used.

Fr: Froude number, $F = \frac{V}{\sqrt{gD}}$

V: Flow velocity, $V = \frac{1}{n} R_H^{0.66} S^{0.5}$
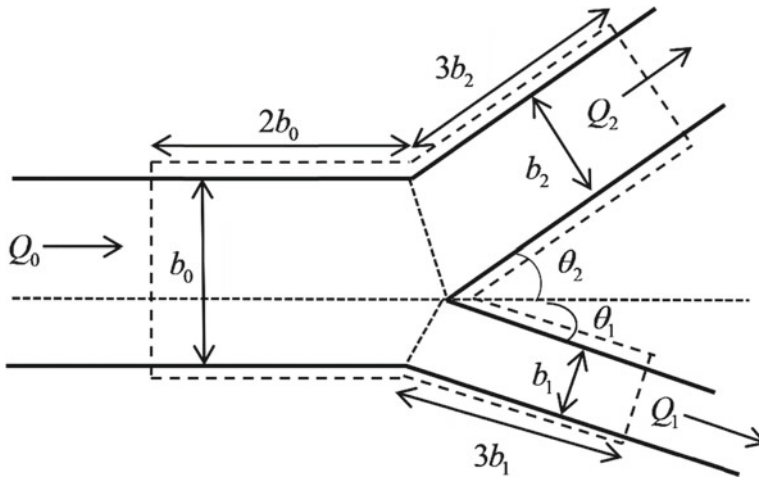
Fig. 1 The schematic layout of open channel dividing flow

D: Hydraulic depth
g: Gravitational acceleration
y: Flow depth
z: Side slope, $z = \frac{kb}{y}$
Q: Discharge
q_r: Discharge ratio
b: Bed width of the channel
B_r: Bed width ratio
y_r: Flow depth ratio
θ: Dividing angles

For the computation and results analysis, model (1) is performed using Maple software.

3   Results and Discussion

In the open channel dividing flow, the amount of discharge ratio depends on many factors such as angles of the channel, Froude number and bed width ratio. At the start of solving (1), all the input values of channel properties used in this study are taken from Zawawi et al. [14]. Since the type of flow is assumed to be subcritical, the Froude number used in the computation is less than one ($Fr < 1$). The angle at channel 1 is restricted to $\theta_1 = 0°$ and $\theta_1 = 15°$ while angle at channel 2 is varied $\theta_2 = 30°, 45°, 60°, 75°, 90°$.

3.1 Relationship Between Discharge Ratio and Froude Number

In this study, the model Froude number is varied between 0.2 and 0.8 while the dividing angles varied between 30° and 90°. The amount of discharge ratio and the Froude number in the main channel with different dividing angles are presented in Tables 1 and 2. It was observed that there is a strong linear relationship between the discharge ratio and the Froude number in all cases.

In subcritical flow, the highest value of the discharge ratio occurs when $\theta_2 = 30°$ with the lowest value of the Froude number, while the lowest discharge ratio is obtained at an angle of $\theta_2 = 90°$ when the value of the Froude number increases. Figures 2 and 3 are illustrated to show the relation between discharge ratio and Froude number. For all angles, it can be seen that the discharge ratio slightly decreases or is almost identical, although the Froude number increases. Moreover, there is a reverse relationship between discharge ratio and Froude number, which is consistent with the results obtained by Sayed [9].

Table 1 The value of q_r when $Fr < 1$ and $\theta_1 = 0°$

θ_1	0°				
θ_2	30°	45°	60°	75°	90°
Fr	q_r				
0.2	0.828318795	0.821292838	0.792674010	0.712372031	0.415985961
0.4	0.828049984	0.820856087	0.792005286	0.711314301	0.413942244
0.6	0.827708637	0.820287001	0.791094295	0.709752504	0.410420486
0.8	0.827288914	0.819586511	0.789969093	0.707779243	0.405142561

Table 2 Results of q_r when $Fr < 1$ and $\theta_1 = 15°$

θ_1	15°				
θ_2	30°	45°	60°	75°	90°
Fr	q_r				
0.2	0.810963847	0.800937750	0.766235915	0.671591456	0.319147330
0.4	0.810777375	0.800595441	0.765685147	0.670702648	0.317431894
0.6	0.810575657	0.800187947	0.764977598	0.669431879	0.314447907
0.8	0.810351511	0.799714233	0.764139290	0.667872749	0.309893820
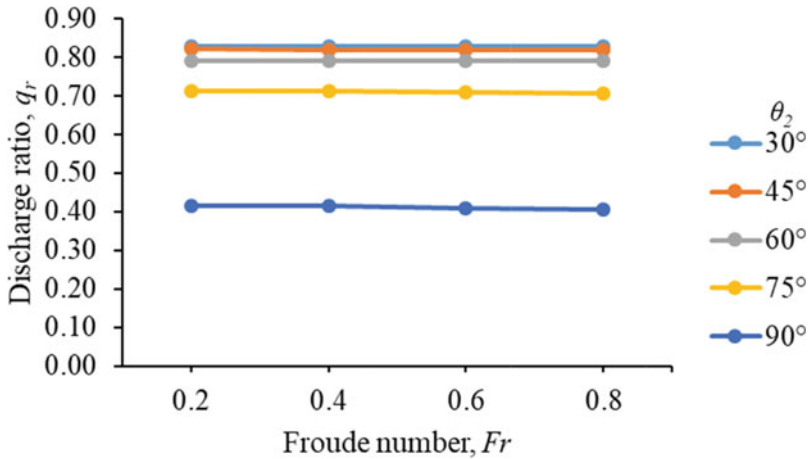
Fig. 2 The relationship between q_r and Fr when $\theta_1 = 0°$
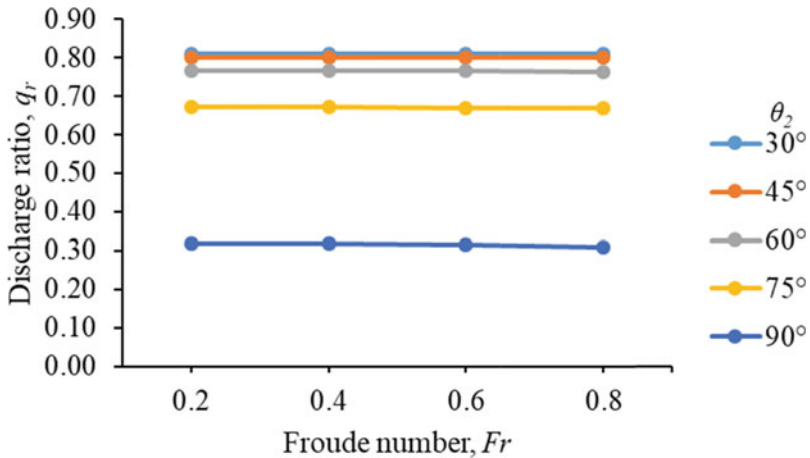
Fig. 3 The relationship between q_r and Fr when $\theta_1 = 15°$

3.2 Relationship Between Discharge Ratio and Bed Width Ratio

This section describes the effect of changing the bed width ratio in channel 1 on the discharge ratio. The values of bed width ratio in channel 1 used are $B_{r1} = 0.5, 0.75, 1.0$ and the fixed value of Froude number, $Fr = 0.174902437$ is used for all dividing angles. The results of the discharge ratio for each different value of bed width ratio are presented in Tables 3 and 4. It shows that the discharge ratio

Table 3 The value of q_r when $\theta_1 = 0°$

θ_1	0°				
θ_2	30°	45°	60°	75°	90°
B_{r1}	q_r				
0.5	0.701032533	0.699174777	0.672261815	0.599287322	0.415990827
0.75	0.629129843	0.633720117	0.613569260	0.553368755	0.415992100
1	0.575530192	0.586478239	0.573462655	0.524776749	0.415992767

decreases when the value of the bed width ratio increases. Surprisingly, the discharge ratio remains unchanged when $\theta_2 = 90°$.

It can be seen that there is a negative linear relationship between discharge ratio and bed width ratio when $\theta_2 = 30°$, $45°$, $60°$, $75°$ as shown in Figs. 4 and 5. Thus, the main factor affecting the discharge ratio in channel 2 is the bed width ratio.

Table 4 The value of q_r when $\theta_1 = 15°$

θ_1	15°				
θ_2	30°	45°	60°	75°	90°
B_{r1}	q_r				
0.5	0.668981300	0.662901011	0.628050739	0.539451609	0.319153203
0.75	0.588078210	0.588231789	0.560038791	0.485296767	0.319154739
1	0.527437495	0.534040069	0.513313603	0.451429146	0.319155545
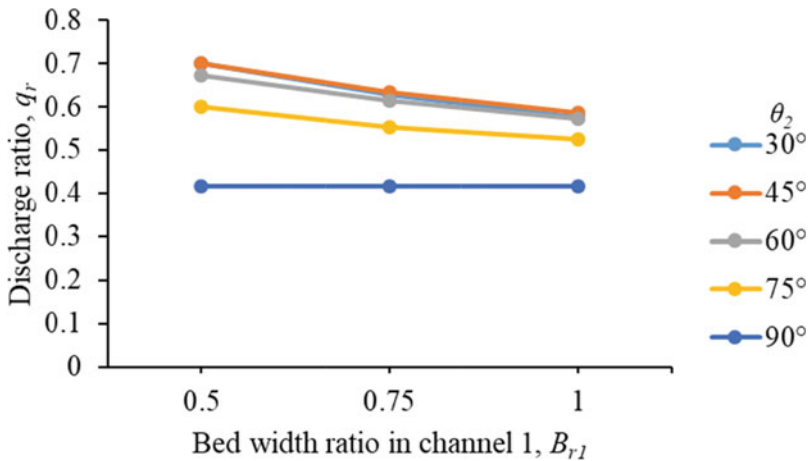
Fig. 4 The relationship between q_r and B_{r1} when $\theta_1 = 0°$
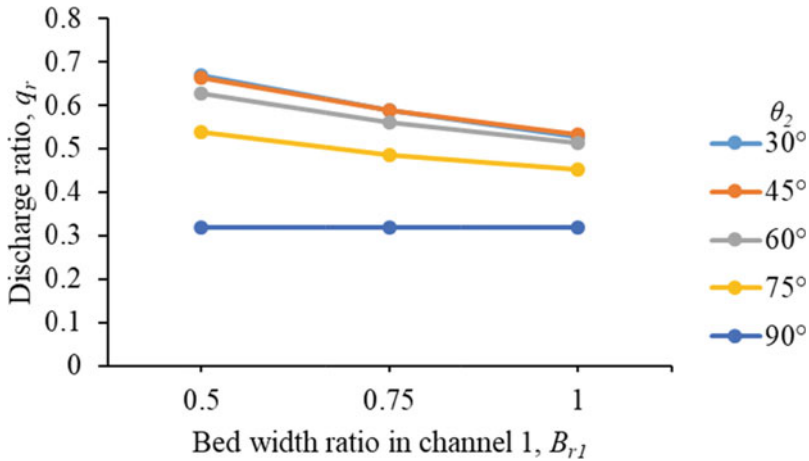
Fig. 5 The relationship between q_r and B_{r1} when $\theta_1 = 15°$

4 Conclusion

In this study, the relationship of the discharge, Froude number and bed width have been investigated using a mathematical model. For the case of subcritical flow, it is shown that there is no significant effect of Froude number on discharge ratio. However, there is a negative linear relationship between discharge ratio and bed width ratio at certain angles. For all values of Froude number and bed width ratio, it could be concluded that the discharge ratio remains constant at the right angle channel. Although the results obtained in this work have not yet been validated by experimental data, it is still applicable as a reference in measuring the dividing flow characteristics. In future studies, another interesting feature of dividing open-channel channel flow that can be considered is the separation zones in the branch channels.

References

1. Barkdoll BBD, Hagen BL, Fellow AJO (1998) January 92–95
2. Grace JL, Priest MS (1958) Division of flow in open channel junctions, Bulletin No 31, Engineering Experiment Station, Alabama Polytechnic Institute, Auburn, 421 pp

3. Ghostine R, Vazquez J, Terfous A, Rivière N, Ghenaim A, Mosé R (2013) A comparative study of 1D and 2D approaches for simulating flows at right angled dividing junctions. Appl Math Comput 219(10):5070–5082
4. Hsu C, Tang C, Lee W, Shieh M (2002) Subcritical 90˚ equal-width open-channel dividing flow. J Hydraul Eng 128(7):716–720
5. Jeppson R (2010) Open channel flow: numerical methods and computer applications. CRC Press, Hoboken
6. Kesserwani G, Vazquez J, Rivière N, Liang Q, Travin G, Mosé R (2010) New approach for predicting flow bifurcation at right-angled open-channel junction. J Hydraul Eng 136(9):662–668. https://doi.org/10.1061/(asce)hy.1943-7900.0000222
7. Pandey AK, Mishra R (2012) Comparison of flow characteristics at rectangular and trapezoidal channel junctions. J Phys Conf Ser 364(1). https://doi.org/10.1088/1742-6596/364/1/012141
8. Ramamurthy A, Tran DM, Carballada L (1990) Dividing flow in open channels. J Hydraul Eng 116(3):449–455
9. Sayed T (2019) An experimental study of branching flow in open channels 93–101. https://doi.org/10.2478/limre-2019-0008
10. Schindfessel L, Creëlle S, De Mulder T (2017) How different cross-sectional shapes influence the separation zone of an open-channel confluence. J Hydraul Eng 143(9):04017036
11. Shahari NA, Husaini Norwaza NA, Mohd Zawawi IS, Mohd Kamarul NA, Said A (2021) Numerical investigation on the behavior of combining open-channel flow. Indones J Electr Eng Comput Sci 23(2):1110–1119. https://doi.org/10.11591/ijeecs.v23.i2.pp1110-1119
12. Taylor EH (1944) Flow characteristics at rectangular open-channel junctions. Trans Am Soc Civ Eng 109(1):893–902
13. Yonesi HA, Omid MH, Haghiabi AH (2008) A study of the effects of the longitudinalarrangement sediment behavior near intake structures. J Hydraul Res 46(6):814–819
14. Zawawi ISM, Abdullah NL, Aris H, Jaafar BA, Norwaza NAH, Mohd Yunos MHF (2019) Mathematical modeling for flood mitigation: effect of bifurcation angles in river discharges

Laboratory Investigations on Porous Concrete Drainage Systems Performance

Feroz Hanif Mohamed Ahmad, Mohamad Hidayat Jamal, Abdul Rahman Mohd Sam, Nuryazmeen Farhan Haron, and Canarisa Nipi Ah Lian

Abstract This research aimed to determine the performance of porous concrete drainage systems, which is focussing on porous concrete permeability and compressive strength. The laboratory investigations have been successfully conducted following appropriate standards and concerned to research for drain cover and cube sample tests with different porous concrete aggregate sizes of 8 and 16 mm. Meanwhile, the porous concrete performance of 4 and 12 mm aggregate sizes have been estimated based on linear regression analysis of 8 and 16 mm for cube sample and drain cover sample, respectively. The finding shows that the highest permeability rate for both cube (20.71 mm/s) and cover drain (8.11 mm/s) samples of 16 mm aggregate size with the highest porosity as compared to other aggregates sizes. The permeability and the porosity of porous concrete increase with the increase of aggregate size. However, the compressive strength decreases as the aggregate size increases, where the compressive strength for 8 mm aggregate size is 3.87 MPa higher than compressive strength for 16 mm aggregate size (3.28 MPa). Thus, the aggregate with a bigger size is good in terms of porous and permeability but low in terms of compressive strength.

Keywords Porous concrete · Drainage system · Permeability · Compressive strength · Porous concrete performance

F. H. M. Ahmad (✉) · M. H. Jamal · A. R. M. Sam · C. N. A. Lian
School of Civil Engineering, Faculty of Engineering, Universiti Teknologi Malaysia, 81310 Johor Bahru, Johor, Malaysia
e-mail: ferozhanifahmad@gmail.com

M. H. Jamal
e-mail: mhidayat@utm.my

A. R. M. Sam
e-mail: abdrahman@utm.my

N. F. Haron
School of Civil Engineering, College of Engineering, Universiti Teknologi MARA (UiTM), 40450 Shah Alam, Selangor, Malaysia
e-mail: nuryazmeen@uitm.edu.my

1 Introduction

Generally, concrete is one of the main materials used in construction. Align with technology being developed, several types of research related to concrete technology also increase [2, 6, 8, 12]. This kind of technology in concrete can be seen by various types of concrete with high performance and environmentally friendly. One of the concrete technology that considers as high performance and environmentally friendly is pervious or porous concrete. Porous concrete is an innovative and alternative technology replacing conventional concrete, which has an interconnected void, so that able to drain water faster and reduce the flood occur.

Porous concrete technology has a larger porosity value, high permeability as compared to conventional concrete [5, 9–11]. Several types of research related to porous concrete technology have been tested in the laboratory. For example, the experiments that have been conducted by Fortes et al. [1], Harshith [3], Hung et al. [4], Mulyono [7]. However, there is lacking the experiments that focus on the porous concrete performance from different sizes of aggregate as part of the concrete design mixture. Thus, this research intends to determine the porous concrete for drainage system performance based on different aggregate sizes. The porous concrete performance that will be determined in this research includes its porosity, permeability, and compressive strength.

2 Materials and Methods

The laboratory investigations were focused on porous concrete permeability and compressive strength based on cube and drain cover samples with different aggregate sizes of 8 mm and 16 mm directly from the experiments (Fig. 1). Meanwhile, the porous concrete performance of 4 mm and 12 mm aggregate sizes have been estimated based on linear regression analysis of 8 mm and 16 mm for cube samples and drain cover samples, respectively.

Fig. 1 Samples of cube (left) and drain cover (right) with different sizes of aggregates

Table 1 Porous concrete mix design proportion for cube samples

Aggregate size (mm)	Cement (kg/m^3)	Aggregate (Kg)	Water (l)	Superplastizer (l)	Rice husk Ash (%)	Polymer adhesive (%)	w/c ratio
8	395	1580	158	0.5	2	5	0.4
16	395	1580	158	0.5	2	5	0.4

For the porous concrete mix design, specifically for cube samples with the size of 100×100 mm, the cement grade of G25 has been used, with a water-cement ratio (w/c) of 0.4. It was considered in the mix proportion with A/C ratio is 1:4. The details of the porous concrete mix design proportion for all cube samples of 8 and 16 mm aggregates are shown in Table 1.

For the permeability test, Darcy's Law has been used to determine the permeability rate, k (mm/s), as indicated in Eq. 1:

$$k = \frac{VL}{hAt} (\text{mm/s}) \tag{1}$$

where: k = permeability rate (mm/s), V = volume of water collection (mm^3), A = cross section area (mm^2), t = duration of water collection (s), L = height of specimen (mm), h = height of water level (mm).

The assumption for these permeability tests, including: i) steady flow (constant flowrate), ii) homogeneous surface area (lined concrete drain), iii) porous concrete aggregate size of 8 mm and 16 mm, iv) bed, is assumed in dry condition with no groundwater present (0% moisture content), and v) volume of collected water is 10 L. Figure 2 shows the experiment to determine the permeability rate for cube and drain cover samples.

Meanwhile, for compressive strength tests at 28 days, the loading rate of 0.3 MPa/s with 100×100 mm area of the specimen subjected to load has been applied in this laboratory investigation in order to determine the porous concrete drainage system performance. Figure 3 shows the experiment to determine the compressive strength for cube samples.

Besides that, the density and the porosity of 8 and 16 mm cube samples also have been done during the investigations. Details of the cube samples density and porosity are discussed in the next section on results and discussion.

3 Results

Firstly, the result from Table 2 shows when the aggregate size increases, the density of the cube sample slightly decreases. Unfortunately, in terms of cube sample porosity, the increase in aggregate size is directly proportional to the porosity (Table 3).
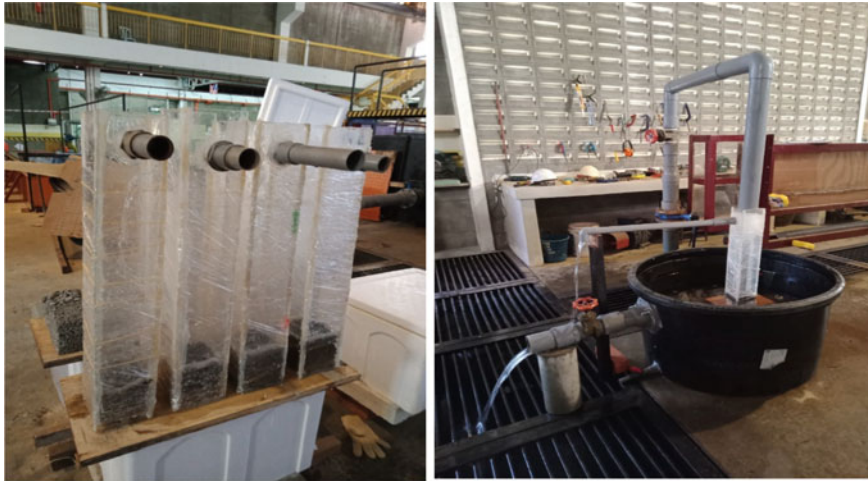
(a) Cube samples
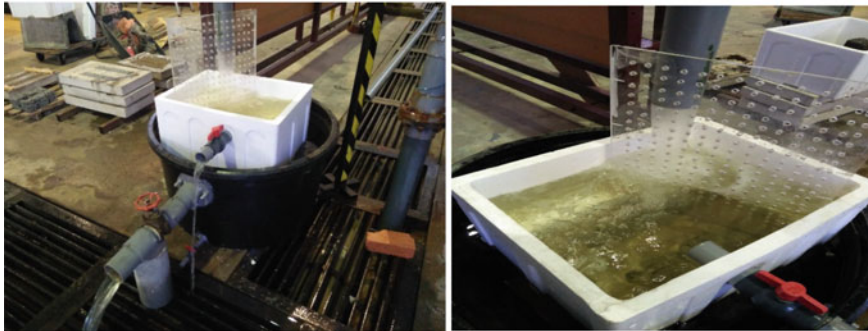
(b) Drain cover samples

Fig. 2 Permeability test for **a** cube and **b** drain cover samples

Similarly, the highest permeability rate of 20.71 mm/s for cube sample, while 8.11 mm/s for drain cover sample was determined for 16 mm aggregate size. Permeability basically is related to porosity and the void size in porous concrete. The results of the permeability test are influenced by the aggregate size. The permeability is calculated using the Darcy equation in order to get the permeability rate, k as shown in Eq. 1. As shown in Figs. 4 and 5, the permeability rate increases with the increases in aggregate size for cube samples as well as for drain cover samples. Meanwhile, the decrease in compressive strength for cube samples when the aggregate size in the mixture increases, as illustrated in Fig. 4.

Meanwhile, the largest compressive strength was found on 8 mm aggregate size porous concrete cube sample with a value of 3.87 MPa for 28 days, as shown in Figs. 4 and 5, Tables 4 and 5. This shows that the compressive strength increases with decreasing aggregate size, similarly with the hardened density of the cube sample.

Fig. 3 Compressive strength test for cube samples with different sizes of aggregates

Table 2 Hardened density of cube sample (kg/m^3)

Size of aggregate, mm	8 mm	16 mm
Mass of cube sample, kg	1.630	1.610
Volume of cube, m^3	0.001	0.001
Density of sample, kg/m^3	**1630**	**1610**

Table 3 Porosity of cube sample

Item/Size of sample	8 mm	16 mm
Dry mass of sample, W_1(kg)	1.630	1.610
Mass of sample saturated in water, W_2 (kg)	0.949	0.962
Bulk volume of sample, V (m^3)	0.001	0.001
Density of water, p (kg/m^3)	1000	1000
Porosity, (100%)	**32**	**35**

The smaller size of aggregate used in the porous concrete mixture, the denser concrete will be produced. This is due to the reduction of voids in the porous concrete so that the mixture gets denser.
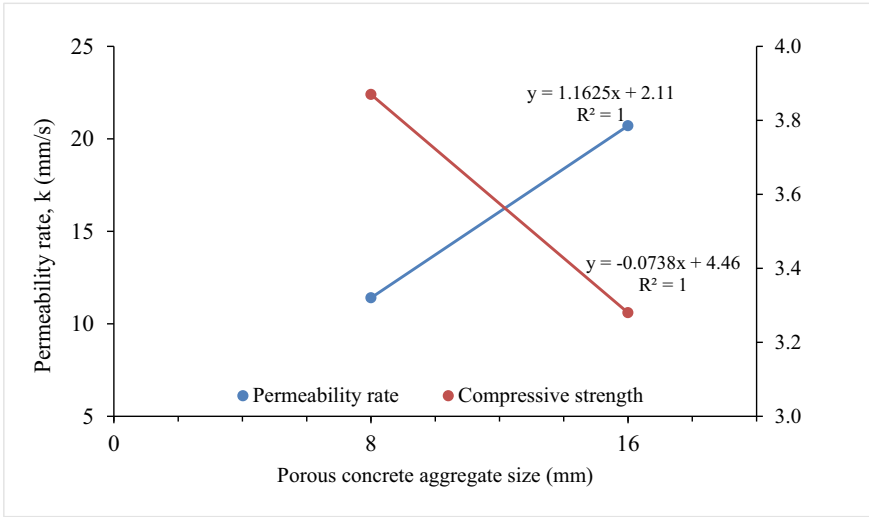
Fig. 4 Porous concrete drainage system performance for cube sample tests
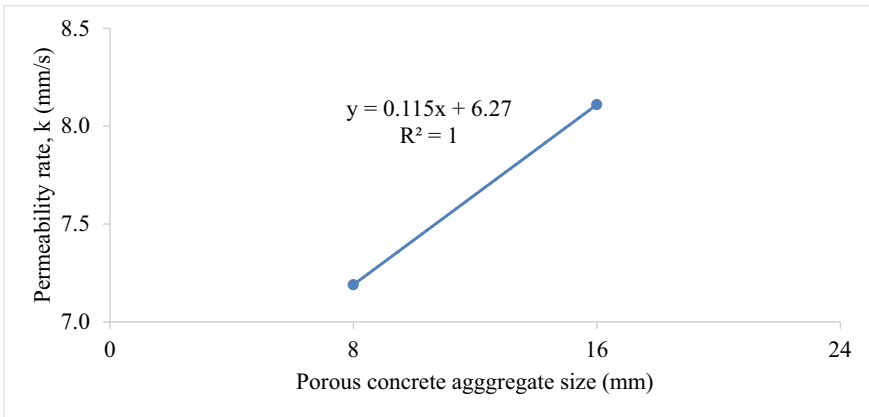
Fig. 5 Porous concrete drainage system performance for drain cover tests

Table 4 Porous concrete drainage system performance for 8 and 16 mm aggregate sizes of the cube and drain cover sample

Type of sample	Cube sample		Cover drain sample	
Aggregate size (mm)	8	16	8	16
Permeability rate, k mm/s	11.41	20.71	7.19	8.11
Compressive strength test (MPa)	3.87	3.28	NIL	NIL

Table 5 Porous concrete drainage system performance for different aggregate sizes of cube and drain cover sample

Type of sample	Cube sample	Cover drain sample
Aggregate size (mm)	Permeability rate, k (mm/s)	Permeability rate, k (mm/s)
4	6.76	6.73
8	11.41	7.19
12	16.06	7.65
16	20.71	8.11

4 Conclusion

In this laboratory investigation, the performance of the porous concrete drainage system has been determined based on the permeability rate, k, and the compressive strength for cube and drain cover samples with different aggregate sizes. The findings show that the highest permeability rate for both cube (20.71 mm/s) and cover drain (8.11 mm/s) samples of 16 mm aggregate size with the highest porosity as compared to other aggregates sizes. The permeability and the porosity of porous concrete increase with the increase of aggregate size. However, the compressive strength decreases as the aggregate size increases, where the compressive strength for 8 mm aggregate size is 3.87 MPa higher than compressive strength for 16 mm aggregate size (3.28 Mpa). Thus, the aggregate with a bigger size is good in terms of porous and permeability but low in terms of compressive strength.

References

1. Fortes RM, Merighi JV, Bandeira AA (2006) Laboratory studies on performance of porous concrete. In: 10th international symposium on concrete roads, vol 18
2. Hassan A, Arif M, Shariq M (2020) A review of properties and behaviour of reinforced geopolymer concrete structural elements-A clean technology option for sustainable development. J Clean Prod 245:118762
3. Harshith (2020) Experimental investigation of porous concrete for concrete pavement. Int J Eng Res V9(08). https://doi.org/10.17577/ijertv9is080267
4. Hung VV, Seo SY, Kim HW, Lee GC (2021) Permeability and strength of pervious concrete according to aggregate size and blocking material. Sustainability 13(1):426
5. Joshi T, Dave U (2021) Construction of pervious concrete pavement stretch, Ahmedabad, India–Case study. Case Stud Constr Mater e00622

6. Marchment T, Sanjayan J (2020) Mesh reinforcing method for 3D Concrete Printing. Autom Constr 109:102992
7. Mulyono T (2019) Laboratory experiment: pervious concrete for permeable pavement, focus in compressive strength and permeability. IOP Conf Ser Earth Environ Sci 366(1):012019
8. Nerella VN, Mechtcherine V (2019) Studying the printability of fresh concrete for formwork-free concrete onsite 3D printing technology (CONPrint3D). In 3D concrete printing technology. Butterworth-Heinemann, pp 333–347
9. Perera IMH, Athapaththu CJ, Mampearachchi WK (2020) Design of a porous concrete mixture for drainage coverslab in pedestrian walkways. Transp Res Procedia 48:3678–3695
10. Ramadhansyah PJ, Mohd Ibrahim MY, Hainin MR, Wan Ibrahim MH (2014) A review of porous concrete pavement: applications and engineering properties. Appl Mech Mater 554:37–41
11. Sanjaya N, Juliantina I, Nurjannah SA (2021) Compressive strength, permeability and porosity analysis of pervious concrete by variation of aggregate and compacting method. J Phys Conf Ser 1783(1):012073
12. Siddika A, Mamun MAA, Ferdous W, Saha AK, Alyousef R (2020) 3D-printed concrete: applications, performance, and challenges. J Sustain Cem-Based Mater 9(3):127–164

Permeability and Mechanical Properties of Pervious Concrete Curb with Different Aggregate Sizes

C. N. A. Lian, M. H. Jamal, and Z. Ibrahim

Abstract Pervious concrete is an environmentally friendly material that can be a feasible option in solving urban drainage problems and mitigating climate change. This research aims to evaluate the mechanical and hydraulics properties of pervious concrete with different aggregate sizes and propose the acceptable aggregate size for road curb. Pervious concrete mixes are prepared with single-sized aggregates (4.75, 8, 12.5 and 16 mm) with constant aggregate cement and water-cement ratios. Furthermore, a series of tests were conducted in this study, such as compressive strength, porosity, and permeability. The experimental result showed that the size of coarse aggregate affects the strength and permeability of the specimens. The permeability and porosity decrease as the aggregate size increases. The smaller aggregate size is beneficial to increase the 28 days compressive strength of pervious concrete. Linear regression relationships were developed to establish relationships between porosity and compressive strength and porosity and permeability. The obtained result showed that the aggregate size of 8 mm performed better than the others in all assessments and could be applied on pervious concrete curb.

Keywords Pervious concrete · Road curb · Permeability · Compressive strength · Porosity · Aggregate size

1 Introduction

Rapid urbanization has risen in impervious surfaces such as highways and roofs, dramatically altering the normal hydrological cycle in urban areas [11, 25, 35]. The

C. N. A. Lian (✉) · M. H. Jamal · Z. Ibrahim
Department of Hydraulics and Hydrology, Faculty of Civil Engineering, Universiti Teknologi Malaysia, Skudai, Malaysia
e-mail: nipi@graduate.utm.my

M. H. Jamal
e-mail: mhidayat@utm.my

Z. Ibrahim
e-mail: zulkfe@utm.my

impact of these changes is related to hydrological and environmental problems, including flash floods due to exceeded discharge capacity of the existing stormwater drainage system [27]. Stormwater drainage system comprises many linking structure such as street gutter and inlet which collect access stormwater from the street and convey it to the underground drainage system. Unfortunately, even though the drainage system has been provided with those inlets, it is still less efficient to remove stormwater on the road surface. Some systems are not fully utilized because of some factors such as clogging the inlet opening by debris [14, 17], the uncertainty design leads to oversize or undersize of the inlet [16, 37] and inappropriate inlet spacing and location [15]. Poorly managed runoff on impervious surfaces will produce some undesirable conditions, such as water spread and ponding onto the roadway which leads to hydroplaning [42]. These conditions will negatively affect vehicle performance and create safety hazards [12, 38], thereby increasing the probability of traffic stagnation and road accidents.

Although various ways have been done to increase the effectiveness of inlets, flood problems still occurred. Among various strategies, pervious concrete pavement technology has been widely used all over the world. Pervious concrete is recognized among the best management practice (BMP) by Environmental Protection Board [7]. This technology provides a solid structure for allowing rainwater to infiltrate naturally into the ground, recharging aquifers and reducing stormwater runoff [47]. Pervious concrete also has been developing in many applications as paving roads, sidewalks and non-structural components [30].

Pervious concrete is a composite with the same essential components as standard concrete engineered to have a large porosity between 15 and 35% [7, 11, 23, 41] and permeability ranging between 1.4 to 12.2 mm/s [20, 44]. Pervious concrete is a combination of Portland cement, coarse aggregate, and water, with or without a limited volume of fine aggregate. Pervious concrete has excellent drainage properties and high noise absorption characteristics [21, 31] due to its high porosity, critical attributes of a quality pavement. Pervious concrete mixtures may have densities ranging from 1600 to 2000 kg/m^3 [33, 40] with the typical compressive strength in the range of 2.8 to 28 MPa [7, 28, 39]. Pervious concrete's poor strength affects the structure's stability and durability because of its vulnerability to frost loss and chemical tolerance. Because of its poor strength, previous concrete has limited application in constructing high traffic highways and low load structures [26]. Porous concrete should achieve maximum function by having efficiency criteria in delivering greater mechanical capabilities while accommodating the porosity of the concrete [8, 19].

Usually, pervious concrete comprises single aggregates in sizes ranging from 19–9.5 mm to obtain sufficient pores in the concrete [7]. However, several studies have used aggregate sizes ranging from 9.5 to 2.36 mm are provided to enhance the strength of PC [11, 29, 43]. Studies conducted by Deo and Neithalath [13], Nguyen et al. [32] have used coarse aggregates with sizes ranging from 16 to 2.35 mm to improve the strength properties. Usage of minor aggregate exhibited compressive and flexural strength, meanwhile, larger aggregate resulted in greater permeability and porosity [9, 19, 45].

Nevertheless, not all areas are capable of providing a pervious concrete road because of its constraints such as expensive cost, less expertise and complicated design [10, 46]. Therefore, the use of pervious concrete technology can be applied for the road curb as an alternative solution, which can provide high permeability compared to the concrete curb to support urban stormwater drainage facilities. Also, by installing a pervious concrete curb on the roadside, the stormwater was supposed to have the self-draining capacity to penetrate the side surface of the porous landscape without relying on the quality and position of the inlet. Thus, this pervious curb would provide as part of the stormwater collection scheme aside from serving as a lane delineation.

The main objective of this study is to evaluate the suitable pervious concrete properties for road curb application. Therefore, several pervious concrete mixes with different aggregate sizes were produced for testing. This information is essential to understand the pervious concrete properties that achieved the standards required to produce road curbs.

2 Materials

The primary experimental materials used are Ordinary Type 1 Portland cement, gravel aggregate and water. In this study, pervious concrete specimens were proportioned using four sizes of coarse aggregate, namely 4.75, 8, 12.5 and 16 mm procured from one distinct source of the quarry. The physical properties of coarse aggregate were measured according to BS EN 1097-6 [4] specification and given in Table 1. The grading was conducted by sieve analysis standard BS EN 12,620 [3] to obtain the size of coarse aggregate. The coarse aggregates are well graded as their sizes are within the grading limit graphically represented in Fig. 1. The polymer adhesive and rice husk ash were used as a binder in the mixture to increase the strength of pervious concrete. A sulphonated naphthalene polymers-based superplasticizer was also applied to the mix to increase the workability of concrete.

Table 1 Physical properties of aggregate

Properties	4.75 mm	8 mm	12.5 mm	16 mm
Water absorption (%)	4.8	4.8	1.3	1.0
Specific gravity	2.3	2.5	2.6	2.7
Bulk density (kg/m^3)	1240	1308	1277	1260
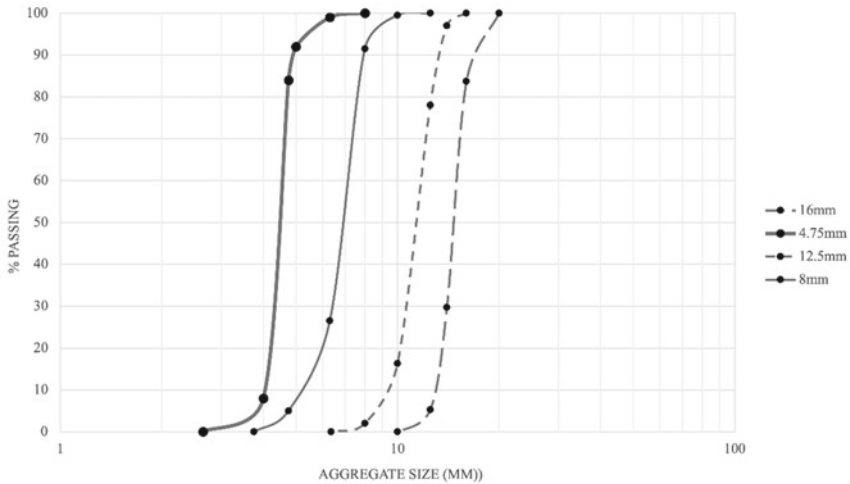
Fig. 1 Particle size distribution curve of aggregate

Table 2 Pervious concrete mix design proportion

Aggregate size (mm)	w/c ratio	a/c ratio	Cement (kg/m^3)	Water (litre)	Superplasticizer (%)	Rice husk ash (%)	Adhesive polymer (%)
4.75	0.4	4	395	158	0.3	5	5
8	0.4	4	395	158	0.3	5	5
12.5	0.4	4	395	158	0.3	5	5
16	0.4	4	395	158	0.3	5	5

2.1 Concrete Mix Design

The pervious concrete mixture, according to Chandrappa and Biligiri [10] is dependent on structural parameters such as a/c ratio, aggregate size, w/c ratio, and aggregate gradation. The a/c ratio, cement content, and w/c ratio values were chosen based on local material properties and trial and error method following the guideline by ACI [7]. The final pervious concrete mix proportion is shown in Table 2.

2.2 Specimen Preparation and Testing

The standard procedure for making and curing cubes was followed according to established [7]. All of the ingredients of pervious concrete consist of cement, coarse aggregate and admixtures, were first weighed as per mix design proportion. The
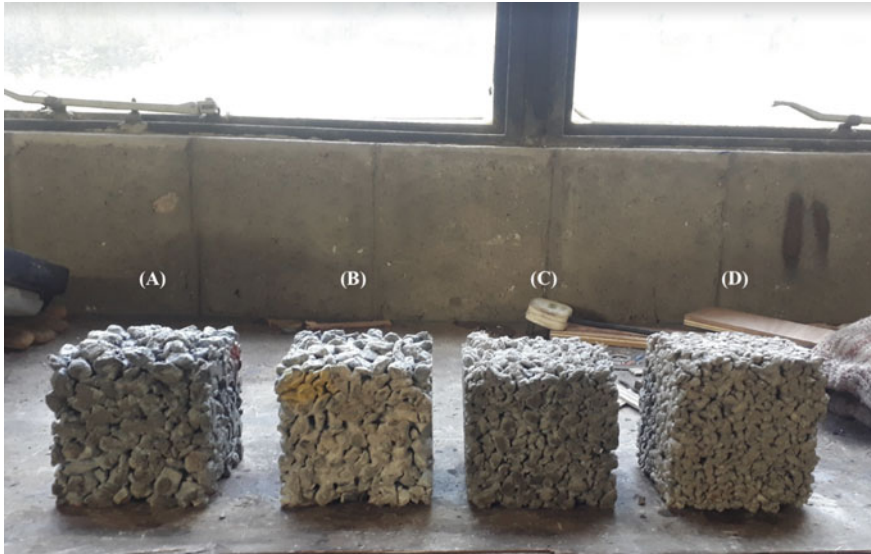
Fig. 2 Pervious concrete cube sample **A** CA20 mm **B** CA16 mm **C** CA8 mm **D** CA4 mm

ingredients were blended for at least two minutes with the aid of a revolving drum mixer to achieve homogeneity of the mixture. The steps are followed by adding the measured amount of water to produce a uniform paste for binding the aggregates together. Finally, the superplasticizer was added altogether with remaining water in the pervious concrete mixture for about another minute, which depended on the workability of the fresh concrete mixture. The concrete mix was compacted using steel tamping rodding in three layers, each of 25 blows, accompanied by vibration on a vibrating table for 2 s to provide proper layer finishing. According to ACI [7], there is no specific requirement for laboratory compaction prepared for pervious concrete sample. After 24 h, the specimens were demolded and placed in a water tank at room temperature for 28 days of water curing. The outcomes of all mixes are shown in Fig. 2.

2.3   Porosity Test

The porosity test was conducted after of 28 days cured specimens and calculated based on Eq. (1) determined by **ASTM C1754,** which is shown below:

$$P = 1 - \frac{m_1 - m_2}{V . \rho_\omega} \times 100 \tag{1}$$

where, P is the porosity, m_1(kg) is the dry sample mass of the oven, m_2(kg) is the sample mass of water saturation, ρ_ω (kg/m^3) is the density of water, and V(m^3) is the total sample volume.

2.4 Permeability Test

A constant head test was designed in the laboratory to evaluate the water permeability of the samples. The ACI [7] recommends the constant head permeability test because it meets the Darcy Law theorem [36]. The value permeability coefficient, k of specimens directly from Darcy's law is determined by Eq. (2).

$$k = \frac{QL}{hAt} \tag{2}$$

where K is the permeability coefficient of the sample (mm/s), Q is the volume of water flow between time (m^3/s), L is the length of the sample (mm), A is the top cross-sectional area of the specimen (mm^2), h is the water head differences (mm), and t is the time measured (s).

2.5 Compressive Strength Test

The compressive strength was tested at 7 days and 28 days after curing, according to BS EN 12390-3 [5] using an automatic compression machine with a loading speed of 3000kN. The compression loaded to failure at a constant rate of 3 kN/s [6, 34] and the maximum load was recorded. The average compressive strength of three samples is taken to perform for each mix proportion. The compressive strength of the specimen was calculated by using Eq. (3).

$$f_i = \frac{P}{A} \tag{3}$$

3 Result and Discussion

The effects of size aggregate of 4.75, 8, 12.5 and 16 mm, were investigated in this result. The density, porosity, water permeability, and compressive strength tests conducted on this sample are summarized in Table 3. Compressive strength was tested at 7 and 28 days. Porosity and permeability tests were carried out for 28 days.

Table 3 Summary of the test value

Aggregate size (mm)	Porosity (%)	Permeability (mm/s)	Compressive strength on 7 days (Mpa)	Compressive strength on 28 days (Mpa)
4.75	30	7.42	3.7	4.4
8	32	12.54	3.5	4.3
12.5	33	13.37	2.9	4.2
16	35	16.43	2.3	3.4

3.1 Porosity

Porosity is the most dependent parameter for invaluable concrete mixes, and therefore, its evaluation of the sample is a requirement in this study. Table 3 shows the results for each sample measured to calculate the porosity. The average void content from smallest to largest size was estimated at approximately 30%, 32%, 33% and 35%, respectively as in Fig. 3. As expected, the largest aggregate size of 16 mm has to produce the highest porosity value up to 35%. The smallest aggregate size of 4.75 mm has contributed the lowest porosity in 30%. The higher porosity occurs due to the inclusion of larger sized aggregates that may have induced more interconnected macropores and possess the largest void spaces within the sample. In other words, the porosity of pervious concrete is closely related to its voids structure. The porosity value of the samples was also found to be in the range of 35 to 30%, which is consistent with the recommended porosity values for pervious concrete mixes [7] and [30].

3.2 Compressive Strength

The size of the aggregates has a significant impact on the compressive strength of pervious concrete. Table 3 show that for 28 days compressive strength of pervious concrete was between 3.4 to 4.4 Mpa. The mixture produces a 4.75 mm aggregate size with the highest compressive strength, followed by 8 mm, 12.5 mm, and 16 mm, respectively. Figure 4 showed a decrease in compressive strength as coarse aggregate size increased. This variation in compressive strength values can be attributed to the increasing amount of voids inside the samples, which play an essential role in determining the strength of pervious concrete mixes. The presence of pore structure in the concrete has a decisive effect on the strength of concrete. Furthermore, it can also be observed that its specific surface area decreases when the aggregate size increases. Hence, the contact points between the aggregates decrease, which makes the strength of the concrete low. The reduction of strength is also because the mixture is free from fine aggregate, and the cement paste coating is the primary source of the compressive strength. Similar result was also observed and well-explained in another
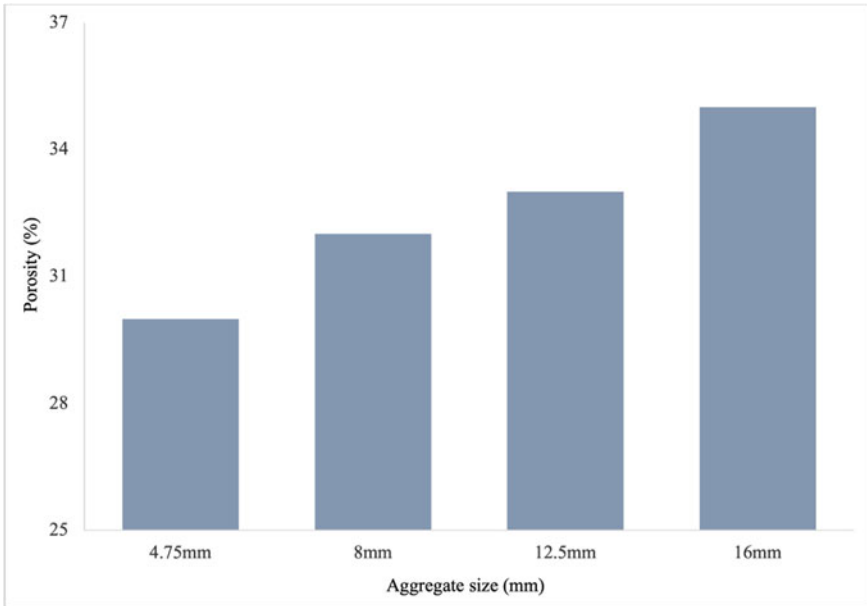
Fig. 3 Porosity of pervious concrete with different coarse aggregate sizes

research [19, 22]. Furthermore, as expected, the 28 days compressive strength were higher than those of 7 days, as the pervious concrete matured. It means strength is directly proportional to time. Therefore, the 28 days compressive strength of all the tested mixes was within the generally acceptable range, which is the compressive strength of conventional pervious concrete is usually lower than 20 MPa. These values also fall within the values stipulated by ACI [7], which is 2.8–28 Mpa. For pervious concrete used as pavement materials, the compressive strengths are restricted from 3.5 to 28 MPa [40, 48]. Therefore, the studied mixes also conform to the compressive strength requirement for curbs application.

The influence of porosity on compressive strength is shown in Fig. 5. As seen in Fig. 5, compressive strength decreases linearly with increasing porosity values. The R^2 value of 0.847 shows a good correlation between compressive strength and porosity. The results verify the generally accepted rule that porosity and compressive strength are inversely related.
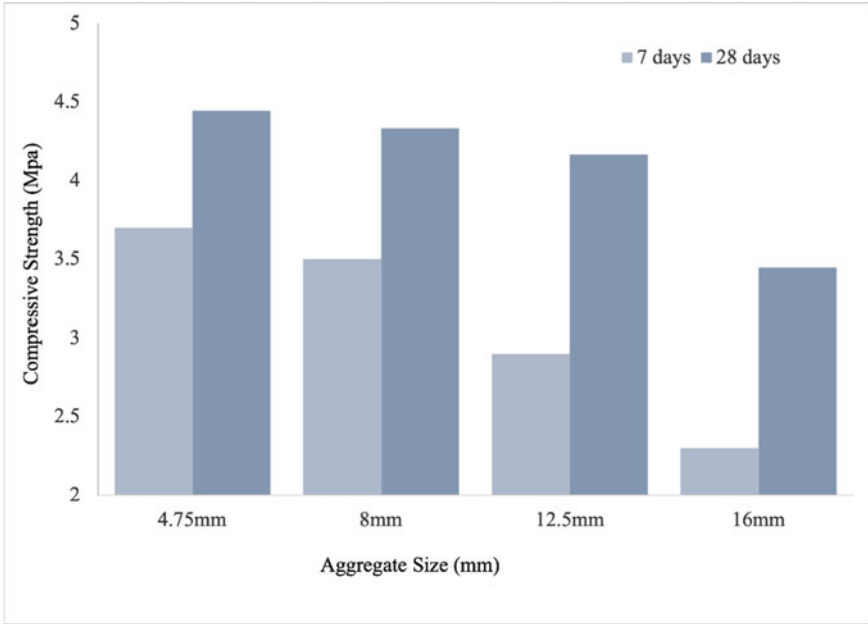
Fig. 4 Compressive strength of pervious concrete with different coarse aggregate sizes
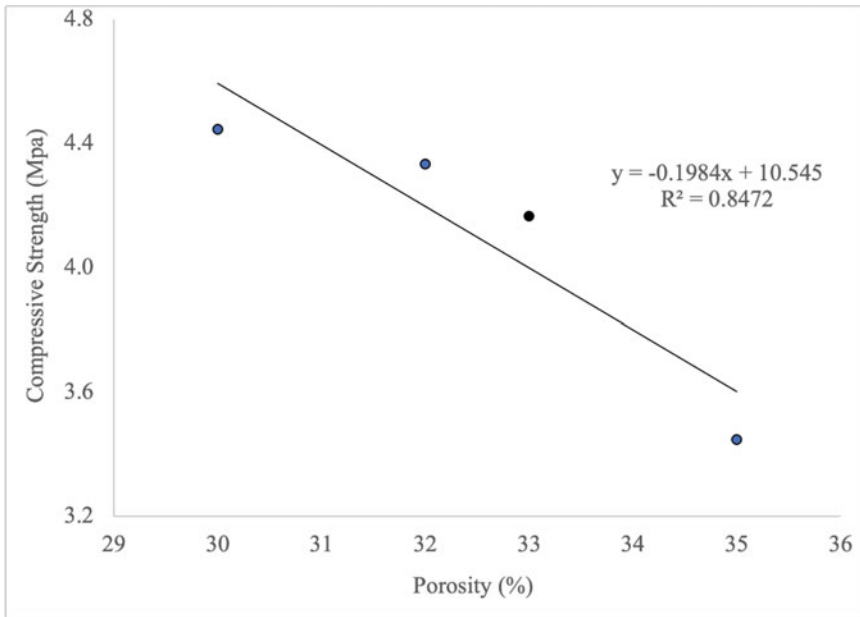
Fig. 5 Relationship between porosity and compressive strength of pervious concrete

3.3 Permeability

Permeability is a critical property in the successful functioning of permeable concrete systems. The permeability of pervious concrete greatly depends on the aggregate size. According to Table 3, the average permeability coefficient for each mix is 16.43 mm/s for size 16 mm, 13.37 mm/s for size 12.5 mm, 12.54 mm/s for size 8 mm and 7.42 mm/s for 4.75 mm, respectively. The permeability coefficient of all samples increases as the aggregate size increases as shown in Fig. 6. As aggregate size increases, bulk density decreases, the contact point between aggregate and cement paste decrease, internal pore diameter increases, pore tortuosity decreases, and more attached pores emerge within, resulting in an improvement in permeability coefficient. A similar result was also observed in Li et al. [24]. Regarding the permeability performance, it was found that all the mixtures had coefficient permeability values obtained between 7 mm/s to 17 mm/s, which is within the acceptable specification of ACI [7].

The relationship between permeability and porosity is a power function following a Cozeny Karmen model. Figure 7 shows permeability as a function of porosity. The significant linearity indicates that the porosity of pervious concrete strongly influences permeability. As the porosity increases, the permeability increases correspondingly, which more void allows more water to sip through the porous concrete. The study used Eq. (3) to estimate permeability with an adjusted R^2 value of 0.9636.

$$k(mm/s) = 1.76x + 44.9$$
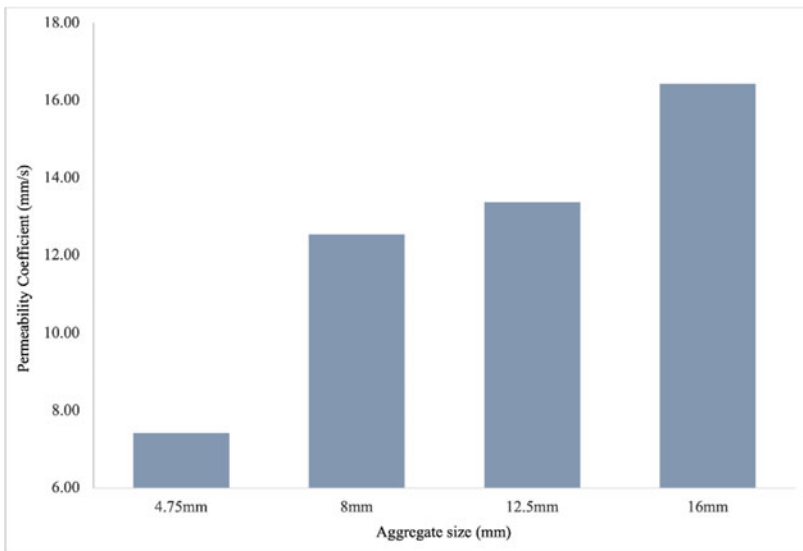
Fig. 6 Permeability of pervious concrete with different coarse aggregate sizes

$$y = 1.7646x - 44.91$$
$$R^2 = 0.9639$$
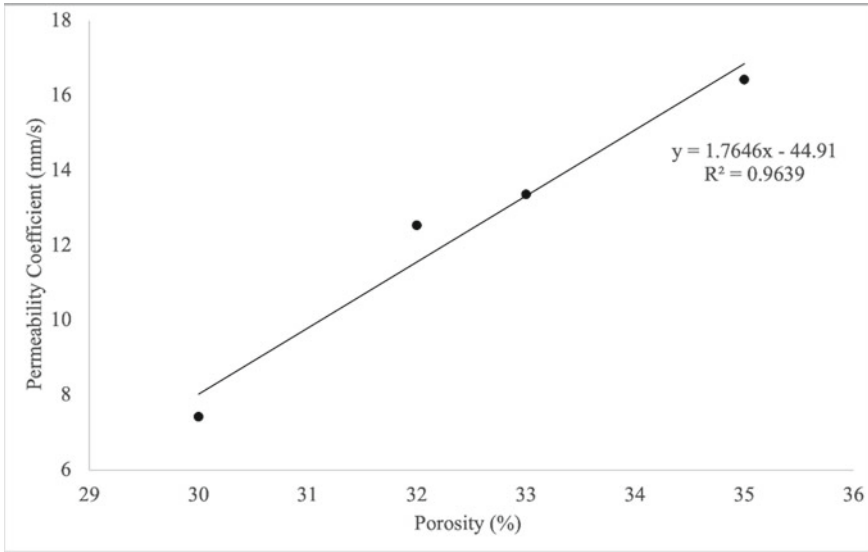
Fig. 7 Relationship between porosity and permeability of pervious concrete

4 Conclusion

An experimental investigation was conducted to examine the influence of aggregate size on pervious concrete's mechanical and permeability characteristics. The study investigated the porosity, compressive strength and water permeability. Based on observed data in this study, the following conclusions have been discussed.

The overall pervious concrete curb performance was chosen based on standard properties requirements and practicality on site. The recommendations were based on the 15 to 25% standard requirement for porous concrete according to porosity property. The selection for permeability characteristics is based on the acceptance criterion, ranging between 1.4 to 12.2 mm/s. For compressive strength, the mixtures should develop compressive strengths in the range of 3.5 to 28 MPa, suitable for a wide range of applications. Based on the overall performance of the static test, all the results were achieved the requirement guidelines by ACI [7]. which applies for the low load structural application as walkways. The aggregate size of 8 mm was considered the most optimum and appropriate size that can satisfy the permeability coefficient of 12.54 mm/s, the porosity of 32% and the compressive strength of 4.3 Mpa.

For the practically on-site, the selection of 8 mm aggregate size can produce a finer texture curb surface which is more aesthetically pleasing for the product. Otherwise, using a larger aggregate size would not be advisable due to the rougher surface and low strength provided. The mixture using 4.75 mm is also not recommended because of low voids and permeability characteristics. Furthermore, the size of 8 mm is also more practical to apply as it has much availability by the local supplier.

References

1. ACI. 522R-13 (2013) Report on pervious concrete. ACI Committee 522
2. American Society for Testing and Materials (2012) ASTM C1754 / C1754M-12, standard test method for density and void content of hardened pervious concrete, ASTM International, West Conshohocken, PA
3. British Standards Institution (2008) BS EN 12620:2002+A1. Aggregates for concrete. BSI, London
4. British Standards Institution (2013) BS EN 1097-6:2013—tests for mechanical and physical properties of aggregates. part 6: determination of particle density and water absorption. British Standards Institution, London
5. British Standards Institution (2009) Testing hardened concrete–Part 3: Compressive strength of test specimens. BS EN 12390-3, London
6. Abd Halim NH, Md Nor H, Jaya RP, Mohamed A, Wan Ibrahim MH, Ramli NI, Nazri FM (2018) Permeability and strength of porous concrete paving blocks at different sizes coarse aggregate. J Phys Conf Ser 1049(1). https://doi.org/10.1088/1742-6596/1049/1/012028
7. ACI (2010) Report on pervious concrete. ACI Commitee 522, March 1–40. https://www.concrete.org/Portals/0/Files/PDF/Previews/522R-10web.pdf
8. Bonicelli A, Giustozzi F, Crispino M, Borsa M (2015) Evaluating the effect of reinforcing fibres on pervious concrete volumetric and mechanical properties according to different compaction energies. Eur J Environ Civ Eng 19(2):184–198. https://doi.org/10.1080/19648189.2014.939308
9. Bright Singh S, Murugan M (2020) Effect of aggregate size on properties of polypropylene and glass fibre-reinforced pervious concrete. Int J Pavement Eng 23(6):1–15. https://doi.org/10.1080/10298436.2020.1836562
10. Chandrappa AK, Biligiri KP (2016) Comprehensive investigation of permeability characteristics of pervious concrete: a hydrodynamic approach. Constr Build Mater 123:627–637. https://doi.org/10.1016/j.conbuildmat.2016.07.035
11. Chandrappa AK, Biligiri KP (2016) Pervious concrete as a sustainable pavement material – research findings and future prospects: a state-of-the-art review. Constr Build Mater 111:262–274. https://doi.org/10.1016/j.conbuildmat.2016.02.054
12. Chang JJ, Yeih W, Chung TJ, Huang R (2016) Properties of pervious concrete made with electric arc furnace slag and alkali-activated slag cement. Constr Build Mater 109:34–40. https://doi.org/10.1016/j.conbuildmat.2016.01.049
13. Deo O, Neithalath N (2011) Compressive response of pervious concretes proportioned for desired porosities. Constr Build Mater 25(11):4181–4189. https://doi.org/10.1016/j.conbuildmat.2011.04.055
14. Despotovic J, Plavsic J, Stefanovic N, Pavlovic D (2005) Inefficiency of storm water inlets as a source of urban floods. Water Sci Technol 51(2):139–145. https://doi.org/10.2166/wst.2005.0041
15. Gómez M, Recasens J, Russo B, Martínez-Gomariz E (2016) Assessment of inlet efficiency through a 3D simulation: numerical and experimental comparison. Water Sci Technol 74(8):1926–1935. https://doi.org/10.2166/wst.2016.326
16. Guo JCY, MacKenzie KA, Mommandi A (2009) Design of street sump inlet. J Hydraul Eng 135(11):1000–1004. https://doi.org/10.1061/(asce)hy.1943-7900.0000094

17. Hao X, Mu J, Shi H (2021) Experimental study on the inlet discharge capacity under different clogging conditions. Water (Switzerland) 13(6). https://doi.org/10.3390/w13060826

18. Huang B, Wu H, Shu X, Burdette EG (2010) Laboratory evaluation of permeability and strength of polymer-modified pervious concrete. Constr Build Mater 24(5):818–823. https://doi.org/10.1016/j.conbuildmat.2009.10.025

19. Hung VV, Seo SY, Kim HW, Lee GC (2021) Permeability and strength of pervious concrete according to aggregate size and blocking material. Sustainability (Switzerland) 13(1):1–13. https://doi.org/10.3390/su13010426

20. Kia A, Wong HS, Cheeseman CR (2017) Clogging in permeable concrete: a review. J Environ Manage 193:221–233. https://doi.org/10.1016/j.jenvman.2017.02.018

21. Kováč M, Sičáková A (2018) Pervious concrete as an environmental solution for pavements: focus on key properties. Environments 5(1):11. https://doi.org/10.3390/environments5010011

22. Leon Raj J, Chockalingam T (2020) Strength and abrasion characteristics of pervious concrete. Road Mater Pavement Des 21(8):2180–2197. https://doi.org/10.1080/14680629.2019.1596828

23. Li J, Zhang Y, Liu G, Peng X (2017) Preparation and performance evaluation of an innovative pervious concrete pavement. Constr Build Mater 138:479–485. https://doi.org/10.1016/j.conbuildmat.2017.01.137

24. Li LG, Feng JJ, Zhu J, Chu SH, Kwan AKH (2021) Pervious concrete: effects of porosity on permeability and strength. Mag Concr Res 73(2):69–79. https://doi.org/10.1680/jmacr.19.00194

25. Liu Y, Tang W, Singh RP (2019) Study on compressive strength and water permeability of steel slag-fly ash mixed permeable brick. Appl Sci (Switzerland) 9(8). https://doi.org/10.3390/app9081542

26. Lori AR, Hassani A, Sedghi R (2019) Investigating the mechanical and hydraulic characteristics of pervious concrete containing copper slag as coarse aggregate. Constr Build Mater 197:130–142. https://doi.org/10.1016/j.conbuildmat.2018.11.230

27. Mohammed BS, Liew MS, Alaloul WS, Khed VC, Hoong CY, Adamu M (2018) Properties of nano-silica modified pervious concrete. Case Stud Constr Mater 8:409–422. https://doi.org/10.1016/j.cscm.2018.03.009

28. Mulyono T, Anisah (2019) Laboratory experiment: pervious concrete for permeable pavement, focus in compressive strength and permeability. IOP Conf Ser Earth Environ Sci 366(1). https://doi.org/10.1088/1755-1315/366/1/012019

29. Neithalath N, Bentz D, Sumanasoorlya M (2010) Predicting the permeability of pervious concrete: advances in characterization of pore structure and transport properties. Concr Int 32(5):35–40

30. Ng CY, Narong AR, Zaman ABK, Mustaffa Z, Mohammed BS, Ean LW (2019) Properties of modified high permeable concrete with a crumb rubber. Open Civil Eng J 13(1):82–91. https://doi.org/10.2174/1874149501913010082

31. Ngohpok C, Sata V, Satiennam T, Klungboonkrong P, Chindaprasirt P (2018) Mechanical properties, thermal conductivity, and sound absorption of pervious concrete containing recycled concrete and bottom ash aggregates. KSCE J Civ Eng 22(4):1369–1376. https://doi.org/10.1007/s12205-017-0144-6

32. Nguyen DH, Sebaibi N, Boutouil M, Leleyter L, Baraud F (2014) A modified method for the design of pervious concrete mix. Constr Build Mater 73:271–282. https://doi.org/10.1016/j.conbuildmat.2014.09.088

33. Obla KH (2010) Pervious concrete - an overview. Indian Concr J 84(8):9–18

34. Oni B, Xia J, Liu M (2020) Mechanical properties of pressure moulded fibre reinforced pervious concrete pavement brick. Case Stud Constr Mater 13:e00431. https://doi.org/10.1016/j.cscm.2020.e00431

35. Patil AR, Darshan SC, Pradeepgouda PP, Vidyashree T, Chm G (2018) Influence of different size of aggregate and water cement ratio on pervious concrete 6(4):1090–1093

36. Sandoval GFB, Galobardes I, Schwantes-cezario N, Berenice M (2019) Correlation between permeability and porosity for pervious concrete Correlación de la permeabilidad y la porosidad para el concreto permeable (CoPe) 86(209):151–159

37. Schalla FE, Ashraf M, Barrett ME, Hodges BR (2017) Limitations of traditional capacity equations for long curb inlets. Transp Res Rec J Transp Res Board 2638(1):97–103. https://doi.org/10.3141/2638-11
38. Shams A, Sarasua WA, Putman BJ, Davis WJ, Ogle JH (2020) Highway cross-sectional design and maintenance to minimize hydroplaning. J Transp Eng Part B Pavements 146(4):04020065. https://doi.org/10.1061/jpeodx.0000213
39. Shukla BK, Gupta A (2020) Mix design and factors affecting strength of pervious concrete. In: Lecture notes in civil engineering, vol 38. Springer Singapore. https://doi.org/10.1007/978-981-13-7615-3_11
40. Tennis P (n.d.) Pervious concrete pavements
41. Torres A, Aguayo F, Gaedicke C, Nerby P, Cavazos M, Nerby C (2020) Developing high strength pervious concrete mixtures with local materials. J Mater Sci Chem Eng 8:20–34. https://doi.org/10.4236/msce.2020.81003
42. Van Vuuren BJ, Van Dijk M, Steyn W (2020) The interception capabilities of slotted drains as pavement surface drainage systems. J South African Inst Civil Eng 62(4):11–19. https://doi.org/10.17159/2309-8775/2020/V62N4A2
43. Vilane BRT, Sabelo N (2016) The effect of aggregate size on the compressive strength of concrete. J Agric Sci Eng 2(6):66–69. http://www.aiscience.org/journal/jase%5Cnhttp://creativecommons.org/licenses/by/4.0/
44. Xie N, Akin M, Shi X (2019) Permeable concrete pavements: a review of environmental benefits and durability. J Clean Prod 210:1605–1621. https://doi.org/10.1016/j.jclepro.2018.11.134
45. Yu F, Sun D, Wang J, Hu M (2019) Influence of aggregate size on compressive strength of pervious concrete. Constr Build Mater 209:463–475. https://doi.org/10.1016/j.conbuildmat.2019.03.140
46. Zaman ABK, Mustaffa Z, Giri LDLA (2019) Infiltration rate of pervious concrete on street curb application. Int J Recent Technol Eng 8(2 Special Issue 2):86–90. https://doi.org/10.35940/ijrte.B1016.0782S219
47. Zhong R, Leng Z, Sun PC (2018) Research and application of pervious concrete as a sustainable pavement material: a state-of-the-art and state-of-the-practice review. Constr Build Mater 183:544–553. https://doi.org/10.1016/j.conbuildmat.2018.06.131
48. Zhong R, Wille K (2015) Material design and characterization of high performance pervious concrete. Constr Build Mater 98:51–60. https://doi.org/10.1016/j.conbuildmat.2015.08.027

Application of Building Information Modelling (BIM) Technology in Drainage System Using Autodesk InfraWorks 360 Software

King Kuok Kuok, Kia Wee Kingston Tan, Po Chan Chiu, Mei Yun Chin, Md. Rezaur Rahman, and Muhammad Khusairy Bin Bakri

Abstract The increased number of physical drainage drawings at Samarahan district, Sarawak for new development areas is difficult to manage and handle by relevant authorities. Hence, this research is conducted to determine the feasibility of Building Information Technology (BIM) to create a proper drainage inventory system to accurately list and record current drainage information using Autodesk Infraworks 360 software. This inventory system will be employed to examine and validate corresponding drainage parameters based on the recorded information. Taman Uni-Central, a residential neighbourhood in Kota Samarahan, has been chosen for this case study. Drainage data, such as drainage size, length, invert level, are entered into GIS-integrated Model Builder in Autodesk InfraWorks 360. Autodesk InfraWorks 360 will conduct a preliminary analysis, including watershed analysis, to delineate the catchment area and drainage performance inspections at rainfall intensities of 2, 5, 10, 20, and 50 years (ARI). Thereafter, the InfraWorks model will be exported into Autodesk Civil3D to conduct a more extensive hydraulic analysis. The results show

K. K. Kuok (✉) · K. W. Kingston Tan · M. Y. Chin
Faculty of Engineering, Computing and Science, Swinburne University of Technology Sarawak Campus, 93350 Kuching, Sarawak, Malaysia
e-mail: kkuok@swinburne.edu.my

K. W. Kingston Tan
e-mail: 100077279@students.swinburne.edu.my

M. Y. Chin
e-mail: mychin@swinburne.edu.my

P. C. Chiu
Faculty of Computer Science and Information Technology, Universiti Malaysia Sarawak, 94300 Kota Samarahan, Sarawak, Malaysia
e-mail: pcchiu@unimas.my

Md. R. Rahman
Faculty of Engineering, Universiti Malaysia Sarawak, 94300 Kota Samarahan, Sarawak, Malaysia
e-mail: rmrezaur@unimas.my

M. K. Bin Bakri
Composites Materials and Engineering Center, Washington State University, 2001 East Grimes Way, Pullman, Washington State 99164, USA
e-mail: m.khusairybinbakri@wsu.edu

that full integration of these two Autodesk software packages had created a proper inventory system of existing drainage information and simulated its sufficiency in catering surcharge runoff from the new development area at the upper catchment.

Keywords Building Information Modelling (BIM) · Inventory management system · Autodesk InfraWorks 360 · Autodesk Civil3D · Average recurrence interval

1 Introduction

Referring to the 2010 Census (Department of Statistics Malaysia, 2010), the total population of Sarawak has experienced a high population growth of 19.3% since the previous Census conducted in 2000. Based on the data obtained, the Samarahan division holds the highest population growth percentage at 27.1%. The Sibu division follows this at 21.8% and the Kuching division at 21.5% [22].

The high population growth rate of Samarahan can be attributed to the rising position of the division as an education hub with its multitude of higher learning institutions and other educational facilities such as Universiti Malaysia Sarawak (UNIMAS), two campuses of University Teknologi MARA Kota Samarahan Campus (UiTM) and Institute of Teacher Education Tun Abdul Razak Campus. According to [20], with the Samarahan District reaching the criteria to be upgraded as a municipal council with a population of over 250,622 people in 2010 [6], the district is undergoing active property development, which will attract even more investors and therefore will bring an increase in construction works and work opportunities.

The current proposed drainage approval process involves submitting all drainage drawings in physical blueprints to the Department of Irrigation and Drainage (DID) Sarawak. The submission of physical blueprints would mean that submitted drawings may scatter around and are difficult to locate when required. The difficulty in retrieving physical drawings of existing drainage plans would delay the planning and approval process. This would cause great hassle when looking for past drawings as a reference before constructing new drainages discharged into the existing drainage system. Additionally, there is a lack of a proper systematic recording system to store the essential drainage information, including flow direction, drain and culvert size, and catchment areas in a master plan. Moreover, there is no system or software available to check and verify the capacity of the existing drainage system after receiving a surcharge from the nearby drainage system. There is a need to revamp our urban drainage management plans by adopting Autodesk InfraWorks, a Building Information Modelling (BIM) infrastructure software, to create an inventory system to record existing drainage information and integrate Autocad Civil 3D for water level forecasting within the drainage system [1, 2, 4, 14].

Autodesk InfraWorks is preliminary conceptual design software that allows users to visualize and render infrastructure models in real-world and real-time environments. It uses cloud-based 3D modelling technology where data can be obtained from

integrated Autodesk sources or manual input [3, 23]. Autodesk InfraWorks provides four main features: generating conceptual design models, contextual modelling, analysis and simulation, and live visualization of models (News [18]. Autodesk Infra-Works can integrate with GIS data for early-stage project planning, and it is interoperability with other BIM-oriented software such as Civil 3D, Navisworks and Revit [8, 9].

Autodesk InfraWorks was utilized in the SmiSto Hydropower Project, Norway, to combine GIS information of topographical information, areal imagery, and available map web services to create a detailed model [19]. Autodesk InfraWorks was also utilized for the rail track rehabilitation project in Portugal due to its accuracy terrain modelling and geolocation of the study site [16]. Autodesk InfraWorks also provided a brief overview of site conditions for the remodelling of the Ebro River bridge project in Spain [5]. Besides, [21] had utilized Autodesk Infraworks to simulate the stormwater runoff depth of the designed space based on the Low Impact Development (LID) principle in Bangkok, Thailand. However, Autodesk InfraWorks has yet to see practicable use within Malaysia.

In this study, Autodesk InfraWorks will be utilized to create an inventory system to systematically store and organize existing drainage information, including drainage size, invert level, flow direction and catchment area. The interoperability of Autodesk InfraWorks and Civil 3D will be demonstrated by importing the created Autodesk InfraWorks model into Civil 3D to check the adequacy of the existing drainage system to receive runoff from new developments at upper catchments. The selected study region is Taman Uni-Central, a mixed development area located at Kota Samarahan, Samarahan.

2   Study Area

Kota Samarahan is located about 30 km southeast of Kuching city. It is a fast-growing suburb in Sarawak, with an area of approximately 508.1 Km^2 [10, 11]. For decades, the main economic activity in Kota Samarahan has been agriculture with thousands of hectares of coconut, oil palm, and pineapples plantations. However, the Sarawak state government had successfully transformed Kota Samarahan into an educational hub in Sarawak that housed Universiti Malaysia Sarawak, two campuses of Universiti Teknologi MARA Kota Samarahan Campus, Tun Abdul Razak Teacher Training Institute, ILPKS Industrial Training Institute and INTAN Training College [12, 13]. With this transformation, the population in Kota Samarahan has grown significantly for the past twenty years. Many new mixed developments were built to accommodate the rapidly increasing population.

One rapidly grown mix development is Taman Uni-Central, located at the North-Western of the Kuching-Samarahan Expressway (refer to Fig. 1). According to [17], the surrounding Uni-Vista and Uni-Garden have been facing rising flash flood occurrences. Residents have commented that this occurrence was attributed to the existing

Fig. 1 Satellite view of Taman Uni-Central, Kota Samarahan

drainage not being improved despite the rapid development of the areas. Additionally, the increase of impervious surfaces due to rapid urbanization also contributed to flash flooding occurrences in the Uni-Central area [7]. The study further showed that the earth drain is insufficient for discharge capacity, which could not cater to the generated peak discharge flow, thus causing the stormwater overflow. Residents also claimed that the floods were also caused by the undersize of the existing drainage system despite the ongoing rapid development.

3   Methodology

Figure 2 shows the research project methodology divided into three main stages. The first stage is data collection, which involves procuring data relevant to the drainage system at Taman Uni-Central. The second stage is plotting the drainage system and conducting initial hydraulics analysis using the Autodesk InfraWorks Drainage Design feature. The third stage is importing the model into Autocad Civil 3D for hydrologic and hydraulic analysis.

Stage 1: Data Collection
The initial site investigation was carried out to understand the general layout of Taman Uni Central. The first stage involves data collection of drainage flow direction, catchment areas, drainage layout, and invert levels through site investigation and application of Google Earth Pro. The catchment areas are then suitably delineated into different sub-basin for hydrology and hydraulic analysis. The coefficients of rainfall intensity duration frequency (IDF) curves with different average recurrence interval (ARI) was also obtained from the Urban Storm Water Management Manual (MSMA) published by the Department of Irrigation and Drainage Sarawak [15].
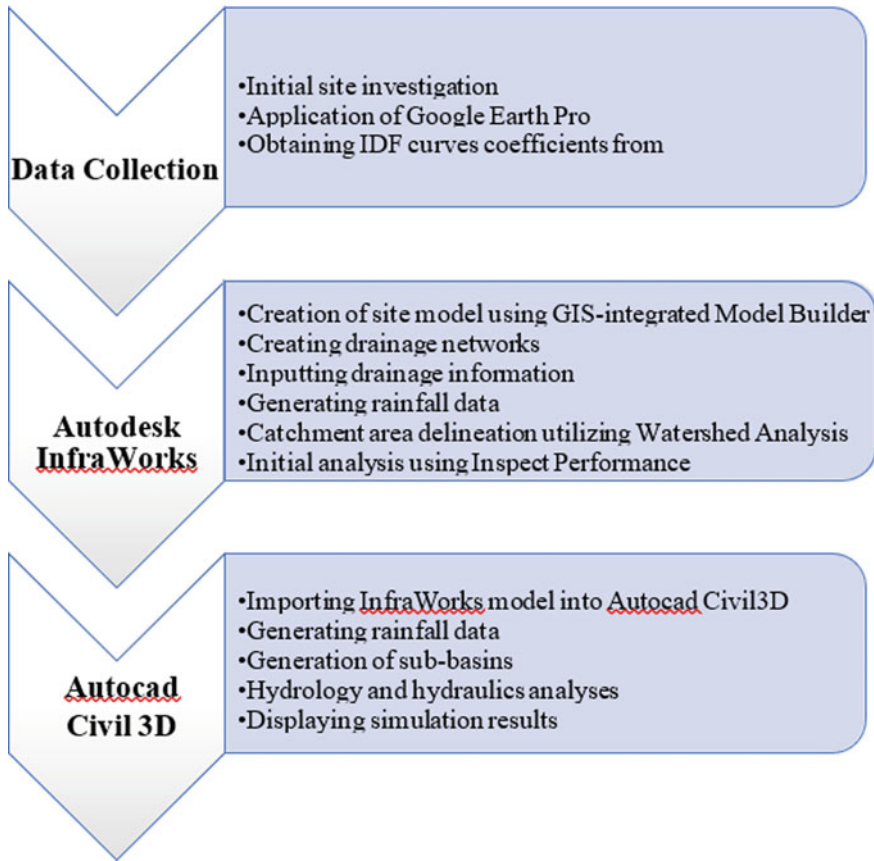
Fig. 2 Overview of research methodology

Stage 2: Autodesk InfraWorks

Autodesk InfraWorks is used to plot the layout of the drainage system of Taman Uni-Central, Kota Samarahan. The modelling procedures of Autodesk InfraWorks are:

a) Determination of Model Extents using Model Builder—The Model Builder feature integrates within InfraWorks is a GIS data source by inputting available data layers from cloud data for model creation. The extent of the model is determined by drawing a rectangle on the model location. Additionally, a coordinate system will be selected to increase the model accuracy. Since Taman Uni-Cental is located within the island of Borneo, the coordinate system with code "BORNEO" for East Malaysia is selected.

b) Creation of Site Model—The site model for Taman Uni-Central can be downloaded from Autodesk Cloud. Figure 3 presents the integrated model builder that already incorporated data layers from OpenStreetMaps and Bing Maps. This

integrated Model Builder function is used to obtain the terrain of the site. The red colouration denotes the low areas of the site terrain, whereas the navy-blue colouration denotes the highest areas of the site terrain. The obtained terrain is vital for the delineation of sub-catchments.

c) The input of coefficients of rainfall Intensity Density Frequency (IDF) Curves – The coefficient of rainfall IDF curves obtained from MSMA, as presented in Table 1 are inputted into Autodesk InfraWorks. The polynomial equation for fitted IDF curves for 5, 10, 20, 50 years ARI is presented in Eq. 1.

$$ln(RIt) = a + bln(t) + c(ln(t))2 + d(ln(t))3 \tag{1}$$

where $^{R}I_t$ is average rainfall intensity (mm/hr) for ARI and duration t, R is average return interval (years) and t is duration in minutes.

d) Plotting of Drainage Layout - The drainage layout can be inputted into the Infra-Works model by inputting the drain sizes, invert levels, bed slope, drainage networks as presented in Fig. 4.
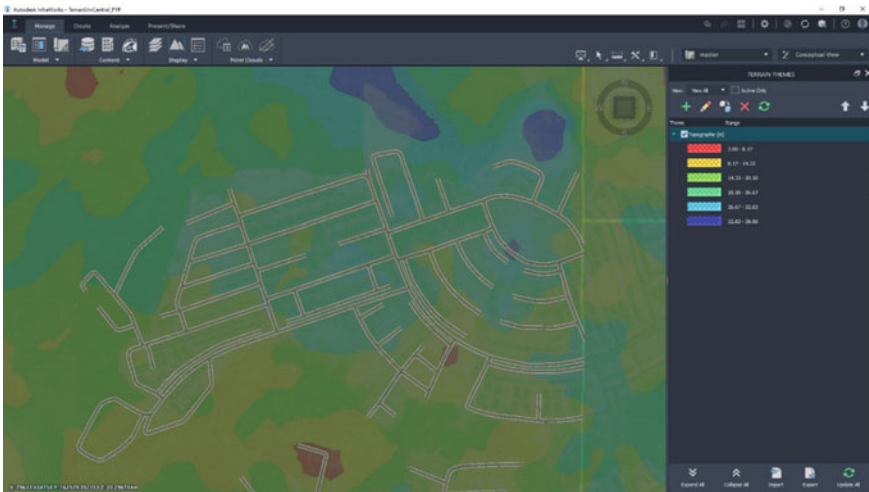
Fig. 3 Terrain theme of Autodesk InfraWorks model

Table 1 IDF polynomial coefficients for different ARI (MSMA, 2000)

Location	ARI parameter (year)	a	b	c	d
Kota Samarahan	2	5.1719	0.1558	0.1093	0.0043
	5	4.8825	0.3871	0.1455	0.0068
	10	5.1635	0.2268	0.1039	0.0039
	20	5.2479	0.2107	0.0968	0.0035
	50	5.278	0.224	0.0932	
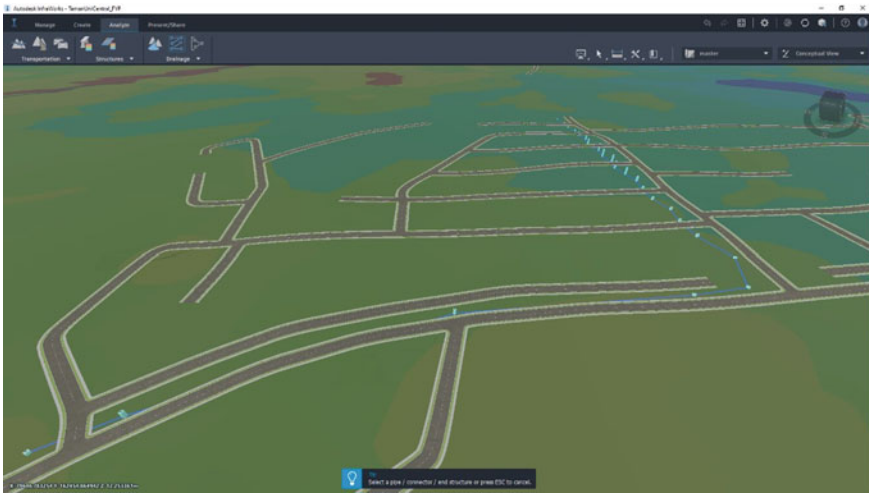
Fig. 4 Plotting of drainage network

e) Watershed Analysis - Autodesk InfraWorks is able to generate the hydraulic and energy grade lines for each drain. Hydraulic grade line (HGL) will help determine probable elevations to which the water would rise under atmospheric pressure occur during a storm event. The energy grade line (EGL) is an imaginary line to measure the total energy including the elevation head, velocity head, and pressure head, along the open channel carrying water.

Stage 3: Autocad Civil 3D (Storm and Sanitary Analysis)
The Autodesk InfraWorks model is imported into Autocad Civil 3D to carry out the Storm Analysis by Storm and Sanitary Analysis (SSA) extension. SSA is typically used to analyze gravity flow-based urban drainage systems. The sub-basins were drawn manually in Autodesk Civil 3D using polylines and converted into parcels after that. The created parcels are then imported into SSA in LandXML files. Figure 5 presents the imported sub-basins into the SSA model.

As SSA focuses primarily on stormwater and urban drainage analysis, all the drainage inventories, including the drainage networks, dimensions, invert levels created in Autodesk InfraWorks, were imported into SSA as Hydroflow Storm Sewers file. The imported drainage networks are imported into SSA is presented in Fig. 6.

The previously created IDF rainfall in Autodesk InfraWorks is also imported into the SSA. The runoff peak is analyzed using the rational method by utilizing the IDF polynomial coefficients for different ARI obtained from the MSMA. The time of concentration (ToC) is determined with the Kirpich method and the flow routing is calculated with the Kinematic Wave method. The analysis options are defined and the analysis is conducted for a duration of one day. Based on the results, the undersized drainage system will then be reanalyzed.
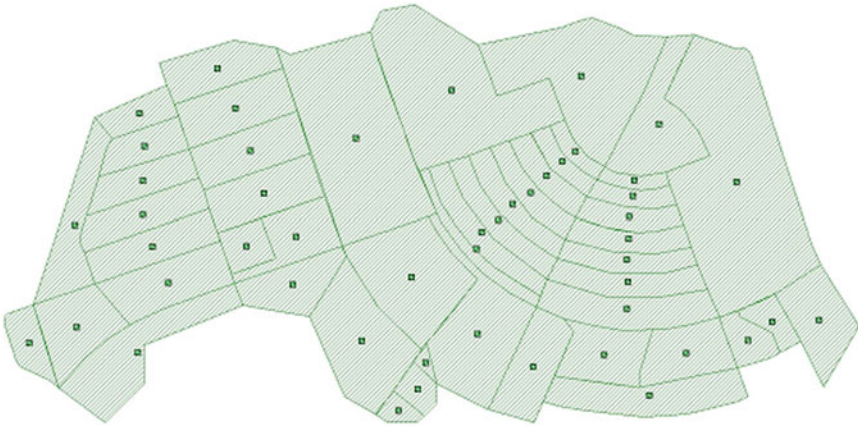
Fig. 5 Imported sub-basin areas into SSA extension
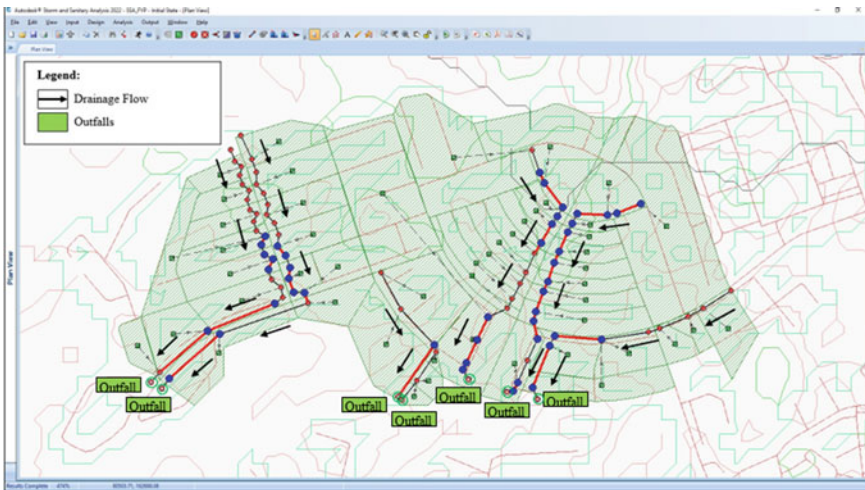
Fig. 6 Import of Autodesk InfraWorks model into SSA

4 Results and Discussion

4.1 Autodesk InfraWorks Analysis

The initial stage of this research project involves modelling the Taman Uni-Central drainage network in Autodesk InfraWorks. Figure 7 shows the successful mapping of the drainage system in Taman Uni-Central. Each drainage network is indicated using different colours and labels systematically according to exact coordinates on-site. Additionally, the existing GIS data sources integrated into Autodesk InfraWorks

Fig. 7 Completed drainage layout of Taman Uni-Central

are able to provide users with a preliminary base map without carrying the on-site topographic or contour survey. The created model is an inventory system to display, record, and list existing drainage information.

It was found that a thriving watershed was generated for Taman UniCentral. Autodesk InfraWorks is also able to detect and identify the culvert locations if the drain is cutting through the roads. Autodesk InfraWorks also designed the culverts' dimensions after imputing the required hydrology data into the models. As a purely conceptual-based modelling software, the analysis features for drainage design using Autodesk InfraWorks are limited. Thus, hydrology and hydraulic analysis are conducted using SSA extension in Autodesk Civil 3D.

Autocad Civil 3D—Storm and Sanitary Analysis (SSA) Extension
Due to the constraints of Autodesk InfraWorks as a conceptual design software with limited analysis options, Autocad Civil 3D in SSA extension will be used to conduct hydrology and hydraulic analysis of stormwater systems.

The first result obtained from the SSA is in the form of a visual plan view of the overall drainage layout plotted from Autodesk InfraWorks. The flooded drainage area will be highlighted in red colour. The flow direction of the drainage networks will be determined by the drain invert levels provided into the SSA extension. Results show that the map plotted in Autocad Civil 3D is successfully imported from Autodesk InfraWorks for model simulation. The properties of nodes, links, sub-catchments, ground level, drain sizes were successfully imported into Autocad Civil 3D and matched the information inputted in Autodesk InfraWorks. By importing the data of the drainage details directly into Autocad Civil 3D, users will not have to key in the required information one by one. This method is extremely effective and efficient when checking existing drainage capacity after connecting with new development areas. Figures 8, 9, 10, 11, 12 and 13 show the drainage network 1, 2, 3, 5, 6 and 7, respectively, with the extreme rainfall intensity of 30 and 50-year ARI with 30, 60, 120 and 360 min duration.

From the simulation results, drainage network 1, network 2, network 3, network 4, network 5, network 6 and network 7 were found to be sufficient to cater for most of the
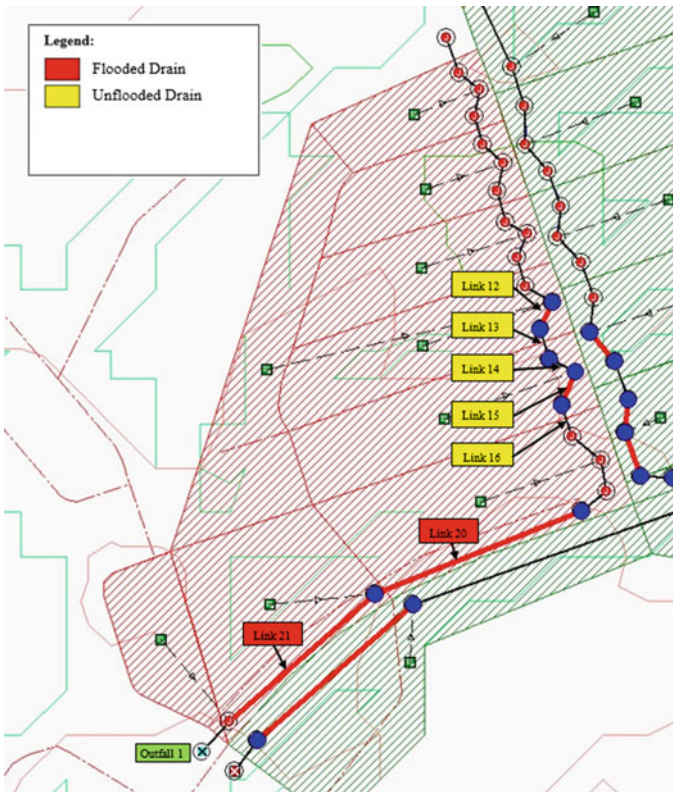
Fig. 8 Locations of highlighted inadequate drainage network 1
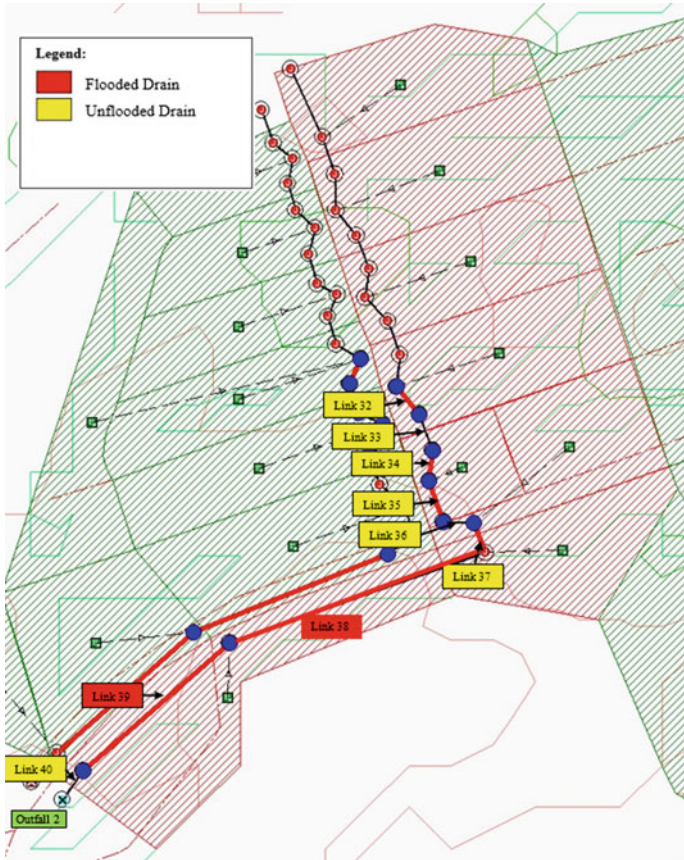
Fig. 9 Locations of highlighted inadequate drainage network 2

rainfall events at different ARIs and durations. However, it was found that drainage network 1 is inadequate to cater for the water flow resulting from the rainfall event of 50 years ARI with 30, 60, 120 and 360 min duration ($^{50}I_{30mins}$, $^{50}I_{60mins}$, $^{50}I_{120mins}$, $^{50}I_{360mins}$) at links 20 and 21. The water level has also overflown the drainage network 2 at links 38 and 39 for rainfall intensity of 50 years ARI with 60, 120 and 360 min
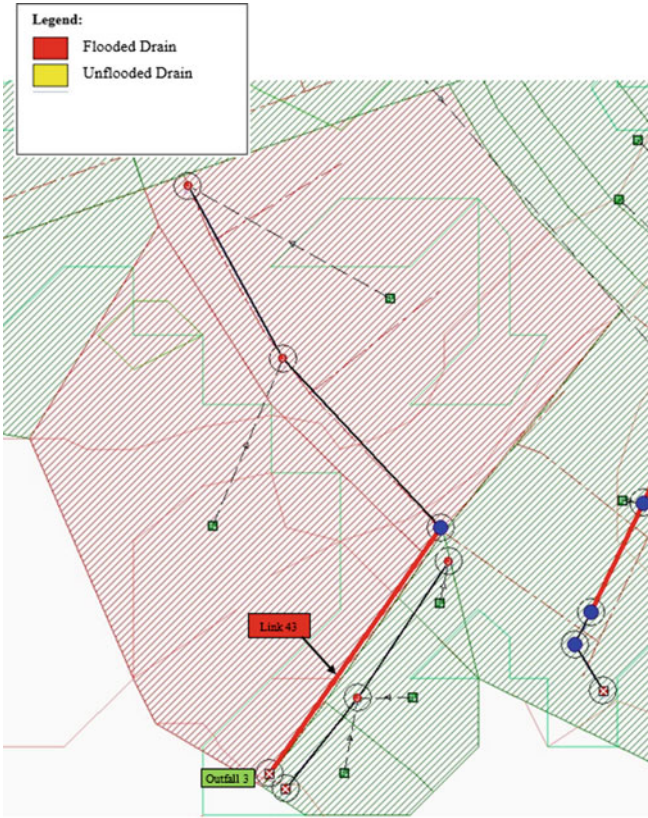
Fig. 10 Locations of highlighted inadequate drainage network 3

duration ($^{50}I_{60mins}$, $^{50}I_{120mins}$, $^{50}I_{360mins}$). Drainage network 3 was flooded as well at link 43 when simulated with rainfall intensity of 50 years ARI with 60 and 120 min duration ($^{50}I_{60mins}$ and $^{50}I_{120mins}$). Drainage network 4 was found to be sufficient to cater to all investigated rainfall intensities at different ARIs and durations. Therefore, no improvement work is required for the Drainage network 4.
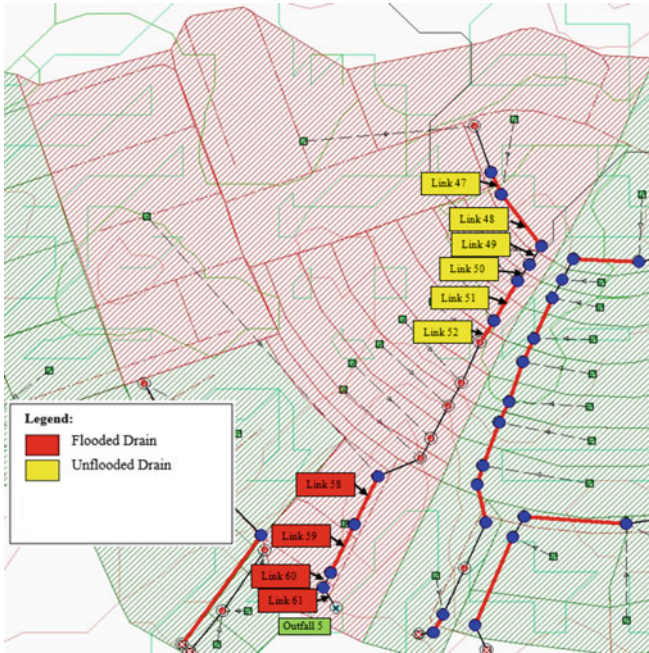
Fig. 11 Locations of highlighted inadequate drainage network 5

The results show that drainage network 5 is able to cater the rainfall intensity at different ARIs and durations except for 50 years ARI at 30, 120, 360 min duration ($^{50}I_{30mins}$, $^{50}I_{60mins}$, $^{50}I_{120mins}$, $^{50}I_{360mins}$) at links 58, 59, 60 and 61. Drainage network 6 is overflowed at links 74, 75, 76 and 77 with the rainfall intensity of 20 and 50 years ARI at 120 and 360 min duration ($^{20}I_{120mins}$, $^{20}I_{360mins}$, $^{50}I_{120mins}$, $^{50}I_{360mins}$). Simulation results also revealed that drainage network 7 is unable to cater for the rainfall intensity of 20 and 50 years ARI with 30, 60, 120 and 360 min duration at links 83, 84, 85 and 86.
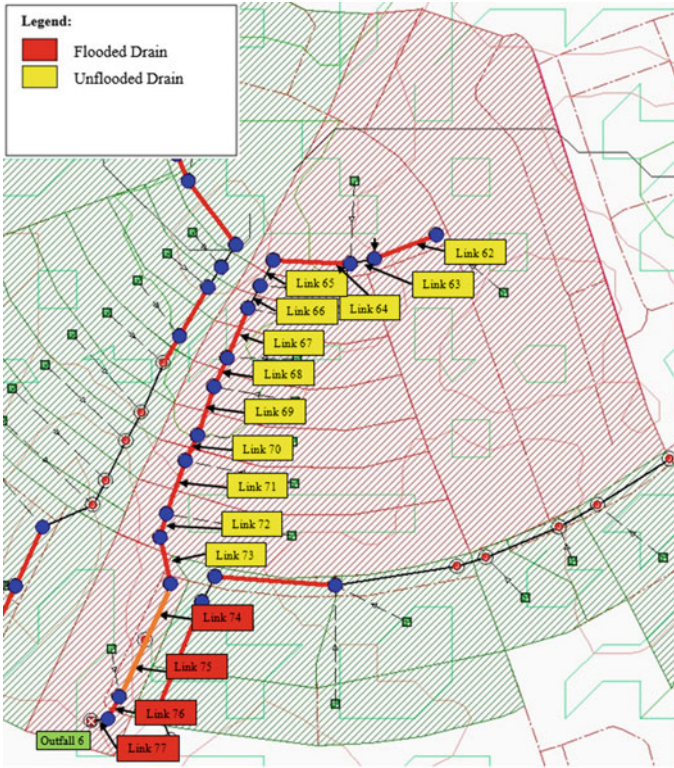
Fig. 12 Locations of highlighted inadequate drainage network 6
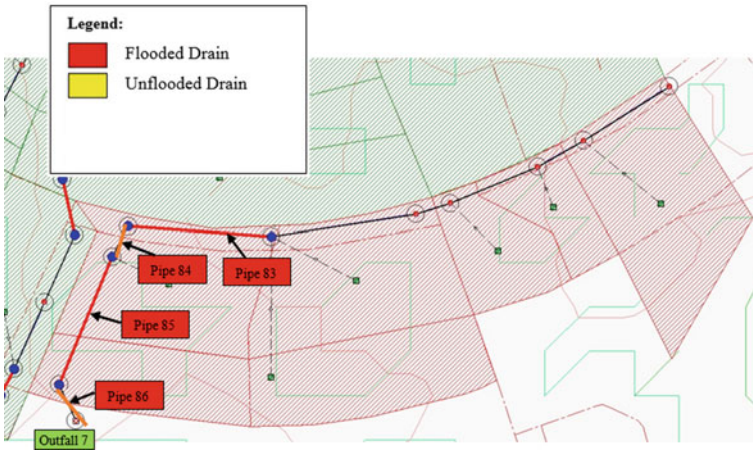
Fig. 13 Locations of highlighted inadequate drainage network 7

5 Conclusion

This research project has shown that the drainage layout of Taman Uni-Central was successfully modelled using Autodesk InfraWorks software, detailing all recorded drainage information. This will help record all the existing drainage neatly and correctly, thus simplifying the process's recording. Whenever drainage from a new development area connects to the existing drainage system, Autodesk InfraWorks will perform as a visual inventory system where all drainage information can be inspected and checked in detail. Autodesk InfraWorks will export the model into Autocad Civil3D under SSA extension to perform hydrology and hydraulics analysis of the drainage networks. This indicates that Autodesk InfraWorks software that performs as BIM for infrastructure works is highly feasible and can be integrated with Autocad Civil3D for performing drainage design processes. Under SSA extension, Autocad Civil3D is able to conduct hydrology and hydraulics analysis with different ARIs and durations to check the adequacy of the existing drainage network in catering the rainfall events.

References

1. Al-Ashmori Y et al (2020) BIM benefits and its influence on the BIM implementation in Malaysia. Ains Shams Eng J. https://doi.org/10.1016/j.asej.2020.02.002. Accessed15 Nov 2020
2. Akeila M, Kuok KKK, Wong NM (2018) Evaluating the visibility of building syrian refugee shelters by 3D printing technology in Jordan. Int J Eng Technol 8(3(2019)):377–385
3. Anderson M (2014) The rising tide: drainage design for Infraworks 360', Autodesk University 2014
4. Autodesk (2020) InfraWorks, Autodesk. https://www.autodesk.com/products/infraworks/features#:~:text=InfraWorks%20enables%20AEC%20professionals%20to,improving%20decisions%20and%20project%20outcomes. Accessed 20 Nov 2020
5. Blanco R, Garcia J, Gonzalez B, Alberti M, Alvarez A (2019) Use of BIM methodology in the remodelling of an existing bridge. Anales de Edificación 5(3):100–106
6. Department of Statistics Malaysia (2010) Population and housing census of Malaysia (Preliminary count report), Department of Statistics Malaysia. https://www.dosm.gov.my/v1/index.php?r=column/cthemeByCat&cat=117&bul_id=Wk81WnBvbXdtQzdJRjdmM2hSNHM3Zz09&menu_id=L0pheU43NWJwRWVSZklWdzQ4TlhUUT09. Accessed 15 May 2021
7. Hauzi E, Lim L, Bong C (2017) A hydrology and hydraulic case study on January 2015 flash fload in UniGarden, Kota Samarahan, Sarawak'. In: 37th IAHR World Congress, Department of Civil Engineering, Universiti Malaysia Sarawak, Sarawak
8. Huang J (2013) Making something from nothing: integrating Autodesk InfraWorks into your design. Autodesk University, Las Vegas
9. Huang J (2017) BIM evolution for wet infrastructure: what if we started Panama Canal expansion today? Autodesk University, Las Vegas
10. Kuok KK, Ziet LZ, PoChan C (2013) Flood map development by coupling satellite maps and three-dimensional drafting software: case study of the Sarawak River Basin. Water SA 39(1):175–182

11. Kuok KK, Harun S, Chiu PC (2011a) Comparison of particle swarm optimization and shuffle complex evolution for auto-calibration of hourly tank model's parameters. Int J Adv Soft Comput Appl 3(3):1–17
12. Kuok KK, Harun S, Chan CP (2011b) Investigation best number of tanks for hydrological tank model for rural catchment in humid region. J Inst Eng 72:1–11
13. Kuok KK, Chiu PC (2018) Indigenous drinking-water consumption pattern of residents in Kuching city: results of a pilot study. J Water Sanit Hyg Dev 8(4):817–824
14. Lee S, Yu J, Jeong D (2015) BIM acceptance model in construction organizations. J Manag Eng 31(3):04014048
15. MSMA–Urban Storm Water Management (2001) Department of Irrigation and Drainage Malaysia, Ministry of Environment and Water, Malaysia
16. Neves J, Sampaio Z, Vilela M (2019) A case study of BIM implementation in rail track rehabilitation. Infrastructures 4(1):8
17. New Star Tribune (2018) Kota Samarahan (P197) Sarawak's education hub, New Star Tribune, 14 April 2018
18. News Desk (2018) InfraWorks collaboration enterprise cloud collaboration with BIM 360, Geospatial World. https://www.geospatialworld.net/news/infraworks-enterprisecloud-collaborationbim-360/. Accessed 20 Nov 2020
19. Nielsen L, Hansen G (2015) Case study: use of InfraWorks and the infrastructure design suite for a hydropower project in Norway. Multiconsult ASA, CI11984
20. Ogilvy G (2016) CM: Kota Samarahan must urbanization growth. The Star, 12 November 2016
21. Rinchumphu D, Choruengwiwat J, Pongsuwan S, Kleatkongmanee N, Yang C, Srivanit M (2019) The eco-efficiency model for outdoor environmental design for the mixed-use real estate development in Bangkok, Thailan
22. Sarawak Government (2020) Sarawak Population, Sarawak Government. https://www.sarawak.gov.my/web/home/article_view/240/175/. Accessed 15 Oct 2020
23. Wei T, Chen G, Wang J (2017) Application of BIM technology in building water supply and drainage design. In: 1st International Global on Renewable Energy and Development, IOP Publishing Ltd., Singapore, vol 100

Comparison of Drag Models in Shallow Flow for Spherical Particle Trajectory

Lavine Wong, Mohamad Hidayat Jamal, and Erwan Hafizi Kasiman

Abstract Numerical models play a significant role in predicting the movement of floating debris. One significant force in predicting a floating object's motion is the drag force. Many empirical methods of drag coefficient (C_D) have emerged over the years to estimate the drag force of spherical particles. This study aims to simulate different C_D of spherical particle trajectory utilizing TELEMAC2D software. The simulation is compared with an Eulerian–Lagrangian one-way coupling discrete element model (DEM). A floating spherical object of radius 0.02 m and density 500 kg ms^{-1} was released in a steady flow of 0.4 m water depth and velocity 0.5 ms^{-1}. The simulated trajectory of the particle within the initial five seconds agrees closely with the DEM simulation, but all six drag coefficient formulas overestimated the distance after five seconds. Therefore, different empirical drag formulas exhibit similar estimations towards the movement of floating debris, and the models' accuracy can be improved with detailed physics of the floating object.

Keywords Floating debris · Drag coefficient · Spherical particle · Eulerian–Lagrangian · One-way coupling

L. Wong (✉) · M. H. Jamal · E. H. Kasiman
School of Civil Engineering, Faculty of Engineering, Universiti Teknologi Malaysia, 81310 Skudai, Johor, Malaysia
e-mail: wlavine2@graduate.utm.my

M. H. Jamal
e-mail: mhidayat@utm.my

E. H. Kasiman
e-mail: erwanhafizi@utm.my

M. H. Jamal · E. H. Kasiman
Centre for River and Coastal Engineering (CRCE), Universiti Teknologi Malaysia, Johor Bahru, Malaysia

1 Introduction

Numerical modelling has been a prevalent research tool to simulate floating debris in shallow and violent flows [12, 20, 24, 28]. These numerical techniques involve internal coupling within the model system or between two different types of models. The interaction can be further simplified into one-way solid to fluid, one-way fluid to solid and two-way dynamic coupling [19, 29]. One way solid to fluid coupling or vice-versa predicts movement of recipient phase to the driving phase. In this case, the dynamics of either the fluid or the solid phase is less predominant than the interaction, and the feedback of the recipient phase is negligible [20, 24, 27]. Two-way dynamic coupling methods consider dynamic interaction between fluids and solids. The motion of the solid imposes a counterforce on the fluid and changes its dynamics as the fluid flow drives the solid. Eulerian–Lagrangian models, force analysis, smooth particle hydrodynamics (SPH or SPH-DEM models are among the methods to determine this two-way interaction [3, 10, 21–23]. Although proven to be successful in simulating the specific type of floating objects, two-way coupling methods are more computational extensive and reproduced only in small scale engineering test-case [18, 22]. Its application to large-scale real-world problems may still be a challenge.

In solid motion dynamics, drag force is one of the crucial forces to determine the interaction between solid and fluid. Evaluation of C_D for floating debris is essential to determine its transport in water applications. Dozens of empirical or semiempirical formulas specifically for spherical particles have been published in the literature [1, 7, 25, 26]. For spherical objects, the influence of drag depends on the Reynolds number (Re). Though some formulas are simple, it is only limited to a certain range of Re. In contrast, those that can be applied at a wide range of Re involves complicated application procedure [4]. Therefore, this study aims to compare the different available drag formulas specifically for spherical object transport in shallow flow employing the Lagrangian–Eulerian approach. The particle trajectory motion is validated as a numerical and analytical outcome from a discrete element method (DEM) model. The numerical prediction of transport of floating bodies is important for better accuracy in future prediction of floating debris using a coastal hydraulic model.

2 Hydrodynamic Model

The hydrodynamic model used in this study is the Telemac 2D model, which solves the free surface flow depth-averaged equation derived by Barre de Saint–Venant at each node of the computation domain. The main results at each node of the computational mesh are the depth of water and depth-averaged velocity components [17]. The equation is solved through a finite-element method over non-structured grids

consisting of triangles [11]. The free surface non-hydrostatic Navier–Stokes equations using mass and momentum conservation is shown in Cartesian coordinates in Eq. (1a), (1b) and (1c) where u^f, v^f represents horizontal components of depth average velocity, t is time, g is the gravity acceleration, υ is the coefficient of kinematic viscosity, ρ^f represents fluid density, F_x, F_y are the friction terms, while x, y denotes the horizontal space coordinates.

$$\frac{\partial (u^f)}{\partial x} + \frac{\partial (v^f)}{\partial y} = 0 \tag{1a}$$

$$\frac{\partial (u^f)}{\partial t} + u^f \frac{\partial (u^f)}{\partial x} + v^f \frac{\partial (u^f)}{\partial y}$$
$$= -\frac{1}{\rho^f} \frac{\partial p}{\partial x} + \upsilon \Delta (u^f) + F_x \tag{1b}$$

$$\frac{\partial (v^f)}{\partial t} + u^f \frac{\partial (v^f)}{\partial x} + v^f V \frac{\partial (v^f)}{\partial y}$$
$$= -\frac{1}{\rho^f} \frac{\partial p}{\partial y} + \upsilon \Delta (v^f) + F_y \tag{1c}$$

The hydraulic variables of the flow are required so that hydrodynamic forces exerted on the body can be calculated. The Eulerian solution of the SWE is coupled with the Lagrangian model for the transport of floating bodies. This means that the flow quantities computed by the SWE module are available at each time step to determine the forces acting on the floating bodies, while the reaction of the bodies on the flow is also taken into consideration.

3 Particle Transport Model

3.1 Solid–Fluid Interaction

The general motion of floating debris in the marine environment is driven by physical forces, gravity force, buoyancy force, drag force which depends on the particle characteristic, most importantly its size, shape and density [5]. A schematic diagram of the general movement of particle transport in a fluid is seen in Fig. 1.

The interaction between phases is also determined based on the strength of coupling between them. If the particle concentration is considered dense, feedback of particles to the driving phase has to be accounted for, and interaction between particles cannot be neglected. This means four-way coupling has to be carried out in order for high order accuracy [13]. For immediate concentration, the interaction between particles can be ignored, but the particle's feedback on the driving
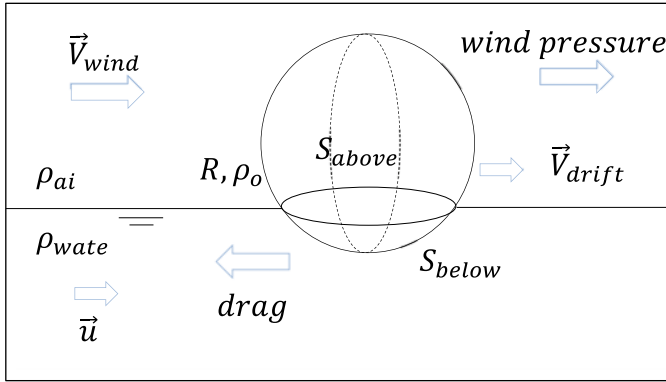
Fig. 1 Notations and forces of a sphere rolling over the water surface

phase need to be considered. Therefore, the two-way coupling is required. In dilute concentrations situations, the fluid flow is considered regardless of the particle's influence [14–16]. According to [8], a method to determine the type of interaction using particle volume fraction, α^p is following the criterion below. With the assumption that the concentration of particles is low enough, the one-way coupling is valid for this comparison.

$\alpha^p < 10^{-6}$, for one-way coupling.

$10^{-6} < \alpha^p \leq 10^{-3}$, for two-way coupling;

$\alpha^p > 10^{-3}$, for four-way coupling.

The interaction between fluid flows and floating objects can be expressed by an ordinary differential equation derived by Oseen from the works of Boussinesq and Basset [6, 30]. Forces considered in the dynamic equation includes the inertial force, buoyancy force, drag force, added mass force and the Basset history force [13, 16]. The Newton law for a spherical particle equation of motion is thus described in Eq. 2 where ρ^P is the density of the particle, D^P is the particle's diameter, and V represents the velocity of the particle, and U is the fluid velocity.

$$\rho^P \frac{dV}{dt} = \rho^P \frac{dU}{dt} + \left(\rho^P - \rho^f\right)g + \frac{3}{4}\frac{\rho^f}{D^P}C_D(U - V)\lceil U - V\rceil$$
$$- \frac{\rho^f}{2}\frac{d(V - U)}{dt} \tag{2}$$

In order to model the transport of particle in the fluid flow, a three-equation model is used as in Eq. 3 in TELEMAC2D where U is the fluid velocity, V is the particle velocity, X is the particle position, T_t is the integral time scale, T_{part} is the particle relaxation time, dt is considered as the numerical time step, i denotes the value at the particular time step, dW_i represents a Weiner process, C_i is the coefficient that regroups the flow components, B_i is the standard deviation of the stochastic term,

F_a is the regrouped force components $F_{i,c}$ coefficient depended on constant values during time t.

$$dU_i = -\frac{1}{T_t}U_i dt + C_i dt + B_i dW_i \tag{3a}$$

$$dV_i = F_a dU_i + \frac{1}{T_{part}}(U_i - V_i)dt + F_{i,c}dt \tag{3b}$$

$$dX_i = V_i dt \tag{3c}$$

3.2 Drag Models

One important stage in Lagrangian particle tracking is considering the proper drag model that works for spherical objects. [4] summarises the different empirical and semi-empirical drag formulas that have been found from literature with Reynolds numbers up to 2×10^5. Amongst the dozens of C_D coefficient derivation, the selected formulas are of high accuracy based on the statistical assessment of average relative error, the sum of squared errors and the sum of deviation [4]. The adopted C_D-Re relationship used as a comparison for a spherical particle in this study is listed in Table 1.

4 Model Set-Up

The hydrodynamic model was set up using Telemac2D, which is a finite element model that computes the results of the depth of water and depth-averaged velocity components at each node of the mesh domain. The dimension of the flume set up is $1 \times 1 \times 20$ m with a discretized domain using a uniform grid of 0.02 m resolution. Prescribed discharge and depth was set at both ends of the boundary conditions to obtain a constant water depth of 0.4 m and velocity 0.5 ms^{-1} (Fig. 2). The constant Manning coefficient is set to be 0.01, and the time step used was 0.001.

5 Preliminary Result and Discussion

The model is compared in one dimensional with a DEM simulation and analytical solution conducted by Xiong et al. 2019. The steady flow is a water depth of 0.4 m and velocity 0.5 ms^{-1}. A small ball of radius 0.02 m and density 500 kg ms^{-1} is released once the flow is steady. The domain was discretised using a uniform grid of 0.1 m

Table 1 Previous drag coefficient formula applicable for the subcritical region

No.	Author	C_D-Re relationship	Eq.
1	[9]	$C_D = \frac{24}{Re}(10Re)^{\propto},$ $\propto = 0.61Re^{0.369} - 0.105Re^{0.431} - \frac{0.124}{1+log^2 Re}$	4
2	[26]	$C_D = \frac{24}{Re}(1 + 0.173Re^{0.657}) + \frac{0.413}{1+42500Re^{-1.16}}$	5
3	[7]	$C_D = \frac{24}{Re}(1 + 0.15Re^{0.687}) + \frac{0.42}{1+16300Re^{-1}}$	6
5	[2]	$C_D = \frac{24}{Re}(1 + 0.15Re^{0.681}) + \frac{0.407}{1+8710Re^{-1}}$	7
6	[1]	$C_D = \lceil \frac{1}{(\varphi_1+\varphi_2)^{-1}+\varphi_3^{-1}} + \varphi_4 \rceil^{1/10}$ Where $\varphi_1 = \left(\frac{24}{Re}\right)^{10} + \left(\frac{24}{Re^{0.67}}\right)^{10} + \left(\frac{4}{Re^{0.33}}\right)^{10} + 0.4^{10}$ $\varphi_2 = \frac{1}{(0.148Re^{0.11})^{-10}+0.15^{-10}}$ $\varphi_3 = \left(1.57 \times \frac{10^8}{Re^{1.625}}\right)^{10}$ $\varphi_4 = \frac{1}{(6x10^{-17}Re^{2.63})^{-10}+0.2^{-10}}$	8
6	[4]	$C_D = \frac{24}{Re}(1 + 0.27Re^{0.43}) + 0.47[1 - exp(-0.04Re^{0.38})]$	9
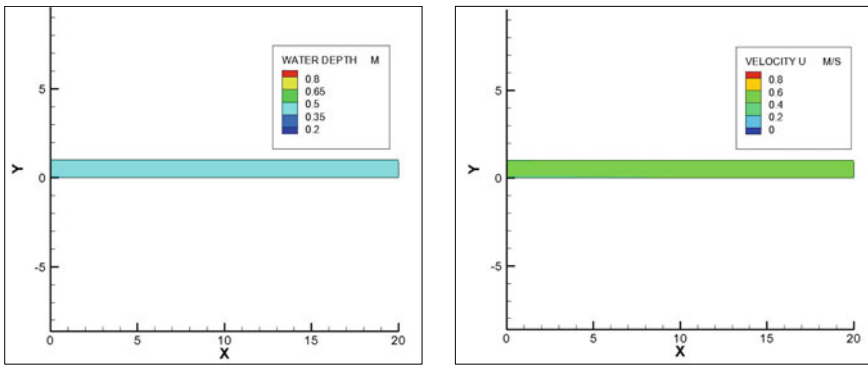
Fig. 2 Constant water depth (left) and constant velocity (right) of flume set up

resolution, and the constant Manning coefficient was set to 0.01. The location of the particle at every second is recorded with the drag formulas as simulated previously, and the results are shown in Fig. 3. [29] replace the drag force with a new method that uses hydrostatic and hydrodynamic forces to encapsulate the fluid–solid interaction using a DEM model. In order to check for accuracy, different empirical formulas of C_D were tested, and the floating particle debris was simulated in TELEMAC2D to analyse its trajectory movement. From Fig. 3, there is no significant difference when a different drag model was implemented in the particle tracking code. Instead, the estimation of drag used by different spherical empirical formulas is higher than the numerical and analytical solutions. At time 20 s, the x-position of the particle is approximate 9 m, which is approximately a meter more than the analytical position. Although experimentally, the proposed drag formulas have shown good agreement with experimental values, numerically, these drag models are still not able to accurately represent the actual phenomenon. This shows that the empirical drag coefficient overestimates the x-position of the particle and is less accurate than what has been predicted by [29]. In DEM models, the kinematics of the body is taken into consideration, which drives the flow and changes the velocity over time. This includes the rotation and translational movement of the body, which translates to higher accuracy results. Meanwhile, in this one-way coupling method, only information from the fluid is imposed on the solid. The information from the solid does not change the velocity of the flow, which contributes to less accuracy of the trajectory motion.
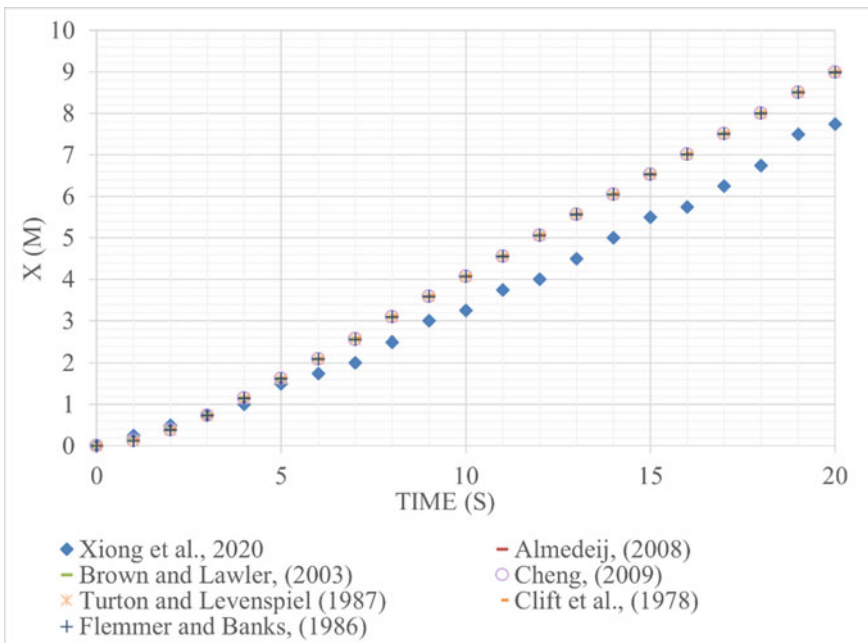
Fig. 3 Comparison of different C_D formulas on floating spherical particle movement

6   Conclusion

The numerical simulation on the trajectory of spherical floating debris is tested with six high statistical assessment accuracies drag coefficient parameters. The model, Telemac2D simulation, was utilized to set up a $1 \times 1 \times 20$ m flume with mesh discretization of 0.02 m resolution, and the simulation was compared with a DEM model. The trajectory movement between the six drag models shows a similar movement but differs from the DEM analytical model solution. Output results initially follow the movement of particle trajectory accurately but appear to overestimate the particle movement after the fifth second. There is a discrepancy of approximately 1 m between both analytical and simulated results possibly contributed by kinematic forces, which were not included in the model. Some suggestion to improve the accuracy of the current model is to add additional forces to the dynamic momentum equation of the particle trajectory coupled with physical experiments to further validate and verify the exact position of the floating object.

References

1. Almedeij J (2008) Drag coefficient of flow around a sphere: Matching asymptotically the wide trend. Powder Technol 186(3):218–223
2. Brown PP, Lawler DF (2003) Sphere drag and settling velocity revisited. J Environ Eng 129(3):222–231
3. Canelas RB, Domínguez JM, Crespo AJC, Gómez-Gesteira M, Ferreira RML (2017) Resolved simulation of a granular-fluid flow with a coupled SPH-DCDEM model. J Hydraul Eng 143(9):06017012
4. Cheng NS (2009) Comparison of formulas for drag coefficient and settling velocity of spherical particles. Powder Technol 189(3):395–398
5. Chubarenko I, Bagaev A, Zobkov M, Esiukova E (2016) On some physical and dynamical properties of microplastic particles in marine environment. Mar Pollut Bull 108(1–2):105–112
6. Coimbra CFM, Rangel RH (1998) General solution of the particle momentum equation in unsteady stokes flows. J Fluid Mech 370:53–72
7. Crift R, Grace JR, Weber ME (1978) Bubbles, Drops, and Particles
8. Elghobashi S (1994) On predicting particle-laden turbulent flows. Appl Sci Res 52(4):309–329
9. Flemmer RL, Banks CL (1986) On the drag coefficient of a sphere. Powder Technol 48(3):217–221
10. Génevaux O, Habibi A, Dischler JM (2003) Simulating fluid-solid interaction. In: Graphics Interface, vol 2003, pp 31–38, June 2003
11. Goeury C et al (2015) Uncertainty quantification on a real case with TELEMAC-2D. In: Proceedings of the XXII TELEMAC-MASCARET Technical User Conference, 15–16 October, 2047, pp 44–51
12. Huang G, Law AWK, Huang Z (2011) Wave-induced drift of small floating objects in regular waves. Ocean Eng 38(4):712–718

13. Hryb D, Cardozo M, Ferro S, Goldschmit M (2009) Particle transport in turbulent flow using both Lagrangian and Eulerian formulations. Int Commun Heat Mass Transf 36(5):451–457

14. Joly A, Violeau D, Minier J (2010) Modelling of the turbulent diffusion of algae in a coastal environment through a stochastic method with an exact integrator. In: Proceedings of the 1st IAHR European Conference, pp 4–6, May 2010

15. Joly A (2011) Modélisation du transport des algues en milieu côtier par une approche stochastique (Doctoral dissertation, Université Paris 6)

16. Joly A, Moulin F, Violeau D, Astruc D (2012) Diffusion in grid turbulence of isotropic macro-particles using a Lagrangian stochastic method: theory and validation. Phys Fluids 24(10):103303

17. Merkuryeva GV, Kornevs M (2013) Water flow forecasting and river simulation for flood risk analysis. Inf Technol Manag Sci 16(1):42–46

18. Nistor I, Goseberg N, Stolle J (2017) Tsunami-driven debris motion and loads: a critical review. Front Built Environ 3:2

19. O'Brien JF, Zordan VB, Hodgins JK (2000) Combining active and passive simulations for secondary motion. IEEE Comput Graph Appl 20(4):86–96

20. Persi E, Petaccia G, Sibilla S, Brufau P, García-Navarro P (2019) Calibration of a dynamic Eulerian-Lagrangian model for the computation of wood cylinders transport in shallow water flow. J Hydroinf 21(1):164–179

21. Ren B, Jin Z, Gao R, Wang YX, Xu ZL (2014) SPH-DEM modeling of the hydraulic stability of 2D blocks on a slope. J Waterw Port Coast Ocean Eng 140(6):04014022

22. Robb DM, Gaskin SJ, Marongiu JC (2016) SPH-DEM model for free-surface flows containing solids applied to river ice jams. J Hydraul Res 54(1):27–40

23. Ruiz-Villanueva V, Bladé E, Sánchez-Juny M, Marti-Cardona B, Díez-Herrero A, Bodoque JM (2014) Two-dimensional numerical modeling of wood transport. J Hydroinf 16(5):1077–1096

24. Stockstill RL, Daly SF, Hopkins MA (2009) Modeling floating objects at river structures. J Hydraul Eng 135(5):403–414

25. Turton R, Clark NN (1987) An explicit relationship to predict spherical particle terminal velocity. Powder Technol 53(2):127–129

26. Turton R, Levenspiel O (1986) A short note on the drag correlation for spheres. Powder Technol 47(1):83–86

27. Wu TR, Chu CR, Huang CJ, Wang CY, Chien SY, Chen MZ (2014) A two-way coupled simulation of moving solids in free-surface flows. Comput Fluids 100:347–355

28. Xiong Y, Mahaffey S, Liang Q (2018) Simulation of floating debris in violent shallow flows. EPiC Ser Eng 3:2375–2382

29. Xiong Y, Mahaffey S, Liang Q, Rouainia M, Wang G (2020) A new 1D coupled hydrodynamic discrete element model for floating debris in violent shallow flows. J Hydraul Res 58(5):778–789

30. Maxey MR, Riley JJ (1983) Equation of motion for a small rigid sphere in a nonuniform flow. Phys Fluids 26(4):883–889

The Relationship Between Flow and Pressure Head of Partially Submerged Orifice Through CFD Modelling Using Flow-3D

**Anas S. Ghamam, Mohammed A. Abohatem,
Mohd Ridza Bin Mohd Haniffah, and Ilya K. Othman**

Abstract Orifices are used as flow control and measuring devices and classified based on their sizes, shapes, and flow conditions. For partially submerged orifice, relatively few studies provide analytical results because it is highly dependent on the orifice's geometry and the net flow head available. The purpose of this study is to determine the relationship between the flow rate and the pressure head of a circular orifice in partially submerged flow conditions using FLOW-3D software. Three cases were considered: Case A, a classical free-flowing circular orifice for validation, Case B, varying upstream and downstream water depth at weir flow conditions; and Case C, partially submerged circular orifice with varying upstream water levels and constant downstream water level at the centre of the orifice. A strong linear relation is obtained between the upstream water level and the flow rate through the orifice for Cases A and C, while the relationship remains valid for Case B unless the water depths exceed the invert of the circle downstream. The percentage of difference in weir flow past orifice between the model and equations derived from previous studies are within 20% with a regression value of 0.99 for all water level differences, except for a couple of cases with small water level differences in which the flow is very complex.

A. S. Ghamam (✉) · M. A. Abohatem · M. R. Bin Mohd Haniffah · I. K. Othman
School of Civil Engineering, Faculty of Engineering, Universiti Teknologi Malaysia, Skudai, Malaysia
e-mail: saganas2@live.utm.my

M. A. Abohatem
e-mail: aaamohammed22@live.utm.my

M. R. Bin Mohd Haniffah
e-mail: mridza@utm.my

I. K. Othman
e-mail: ilya@utm.my

I. K. Othman
Center for Coastal and Ocean Engineering (COEI), School of Civil Engineering, Faculty of Engineering, Universiti Teknologi Malaysia, Skudai, Malaysia

1 Introduction

An orifice is a small opening of any cross-section, which allows the fluid to flow through. Orifices can be classified as large or small based on the ratio of their size and the head of fluid measured from the centre of the orifice. They are also classified based on the shape of the upstream edge of the orifice as a sharp-edged or bell-mounted edge [1]. In general, orifices are used as flow control and measuring devices and can be found in pipes, channels, tanks, and large reservoirs. According to [3], when the water level increases from $y = 0$ to $y = D$, where y is upstream flow depth relative to the invert of the orifice and D is the diameter of the orifice, the flow goes through a transition from weir flow when the flow head is shallow to orifice flow when the flow head is deep and the flow leaving the orifice is a mix of both. [5] stated that orifice flow occurs only if the crown of the orifice is submerged and therefore when the flow head is anywhere under the crown for the partially submergence case, it will behave as a weir. Hussain et al. (2016) stated the following: "If the upstream water level drops below the top of the opening, it no longer performs as an orifice but as a weir." [5] has developed empirical equations that determine the discharge at different conditions of the orifice. The author derived the discharge relation for both small and large orifices using the energy equation. Then, he derived the head-discharge relation for a circular weir using the energy equation for a horizontal elemental strip. Brandes and Barlow (2011) worked on the development of a model that is conceptually simple and easy to apply for estimating discharge from detention facilities through thin-walled orifices under partial submergence conditions. The developed models were named the top-width approach and the equivalent rectangular area weir approach. They treat orifice in partial submergence case as an equivalently sized rectangular weir. Furthermore, the result has shown that the top-width approach provides a better fit to the data than the equivalent rectangular area weir approach. Hence, they recommended using it for the modelling of an orifice in partial submergence conditions as it is both more accurate and easier to apply than the other method. [6] argued that it is hydraulically meaningless for C_w to be greater than unity as it would mean that there are no losses, and the actual discharge will be idealized more than the theoretical discharge which is logically impossible. Rather, they developed a discharge equation and by solving it for full submergence condition and partial submergence condition at $y/D = 1$. After eliminating all the values of $C_w > 1$ and by using the curve fitting technique, they obtained an equation that is valid for both C_d and C_w for all the values of $y/D \geq 0.25$. The maximum percentage error of this equation was obtained to be less than 6.4% comparing with experimental data. Hussain et al. (2016) carried out an analytical and experimental study on sidewall circular orifice with sharp-crested edges and in an open channel to determine the coefficient of discharge for partially submerged flow circular orifice, by using the least square method and separating the flow into free and fully submerged. Three different diameters, six heights of orifice crest, and different discharges in the main channel were applied to produce a set of data with the use of a common practice to propose the coefficient. 70–75% of the data was used to propose the relationship between the difference in water level with flowrate

and the rest to validate it. Out of 458 data sets of free-flow discharge, there was a $\pm5\%$ difference between the observed and computed discharge. The difference was $\pm10\%$ for a 170 set of data in the submerged condition. Meanwhile, in the partially submerged condition, the difference was $\pm20\%$.

When an outlet is continuously drained away, it will establish a steady state with the different water levels at both sides of the orifice. Hence, the challenge is finding a relationship that relates the steady state of flow rate across the orifice with varying water levels and orifice dimensions on both sides of the orifice. This study is dedicated to the computational modelling of flow through the orifice to determine the relationship between the difference head (upstream and downstream) of a partially submerged circular orifice with its flow rate with the aid of FLOW-3D software. The water level was maintained in the upstream and downstream tanks. The water depth in the upstream part is always kept high. Moreover, the upstream tank does not have flow in the horizontal direction, except the flow out of the orifice while the downstream tank is in a steady state. Free fall flow case was used to validate the modelling of FLOW-3D.

2 Concept of Calculation of Flow Through Orifice

The rate of flow through the orifice opening at any given time will be highly dependent mainly on three factors which are pressure difference, shape, and size of the orifice. The first case of free flow is very important to validate the model because the flow equation is known. For a fully submerged orifice with free fall condition, the flow can be calculated using the following equation:

$$Q = C_d A \sqrt{2gh_0} \tag{1}$$

where, Q is the volume of flow rate through the orifice in cubic meters per second (m^3/s); C_d is dimensionless discharge coefficient; A is the area of the orifice in square meters (m^2); g is acceleration due gravity (m/s^2); and h_0 is effective head on the orifice measured from the centroid of the opening (m). According to Urban Stormwater Management Manual. (MSMA). 2nd Edition. (2012) a value between 0.6–0.62 should be considered for circular orifice. Another study also suggested that values of C_d in the range of 0.6–0.65 [2].

Meanwhile, [5] proposed a method to calculate the theoretical flow rate, as shown in Eq. 2. It is applicable for a fully submerged circular orifice or when the water depth ratio, $\eta = y/D$ is more than 1, where y is the depth of water from the bottom of the orifice and D is the diameter of the orifice.

$$Q = 0.79 C_d \sqrt{2g D^5 (\eta - 0.54)} \tag{2}$$

where, Q_w is the actual weir discharge and C_w is the coefficient discharge for the weir.

The coefficient of discharge introduced by [6] is valid for values of $\eta \geq 0.25$ and is shown in Eq. 3

$$C = \frac{1.06 + 5.11\eta^{1.8}}{1 + 8.04\eta^{1.8}} \tag{3}$$

3 Flow-3D and Modelling Set-Up

FLOW-3D is a computational fluid dynamic (CFD) software that uses the equations of Navier–Stokes and the method of the volume of fluid (VOF) to simulate a fluid-based problem and obtain all the outcomes to analyse the problem.

Setting up the model starts with the geometry set up, whereby two chambers are used, and they are separated by the circular orifice plate. The diameter of the orifice is set to 40 mm, the thickness of the orifice plate is set as 5 mm, and the width of the channel or chambers is 0.5 m.

The whole domain can be divided into multiple mesh blocks with different mesh cell sizes, and that could be defined by the location of interest. For this study, two main mesh blocks with the same mesh cell sizes are introduced, one for the upstream and one for the downstream away from the plate. Two other mesh blocks surrounding the orifice hole with a smaller mesh cell size were applied to capture the shape of the orifice. FAVORize tool is used to give a preliminary evaluation of the model geometries.

Boundary conditions were set for each mesh block as in Fig. 1. The intermediate mesh blocks surrounding the orifice hole will have symmetric boundary conditions; sides and bottom of the upstream and downstream mesh blocks are defined as walls. The boundary of the inlet section of the upstream mesh block and the outlet section of the downstream mesh block was defined using specified pressure boundary condition that uses the fluid elevation to keep the water level constant while the top boundary condition was set to be specified pressure allowing fluid to flow or splash. Fluid properties are then defined from the built-in data as water in normal condition with 20 °C and 0.001 kg/m/s viscosity.

A preliminary check was done using pre-processing, which gives more information about diagnostics and errors in all aspects of the model, boundary conditions, physics, and other properties. Measuring devices in FLOW-3D were used to record the flow rate and the water depth in a defined location as shown in Fig. 2.
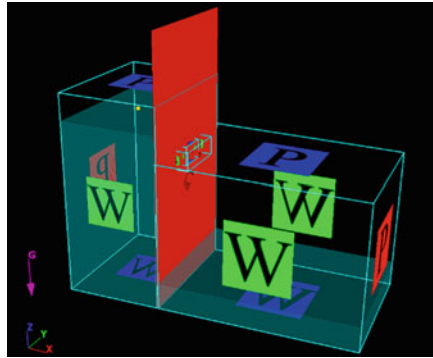
Fig. 1 Boundary, and initial conditions
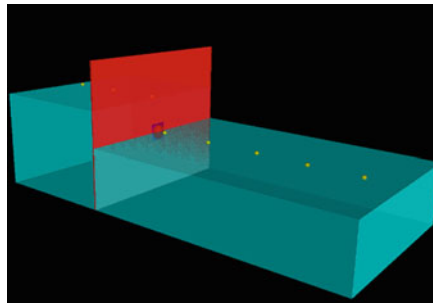
Fig. 2 Probes and flux devices

4 Convergence Study

A convergence study was undertaken to find the optimal cell size of the mesh. A trial study that begins with large mesh cell size and refining it until the simulation results change is insignificant. After obtaining this optimal cell size, it is then used for all simulations and any further decrease in cell size is unnecessary.

5 Data Samples

Three types of cases were considered to accomplish the purpose and objective of this study (Table 1).

1. **Case A**: Orifice Flow—Free Fall Flow Condition
   Table 1 represents the effective height which is the difference between upstream and downstream heights. For free-fall flow conditions, the downstream has no effect on the flow, as shown in Fig. 3. Hence the water level downstream was set

Table 1 Data case A

Case A
Effective height, y (m)
0.38
0.33
0.28
0.23
0.08
0.06
0.02

to 0.15 m, in which the height of the centre of the orifice is 0.52 m from the bed. Varying effective heads were established.

2. **Case B**: Weir Flow—Partially Submerged Orifice
   For this case, the water level upstream is below the crown of the orifice, while the downstream water level is the same as the bottom of the orifice. Details of the parameters simulated are as in Table 2 and shown in Fig. 4.

3. **Case C**: Orifice Flow—Partially Submerged Orifice
   For Case C, the water level upstream is higher than the crown of the orifice, while the water level downstream is the same as the bottom of the orifice. The height of the tank was shortened to save computational time. The centre of the
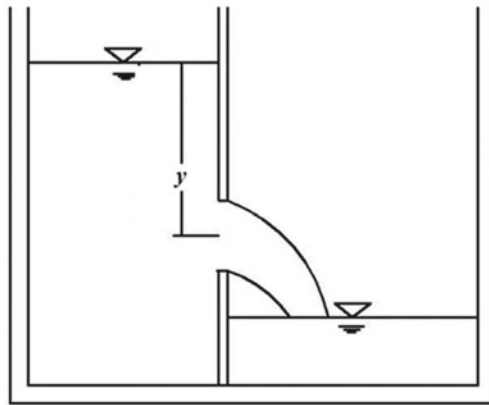
Fig. 3 Free flow condition

Table 2 Data case B

Case B		
Upstream head (m)	Downstream head (m)	Effective head, y (m)
0.535	0.5	0.035
0.53	0.5	0.03
0.52	0.5	0.02
0.515	0.5	0.015
0.51	0.5	0.01
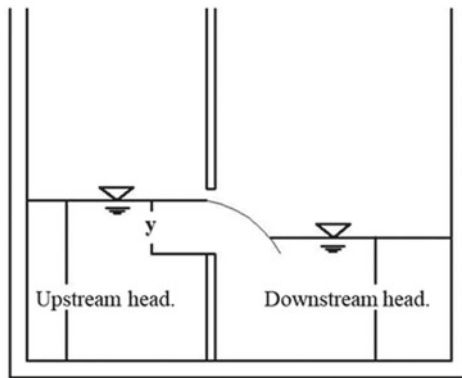
Fig. 4 Partially submergence condition—weir flow

orifice and also the downstream head is 0.17 m from the bed. Details are shown in Table 3 and Fig. 5.

6 Results and Discussion

6.1 Convergence Study

A convergence study was conducted to determine the optimum mesh cell size, which produces accurate results in a reasonable amount of time, or the results are not affected by the mesh anymore (mesh independent). It should be highlighted that all water depths upstream and downstream were kept constant, and the only changing variable was the mesh cell size. From Table 4, seven mesh sizes were simulated successfully except for the finest mesh, in which the simulation was very slow and stopped at only 2% completion from the total time. The convergence was achieved at a mesh size of about 0.00125 m, as better shown in Fig. 6. Therefore, it was concluded that the most suitable mesh cell size that should be used is 0.0015 m, which gives

Table 3 Data sample case C

Case C
Effective height, y (m)
0.03
0.04
0.05
0.06
0.07
0.08
0.09
0.1
0.16
0.46
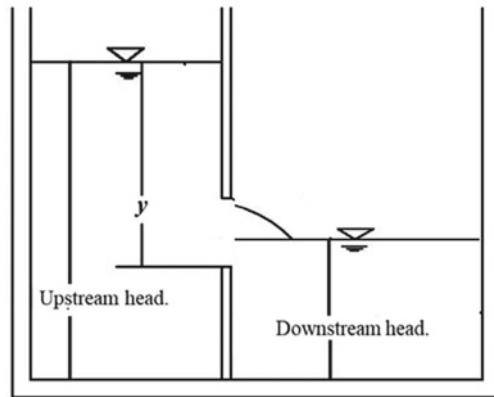
Fig. 5 Partially submergence condition—orifice flow

accurate results with a lesser amount of computational time as compared to the other converged and finer meshes.

Case A: Orifice Flow—Free Fall Flow Condition

Table 5 shows the result of theoretical discharge obtained by Eq. 1 and the modelling discharge. The theoretical discharge is consistently higher than the modelling discharge because the coefficient of discharge has not been implemented in it, or it is assumed to be 1. The actual C_d are obtained by the division of the discharge obtained by modelling and the theoretical discharge, while $C_{dcalculated}$ are calculated via Eq. 3. It can be seen from Fig. 7 that the $C_{dcalculated}$ is at its peak at a value of 0.68 for the lowest effective head, and the value becomes more stable as the effective head increases. Meanwhile, the actual C_d fluctuates between 0.73 and 0.75. It is believed that the results of the actual coefficient of discharge are acceptable, although it is not

Table 4 Results of convergence study

Finest mesh cell size (m)	$Q_{Modelling}$	Time	Status of completion (%)
0.00078125	2.48E-03	04 h:11 m:45 s	2.00
0.001	2.52E-03	1d:4 h:14 m:42 s	100.00
0.00125	2.42E-03	02:12:04:18	100.00
0.00156	2.43E-03	00:22:30:59	100.00
0.00188	2.69E-03	00:16:01:05	100.00
0.00219	2.57E-03	00:05:38:11	100.00
0.00250	2.71E-03	00:03:11:32	100.00
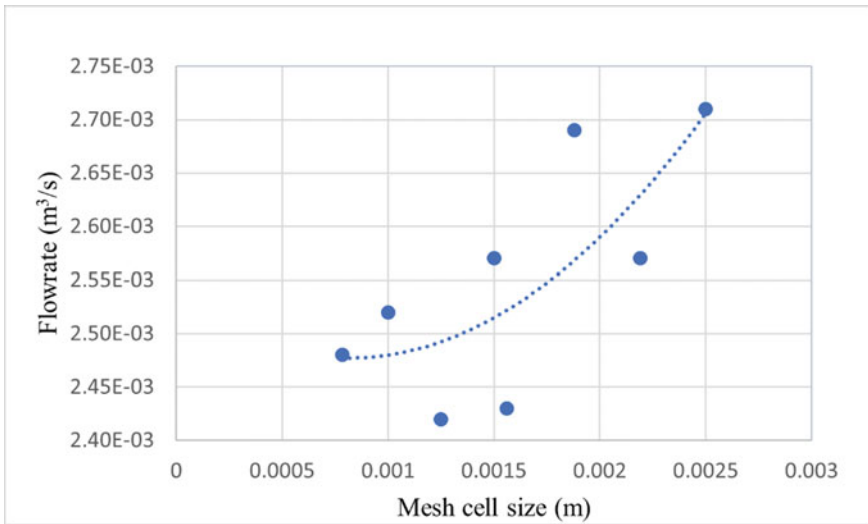
Fig. 6 Graph of flow rate vs mesh cell size

as suggested. The slight difference may be due to variables such as thickness, size, and shape of the orifice. C_d of 0.62 is suggested by Urban Stormwater Management Manual (MSMA) [4].

Figure 8 shows that the modelling discharge increases at a similar rate as the theoretical discharge and that both discharges have strong relationship of 0.98 as obtained by regression line. Moreover, the percentage of error of both discharges is within 14.8 and 17.8%. This agreement of results reflects the suitability and the validation of the model.

Case B: Weir Flow—Partially Submerged Orifice

Table 6 shows the result of theoretical discharge obtained by Eq. 3 and the modelling discharge. The theoretical discharge is consistently higher than the modelling discharge because the coefficient of discharge has not been implemented in it, or

Table 5 Results of case A

Effective height, y (m)	η_L	Q_T (m^3/s)	$Q_{Modelling}$ (m^3/s)
0.38	10	2.13E-03	2.57E-03
0.33	8.75	1.98E-03	2.37E-03
0.28	7.5	1.83E-03	2.18E-03
0.23	6.25	1.66E-03	2.01E-03
0.08	2.5	9.76E-04	1.15E-03
0.06	2	8.45E-04	1.00E-03
0.02	1	4.88E-04	5.81E-04
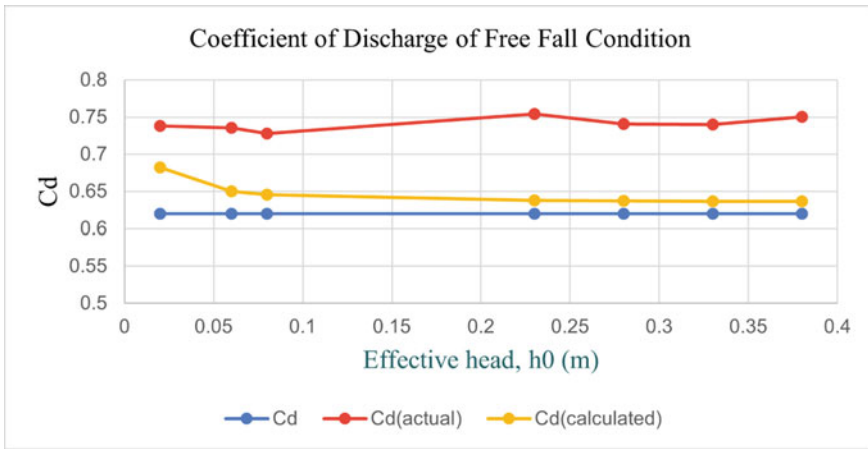
Fig. 7 Coefficient of discharge for case A

it is assumed to be 1. The actual C_d are obtained by the division of the discharge obtained by modelling and the theoretical discharge, while $C_{dcalculated}$ are calculated via Eq. 3. Figure 9 represents a comparison between the coefficient of discharge obtained by modelling and the one that was computed using Eq. 3. It is noticed that both curves show higher values of C_d at the low effective head. The curve of the actual C_d exceeds one, means that the modelled results might not be correct in which a smaller or finer mesh size needs to be applied (Fig. 9). Figure 10 shows a strong proportional relationship between the discharge and the head difference.

Case C: Orifice Flow—Partially Submerged Orifice
Data obtained for partially submerged flow conditions is shown in Table 7. It is obvious that the general relation between the water head and the discharge rate is proportional and direct, as shown in Fig. 12. However, the low upstream levels cause a small fluctuation in the values of flow rate within their simulations, and that is expected to be caused by backwater from the downstream chamber. Figure 11 shows the discharge coefficient for both the modelling and theoretical, in which
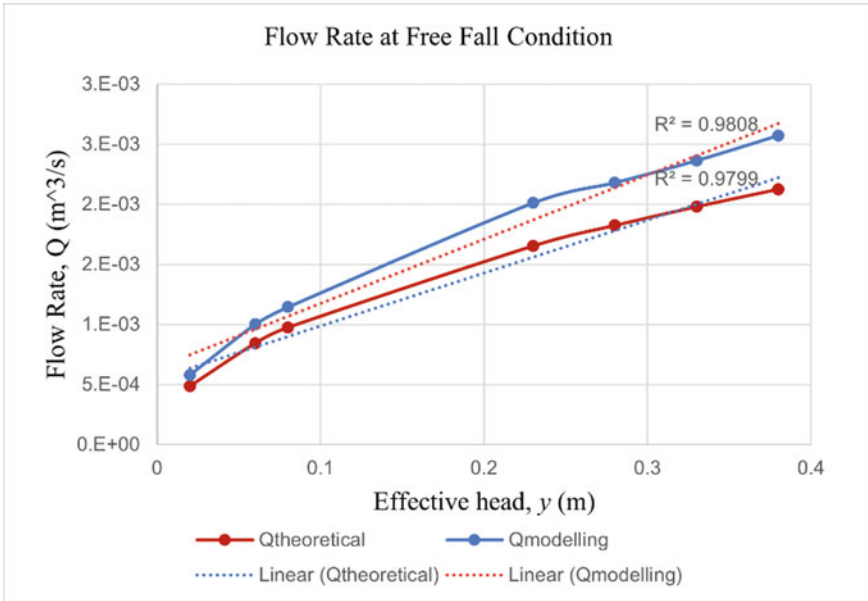
Fig. 8 Flow rate of case A

Table 6 Results of case B

Effective height, y (m)	η	Q_T (m^3/s)	$Q_{Modelling}$ (m^3/s)
0.035	0.88	6.23E-04	5.44E-04
0.030	0.75	4.86E-04	4.34E-04
0.020	0.50	2.39E-04	2.37E-04
0.015	0.38	1.41E-04	1.43E-04
0.010	0.25	6.51E-05	8.28E-05

the calculation follows the previous two cases. Although there is some deviation in results, the values are between 0.64 and 0.74, with an average discharge coefficient for the partially submerged orifice flow of 0.67.

Moreover, three extra simulations were conducted for Case C; two simulations for a higher upstream level of 0.33 and 0.63 m to ensure FlOW-3D is capable of getting accurate results for higher upstream levels, while another simulation with an upstream level of 0.2 m (which is the same as before) but with a wider downstream tank, as shown in Fig. 13. This is to investigate the effect of the downstream boundaries on the flowrate. Figure 14 shows the algorithmic trend line for modelling water discharge for all partially submerged simulations. The trendline looks very promising, indicating that the study was able to capture the relationship for this partially submerged orifice. The results for the wider downstream tank show that the discharge coefficient increased from 0.59 to 0.63, which is closer to the average
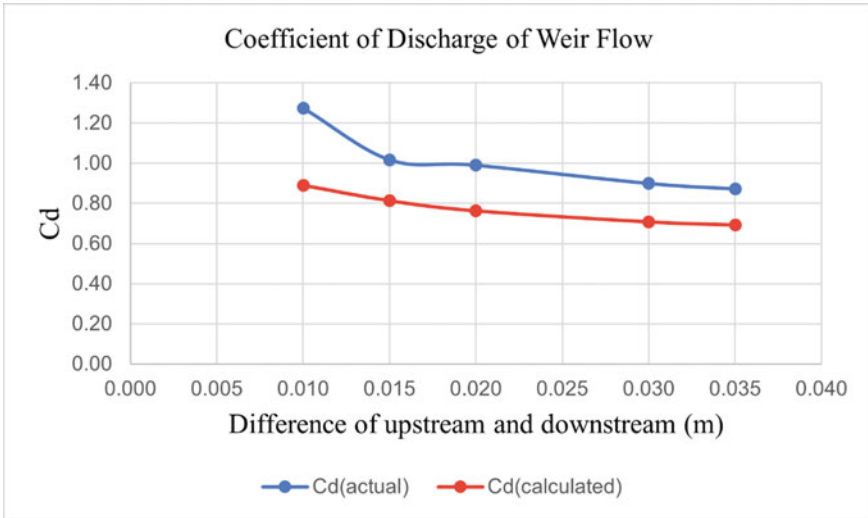
Fig. 9 Coefficient of discharge for case B
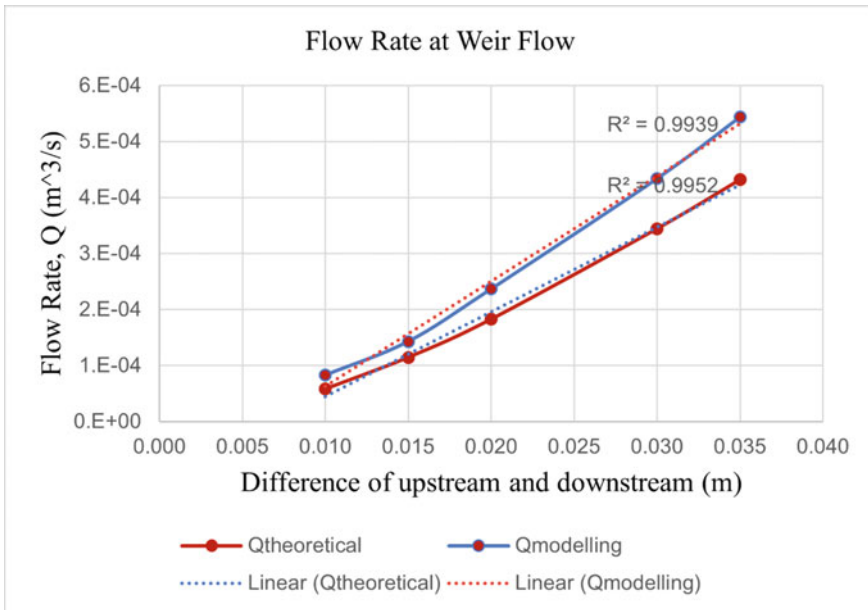
Fig. 10 Flow rate of case B

Table 7 Results of case C

Effective height, y (m)	n	Q_T (m^3/s)	$Q_{Modelling}$ (m^3/s)
0.03	1.25	9.44E-04	5.59E-04
0.04	1.5	1.10E-03	6.89E-04
0.05	1.75	1.23E-03	8.56E-04
0.06	2	1.35E-03	8.91E-04
0.07	2.25	1.46E-03	1.02E-03
0.08	2.5	1.57E-03	1.08E-03
0.09	2.75	1.66E-03	1.12E-03
0.1	3	1.76E-03	1.22E-03
0.16	4.5	2.23E-03	1.55E-03
0.46	12	3.79E-03	2.84E-03
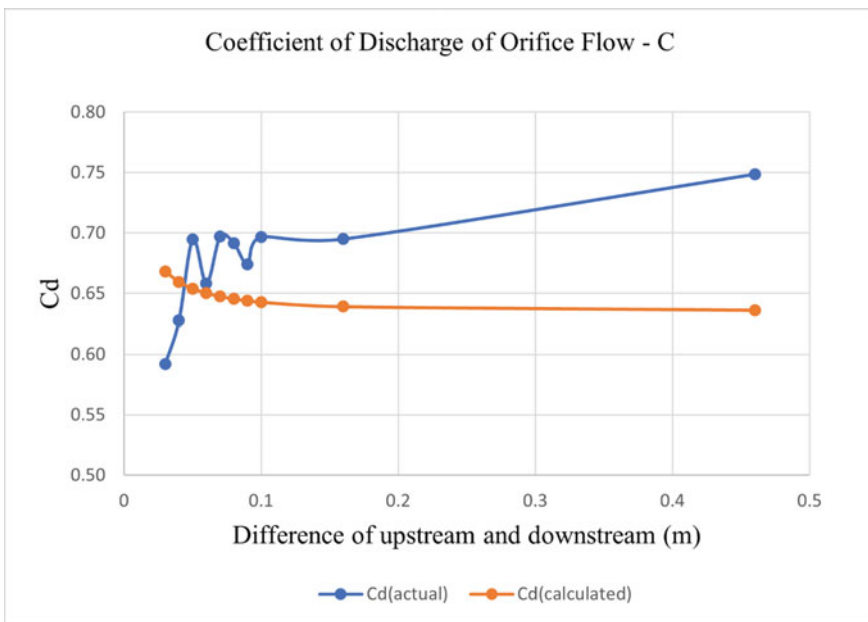
Fig. 11 Coefficient of discharge for case C

coefficient of discharge. It seems that as the water levels became lower, the current
mesh was not able to capture the whole physics of the flow. A finer mesh needs to
be implemented for very low water levels.
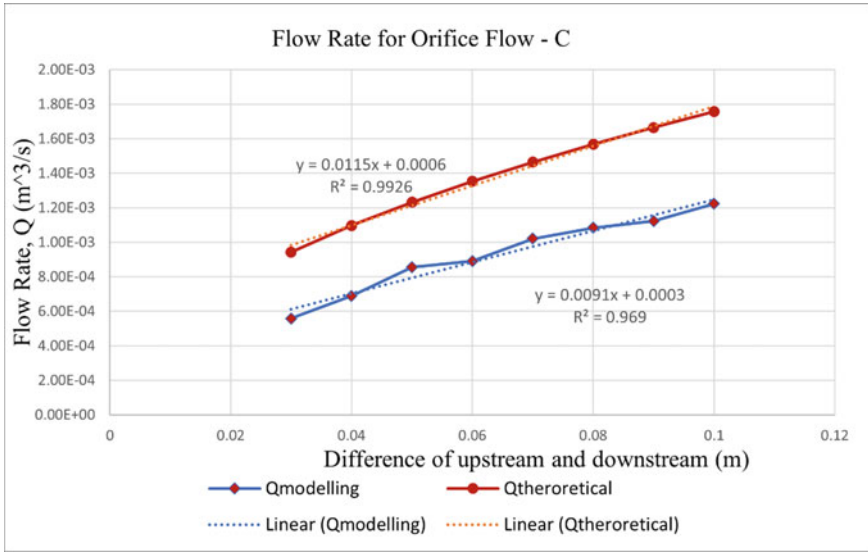
Fig. 12 Flow rate of case C
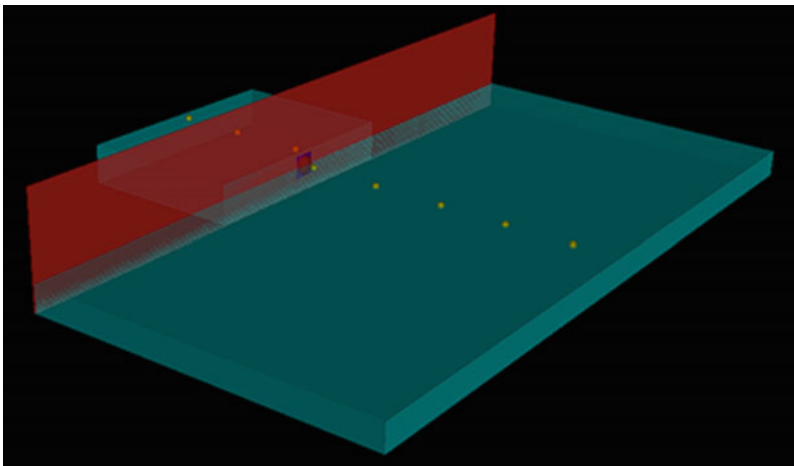
Fig. 13 Wide downstream channel
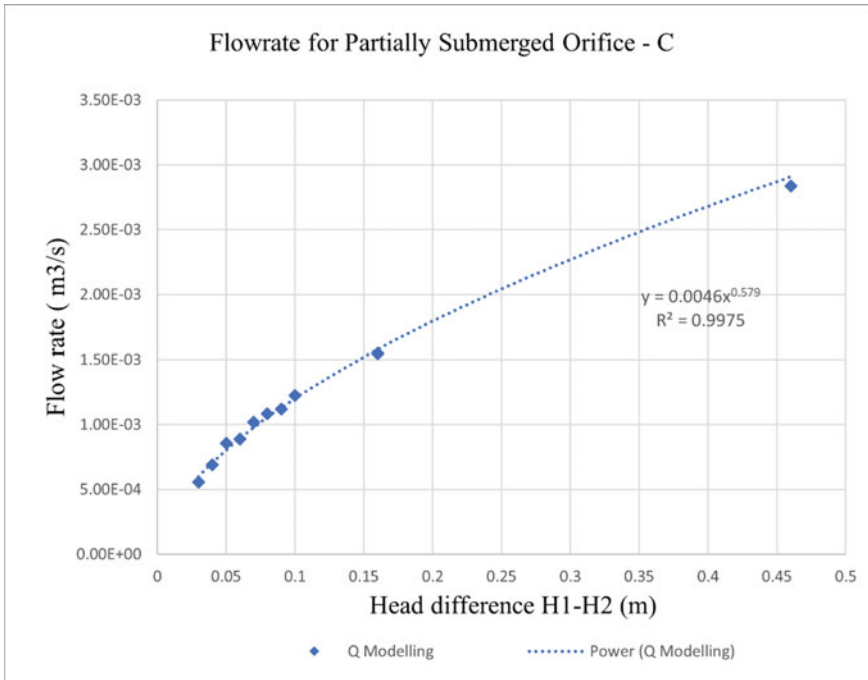
Fig. 14 Power trend line for Q modelling

7 Conclusion

A computational model for the partially submerged circular orifice between two industrial chambers using FLOW-3D was developed. In general, increasing the difference head will increase the flow rate of the orifice in both free flow and partially submerged flow conditions. Findings concerning the objectives of the study are as below:

1- A higher effective head causes a steady flow rate through the orifice of case A. This justifies the fluctuation of flow in Case B and C, where the pressure head is lower.

2- Although a general trend has been obtained in Case BII via modelling, Vatankah (2018) discharge equation produced unrealistic results due to its neglect of the effect of water elevation downstream.

3- In partially submerged orifice flow, the fluid flow rate will increase with the increase of pressure head is represented in a powerful manner as $= 0.0046(H_1 - H_2)^{0.579}$, where H_1 and H_2 are head from the lower crust of the circular orifice.

4- Even though [6] equation of coefficient of discharge is valid for all the values of $\eta \geq 0.25$, its result require further investigation at the range of $0.25 \leq \eta \leq 1$ as the results increase with the drop of pressure head.

This study concludes that Head difference level has a direct relation with orifice flow rate. Backwater from downstream affects the flow rate significantly in low upstream levels. It is recommended to study the effect of downstream water at the flow rate when its height is above the invert of the orifice for weir flow. Also, it is suggested to do further study on the low upstream levels and consider other variables such as channel width.

References

1. Bansal RK (2010) Fluid mechanics & hydraulic machines, pp 853–944
2. Brandes D, Barlow WT (2012) New method for modeling thin-walled orifice flow under partially submerged conditions. J Irrig Drain Eng 138(10):924–928. https://doi.org/10.1061/(asce)ir.1943-4774.0000488
3. Guo JCY, Stitt RP (2017) Flow through partially submerged orifice. J Irrig Drain Eng 143(8):06017006. https://doi.org/10.1061/(asce)ir.1943-4774.0001192
4. Urban Stormwater Management Manual (MSMA), 2nd edn., p 373 (2012)
5. Vatankhah AR (2018) Discussion of flow through partially submerged orifice by James C. Y. Guo and Ryan P. Stitt. J Irrig Drain Eng 144(5):07018022. https://doi.org/10.1061/(asce)ir.1943-4774.0001296
6. Vatankhah AR, Bijankhan M (2012) Discussion of new method for modeling thin-walled orifice flow under partially submerged conditions by David Brandes and William T. Barlow. J Irrig Drain Eng 138(5):476–480. https://doi.org/10.1061/(ASCE)IR.1943-4774.0000427

Prediction of Flow Structure in Axial Flow Submersible Pumps During Intake by Numerical Simulation

T. A. Norizan, H. Ghazali, R. Abu Seman, and Z. Harun

Abstract Intake flow is the main factor that determines the functionality of submersible pumps that withdraw fluid in sumps. It is important that the prediction of flow characteristics of the pump intake is made prior to the construction of the pumping system to identify any hydraulic problem that may arise after installation. In this study, the flow structure in an axial flow submersible pump during intake is analyzed using ANSYS Fluent. A numerical model of the pump with a single-bay intake sump was constructed and simulated with boundary conditions associated with typical on-site pumping operation. The simulation was conducted with two settings; the first one involved pump operation without any flow modification, and the other was included with the installation of a flow correction device called the floor splitter. Data from experiments were used to validate the results, and the analysis was performed by evaluating the numerical results from the aspects of vortex formation, flow vorticity and uniformity. The results showed that the flow structure of the intake flow displayed a swirling motion with the presence of a vortex and that the installation of a floor splitter has successfully eliminated the vortex and improved the uniformity of the flow.

Keywords Pump intake flow · Pump sump model · Computational fluid dynamics

T. A. Norizan (✉) · H. Ghazali · R. Abu Seman
Mechanical and Electrical Services Division, Department of Irrigation and Drainage, Kuala Lumpur, Malaysia
e-mail: tajul@water.gov.my

H. Ghazali
e-mail: hapida@water.gov.my

R. Abu Seman
e-mail: rosazlan@water.gov.my

Z. Harun
Faculty of Engineering and Built Environment, National University of Malaysia, Bangi, Malaysia
e-mail: zambri@ukm.edu.my

251

1 Introduction

Study on pump sump hydraulics has long been the subject of discussion not only among researchers but also practitioners. This is because the flow in pump sumps during intake is a complex structure that is highly dependent on the shape and orientation of the intake sump and cannot be generalized for the purpose of design guidance (Padmanabhan, 1987) [5]. Among the decisive factors include pump sump geometry [13], pump inlet submergence [6] and approach flow condition [3].

The study has been conducted with physical models, but since the commercialization of computational fluid dynamic (CFD) software, numerical models have increasingly been used as an alternative. [2], for example, have conducted an experiment to investigate the influence of cross-flow on the formation of vortices in pump sump by using a physical model. A quantitative study focusing on the vortex formation in the vicinity of the pump inlet was performed by [12] using particle image velocimetry (PIV) on a single intake pump sump model. Nowadays, the advantages of numerical simulation have been utilized by researchers to obtain valuable information and understanding of pump sump hydraulics. These studies focus on relevant subjects such as air entrainment in pumps caused by free surface vortices during intake [7], the influence of flow correction devices on the improvement of intake efficiency [10] and comparison of performance for several anti-vortex devices in terms of the effectiveness of vortex suppression in pump sump [4].

The methods to perform numerical simulation have also been improved for the past decades, and the accuracy of results are comparable, in some cases, to the results from the physical model study. The important criteria for accurately acquiring simulated results are turbulence models, mesh quality, and boundary conditions [14]. In this paper, the numerical simulation of a single bay pump sump model with axial flow submersible pump is discussed.

2 Methodology

A numerical pump sump model with a single intake bay and the floor was modified to create a 30° horizontal slope as well as a 30° sloped expansion on the left side of the wall. The settings of the model were based on a typical pump intake sump design to emulate the flow in actual pump sumps. It was the model, as shown in Fig. 1, which was used in an experimental study by [11] as validation to the current numerical model.

The design of the pump sump model is illustrated in Fig. 2, and its respective dimensions are listed in Table 1. At the suction pipe outlet, a flow rate of 2100 l/s is applied to induce the intake flow, a flow capacity similar to the actual pump used on site.

The numerical study was a steady-state simulation performed using ANSYS Fluent. Boundary conditions have been defined to the numerical model as mass

Fig. 1 Experimental pump sump model
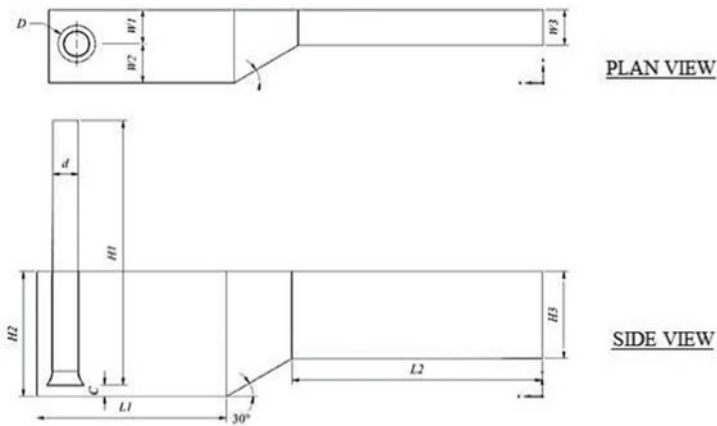
Fig. 2 Numerical pump sump model

flow inlet at the pump sump inlet, pressure inlet at the sump surface, mass flow outlet at the pump outlet and fixed wall at the sump walls to simulate the intake flow in the pump sump. Figure 3 shows the concept for boundary conditions applied to the numerical model.

The numerical model was divided into tetrahedral meshes with refinements at critical locations such as near the suction inlet to improve the accuracy of the results. Another variant of the model was built in which a flow correction device called the floor splitter was installed underneath the suction pipe. The use of a floor splitter in the pump sump is a common practice that is convenient for improving intake flow

Table 1 Dimensions of the pump sump model

Parameter	Dimension [mm]
Inlet diameter D	1275
Intake pipe diameter d	850
Left side distance $W1$	1190
Right side distance $W2$	1360
Entrance width $W3$	1275
Suction pipe height $H1$	9350
Sump height $H2$	4250
Entrance height $H3$	2975
Base length $L1$	6375
Entrance length $L2$	8417
Clearance C	383
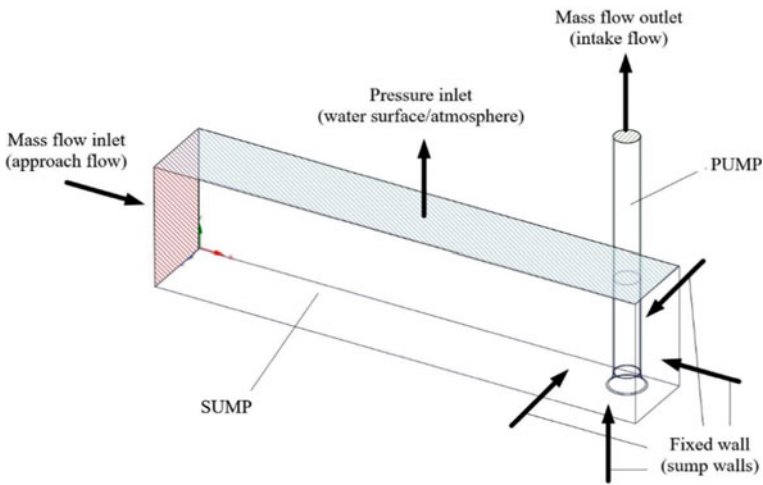
Fig. 3 Boundary conditions for the numerical model

conditions. Figure 4(a), (b) and (c) show the entire pump sump domain, domain without floor splitter and domain with floor splitter, respectively.

To address the formation of vortices that may be formed in the pump sump, the volume of fluid (VOF) method was employed due to the existence of a mixture of fluid and gas within the simulation domain. For the selection of turbulence model, the k-ω model was chosen as it is the best turbulence to simulate flow in the pump sump model [7–9].
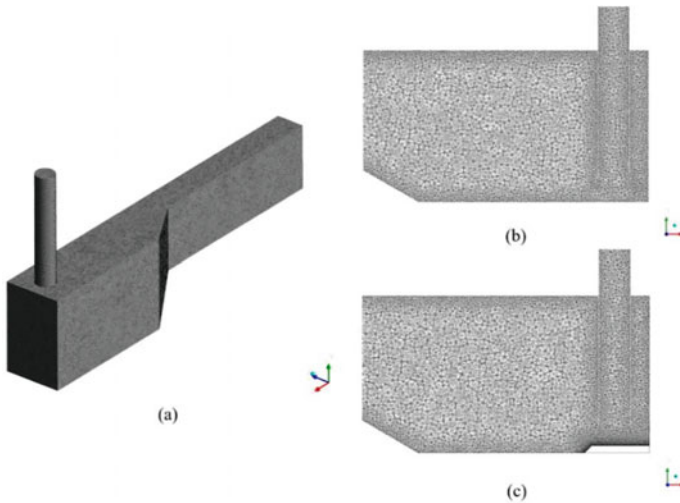
Fig. 4 Meshed numerical models; **a** the entire pump sump domain, **b** domain without floor splitter, **c** domain with floor splitter

3 Results and Discussion

Three evaluation criteria were selected to characterize the flow structure in the pump from the simulation, namely vortex formation, flow vorticity and uniformity. Figure 5 shows the vortex formed at the pump inlet, which originates from the sump floor and continues its way through the pump. This indicates that the intake flow of the pump is highly rotational, and the flow structure is formed due to the sloped floor and wall of the sump.

Streamlines within the pump are plotted in both cases to observe the flow structure more clearly, which are sump without and with the installation of floor splitter as displayed in Fig. 6 (a) and (b), respectively.

From Fig. 6, it can be clearly seen that the installation of the floor splitter has improved the swirl and uniformity of the intake flow. The mechanism of flow straightening effect introduced by the floor splitter originates from the principle of splitting the flow to break the vortex core that occurred as a result of non-uniform and highly rotational intake flow. The disappearance of the vortex core can be observed from Fig. 7 (a) and (b), which is indicated by the region with high vorticity (red coloured zone) reduced to lower vorticity (green coloured zone) on the x–y plane when installed with floor splitter. Similar results can also be observed on the y–z plane as displayed in Fig. 8 (a) and (b).

The elimination of the vortex attached to the floor can be perceived by plotting the vorticity at the sump floor on the x–z plane, as shown in Fig. 9. The dashed lines represent the inlet of the pump through which the pumped fluid flows in an upward direction (flow direction is into the paper). From Fig. 9(a), we can see that
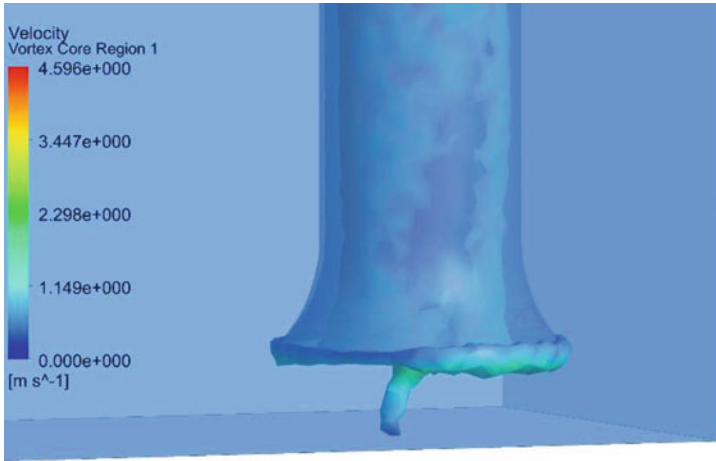
Fig. 5 Vortex core at the inlet
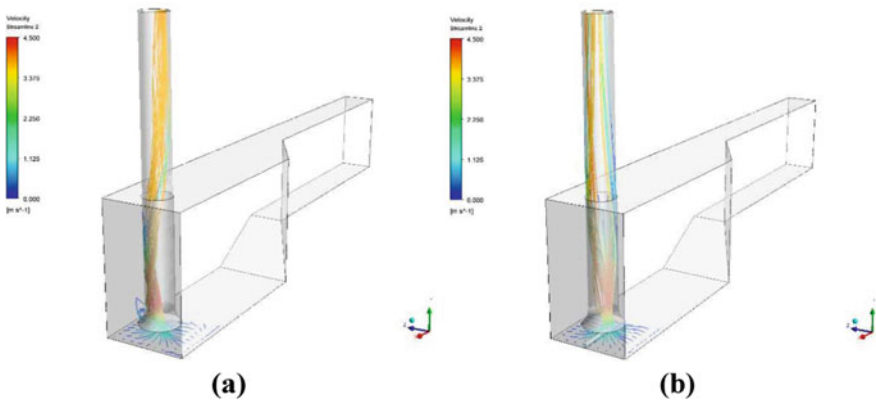
Fig. 6 Streamlines indicating the flow structure; **a** without floor splitter, **b** with floor splitter

the vortex core is located at a position offset from the centre of the inlet diameter. This occurrence is due to the fact that the sloped wall is only on one side, and the inlet is situated near the back wall. When the floor splitter is installed, as shown in Fig. 9(b), the streamline of the flow is directed towards the centre of the inlet, which results in a more uniform intake flow.
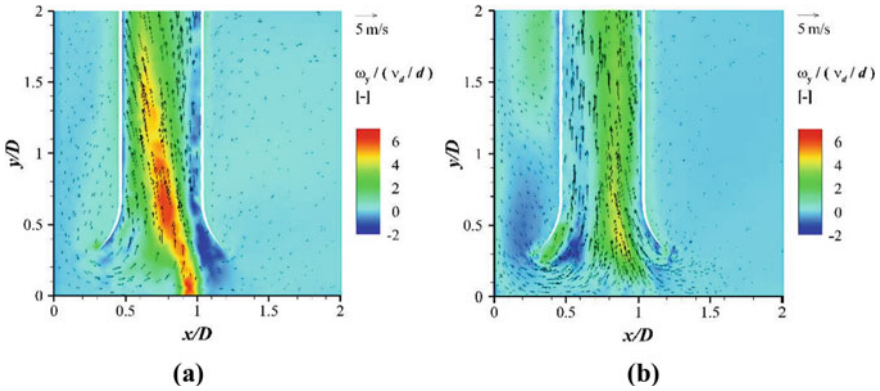
Fig. 7 Vorticity plot of the flow structure through the vortex core on x–y plane; left side **a** without floor splitter, right side **b** with floor splitter
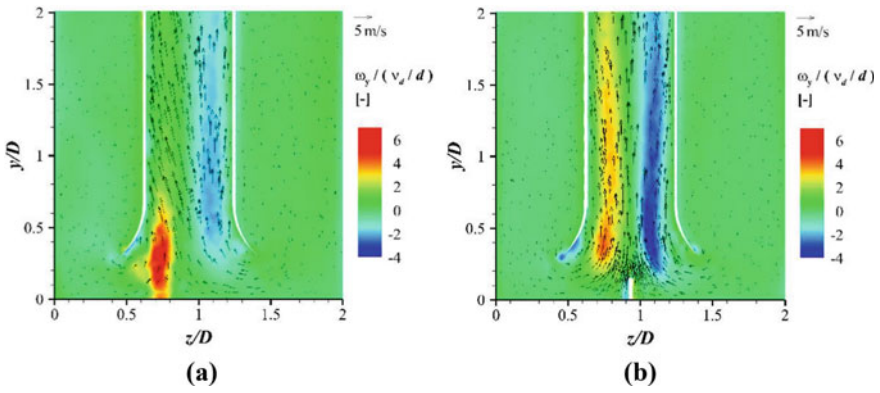
Fig. 8 Vorticity plot of the flow structure through the vortex core on the y–z plane; left side **a** without floor splitter, roght side **b** with floor splitter

The final evaluation is the uniformity of the intake flow, which is compared in Fig. 10 (a) and (b). The vorticity in the case without a floor splitter is obviously higher than the case with a floor splitter, and therefore the intake flow is more uniform and less swirl with the installation of the floor splitter. One of the methods to determine how strong is the swirling flow of the intake by experimental approach is by measuring the swirl angle θ of the flow. The definition of θ is simply the angle between the tangential component of the flow velocity to the axial velocity component. A bigger swirl angle indicates stronger swirling flow, and this value is measured at a level recommended in the American National Standards Institute (2018) [1], which is at a distance about four times the inner diameter of the suction pipe from the pump inlet. Based on Fig. 11, the values of θ for the case with and without floor splitter are 7.58 and 4.27°, respectively. According to ANSI/HI 9.8, the value of θ shall be
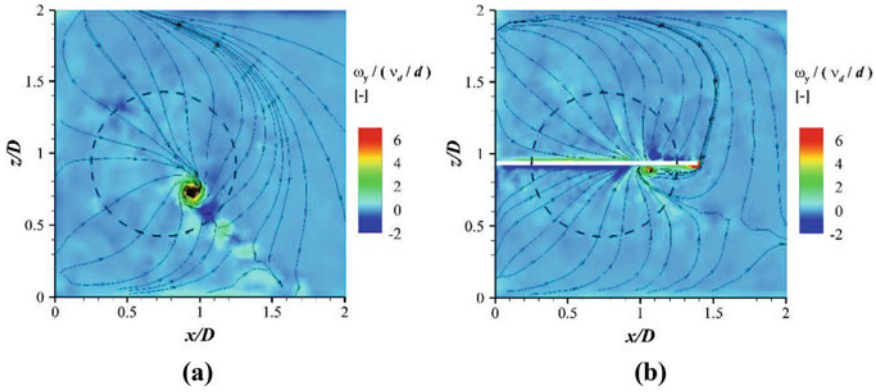
Fig. 9 Vorticity plot of the flow structure at the sump floor on the x–z plane; left side **a** without floor splitter, right side **b** with floor splitter
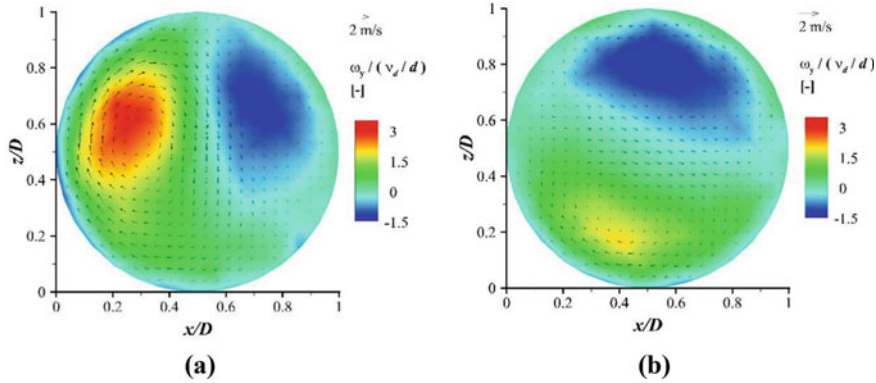
Fig. 10 Vorticity plot of the flow structure at the swirl angle measurement level; right side **a** without floor splitter, left side **b** with floor splitter

less than 5° to ensure that the intake flow is optimized and does not potentially cause any damage to the pump impeller. Therefore, it can be concluded that a sump with a floor splitter displays intake flow with a smaller swirl angle compared to intake flow in a sump without a floor splitter and from the aspect of hydraulics, it is better for the operation of the pump.
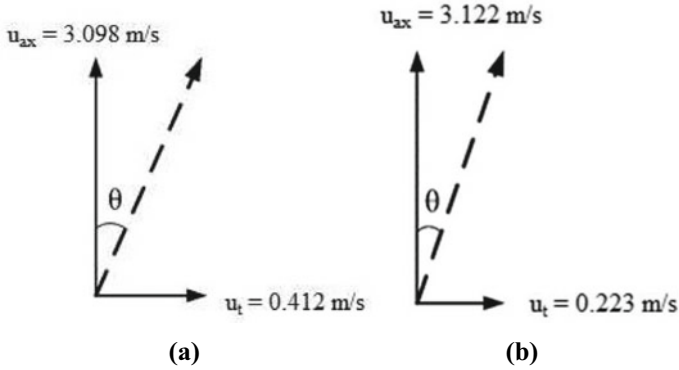
Fig. 11 Velocity diagram for intake flow at swirl angle measurement level; left side **a** without floor splitter, right side **b** with floor splitter

4 Conclusion

A numerical study of the intake of an axial flow submersible pump in a sump complemented with the installation of a floor splitter for flow improvement is presented. The aim of the study is to predict the flow structure in the submersible pump during intake by means of CFD. The numerical model was validated with experimental data to ensure the accuracy and reliability of the simulation results. Boundary conditions similar to on-site pumping operation are applied to the model to simulate the pump intake flow. Without the installation of a floor splitter, the intake flow is highly rotational, and a vortex with an air core is formed at the sump floor, which extends into the pump and affects the pump impeller. By installing a floor splitter, the vortex is eliminated, and the uniformity of the intake flow is improved, which is visualized with a streamlined plot within the suction pipe connected to the pump. An evaluation of swirl angle, which characterizes the level of swirling in the intake flow, is made based on ANSI/HI 9.8, and the results show that by installing a floor splitter, the swirl angle can be reduced to an acceptable value. The result of this study can be used to implement a flow correction method that does not require a total pump sump modification but rather a localized approach.

References

1. American National Standards Institute (2018) Rotodynamic Pumps for Pump Intake Design. Standard No. ANSI/HI 9.8, Hydraulic Institute, Parsippany, US

2. Ansar M, Nakato T (2001) Experimental study of 3D pump-intake flows with and without cross flow. J Hydraul Eng 127(10):825–834

3. Arboleda G, El-Fadel M (1996) Effects of approach flow conditions on pump sump design. J Hydraul Eng 122(9):489–494

4. Arocena VM, Abuan BE, Reyes JGT, Rodgers PL, Danao LAM (2020) Reduction of entrained vortices in submersible pump suction lines using numerical simulations. Energies 13(22):1–20

5. Padmanabhan M (1987) Design recommendation: Pump Sump. In: Knauss J (ed) Swirling Flow Problems at Intakes, pp 101–113. Taylor & Francis, New York

6. Gulliver J, Rindel AJ (1987) Weak vortices at vertical intakes. J Hydraul Res 112(9):610–620

7. Guo ZW, Chen F, Wu PF, Qian ZD (2017) Three-dimensional simulation of air entrainment in a sump pump. J Hydraul Eng 143(9):04017024(1–9)

8. Kim HJ, Park SW, Rhee DS (2017) Effective height of a floor splitter anti- vortex device under varying flow conditions. Sustain (Switz) 285(9):1–14

9. . Lomakin VO, Kuleshovav MS, Bozh'eva SM (2016) Numerical modelling of liquid flow in a pump station. Power Technol Eng 49(5):324–327

10. Norizan TA, Reda E, Harun Z (2018) Enhancement of vorticity reduction by floor splitter in pump sump to improve pump efficiency. Sustain Energy Technol Assess 26:28–36

11. Norizan TA, Harun Z, Abdullah S, Wan Mohtar WHM (2019) Effects of floor splitter height on the effectiveness of swirl angle reduction in pump intake. J Adv Res Fluid Mech Therm Sci 57(1):32–39

12. Rajendran VP, Patel VC (2000) Measurement of vortices in model pump-intake bay by PIV. J Hydraul Eng 126(5):322–334

13. Tullis JP (1979) Modelling in design of pumping pits. J Hydraul Div ASCE 105(9):1053–1063

14. Versteeg H, Malalasekara W (2007) An Introduction to Computational Fluid Dynamics: The Finite Volume Method, 2nd edn. Pearson, London, UK

Numerical Analysis of Flow Characteristics for Idealised Y-Shaped Channels

Zi Xin Foh, Cha Yao Tan, Mohd Ridza Mohd Haniffah, Erwan Hafizi Kasiman, and Fang Yenn Teo

Abstract Channel confluence and bifurcation flows are common phenomena in a natural river. Understanding the characteristics of these dividing flows can help engineers to make decisions on flood risk reductions. In this study, a numerical model has been applied for idealised Y-shaped channels in both cross-sections of rectangular and trapezoidal. InfoWorks ICM software is used to run the numerical analysis on the proposed model. The model included the main channel upstream with a bifurcated angle of 45° at each downstream channel. A series of simulations have been carried out to investigate the effects of various flow characteristics on the water depths and flow velocities. These characteristics are manning's roughness coefficient, the width of the channel, and the shape of the channel cross-section. Results show that the increase in manning's roughness coefficients caused a decrease in flow velocities and increased the water depths for both rectangular and trapezoidal cross-sections. Furthermore, increases in channel widths have caused decreases in flow velocities and water depths for both rectangular and trapezoidal cross-sections. In addition, the rectangular cross-section showed lower flow velocities and water depths compared to the trapezoidal cross-section. The findings from this study may provide a good understanding of the flow characteristics in a bifurcation river to mitigate floods.

Z. X. Foh · C. Y. Tan (✉) · F. Y. Teo (✉)
Faculty of Science and Engineering, University of Nottingham Malaysia, 43500 Semenyih, Selangor, Malaysia
e-mail: keey5tcy@nottingham.edu.my

F. Y. Teo
e-mail: fangyenn.teo@nottingham.edu.my

Z. X. Foh
e-mail: efyzf1@nottingham.edu.my

M. R. M. Haniffah · E. H. Kasiman
School of Civil Engineering, Faculty of Engineering, Universiti Teknologi Malaysia, 81310 Johor Bahru, Johor, Malaysia
e-mail: mridza@utm.my

E. H. Kasiman
e-mail: erwanhafizi@utm.my

261

Keywords Y-shaped channel · Bifurcation · Numerical modelling

1 Introduction

River bifurcation is defined as dividing flow at a point of bifurcation where a single stream of water divides into two or more individual streams. River bifurcation can be found in nature and can be constructed to diverge existing flow to form a new stream. Bifurcation occurs in four natural settings, which are braided rivers, alluvial fans, lowland river plans and deltas [4]. Common engineering designs include artificial structures to redirect the flow for flood control, irrigation, navigation, and other hydraulic applications in floodplains [2, 3, 9, 11, 14]. The common examples of artificial structures with river bifurcation are the side channel, irrigation canal, and longitudinal wall. Other research works also described the morphological processes and their stability on a series of natural bifurcations [1] and artificial bifurcation [12].

2 Artificial Channel Bifurcation

Side-channel construction has been done in rivers to increase the river's conveyance capacity as well as to increase ecological value. [12] carried out a morphodynamic assessment of a side-channel system using a 1D bifurcation model and aerial images. This research uses a 1D model to predict the changes of the side channel. Likewise, it also assesses the condition where the side channel aggrades or degrades as well as the characteristics timescale of morphological change. The result is then compared with the aerial images. A stability diagram was obtained from this research, and it can be used for future design and maintenance. Other than that, [10] idealised a model of gravel-sand river bifurcation based on nodal point relation and analysed its stability properties. The model predicts the changes in bed elevation and bed surface gravel content in the two bifurcates. It proves that mixed-size sediment reveals a more complex behaviour than uni-size sediment. This research uses [13]'s approach and the nodal point relation with specific limitations. There are two cases in this research. One of the cases is where a channel bifurcates into two channels flowing into the lake with the same base level [13], and the other is a side channel.

Longitudinal wall has been proposed by engineers as an alternative to the transverse groynes. This is to maintain a navigable channel and to improve the river's conveyance. The main idea of this proposal is to allow more water flow in the secondary channel behind the training wall when discharge is high. This is to reduce the main channel erosion and to reduce water levels during floods. [5] analyse the stability of the river bifurcation created by the longitudinal wall. In this research, a numerical investigation approach has been used. The Delft3D code has been used to perform the numerical analysis. It has been proven in this research that a bifurcated channel created by a longitudinal wall may be unstable. The main factor affecting it

is the location of the bifurcating point. Another research by [5] is to determine the long-term morphological changes on the river by a longitudinal wall. The aim of this research was to observe the possibility of dividing the flow using longitudinal walls and the long-term morphological development of the river with the presence of bars. Laboratory experiments and numerical investigation using Delft3D code has been done. The result in this research has also proved that bifurcated channels divided by the longitudinal wall have the tendency to be unstable.

3   Flow Characteristics of Channel Bifurcation

Flow characteristics in open channels and closed channels are studied to understand the behaviour of a fluid. Most of them used idealized channels and related them to the river as rivers are considered open channels. Throughout the years, engineers have used experiments, mathematical modelling, and numerical analysis to understand the behaviour of rivers. Flow patterns depend on the characteristics of the fluid, speed of the flow and the shape of the channel. Characteristics of the fluid are viscosity, density, and compressibility. As mentioned earlier, river bifurcation consists of a junction. Discharge ratio, velocity and depth of water at the junction are considered important in the study of river behaviour. This field of study is important in the aspect of river management.

The two main cross-section channels that are widely studied in rivers are the trapezoidal and rectangle. [8] compare the flow characteristics at rectangular and trapezoidal channel junctions. This paper investigates the complex features of combining and diving flow for both different channels analytically. Parametric investigations are also carried out to establish the dependence of depth ratio on various parameters for both cross-sections. From the results obtained, for equal discharge, the depth ratio at the rectangular channel increases more compared to the trapezoidal channel. For equal discharge with the same flow area, the depth ratio at the rectangular channel has a smaller increase compared to the trapezoidal channel.

The study was done by [6] to investigate the suitability of trapezoidal cross-section with segment base in drainage system design. Saint–Venant partial differential equations of continuity and momentum governing free surface flow in open channels are solved using the finite difference approximation method. This research studies the effects of channel radius, area of cross-section, water depth and the manning's roughness coefficient on the flow velocity. The study shows that an increase in cross-section leads to a decrease in flow velocity. This also applies to channel radius, area of cross-section and manning's roughness coefficient. However, the increase in water depth leads to an increase in velocity.

4   Methodology

An idealised 1D river bifurcation numerical model was simulated by InfoWorks ICM. The river model is a Y-shaped bifurcation with a 90° bifurcation angle (i.e. 45 deviations angle for both downstream), as shown in Fig. 1. To avoid confusion, upstream, left and right downstream were named as Main Channel, Channel 1, and Channel 2. The length of all channels was set as 600 m, the width of the Main Channel was set as 300 m, and the height of all channels was set as 3.5 m.

The variable factors in this study are designated as the width of Channel 1 and Channel 2, cross-section shape, and manning's roughness coefficient as shown in Table 1. 100, 150, 200, and 300 m are designated as Channel 1 and Channel 2 width in different combination as shown in Fig. 2. The shapes of the cross-section are rectangular and trapezoidal. The width of the trapezoidal cross-section was referred to as the top width of the channel; the bottom width of the channel was set as 50 m, lesser than the top width for all scenarios. The manning's roughness coefficients are 0.013, 0.03, and 0.06.

The simulation duration was assigned as 24 hours, with 100 m^3/s inflow at the beginning of the simulation, and the inflow was slowly increased by 100 m^3/s with an interval of 4 h up to 700 m^3/s at the time of 24:00:00. The water level at the end node of both Channel 1 and Channel 2 was set as a 2.5 m boundary condition. The analysis is run according to time with an increment of 1 hour and stop at the time of 24:00:00.
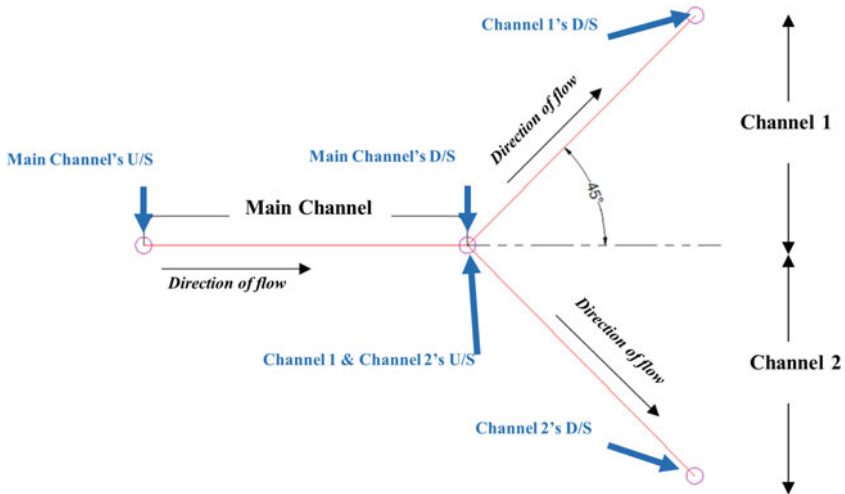
Fig. 1   Model setup (not to scale; U/S: upstream; D/S: downstream)

Table 1 List of variable factors

Scenario	Width of channel 1 (m)	Width of channel 2 (m)	Shape of cross section	Manning's roughness coefficient
1a	150	300	Rectangular	0.013
1b				0.03
1c				0.06
1d			Trapezoidal	0.013
1f				0.03
1g				0.06
2a	100	300	Rectangular	0.013
2b				0.03
2c				0.06
2d			Trapezoidal	0.013
2f				0.03
2g				0.06
3a	100	200	Rectangular	0.013
3b				0.03
3c				0.06
3d			Trapezoidal	0.013
3f				0.03
3g				0.06
4a	300	300	Rectangular	0.013
4b				0.03
4c				0.06
4d			Trapezoidal	0.013
4f				0.03
4g				0.06

5 Result and Discussion

5.1 Effect of Manning's Roughness Coefficient

The results from Figs. 3, 4, and 5 show increase in Manning's roughness coefficient causes a decrease in flow velocity. This finding applies to both rectangular and trapezoidal cross-sections. Manning's roughness coefficient is the channel surface roughness to the flow in the channel. Higher Manning's roughness represents a rougher surface, more vegetation on channel and channel irregularity. Thus, a slower flow rate resulted in a decrease of flow velocity. The results obtained are similar to the studies by [6] and [7].
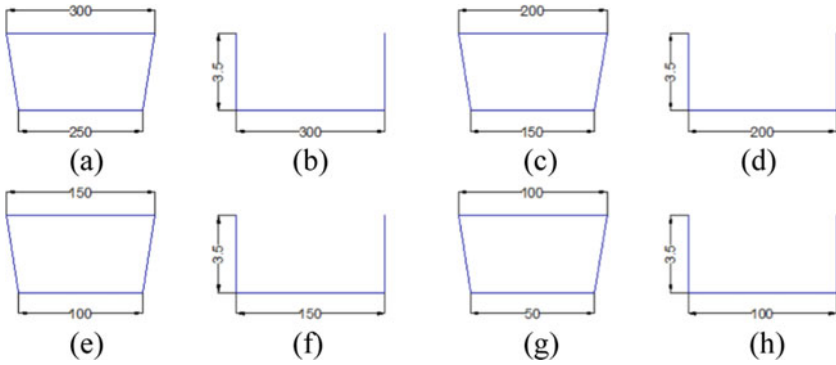
Fig. 2 Types of cross section for rectangular and trapezoidal section (not to scale and all value are in metre)
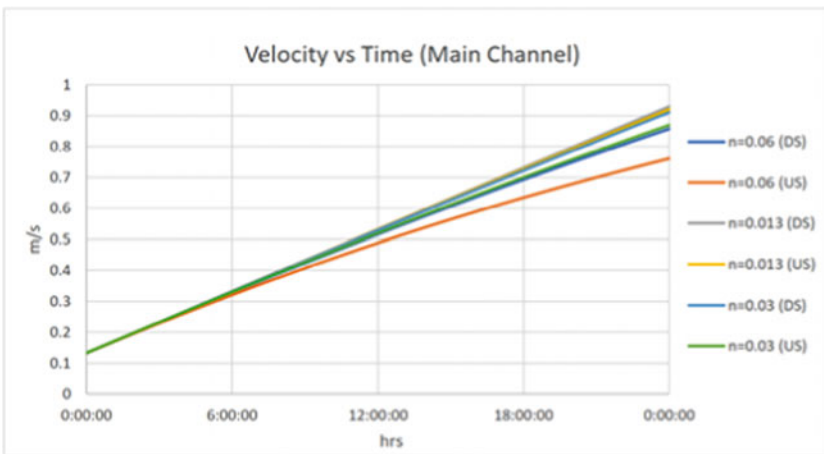
Fig. 3 Velocity profile of main channel with various manning's coefficient (Rectangular cross-section and Scenario 1)

Other than velocity, an increase in Manning's roughness coefficient leads to an increase in water depth for both rectangular and trapezoidal cross-sections. The water depth for $n = 0.06$ is much higher than the water depth for $n = 0.013$ and $n = 0.03$.
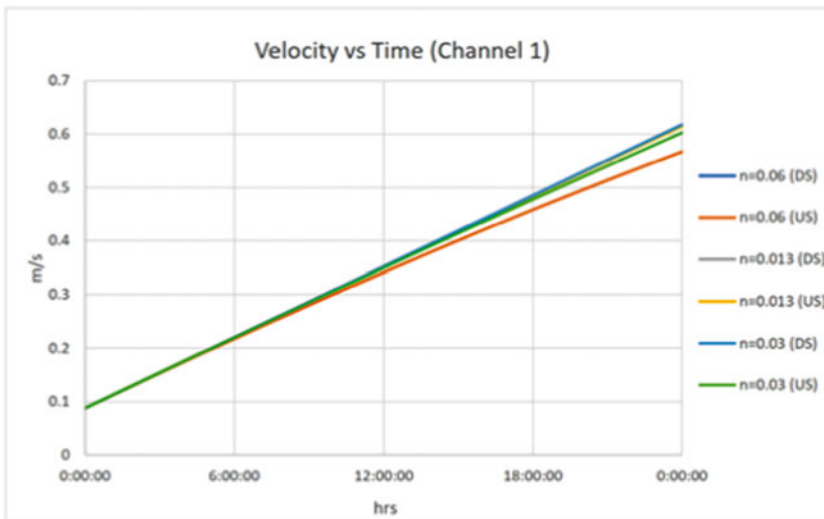
Fig. 4 Velocity profile of channel 1 with various manning's coefficient (Rectangular cross-section and Scenario 1)
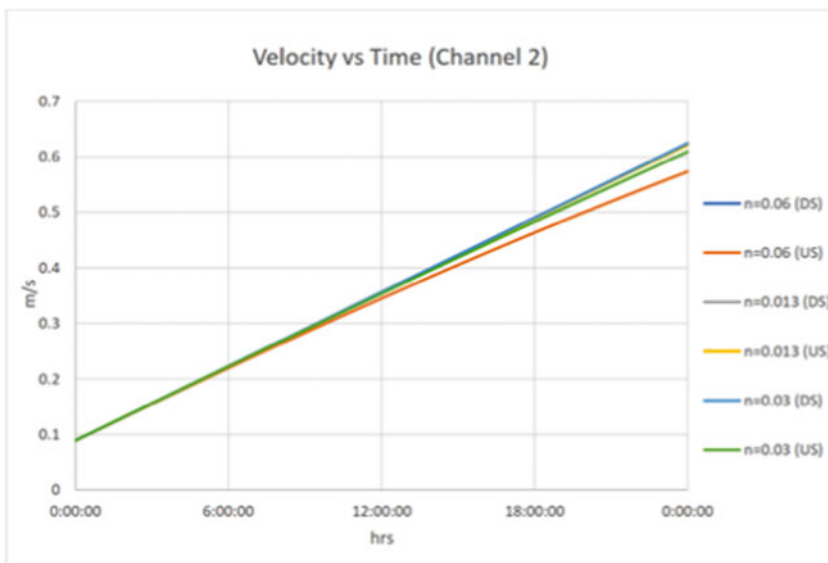
Fig. 5 Velocity profile of channel 2 with various manning's coefficient (Rectangular cross-section and Scenario 1)

5.2 Effect of Cross Section Shape

For channels with equal width and Manning's roughness coefficient, the flow velocity in a rectangular cross-section is lower compared to the trapezoidal cross-section. This applies to all three of Manning's roughness coefficients. The results obtained contradicted the results obtained from the studies by [6] and [7].

For channels with equal width and Manning's roughness coefficient, the water depth in rectangular cross-section is lower compared to the trapezoidal cross-section. This applies to all three of Manning's roughness coefficients.

5.3 Effect of Channel Width

Channels in each scenario are compared individually. For Main Channel, the channel width is the same for all four scenarios. However, the flow velocity in Scenario 4 is the largest, followed by Scenario 1, Scenario 2, and Scenario 3. This is due to the continuity equation:

$$V_{upstream} \ A_{upstream} = V_1 A_1 + V_2 A_2 \tag{1}$$

The channel width of the Channel 1 will affect the velocity in the Main Channel. Figure 6 showed the flow velocity at Main Channel with different scenarios. By comparing the Main Channel' DS, the flow velocity of Scenario 4 (Channel 1 width = 300 m) is faster than Scenario 1 (Channel 1 width = 150 m), and Scenario 1 is faster than Scenario 2 (Channel 1 width = 100 m). Thus, the larger channel width of the Channel 1 will result in a larger flow velocity in the main channel.

From Figs. 7 and 8, as for Channel 1 and Channel 2, the flow velocity in Scenario 3 is the largest, followed by Scenario 2, Scenario 1, and Scenario 4. This is due to an increase in channel width that causes a decrease in flow velocity. For Channel 2, the channel width is the same in Scenario 1, Scenario 2 and Scenario 4. This is also due to the continuity equation (Eq. 1). In all scenarios except Scenario 3, the flow velocity of Channel 1 is always smaller than Channel 2 due to the width of Channel 1 being always smaller than Channel 2 (except Scenario 3). The results obtained apply to both rectangular and trapezoidal cross-section.
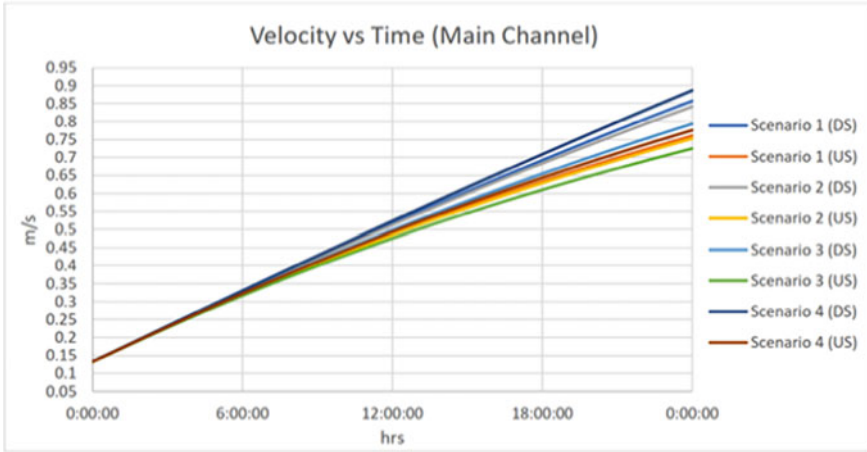
Fig. 6 Velocity profile of main channel with various scenario (Rectangular cross-section and n = 0.06)
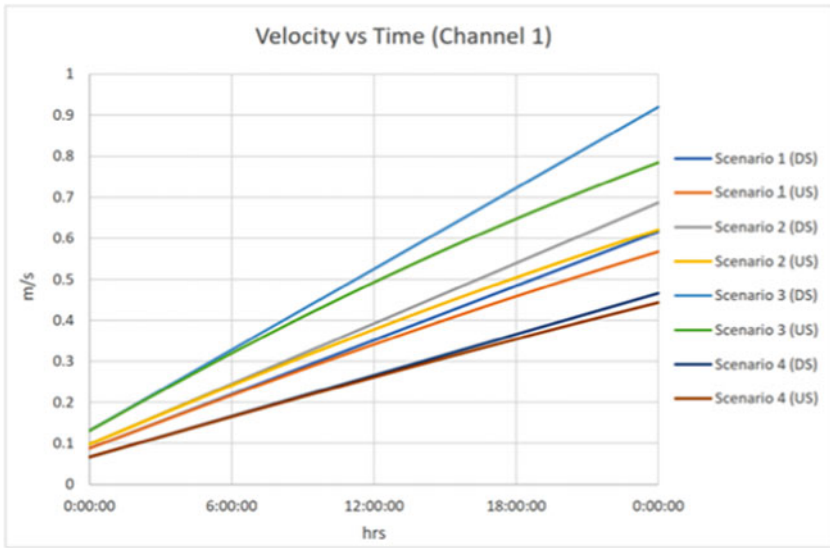
Fig. 7 Velocity profile of channel 1 with various scenario (Rectangular cross-section and n = 0.06)

All three channels shared the same results for water depth. The water depth in Scenario 3 is the highest, followed by Scenario 2, Scenario 1, and Scenario 4. Scenario 3 has the highest water depth because Channel 1 and Channel 2 have the smallest channel width compared to other scenarios. Since the channel width is fixed, the variable will be the height of the water. Therefore, it can be concluded that smaller
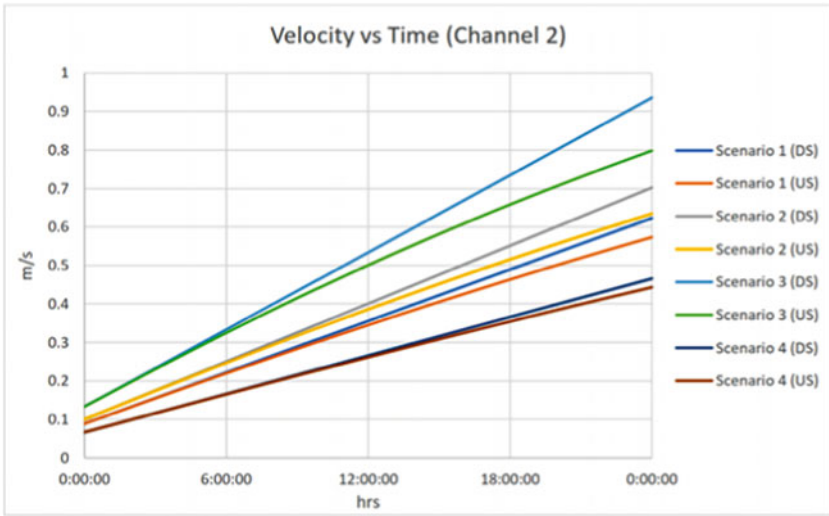
Fig. 8 Velocity profile of channel 2 with various scenario (Rectangular cross-section and n = 0.06)

channel width results in higher water depth. The results obtained apply to both rectangular and trapezoidal cross-sections.

6 Conclusion

In this study, the attention is focused on the morphodynamics of a river with a Y-shaped bifurcation. Y-shaped open channel model is used to run the numerical analysis as rivers can be presented as an open channel. This study has provided a better understanding of the behaviour of open channel flow with bifurcation and assists engineers in mitigating floods. These findings clearly showed how different parameters affect the water depth and flow velocity. The water depth and flow velocity are observed individually. From the results obtained, a rectangular cross-section is preferable in mitigating flood compared to a trapezoidal cross-section. It shows contradiction with past research as it has shown that a trapezoidal cross-section is preferable. This may be due to not taking into consideration of the side slope ratio in the trapezoidal cross-section when designing the model. However, all results of other parameters show the same patterns when compared with past research.

References

1. Bertoldi W, Tubino M (2007) River bifurcations: experimental observations on equilibrium configurations. Water Resour Res 43(10). https://doi.org/10.1029/2007WR005907
2. Caddis B, Nielsen C, Hong W, Tahir PA, Teo FY (2012) Guidelines for floodplain development–a Malaysian case study. Int J River Basin Manag 10:161–170
3. Cheah R, Billa L, Chan A, Teo FY, Pradhan B, Alamri AM (2019) Geospatial modelling of watershed peak flood discharge in Selangor, Malaysia. Water 11(12):2490
4. Kleinhans MG, Ferguson RI, Lane S, Hardy RJ (2013) Splitting rivers at their seams: bifurcations and avulsion. Earth Surf Proc Land 38(1):47–61. https://doi.org/10.1002/esp.3268
5. Le TB, Crosato A, Uijttewaal WSJ (2018) Long-term morphological developments of river channels separated by a longitudinal training wall. Adv Water Resour 113(May 2017):73–85. https://doi.org/10.1016/j.advwatres.2018.01.007
6. Marangu PK, Mwenda E, Theuri DM (2016) Modeling open channel fluid flow with trapezoidal cross section and a segment base. J Appl Comput Math 05(01):1–5. https://doi.org/10.4172/2168-9679.1000292
7. Natasha G, Suharjito NV (2019) Saint-venant model analysis of trapezoidal open channel water flow using finite difference method. Procedia Comput Sci 157:6–15. https://doi.org/10.1016/j.procs.2019.08.135
8. Pandey AK, Mishra R (2012) Comparison of flow characteristics at rectangular and trapezoidal channel junctions. J Phys Conf Ser 364(1). https://doi.org/10.1088/1742-6596/364/1/012141
9. Shah SMH, Mustaffa Z, Teo FY, Imam MAH, Yusof KW, Al-Qadami EHH (2020) A review of the flood hazard and risk management in the south Asian region particularly Pakistan. Sci Afr 10:e00651
10. Schielen RMJ, Blom A (2018) A reduced complexity model of a gravel-sand river bifurcation: equilibrium states and their stability. Adv Water Resour 121(January):9–21. https://doi.org/10.1016/j.advwatres.2018.07.010
11. Teo FY, Xia J, Falconer RA, Lin B (2012) Experimental studies on the interaction between vehicles and floodplain flows. Int J River Basin Manag 10(2):149–160
12. Van Denderen RP, Schielen RMJ, Blom A, Hulscher S, Kleinhans MG (2018) Morphodynamic assessment of side channel systems using a simple one-dimensional bifurcation model and a comparison with aerial images. Earth Surf Proc Land 43(6):1169–1182. https://doi.org/10.1002/esp.4267
13. Wang ZB, Vries MD, Fokkink RJ, Langerak A (1995) Stability of river bifurcations in 1D morphodynamic models. J Hydraul Res 33(6):739–750
14. Xia J, Teo FY, Falconer RA, Chen Q, Deng S (2018) Hydrodynamic experiments on the impacts of vehicle blockages at bridges. J Flood Risk Manag 11(S1):S395–S402. https://doi.org/10.1111/jfr3.12228

Modelling of an Embankment Failure Using Flow-3D

M. Y. Zainab, A. L. S. Zebedee, A. W. Ahmad Khairi, I. Zulhilmi, and A. Shahabuddin

Abstract Embankment dam failures are concerning to many people in society today, including dam engineers, federal, state, and local officials. The effects of dam failure will cause more harm than good, leading to the losses of lives, properties being damaged, economic and environmental issues. The embankment dam breaching is a complex process between hydraulics and soil erosion processes that requires an analysis of hydrodynamic parameters such as breach outflow hydrograph, peak outflow rate and failure time, and geometric parameters; breach depth, H_b, and top breach width, B_t. . With the aid of simulation techniques such as Computational Fluid Dynamics (CFD), it is possible to understand the behaviour of embankment breaching processes. In this paper, modelling of an embankment breaching using FLOW-3D allows modellers to open doors to plenty of experiments to breaching in the near future. This paper focuses on analyzing the modelling breaching embankment for different sediment sizes of embankment material to investigate the patterns of breached outflow, breach width, dam breach depth. Moreover, the study also investigates the hydrostatic pressure, free surface elevation and shear stress on embankment during the breaching failure processes.

M. Y. Zainab (✉)
Eco-Hydrology, School of Civil Engineering, Faculty of Engineering, Universiti Teknologi Malaysia, Johor Bahru, Malaysia
e-mail: zainabyusof@utm.my

A. L. S. Zebedee
School of Civil Engineering, Faculty of Engineering, Universiti Teknologi Malaysia, Johor Bahru, Malaysia

A. W. A. Khairi · I. Zulhilmi
Centre for River and Coastal Engineering (CRCE), Faculty of Engineering, Universiti Teknologi Malaysia, Johor Bahru, Malaysia
e-mail: akhairi@utm.my

I. Zulhilmi
e-mail: zulhilmi@utm.my

A. Shahabuddin
Department of Geoinformation, Faculty of Built Environment and Surveying, Universiti Teknologi Malaysia, Johor Bahru, Malaysia
e-mail: shahabuddin@utm.my

1 Introduction

Dam failures, either from accidents or deliberate acts, may cause disastrous damage towards downstream areas. Major flood waves brought by the dam failure may cause serious damage or destroy industrial or power plants, houses and bridges; transportation, navigation, irrigation and social economy activities; and may cause loss of life, spoiling of agricultural land, and adversity of ecological and environmental impacts.

According to [1], approximately 34% of dam failures are caused by overtopping, 30% by foundation defects, and 28% by piping. Overall, the most common causes of embankment failure are overtopping and internal erosion. [5] indicates that there are approximately 57 000 dams in the United States that have the potential for overtopping. In obtaining breach parameters from regression analysis, [6] stated dam erodibility plays a significant role in influencing the results of breaching parameters. Sand has high erodibility compared to clay which has low erodibility, and hence higher resistance to fast-moving water.

Data collected by the Association of State Dam Safety Officials (ASDSO, 2020) between 2010 and 2019 showed that dam failure by overtopping ranked the highest for a number of incidents and followed by piping. Overtopping is caused when water spills over the top of the dam and causes erosions. Overtopping may occur due to inadequacy of spillway design, blockage by debris at the spillway, or settlement of the dam crest.

Overtopping is a result of insufficient spillway capacity or an event of extreme rainfall, which causes the water level to exceed design criteria. The water flow over the embankment from overtopping introduces tractive shear stress on the downstream surface [4]. The erosion process begins at a weak spot where the tractive shear stress exceeds a critical resistance that keeps the soil material in place [3, 7]. The process will continue under the action of flowing water while soil materials are being transported downstream. The initial breach is often V-shaped and becomes larger as the erosion progresses, which finally results in an inverse trapezoidal shape. The extent of breaching usually depends on the duration of overtopping and the structure of the embankment. In fact, the erosion characteristics are different for granular and cohesive embankments. Granular soil is non-cohesive soil such as sand or small gravel, whereas an example of cohesive soil is clay.

For non-cohesive embankments, the overtopping flow of water on downstream slope causes surface slip to take place quickly, hence resulting in non-cohesive materials to be removed rapidly, layer by layer. Usually, the end result for breaching in this manner tends to become flattened, depending upon the material and the longitudinal slope of the foundation surface. For cohesive embankments, erosion often starts at the embankment toe and advances upstream, undercutting the slope and in turn causing the removal of large chunks of materials due to tensile or shear failure of the soil on the over-steepened slope. In certain cases, a series of stair-step head-cuts develop at the downstream face.

2   Breaching Embankment Modelling

In this study, FLOW-3D v11.2 [2], which was developed by Flow Science, Inc. USA, is used to investigate the breaching processes to analyse the breaching parameters such as shear stress, hydrostatic pressure and free surface elevation. The output of breaching outflow hydrographs and comparison of sediment sizes of the embankment is also modelled to predict the breach patterns and breach outflows.

The embankment is modelled using AutoCad 3D before importing into FLOW-3D for meshing generation. Figure 1 shows the geometry of the embankment and the model setup. The model setup has a total channel length of 12 m with upstream and downstream lengths of 8.5 and 1.815 m, respectively. A structured and uniform mesh size of 0.02 m is used where the finer mesh is located in the embankment area to get more accurate simulation results.

The simulation was run for 400 s using the sediment scour physical model. The embankment sediment was set to be 0.1 (fine), 0.4 (medium) and 0.8 mm (coarse) with an inflow rate of 0.012 m³/s. The initial state of the solution for transient fluid flow problems must be known in order to find a solution and, in a manner similar to what is done with boundary conditions, the initial conditions are assumed, approximating the true state at time $t = 0$. The Boundary conditions used are Volume Flow Rate (Q), Outflow (O), Symmetry (S), Wall (W) and Specified pressure (P), and the location to apply the boundary conditions is shown in Fig. 2.

(a)

(b)
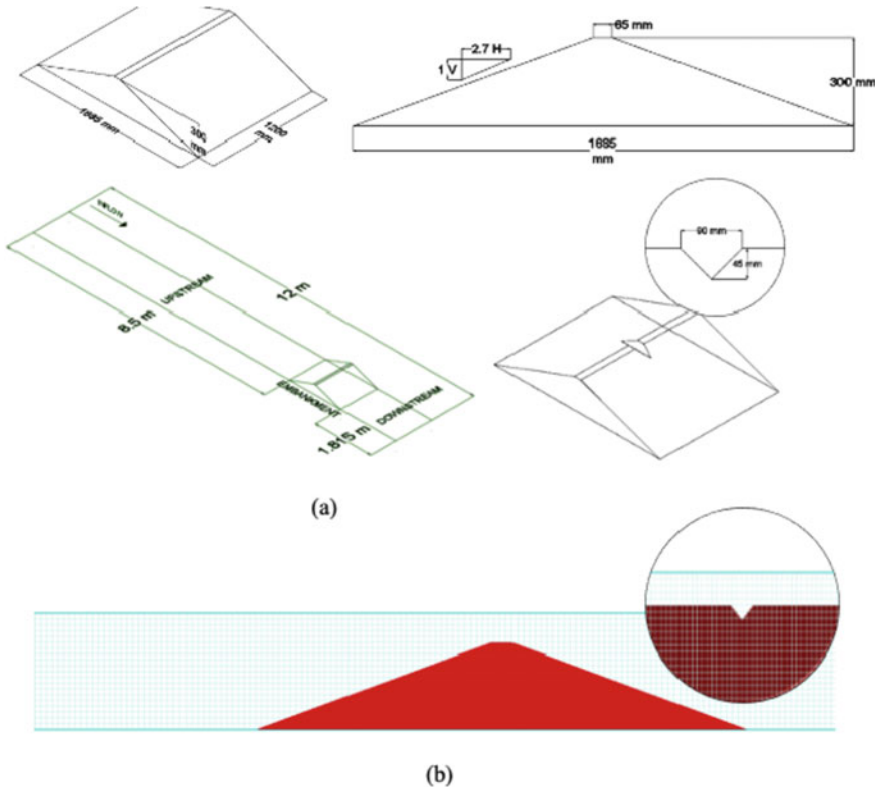
Fig. 1 Model setup **a** Embankment geometry, and **b** Meshing size
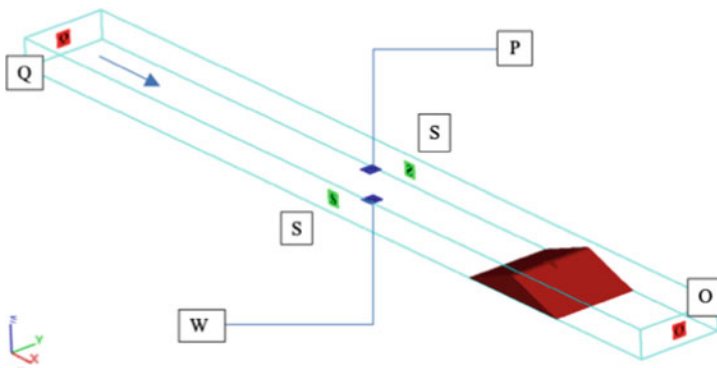
Fig. 2 Boundary conditions of the model setup
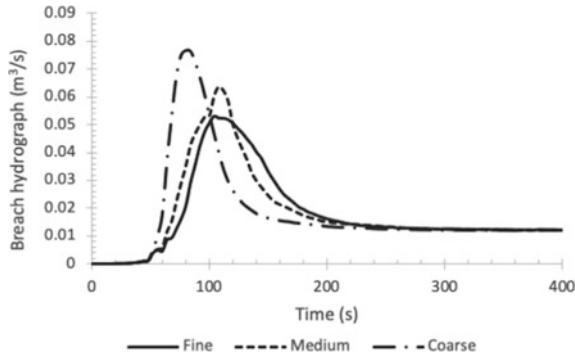
Fig. 3 Breach outflow hydrograph for different sediment sizes

3 Results and Discussions

The modelling of breaching embankment with different sizes of sediments diameter showed that the breaching occurs slower when the sediment is finer as compared to larger sediment embankments. This is because the fine sand seems to be more resistant to erosion. Figure 3 shows the peak outflow hydrograph for coarse sand with a diameter of 0.8 mm is 0.0768 m^3/s, and for fine sand with a diameter of 0.1 mm, the peak is 0.0532 m^3/s. The outflow hydrograph is measured at the outlet of the channel where the v-notch is installed. Meanwhile, for medium sand with a diameter of 0.4 mm, the peak outflow hydrograph is 0.0638 m^3/s. As for the failure time where the breaching started, the coarse sand obtained a failure time of 80 s, while that of the fine sand had a failure time of 104 s. The failure time for the medium sand is 108 s which is almost as similar to the failure time for the fine sand (Fig. 5).

In the breaching process, the flowrate plays an important role in the erosion and scour of the embankment, the widening and deepening process of the breach, and the flood propagation process downstream. Figure 4 illustrates the breach profiles – failure lines patterns with sediment size of 0.4 mm and inflow rate of 0.012 m^3/s at time 40, 60, 80, 100, 120 and 140 s, respectively. As breach depth increases and the height of the embankment reduces, the downstream slope angle of the embankment decreases, as can be observed in Fig. 4. The details of the breach patterns with respect to the free surface profiles and hydrostatic pressure is shown in Fig. 6.
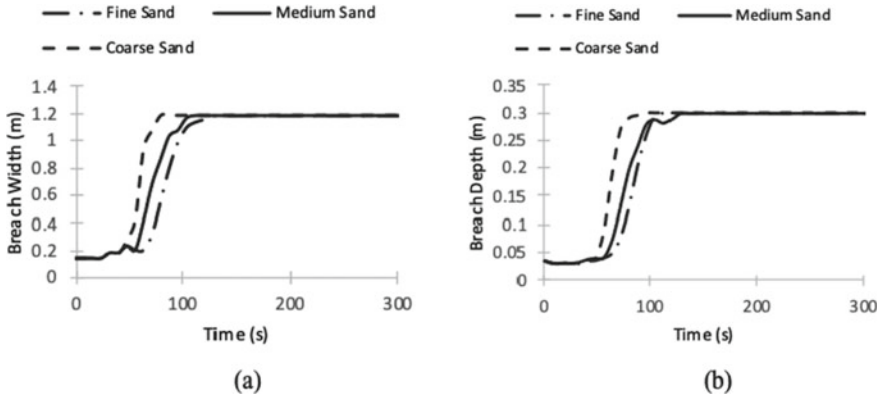
Fig. 4 **a** Breach width and **b** breach depth against time
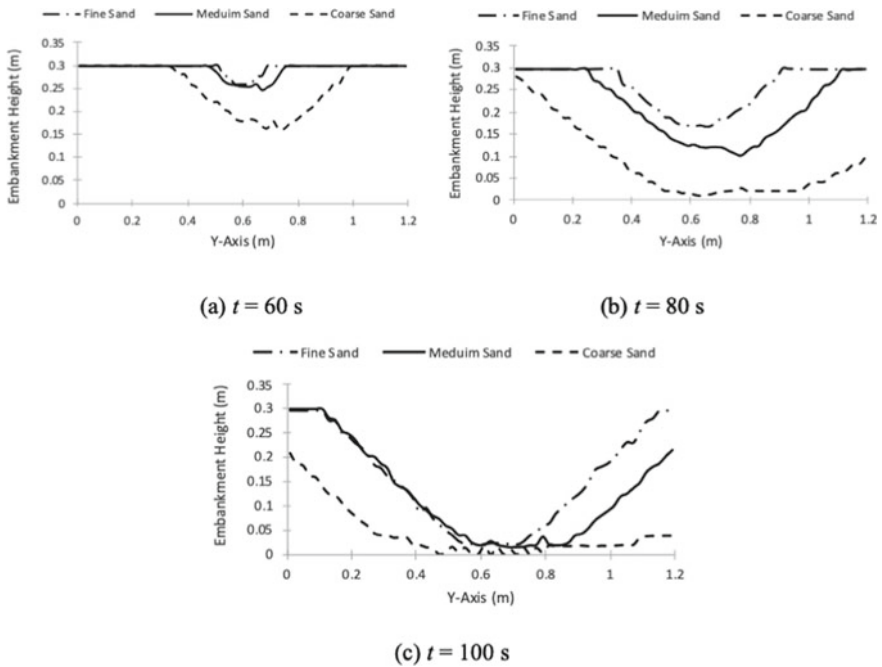
Fig. 5 Breach growth for **a** $t = 60$, **b** $t = 80$ and **c** $t = 100$ s

Meanwhile, for hydrostatic pressure analysis, there is an increment in bottom pressure from $t = 40$ s to $t = 60$ s. This is due to a rising in water elevation during the overtopping flow. Since the erosion rate at this condition is still slow, the embankment height shows little change, which results in hydraulic jump and an increase in water elevation. At $t = 80$ s, the hydrostatic pressure at the bottom decreases as
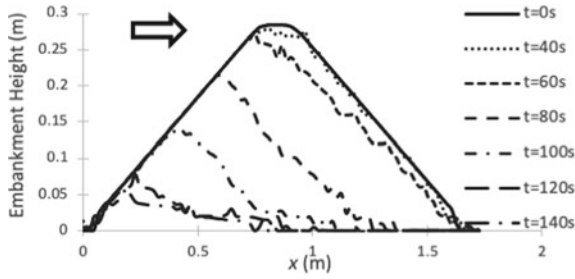
Fig. 6 Progression of breaching profiles at various time intervals

the embankment height decreases due to erosions, from the result of lower water elevation. As the erosion continues, the hydrostatic pressure at the bottom continues to decrease as the embankment height decreases due to erosion. This can be seen at $t = 120$ s to $t = 140$ s. This progression can be observed in Fig. 7 for time intervals of 40, 60, 80, 100, 120, and 140 s.

Meanwhile, the shear stress results of 3D modelling of the embankment are shown in Fig. 8. Through the observation of the 3D model results of shear stress, erosion
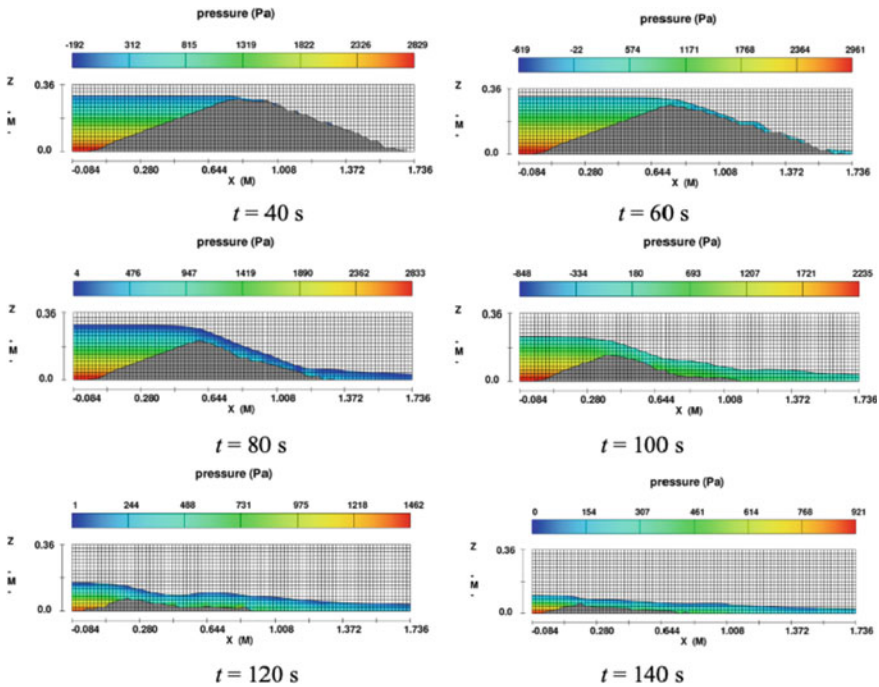
Fig. 7 Changes of free surface elevation with hydrostatic pressure variation during the embankment failure

occurs when shear stress is present. This illustrates how shear stress influences the erosion process in embankment breaching. Also, due to erosion beginning at the canter y-axis of the embankment, the erosion pattern of the embankment resembles a V-shape when looking from a plane view at the embankment downstream.
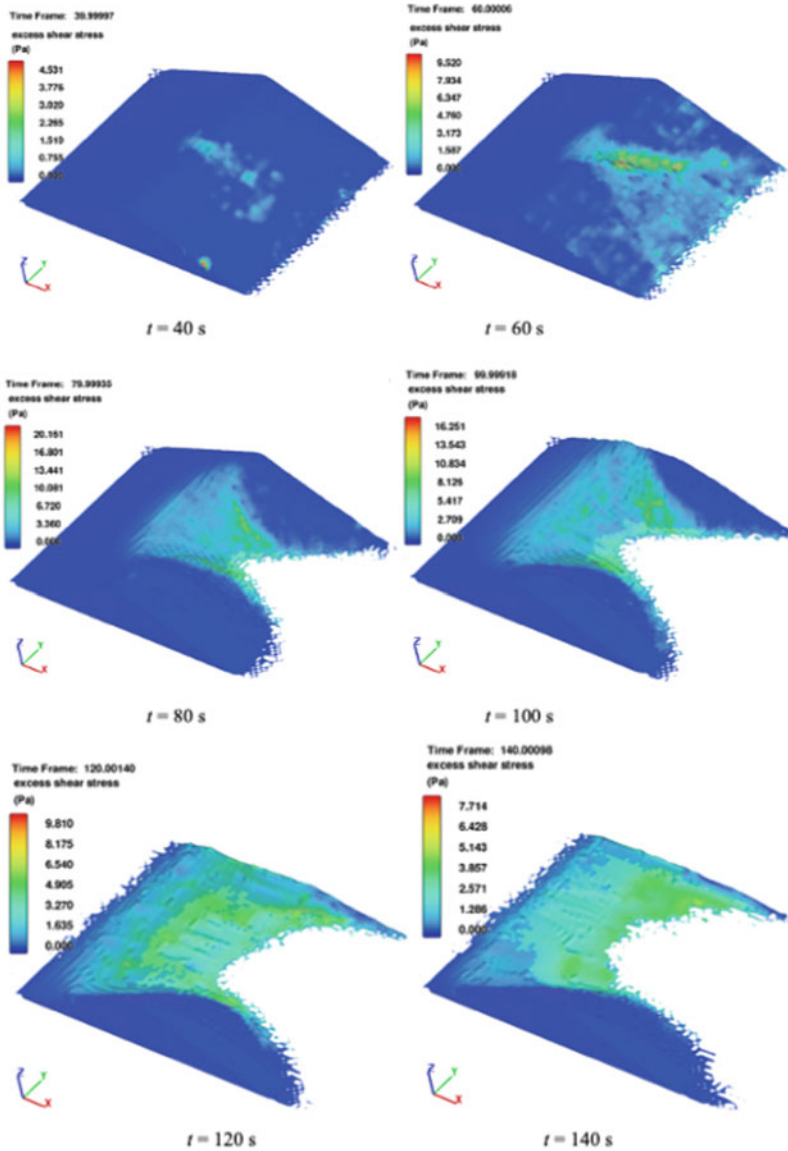
Fig. 8 Shear stress changes of an embankment breaching
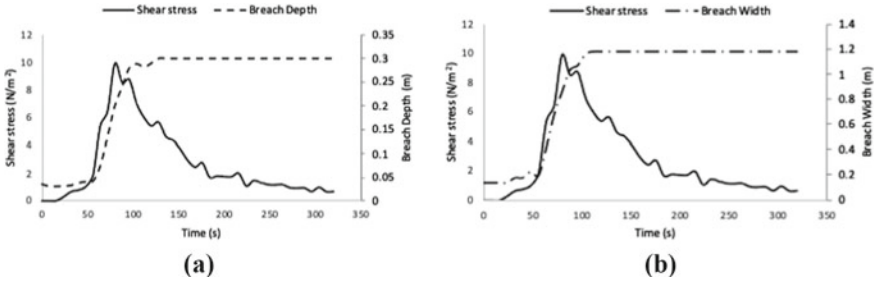
Fig. 9 Shear stress against **a** breach depth and **b** breach width

Table 1 Summary of maximum shear stress, breach depth, and top breach width

Time, t (s)	Maximum shear stress, τ (N/m^2)	Breach depth, H_b (m)	Top breach width, B_t (m)
40	0.76	0.04	0.18
60	5.83	0.05	0.31
80	9.87	0.20	0.86
100	8.84	0.28	1.12
120	5.37	0.29	1.18
140	4.51	0.30	1.18

The maximum value of shear stress at cross-section is plotted against time and compared with breach depth and breach width, as shown in Fig. 9. The results indicate an increasing gradient of the curve of the rate of shear stress, the breach depth and the breach width at the beginning of breaching, then slowly, the rate of shear stress starts showing a decreasing gradient. At this point, the breach depth and the breach width hit a constant, reaching their maximum depth and width. Table 1 indicates the summary of the maximum shear stress obtained in relation with breach width and breach depth for $t = 40$ s, $t = 60$ s, $t = 80$ s, $t = 100$ s, $t = 120$ s, and $t = 140$ s.

4 Conclusion

The peak outflow hydrograph is higher and has a shorter failure time for embankment with larger sediment sizes and lower peak outflow hydrograph and longer failure time for embankment with finer sediment sizes. Finer particles are able to provide a greater surface area of contacts between other particles, thus having increased interlocking between soil particles and hence higher resistance to soil erosion. Embankment dams with large sediment sizes will have larger breach depth and width as compared to embankment dams with finer sediment sizes at the end of the breaching process. The breach depth and breach width also show an increment when the shear stress

increases. The shear stress exerted by the flowing water exceeds the critical erosive shear stress of the soil resulting in the erosion of the embankment. The hydrostatic pressure upstream is greater than the hydrostatic pressure downstream. As a result, the surface of the embankment during breaching keeps on eroding and changes shape, which leads to variations in the flow depth.

References

1. Costa JE (1985) Floods from dam failures. Open-File Rep. No. 85-560, USGS, Denver, p 54
2. FLOW-3D (2016) FLOW-3D v11.2 Documentation. Flow Science Inc.
3. Mat Lazin NA (2013) Erodible Dam Breaching Patterns Due to Overtopping. Master thesis, Johor Bahru: Universiti Teknologi Malaysia
4. Powledge GR, Ralston DC, Miller P, Chen YH, Clopper PE, Temple DM (1989) Mechanics of overflow erosion on embankments II: hydraulics and design considerations. J Hydraul Res 115(8):1056–1075
5. Ralston DC (1987) Mechanics of embankment erosion during overflow hydraulic engineering. In: Proceedings of the 1987 National Conference on Hydraulic Engineering, ASCE Reston VA, pp 733–738
6. Xu Y, Zhang LM (2009) Breaching parameters of earth and rockfill dams. J Geotech Geoenviron Eng 135(12):1957–1970
7. Zhao G, Visser PJ, Ren Y, Uijttewaal WSJ (2015) Flow hydrodynamics in embankment breach. J Hydrodyn 27(6):835–844

Water Distribution System Modelling in Pasir Gudang, Johor with EPANET

J. H. Lee, P. Jeevaragagam, N. K. Max Mulwan, A. Aris, and M. Anjang Ahmad

Abstract This paper presents a water supply distribution system for the Pasir Gudang area in Johor by using EPANET software. The requirements for this study are Pasir Gudang water distribution layout, water demand based on each area, the elevation of tank locations and length and diameter of the pipes. The required water demand, the elevation of the tank and the main pipe diameter are obtained from Ranhill SAJ Sdn Bhd. The water distribution network that is modelled with EPANET consists of 26 water tanks, 38 junctions, 65 pipes and one water treatment plant. The total amount of Epanet computed water demand is 215,160 million litres per day, which is higher than the required water demand of 206,070 million litres per day. Therefore, there is no shortage of water to affect in Pasir Gudang area.

Keywords Water distribution network · Water demand · EPANET

1 Introduction

Water Distribution System (WDS) is one of the imperative city foundation systems within the world. The WDS passes on consumable water through an organised of

---

J. H. Lee · P. Jeevaragagam (✉) · N. K. Max Mulwan · A. Aris
Department of Water and Environmental Engineering, School of Civil Engineering, Faculty of Engineering, Universiti Teknologi Malaysia, 81310 Johor Bahru, Johor, Malaysia
e-mail: ponselvi@utm.my

J. H. Lee
e-mail: jun.hao@graduate.utm.my

N. K. Max Mulwan
e-mail: nikitakhairina@graduate.utm.my

A. Aris
e-mail: azmi.aris@utm.my

M. Anjang Ahmad
Faculty of Civil Engineering and Built Environment, Universiti Tun Hussein Onn Malaysia, 86400 Parit Raja, Batu Pahat, Johor, Malaysia
e-mail: mustafa@uthm.edu.my

channels and other components from the treatment plants to commercial, family units, and mechanical clients. The water is supplied continuously and at a satisfactory pressure and stream, complying with microbial and chemical quality measures [1]. The WDS is not scheduled to meet peak demands in the long term but to effectively operate water distribution over short time periods. EPANET is a computer program that performs an extended period simulation of hydraulic and water quality behaviour within pressurized pipe systems. The program computes water flow in each pipe, pressure at each node, height of water in each tank and concentration of a chemical species [4]. It provides an integrated environment for editing network input data, executing hydraulic and water quality simulations, and viewing the results in a variety of formats [11]. Furthermore, it is designed as an investigative apparatus to evaluate the development and destiny of drinking water constituents in a water distribution system. Thus, EPANET can be used for decision support in a network of water distribution systems to evaluate alternative management strategies for improving water quality and quantity. The water distribution network model can be used to compare and analyse the existing, the present required water demand, and the water supply to prevent the shortage of water happening in future.

The demand for water resources in Malaysia for agricultural, industrial and domestic activities have been increased steadily from 8.9 billion m^3 in 1980 to 15.5 billion m^3 in 2000 [7]. The agriculture sectors use an estimated 76% of available water as well as in heavy industrialisation in developed states. The increasing population and urbanisation have also affected water demands [3]. In Johor, many developments and investments in manufacturing, modern agriculture, technology and others are expected in the near future. The rapid development and economic growth, especially in Pasir Gudang, Johor, Malaysia, have caused an increase in water demand. As populations are growing within years, the changes in water demand consumption are also significant [6]. Contaminated water sources and seawater are more expensive than other water treatment methods. Water scarcity has become the greatest challenge, particularly during extremely hot weather in Pasir Gudang, Johor [9]. In 2011, the water supply to Pasir Gudang has disrupted for about 15 h and affected several residential and industrial areas [12]. In 2017, several industrial areas in Pasir Gudang again had been disrupted by the pipe leakage near the Sultan Iskandar Water Treatment Plant in Sungai Layang [5].

A reliable water distribution system is needed to evaluate the water supply and the water demand for the Pasir Gudang area and to help avoid water shortages. The main purpose of this study is to develop a new water distribution model for the Pasir Gudang area by using EPANET. The existing water demand information that is obtained from Ranhill SAJ Sdn Bhd will be compared to the new water demand model computed by EPANET.

2 The Methodology

2.1 Study Area Description

Pasir Gudang is located in Mukim Plentong, Johor, Malaysia with an estimated population of 533,868 people [10]. The climate in the Pasir Gudang area can be summarized as hot, humid and wet, daytime maximum temperatures average around 31 °C, whilst at night 24 °C is normal. The city receives an average rainfall of 155 mm. It is one of Malaysia's most important economic hubs for logistics, transportation, shipbuilding, petrochemical manufacturing, palm oil storage and heavy industries.

2.2 Preparation of Water Distribution Network Layout

The layout of the water distribution network and the pipe specification are obtained from the Ranhill SAJ Sdn Bhd. The sketch of the water distribution layout is shown in Fig. 1. The map covers the recent water distribution layout of the Pasir Gudang area, which includes pipe lengths of the network and their respective positions.
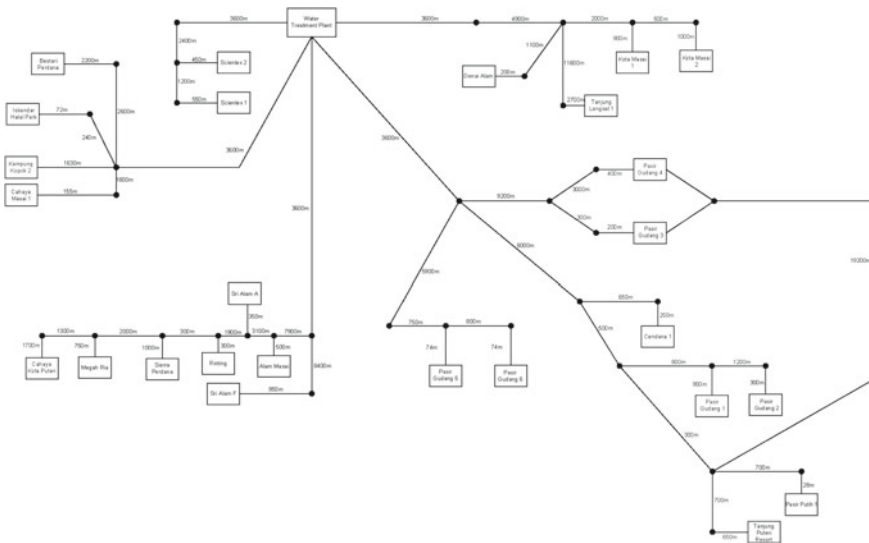
Fig. 1 The sketch of water distribution layout

2.3 Google Earth Pro

The data of pipe length between tank(s) to tank(s), junctions(s) to tank(s) and longitude(s) and latitude(s) for Pasir Gudang area are determined by using the Google Earth Pro, which is a Google Earth desktop application. The Google Earth Pro has many features, including displaying satellite and aerial imagery, a set of layers of mappable data, the ability to import ESRI shapefiles and MapInfo tab files, measuring distance and elevation and others.

2.4 Construct the Water Distribution Network into EPANET

The water distribution network of the Pasir Gudang area is constructed into the EPANET, as shown in Fig. 2. Based on the hydraulic scheme design, the total demand from reservoirs or tanks is firstly evaluated. The nodes and pipes are thoroughly checked to make sure it is connected to the intersections and reservoir nodes. Furthermore, all the piping specification values are inputted into the network modelling, such as the water demand of tanks, pipe length, pipe diameter and elevation of tanks. After all the necessary information have been assigned and calibrated, the model can be used to simulate the present water demand and future water demand in the case the tank is not functioning.
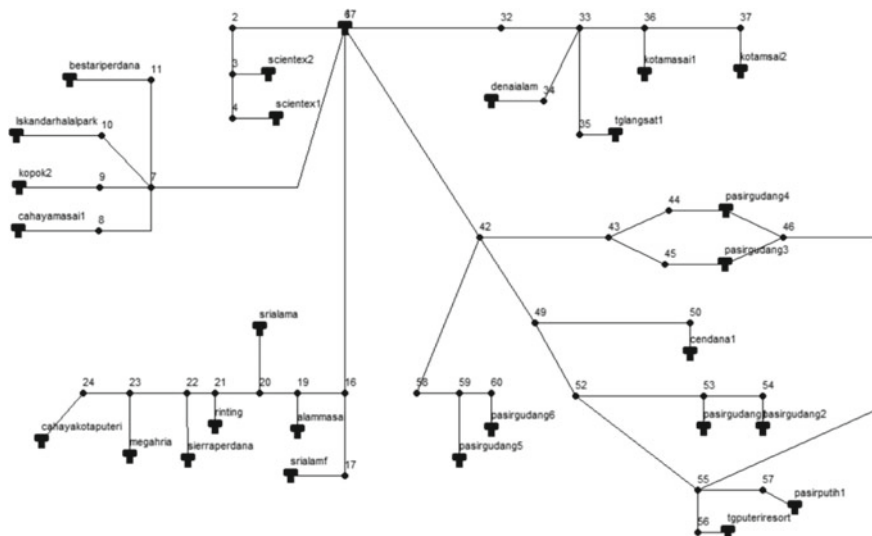
Fig. 2 Water distribution network in EPANET

2.5   Data Analysis

The data is initially analyzed by using EPANET to conduct the water distribution modelling. Microsoft Excel is used to perform the graph of the water demand of tanks in Pasir Gudang. The maximum allowable velocity is limited to 2.6 m/s to prevent erosion caused by high-speed turbulence [2]. The continuity equation and the energy conservation equation at the node and in the loop are the two basic equations for pipe network flow analysis [8]. The Hazen-William equation [13] is used to calculate the head loss (h_L) due to pipe friction and the flow rate in the pipe. The general h_L is as given in Eq. (1).

$$h_L = K Q^n \tag{1}$$

where K is the pipe constant, Q is the flow rate (m^3/s), and n is the coefficient of the flow that equals 1.85. The pipe constant, K is then given in Eq. (2).

$$K = \frac{10.69L}{C^{1.85} d^{4.87}} \tag{2}$$

where L is the length of pipe (m), d is the diameter of the pipe (mm), and C is a Hazen Williams coefficient. Bernoulli's equation is used to calculate the residual pressure head at each node, as given in Eq. (3).

$$\frac{P_2}{pg} = \frac{P_1}{pg} + z_1 + z_2 - \sum h_L \tag{3}$$

where $\frac{P_1}{pg}$ and z_1 are pressure head (m) for datum at node 1, while $\frac{P_2}{pg}$ and z_2 are pressure head (m) for datum at node 2, respectively, in the same pipe.

3   Results and Discussion

The results of the development of water distribution modelling in evaluating the water demand in Pasir Gudang are discussed herein. The water distribution network of the Pasir Gudang area consists of 26 water tanks, 38 junctions, 65 pipes and one water treatment plant.

3.1   Water Demand Report

The water demand and elevation of tanks in the Pasir Gudang area are given in Table 1. The water is supplied from the water treatment plant to the main tanks of the Pasir Gudang areas. The highest water supply is from the tank Taman Kota

Table 1 The water demand and elevation of the tank

Tank	Water demand (million litre/day)	Elevation (m)	Tank	Water demand (million litre/day)	Elevation (m)
Scientex 2	13.00	71.00	Taman Denai Alam	1.42	34.00
Scientex 1	4.50	71.00	Tanjung Langsat 1	27.26	44.80
Taman Bestari Perdana	5.09	66.00	Taman Kota Masai 1	36.20	51.30
Iskandar Halal Park	1.64	66.00	Taman Kota Masai 2	8.35	70.75
Kampung Kopok 2	0.85	53.30	Pasir Gudang 4	13.55	54.86
Taman Cahaya Masai 1	2.38	46.70	Pasir Gudang 3	13.37	54.86
Taman Cahaya Kota Puteri	2.32	46.00	Taman Cendana 1	4.45	50.00
Taman Megah Ria	9.09	53.81	Pasir Gudang 1	3.49	49.96
Taman Sierra Perdana	6.88	55.80	Pasir Gudang 2	1.71	73.25
Taman Rinting	11.26	51.83	Taman Pasir Putih 1	8.95	43.64
Bandar Sri Alam A	9.02	52.00	Taman Tanjung Putri Resort	9.00	46.04
Taman Alam Masai	3.74	50.00	Pasir Gudang 5	4.47	54.86
Bandar Sri Alam F	11.09	55.63	Pasir Gudang 6	2.08	73.00

Masai 1 with 36.20 million litres/day, while the tank Kampung Kopok 2 shows the lowest demand of 0.85 million litres/day. This is because Kopok 2 have the lowest population among other areas. Other areas are in the range of 1.42 to 27.26 million litres/day. Pasir Gudang 2 has recorded the highest elevation of 73.25 m, while the lowest elevation of 34.00 m is Taman Denai Alam.

3.2 Pipe Report

The pipes convey the water from the source to the consumers through connecting the junctions. Based on the Hazen Williams Equation, the flow rate in the pipes is obtained. Table 2 shows the length, diameter, flow rate, velocity and head loss in a

Table 2 Flow rate in pipes

Pipe	Flow rate (million litre /day)	Velocity (m/s)	Unit head Loss (m/km)	Pipe	Flow rate (million litre /day)	Velocity (m/s)	Unit head loss (m/km)
1	−0.28	0.00	0.00	36	0.33	0.22	8.88
2	−0.28	0.64	7.00	37	0.29	0.19	0.19
3	0.36	0.23	0.50	38	1.46	2.60	5.63
4	13.00	0.77	1.10	39	27.29	0.82	0.84
5	4.50	0.33	0.30	40	36.55	0.54	0.25
6	−0.75	0.50	1.00	41	8.35	0.77	1.49
7	−0.36	0.24	2.60	42	−0.10	0.07	0.00
9	−0.02	0.01	4.40	43	0.07	0.05	0.07
10	−0.54	0.36	5.90	44	−0.04	0.03	0.02
11	0.17	0.11	1.10	45	0.12	0.08	0.02
12	5.09	0.37	0.30	46	13.55	0.41	0.23
13	1.64	0.20	0.00	47	13.59	0.41	0.24
14	0.85	1.25	3.00	48	−0.14	0.09	0.00
15	2.38	2.43	5.60	49	−0.14	0.09	0.00
16	−0.04	0.02	0.00	50	0.47	0.31	0.75
17	−0.27	0.18	0.30	51	−0.14	0.09	0.18
18	0.24	0.16	0.30	52	0.61	0.40	1.51
20	−0.03	0.03	0.00	53	−0.61	0.41	2.19
21	−0.16	0.30	1.40	54	−0.57	1.30	8.62
22	−0.06	0.02	0.00	55	1.22	0.81	6.63
23	0.33	0.22	0.50	56	0.68	0.45	0.79
24	0.32	0.21	0.40	57	1.06	0.70	3.28
25	11.09	1.02	2.50	58	0.15	0.10	0.41
26	3.74	1.14	6.20	59	−0.15	0.10	0.41
27	9.02	1.08	3.30	60	−0.22	1.15	6.52
28	11.26	2.04	13.00	61	4.59	0.75	3.80
29	6.88	0.28	0.10	62	2.08	0.49	0.00
30	9.09	0.93	2.20	63	9.27	0.55	0.58
31	2.32	1.52	17.00	64	9.07	0.37	0.24
32	−0.06	0.04	0.00	65	4.53	0.33	0.26
33	0.44	0.29	0.00	66	1.71	0.38	0.83
34	−0.19	0.12	6.70	67	0.51	0.18	0.00
35	−0.74	1.09	14.00				
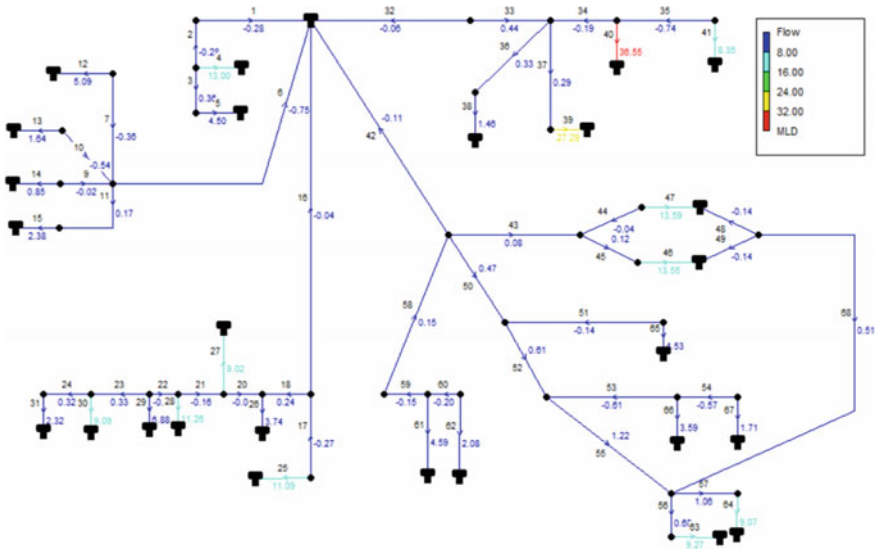
Fig. 3 Pipe flow rate and flow direction in EPANET

unit of each pipe. The head loss is occurred due to the pipe friction over the length of the pipe. Fig. 3 shows the pipe flow rate and flow direction in EPANET software. The flow rate flows with a negative sign, showing the flow is in the opposite direction. For example, if water is flowing from the "start node" to the "stop node", the flow arrow will point that way, and the flow result will be in positive value. If water is flowing from the "stop node" to the "start node", the flow arrow will point that way; thus, the flow result will be a negative value. The velocity for each pipe is acceptable since the maximum allowable flow velocity in any pipeline is 2.6 m/s. All the velocities in the pipes are shown as acceptable since each pipe's velocity is less than the maximum allowable velocity of 2.6 m/s. Furthermore, the flow rate in the pipes ranges from −0.61 to 36.55 million litres/day. The maximum head loss of pipe is P31, which comprises 17.00 m/km, while other pipes mostly present the head loss ranging from 0 to 14.00 m/km.

3.3 Node Report

The Pasir Gudang area consists of condominiums, shops, petrol stations, mosques, factories, one storey and double-storey houses and other facilities. According to the Johor Water Authority, if the value of the residual pressure head at the node is passing above the required pressure head of 11.7 m, thus it is considered sufficient. From Table 3, all the values of residual pressure heads at nodes are found higher than

Table 3 Pressure head in nodes

Node	Residual pressure head (m)	Required pressure head (m)	Sufficiency	Node	Residual pressure head (m)	Required pressure head (m)	Sufficiency
2	55.00	11.7	Sufficient	35	47.16	11.7	Sufficient
3	71.76	11.7	Sufficient	36	51.49	11.7	Sufficient
4	71.15	11.7	Sufficient	37	72.24	11.7	Sufficient
7	64.87	11.7	Sufficient	42	55.22	11.7	Sufficient
8	64.63	11.7	Sufficient	43	54.93	11.7	Sufficient
9	64.87	11.7	Sufficient	44	54.96	11.7	Sufficient
10	66.10	11.7	Sufficient	45	54.91	11.7	Sufficient
11	66.29	11.7	Sufficient	46	54.95	11.7	Sufficient
16	55.04	11.7	Sufficient	49	49.91	11.7	Sufficient
17	57.77	11.7	Sufficient	50	50.13	11.7	Sufficient
19	53.09	11.7	Sufficient	52	49.20	11.7	Sufficient
20	53.15	11.7	Sufficient	53	50.34	11.7	Sufficient
21	55.88	11.7	Sufficient	54	73.30	11.7	Sufficient
22	55.88	11.7	Sufficient	55	47.65	11.7	Sufficient
23	55.49	11.7	Sufficient	56	46.43	11.7	Sufficient
24	55.18	11.7	Sufficient	57	43.76	11.7	Sufficient
32	55.08	11.7	Sufficient	58	55.87	11.7	Sufficient
33	51.33	11.7	Sufficient	59	55.94	11.7	Sufficient
34	50.84	11.7	Sufficient	60	73.08	11.7	Sufficient

11.7 m. Hence, the water distribution network model that is developed with Epanet can be used to supply water sufficiently to all areas in Pasir Gudang.

3.4 Comparison of Water Demand in Pasir Gudang Area

The water demand for each area in Pasir Gudang is presented in Fig. 4. The total amount of water demand to these consumers based on the EPANET modelling is 215.16 million litres per day. The area of highest in water demand is Taman Kota Masai 1, with 36.20 million litres per day. Meanwhile, Kampung Kopok 2 shows the lowest water demand of 0.85 million litres per day. It is because Kampung Kopok 2 has recorded the lowest population and less demand requirement in the Pasir Gudang area. The difference between the highest and lowest water demand is about 35.35 million litres per day. Moreover, the Scientex 2, Pasir Gudang 4 and Pasir Gudang 3 have shown a moderate amount of water demand with 13 million litres per day, 13.55 million litres per day and 13.37 million litres per day, respectively. The Taman Rinting, Bandar Sri Alam F and Tanjung Langsat 1 are presented slightly higher
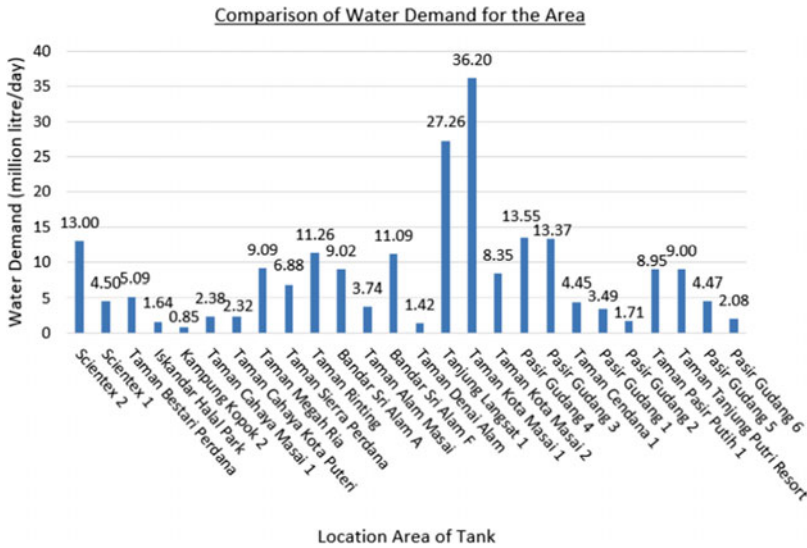
Fig. 4 Comparison of water demand for the Pasir Gudang area

than 10 million litres per day of water demand when compared to the other areas like Scientex 1, Taman Bestari Perdana, Taman Megah Ria, Taman Pasir Putih 1 etc., which mostly show below 10 million litres per day.

The total water demand for the Pasir Gudang area based on EPANET modelling is 215.16 million litres per day. From the data of Ranhill SAJ Sdn Bhd, the total demand consumption is 206,070 million litres per day. Thus, it shows that the total demand consumption is less than the demand of EPANET modelling. The result shows the water distribution model can sustain the water demand in all the areas in Pasir Gudang.

3.5 Case Study of One of the Tanks is not Function

Fig. 5 shows the comparison of water demands when the tank of Kampung Kopok 2 is not functioning, and its water demand is zero. This will result in a slight impact on the water demand to nearby tanks of Taman Bestari Perdana, Iskandar Halal Park and Cahaya Masai 1 with 5.32, 2.08 and 2.51 million litres per day, respectively. The water from Kampung Kopok 2 will flow to the nearest tank due to the loop of the network. The other tanks, such as Scientex 1, Scientex 2, Taman Cahaya Kota Puteri etc., will not be affected since the loop of the network is different.
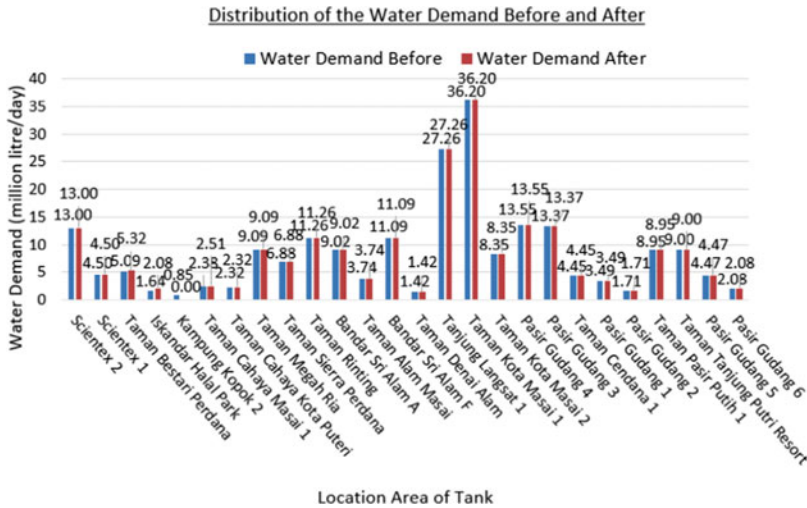
Fig. 5 Comparison of demand before and demand after the tank of Kampung Kopok 2 is not function

4   Conclusion

This study has developed a water distribution network modelling by using EPANET software to evaluate the water demand for the Pasir Gudang area. The water distribution model consists of 26 water tanks, 38 junctions, 65 pipes and one water treatment plant. The total amount of computed water demand obtained from EPANET modelling is 215,160 million litres per day. According to Ranhill SAJ Sdn Bhd, the total water demand required by the consumers in Pasir Gudang is 206,070 million litres per day, which is lower than 215,160 million litres per day of the EPANET computed water demand. Thus, the water can constantly be supplied without any issue on water shortage at any area in Pasir Gudang.

References

1. Abdulkadir TS, Sule BF (2012) Improving the hydraulic system for water supply to the University of Ilorin academic buildings. J Eng Res 17(2):56–65
2. Amat S (2013) The Design of Water Reticulation, pp 1–55. Penerbit UTM Press, Johor, Malaysia
3. Anang Z, Padli J, Abdul Rashid NK, Mat Alipiah R, Musa H (2019). Factor affecting water demand: macro evidence in Malaysia. Malays J Econ 53((1)2019):17–25

4. Arjun K (2015) Design of water distribution system using EPANET. Int J Adv Res 3(9):789–812
5. Bernama B (2017) Water supply disruption at several areas in Pasir Gudang. New Straits Times. https://www.nst.com.my/news/nation/2017/04/229259/water-supply-disruption-several-areas-pasir-gudang. Accessed 10 Dec 2021
6. Chan NW (2000) 1997/98 Nationwide water crisis in Malaysia: what are the real causes and lessons to be learnt. In: Proceedings of the International Conference on Disaster Management, Lessons to Be Learnt, Langkawi Malaysia 29–30 April 2000, pp 270–284
7. Ferdoushi A, Chamhuri S, Rawshan AB (2014) Water resources in Malaysia: issues and challenges. J Food Agric Environ (JFAE) 12(2):1100–1104
8. Jha K, Mishra MK (2020) Object-oriented integrated algorithms for efficient water pipe network by modified Hardy Cross technique. J Comput Des Eng 7(1):56–64
9. Khan P, Hangzo K, Ewing J (2013) Will rapid development in Johor impact water access, quality or price in Singapore? NTS Insights. Centre For Non Tradisional Securities Studies
10. Kaur S (2020) City status for Pasir Gudang should enhance developments. The New Straits Times. https://www.nst.com.my/property/2020/11/643525/city-status-pasir-gudang-should-enhance-developments. Accessed 23 Nov 2020
11. Rossman LA (2000) EPANET 2 User's manual. U.S. environmental protection agency, National Risk Management Research Laboratory, Office of Research and Development, Cincinnati, OH
12. Wong MK (2011) 15 hours water supply disruption in Pasir Gudang. Citiz J. https://cj.my/9475/15-hours-water-supply-disruption-in-pasir-gudang/. Accessed 9 Nov 2021
13. Williams GS, Hazen A (1933) Hydraulic Tables, 3rd edn., pp 1–8 (Revised). Wiley, New York, United States of America

Removal of Ammoniacal Nitrogen from Aqueous Solution Using Clinoptilolite as Adsorbent

Najihasuhada Abi Jihat and Mohd. Hafiz Puteh

Abstract Removal of ammoniacal nitrogen from aqueous solution using clinoptilolite was investigated by influence factors of particle size, initial concentration, contact time, and adsorbent dosage. One-factor-at-a-time (OFAT) approach was used for experimental design to obtained maximized ammoniacal nitrogen removal and rate of ammoniacal nitrogen adsorption of clinoptilolite from aqueous solutions. Adsorption isotherm then was analyzed by using Langmuir and Freundlich model to determine the relationship between adsorption and adsorbate surface. The results show that smaller clinoptilolite particle size gives a higher rate of removal of ammoniacal nitrogen and adsorption capacity which are 66.67% and 9.39 mg/g respectively. The initial concentration of 100 mg/l gives better removal and adsorptions with a higher contact time which is at 60 min. Based on the comparison of data, the rate of ammoniacal nitrogen adsorption by clinoptilolite was well-fitted with Freundlich isotherm instead of Langmuir isotherm. The study found that clinoptilolite with the smallest particle size was more efficient in removing ammoniacal nitrogen and procuring a high rate of ammoniacal nitrogen adsorption.

Keywords Zeolite · Ammoniacal nitrogen · Clinoptilolite · Particle size · Adsorption isotherm

N. A. Jihat (✉) · Mohd. H. Puteh
School of Civil Engineering, Faculty of Engineering, Universiti Teknologi Malaysia (UTM), 81310, Johor Bahru, Johor, Malaysia
e-mail: najihasuhada2@graduate.utm.my

Mohd. H. Puteh
e-mail: mhafizputeh@utm.my

Mohd. H. Puteh
Centre for Environmental Sustainability and Water Security (IPASA), Universiti Teknologi Malaysia UTM, 81310 Johor Bahru, Johor, Malaysia

1   Introduction

Ammonia is well known to be a great threat to the environment due to its consequences not only to human health but also to the environment and other habitats [7, 8, 10]. Commonly, ammonia causes excessive algae to bloom and leads to eutrophication, directly disrupting water treatment. Improvement of technologies for wastewater treatment systems is usually associated with a great effort of creating environmentally friendly materials, low-cost resources, and simple operational implementation [1, 15, 23]. The innovations were mostly physio-chemical processes consisting of various methods based on their focus. Ammonia removal alternatives have been developed continuously from before as conventional methods do not respond well to the current wastewater treatment system [12, 17, 25, 27]. One of the promising technologies that has been adapted to the wastewater treatment system is utilizing zeolites.

The application of zeolite in the adsorption process has been proved efficient in ammonia removal previously. The most well-known alternative is the application of zeolites in wastewater treatment. Zeolites were introduced in 1954 as adsorbents and were widely used for industrial purifications [18]. Zeolites are very stable solids as they can resist any kind of environmental conditions such as temperature, pressures, and reactivity. Their positive capabilities make them do not have any harmful environmental impact [2, 20].

Among the zeolites, clinoptilolite is the most abundant natural zeolite and is widely used in the world [3, 19, 24]. Clinoptilolite was classified as heulandite (HEU) group [21] and is known for its attributes of having impressive adsorption, high ion exchange, and outstanding molecular sieving [11, 13, 17]. Clinoptilolite has been utilized in many niche areas, including agriculture and environmental preservations. Therefore, clinoptilolite capability was proposed for primary treatment of effluent and pilot plant scale. It is difficult to deduce the range of the effects of the parameters on the adsorption capacity as there is still a lack of detailed comparisons regarding adsorption properties between influence factors [5, 21]. The objectives of this study are to understand the influence factor of ammoniacal nitrogen removal and to verify the use of isotherm and kinetic study for adsorption of ammoniacal nitrogen from an aqueous solution.

2   Materials and Methods

2.1   Materials

Clinoptilolite was purchased from a manufacturer. Clinoptilolite was washed using distilled water and dried at a temperature of 110 °C for 24 h. After the drying process was completed, clinoptilolite was crushed using a mortar and sieved into <1.18, <0.6, <0.3, and <0.075 mm sizes. The aqueous solution was prepared using 3.82 g of anhydrous NH_4Cl by dissolving it into 1 L of deionized water in a volumetric

flask. The aqueous solution was diluted (20, 40, 60, 80, and 100 mg/L), and different amounts of adsorbent (1, 2.5, and 4 g) was weighed for adsorption experiments.

2.2 Adsorption Experiments

Adsorption batch-test were conducted at 27 °C with NH4Cl stock solution that had been diluted into 20, 40, 60, 80, and 100 mg/l. The adsorption was performed in 400 mL of ammonia chloride aqueous solution loaded with a different mass of adsorbent in a beaker and shaken at 120 rpm for 120 min. The sample was taken from the beaker at a certain time interval and was analyzed using Nessler Method (US EPA, Method 350.2) and spectrophotometer (HACH DR6000, US) for ammoniacal nitrogen removal reading.

Equations (1) and (2) were used to obtain the percentage of ammoniacal removal (%) and adsorption capacity (mg/g). The equation for ammoniacal nitrogen removal percentage can be expressed below:

$$\text{Removal percentage, \%} = [(Co - Cf)/Co] \times 100\% \tag{1}$$

where Co is the initial concentration of an aqueous solution (mg/l) and Cf is the final concentration of an aqueous solution (mg/l), while ammoniacal adsorption capacity (mg/g) can be expressed using the equation below:

$$\text{Adsorption capacity, } q = [(Co - Cf)/M] \times V \tag{2}$$

where q is adsorbent adsorption capacity (mg/g), M is the mass of clinoptilolite (g), and V represents the volume of aqueous solution (L).

3 Results and Discussion

3.1 Adsorption of Ammoniacal Nitrogen

3.1.1 Effect on Particle Size

Percentage of removal can be defined as a measure of performance of clinoptilolite to remove ammoniacal nitrogen from aqueous solution, where adsorption capacity is the ability to hold ammonium ions at clinoptilolite's surface. A constant value of other variant parameters was decided to observe the specific effect of particle size on ammoniacal nitrogen removal,. Other parameters related to the experiment were set to constant such as initial concentration, clinoptilolite dosage, and contact time which are 100 mg/l, 2.5 g, and 60 min. Based on Fig. 1, clinoptilolite < 0.075 mm

Fig. 1 Effect of particle size on removal efficiencies and adsorption capacity
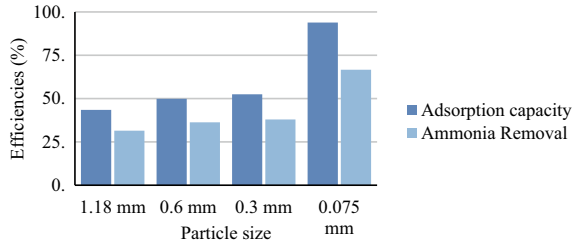
size have 66.67% of ammoniacal nitrogen removal compared to < 1.18 mm size, which only has 31.48% removal with 9.39 mg/g and 4.35 mg/g, respectively. This is aligned with Chuan-hsia Liu (2000), that obtained 66.6% removal with particle size < 0.5 mm. It is clearly shown that the results are directly proportional, indicating that the smaller particle size of clinoptilolite increased the percentage of ammoniacal nitrogen removal and also clinoptilolite's adsorption capacity.

Hypothetically, a smaller particle size gives a larger surface area which leads to a high percentage of ammoniacal nitrogen removal. Clinoptilolite consists of tetrahedral cages that can occupy ammonium ions temporarily. When the size is reduced, only the external surface layer is affected. The internal surface area of clinoptilolite won't be affected and there were no changes in structural sites but increased in available occupied sites for ions to engage (Erdoğan et al. 2011).

Larger surface area contributes to high efficiencies of removal rates and also adsorption capacity, which are associated with mass transfer rate and diffusion path. Smaller particles size escalate mass transfer rate and shorten the diffusion path that leads to facile cations exchange in the aqueous solution. The increased surface area gives ample active sites for ammonium ions to occupy (Lebedynets et al. 2004). Therefore, particle size plays a major role in the efficiency of ammonia removal through aqueous solutions and smaller particle size gives better removal of ammoniacal nitrogen.

3.1.2 Effect on the Initial Concentration

Based on Fig. 2, the highest removal percentage of ammonium was achieved at 100 mg/l, which is 66.7% with 9.39 mg/g adsorption capacity, while the lowest removal percentage of ammonium removal was at 20 mg/l, which is 36.96% with 5.31 mg/g adsorption capacity. The results obtained were similar with [16], which were found an increased removal of ammoniacal nitrogen from 35 to 60% with 25 mg/l to 500 mg/l of initial concentration removal. Parameters involved, such as particle size, adsorbent dosage, and contact time, was set to a constant, which are < 0.075 mm clinoptilolite's size, 2.5 g of adsorbent dosage, and 60 min of contact time, respectively. The graph showed that the interaction between initial concentrations and removal efficiencies are directly proportional as the percentage removal of

Fig. 2 Effect of initial concentration on removal efficiencies and adsorption capacity
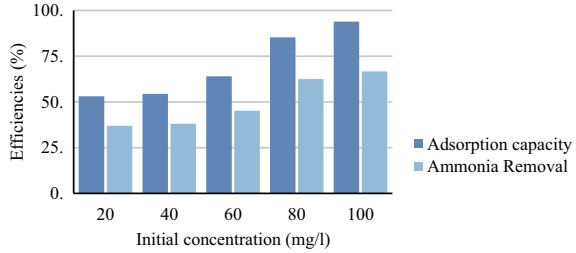
ammonium and adsorption capacity increase when the initial concentration of the aqueous solution increase.

Principally, initial concentrations were highly associated with the driving force of mass transfer in an aqueous solution. The driving force for a mass transfer indicates the difference concentration between two compounds, which affects the rate of ammoniacal nitrogen removal efficiencies. Logically, the higher concentration of adsorbate comprises a bigger driving force that helps to enhance ion exchange between ammoniacal nitrogen and available active sites. It provides sufficient energy for ammoniacal nitrogen to engage with the active site in a short time as high energy leads to a shorter diffusion path that creates a faster breakthrough for ample exchanged amount of ammonium ions per contact time (Annelie Herdström, 2001).

3.1.3 Effect of Contact Time

Effect of contact time on ammoniacal nitrogen removal was a crucial part of the adsorption process. Contact time was monitored to determine the equilibrium condition of both adsorbate and adsorbent. The longer contact time allowed more time for the ion exchange process to occur and reach equilibrium. Based on Fig. 3 shown, the rate removal of ammoniacal nitrogen difference between the first 30 and 60 min shows significant changes with a 31.35% difference. For the first 15 and 30 min, there is minimal difference in removal rate, which is 5.50% and towards 120 min, the process shows the decrease in removal rate as the process approaches equilibrium condition, which is a 6.57% difference.

Fig. 3 Effect of contact time on removal efficiencies and adsorption capacity
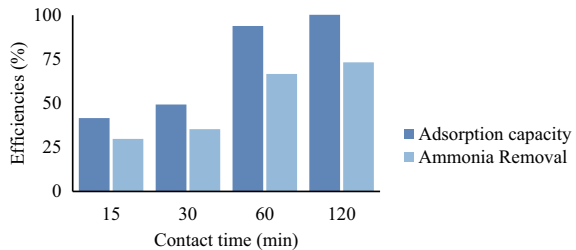
However, due to the smallest particle size were used, the process reached its equilibrium in a short amount of time. Therefore, in 120 min, the process has the highest removal of ammoniacal nitrogen, which is 73.24% with 10.24 mg/g adsorption capacity compared to the first 15 min. Overall, the removal percentage of ammoniacal nitrogen dropped about 36% as the ion exchange process reached its equilibrium, and this is aligned with M. Sarioglu (2005). This achieved results also was proven by Nurul [26].

Contact time influence was determined by removal rate between the time interval as the differences indicates the adsorption process rate. For first 15 to 30 min shows rapid removal rate and adsorption capacity, while later, up to 120 min, the rate of removal decreases slowly. This is because, at the first 15 min, there were plenty of vacant active sites of clinoptilolite that led to faster diffusion of ions onto clinoptilolite. Approaching 120 min, the rate of removal decreased as all the vacant sites were almost occupied by ammonium ions and reached their equilibrium. The effect of contact time could be varied between the particle size as available surface area for adsorption sites changes with sizes. Therefore, contact time contributes a significant link as the particle size decreased the adsorption time for the process to reach its equilibrium decreased and simultaneously increased the efficiencies of ammoniacal removal (Nurul [26]. Eventually, 120 min was counted as the optimum contact time for the adsorption process to have better ammoniacal removal.

3.1.4 Effect of Adsorbent Dosage

Based on Fig. 4 show that the adsorbent dosage at 1 g gives the highest removal of ammoniacal nitrogen, which is 67.36% with 18.61 mg/g, whereas 4 g of adsorbent dosage gives the lowest, which are 55.77% removal with 5.84 mg/g adsorption capacity. For 1 g of adsorbent dosage, the adsorption capacity of clinoptilolite is greater than its ammonia removal efficiencies, while 4 g of adsorbent dosage shows a very minimal difference between adsorption capacity efficiencies percentage. This aligned with [4], which was obtained only 50% of ammoniacal nitrogen removal as the adsorbent dosage increased. In order to have optimum results, it is vital to ensure that adsorption capacity and removal efficiencies have minimal difference; otherwise, it would affect the adsorption process. [27] proved that higher adsorbent dosage increases removal, which shown by their results increased by 5% from 1 g of adsorbent to 2 g of adsorbent.

To observe the influence of adsorbent dosage in the removal of ammoniacal nitrogen efficiencies, optimum value from other influence factors were considered which are <0.075 mm particle size, 100 mg/l initial concentration, and 120 min of contact time. Figure 3 proved that with the higher amount of adsorbent dosage used for the adsorption process, the efficiencies of ammoniacal nitrogen removal decreased alongside its adsorption capacity. This is due to the possibilities in agglomerations of the particles. The particle size used for the adsorption process was very fine which leads to aggregations that could decrease in surface area. The surface area plays a crucial role in efficiencies of ammoniacal nitrogen removal as it holds the availability

Fig. 4 Effect of adsorbent dosage on removal efficiencies and adsorption capacity
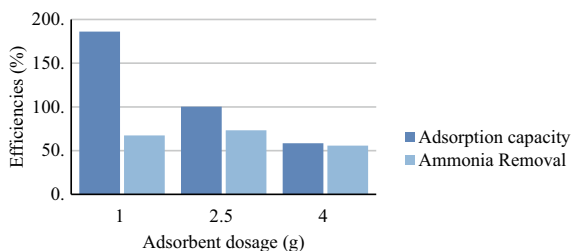
of vacant active sites of clinoptilolite. Agglomerations occur as the very fine particles clump together and decreased the surface area which is directly effected the removal efficiencies. This phenomenon could lead to lower the possibility of molecule contact to the adsorption sites fully [14]. On the other hand, the lower amount of adsorbent dosage won't lead to better results either due to the imbalance of adsorption capacity and the percentage of ammoniacal nitrogen removal. Therefore, 2.5 g was considered a better option as an adsorbent dosage for the removal of ammoniacal nitrogen.

3.2 Adsorption Isotherm

To justify the adsorption process, results obtained from the conducted experiments were applied to the Langmuir and Freundlich isotherm equations. The Langmuir equation can be expressed:

$$1/qe = 1/(KLqmaxCe) + 1/(qmax) \qquad (3)$$

where qe is the equilibrium amount of ammoniacal nitrogen adsorbed (mg/g), KL is the adsorption energy constant (L mg/g), Ce is the equilibrium constant (mg/l) and qmax is the maximum adsorption capacity (mg/g). Langmuir-type adsorption is considered to be a monolayer process. On the other hand, Freundlich-type adsorption is considered to be a multi-layer process in which the amounts of adsorbed solute per unit adsorbent mass increase gradually [6]. The Freundlich equation is expressed below:

$$lnqe = lnKF + 1/nlnCe \qquad (4)$$

where q_e represents the equilibrium amount of ammonia adsorbed (mg/g), KF is the Freundlich constant (mg/g), n represents the diversity factor and Ce represents equilibrium concentration (mg/l). All the values calculated by using the Eq. (3) and (4) were listed in Table 1. The values of KL and q_{max} were obtained from the intercept and slope plot of 1/qe vs. 1/Ce graph and the values of KF and n were obtained from the intercept and slope plot of ln qe vs. ln Ce graph. Correlation R2 of both graphs were used to suggest the adsorption phenomena of the clinoptilolite in ammoniacal nitrogen removal.

Table 1 Langmuir and Freundlich isotherm constants

Coefficients	Langmuir model			Freundlich model		
	q_{max}	K_L	R^2	$1/n$	K_F	R^2
	0.2681	−4.833	0.954	5.0273	−0.8273	0.9785

Fig. 5 Linear line plotting **a** $1/q_e$ vs. $1/C_e$ and **b** $\ln q_e$ vs. $\ln C_e$ for adsorption of ammoniacal nitrogen onto clinoptilolite from aqueous solution

(a)

(b)
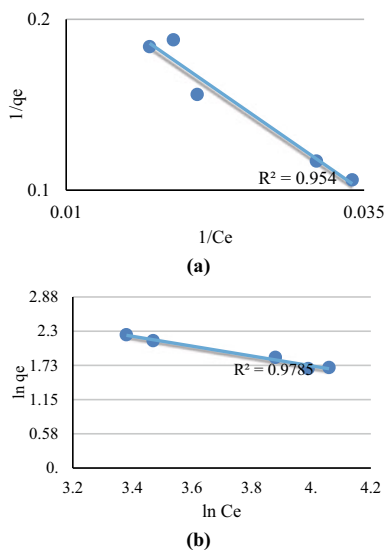
Based on Fig. 5(a) and (b), shows the correlation R^2 for Freundlich isotherm fitted more than Langmuir isotherm which is 0.9785. The value of R^2 was used to explain the adsorption phenomena which is in this case Freundlich equations gives a better R^2 value compared to Langmuir equations. This clarifies that the adsorption process occurred at the multi-site which is not homogeneous. It suggested that when the concentration of the aqueous solution is low, high energy sites will be occupied first then followed by weaker sites.

3.3 Adsorption Kinetics

Adsorption kinetics then were used to explain the mechanism between adsorbent and adsorbate of the adsorption process. Two types of kinetics modeling can be applied which are pseudo-first-order kinetic model and pseudo-second-order kinetic model. The pseudo-first-order equations can be expressed below:

$$ln(qe - qt) = ln(qe) - K1ti \tag{5}$$

where q_e is the equilibrium amount of ammoniacal nitrogen adsorbed (mg/g), q_t is the amount of ammoniacal nitrogen adsorbed at adsorption time (mg/g), K_1 is a rate constant of pseudo-first-order equation and t_i is the adsorption time (minutes). The pseudo-second-order equations can be expressed below:

$$ti / qt = 1/(K2qe2) = ti / qe \tag{6}$$

where q_e is the equilibrium amount of ammoniacal nitrogen adsorbed (mg/g), q_t is the amount of ammoniacal nitrogen adsorbed at adsorption time (mg/g), K_2 is a rate constant of pseudo-second-order equation and t_i is the adsorption time (minutes). All the values calculated by using the Eq. (5) and (6) were listed in Table 2. The values of K_1 and ln q_e were obtained from the intercept and slope plot of ln (q_e-q_t) versus t_i graph and the values of K_2 and q_e were obtained from the intercept and slope plot of t_i/q_t versus t_i graph. Correlation R^2 of both graphs were used to suggest the adsorption mechanism of ammoniacal nitrogen onto clinoptilolite.

Figure 6(a) and (b) show linear line plotting for the pseudo-first-order model and pseudo-second-order model respectively. As shown in Table 2, the correlation R2 for pseudo-second-order model value was higher compared to a pseudo-first-order model which is 0.8954. These results clarify mainly the adsorption mechanism of clinoptilolite in ammoniacal nitrogen as chemisorption. Chemisorption can be described as an adsorption process which is involved electrons sharing between adsorbents and adsorbates that create a chemical bond.

Fig. 6 Linear line plotting **a** ln (qe-qt) versus ti and **b** ti/qt versus ti for adsorption of ammoniacal nitrogen onto clinoptilolite from aqueous solution
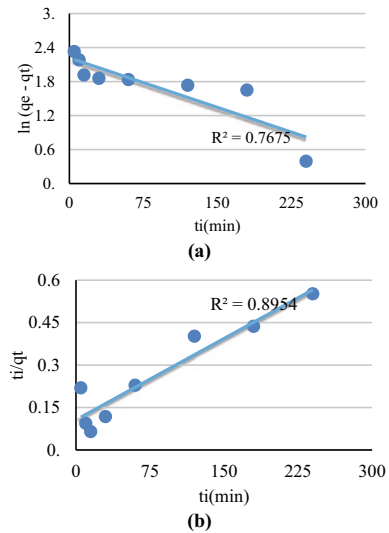
Table 2 Kinetic parameters for the adsorption of ammoniacal nitrogen

	Pseudo-first-order model (PFO)			Pseudo-second-order model (PSO)		
Coefficients	q_e	K_1	R^2	q_e	K_2	R^2
	−0.0058	2.216	0.7675	0.1061	0.0018	0.8954

4 Conclusion

In this conducted experiment, it can be concluded that there is four major influence on the removal of ammoniacal nitrogen and adsorption capacity which are particle size, initial concentration, contact time, and adsorbent dosage. Although they are separately accessed, without a doubt they are associated with each other. For instance, smaller particle size enhances more ammoniacal removal with ample driving force provided by higher initial concentration. In addition, particle size also has a major influence on the time for adsorbents to achieve equilibrium as smaller sizes allocate more surface area for ammonium ions to engage. Furthermore, with a smaller size of clinoptilolite, there is no need to use for a large amount per adsorption batch due to the possibility of agglomerations. This not only helps in reducing contact time but also reduced materials cost for application later in the large-scale industry.

The mechanism and adsorption phenomena were clarified by adsorption isotherms and pseudo-kinetic-model equations. From the results, it can be finalized that the adsorption batch was well fitted with Freundlich isotherm which indicates heterogeneity of the adsorbent surface. The mechanism of the adsorption process was suggested by the pseudo-second-order kinetic model as the correlation of R^2 fitted well with this equation better compared with the pseudo-first-order kinetic model. The findings suggested that the mechanism of the adsorption batch is chemisorption which is created by chemical bonds due to electron sharing.

References

1. Adam MR, Othman MHD, Samah RA, Puteh MH, Ismail AF, Mustafa A, Jaafar J (2019) Current trends and future prospects of ammonia removal in wastewater: a comprehensive review on adsorptive membrane development. Sep Purif Technol 213:114–132
2. Akpor OB, Otohinoyi DA, Olaolu TD, Aderiye BI (2014) Pollutants in wastewater effluents: impacts and remediation processes. Int J Environ Res Earth Sci 3:50–59
3. Almutairi A, Weatherly LR (2015) Intensification of ammonia removal from wastewater in biologically active zeolitic ion exchange columns. J Environ Manag 160:128–138
4. Burgess RM, Perron MM, Cantwell MG, Ho KT, Serbst JR, Pelletier MC (2004) Use of zeolite for removing ammonia and ammonia-caused toxicity in marine toxicity identification evaluations. Arch Environ Contam Toxicol 47:440–447
5. Chen HF, Lin YJ, ChenBH YI, Liou SYH, Huang RT (2018) A further investigation of NH4+ removal mechanisms by using natural and synthetic zeolites in different concentrations and temperatures. Minerals 8(11):499

6. Chung HK, Kim WH, Park J, Cho J, Jeong TY, Park PK (2015) Application of Langmuir and Freundlich isotherms to predict adsorbate removal efficiency or required amount of adsorbent. J Ind Eng Chem 28:241–246

7. Daud Z, Ibrahim FND, Latiff AAA, Ridzuan MB, Ahmad Z, Awang H, Marto A (2016) Ammoniacal nitrogen and COD removal using zeolite-feldspar mineral composite adsorbent. Int J Integr Eng 8:9–12

8. Delkash M, Bakhshayesh BE, Kazemian H (2015) Using zeolitic adsorbents to cleanup special wastewater streams: a review. Microporous Mesoporous Mater 214:224–241

9. Huang H, Xiao X, Yan B, Yang L (2010) Ammonium removal from aqueous solutions by using natural Chinese (Chende) zeolite as adsorbent. J Hazard Mater 175(1–3):247–252

10. Ismail MHS, Dalang S, Syam S, Izhar S (2013) A study on zeolite performance in waste treating ponds for treatment of palm oil mill effluent. J Water Resour Prot 5(07):18

11. Jha VK, Hayashi S (2009) Modification on natural clinoptilolite zeolite for its NH4+ retention capacity. J Hazard Mater 169(1–3):29–35

12. Jorgensen TC, Weatherley LR (2003) Ammonia removal from wastewater by ion exchange in the presence of organic contaminants. Water Res 37:1723–1728

13. Lenntech (2018). Zeolites-applications. https://www.lenntech.com/library/media-filtration/zeolites-applications.html. Accessed 8 Aug 2020

14. Manikam MK, Halim AA, Hanafiah MM, Krishnamoorthy RR (2019) Removal of ammonia nitrogen, nitrate, phosphorus and COD from sewage wastewater using palm oil boiler ash composite adsorbent. Desalin Water Treat 149:23–30

15. Margeta K, Logar NZ, Šiljeg M, Farkaš A (2013) Water Treatment. IntechOpen Limited, London

16. Millar GJ, Winnett A, Thompson T, Couperthwaite SJ (2016) Equilibrium studies of ammonium exchange with Australian natural zeolites. J Water Process Eng 9:47–57

17. Montalvo S, Guerrero L, Borja R, Sanchez E, Milan Z, Cortes I, Rubia MA (2012) Application of natural zeolites in anaerobic digestion processes: a review. Appl Clay Sci 58:125–133

18. Peskov M (2018) Zeolites. https://asdn.net/asdn/chemistry/zeolites.php. Accessed 5 Sept 2020

19. Prajapati S (2014) Cation exchange for ammonia removal from wastewater. Master of Science Thesis. Tampere University of Technology

20. Rahmani AR, Malvi AH, Mesdaghinia AR, Nasseri S (2004) Investigation of ammonia removal from polluted waters by clinoptilolite zeolite. Int J Environ Sci Technol 1:125–133

21. Roth WJ, Nachtigall P, Morris RE, Čejka J (2014) Two-dimensional zeolites: current status and perspectives. Chem Rev 114(9):4807–4837

22. Samer M (2015) Wastewater Treatment Engineering. IntechOpen Limited, London

23. Segweni D (2017) Options for Treatment of Ammonia in Landfill Leachate. Master Thesis. University of Canterbury

24. Wang S, Peng Y (2010) Natural zeolites as effective adsorbents in water and wastewater treatment. Chem Eng J 156(1):11–24

25. Wen J, Dong H, Zeng G (2018) Application of zeolites in removing salinity/sodicity from wastewater: a review of mechanisms, challenges, and opportunities. J Clean Prod 197:1435–1446

26. Widiastuti N, Hongwei W, Ang HM, Zhang D (2011) Removal of ammonium from greywater using natural zeolite. Desalination 277:15–23

27. Zabochnicka-Światek M, Malińska K (2010) Removal of ammonia by clinoptilolite. Global NEST J 12:256–261

Determination of the Relationship Between River Ecosystems and Benthic Macroinvertebrate Ecological Indices as a Basis for River Health Assessment

Aweng Eh Rak, Sharifah Aisyah Syed Omar, Muhammad Abdul Salam, and Mior Izuddin Baharuddin

Abstract In Malaysia, physical and chemical components have been used as an indicator for river health monitoring and rehabilitation programme for many years as a basis and reference without any proven successful results. Therefore, this study aims to identify the relationship between river ecosystems and benthic macroinvertebrate ecological indices for river health assessment. There were a total of five sampling sites selected along Sungai Mengkibol, Sungai Madek and Sungai Dengar in Johor. Benthic macroinvertebrates and six in-situ parameters were collected and measured. Meanwhile, riparian river compositions, canopy cover, large woody debris, substrate compositions and velocity were measured for assessing the river habitat. Ecological indices were analysed and correlated with other parameters. The results obtained reaffirms that river discharge had an influence ($p < 0.05$) on the composition of the benthic macroinvertebrates caught in the sampling area. Rivers that have reached canopy cover recorded a higher diversity, richness, evenness indices and EPT taxa compared to the least or those of poor canopy cover. The results obtained from the chi-square test shows that there is a significant association ($p < 0.05$) between physicochemical water quality with dominance index, evenness index and EPT composition. Thus, it can be concluded that benthic macroinvertebrates can be used as bio-indicator to assess river health.

Keywords River health · River rehabilitation · River ecosystems · Ecological index · Biological indicator

A. Eh Rak (✉) · S. A. S. Omar
Faculty of Earth Science, Universiti Malaysia Kelantan, Kota Bharu, Malaysia
e-mail: aweng@umk.edu.my

M. A. Salam
Department of Environmental Science and Disaster Management, Faculty of Science, Noakhali Science and Technology University, Noakhali, Bangladesh

M. I. Baharuddin
Department of Environment Perak, Perak, Malaysia
e-mail: 4mib@doe.gov.my

1 Introduction

From the literature, it is evident that a river ecosystem is a fragile ecosystem where even minimum changes made will cause a dramatic impact on the health of the river. Different land uses have produced various pollutants. Normally, physicochemical parameters are used as an indicator to show whether the river water quality is in good or bad condition [36]. Salam et al. [29] determined the heavy metals component in Perak River Malaysia as one of the parameters to gauge the Perak River's water quality status. They expect the source to come from wastewater and industrial discharges. This is in line with the findings of Camara et al. [9] in their study, where they found agricultural and forest-related activities as a cause of river pollution.

Lately, more and more studies are being conducted by researchers to look at the river's physicochemical quality and health. This is done by correlating aquatic life, especially benthic macroinvertebrates, with physicochemical water quality [4] and other ecological attributes such as substrate compositions, canopy, and riparian cover, channel morphology, large woody debris, and many others. Several investigators have studied and analysed the relation between river bed grain size and benthic macroinvertebrate diversity indices (Athirah et al. 2018). Some have studied the grain size distribution caused by land-use changes [18], which was the consequence of determining the composition of benthic macroinvertebrate assemblages. A similar study was conducted by Ehrhart et al. [12], but the impact was from the sedimentation basins discharge. The results have shown that there was no significant change in the number of macroinvertebrate individuals as a result of the sedimentation basin discharge. Still, there was a huge decrease in the number of taxa observed in the receiving stream directly below the basin outlet. However, this observed reduction in species richness was not significant 100 m downstream from the basin discharge pipe. Richards [22] found that instream conditions such as substrate composition, channel morphology, and woody debris were the factors influencing benthic macroinvertebrate community structure. Merckx et al. [17] had found that species richness was affected by the amount of sand extraction and the amount of gravel settled at the sea or river bed, while the work by Spindler (2004) showed that the increase in per cent composition by oligochaetes and chironomidae occurred when median particle sizes were the smallest. Nevertheless, it is also essential to look at the distribution and assemblages of benthic macroinvertebrates in rivers that are affected by various land uses. These rivers are located in highland areas (Sharifah Aisyah et al. 2014), recreational areas [28], passing through municipal areas, agricultural land and logging areas. With the distribution information, many also suggest using benthic macroinvertebrates as a biological indicator [3] component to assess river water quality. Moreover, studies on the influence of habitat on the distribution and assemblage of benthic macroinvertebrates were conducted [21], in addition to many other related studies to improve the usability of benthic macroinvertebrates as biological indicators. All the studies showed that benthic macroinvertebrates have different organisms, distributions and compositions depending on the type of watershed and ecoregions. Therefore, this study focused on identifying the relationship between

river ecosystems and benthic macroinvertebrate ecological indices as a basis for a river health assessment at the three tributaries of Sungai Sembrong.

2 Materials and Methods

This study was conducted within the Sungai Endau watershed in the districts of Segamat, Kluang and Mersing in the state of Johor. The main tributary of these catchments is Sungai Sembrong which is fed by several tributaries such as Sungai Madek, Sungai Mengkibol and Sungai Dengar (Figs. 1, 2, 3, 4 and 5) (Table 1).

Surber Net was used to sample benthic macroinvertebrates, whereas Karr's Aquatic Insect Stream Sampling Protocol [14] was followed with minor modifications to suit local conditions. Benthic macroinvertebrates were identified by using
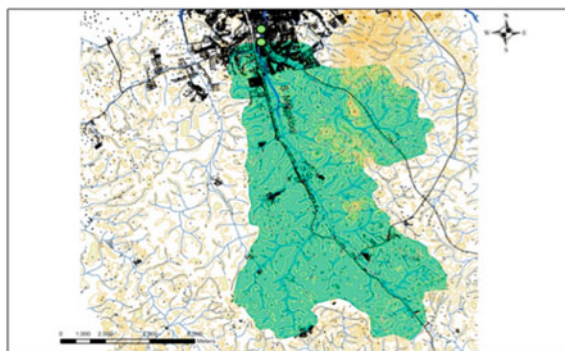
Fig. 1 Sampling stations at Sungai Mengkibol
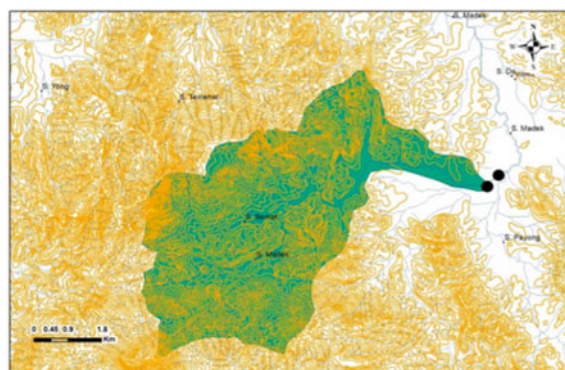
Fig. 2 Sampling stations at Sungai Madek
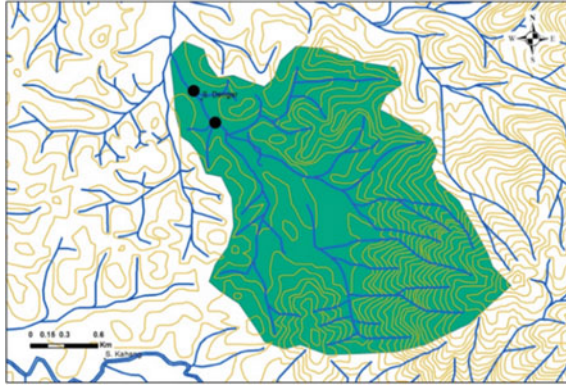
Fig. 3 Sampling stations at Sungai Dengar
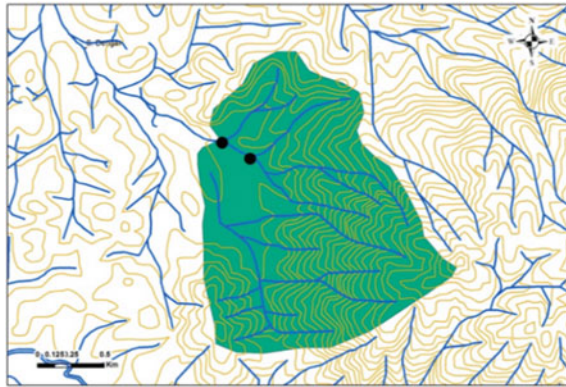
Fig. 4 Sampling stations at Sungai Hulu Dengar
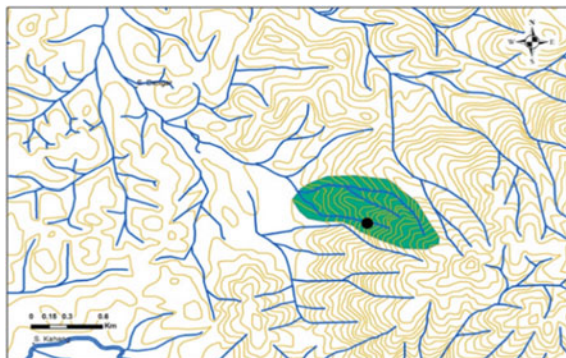
Fig. 5 Sampling stations at Sungai Gunung

Table 1 Sampling site descriptions

Station	River	Stream order	Water depth (m)	Width (m)	Land use	Riparian vegetation	Catchment size (km^2)
Impact	Mengkibol	3	0.11–0.39	14	Urban	Grass	72.7
	Madek	3	0.11–0.38	12	Logging	Tree and shrub	33.1
	Dengar	2	0.15–0.45	7	Oil palm	Grass and shrub	5.4
(Pristine stations)	Hulu Dengar	2	0.08–0.16	12	Forest	Tree	2.9
(Pristine–pristine station)	G. Berlumut	1	0.04–0.10	0.83	Forest	Tree	0.5

a streo-microscope with morphology identification methods based on several identification books. Species diversity and richness indices, including EPT that was based on Shannon Diversity Index [24], Margalef Index [15], Hill Index [13], Wallace et al. [34], Poff et al. [20] and Simpson Index [23] were used to analyse the data on benthic macroinvertebrates. On the other hand, Multiparameter probe Model Yellow Springs Instrumentations (YSI) 6920 with 650 MDS Display/Logger and single parameter probe were used for in-situ determination of river water quality [11]. Meanwhile, water sampling for laboratory analysis was carried out based on the standard procedure provided by the USEPA [32]. Analyses were carried out according to procedures given by the Standard Methods for the Examination of Water and Wastewater [5]. At the same time, habitat characteristics were also assessed using a field survey form adopted from Barbour [7]. Canopy cover and riparian vegetation assessment was followed as given by "Field Methodology for the Christchurch River Environment Assessment Survey (CREAS)" and also from the study conducted by Timbol et al. [30]. Valeport' Braystoke' Model 001 Flow Meter was used to gauge the river (Thandaveswara 2011), and the Area Method was used to calculate river discharge [10]. According to the Pebble Count Procedure published by Bevenger and King [8] and Wolmen [35], Pebble Count was adopted to determine river substrate compositions. On the other hand, LWD, which measured the size, including diameter and length of the whole tree, logs or root wads, was carried out using a measuring tape, ruler, and vernier calliper. The measurement was conducted within a 500-m stretch between upper and lower stations. All measurements and observations of LWD were recorded in the field data sheet prepared.

The Chi-square test was performed to determine the association level between one variable with another [33]. Pearson Chi-Square Value or P-value was used to determine the level of association. The P-value smaller than 0.05 indicates that there is some association between the components with a 95% confidence level [25]. On the other hand, when Pearson's R-value negative result means that the correlation is negative and vice versa. At the same time, the value itself represents the correlation level, whether it is strong or weak. Pearson's R-value greater than 0.5 shows a strong

correlation, and the relation or correlation is stronger as the R-value increases. R-value below 0.5 is considered to have a weak correlation.

Numerical data or quantitative data were transformed into categorical data where the data was categorised into different categories, and the value of each data was then categorised into simple coding. Each coding represents the range of value or description. The steps involved in the analysis are first defining the variable properties and then keying in all the variables and variables' properties in the variable worksheet. The next step is to key in all the codes assigned for each parameter into the data worksheet. The main requirement for this type of analysis is that all the cells in the data worksheet must have a value. The next step is data analysis, where for this purpose, cross-tabs analysis was performed to generate P-value and Pearson's R-value. Cross-tabulation analyses are basically a test carried out to determine the significance and level of association between variables or to determine the correlation between the variables.

3   Results and Discussion

This study revealed that more diverse species were found in rivers with good canopy cover than the river with the least or poor canopy cover. The highest number of species was found under a good canopy cover, and the species were also evenly distributed in contrast to the river with the least canopy cover when only a certain number of species dominated in that area. This is in agreement with the study conducted by Azrina et al. [6], where they reported that the total number of benthic macroinvertebrates taxa and their overall richness and diversity indices were significantly higher ($p < 0.05$) at the upstream than at the downstream stations. The species of benthic macroinvertebrates collected from the undisturbed (reference) river and the polluted river was also similar to the findings of Ahmad et al. [2]. The species which was found at the upstream station (undisturbed) were ephemeroptera, plecoptera, trichoptera, diptera and coleoptera. In contrast, species which was found downstream (polluted) were resistant species like oligochaeta, mollusca, nematoda and annelida. Furthermore, this result also complies with the findings of Shabdin and Abang [26], where they collected EPT, coleopteran and dipteral at the clean and healthy river located in Bario, Sarawak. The results of this study are also in agreement with the findings of Narumon and Wiroj [19], who found that EPT and dipteral were the three most abundant benthic fauna at a good water quality station. The absence or the presence of very few numbers of plecopteran at the certain river was also due to one of the influences of poor or minimal canopy cover, and this finding is in agreement with Suhaila and Che Salmah [27]. They reported that the number of plecoptera decreased at the open water surface area. On the other hand, substrate composition, specifically the D_{50} value, also played a very important role in determining the composition of the benthic macroinvertebrate.

Riparian cover and compositions and canopy were the main factors that contributed to changes in the ecosystem, such as large woody debris, substrate

compositions, river discharges, riverbank types, shapes of river channel river mean-ders, physicochemical water quality and aquatic life forms. The added advantage of determining each of them will indicate how a river system has been abused by human intervention. For example, the information gained on the presence of large woody debris (LWD) will give insight into its influence on substrate compositions and river discharge and, consequently, alter the benthic macroinvertebrate composi-tion. The results obtained reaffirms that river discharge had an influence ($p < 0.05$) on the composition of the benthic macroinvertebrates caught in the sampling area. In one sampling event, at least two species were caught at all the stations when the river discharge was at its lowest, while sampling made more than six months later when the river discharge recorded was highest had recorded no species being caught at one of the rivers. As for riparian river cover, this acted as a filter for suspended solids before water flowed into a river and helped to impede and slow down the flow, indirectly helping to minimise riverbank erosion. River meanders also retards the water flow down the course and create a localised habitat for aquatic lives to thrive. On the other hand, the river canopy provides shelter for aquatic lives and reduces water temperature. This is amply exhibited from the results obtained whereby rivers that have reached canopy cover recorded a higher diversity, richness, evenness indices and EPT taxa compared to the least or those of poor canopy cover. Usually, the undisturbed river, which is located uppermost of the stream channel, has good canopy cover compared to those located at the downstream channel, which is almost always with poor canopy due to human encroachment. Even this may be true: rivers with poor canopy cover have a higher dominance index than rivers with good ones. Marta González et al. [16] also mentioned how the riparian play important roles in improving the hdromorphology and stress out the integrations relationship between riparian, flow regime and channel morphology.

Results of this study have shown that the D_{50} value of a river ranging from 51 to 70 mm and plecoptera was found to be embedded in the sand. The abundance of plecopteran found is in agreement with the findings obtained by Suhaila and Che Salmah [27]. This study has found that plecoptera prefer gravel substrates embedded in the sand but not those dominated by boulders and cobbles.

The results obtained from the chi-square test shows that there is a significant asso-ciation ($p < 0.05$) between physicochemical water quality with dominance index, evenness index and EPT composition. The correlation between physicochemical water quality with dominance index and EPT composition is found to be very strong with Pearson's R-value of 0.673 and 0.626, respectively. However, the correlation between physicochemical water quality with evenness index is weak with Pearson's R-value of 0.226. On the other hand, the canopy cover is associated ($p < 0.05$) with diversity index, richness index, evenness index and EPT composition, but the associ-ation between canopy cover and evenness index is weak (Pearson's R-value = 0.288). The correlations between canopy cover with diversity index, dominance index, rich-ness index and EPT composition are strong with Pearson's R-value of 0.595, 0.529, 0.563 and 0.808, respectively. Substrate composition or specific D_{50} is associated ($p < 0.05$) with diversity index and EPT composition. The correlation between D_{50} and EPT composition is strong (Pearson's R-value = 0.598) but has a weak diversity

index (Pearson's R-value = 0.391). At the same time, LWD has a significant association (p < 0.05) with diversity index, dominance index, richness index, evenness index and EPT composition. However, the correlation between LWD with diversity index (Pearson's R-value = 0.428) and evenness index is weak (Pearson's R-value = 0.277). Nevertheless, there is a strong correlation with dominance index (Pearson's R-value = 0.597), richness index (Pearson's R-value = 0.533) and EPT composition (Pearson's R-value = 0.611). The riparian composition is also associated (p < 0.05) with diversity index, richness index and EPT composition but generally weak. The correlation between riparian composition and diversity index have recorded Pearson's R-value = 0.019, dominance index recorded Pearson's R-value = 0.235, richness index recorded Pearson's R-value = 0.155, evenness index recorded Pearson's R-value = 0.036 and EPT composition recorded Pearson's R-value = 0.068. On the other hand, cross-tabulations between river discharge and all the biological indices shows that it is only associated (p < 0.05) with EPT with Pearson's R-value = 0.461 (Fig. 6).

River health is usually associated with good physical and chemical water quality, maintenance of natural habitat, natural river morphology and sustainable aquatic life.
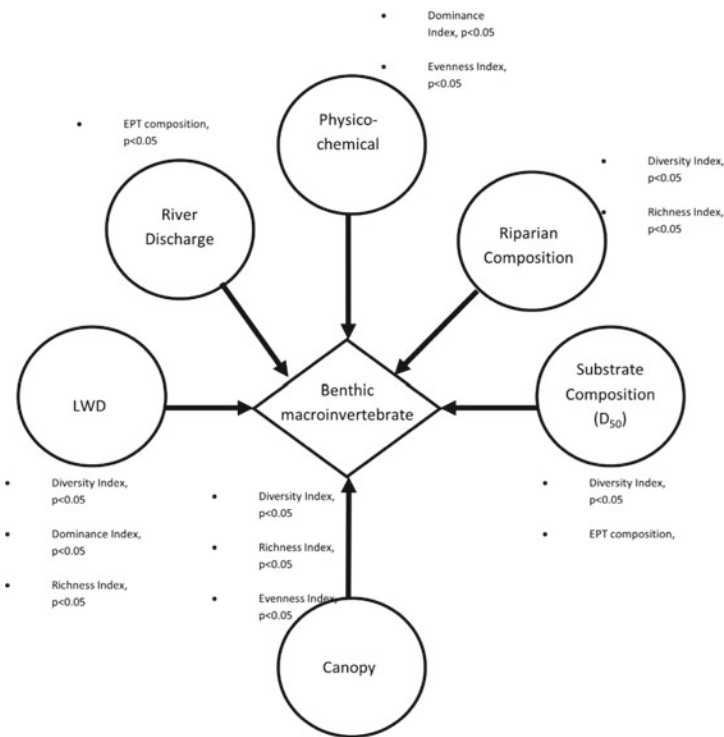
Fig. 6 Correlation between benthic macroinvertebrate with substrate compositions, riparian composition, physicochemical water quality, river discharge, LWD and canopy cover

Merely considering the physicochemical parameters alone to represent the quality or health of a river as a whole is not quite proper; neither is acceptable as was practised in the past. For a complete and proper assessment of river health, other parameters such as biological components, habitat characteristics, and substrate size distribution have to be considered integrally with physicochemical water quality and not on an isolated basis. Changes in land use will lead to catchment characteristics, river habitat patterns, and in-stream characteristics. Consequently, these changes would usually lead to physicochemical water quality changes. The end result will ultimately lead to perceptible changes in aquatic life forms and compositions. In this regard, using a single attribute for assessing the health of a river is not appropriate as each attribute is limited to only answering specific objectives, whilst a general assessment for river health would require a multidisciplinary approach. Each attribute was previously developed purely on a specific basis. Attributes for river morphology and hydrology were developed basically to assess river flow, discharge, cross-section, bank conditions and sediment transport concerning hydrology and fluvial hydraulics [16]. Habitat assessment attributes were developed to assess various components of biodiversity such as river riparian, canopy cover, land use, substrate size distributions, woody debris and river meander. For ecology, a biological attribute was made available to quantify aquatic life in the river. All these attributes should be evaluated one by one to get the current status to conclude whether a river is healthy or not. Nonetheless, these assessments require a lot of money, a long time and require a variety of expertise.

4   Conclusion

Based on the results obtained, it can be concluded that all river ecosystem attributes have a significant correlation to the population of benthic macroinvertebrates in a river body. This suggests that benthic macroinvertebrates can be used as indicators to assess water quality and river health.

References

1. Abas A, Rak AE, Omar SAS, Kumaran JV (2018) Correlation between benthic macroinvertebrate distribution and substrate composition in selected recreational rivers in Kelantan, Malaysia. J. Sustain Sci Manage 13(1):39–48

2. Ahmad AK, Abd Aziz Z, Fun HY, Ling TM, Suhaimi Othman M (2013) The use of benthic macroinvertebrates as bio-indicator at Sungai Kongkoi, Negri Sembilan, Malaysia. Sains Malaysiana 42(5):605–614

3. Kutty AA, Fauzi NM, Nurhafizah-Azwa S, Rak AE, Omar SAS (2019) Potensi Makroinvertebrat Bentik Sebagai Penunjuk Biologi di Ekosistem Sungai Rekreasi. Serangga 24(1):42–57

4. Appalasamy S, Arumugam N, Sukri S, Eh Rak A (2018) Physico-chemical water quality and macroinvertebrate distribution along Sungai Asah in Pulau Tioman, Johor, Malaysia. Songklanakarin J Sci Technol 40(6)

5. APHA (1995) Standard methods for the examination of water and wastewater method, 19th edn. United States of America: American Public Health Association and American Water Works Association and Water Environment Federation

6. Azrina MZ, Yap CK, Rahim Ismail A, Ismail A, Tan SG (2006) Anthropogenic impacts on the distribution and biodiversity of benthic macroinvertebrates and water quality of the Langat River, Peninsular Malaysia. Ecotoxicol Environ Safety 64(3):337–347

7. Barbour MT, Gerritsen J, Snyder BD, Stribling JB (1999) Rapid bioassessment protocols for use in streams and wadeable rivers: Periphyton, Benthic Macroinvertebrates, and Fish, 2nd edn. EPA, USEPA, Washington, D. C.

8. Bevenger GS, King RM (1995) A pebble count procedure for assessing watershed cumulative effects. Res. Pap. RM-RP-319. Fort Collins, CO: U.S. Department of Agriculture, Forest Service, Rocky Mountain Forest and Range Experiment Station. 17 p

9. Camara M, Jamil NR, Abdullah AFB (2019) Impact of land uses on water quality in Malaysia: a review. Ecol Processes 8(10)

10. Chitale SV (1974) Discharge measurement - technology and data analysis, hydraulics of alluvial streams, central board of irrigation and power. Status report Number 3, New Delhi

11. Cieszynska M, Wesolowski M, Bartoszewicz M, Michalska M, Nowacki J (2011) Application of physicochemical data for water-quality assessment of water courses in the Gdansk Municipality (South Baltic Coast). Environmental Monitoring Assessment. Epub ahead of print

12. Ehrhart BJ, Shannon RD, Jarrett AR (2002) Effects of construction site sedimentation basins on receiving stream ecosystems. Am Soc Agric Biol Eng 45(3):675–680

13. Hill MO (1973) Diversity and evenness: a unifying notation and its consequences. Ecology 54(2):427–432

14. Karr JR (1998) Draft: Karr's aquatic insect stream sampling protocol. salmon web. http://www.cbr.washington.edu. Accessed 05 Aug 2021

15. Margalef R (1958) Information theory in Ecology. Int J Gen Syst 3:36–71

16. Marta González T, Vanesa MF, Francisca CA, Walter B, Simon D, Diego García J, Virginia GG, Dejan M, Patricia MRG (2021) Improving river hydromorphological assessment through better integration of riparian vegetation: Scientific evidence and guidelines. J Environ Manage 292:112730

17. Merckx B, Geothals P, Steyaert M, Vanreusel A, Vincx M, Vanaverbeke J (2009) Predictability of marine nematode biodiversity. Ecol Model 220(11):1449–1458

18. Miller SW, Wooster D, Li JL (2009) Does species trait composition influence macroinvertebrate responses to irrigation water withdrawals: evidence from the Intermountain West, USA. River Research and Applications. Wiley InterScience

19. Narumon S, Wiroj N (1998) Preliminary study of benthic macroinvertebrate fauna in Yakruea and Phromlaeng Streams at Nam Nao National Park, Thailand. KKU Res J 3(1):1–15

20. Poff NL, Bledsoe BP, Dean D (2007) Final report: linking watershed characteristics with flow region and geomorphic context to diagnose water quality impairment at multiple spatitemporal scales. Colorado State University

21. Rak AE, Omar SAS, Kutty AA (2017) Influence of habitat characteristics on the assemblage and distribution of Ephemeroptera, Plecoptera and Trichoptera (EPT) at selected recreational rivers in Kelantan, Malaysia. J Fund Appl Sci 9(7S):37–48

22. Richards C, Host G (1994) Examining land use influences on stream habitats and macroinvertebrates: a Gis approach. Water Resour Bull 30(4):729–738

23. Simpson EH (1949) Measurement of diversity. Nature 163:688
24. Shannon CE, Wiener W (1963) The mathematical theory of communication. University Illinois Press, Urbana
25. Scheaffer RL (1999) Categorical data analysis. University of Florida, NCSSM Statistics Leadership Institute
26. Shabdin ML, Abang F (1999) The benthic invertebrate community of rivers in Bario, Kelabit Highlands, Sarawak. ASEAN Rev Biodiversity Environ Conserv UMS
27. Suhaila AH, Che Salmah MR (2011) Stoneflies (Insecta: Plecoptera) in Malaysian tropical rivers: diversity and seasonality. J Entomol Nematol 3(2):30–36
28. Sharifah Aisyah SO, Aweng ER, Razak W, Ahmad Abas K (2015) Preliminary study on benthic macroinvertebrates distribution and assemblages at Lata Meraung Waterfall, Pahang, Malaysia. Jurnal Teknologi 72(5):1–4
29. Salam MA, Kabir MM, Yee LF, A/l Eh Rak A, Khan MS (2019) Water quality assessment of Perak river, Malaysia. Pollution 5(3):637–648
30. Timbol AS, Kido MH, Heacock DE (1989) A descriptive study of selected biological and physicochemical characteristics of Limahuli stream, Kauai. Report prepared for Limahuli Garden and Preserve (National Tropical Botanical Garden)
31. Omar SAS, Rak AE, Sanusi AFA, Yusoff AM (2014) Benthic macroinvertebrates composition and distribution at sungai dawai and sungai dekong in lojing highland, Gua Musang, Kelantan. Jurnal Teknologi, 68(3)
32. USEPA (2007) Benthic Macroinvertebrate Identification. Biological Indicators of Watershed Health. http://www.epa.gov/owow/monitoring/. Accessed 05 Aug 2021
33. Vicki FS (1979) Statistics for the social sciences. Little, Brown, the University of Michigan
34. Wallace JB, Grubaugh JW, Whiles MR (1996) Biotic indices and stream ecosystem processes: results from an experimental study. Ecol Appl 6(1):140–151
35. Wolman MG (1954) A method of sampling coarse river-bed material. Trans Am Geophys Union (EOS) 35:951–956
36. Shamsul ZNM, Rak AE, Hajisamae S, Omar SAS, Afip LA (2018) Assessment of physico-chemicals water quality, substrate compositions and phytoplankton in relation to the density of *Corbicula fluminea* in Pattani river, Southern Thailand. Int J Pure Appl Math 118(24):1–13

A Holistic Approach for Establishing Resilient Dams for Malaysia

Lariyah Mohd Sidek, Hidayah Basri, Mohammad Marufuzzaman, Norziana Jamil, Zeittey Karmilla Kaman, Muhammad Izzat Azhar Khebir, Siti Mariam Allias Omar, and Mohd Hazri bin Moh Khambali

Abstract The dam related disaster caused thousands of people's lives and billions of property damages in the world and in Malaysia. The loss of life and property damages is mostly happened due to dam failure and the lack of timely evacuation procedures. Currently, insufficient integrated and comprehensive research are being done in Malaysia, including the impact of dam failures. The interconnection and interdependence of these elements are vital to ensure holistic solutions for dam safety. In this research, we proposed a resilient and intelligent dam safety management program that integrates engineering, cybersecurity and socioeconomic elements to minimize the risks of dam failure. A comparatively new approach named Risk-Informed Decision-Making is proposed in this research which will use the likelihood of loading, dam fragility, and consequences of failure to estimate the risk related to Batu Dam. Investigation of cyber security in dam data will be portrayed to assist in strengthening the security of dam control systems against sophisticated attacks such as APT. Finally, an effective evacuation procedure will be proposed to complete the holistic solution that benefits the nations, dam owners and other related authorities, but more importantly, it will help keep the community safe.

L. M. Sidek · H. Basri (✉) · M. Marufuzzaman · M. I. A. Khebir · S. M. A. Omar
Institute of Energy Infrastructure, Universiti Tenaga Nasional, Kajang, Malaysia
e-mail: Bhidayah@uniten.edu.my

L. M. Sidek
e-mail: Lariyah@uniten.edu.my

M. I. A. Khebir
e-mail: izzat.azhar@uniten.edu.my

N. Jamil
College of Computing and Informatics, Universiti Tenaga Nasional, Kajang, Malaysia
e-mail: Norziana@uniten.edu.my

Z. K. Kaman
Institute of Energy Policy and Research (IEPRe), Universiti Tenaga Nasional, Kajang, Malaysia
e-mail: Zeittey@uniten.edu.my

M. H. M. Khambali
Department of Irrigation and Drainage, Kuala Lumpur, Malaysia
e-mail: mohdhazri@water.gov.my

1 Introduction

Dam-reservoir systems play a key role in providing multiple services for society, including water supply, irrigation, flood protection and hydropower generation worldwide, and East Asia is not an exception [2, 13, 18]. Hydropower production is a cleaner, renewable energy source, and it is one form of powering developing countries. In addition, dams contribute to achieving the established Sustainable Development Goals (SDGs), adopted by all United Nations Member States in 2015, providing resources and services to reduce poverty, improve health and well-being, and boost economic growth, among others. However, there is a probability of the potential failure of these infrastructures, resulting in devastating damages downstream. The potential consequences of a dam failure may include social, economic and environmental damages, among which the potential life lost is the most crucial aspect.

Recent examples of dam failure in East Asia include the collapse of Laos' Saddle Dam in July 2018. This auxiliary dam is part of the Xe-Pian Xe- Namnoy hydroelectric project, a 410 megawatts (MW) project, in construction since 2013 by a consortium of South Korean, Thai and Laotian firms, which was near to completion when heavy rains, linked to the tropical storm Son-Tinh, filled the site beyond capacity, sending more than 170 billion cubic feet of water downstream. As of September 25, 40 people were confirmed dead, at least 98 more were missing and more than 6,600 others were displaced due to the dam failure [20].

The collapse of Machhu Dam II in Gujarat (India) in 1979 occurred on August 10 during the monsoon storms, although not uncommon in this part of India, which were larger than the usual events. The flow began to increase down the Machhu river, first hitting Machhu Dam I and then turning downstream to Machhu Dam II. As the storm intensified, operators at the Machhu Dam II began to open gates to keep the dam from rising above maximum levels. By 1:30 AM, all the gates were opened fully, except for three gates that were not properly functioning. Despite the non-operational gates, the dam was passing 196,000 cubic feet per second (cfs), very close to its full capacity of 200,000 cfs. However, the water continued to rise and the day after, water overtopped the earthen embankments on both sides of the masonry spillway leading to dam failure. The flood wave destroyed buildings, killed livestock and took lives. Life-loss estimates range from 1,800 to as high as 25,000 people [20].

Today, society demands an increase in the safety and reliability levels of such infrastructures considered essential. The only way to respond positively to these expectations is to integrate the dam's design, construction and operation in a framework of risk management that ensures effective mitigations of natural and anthropic threats [4]. Risk analysis is a way of managing the life cycle of dams and reservoirs, from their conception to their exploitation and maintenance, allowing them to optimise their capacities, minimise their risks and carry out truly smart governance. The

owner becomes an active part in making decisions through a set of methodologies and technologies that will allow getting better projects, adjusting costs, improving sustainability and demonstrating in any moment that the way of proceeding follows the best practices worldwide.

From the previous study by UNITEN in 2018 for TNB Hydro schemes (Cameron Highlands, Kenyir, Sg Perak and Pergau), the revised PMF Inflow (m^3/s) values exceeded the original design, especially Kenyir and Jor Dam except for Pergau dam. Meanwhile, the revised spillway outflow at PMF values exceeded all dams except Kenyir and Susu dam. These findings showed that the Inflow design flood (IDF) used for design have increased, and currently, some TNB dams would be overtopped and possibly fail using the latest calculated PMF at each dam site [22]. A similar situation has been experienced by US dams as the probable maximum flood (PMF) currently served as the design standard for many US dams. Therefore, IDF used for design have increased, and currently, thousands of dams in the US would be overtopped and possibly fail using the latest calculated PMF at each dam site. Some researchers have suggested that modifying dams to accommodate the PMF could be wasteful [8].

Consequently, global strategies of risk management have gained great importance during the last years worldwide. Efforts carried out to implement them systematically include aspects such as sustainability, resilience and public participation. In this sense, some of the most important agencies and organisations in the dam safety field are implementing risk assessment methodologies. Some examples are USACE, Bureau of Reclamation and FERC in the USA, Canadian Dam Association, Australian National Committee on Large Dams, United Kingdom Environmental Agency, Spanish National Committee on Large Dams or current dam safety ICOLD, 2017 legislation in France [1, 6, 8, 21, 23, 24]. Risk-Informed Decision-Making (RIDM) is a method of dam safety evaluation that uses the likelihood of loading, dam fragility, and consequences of failure to estimate the risk (Rodríguez et al. 2015). This risk estimate is used along with standards-based analyses to decide if dam safety investments are justified or warranted. This approach has many benefits, including a greatly improved understanding of the safety of the dam and identifying dam safety vulnerabilities that have not been identified using standards-based evaluation techniques. Moreover, the mathematical representation clearly shows the nonlinear mapping relationship between dam structural behaviour (effect-quantity) and its cause (influence-quantity). Therefore, machine learning (ML) algorithms can be useful in evaluating the data related to the risks involved in dam failure [7]. The construction of the monitoring model can be equivalent to an ML problem [17, 19]. Dam effect-quantity and its influence-quantity are regarded as an output vector and input vector of one learning machine. The observed data consist of a training sample set whereby the data analytic method will be processed using the ML algorithm [18]. The training operation is implemented to obtain one learning machine, which is essentially an implicit expression of the monitoring model of dam safety. The prediction of the failure of the dam will be more efficient, and the data analysis will be more effective.

However, while storing so much data related to dams for RIDM modelling, another important feature need to be considered, i.e., security. Because the interconnection

of the cyber-physical system has opened a door for more exposure to cyber threats and cyber-attacks. This is shown in the number of real cyber-attacks on critical infrastructure that has been increased over the years. In 2010, a sophisticated killing chain of a worm, Stuxnet, propagated itself in Iran's nuclear facilities and damaged almost one-fifth of the facilities [14]. This cyber-attack is one of the most powerful attacks, and it is called Advanced Persistent Threat (APT). APT is a multi-stage attack that has been a major concern worldwide. In the past, attackers attacked information systems with personal and financial motives. However, nowadays, the motives are more towards political interest and normally been financially supported by a particular country. Attackers engaged with a different sophisticated method of attack towards the target to steal confidential and sensitive information (4). Their objective is to make a destructive impact on the targeted industry or countries, specifically on critical infrastructure.

Stuxnet has given more births to more variants of APT, specifically to attack industrial plants. In 2014, the German steel plant was cyber-attacked which caused significant damage to the plant [15]. APTs are seen as a serious threat to industrial plants such as water dams. The failure to detect the existence of APT in the industrial plant would risk a serious and significant negative impact to the people as well as to the country. Since then, many approaches have been proposed by researchers to detect the existence of APT attacks in their early stage so that early notification can be sent to the network administrator and, thus, necessary action can be made. Currently, there are two approaches applied in general cyber-attack detection method; an offline detection method that uses a sandbox technique where a program or system been deployed in an isolated environment for a separate analysis to detect anomaly which is not suitable for APT detection since it is unable to detect a real-time attack. Another approach is the Real-time detection method consists of a few approaches, which are signature-based analysis, anomaly-based detection and correlation analysis. However, signature-based analysis, anomaly-based detection is not suitable for a zero-day attack like APT since both are based on the stored signature and known malware patterns. On the other hand, APT has dynamic characteristics that cause its detection becomes very challenging. On the other hand, correlation analysis seems to be the most applicable method for APT detection. However, there are still some weaknesses, such as slow computation which needs to be addressed in more detail.

Other approaches that are used for intrusion detection are also studied. For example, a statistical analysis approach by Han et al. uses a provenance graph to record every detailed activity that happened at the kernel level of the computer system [12]. It is a good approach since it is able to capture data up to security-related interaction rather than just intercepting system calls. However, the problem faced by the method is that it requires high computation power at the host. Aside from that, as the provenance graph provides a detailed structure for every activity, the graph will be more difficult to be understood by a network administrator for a complex system. This can lead to misinterpretation of the graph itself. [3] proposed almost a similar approach with slight enhancement, i.e., adding an algorithm called Attribute Value Frequency (AVF). The AVF models the data and assigns a score to it. However, the problem with this approach is each of the data received must be manually interpreted

by a network administrator/system analyst to indicate whether the process contains attacks or otherwise. This practice is not practical because it is time-consuming and can also lead to misinterpretation.

APT indicators of compromise commonly span broad system-level behaviours. There are several approaches to monitor provenance in a single application, such as using Hadoop Apache and single language runtime such as Java. The system-level provenance system will generate a significantly higher volume of data that leads to potentially significant scalability challenges and storage constraints. Han et al. introduced an enhancement to their previous work by adding baseline profile phases whereby comparison is made between host behaviour during normal and abnormal activity [12]. However, it only works well in a domain with homogenous normal activity and if a host involves various activities, the method will raise a false alarm.

[9] developed a machine learning-based system called MLAPT (Machine Learning APT) that consists of 3 phases, which are (1) Threat detection, (2) Alert Correlation, and (3) Attack Prediction. The method is able to process and analyze network traffic in real-time without needing to store the data. However, it tends to create false alarms and also some type of 'APT failed to be detected' if the alert clustering was incorrectly done during phase (2). The author suggested that the alert from an external IDS be used as an input to the MLAPT during phase (1) instead of using sensors on MLAPT itself. As we noted earlier, IDS is using signature-based detection and due to that, the detection of APT will not be highly precise.

[10] proposed a framework to detect and predict APT based on Cyber Kill Chain (also known as Intrusion Kill Chain. The model itself consists of 7 phases, which are (1) Reconnaissance, (2) Weaponization, (3) Delivery, (4) Exploitation, (5) Installation, (6) Command and Control and (7) Act on Objective. The limitation of this method is on phase (1), whereby the author needs to manually include the list of detection methods such as DNS Honey Tokens, Detection of Access to robot.txt Files, Detection of Web Server and a few others. Hence, not all APTs can be detected since the detection is solely done based on patterns included in the lists. This approach is almost similar to signature-based detection.

Despite the increasing safety of dams resulting from the improved engineering knowledge and better construction quality, a full non-risk guarantee is not possible and accidents can occur owing to natural hazards, human actions or dam ageing. The societal life risk is one of the characteristics that could have been affected by hazardous activity in combination with the surrounding population. [16] presented the results of a research project that evaluated the potential roles of two risk metrics, individual and societal life risks, to support decision making on new flood safety standards and presented preliminary estimates of the nationwide levels of societal life risk. [11] established integrated dam failure risk criteria that comprehensively considered the risks caused by a dam failure in the areas of life, economy, environment, and society. From a technical perspective, [5] adopted the societal criterion named Expected Average Number of Casualties per year as the highest priority among the criteria used to make decisions on flood management. [11] proposed societal life risk criteria based on the safety conditions of dams in China, public safety and the acceptance of dam risks, historical dam breach data and current design standards. In line

with the current situation, this study argues on Malaysia's preparedness on potential risks which might be occurred due to dam failure in terms of socio-economic impact towards public safety around the dam. Some of the questions being raised: What are the potential risks due to dam failure? How can the impacts be measured? What is the prevention or action plan that needs to be established in order to safeguard the life of the community at large?

Therefore, this research proposed a concept of quantitative RIDM and generated the dam-break flood inundation map for reducing the risk of dam failure. The research data will be protected using the context-based ML method for strengthening the security of dam control systems against sophisticated attacks such as APT. Finally, the proposed research will conduct a socio-economic impact assessment related to dam failure and help the dam owners to make decisions quickly. This Quintuple Helix innovation model of this research ultimately cover all the aspects related to dam failure and its consequences as well as help to build a resilient, intelligent and secure dam safety management system, including big data for dams in Malaysia.

2   Methodology

The goal of this research is to ensure resilient dams for Malaysia. The research will be conducted in one of the many dams of Malaysia and eventually expanded for other dams of Malaysia. The name of the study area is Batu Dam which is classified as a high hazard dam as the dam is a large dam and highly urban downstream area is populated approximately 1.25 million people by a mix of industry, water treatment plant and housing scheme. This methodology is based on the integral and continuous management of dam safety, linking the existing information contained in the Dam Safety Technical File with the qualitative and quantitative analysis of the system, which allows analysing and evaluating the existing risk, as well as evaluating the impact of different risk reduction measures to establish the optimal sequence of implementation. The overall concept of the proposed research project is shown in Fig. 1, where the overall project is divided into three sub-projects named P1, P2 and P3.

According to Fig. 1, the P1 part will develop the RIDM framework and implement the ML model to identify the failure modes. On the other hand, the P2 part of the project will solely work on the Cybersecurity area and ensure the dam data is safe from the APT. Finally, the last part, i.e. P3, is more on implementing the socio-economic analysis where the potential loss of lives, damage to physical assets and other potential consequences will be assessed to determine the impact. As a whole, the research will ensure resilient and intelligent dam safety for the betterment of the community. The research will engage different sectors and niche areas and develop an Intelligent Dam Safety Management database that is capable of managing information from multiple sources. The overall data sharing plan is depicted in Fig. 2.

The research will collect primary and secondary data such as Hydrological data (rainfall, water level and flow), Inspection and Monitoring data (e.g., piezometers
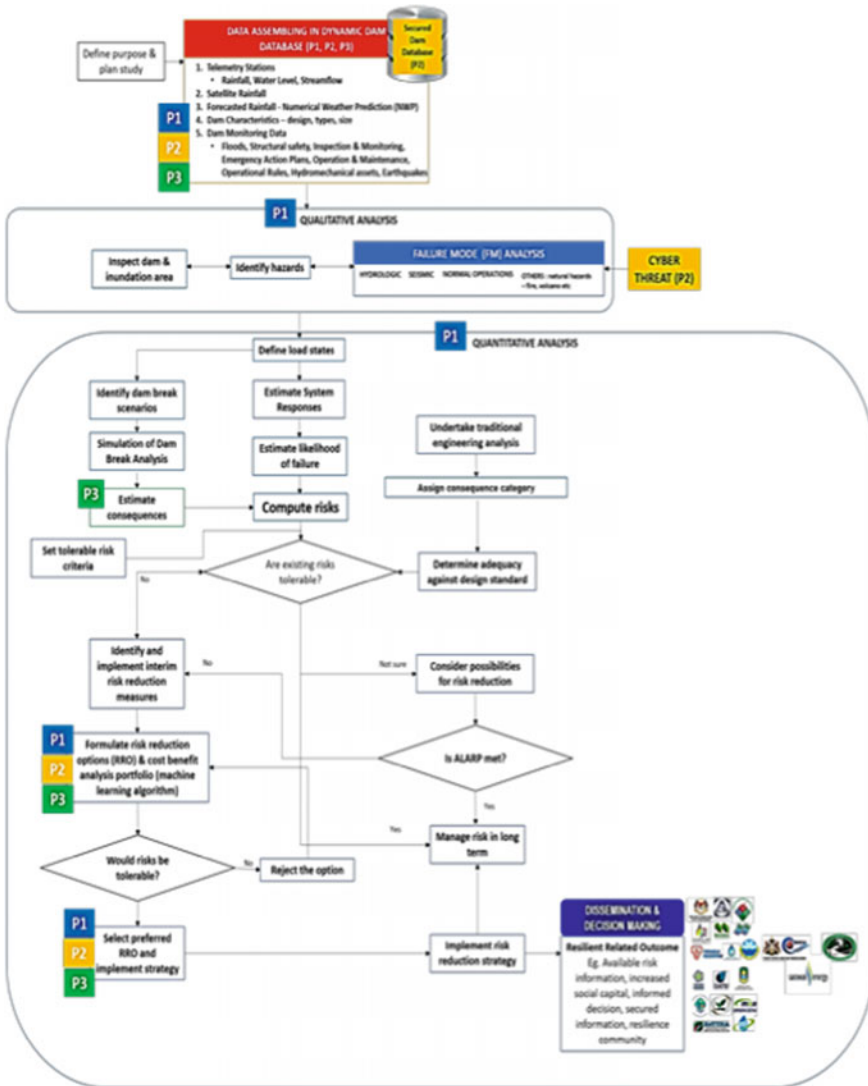
Fig. 1 The overall framework of the proposed research

and inclinometer), Structural Safety data, Operational Rules, Floods, Earthquakes, Hydromechanical Assets, Operation and Maintenance, Emergency Action Plans and others. After processing the information, the research will compile and integrate as big data to share with JPS, NADMA and other Dam owners for decision making. Only with the help of RIDM that it is possible to compile the key data in a way that reliable decision making is available at all times for various scenarios. All collected data will be digitized and stored securely against unauthorised disclosure, modification or
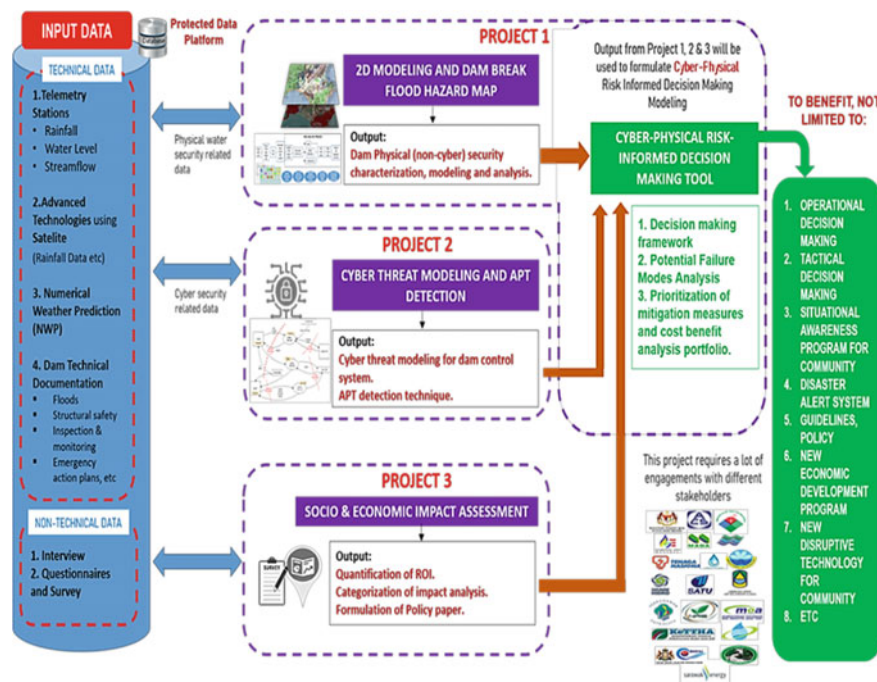
Fig. 2 Data sharing architecture of the proposed research

destruction with the help of Subproject 2, i.e., cybersecurity. The data collected under P1 will be shared among P2 and P3 for building a secured digital database for dams in Malaysia. Finally, the project outcomes will be integrated with the dam owner's hazard mitigation plan to effectively implement mitigation action and eliminate future risks.

The first part of the project is the quantitative dam safety risk-informed decision-making model for reducing the risk of dam failure. The proposed methodology of this part of the project has three phases: the first phase will generate the development and application of methodologies and practical tools for risk analysis applied to dam safety management. The methodology for the analysis and evaluation of risk in dam-reservoir systems will be based on international best practices. Besides, the fundamentals are aligned with publications developed in recent years, such as the Technical Guide No. 8 on Dam Safety published by the Spanish National Committee on Large Dams (SPANCOLD) in 2012 and the CWC Guidelines for Assessing and Managing Risks Associated with Dams published by Indian Central Water Commission in 2019. This methodology is based on the integral and continuous management of dam safety, linking the existing information contained in the Dam Safety Technical File with the qualitative and/or quantitative analysis of the system, which allows analysing and evaluating the existing risk, as well as evaluate the impact of

different risk reduction measures to establish the optimal sequence of implementation. The second phase will be enhancing the performance of the RIDM model. As the RIDM modelling is based on statistical analysis and using big data as an input, thus classification-based ML algorithm will be implemented for data analysis and risk prediction. This enhancement will make the model more accurate and substantially reduce execution time. The third phase will be the enhancement of the 2D dam-break flood hazard map. The 2D modelling module will simulate water level variations and flows in the river and the floodplain maps during the dam operational release and dam break scenarios. The RIDM modelling will fetch the output from this 2D hydrodynamic model to calculate the probable risks of dam failure.

The second part of the proposed research will be cyber threat modelling and APT detection using a context-based approach and ensemble method of ML models with a discrete probability distribution. This part of the project involves four phases too. The first phase will be the preliminary investigation, an in-depth study to understand the dam control system will be carried out. This includes a study on dam control system reference architecture adopted in Malaysia, assets in every layer in dam control system architecture, communication protocols, communication network, identification of vulnerabilities in each layer, identification of potential threats, existing security controls implemented and dam control system requirements (such as data transfer rate and tolerated latency range). After obtaining the understanding, a reference architecture for the dam control system will be produced. The dam control system will be modelled as a Processor Data Flow Diagram following a correctly identified threat modelling framework and an attack tree that describes the dependencies of all the gathered to indicate cyber threats to the dam control system will be constructed. The second phase will be the design and formulation phase. Characteristics of APT from its many types will be studied in detail and identified. Network traffic datasets and some other data useful for constructing APT datasets will be gathered from the dam control system and public databases, an ensemble method of ML models useful to forecast vulnerabilities will be identified, and a context-based approach will be designed and formulated. After this, the test and analysis validation phase will be performed where the APT datasets will be trained and tested using several machine learning approaches, with the focus on time series analysis using a recurrent neural network model. In this phase, the ensemble method is used to strengthen the accuracy of detection done earlier by a context-based approach. The PhD candidate should be able to improve the accuracy of detection exhibited by an ensemble of identified machine learning models. Next, the conditional probabilities to determine APT propagation and cascading effects, a discrete probability distribution method will be used. The overall technique will then be compared with the performance of other researchers. In the last phase, the output from Phase 1 to Phase 3 will be integrated holistically as a framework that will appear as a tool to help the state government or dam owner to understand further the cyber threats of dam control systems and be alert of APT existence.

The last part of the proposed research will be determining the dam failure hazard risk and socioeconomic impact assessment. The dam failure hazard impact assessment study deals with the consequences of flooding and flood inundation caused

by dam failure on the downstream population and environment within the impacted area, as well as potential snowball economic impact at a regional level. The potential loss of lives, damage to physical assets and other potential consequences will be assessed to determine the impact. The assessment will provide a link between the different scenarios of dam failure with potential social, economic and environmental impact. Consequently, risk-based option appraisals involving modification of variables that describe the flood system and the consequences will be developed and contribute to short- and long-term decisions related to flood risk management. Given the intense nature of water infrastructure investment and the importance of public safety, a strategic decision based on comprehensive flood risk analysis and its socioeconomic impact is considered crucial.

3   Results and Discussion

In this research, a dam safety risk analysis system incorporating risk calculations and analyses will be developed using a renowned and established software named as iPresas. Some pilot results are described in this section. The tools can be applied for asset and portfolio dam risk analysis. Risk models will be performed, and risk outcomes will be used as an example of how investments for dam rehabilitation and maintenance can be prioritised at a portfolio scale, as shown in Fig. 3.

The use of iPresas software tools will allow quantifying, representing and evaluating risks and comparing risk outcomes with international tolerability recommendations. There were no complete results for this project. In this section, a preliminary result and findings from all three projects that have been produced from his research will be presented.
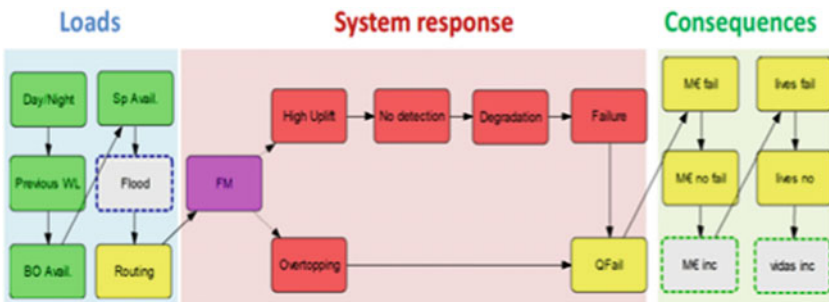
Fig. 3 Example of risk model architecture (2 failure modes) (iPresas, 2017)

3.1 Preliminary Result for Project 1

For the preliminary result on project 1, hydrological data for stations at Kg. Sg. Tua at Wilayah Persekutuan (Station. No. 3216001), Ibu Bekalan KM16 Gombak, Kuala Lumpur (Station. No. 3217001) and Genting Sempah, Kuala Lumpur (Station. No. 3317004) which is located near Batu Dam. The station that is being used is considered for its long records and quality of data. Base Fig. 4 is an isohyet map that has been plotted, and it can be observed that the maximum areal rainfall for all three stations ranges from 130 to 195 mm. Table 1 and Figure show the detail on the values for the highest recorded point of rainfall for all durations.

Besides that, a PMP review is done to compute the Probable Maximum Flood (PMF) for checking the spillway adequacy of the dam in case of a flood rise inherent during current conditions. The PMF derived from the PMPs is the design flood inflow into the reservoir where no risk of failure of dam structure is anticipated. The PMP is defined as the greatest precipitation depth for a given duration that is meteorologically possible over a given station or a specified area. There are two methods used to calculate the magnitude of the PMP. The first is the physical approach in which the PMP for the different duration is determined by maximizing the major historical
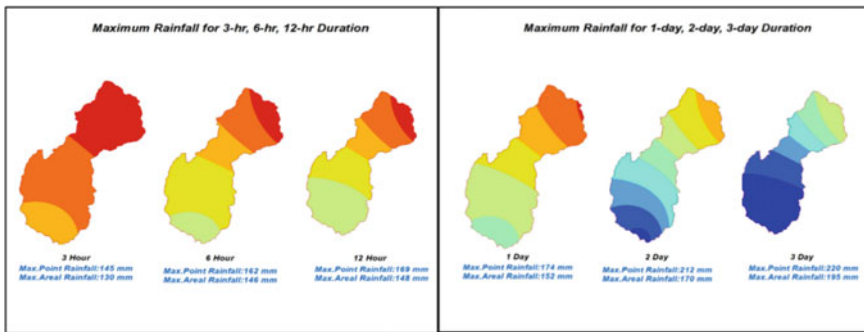
Fig. 4 Isohyets map for the highest recorded rainfall

Table 1 Highest recorded point of rainfall

No	Duration	Rainfall station		
		3,216,001 Kg Sg Tua at Wilayah Persekutuan	3,217,001 Ibu Bekalan KM 16	3,317,004 Genting Sempah
1	3-h	144.8	126.5	118.0
2	6-h	162.0	157.5	118.1
3	12-h	168.5	157.5	118.5
4	1-day	173.5	158.0	123.0
5	2-day	212.0	160.0	137.0
6	3-day	220.0	215.0	150.0

storm events. Storm transposition and envelopment techniques are incorporated to achieve the level of PMP in order to compensate for the lack of an adequate storm database. Over the past 20 years, many estimates of PMP have been made for dam sites in Peninsular Malaysia using transposition and maximization techniques.

The statistical approach is employed to estimate the PMP rainfall at a particular location or area, determined from the frequency distribution fitted to the annual maximum rainfall data. Hershfield 's statistical techniques are extensively used to estimate PMP for stations with a long rainfall record period. It is therefore considered desirable to carry out a study on the estimation of PMP for 1, 3, 6, 12-h, 1, 2, 3, and 5-day duration using the Hershfield technique for the station in Batu Dam Catchment where daily rainfall data are available for an extended period.

Then, the probable maximum flood (PMF) in Batu Dam Catchment will be simulated using HEC-HMS 4.8 by using the estimated probable maximum precipitation (PMP) as the design rainfall input. The deterministic methodology generates the PMF hydrograph by modelling the study area's physical atmospheric and drainage basin hydrologic and hydraulic processes. HEC-HMS 4.8 is adopted in this study due to its successful and worldwide acceptance and local applications in hydrological simulation. Figure 5 and Table 2 show the model setup on HEC-HMS 4.8 and the value of PMP and PMF.

Fig. 5 Model setup on HEC-HMS 4.8 software

Table 2 Highest recorded point of rainfall

UNITEN 2021		
Duration (hr)	PMP (mm)	PMF (mm)
1	232.60	512.80
3	259.71	522.70
6	298.08	453.70
12	323.03	314.90
24	347.42	234.10
48	458.50	193.10
72	478.05	126.90
120	543.07	87.2

3.2 Preliminary Finding for Project 2

We gather information on the real cyber incidents in the dam sector to understand the motive and modes of operation. Table 3 shows the summary of the gathered information.

From the information shown in Table 3, it can be seen that the tactics used by the hackers range from gaining unauthorized access to the system ransomware and vulnerabilities that were exploited by internal threats. Note that the software vulnerabilities also become the targeted source of the attack. This drives us to then model the threats for the water sector and countermeasures as summarized in Table 4.

Table 3 Summary on information gathering

Cyber incidents	Year	Perceived cause of the cyber incident	Impact	Mitigation action taken
Illinoiswater Plant Pump Station, United States	2011	The apparent connections to foreign IP addresses in the log files. Investigation of the log files and interviews with the personnel collectively concluded that the reported attack was a false alarm	The pump kept turning on and off and eventually burnt out	The issue could have been prevented through a timelier consideration of the employee's international travel and pump malfunctioning history

Table 3 (continued)

Cyber incidents	Year	Perceived cause of the cyber incident	Impact	Mitigation action taken
Key Largo Wastewater Treatment District, United States	2012	An illegal access to the district's computer system to download emails and other personal documents. He performed these actions using the credentials of other employees after the district did not renew his contract	The attack was limited to the IT systems of the facility, with no other malicious activity or disruptions to the district's operations	Implementation of two-factor authentication
Bowman Avenue Dam, United States	Aug, 2013	"Unauthorized remote access" to the SCADA system; a cyber-attack that allowed hackers to gather information on water levels, temperature, and the status of the sluice gate	The hackers exploited the unprotected modem connection and lack of security controls for the Dam's systems. Fortunately, the hackers only accessed a small sluice gate, but were able to manipulate the SCADA controllers expertly. The attack was not necessarily complex in nature but was deemed to be more of a penetration test to probe for weaknesses	Critical infrastructure controllers are kept separate from the internet at all costs

Table 3 (continued)

Cyber incidents	Year	Perceived cause of the cyber incident	Impact	Mitigation action taken
Five Water Utilities, United States	2014	The attack was caused by a fired employee of the company that manufactured the smart water meters who gained unauthorized access to protected computers	Inaccurate water bills and the deactivation of the Tower Gateway Base Stations (TGB), which receive signals from the water meters and transfer them to centralized facilities for monitoring and billing purposes. The first incident was reported by Kennebec Water District (Maine), where the utility could not connect to the TGB. Other nine attacks were reported in Spotswood (New Jersey), Egg Harbor (New Jersey), Aliquippa (Pennsylvania), and New Kensington (Pennsylvania)	Implementing access control and revoking access rights when someone is laid off
Kemuri Water Company (A Pseudonym), United States	2016	Possible unauthorized access to the systems (including an outdated mid-range computer system (AS400) system that served a number of critical OT and IT functions) as well as a series of unexplained valve manipulation patterns	Actual exploitation of the internet-facing payment application server and the subsequent manipulation of the utility's valve and flow control application. In synthesis, the incident resulted in the exfiltration of 2.5 million unique records and manipulation of chemicals and flow rates	Should not deploy the outdated systems (AS400), and install the security patches. Also, there should be a monitoring mechanism in place that oversees the transfer of data to enable early detection and response

Table 3 (continued)

Cyber incidents	Year	Perceived cause of the cyber incident	Impact	Mitigation action taken
An Undisclosed Drinking Water Utility, United States	2016	The cause of the attack may stand in the Sixnet BT Series Hard-coded Credentials Vulnerability (identified by the DHS in May 2016). The use of hard-coded credentials by the routers manufacturer and the failure of the water authority to install the patches proved to be major contributors to this incident	The hack was believed to be an opportunistic action to steal valuable internet bandwidth, resulting in the authority's cellular data bill soaring from an average of $300 a month to $45,000 in December 2016 and $53,000 in January 2017	Sixnet produced patches and new firmware to mitigate this vulnerability
A Regional Water Supplier, United Kingdom	2017	The funds were used to purchase Bitcoins, which were then transferred to addresses associated with a Bitcoin mixing service, thus preventing any subject from being identified by following this trail further	A regional water supplier was notified by several of its clients that their online account details were changed. After the client's credentials were reset, it emerged that the details of some registered bank accounts were also changed so that refunds issued to the customers were transferred fraudulently to these new bank accounts	Ensuring that partners having access to critical data perform stringent background checks on their employees

Table 3 (continued)

Cyber incidents	Year	Perceived cause of the cyber incident	Impact	Mitigation action taken
Onslow Water And Sewer Authority, United States	2018	Ransomware	The attack escalated into a sophisticated ransomware attack that locked out employees and encrypted databases, leaving the utility with limited computing capabilities. The hack began with persistent cyber-attacks through a virus known as EMOTET	The authority had multiple layers of protection in place, including firewalls and antivirus/malware software when the hackers struck. In this incident, the utility decided not to pay a ransom. This is in accordance with the federal guidelines—the US Government does not encourage paying a ransom to criminal actors
Fort Collins Lovelandwater District, United States	2019	Ransomware cyber-attack. The hackers demanded a ransom to restore access (the amount of ransom payment demanded has not been disclosed to the public)	The staff of the Fort Collins Loveland Water District and South Fort Collins Sanitation District were unable to access technical data	The district declined to pay the ransom. Data segmentation and segregation have proven to be a helpful practices in safeguarding sensitive customer and daily operation data
Riviera Beach Water Utility, United States	2019	Riviera Beach, a small city of 35,000 inhabitants located north of West Palm Beach (Florida), was hit by a crippling ransomware attack after an employee of the police department opened an infected email	Paralyzing computer systems of the police department, city council and other local government offices, the ransomware sent all operations offline and encrypted their data. The attack also spread to the water utility, compromising the computer systems controlling pumping stations and water quality testing, as well as its payment operations	Provide cybersecurity training and never pay the ransom as it only encourages future criminal activity

Table 4 Summary on the threats for water sector and its countermeasures

Threat category	Threats	Countermeasures
Spoofing	Spoofing the SCADA server process Spoofing of destination data store controller spoofing the human user external entity	Authentication
Tampering	Application server process memory tampered Cross-site scripting Controlled data store could be corrupted	Application hardening
Logging	Data Stores denies gateway Potentially writing data Potential data repudiation by application server	Logging
Information disclosure	Weak credential transit Data store inaccessible Potential process crash or stop for SCADA server	Segregation, encryption
Denial of service	Data flow serial Communication is potentially interrupted	Redundancy
Elevation of PRIVILEGE	Elevation by changing the execution flow in application server Cross-site request forgery Elevation using impersonation SCADA system may be subject to elevation of privilege using remote code execution	Device or application hardening

3.3   Preliminary Finding for Project 3

In order to reduce the risks of a dam failure, this project is calculated and quantify the losses that need to be bare by the stakeholder, which requires holistic studies on socioeconomic factors and situations. The highlights are especially for the communities in inundation areas where they were the most vulnerable to the dam break flood catastrophe. While downstream of the Batu Dam consists of various business industries (small, medium, and large enterprise), housing, and water treatment plants; social and economic factors need to be considered to get a reliable result of the impact of dam break for almost 1.25 million population lives under the 5 km range of the Batu Dam. MyDAMS (DID, 2017) has underlined six main risks of the dam itself to the inundation areas, which are:

I.   Loss of life
II. Economic losses

III. Environmental losses
IV. Cultural losses
 V. Cascade projects
VI. Incremental and total consequences

Nevertheless, economic losses play a significant role in contributing to the total loss and consequences of the dam break, making it our focus. While the elements considered under the economic losses were household income, dam benefit losses, property damage, and labour reduction, as it covered almost all the economic aspects for the community. The result will give a more holistic approach in determining the risk of dam failure not only based on the engineering aspect but also the real-life impact that could happen, which is the socioeconomic itself.

3.4 Overview of Overall Project

An example screenshot of the iPresas calc software tool is shown in Fig. 6. In this figure, the risk model is developed for two failure modes.

Risk-informed dam safety management: lessons learned from portfolio risk analyses in Europe, Third National Dam Safety Conference (3NDSC), 2017. Results from pilot dam risk models will be integrated using iPresas Manager software tool to show how risk outcomes can be used to prioritise investments based on multiple criteria (e.g., efficiency, equity, reduction of dam failure probabilities, etc.). For example, in hydrologic failure modes, the system will incorporate results of water level forecast in Temengor Inflow Forecasting system (TIFS) to the risk model architecture, as shown in Fig. 7. This will enable advanced operational decisions for the dam to reduce the risk of dam failure.
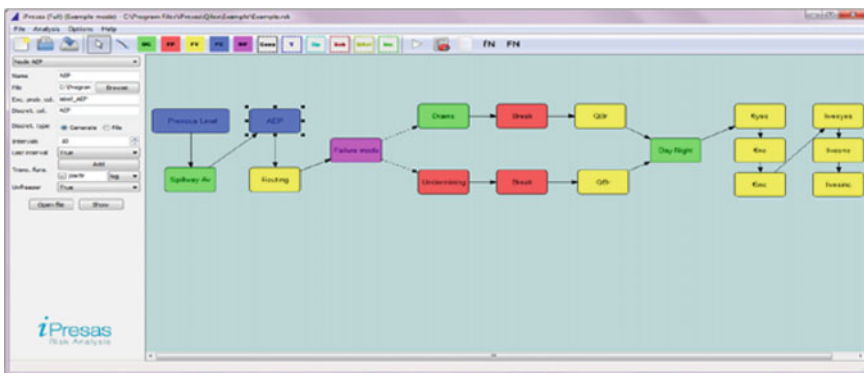
Fig. 6 Example of a screenshot of the iPresas Calc software
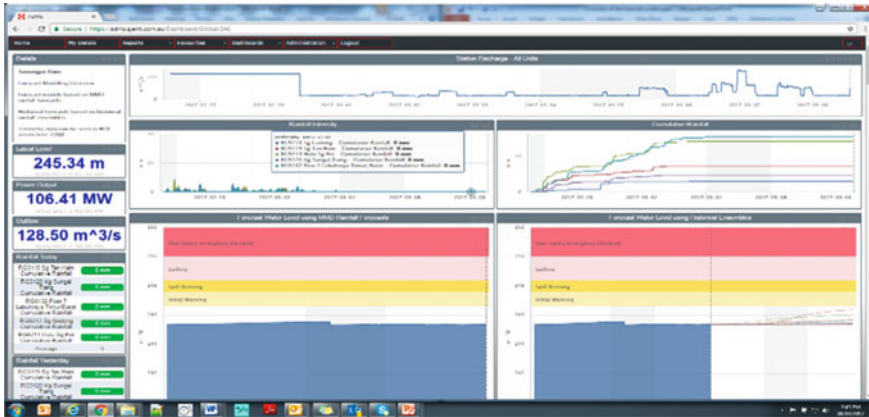
Fig. 7 Temengor inflow forecasting system

4   Conclusion

In this proposed research project, the application of risk analysis techniques to dam safety management will be made. The research will integrate all information on the dam in a secure and smart data management platform owned by TNB and assess its safety against current design standards. Also, it will promote more efficient and useful instrumentation and monitoring systems and inspection procedures to ensure the safety of the dams. Moreover, the screening tools allow a quick and homogeneous first estimation of the risk of a large group of dams and able to manage a portfolio of dams in an efficient and justified way, prioritising the rehabilitation of dams that allow reducing risk more at a lower cost. The research will optimise the design of rehabilitation measures and produce a conceptual design based on risk results and reinforce legal protection for dam safety managers through transparent and efficient decision making based on reports and risk results. Finally, this research will boost innovation not only through models, engineering solutions and technologies but also in terms of policies and efficient and effective decision-making.

The main objective of the proposed research is resilient dams for Malaysia. The proposed research will develop physical resilient and intelligent dam safety management systems for safe communities and water supply sustainability by developing smart monitoring systems for evaluating the dam performance under various failure modes. The research will also provide a means to quantify, communicate, mitigate current and avoid the future risk associated with dams through social engagement and leveraging industry best practices across the dam safety community and a framework in which the public's awareness of the risks associated with living within the risk area of a dam failure will result in effective mitigation of current and future risk. By doing this research, a process will be developed for effectively conducting routine dam risk assessments and measuring reductions in risk and creating partnerships that successfully leverages Emergency Management and Dam Safety programs with

NADMA's Mitigation and Dam Safety programs. The research will integrate project outcomes into the Dam owner's hazard mitigation plan and use project results to effectively implement mitigation action, thus eliminating future risks and assisting the Government agencies/regulators such as JPS/BBA/KASA etc. in preparing standardized best practices for dam related risk assessments, emergency action planning, catastrophic long-term recovery planning, and risk communication. The research will come up with decision support models to assist in making risk-informed decisions to reduce overall dam risks and support Industrial Revolution 4.0 through dam data management, including cybersecurity.

The research supports Sustainable Development Goals (SDG) by ensuring availability and sustainable management of water and sanitation for all. (SDG 6), build resilient infrastructure, promote inclusive and sustainable industrialization and foster innovation. (SDG 9 and 11) and combat climate change and its impact (SDG 13). Moreover, the research supports the Sendai Framework by supporting DRR initiatives, strengthening disaster preparedness and increasing capacity in disaster response. Finally, we can conclude that the research will integrate all the five elements of the Quintuple Helix model, which represents Government, University, Industry, Civil Society and Environment and will establish a resilient and intelligent dam safety management.

References

1. ANCOLD, Australian National Committee on Large Dams (2003) Guidelines on Dam Safety Management, Australia
2. Basri H, Marufuzzaman M, Mohd Sidek L, Ismail N (2019) Investigation of multimodel ensemble performance using machine learning method for operational dam safety. In: International conference on dam safety management and engineering. Springer, Singapore, pp 625–632
3. Berrada G, Cheney J, Benabderrahmane S, Maxwell W, Mookherjee H, Theriault A, Wright R (2020) A baseline for unsupervised advanced persistent threat detection in system-level provenance. Futur Gener Comput Syst 108:401–413
4. Castillo-Rodríguez JT, Morales-Torres A, Escuder-Bueno I (2013). A risk-informed journey towards improved dam safety governance in Spain. In: De Andrés Rodríguez-Trelles M, Mazaira JP (eds) Second international dam world conference, Lisbon, pp 22–27
5. Chitsaz N, Banihabib ME (2015) Comparison of different multi criteria decision-making models in prioritizing flood management alternatives. Water Res Manag 29(8):2503–2525
6. Canadian Dam Association (2013) Dam Safety Guidelines. CDA, Canada
7. Fazli B, Abdullah MF, Zulkifli H, Kasim MF, Lee HL, Noh M, Yahya F (2019) Improvement of dam management in terms of WAM using machine learning. In: International conference on dam safety management and engineering. Springer, Singapore, pp 226–236
8. FERC, Federal Energy Regulatory Commission, Chapter 14 (2005) - Engineering Guidelines for the Evaluation of Hydropower Projects

9. Ghafir I, Hammoudeh M, Prenosil V, Han L, Hegarty R, Rabie K, Aparicio-Navarro FJ (2018) Detection of advanced persistent threat using machine-learning correlation analysis. Future Gener Comput Syst 89:349–359

10. Garba FA, Junaidu SB, Ahmad I, Tekanyi MS (2018) Proposed framework for effective detection and prediction of advanced persistent threats based on the cyber kill chain. Sci Pract Cyber Secur J 3(3):1–11

11. Ge W, Qin Y, Li Z, Zhang H, Gao W, Guo X, van Gelder P (2020) An innovative methodology for establishing societal life risk criteria for dams: a case study to reservoir dam failure events in China. Int J Disast Risk Reduct 49:101663

12. Han X, Pasquier T, Bates A, Mickens J, Seltzer M (2020) Unicorn: Runtime provenance-based detector for advanced persistent threats. arXiv preprint arXiv:2001.01525

13. Hossain M, Nair M, Mohd Sidek L, Marufuzzaman M (2019) A pre-release concept for reservoir management and the effect analysis on flood control. In: International conference on dam safety management and engineering. Springer, Singapore, pp 556–566

14. Huong TT, Bac TP, Long DM, Luong TD, Dan NM, Thang BD, Tran KP (2021) Detecting cyberattacks using anomaly detection in industrial control systems: a federated learning approach. Comput Ind 132:103509

15. International Water Power and Dam Construction (2019)Hydropower facilities: vulnerability to cyber attacks. https://www.waterpowermagazine.com/features/featureunder-cyber-attack-705 1600/

16. Jonkman SN, Jongejan R, Maaskant B (2011) The use of individual and societal risk criteria within the Dutch flood safety policy—nationwide estimates of societal risk and policy applications. Risk Anal Int J 31(2):282–300

17. Marufuzzaman M, Bin Ibne Reaz M, Rahman LF, Farayez A (2017) A location based sequence prediction algorithm for determining next activity in smart home. J Eng Sci Technol Rev 10(2):161–165

18. Marufuzzaman M, Tumbraegel T, Rahman LF, Sidek LM (2021) A machine learning approach to predict the activity of smart home inhabitant. 271–283

19. Marufuzzaman M, Reaz MBI (2013) Hardware simulation of pattern matching and reinforcement learning to predict the user next action of smart home device usage. World Appl Sci J 22(9):1302–1309

20. Sanit W, Weesakul U (2020) Application of IRIC software for flash flood disaster prediction in Laos and Thailand. In: Proceedings of the 22nd IAHR-APD congress 2020, Japan, pp 1–7

21. Sidek LM, Yalit MR, Djuladi DA, Marufuzzaman M (2021) Flood damage assessment for pergau hydroelectric power project using HEC-FIA. In: IOP conference series: earth and environmental science, vol 704, no 1. IOP Publishing, p 012002

22. Sidek LM, Marufuzzaman M, Rakhecha PR, Radzi MRM, Hossain MS, Zawawi H (2019) PMP driven probable maximum flood for 4 dams in sungai perak hydroelectric scheme. In: International conference on dam safety management and engineering. Springer, Singapore, pp 76–89

23. Sidek LM, Basri H, Mohammed MH, Marufuzzaman M, Ishak NA, Ishak AM, Omar BZC, Osman S, Ramly S, Hassan MH (2021) Towards impact-based flood forecasting and warning in Malaysia: a case study at kelantan river. In: IOP conference series: earth and environmental science, vol 704, no 1. IOP Publishing, p 012001

24. US Bureau of Reclamation (1989) Policy and Proceedings for Dam Safety Modification Decision Making, USBR

Sentiment Analysis and Topic Modeling for Identifying Key Public Concerns of Water Quality/Issues

Dwijendra Nath Dwivedi, Ghanshyama Mahanty, and Anilkumar Vemareddy

Abstract A Slovakian proverb says, "Pure water is the World's first and foremost medicine". Public opinion on water quality can play a critical role in the policy process, primarily because water quality determines the quality of health. The goal of the paper is to analyze Twitter data to extract feelings and opinions into unstructured text. We perform the topic extraction that discovers the keywords in sentiments that capture the text's recurring theme and is widely used to analyze large sets of sentiments to identify the most common topics quickly and efficiently. The main purpose of the article is to collect public opinion on Twitter to understand critical issues related to water quality. We used a few weeks of Twitter data and applied the principle of latent semantic analysis and decomposition of singular values to group key water quality questions that impact people's lives. People do realise that bad water deteriorates the quality of life, particularly for children. Also, there is a looming fear about imminent water, which bothers them a lot. They are hopeful that some of the measures like the Swatch Bharat Mission, Rally for River, Water Kiosk and applying Machine Learning and Artificial Intelligence solutions to provide safe and clean water could solve the crisis.

Keywords Water quality · Drinking water · Water pollution · Sentiment analytics · Twitter · Text clustering · Topic modeling

1 Introduction

Clean water and availability have been vital challenges and significant global goals across countries and agencies. The accessibility of water has been a concern at the

---

D. N. Dwivedi (✉)
Krakow University of Economics, Rakowicka 27, 31-510 Kraków, Poland
e-mail: dwivedy@gmail.com

G. Mahanty
Department of Analytical and Applied Economics, Utkal University, Bhubaneswar, India

A. Vemareddy
University of Agricultural Sciences, Bangalore, India

same time the quality of water as well. Water scarcity has also been caused by human-made poor water quality due to increased pollution, mainly releasing untreated large quantities of industrial waste. Emerging pollutants that include personal care products and pharmaceuticals, pesticides, and industrial and household chemicals, combined with future changes in climate patterns, may also exacerbate current and create new water quality challenges that still have unknown long-term impacts world's ecosystems and humans health (UNEP 2016).

Sentiment analysis is the process of detecting positive or negative sentiment in text. It's often used by businesses to detect social data sentiment, gauge brand reputation, and understand customers. Sentiment analysis models focus on polarity (positive, negative, neutral) but also on feelings and emotions (angry, happy, sad, etc.), urgency (urgent, not urgent), and even intentions (interested v. Not interested). This study wants to understand and analyze the sentiments of the public regarding the water quality challenges. The idea is to know if the majority of the tweets have positive sentiments or negative sentiments. At the same time, it would be essential to understand the key clusters and segments of positive and negative tweets.

The research aims to address the following primary question:

1. What is the distribution of positive and negative sentiments emerging from public tweets in the context of water quality challenges?
2. What are the key segmentations and clusters in the positive and negative sentiments?

2 Literature Study

Here is the referenced literature for the two steps and stages in our work.

2.1 Water Quality Challenges

Agricultural activities and domestic sewage are two main reasons for water pollution [22, 32]. Simultaneously, increasing personal care and pharmaceutical products is another water challenge source [4, 9, 18]. As per FAO, The Pesticides Use database includes data on significant pesticide groups (Insecticides, Herbicides, Fungicides, Plant growth regulators, and Rodenticides) and relevant chemical families. Data report the quantities (in tonnes of active ingredients) of pesticides used in or sold to the agricultural sector for crops and seeds. Information on amounts applied to single crops is not available—Food and Agriculture Organization of the United Nations (FAO). The current primary considerations safeguard public health and protect the aquatic environment [8, 19].

2.2   Sentiment Analytics Using Twitter

[1] analyzed consumers' views for major automobile Brands Using Twitter Data. He found that Audi has 87% of the positive tweets compared to 74% for BMW, 84% for Honda, 70% for Toyota, and 81% for Mercedes Guide. Andreea Kamiana (2015) explored the general sentiments and information dissemination concerning electronic cigarettes or e-cigs using Twitter and found that Twitter users are mainly concerned with sharing information (33%) and promoting e-cigs (22%). [28] found it is able to capture individuals' sentiments as they evolve while Exploring political sentiments on Twitter for opinion mining. [12] used Twitter data to determine the popularity of city locations of interest and public spaces in general. [17] compared the performance of the Naïve Bayes and Maximum Entropy classification methods for predicting market trends. [10] performed Sentiment analysis for tracking breaking events and found that his study offers diverse evidence to prove that Twitter has valuable information for monitoring breaking news worldwide. [31] evaluated public opinion tweets in driving investment decisions. [33] analyzed the sentiment and content Analysis of Twitter Content regarding Antibiotics' use in Livestock.

2.3   Text Clustering Methods

In order to manage the explosion of electronic document archives, new techniques or tools are required to organize, search, index, and review extensive data collections in a time-efficient manner [2]. As a generalization, there are two broad approaches to processing text- natural language processing (NLP) and statistics-based programs like topic modelling [24]. Unlike NLP methods that tag parts-of-speech and grammatical structure, statistical-based models like topic models are based mainly on the 'bag-of-words (BoW) assumption. In BoW models, the collection of text documents is quantified into a document-term matrix (DTM) that counts the occurrence of each word (columns) for each document (rows). [11] presented one of the first topic models using latent semantic analysis (LSA) and singular value decomposition (SVD), in which a large DTM is decomposed into a set of about 100 orthogonal factors from which the original matrix can be approximated by linear combination. They assumed some underlying latent semantic structure and used statistical techniques to estimate this latent structure.

[6] presented a framework to leverage the topic modelling technique for performing an exploratory literature review of an extensive collection of papers. The framework proposed by them enables a large volume of documents to be reviewed in a transparent, efficient, and reproducible way using the LDA method. In general, there are two methods for automatically processing documents- Supervised learning and unsupervised learning. Supervised learning includes manually coding a collection of documents before conducting an analysis, which involves a high amount of time to achieve the result. On the other hand, unsupervised learning methods, such

as topic modelling, do not have the prerequisites to manually code the documents, saving a lot of time for an exploratory review of the extensive collection of papers. Leverage topic modelling and data visualization methods to analyze student feedback comments from seven undergraduate courses taught at Singapore Management University. They assessed rule-based methods and statistical classifiers for extracting the topics. [3] further proposed an opinions sandbox for topic extraction, sentiment analysis for pulling issues and their associated sentiments from a database. They used LDA for topic extraction and the "bag-of-words" sentiment analysis algorithm, where polarity is determined based on the frequency of positive/negative words in a document. [7] highlight the standard approaches of sentiment analysis in social media streams and related cloud computing issues. Big data is divided into four features, namely four V's of big data- volume, velocity, variety, and Veracity. Volume is the most considerable amount of data that should be stored and processed. Velocity is the frequency of the incoming data. Variety describes different data types, whereas Veracity refers to the trustworthiness and accuracy of the data available.

Ajeet Ram [29] proposed approach is that it works at the sentence level to extract the topic using online latent semantic indexing with regularization constraints. Md. Mokhlesur [30] attempted to explore the factors associated with positive and negative sentiments of the people about reopening the economy in the United States (US) amidst the COVID-19 global crisis. It took into consideration the situational uncertainties (i.e., changes in work and travel patterns due to lockdown policies), economic downturn and associated trauma, and emotional factors such as depression. [26] showed that consumers overreact to negative news and negative pre-news sentiment intensifies such overreaction, leading to negative herding. Tirta Hema Jaya [23] research was conducted to analyze the public's sentiment about this development which was divided into three categories: pro, contra, and material related to development on Rinca Island by the Indonesian Government. [35] used online reviews of air purifiers in the Chinese market to identify multi-word product attributes. [27] examined tourist public responses to crisis communications during the early stages of Covid-19. Using the social-mediated crisis communication model. [21] attempted to use contextual text analytics to identify product or service features that drive the sentiment of the user. [13] perfomed sentiment analytics and topic modeling on government actions and document post COVID comparing united arab emirates and Kingdom of Saudi Arabia. [16] performed topic and sentiment analysis using twitter data to identify key concern on data quality and data impurity. [14] attempted to use contextual text analytics to categorize Twitter data to understand the positive or negative sentiments for COVID vaccinations and wish to highlight key concerns. [15] analyzed approved areas of medical research related to COVID-19 from the United Arab Emirates (UAE) and World Health Organization (WHO) in order to identify key topics and themes for these two entities.

Fig. 1 Process flow for
topic modeling
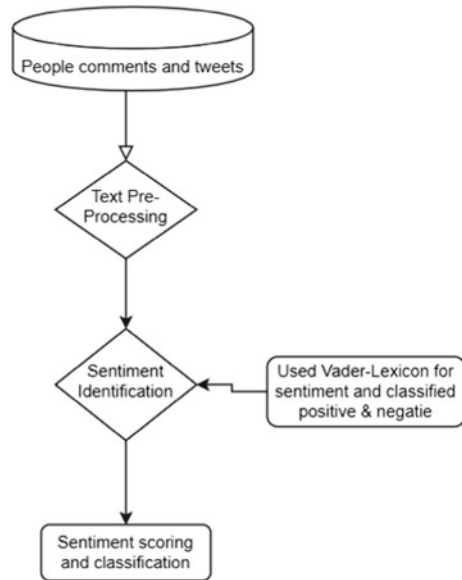
3 Data Source

Our study has extracted the people's tweets regarding the drinking water quality, water crises, and pollution issues in recent years. We have focused on people's opinions, attitudes, and emotions toward an entity. The entity can represent individuals, events, or topics.

This dataset has been extracted from Twitter and includes 9700 tweets from different parts of the world. All the tweets are related to the water quality challenges. We analyzed these tweets regarding water challenges from Feb 2021 to March 2021. Data collection was done from Twitter Firstly. We decided on the specific words/related words (#hashtags) for the study. We have collected more than 9700 tweets on water quality, drinking water, and other associated words (Fig. 1).

4 Results

4.1 Preprocessing Text

The data have been extensively cleaned before the sentiment polarity calculations. The steps included.

This step is needed for the text analysis to transform human language into a machine-readable format for further processing and analysis. There are a few mandatory steps to apply for cleaning the texts, which are listed below.

- Convert all the text to lower case
- Removing stop words, sparse terms, and particular words
- Convert numbers into words or remove the numbers
- Removing white spaces (leading and ending spaces)
- Removing punctuation (all types of special characters or symbols)

Firstly, we started removing the duplication of rows, and it's essential to remove the duplicate data or rows to avoid unbiased results. Convert all the text into lower cases to prevent multiple copies of the same word. For example ("drinking water" Drinking water" will be considered as two different words).

We were removing punctuation because it does add any extra information while handling text data. And also, it will reduce the size of the training dataset. We are eliminating stop words that are frequently occurring words in the text or creating the list of stop words, or using predefined libraries. We have used stopword and text, blob libraries which will handle the stopwords. In the steward's, we removed commonly occurred words in the general scenario, but we can also remove the naturally occurring comments from our text data. So we can check the ten words frequently occurring words, then decide which one to remove.

Spelling correction of the text, we have considered the tweets, we have seen the tweets with many spelling mistakes, or short words will be used. In this situation, the spelling correction step is beneficial in reducing multiple copies of the word. For this, we have a Textblob library it will handle spelling mistakes.

Tokenization refers to dividing the text into a sequence of words or sentences. In our example, we have used the text blob library to transform our tweets into a blob and then convert them into a series of words.

Stemming refers to the removal of suffices, like "ing," "ly," "s," etc., by a simple rule-based approach. For this purpose, we will use PorterStemmer from the NLTK library.

Lemmatization is a more practical option than stemming because it converts the word into its root word, rather than just stripping the suffices. It makes use of the vocabulary and does a morphological analysis to obtain the root word. Therefore, we usually prefer using lemmatization over stemming.

We have done all the basic preprocessing steps to clean the text, and now we need to extract the features using natural language techniques.

N-Grams are defined as a combination of multiple words used together. We have used N-grams, bigrams, and trigrams. Unigrams will not do not have much information as compared to bigrams and trigrams. We use these bigrams or trigrams to capture the language's structure, like what letter or word is likely to follow the given one. These Ngrams will depend on the application of our study. Sometimes, if we use low grams and fail to capture the essential differences or sometimes take long grams, it will fail to capture the sentence's general meaning.

Part-of-Speech Tagging (POS)
Part-of-speech tagging mainly assigns speeches to each word of the text based on its context and definition (nouns, verbs, adjectives, and others) (Figs. 2 and 3).
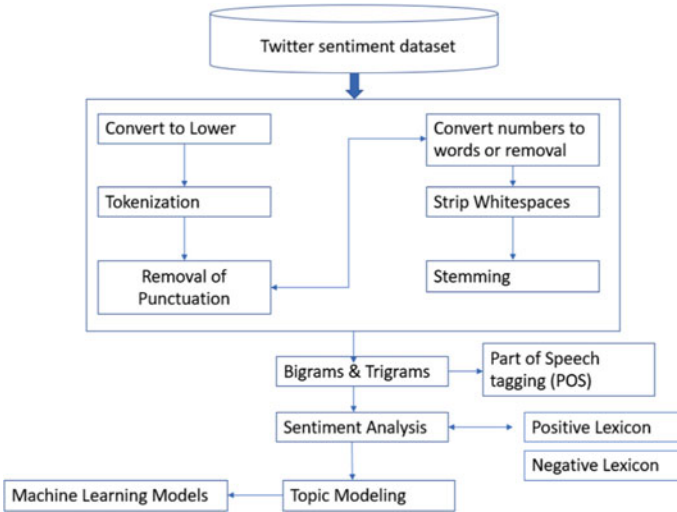
Fig. 2 Pre-processing process for sentiment analysis

Fig. 3 Word cloud before sentiment analysis and topic modeling

Sentiment analysis is a natural language processing technique used to determine whether data is positive, negative, or neutral. Sentiment analysis for free-flowing text like Twitter data can effectively combine natural language processing (NLP) and machine learning algorithms to deduce sentiment scores to a sentence or phrase. Sentiment analysis can give an idea about public opinion, brand reputation, key concerns, customer experience, customer perception, and an overall index of how optimistic the common public is about a topic of interest, which is the people's attitude towards covid vaccinations.

4.2 Sentiment Analysis

There are four layers of a sentiment analysis engine: the first step is to break down the raw text into a list of different components that are sometimes referred to as tokens. The tokenization process breaks down the introductory text into keywords, meaningful keywords that reflect the person's emotions. The next step is to isolate art or the tokens which are sentiment bearing and ignore the rest. The third step is to assign polarity scores to each component of the tokens. This is done by referring to different sentiment libraries depending on the program employed. For example, we utilized the text-blob library in Python to calculate each tweet's sentiment polarity in our data. We transformed the text data and created word vectors. We then used the text blob library to calculate the sentiment scores for the tweets. Text blog uses naive Bayes (probabilistic algorithms that use Bayes's Theorem to predict a text's category) classifier to assess a sentence's polarity. It generates a score ranging between -1(strongly negative) to +1 (strongly Positive). This is the crucial aspect of sentiment analysis as it tries to understand the opinion or the Orientation of the sentiments expressed in a text. This aspect is quantified with a positive or negative value, called polarity. Identifying the range of polarity scores to be classified as Positive, Neutral, or Negative Sentiment: Read its extensive analysis of the polarity scores and looked at the distribution of these scores and man Willie eyeballing the sentiment expressed in a text. Furthermore, we created score ranges that define whether a text's sentiment was very positive, positive, neutral, very negative, or negative.

Following is the data distribution of the sentiments in the data (Figs. 4, 5 and 6):

Sentiments	Counts
Neutral	4050
Positive	2481
Very positive	2126
Negative	615
Very negative	436

Fig. 4 Sentiments segmentations
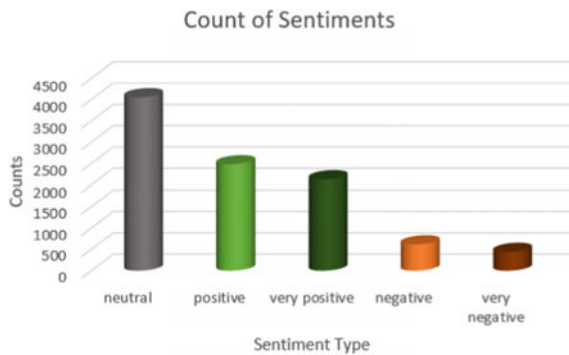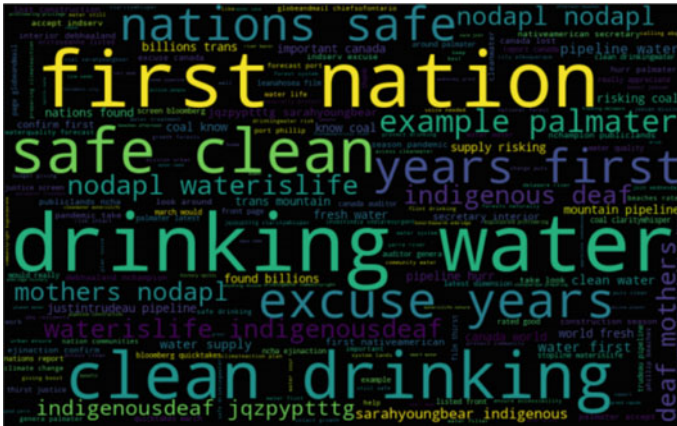
Fig. 5 Word cloud for positive sentiments

Fig. 6 Word cloud for negative sentiments

Here is the word cloud for positive and negative sentiments.

4.3 Topic Modelling

The fundamental idea of applying classical data mining techniques to topic modeling relies on transforming text data (unstructured) to numbers (structured). Topic modeling is the process of extracting or obtaining required features from the bag of words. This is very important because each word present in the corpus has considered a feature in natural language processing. This feature reduction will help us to

focus on the right content instead of going through the entire text in the training data. Many methods are used for topic modeling in that LDA is one of the ways we have used in our study. LDA Latent Dirichlet Allocation is a statistical and graphical model used to obtain relationships between multiple documents in a corpus. It is developed using the Variational Exception Maximization algorithm for obtaining the maximum likelihood estimate from the whole corpus of text. Traditionally, this can be solved by picking out the top few words in the bag of words. However, this completely lack the semantics in the sentence. This model follows the concept that the probabilistic distribution of topics can describe each document, and the probabilistic distribution of words can explain each topic. Thus, we can get a much clearer vision of how the topics are connected. It will consider all corpus of entire documents in the data. After preprocessing of the corpus, each bag of words consists of common words. Using this LDA model, we can determine the topics related to each document, and it will group all corpus into a particular group. We can see in the below screenshot our study results.

5 Topic Modeling of Negative Sentiments

5.1 Model Performance Checking Using Perplexity

The measure traditionally used for topic models is the \textit{perplexity} of held-out documents wd defined as

$$\text{perplexity(test set w)} = \exp\{-L(w)/\text{count of tokens}\}$$

which is a decreasing function of the log-likelihood L(w) of the unseen documents wd; the lower the perplexity, the better the model. We have got a very low confusion and Coherence score.

Perplexity: -9.508201741554696
Coherence Score: 0.4371544825332605

Topic models play an essential role in exploring text data when we have a large volume of data to understand the structures and groups that we could find. From Table 1, we have seen the negative sentiments and related topics discussed in the Twitter text data about drinking water destroys due to not following basic rules and regulations. Other topic groups say polluted water is more dangerous and deadly. Globally, more than 700 million people don't have drinking water accessibility, and the catholic water relief services are working on these. The topic has discussed in Flint water crisis case has a significant effect on the health failure to provide quality drinking water and supplied highly contaminated flint river water many small children harmed due to the poisoning.

Table 1 Cluster: negative sentiments segmentations

Segments	Topic modeling: negative sentiments
	0: "transboundary, +lawmaker, +relax, +livingshoreline, +sewageoverflow",
	1: "supply_link, +limits_cancer, +smartdissent_destroye, +that_pollute, +causing_coalash",
	2: "unpleasant_deadly, +close, +catholicrelief_pollute, +drink, +people",
	3: "personal +hiking, +lifestraw, +camping, +travel",
	4: "state, +community, +climatesolution, +essential, +cleanenergy",
	5: "justintrudeau, +promise, +border, +dictator, +medium",
	6: "aguaclan, +limited, +ncoimbatore, +nsomayampalayam, +elanxozdgp",
	7: "damaging, +push, +winter, +storm, +anywhere",
	8: "flintwatercrisis, +governor, +say, +michigan, +duty",
	9: "ulhsno, +tfjwppn, +clean, +more, +ntap"

5.2 Key Identified Negative Topics

The grave water crisis in Bangladesh with almost more than 60 percent do not have access to safe drinking water. Large city to face Water scarcity, High pneumonia, Taster, odor, Straining cloths Nuke dump illegal dump and landfill. Over 6,500 new cases of bladder cancer in Europe are caused by exposure to chemicals called trihalomethanes (THM) found in drinking water. This number adds up to almost 5% of all bladder cancers in the continent.

6 Topic Modeling of Positive Sentiments

(See Table 2).

6.1 Model Performance Checking Using Perplexity

Perplexity: -10.002978035181536

Table 2 Cluster: positive sentiments segmentations

Segments	Topic modeling: positive sentiments
	0: "good, +rate, +bharat_mission, +nurban_swachh, +solid_liquid",
	1: "cleanwat, +cleanwater, +join, +support, +thank",
	2: "coal, +fresh, +sure, +join, +stopline",

(continued)

Table 2 (continued)

Segments	Topic modeling: positive sentiments
	3: "example, +palmater, +nation, +excuse, +there",
	4: "restore, +health_improve, +roads_national, +forest_system, + lands_decommissione",
	5: "flintwatercrisis, +flint, +still, +protect, +safe",
	6: "would_really, +appreciate, +quicktakes_march, +cleanwater, + provide",
	7: "nature, +dharamifs_anythe, +divine_planet, +life, +visit",
	8: "open, +flows_built, +moment_every, +tell, +receive",
	9: "supply, +canada, + world, +important, +risk"

Coherence Score: 0.33237480772989636

From the table two above topic results to improve the water quality, new schemes and initiatives are taken in the urban community and succeed. As humans, we all need to join our hands in part of any initiatives or strategies. From topic four of the discussions, we can restore the water resources to improve health by protecting the land's natural forests and water levels. We can identify the water crisis and clean and safe water protection in public from the other issues.

6.2   Key Identified Positive Topics

People are generally happy about some of the new initiatives governments are taking around the world. One such program is called the "Swachh Bharat Mission initiative introduced by the Government of India in 2014. Under this program, there has been a comprehensive plan not only to provide clean drinking water to reduce groundwater contamination by checking open defecation and putting efficient, solid and liquid waste management policies in place (Ministry of Drinking Water and Sanitation 2017). Americans have been buoyant about Present Biden reversing earlier president Trump's 'dirty water rule'. President Biden pledged to protect America's 30 percent of the nation's land, freshwater, and ocean area by 3030 which he calls a "30X30" challenge. There has been a lot of positive discussions around adopting smart water management system power by machine learning and artificial intelligence technologies. IoT and Machine learning solutions can be applied to measure water quality parameters like pH, turbidity, color, DO, and conductivity [5]. Women leadership started playing a critical role in the water management area. Men are often away from home and it's the female members play a critical role in the day-to-day management of water in the household. Women representation and participation in the overall over management and sanitation. "Rally for the River" is India's most revered campaign to connect rivers for better management of water resources. One

of the most effective means to enlarge the irrigation potential of river command areas is the Inter Basin Water Transfer (IBWT). It refers to the water transfer from water surplus rivers to the water deficit rivers or regions. Water Kiosk or water ATMs seem to be a positive solution for countries in Sub Sharan Africa and the Asia Pacific continents.

Discussions around Blue-Green Infrastructure (BGI) for stormwater management in the urban centers are another super alternative to piped water management across six municipalities in Bejing and Copenhagen.

7   Conclusion

The democratic process allows people to form and communicate their opinion on many issues that impact their lives. Social media platforms are easier to express their opinion and feelings about issues. We have used Twitter data and natural language modelling techniques to group these themes to appreciate the effort and initiatives the public policymakers took and convey their grievances relating to exact water quality issues that negatively impact current and future generations.

Our sentiment and topic models have pinpointed some of the key challenges from negative sentiments. The policymakers need to take these themes and expect to initiate dialogue with the masses to get to the bottom of the issues and formulate better and meaningful solutions. The paper's key contribution is to use the latest text mining principles and identify these themes from social media platforms like Twitter.

Our study has considered all the aspects of water issues covering water shortage, pollution, and crisis. The study usages two weeks of data from the Twitter platform and applies the LDA model for topic modelling and sentiment analysis for identifying key issues that need urgent attention from policymakers.

We observe that government initiatives worldwide have created positive differences in the quality and availability of water, which need to be appreciated and further expanded. The paper's key contribution is the identification of such relevant themes from social media. People are concerned that there should be a focus on saving drinking water and protecting water quality. However, the government and other NGOs have issued many schemes and initiatives to create awareness to save water and human lives. The human community should be responsible for following the rules and other practices to protect the water quality.

References

1. Asghar Z, Ali T, Ahmad I, Tharanidharan S, Nazar SKA, Kamal S (2019)Sentiment analysis of automobile brands using twitter data. In: Communications in computer and information science, vol 932. Springer, Singapore. https://doi.org/10.1007/978-981-13-6052-7_7

2. Alghamdi R, Alfalqi K (2015) A survey of topic modeling in text mining. Int J Adv Comput Sci Appl 6(1):147–153. https://doi.org/10.14569/ijacsa.2015.060121

3. Al-Obeidat F, Kafeza E, Spencer B (2018) Opinions sandbox: turning emotions on topics into actionable analytics. In: Lecture notes of the institute for computer sciences, social-informatics and telecommunications engineering, LNICST, vol 206, pp 110–119. https://doi.org/10.1007/978-3-319-67837-5_11

4. Aristizabal-Ciro C, Botero-Coy A, López F, Peñuela G (2017) Monitoring pharmaceuticals and personal care products in reservoir water used for drinking water supply. Environ Sci Pollut Res 24:7335–7347

5. Ashwini K, Vedha JJ, Priya MD (2019) Intelligent model for predicting water quality. Int J Adv Res Ideas Innov Technol 5(2):70–75

6. Asmussen CB, Møller C (2019) Smart literature review: a practical topic modeling approach to exploratory literature review. J Big Data 6(1). https://doi.org/10.1186/s40537-019-0255-7

7. Benedetto F, Tedeschi A (2016) Big data sentiment analysis for brand monitoring in social media streams by cloud computing. In: Studies in computational intelligence, vol 639. https://doi.org/10.1007/978-3-319-30319-2_14

8. BoydD (2006) The water we drink: an international comparison of drinking water standards and guidelines. David Suzuki Foundation, Vancouver, p 34

9. Chèvre N (2014) Pharmaceuticals in surface waters: sources, behavior, ecological risk, and possible solutions. case study of lake Geneva, Switzerland. WIREs Water 1:69–86

10. Choi D, Kim P (2013) Sentiment analysis for tracking breaking events: a case study on Twitter. In: Lecture notes in computer science (including subseries lecture notes in artificial intelligence and lecture notes in Bioinformatics), vol 7803 LNAI(PART 2), pp 285–294. https://doi.org/10.1007/978-3-642-36543-0_30

11. Deerwester S, Dumais ST, Furnas GW, Landauer TK, Harshman R (1990) Indexing by latent semantic analysis. J Am Soc Inf Sci 41(6):391–407

12. Dinkić N, Džaković N, Joković J, Stoimenov L, Đukić A (2018) Using sentiment analysis of Twitter data for determining the popularity of city locations. Adv Intell Syst Comput 665:156–164. https://doi.org/10.1007/978-3-319-68855-8_15

13. Dwivedi DN, Anand A (2021) The text mining of public policy documents in response to COVID-19: a comparison of the United Arab Emirates and the Kingdom of Saudi Arabia. Public Govern/Zarządzanie Publiczne 55(1):8–22. https://doi.org/10.15678/ZP.2021.55.1.02

14. Dwivedi DN, Pathak S (2022) Sentiment analysis for COVID vaccinations using twitter: text clustering of positive and negative sentiments. In: Hassan SA, Mohamed AW, Alnowibet KA (eds) Decision sciences for COVID-19. International series in operations research & management science, vol 320. Springer, Cham. https://doi.org/10.1007/978-3-030-87019-5_12

15. Dwivedi DN, Anand A (2022) A comparative study of key themes of scientific research post COVID-19 in the United Arab Emirates and WHO using text mining approach. In: Tiwari S, Trivedi MC, Kolhe ML, Mishra K, Singh BK (eds) Advances in data and information sciences. Lecture notes in networks and systems, vol 318. Springer, Singapore. https://doi.org/10.1007/978-981-16-5689-7_30

16. Dwijendra ND, et al (2021) Identification of key concerns and sentiments towards data quality and data strategy challenges using sentiment analysis and topic modeling. In: 30th SKAD conference, Poland

17. Esiyok C, Albayrak S (2015) Twitter sentiment tracking for predicting marketing trends. Adv Comput Vis Pattern Recogn 66:47–74. https://doi.org/10.1007/978-3-319-14178-7_2

18. Ebele A, Abdallah M, Harrad S (2017) Pharmaceuticals and personal care products (PPCPs) in the freshwater aquatic environment. Emerg Contam 3:1–16

19. EPA – Environmental Protection Agency (2001) Parameters of water quality. Interpretation and standards. Environmental Protection Agency, Wexford, p 132

20. Godea AK, Caragea C, Bulgarov FA, Ramisetty-Mikler S (2015) An analysis of Twitter data on e-cigarette sentiments and promotion. In: Lecture notes in computer science (including subseries lecture notes in artificial intelligence and lecture notes in bioinformatics), vol 9105, pp 205–215. https://doi.org/10.1007/978-3-319-19551-3_27

21. Gupta A et al. (2021) Understanding consumer product sentiments through supervised models on cloud: pre and post COVID. Webology 18(1): 406–415. https://doi.org/10.14704/web/v18i1/web18097

22. Habersack H, Samek R (2016) Water quality issues and management of large rivers. Environ Sci Pollut Res 23(12):11393–11394

23. Hidayat THJ, Ruldeviyani Y, Aditama AR, Madya GR, Nugraha AW, Adisaputra MW (2022) Sentiment analysis of twitter data related to Rinca Island development using Doc2Vec and SVM and logistic regression as classifier. Procedia Comput Sci 197:660–667

24. Hofmann T (2001) Unsupervised learning by probabilistic latent semantic analysis. Mach Learn 42(1–2):177–196. https://doi.org/10.1023/A:1007617005950

25. Jeet P, Kumar A, Sundaram, PK (2020) Interlinking of river: issues and challenges. Hydrology

26. Kim JJ, Dong H, Choi J, Chang SR (2022) Sentiment change and negative herding: evidence from microblogging and news. J Bus Res 142:364–376. https://doi.org/10.1016/j.jbusres.2021.12.055

27. Obembe D, Kolade O, Obembe F, Owoseni A, Mafimisebi O (2021) Covid-19 and the tourism industry: an early stage sentiment analysis of the impact of social media and stakeholder communication. Int J Inf Manag Data Insights 1(2):100040

28. Olorunnimbe MK, Viktor HL (2015) Tweets as a vote: exploring political sentiments on Twitter for opinion mining. In: Lecture notes in computer science (including subseries lecture notes in artificial intelligence and lecture notes in bioinformatics), vol 9384, pp 180–185. https://doi.org/10.1007/978-3-319-25252-0_19

29. Pathak AR, Pandey M, Rautaray S (2021) Topic-level sentiment analysis of social media data using deep learning. Appl Soft Comput 108:107440

30. Rahman MM, Ali GMN, Li XJ, Samuel J, Paul KC, Chong PH, Yakubov M (2021) Socioeconomic factors analysis for COVID-19 US reopening sentiment with Twitter and census data. Heliyon 7(2):e06200

31. Rao T, Srivastava S (2014) Twitter sentiment analysis: how to hedge your bets in the stock markets, pp 227–247. https://doi.org/10.1007/978-3-319-05912-9_11

32. Smith V (2003) Eutrophication of freshwater and coastal marine ecosystems is a global problem. Environ Sci Pollut Res 10:126–139

33. Steede GM, Meyers C, Li N, Irlbeck E (2018) *A Sentiment and Content Analysis of Twitter Content Regarding the use of Antibiotics in Livestock*. *102*(4).

34. Wesslen R (2018) Computer-assisted text analysis for social science: topic models and beyond. ArXiv

35. Zhang J, Zhang A, Liu D, Bian Y (2021) Customer preferences extraction for air purifiers based on fine-grained sentiment analysis of online reviews. Knowl-Based Syst 228:107259

Islamic Institutional Arrangements of the Aflaj Systems Maintenance in Sultanate of Oman: Operation of the Different *Aflaj* Type Case Study

Ahmed S. Al-Marshoudi and Jasni Sulong

Abstract The *aflaj* (singular *falaj*) among the most ancient system in Sultanate of Oman, not only collect/extract water from alluvial aquifers, but characterized by holding traditional knowledge/institutional arrangements based upon Muslim jurist view. Since there exists physical water extraction variation over these aquifers, three aflaj type normally classified known as *daudi, ghaili* (oasis) and *ayni* (spring). This paper used a sample of these three types to capture the physical-extraction variation in the aim to examine and document the historical methodology undertaken to develop different institutional arrangements. Although there exist three water-extraction processes in Oman, the finding clearly classified the three *aflaj* types with respect to institution for maintenance into two main categories. The first category considered more complex and hold several sophisticated components or its main water source were constructed near oasis which cause severe damage from the occasional heavy rain flood. Because of this, forced the local to develop institution based on water market. The second category was identified of being simple and was constructed away from flooded areas. This thought to require less financial support for maintenance. Hence, the survey provided evidence by which places *daudi* and *ghaili* within the first category and *ayni* system in the other.

Keywords Institutional arrangements · Scarcity · Water allocation · Water rights

1 Introduction

While several regions in the northern part of Sultanate of Oman rely heavily upon a single community-owned *falaj* for irrigating their date gardens and other annual crops [1], historically these communities characterized by a legal boundary defined over Muslim legal law. [21] used a term locally known as *sawadir al-bilad* (literally means

A. S. Al-Marshoudi (✉) · J. Sulong (✉)
Islamic School, School of Humanities University Sains Malaysia, 11800 Pulau Pinang, Malaysia
e-mail: almarshoudi4@gmail.com

J. Sulong
e-mail: jasni@usm.my

the village boundary) as he included things like walls, channels, bridges, building and gardens. Zekri and al-Marshudi [23] referred it as falaj protected zone and sited (Caponera 1978) to define such zone, stated: customary laws were commonly used as a legislative tool to declare a protected area extending over a 25 m radius around the falaj infrastructure where well digging is not allowed because it affects the falaj flow" (P. 355). These Muslim developed boundaries created a more permanently administered villages which suited the development of water rights since millenniums. Along these physical legal boundaries, there exist what known as aflaj traditional knowledge/institutional arrangements [16]. This knowledge was, and still form the core for the community, not only provided/developed tools to generate income for maintenance, motivated all member to participate in protecting the whole system. For example, since frequencies of the drought period can damage the whole systems, continuous cooperation by all members of the community is required [3, 5]. In the past [19] linked this knowledge in generating income for system survival, stated "…by tradition the *falaj* institution owns property from which the income necessary for its continued survival comes" (P. 9). Whereas [16] discussed the aflaj traditional knowledge with the adaptation toward the country agricultural modernization; She wrote "… after the modernization of agriculture resulted in competing interests over water, mean that traditional knowledge systems need to adapt to this challenge" Page. 135. However, much have been written about aflaj-physical structural setting [1, 2], with little information with respect to the aflaj tradition knowledge/institutional arrangements, a part of [16] more recent study. Hence, in this paper, we suggest that we can now begin to move beyond the simple descriptive way to a rather sophisticated analysis. It is worth noting that [16] placed the *aflaj* with a common management collective action framework from two supportive claims: 1) the first aspect is concerned with the fact that the main source of the water (in this case is the aquifer) can be considered as forming a collective action for the whole community. 2) the second aspect is related to social organization in forming a cooperative collective action by distributing water equitably. This paper provides further investigation of the management and development of the *aflaj* institutional arrangements from Islamic point of view. The primary objective of this study is to further investigate this institution within the context of physical water extraction variation. To do this, it is important to include a sample comprised the three existing *aflaj* types. The fieldwork was conducted over a period of four years; 2014 to 2018 in several governing region at the Northern part of Oman.

2   Problem Background

There is agreement among researchers that in order to solve the ever-growing water demand (water scarcity) globally, it requires to introduce regulatory measures. There have been several of these measures. However, the most discussed and analyzed is

what referred as tradable water rights. This have been introduced/proposed within the efficiency concept and the related water-market approach [24]. Here the arguments have been viewed from two different angles: water can be treated as an economic good/commodity which can be evaluated within the efficiency criteria [4, 6], or the price of water will reflect its true scarcity and its opportunity cost [13, 14]. Another evaluating criteria used in examining water is the concepts of equitably. This is very much concerned with the social aspects with respect in distributing water equitably so that disputes among beneficiaries are minimized. Although extensive coverage of the efficiency concept and the market-oriented strategy [4, 24], difficulty in adjusting between social (equitably) and the private benefit (efficiency) have been observed. For instance, while several researchers have been calling for tradable water rights and to propose/develop a water market within the efficiency water pricing approach [17, 18], other are against the idea of establishment of a water market because, as they think on one hand, water is a social commodity [7] and on the other hand may be prone to a market failure due to physical characteristic of a watercourse [10, 15, 22]. With this in context, many researchers and water proficiencies studied several of the ancient small community-managed irrigation systems worldwide. For example, the Nepal farmer-managed irrigation system [12], the communal tenure in Swiss villages [11], canal irrigation system in India [9] and indigenous water distribution system in Andean village, Peru [20]. Although these provided much discussion with respect to the indigenous knowledge of water distribution, limited insight provided concerning the development of water rights and their associated institutional arrangements. However, it believed that the ancient aflaj system (singular falaj) in Oman have been studied over a wider contribution matter with regard to the water rights and associated legal context since millennium [23]. Although studies such as [1] and [23] placed the system within a competitive market and tradable water rights frameworks, provided limited insight into institutional arrangements. It is acceptable to place the system within the context of competitive tradable water rights, but these institutional arrangements must be evaluated within the three aflaj type's physical variation (see below).

3   Overview of the Aflaj System Water Extraction Process

[8] classified *aflaj* into three different types and cited Costa (1983) definition for each: *daudi* drain water from aquifers, *ghaili aflaj* channeling surface from *wadis* (oasis), and *ayni* ones are connected to springs. Despite the fact that *daudi* and *ayni* type originate/extract their water from aquifer/underground, differ in extraction method. For example, for the daudi type an underground tunnel, extending deep into the aquifer (but was constructed at a level of the upper part of the aquifer to allow natural flowing by gravity over the tunnel) with serial of vertical-*shaifts* (for ventilation and maintenance) were built. Whereas the *ayni* water sources naturally (mainly in limestone rocks) come up to the surface, as can be seen, with a short open channel constructed to convey water to the irrigated areas. In contrast, the

situation for the *ghaili* type is completely different as follow: it extracts water from surface of an oasis (*wadis)* 2) uses open short channel in transporting water to the irrigated areas. These then offers a useful requirement to evaluate the aflaj institutional arrangements. We argued that since the *daudi* type extract water from deep of the aquifer/away from irrigated areas, a more complex institutional arrangements with high community involvement is expected. In contrast, since the ayni and ghaili type extract water from short distance of the irrigated areas with open simple channel, less complex institutional arrangement is expected.

4   Method and Study Site

To investigate the aflaj traditional knowledge/institutional arrangements) for its maintenance, the physical extraction variation among the three types must be included. First, we need to evaluate how aflaj institutional arrangements embedded its physical extraction variation. To do this, require providing thorough understanding of the three-water extraction processes for the three aflaj. Second, based on survey finding to what extent these three methods can be further classified. The study used primary as well as secondary sources of information. These sources were structured over the preparatory data collection framework. First, information related to the primary sources which is based on in-depth interview in the various villages, with repeated visits and time spent interacting with people in these communities. Second, to identify the main stakeholder's bodies which have close contact with the system. These can be divided into two main categories: the private stakeholders including private community members, such as the aflaj committee members (wakeels, areefs, auctioneers, recorders and aflaj historical expertise) and individual farmers, and the public official bodies, such as the most relevant Omani official Ministries. Using a case study approach, nine aflaj among the three types were selected. These aflaj located in four main areas: Nizwa, Smail, rustaq and Tawwi, all of which situated in the northern part of the country (Along the main sample of the five aflaj (which were included on the UNESCO heritage list in the year 2006 (MRMWM 2008)). In addition, these areas belong to three main regions: Dakhiliya (the interior) hold the area of Nizwa and Smail, Southern Al-Batinah hold the area of Rustaq and Al-Sharqyah hold the area of Tawwi (Fig. 1). The main selective criteria are the popularity of each falaj within their category. For example, falaj daris in Nizwa, by which considered as the largest in the region, selected to represent the daudi type. Similarly, falaj al-samdi in Samail represent an example of the oasis falaj type.
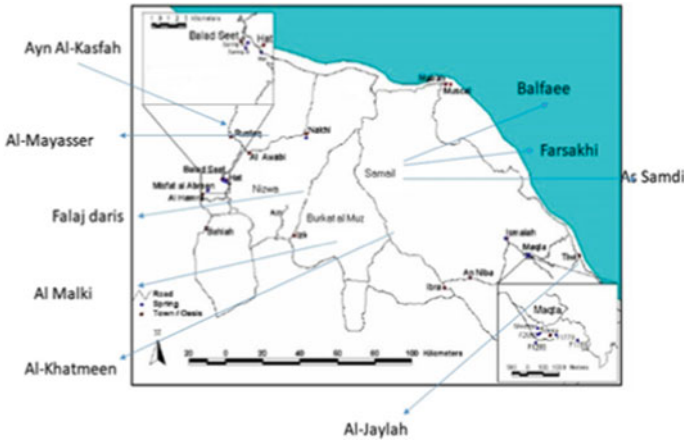
Fig. 1 Location of the studied aflaj over the Northern part of Oman

5 Result

In Oman the natural water storage and infiltration occurred primarily due to the presence of the mountainous wide range. This is represented by the presence of two main mountains: al-*hajir* mountain range and al-*jebal akhdar* (Green Mountain). This study identified, in general, that there are three different water extraction processes, close linked to the existence of the mountainous range indicated above, in northern Oman. The first source is characterized by perennial water-flow by which is water extracted from the upper part of the aquifer in the mountains, by which it is achieved through the use of a long underground tunnel. Hence, the local use the term *daudi* to refer to this traditional construction-engineer of a long tunnel. Special visit was arranged to view this type of aflaj. For example, *falaj khatmeen* in the village of *burkat al-mouz* and *falaj al-malki* in the town/wilayat of Izki were visited to view their physical-constructive layout (see Fig. 2).

The second source normally extracts water from the surface of wadi (oasis). This is considered as seasonal fluctuated flow. Hence, the word *ghail* has been employed by the locals referring to all *ghaili aflaj* system which uses the flow of the permanent oasis flow. During the survey, particular visits were paid to view this water source in Oman represented by viewing *falaj as-samdi* in *Samail* (see Fig. 4). The third source known as perennial natural-spring flow extracts water from a spring that naturally comes to the surface, mainly in limestone rocks. Hence, ayn is a word very often employed by the local refer to a natural occurring phenomenon of perennial flow since millennium. Again, a particular visit was paid during the field survey to view the most ancient *ayni falaj*, *ayn al-khasfah* (see Fig. 3).

Fig. 2 Field survey constructed *daudi* identified components. The picture (left side) indicated a man-waking tunnel for *falaj al-khatmeen* in the district of *burkat al-mouz* (approximately 2,450 m long with a two-meter width and one meter height), as indicated above. The second picture (right site) shows author viewing, along with *falaj al-malki* wakeel (administrative agent), a one ventilation shaft which deeply is attached to the tunnel forming a horizontal tunnel attached with serial of these shafts. The main function of these is to allow air inside the tunnel and also as a means to get rid of the dirt from the tunnel construction, and later used as access for maintenance
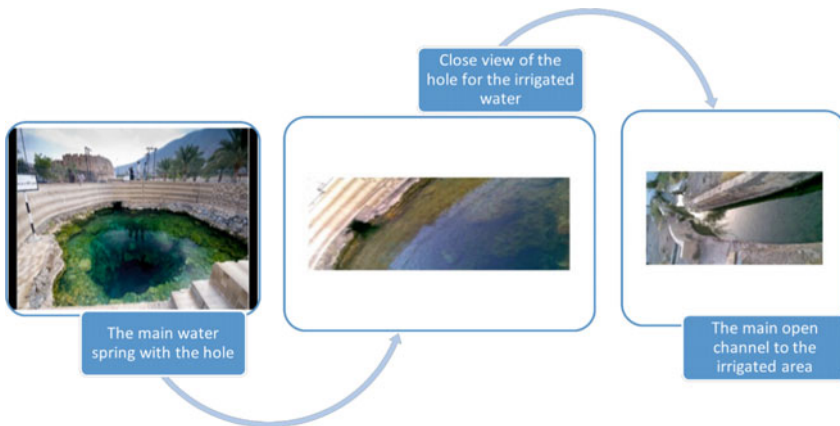
Fig. 3 The first picture (left) shows how the water is coming from the volcanic limestone rocks and is highly protected (by the government) due to its high temperature from the locals and tourists to enter. As can be seen, there is strong metal fence along with warning signs so any visitor only can view it from above. The second picture (middle) is an old hole which was constructed at the top-edge of the main spring to convey flow through an open channel (left side) constructed (strong cement dam) with the aim of conveying water continuously day and night to the irrigation area
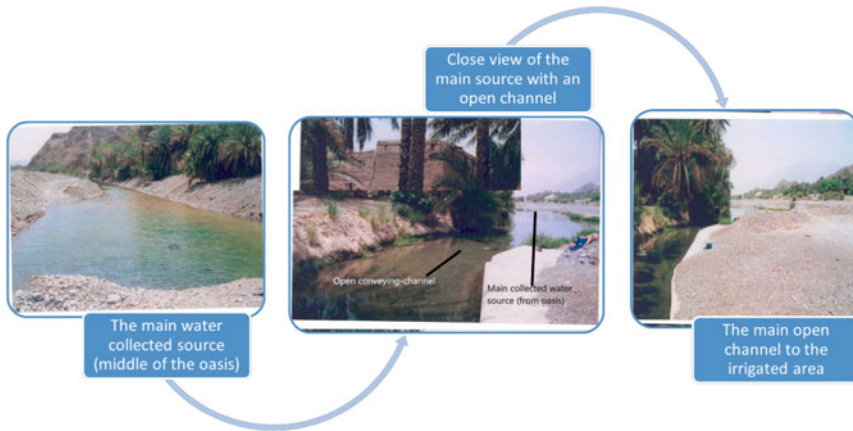
Fig. 4 Water extraction process of the wadis (oasis) surface source: falaj al-samdi. The first picture (left) shows how the water is collected from the main source in the middle of the oasis (*wadi*). Since it is difficult to be protected from the heavy rain (flood), monitoring and maintenance must be there. The second picture (middle) which is an open water-flow conveying channel was constructed at the top-edge of the main water source to convey flow through an open channel (left side) with strong cement dam) with the aim of conveying water continuously day and night to the irrigation area

5.1 Maintenance Institutional Arrangements

From the above illustrative account of the identified water extraction/collection processes, a very important element with respect to aflaj maintenance institution was apparent. First, it has been found that a particular pattern was developed historically based upon physical characteristic of the system. 1) the three *aflaj* collection processes can be combined into two major constructive physical networks. It is noteworthy to state that the primary purpose of such constructive network is to convey/transport water to the villages/irrigated areas. The first process/method is found to be more complex and hold a number of sophisticated components. This is normally implied for the *daudi* type with long tunnel, as discussed above. The reason for such sophisticated components because these types are characterized by holding a high rate (powerful discharge rate) and a constant water flow (high reliability). 2) another constructive process has been found as less complex with short open channels. This is normally applied for the *ghaili* and *ayni aflaj* types. Combination of the physical network construction pattern and the requirement for maintenance provide thorough understanding of how each category developed its own institutional arrangements. The survey provided evidence which places *daudi* and *ghaili* within one category and *ayni* system in another. These are shown in Fig. 3 and Fig. 4. For example, from the view of the *ayn al-kasafah* (Fig. 3) and al-samdi (Fig. 4), several noteworthy institutional arrangements could be seen. First, since the *ayni*-type *aflaj* are usually found in mountainous areas that are not prone to flooding, limited financial support is required for their regular maintenance. In addition, their channel

layout prevents extensive water damage. Second, although the main water source (mother-well) in *as-samdi* appears simple and does not require complex construction, they tend to capture tremendous amounts of sand that remains after flash floods. As a result, sand removing machines need to be used on a daily basis, which can be costly. This system also requires monthly flow monitoring, including main channel cleaning and repairing any damage to the channel bridges and junctions.

5.2   Islamic Time-Share Water Market

The institutional arrangements currently in place for *aflaj* maintenance and damage prevention as a result of heavy floods have forced the locals to develop unique water market based on Muslim jurist view. First, the primary operational mechanism of this market is to rent a whole day (24 h), known as a common (renting) right. This is operated as follows: since *falaj* water flows continuously day and night, the overall flow distribution/rotation is expressed on time-share not volume. A whole day (24 h) set aside to generate income. This is different among the two *aflaj*-types. For example, since the *ghaili*-type is characterized by low flow, the common (renting) day is implicitly set aside from the seventh simple-days circulation. Whereas, because the *daudi aflaj* is characterized by holding a high discharge rate, an explicit common (renting) right is set aside with locally innovated measuring units—known as *athar* (see below). Second, since such right belonged (owned) to the falaj itself to generate income, must be rented only through falaj wakeel (administrative agent organization) not individual. This is crucially important to prevent the free-riding problem if the individual were allowed to rent their share. Hence, all individual seeking an extra of what usually is rented from the falaj common right, and the generating revenue normally used for whole system maintenance.

Data shown in column 3 of Table 1 is the identified weekly water market; expressed on time share 24-h) but using two types of water rights (explicit for the daudi type and implicit for the ghaili type aflaj as indicated above). Data in column 4 and 5 of Table 1 shows the annual water market. The survey identified two annual water rights: *muzyadah* (meaning the bit left over) and *murboutah* (meaning tightened water rights to its leases) also stated as: Three aflaj attached with muzyadah. These are falaj *daris* (19.5 *athar*), *falaj al-mayasser* (96 *athar*) and *falaj al-malki* (51.5 *athar*). Whereas only two aflaj were linked with *murboutah* annual market; these are falaj daris (2.5 athar) and *falaj al khatmeen* (96 *athar).* Our interpretation of the finding as follow: since not all aflaj-type require maintenance, co-existence of a water market varies. According to Table 1 in general traditional water market has been found mainly with the daudi and ghaili aflaj and does not exist with ayni type. This proves the finding above that not much financial support is required for the ayni-type because they were constructed away from a flooded area with simple channel layout. In addition, more complex market transactions are usually associated with the *daudi*-type relative to *ghaili aflaj.* This to refer to the attachment of annual water market. This can be interpreted from the fact that these types aflaj (daudi) characterized by

Table 1 The identified tradition water market within the studied sample

Falaj name/inventory number	Location/wilayat	Water market		
		Weekly	Annually	
			Muzyadah	Murboutah
Daudi Aflaj				
Daris (F0500)	*Nizwa*	Exist/explicit 24 h	19.5	2.5
Al-mayasser (F1446)	*Rustaq*	None	96	
Al-malki (F0606)	*Izki*	Exist/explicit 24 h	51.5	96
Al-khatmeen (F3071)	*Burkat-al-mouz*	None	None	
Ghaili Aflaj				
As-samdi (F1714)	*Samail*	Exist/explicit 24 h	None	
Al-farsakhi (al-alayah)	*Samail*	Exist/explicit 24 h	None	
Balfaee (Asifalah)	*Samail*	Exist/explicit 24 h	None	
Ayni Aflaj				
Ayn al-kasfah (F2750)	*Rustaq*	None	None	
Al jaylah	*Sur*	None	None	

holding high discharge rate (high reliability) by which provide more water rights for renting purposes.

6   Conclusion

An investigation of the *aflaj* maintenance institutional arrangements is, in many respects, an assessment of the overall *aflaj*-shared community threating risk/uncertainty within an arid harnessed environment. However, our field survey found that careful institutional arrangements concerning with the whole system maintenance have been developed in accordance with the physical extraction variation among the three *aflaj* types in Oman. First, although certain of these types (ghaili) were constructed with a simple short physical-network layout, received a well-developed institutional arrangement for maintenance. This is attributed to the fact that they are prone to drought and greatly influenced by the occasional heavy rainfall flood. In contrast, *aflaj* constructed over mountainous areas away from heavy flooded areas, were found with less arrangement for maintenance. Second, the development/co-exist of a traditional water market within certain aflaj type is not merely to meet the efficiency criteria of water usage, but whether the original of the water extraction variation have been represented by the law of water supply. This is significantly important in the process of prices determination. The picture drawn from this investigation indicates that while there are co-exist two several methods in determining prices (weekly auction, *murboutah* and *muzayadah*), prices determined freely within a competitive water market. For example, in a situation where

the flow is regular and water supply fairly stable, community developed two type of water market: weekly and annually, while where the flow very low and irregular they developed only one type (implicit weekly water market).

References

1. Abdel Rahmnn HA, Omezzine A (1996) Aflaj water resources management: tradable water rights to improve irrigation productivity in Oman. Water Int 21:70–75
2. Al-Marshudi AS (2001) Traditional irrigated agriculture in Oman. Water Int 26:259–264
3. Al-Marshudi AS (2007) The falaj irrigation system and water allocation markets in Northern Oman. Agric Water Manag 91:71–77
4. Araral E (2009) The failure of water utilities privatization: synthesis of evidence, analysis and implications. Policy Soc. 27:221–228
5. Birks S (1978) The mountain pastoralists of the Sultanate of Oman. Dev Chang 9:71–86
6. Hansen K., Howitt R, Williams J (2015) An econometric test of water market structure in the Western United States
7. Larson BA, Bromley DW (1990) Property rights, externalities, and resource degradation: locating the tragedy. J Dev Econ 33:235–262
8. Megdiche-Kharrat F, Moussa M, Rejeb H (2017). Aflaj water management in Oman: the case of Falaj Al-Khatmeen in Birkat Al-Mouz, Wilayat Nizwa. In: Water and land security in drylands. Springer, Cham, pp 119–128
9. Meinzen-Dick R, Raju KV, Gulati A (2002) What affects organization and collective action for managing resources? evidence from canal irrigation systems in India. World Dev 30:649–666
10. Milliman JW (1959) Water law and private decision-making: a critique. J Law Econ 2:41–63
11. Netting RM (1976) What alpine peasants have in common: observations on communal tenure in a swiss village. Hum Ecol 4:135–146
12. Ostrom E, Gardner R (1993) Coping with asymmetries in the commons: self-governing irrigation systems can work. J Econ Perspect 7:93–112
13. Perry C (2001) Water at any price? issues and options in charging for irrigation water. Irrig Drain 50:1–7
14. Randall A (1981) Property entitlements and pricing policies for a maturing water economy. Aust J Agric Econ 25:195–220
15. Randall A (1983) The problem of market failure. Nat Resour J 23:131–148
16. Remmington G (2018) Transforming tradition: the aflaj and changing role of traditional knowledge systems for collective water management. J Arid Environ 151:134–140
17. Rosegrant MW, Binswanger HP (1994) Markets in tradable water rights: potential for efficiency gains in developing country water resource allocation. World Dev 22:1613–1625
18. Rosegrant MW, Schleyer RG, Yadav SN (1995) Water policy for efficient agricultural diversification: market-based approaches. Food Policy 20:203–223
19. Sutton S (1984) The falaj-a traditional co-operative system of water management. Waterlines 2:8–12(5)
20. Trawick PB (2001) Successfully governing the commons: principles of social organization in an andean irrigation system. Hum Ecol 29:1–25
21. Wilkinson JC (1977) Water and tribal settlement in South-east Arabia: a study of the Aflaj of Oman. Clarendon Press, p Oxford
22. Young RA (1986) Why are there so few transactions among water users. Am J Agr Econ 68:1143–1151

23. Zekri S, Al-Marshudi A (2008) A millenarian water rights system and water markets in Oman. Water Int 33:350–360
24. Zekri S, Kotagama H, Boughanmi H (2006) Temporary water markets in Oman. 11(8)

Coastal Engineering and Management

The Coastal Engineering and Management section includes a few more papers that provides valuable information for current research work specialising in coastal and estuary. It is also suitable for anyone having any basic engineering or science background. The topics presented here covers observation on-site and numerical simulation. The first topic discusses about estuary and salinity intrusion in the river, followed by mangrove habitat on the muddy coastal area. The physical and chemical properties that are suitable for mangrove growth are discussed. The coastal reservoir is an alternative source of freshwater in the downstream area and this paper discussed the potential development of a coastal reservoir in Malaysia. Next, numerical simulations of wave generation and propagation to the nearshore are presented in three papers. It started with the numerical study of wave groups in wind-swell seas and then wave diffraction on a low-crested structure. The last paper on this topic is the numerical simulation on wave run-up and overtopping on a breakwater. Finally, assessment on marine debris and clean coast index for a few coastal areas in Malaysia were reviewed and discussed. The papers presented and discussed in this section may give a general overview of the current's situation and research work in the estuary and coastal area.

Salinity Behavior and Intrusion in Kelantan River Estuary

N. A. Mohamad, I. K. Othman, M. H. Jamal, R. Sa'ari, K. V. Annamala, and M. F. Ahmad

Abstract An estuary is a unique environment influenced by tidal and freshwater mixing. Saltwater intrusion during the wet season is less studied in Kelantan River despite occasional flooding from high tides. Thus, this study presents one month's water level measurements at three locations and two days horizontal, vertical and longitudinal salinity profile measurements at seven cross-sections along approximately 11 km upstream of the Kelantan River estuary. Salinity measurements were taken using the YSI Water Quality meter by moving boat method before the North-East Monsoon in October 2015. The maximum tidal range computed from water level data is around 1.32 m on average and can be classified as microtide, characterised by delta formation from upland discharged sediments. The vertical salinity profile was measured every 0.5 m water depth and the inflexion point where mixing starts to occur increases from around 2 m at the river mouth to 4.5 m at 8.3 km upstream. The longitudinal salinity structure indicates Kelantan estuary as salt wedge maximum saltwater intrusion around 9 km upstream. The data provides a preliminary understanding of longitudinal and vertical salinity structure. During wet and dry seasons, higher or lower river discharge may alter the mixing process and saltwater intrusion length.

Keywords Kelantan River Estuary · Saltwater intrusion · Estuary classification · Monsoon

N. A. Mohamad · I. K. Othman (✉) · M. H. Jamal · R. Sa'ari · K. V. Annamala · M. F. Ahmad
Department of Water and Environmental Engineering, School of Civil Engineering, Faculty of Engineering, UTM, Johor Bahru, Malaysia
e-mail: tyra.mohamad90@gmail.com; radzuans@utm.my; faizal_9273@yahoo.com; ilya@utm.my; mhidayat@utm.my; kogila@utm.my

I. K. Othman · M. H. Jamal
Center for Coastal and Ocean Engineering (COEI), UTM, Johor Bahru, Malaysia

K. V. Annamala
Centre for Environmental Sustainability and Water Security (IPASA), UTM, Johor Bahru, Malaysia

1 Introduction

In estuaries, saltwater intrusion is caused by tidal movements where the difference in water density, freshwater discharge and tidal current allows the saltwater to intrude inland. Saltwater intrusion may reach a great distance from the river mouth, especially when ocean flows are higher than river flows [5]. Besides indicating the extent of salt and fresh water mixing, the distance of tidal intrusion also provides information for the locals regarding the areas possibly influenced by the tides. Saltwater intrusion, particularly in delta areas, has become a major concern as an effect of climate change and human activities [4]. If there is an insufficient water supply from upstream, saltwater intrusion would reduce water availability and degrade the water quality [4] if the intrusion reaches near the water intake point. Understanding the streamwise salinity profile will help determine the salt intrusion length that may influence the design of water intake location. At the same time, the horizontal velocity gradient provides more in-depth into how saltwater intrudes, mixes and evolve from the river mouth upstream. At the time of writing, there are very few studies on the salinity intrusion into the river in Malaysia especially on the salinity profile in Sg Kelantan. Previous local studies focused on saltwater intrusion effect on the groundwater around the estuary environment [1–3, 6] but did not carry out detailed salinity measurements.

The present study describes the methodology for the field data collection, followed by the horizontal and vertical salinity profile results. The vertical salinity structure for all points is combined to form the longitudinal salinity structure for further estuarine classification. The last section gives the overall conclusion of the estuarine classification based on the salinity profile.

2 Materials and Methods

2.1 Overview of the Study Area

Kelantan River basin is located in the North-Eastern of Peninsular Malaysia in between latitudes ($4^\circ 40'$ to $6^\circ 12'$) N and longitudes ($101^\circ 20'$ to $102^\circ 20'$) E. The river is approximately 248 km long, and the average runoff is about 500 m^3/s. It drains into an approximately 12,000 km^2 (upstream of Guillemard Bridge) catchment area to two main streams that are Lebir and Galas upstream and then splits into two branches downstream. The first branch of the river flow towards Geting, and the second branch of the river flow towards the Kelantan River estuary (Fig. 1). Both branches flow northwards into the South China Sea (Fig. 1). The river is exposed to the dry season from March to May during South-West Monsoon and from November to March during North-East Monsoon. The climate is hot and humid all year round, with an annual rainfall of more than 2,500 mm [8].

Fig. 1 Maps of Kelantan River estuary (Google earth 2021)

2.2 Salinity and Water Level Measurement

The salinity measurements were carried out prior to the North-East Monsoon for two consecutive days, 24 October 2015 during ebb tides to 25 October 2015 during flood tides. There was light rain on both sampling days. Transverse salinity measurements were recorded manually at seven cross-sections downstream of the Kelantan River (Fig. 2). Navigation from one cross-section to another cross-section was guided by using Garmin GPS Navigation System. The first measurements station was taken at the inlet and progressed upstream until approximately 11 km for the last station, as shown in Fig. 2. The cross-sections range are approximately 11 km except for the last two stations close to the river mouth, distant at 1 km. Inconsistencies distances range occurs due to the boat drifting away by the strong river current and shifting actual location planned. Field salinity data sampling for every cross-section consists of three sampling points, namely: P1 (left), P2 (middle) and P3 (right), respectively. The field data sampling process takes up to 5 h to complete from C1 to C7 at all P1, P2 and P3. Table 1 shows the list of geographical coordinates of salinity sampling points (P1, P2 and P3) from C1 to C7.

Salinity was measured by using the YSI Water Quality instrument in the unit of part per thousand, as shown in Fig. 3(a). This instrument can also measure the other parameters such as temperature, pH, dissolved oxygen (DO), pressure, conductivity, total dissolved solids, and ammonium. The YSI water quality sensors are immersed into water for every 0.5 m depth until reaching the river bed. A cylindrical cement block was fastened to YSI to minimise drifting during immersion into the river (Fig. 3(b)). The YSI was synchronised to GPS time.
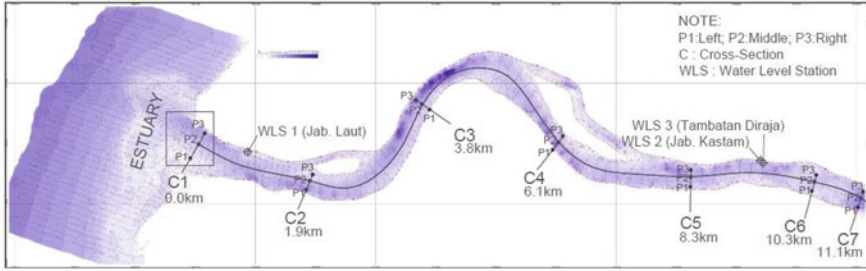
Fig. 2 Location of salinity sampling points and water level stations

Table 1 The list of the geographical coordinate of salinity sampling points

Cross section	Coordinates in WGS-84 coordinate system		
	P1 (Left)	P2 (Middle)	P3 (Right)
C1	N 06°13′00.7″ E 102°14′00.6″	N 06°13′02.4″ E 102°14′13.3″	N 06°13′08.1″ E 102°14′16.1″
C2	N 06°11′58.8″ E 102°13′47.1″	N 06°12′00.2″ E 102°13′53.5″	N 06°11′58.2″ E 102°14′01.5″
C3	N 06°10′53.2″ E 102°14′36.7″	N 06°10′58.9″ E 102°14′34.6″	N 06°11′03.9″ E 102°14′35.1″
C4	N 06°09′47.8″ E 102°14′13.6″	N 06°09′45.0″ E 102°14′14.6″	N 06°09′40.2″ E 102°14′14.5″
C5	N 06°08′35.0″ E 102°13′50.2″	N 06°08′33.5″ E 102°13′56.1″	N 06°08′34.0″ E 102°14′00.9″
C6	N 06°07′28.1″ E 102°13′47.8″	N 06°07′26.8″ E 102°13′52.0″	N 06°07′28.1″ E 102°14′00.9″
C7	N 06°07′01.5″ E 102°13′38.0″	N 06°07′01.6″ E 102°13′41.6″	N 01°32′26.5″ E 103°39′26.6″
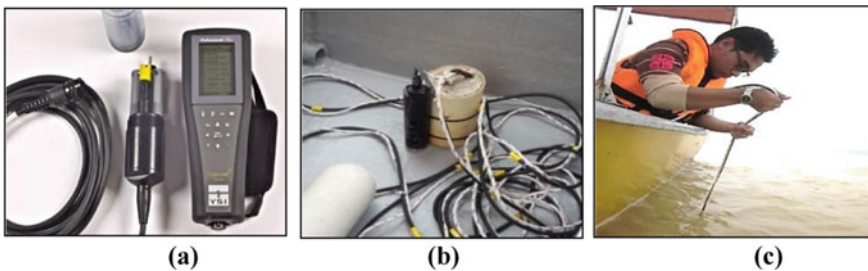
Fig. 3 Salinity measurements equipment and process. **a** YSI Water Quality Sensors tools fastened on cement blocks **c** YSI water quality sensors immersed into water
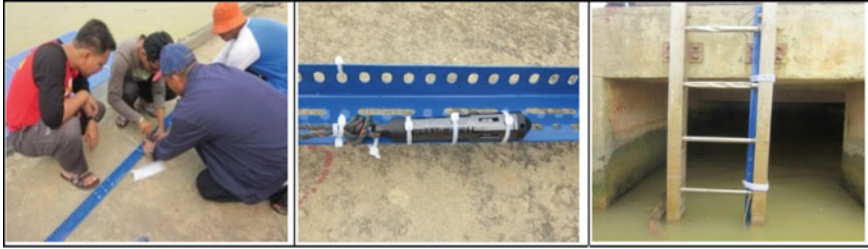
Fig. 4 Installation of water level data logger (CTD diver)

The water level data used consist of two sets: (i) the primary data is from field measurements that were carried out for a month, from 23 October 2015 until 22 November 2015; and (ii) the secondary data set is from one station from Department of Irrigation and Drainage, DID. The primary data set is from two stations, Jabatan Laut (WLS 1) and Tambatan Di Raja (WLS 2), recorded at the frequency of 5 min using CTD Diver. The location is selected randomly based on the suitability and safety to install the water level monitoring device (Fig. 4). The secondary data set is at station Jabatan Kastam (WLS 3) obtained at an hour frequency from DID portal. The approximate locations of the water level measurement are illustrated in Fig. 2.

3 Result and Discussion

3.1 Water Level

Figure 5 shows that the neap and spring tides occurred twice throughout the observation period (23 October 2015 to 22 November 2015). Qualitative observation of the water level trend demonstrates that the neap tides (smaller tidal range) occurred around 23–31 October 2015 and 8–14 November 2015. There are two phases of different tidal patterns that occur during the observation period (Table 2). The first phase, 24 October–1 November 2015 and 8–16 November 2015, show mixed predominantly semidiurnal. The second phase, from 2–7 November 2015 and 17–21 November 2015, illustrate the diurnal pattern for all stations. From overall observation of tidal patterns, it can be concluded that the first phase will occur when there are changing times from neap to spring tides and vice versa for the second phase. The tidal pattern is characterised based on the qualitative observation of the number of ebb-tide and flood-tide per day. Based on the higher high water and lower low water, a maximum tidal range for every location can be computed throughout the record. The maximum tidal range for Kelantan River Estuary is around 1.32 m on average and can be classified as microtide. The microtide estuary is usually characterised by the formation of the delta from upland discharged sediments. In the river mouth, the waves forcing produces spits, barrier islands and bar-built formations.
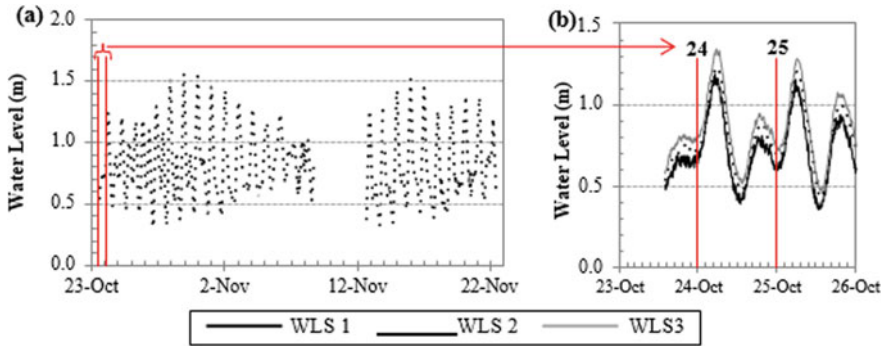
Fig. 5 Water level at three different locations along the Kelantan River from 23 October 2015 to 22 November 2015

Table 2 Summary of tidal pattern at observation stations

Date	Station	Tidal pattern
24 Oct–1 Nov) & (8–16 Nov)	WLS 1, WLS 2, and WLS 3	Mixed semidiurnal
(2–7 Nov) & (17–21 Nov)	WLS 1, WLS 2, and WLS 3	Diurnal

3.2 Longitudinal Salinity Profile

Figure 6 shows the different average horizontal salinity profile patterns at the river's left, middle, and right sides. The exact location is given in Table 1. The horizontal salinity is asymmetrical between the right and left side but indicate the same profile on both sampling days. The maximum intrusion length is approximated at around 9 km upstream at all sides of the river. The salinity profile fluctuates between 2 and 4 km as the river starts to meander at 2 km. The meander may have dampened the speed and concentration of saltwater intrusion. However, the salinity pattern decreases linearly in between 4 and 6 km meander. The salinity decreased from the estuary to the upstream of the river and all sides of the river. Overall point (left, middle and right) shows the salinity reduces to 0.0 ppt when approaching 9 km upstream. The linear reduction of salinity indicates a positive and normal estuary [7]. There is less fluctuation in the salinity profile in the middle of the river and thus used for further comparison for vertical salinity profile in the next section.

3.3 Vertical Salinity Profile

Figure 7 shows the different patterns of salinity and vertical profile between three measurement points, left (P1), middle (P2) and right (P3) side of the river at seven cross-sections, C1 until C7. The upper layer is dominated by the freshwater moving
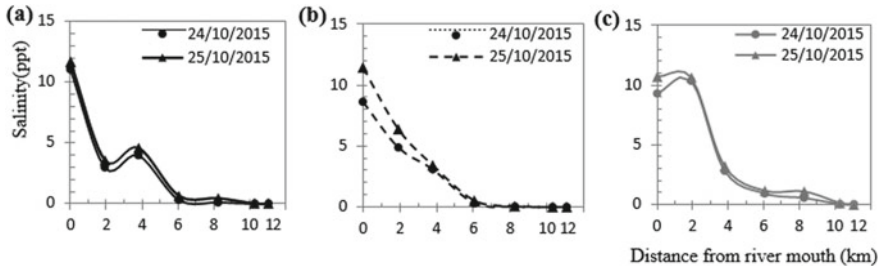
Fig. 6 Average salinity along the downstream of Kelantan River at different sampling points on 24 and 25 October 2015. **a** Salinity at left (P1), **b** Salinity at the middle (P2), **c** Salinity at right (P3)

seaward, and the salty ocean water moving landward dominates the lower layer. This is a common feature as dense saltwater intrudes towards the bottom, and salinity becomes higher at increasing depth. Between the upper freshwater layer and the salty bottom layer, an inflection point separated the two different layers of different water densities. The inflection depth increases from about 2 m at the river mouth (C1), 3 m at C2, 3.5 m at C3, 4 m at C4, and 4.5 m at C5 and none at C6 and C7. The increment of the inflection depth indicates the decreasing strength of seawater intrusion (seawater discharge) and increasing strength of river discharge, both in landwards direction. For instance, the river mouth (cross-Sect. 1, C1) vertical profile illustrates that there are 0.5–2 m depth layers of buoyant freshwater flows on top of saline water. The depth layer of buoyant freshwater becomes higher further upstream. Saline water moves along the bottom towards the upstream of the river and ceases somewhere between C4 and C5. From C5 onwards (i.e. C5, C6 and C7), no seawater intrusion is indicated by the 0 ppt vertical salinity profile. It is estimated that the maximum seawater intrusion or intrusion length in Sg Kelantan is between 8.3 to 10.3 km before monsoon season from Fig. 5. However, as determined earlier using a horizontal salinity profile, the intrusion length is around 9 km. A finer resolution measurement of less than 2 km is required for the exact estimation of the intrusion length. The intrusion length will vary with different tidal and river water levels during drought season. Hence, a complete salinity measurement is required for at least one tidal cycle in each drought and monsoon season. The vertical salinity profiles on 24 October 2015 is relatively more consistent than on 25 October 2015 at C1 and C2 due to greater flood tidal currents on the 25th than ebb tidal currents on the 24th.

3.4 Longitudinal Salinity Structure Along Kelantan River

Figure 8 shows the longitudinal salinity structure along 11 km and can be classified as a salt wedge estuary. Overall, the interfacial friction is pronounced at around 2.3 m depth, where the relative velocity between the fresh and salty water is intense. This creates turbulence that mixes the upper and lower layer of water through the vertical
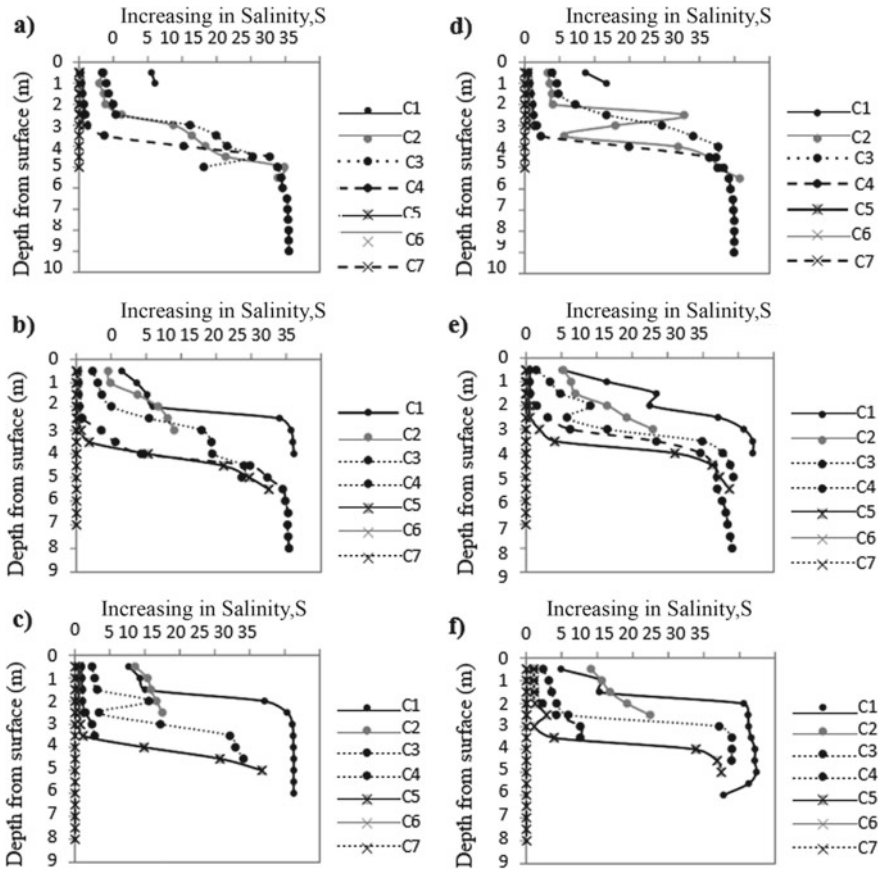
Fig. 7 Average salinity from the river mouth to downstream (C1 to C7) in ascending depths at three different points left, P1 (a and d), middle, P2 (b and e), and right P3 (c and f) on 24 October 2015 (a–c) and 25 October 2015 (d–f)

and horizontal advection. The salinity profile shows the slope of salinity (salinity gradient) increases rapidly at the river mouth and declines almost instantly at 8.3 km upstream. Although no discharge measurements were made, it is estimated that the river discharge is much higher than the oceanic discharge at the river mouth indicated by the rapid increase in salinity (or high salinity gradient). The sharp dent in the bed profile just after 3.8 km indicates insufficient bathymetry data and the possibility of sand mining at this location. Sand mining in the Kelantan River is common and so do in most Malaysian rivers.
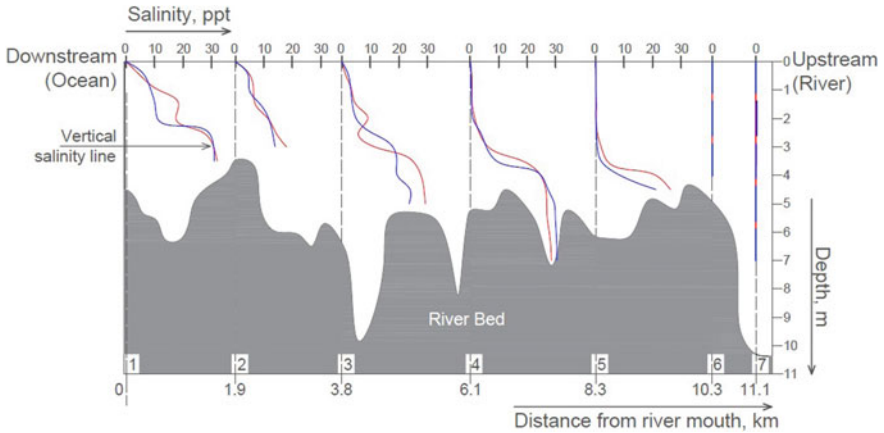
Fig. 8 Longitudinal salinity structure along Kelantan River estuary, 24 October 2015 (blue line) and 25 October 2015 (red line)

4 Conclusion

This paper focuses on the preliminary understanding of the horizontal and vertical salinity profile of saltwater intrusion Kelantan River Estuary. Fieldwork measured salinity (24–25 October 2015) and water level (23 October–22 November 2015). The salinity was measured using a moving boat at three points on the left, middle and right sides of the river along seven cross-sections traversing 11 km from the river mouth. One-month water level measurements were measured at Jeti Kastam and Tambatan Di Raja and cross-checked with secondary data from DID at Jabatan Kastam. The maximum tidal range for Kelantan River Estuary is around 1.32 m on average and can be classified as microtide. The microtide estuary is usually characterised by the formation of the delta from upland discharged sediments, which is visible from the morphology of the Kelantan River estuary. There is fluctuation in the average horizontal salinity readings on the right and left sides in between 2 to 4 km, which may be caused by the dampening of the saltwater intrusion by the river meander around 2 km upstream. Overall, the average horizontal salinity reduces upstream, which indicates a positive and normal estuary. The vertical salinity profiles indicate an increase in inflection point at 2 m depth at the river mouth to 4.5 m depth at 8.3 km upstream. The inflection point indicates the mixing point of the salt and fresh water. The increases in the depth of the inflection point upstream reflect the stronger ocean currents at the mouth than river discharge and gradual domination of river discharge and mixing upstream. The longitudinal salinity structure shows the salinity gradient increases rapidly at the river mouth and decline almost instantly at 8.3 km upstream, which is a typical characteristic of a salt wedge type estuary. Based on the vertical and horizontal salinity profile, the maximum salinity intrusion reach 9 km upstream from the river mouth. Further salinity measurement at a longer timescale is required

to confirm this estuary's intrusion length and type. The salinity profile may change during low river flow or drought season where salinity intrusion is greatest.

References

1. Aris AZ, Abdullah MH, Kim KW, Praveena SM (2009) Hydrochemical changes in a small tropical island's aquifer: Manukan Island, Sabah, Malaysia. Environ Geol 56(8):1721–1732
2. Baharuddin MFT, Taib S, Hashim R, Abidin MHZ, Rahman NI (2013) Assessment of seawater intrusion to the agricultural sustainability at the coastal area of Carey Island, Selangor, Malaysia. Arab J Geosci 6(10):3909–3928
3. Kura NU, Ramli MF, Ibrahim S, Sulaiman WNA, Aris AZ (2014) An integrated assessment of seawater intrusion in a small tropical island using geophysical, geochemical, and geostatistical techniques. Environ Sci Pollut Res 21(11):7047–7064
4. Liu D, Chen X, Lou Z (2010) A model for the optimal allocation of water resources in a saltwater intrusion area: a case study in Pearl River Delta in China. Water Resour Manag 24(1):63–81
5. Nguyen AD (2008) Salt Intrusion, Tides and Mixing in Multi-Channel Estuaries, PhD Thesis, UNESCO-IHE Institute, Delft. CRC Press
6. Samsuddin AR, Haryono A, Hamzah U, Rafek AG (2008) Salinity mapping of coastal groundwater aquifers using hydrogeochemical and geophysical methods: a case study from North Kelantan, Malaysia. Environ Geol 55(8):1737–1743
7. Savenije HHG (2012) Salinity and Tides in Alluvial Estuaries, completely revised, 2nd edn. Delft University of Technology, Netherlands
8. Tan ML, Yusop Z, Chua VP, Chan NW (2017) Climate change impacts under CMIP5 RCP scenarios on water resources of the Kelantan River Basin, Malaysia. Atmos Res 189:1–10

Physical and Chemical Variability of Mangrove Island: A Case Study of Pulau Kukup, Johor

Abdul Al-Hafiis Abdul Rahman Lim, Mohamad Hidayat Jamal, Daeng Siti Maimunah Ishak, Shamila Azman, Myzairah Hamdzah, and Nor Suhaila Rahim

Abstract This paper highlights a preliminary review study on the species distribution using spatial analysis at the mangrove area. Fourteen sampling plots were established at the study area to determine the variability of physical and chemical properties of the soil. The interpolation process was conducted in ArcGIS spatial analysis to interpolate the value of elements where the field data collection is inaccessible. A number of tests were conducted on common soil physical and chemical parameters such as salinity, pH, conductivity, nutrient, and particle size distribution of soil. The results determined that soils are categorized as very saline-sodic, and most of the soil determined at the study area was classified as silt loam soil. In conclusion, this type of soil is most suitable for *Brugueira cylindrica* and *Rhizophora mucronate* species due to the high number of sapling species found in the plots. However, inaccessibility to the whole Pulau Kukup had led to the lack of sample collected during

A. A.-H. A. R. Lim (✉) · M. H. Jamal · S. Azman
School of Civil Engineering, Faculty of Engineering, Universiti Teknologi Malaysia, Johor Bahru, Malaysia
e-mail: abdulal-hafiis@graduate.utm.my

M. H. Jamal
e-mail: mhidayat@utm.my

S. Azman
e-mail: shamila@utm.my

M. H. Jamal · S. Azman
Department of Water and Environment Engineering, School of Civil Engineering, Faculty of Engineering, Universiti Teknologi Malaysia, Johor Bahru, Malaysia

M. H. Jamal · D. S. M. Ishak · N. S. Rahim
Centre for River and Engineering, Research Institute For Sustainable Environment, Universiti Teknologi Malaysia, Johor Bahru, Malaysia
e-mail: maimunah.kl@utm.my

N. S. Rahim
e-mail: nsuhaila@utm.my

D. S. M. Ishak · M. Hamdzah · N. S. Rahim
Research Institute For Sustainable Environment, Universiti Teknologi Malaysia, Johor Bahru, Malaysia
e-mail: myzairah@utm.my

the sampling process. Therefore, for future improvement, it is suggested to use the data collected from the secondary and archive data while increasing the data input, thus producing a more precise interpolation output map.

Keywords Mangroves species · Distribution · Spatial analysis · Physical and chemical parameters

1 Introduction

The Southeast Asian countries of such as Brunei Darussalam, Cambodia, Indonesia, Malaysia, Myanmar, Philippines, Thailand, and Vietnam has accounted for 35% of the world's mangrove forests. It is reported that the total number of mangrove distribution was 18 million hectares [11]. In Asia, the mangrove forest conversion to shrimp ponds, settlements, salt beds, and overexploitation has resulted in significant rates of mangrove destruction over the last three decades. The destruction of mangroves ranges from 25% in Malaysia to 50% in Thailand [13, 15]. In 1987, a total of 102,000 hectares of mangroves area were cleared in Vietnam alone [12] (Honculada et al. 2019). Whereas, in Thailand, between the year 1961 to 1993, it is estimated around 150 ha from the total of 203,600 ha of mangrove area were destroyed [14].

The mangrove area offers valuable protection for people at risk from sea-level rises and severe weather caused by climate change [4]. The coastal forests act like carbon sinks help to fight against global warming by eliminating carbon dioxide from the atmosphere, in which most of it was stored in the mangrove plant [2]. The ecotourism of mangrove areas also depends on the mangrove resources. Besides the mangrove exhibition of the mangrove species that attract visitors, the durability of the mangrove wood is also useful for the infrastructure development of the area. Therefore, it is important to protect the mangroves instead of clearing them for ecotourism development [1]. Moreover, they are rich in biodiversity and a home-based to an array of nesting, breeding and migratory of wildlife [6].

According to the findings, four environmental parameters (frequency of tidal currents, salinity, groundwater, and temperature) in the Semarang-Demak coastal area continue to encourage mangrove growth. On the other hand, waves and rainfall require special attention because they have a propensity to intensify, which might result in abrasion. Eventually, the mangroves will collapse, and the erosion continues from the effect of waves and rainfall [5]. *Avicennia marina, Avicennia alba, Rhyzophora mucronata, Rhyziphora stylosa,* and *Sonneratia caseolaris* are the five-mangrove species dominating the Semarang-Demak coastal area [3]. The current and historical distributions of numerous mangrove species across the continent are thought to be the result of intricate interactions between biological, chemical, and physical conditions [10].

Mangroves play an important role in mitigating storm surges and tsunamis through wave attenuation in coastlines. Numerous studies show that mangroves provide a nursery. Yet the study has been made in the past, but not all the mangrove species have been analysed because the tolerance of mangrove species would be different and depends on their specific growth rate, climate change, and suitable environmental factor. The study focuses on physical and chemical parameters, which are tide, temperature, and light intensity. While for soil is salinity, pH, conductivity, nitrate, phosphate, potassium, and particle size distribution for sampling distribution. The aim of this paper is to present the results of the application of the interpolation process within ArcGIS spatial analysis to interpolate the value of physical and chemical parameters where the field data collection is inaccessible.

2 Methodology

This study highlights the application of interpolation in ArcGIS spatial analysis. It is a method to estimate the value of absence data for the distribution at locations that is inaccessible. The interpolation method will be based on the available process within the ArcGIS software.

2.1 Study Area

Data collection was conducted at Pulau Kukup, Johor, which is 6.4 km^2 in area (Fig. 1) and located at longitude and latitude 1.322, 103.424. Pulau Kukup is an island that is dense with mangrove trees, there were 24 mangrove species recorded in Pulau Kukup and *Rhyzophora apiculata, Rhyzophora mucronata*, and *Bruguiera cylindrica* contributed the most biomass to the Pulau Kukup research plot in terms of species [9]. From 40 points marked, 14 points are accessible and have been plotted. Sampled point are 10, 12, 13, 14, 15, 16, 19, 20, 31, 32, 33, 35, 36, and 40 (Fig. 2). Mangrove sapling was identified and recorded within a 10 × 10 m plot. Selected mangrove saplings were identified based on the range height, which is 1.3 to 4 m. The information of tree circumference, height, species and coordinate locations is recorded for further analyses. Approximately one kilogram of soil is collected from the centre point of the plot as the sediment sample at an interval depth of 0.5 to 1.0 m. It is collected using a hand auger.

Overall, a total of 24 soil samples are collected for both depths, which are 50–100 cm depth. Soil samples are placed in a plastic container and brought back for laboratory analysis. Laboratory analyses were conducted to identify the salinity, pH, conductivity, particle size distribution, and nutrient content. The specific nutrient content analyses for this study are Nitrate, Phosphate, and Potassium (NPK). The concentration gradient of the physical–chemical parameter of the study area will be

Fig. 1 Location of Pulau Kukup, Johor, Malaysia

interpolated using Kriging, Inverse Distance Weighted (IDW) and other available interpolation tools in ArcGIS.

2.2 Laboratory Test

The soil tests are separated into two processes. The first process was conducted in Environment Laboratory, Universiti Teknologi Malaysia Johor, which consists of salinity, pH, and conductivity test. Every sample of soil will be weighed 200 g. Place the soil sample was weighing in the beaker with distilled water 200 ml. The sample is stirred, and the sample is left for 24–48 h. Soil water samples were separated into different beakers. The salinity, pH and conductivity will be measured using YSI Dissolved Oxygen Meter (Fig. 3). Whereas the determination of nutrient content and particle size distribution was conducted at Castconsult Sdn Bhd Laboratory.
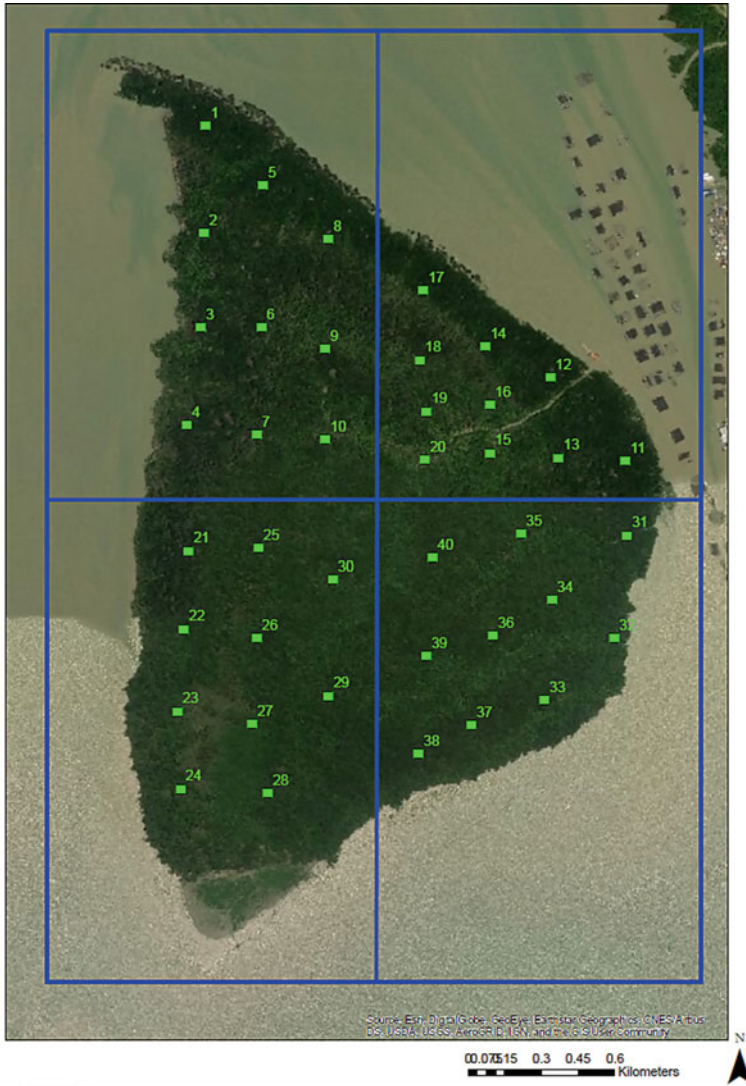
Fig. 2: 40 plots that were randomly marked on the Pulau Kukup map. Location of Pulau Kukup, Johor, Malaysia

2.3 Particle Size Distribution (Hydrometer Method)

The soil samples were oven-dried at 110 °C, then the samples were weighted to take the initial mass. After that, the sample is placed in the wide-mouthed conical flask and shake the sample 100 mL of dispersant solution thoroughly until the soil is in suspension. Shake the flask for at least four hours or overnight before transferring
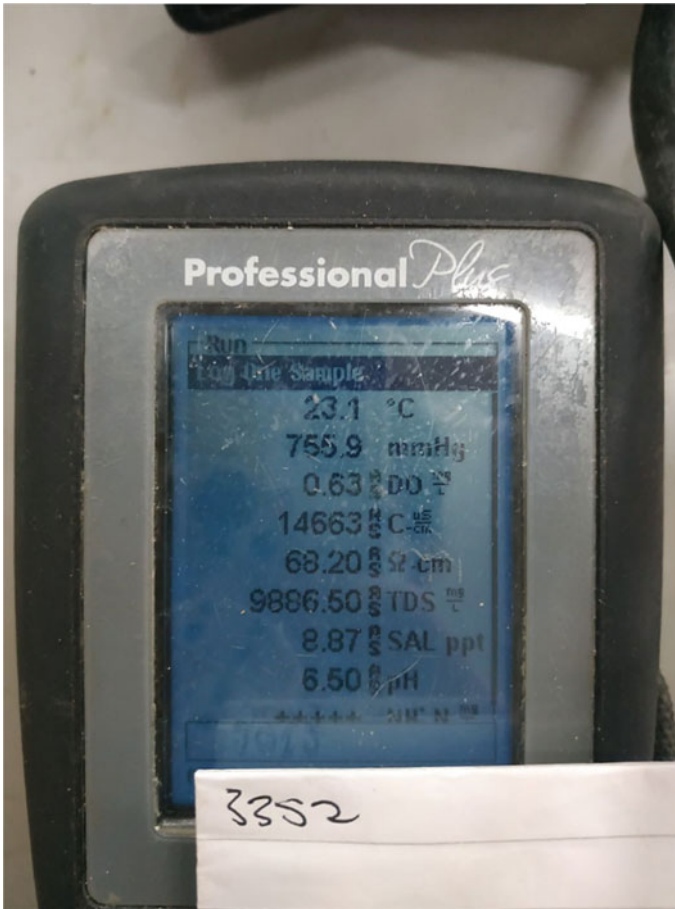
Fig. 3 Reading of salinity, pH and conductivity using YSI Dissolved Oxygen Meter

the suspension to the 63 μm test sieve placed on the receiver and wash the soil in the sieve using distilled water (shall not exceed 500 mL). The suspension that has passed through the sieve to the 1L measuring cylinder and made up to the 1L distilled transferred and make-up to the 1L distilled water. Use this suspension for the sediment analysis. Next, transfer the material retained on the 63 μm test sieve to an evaporating dish and dry in the oven at 110 °C when the sample cooled, re-sieve the material on the sieve down to the 63 μm size. Weight the material retained on each sieve to 0.01 g. Add any material passing the 63 μm test sieve to the measuring cylinder, then shake the cylinder containing the soil suspension at the constant temperature at least up to the 1L graduation mark. After that, add 100 mL of dispersant solution to the second 1L sedimentation cylinder and dilute with distilled water to exactly 1L. Place the cylinder in the constant temperature. After at least one hour or when the

cylinder and contents have reached the temperature, shake it vigorously end-over-end about 60 times in two minutes. Instantly start the timer while the hydrometer is immersed in the suspension to a depth slightly below its floating position and allow it to free float. Take and record the hydrometer slowly, rinse in distilled water with dispersant at the same temperature as the soil suspension. Reinsert the hydrometer in the soil suspension, take and record the reading after periods of eight minutes, 30 min, two hours, eight hours, and 24 h from the start sedimentation and twice during the following day if appropriate.

2.4 Determination of Potassium in Soil Sample

The soil sample dried up in the oven at 103 °C for two hours. After that, weigh 1.0 g of dried sample in porcelain crucible and ash in the furnace at 550 °C for two hours. Digest the ash at hotplate with 5 mL concentrated Hydrochloric Acid and %mL concentrated Nitric Acid for 5 min. Next, cool and digested sample and filter into 100 mL volumetric flask. Lastly, mark up to volume with distilled water and proceed for Atomic Absorption Spectroscopy (ASS) inspection.

2.5 Determination of Phosphate in Soil Sample

The soil sample dried up in the oven at 103 °C for two hours. After that, weigh 1.0 g of dried sample in porcelain crucible and ash in the furnace at 550 °C for two hours. Digest the ash at hotplate with 5 mL concentrated Hydrochloric Acid and %mL concentrated Nitric Acid for 5 min. Next, cool and digested sample and filter into 100 mL volumetric flask. Lastly, mark up to volume with distilled water and proceed for Atomic UV–Vis inspection.

2.6 Determination of Soluble Nitrate in Soil Sample

The soil sample dried up in the oven at 103 °C for two hours. After that, weigh 5-10 g sample and mix the 100 mL distilled water. Stir the mixture with a magnetic stirrer for one minute. Next, filter the sample using filter paper and funnel. Collect filtrate 50 mL and add 1 mL 1 M Hydrochloric Acid. Finally, proceed for UV–Vis inspection by using distilled water as blank.

2.7   Mapping and Interpolation

Recorded saplings and sediment extraction coordinate locations will be transferred into ArcGIS in the comma-delimited (.csv) form for the spatial analysis process. The physical–chemical parameters related to the sapling distribution was used to project the suitable location for the mangrove sapling. The concentration gradient of a physical–chemical parameter of the study area will be interpolated by using Kriging, Inverse Distance Weighted (IDW) and other available interpolation tools in ArcGIS. Finally, the accuracy assessment will be conducted for numbers of interpolation results, and the highest percentage of accuracy level will be selected to represent the study area.

3   Results and Discussion

Data collection was conducted in the eastern part of the island. Based on the data, the majority of sapling species at the eastern side of the island is *Brugueira cylindrica* and *Rhizophora mucronata* (Fig. 4). Figure 5 shows the interpolation of species distribution in Pulau Kukup. Each species found is given a number 1 to 8 to be able to interpolate the data. As stated above, the *B. cylindrica* was founded as dominant in Pulau Kukup, which set the value as 3.
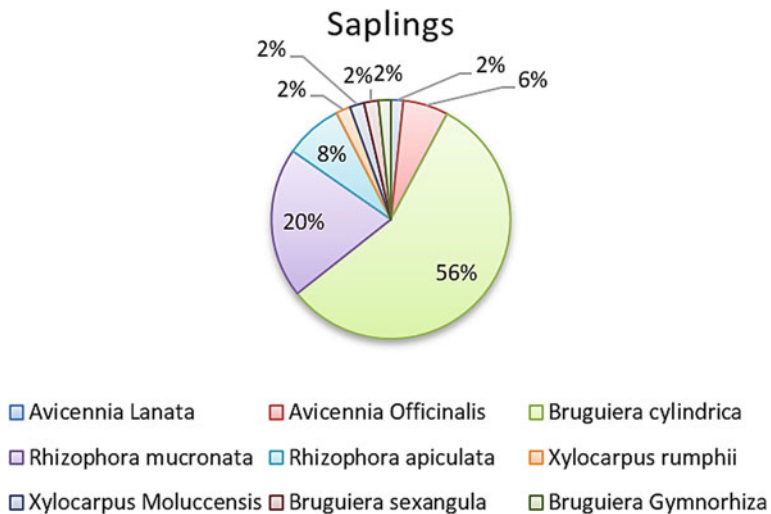
Fig. 4   Percentage of mangrove sapling species from 14 plot

■	1.296200156 - 2.159018842
■	2.159018843 - 3.021837527
□	3.021837528 - 3.884656213
□	3.884656214 - 4.747474898
□	4.747474899 - 5.610293583
□	5.610293584 - 6.473112269
■	6.47311227 - 7.335930954
■	7.335930955 - 8.19874964
■	8.198749641 - 9.061568325
□	9.061568326 - 9.924387011
□	9.924387012 - 10.7872057

Species Value
1 – A. lanata
2 – A. officinalis
3 – B. cylindirica
4 – R. mucronate
5 – R. apiculate
6 – X. Moluccensis
7 – B. sexangular
8 – B. gymnorhiza

Fig. 5 IDW interpolation mangrove sapling species distribution at Pulau Kukup

3.1 Soil Salinity, pH and Resistivity

Soil salinity is the main soil characteristic of mangrove mud due to direct exposure to seawater during the tidal process. Mangrove soils are usually high in soil salinity. We tested the hypothesis by determining the level of soil salinity of two depths which is sediment surface and 50 to 100 cm depth. The test result shows that the range of salinity at sediment surface is between 6.51 to 10.00 ppt with an average of 7.64 ppt while at 50–100 m, is a range at 6.95 to 9.02 ppt with an average of 9.02 ppt. Some of the soils have higher salinity levels at sediment surfaces, while other soils have higher salinity values at deeper depths (50–100 cm) (Fig. 6). This clearly shows that the lower salinity occurs near the intertidal creeks due to continuous contact with seawater and freshwater mixing. Hence the salinity is diluted compared to the sites that are a distance from the creeks.

From the analysis, the average pH at the sediment surface is 6.54, whereas the mean value at 50–100 cm was 6.57. There are slight differences between pH values at the two-layer depths. The pH values at 50–100 cm were ranged from 6.43 to 6.75 (Fig. 7). From the literature studies, it is found that the common pH level for the optimum mangrove growth ranges from 6.7 to 7.3. It is concluded that Pulau Kukup the values of soil pH varied slightly among the sites.

Figure 8 show the summary of the soil conductivity of the study area. From the result, soil conductivity at the sediment surface ranges from 67.17 to 91.94 Ω.mm
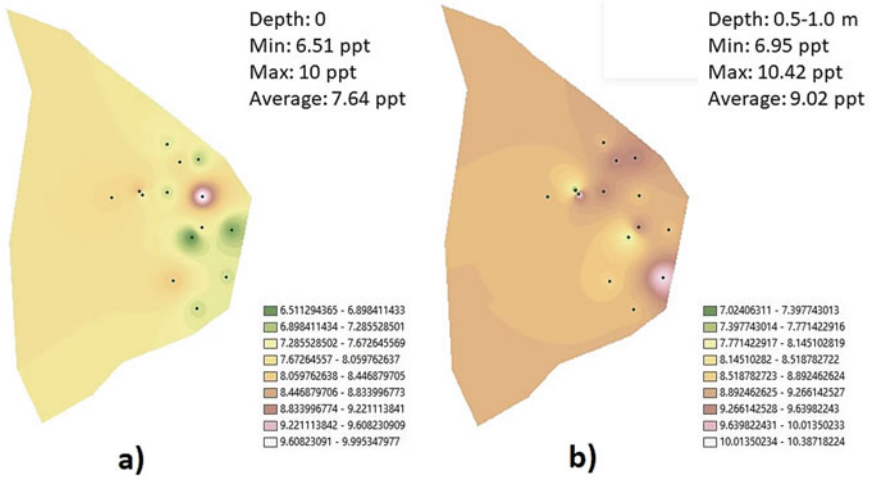
Fig. 6 IDW spatial analysis on salinity from 14 points. **a** for sediment surface, **b** for 50 to 100 cm depth
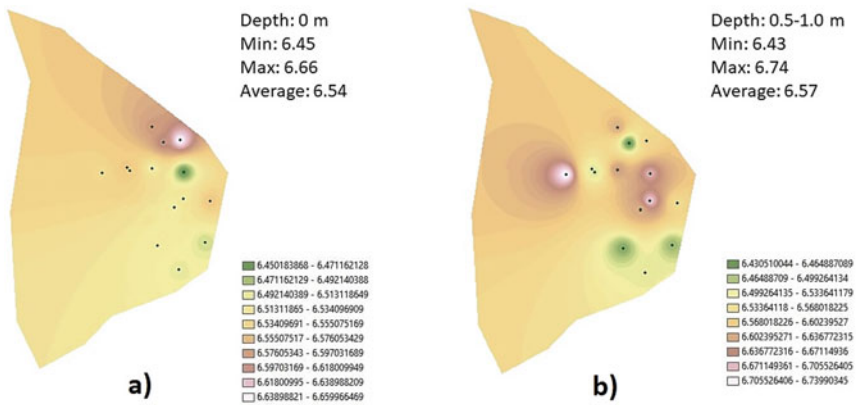
Fig. 7 IDW spatial analysis on pH from 14 points. **a** for sediment surface, **b** for 50 cm to 100 cm depth

while range at the depth 50–100 cm is 59.1 to 86.99 Ω.mm. The respective average for each depth was recorded at 79.92 and 67.95 Ω.mm (Fig. 8).
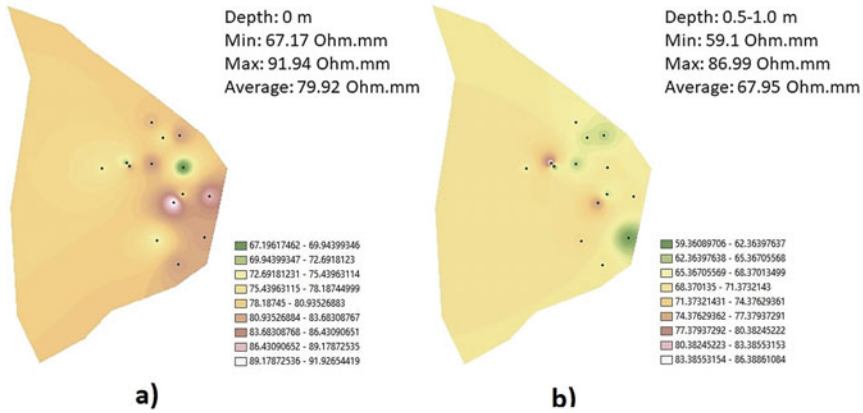
Fig. 8 IDW spatial analysis on conductivity from 14 points. **a** for sediment surface, **b** for 50 to 100 cm depth

3.2 Nutrients

There are 16 essential nutrients required for plants' growth and development. The most vital nutrients are namely carbon (C), hydrogen (H) and oxygen (O) from air and water (H_2O), while the other 13 nutrients are grouped into two main categories depending on the various amount needed for the plants. The first category is the macronutrients. In fact, nitrogen (N), phosphorus (P), and potassium (K) are the primary nutrients within the group of macronutrients. According to [7], the availability of soil nutrients to microorganisms and vegetation is involved by geochemical processes. From our analysis, it is found that the nitrogen. Range between 0.001 to 0.28% with the average 0.04% (Fig. 9). The high concentration of nitrogen can be related to organic-rich mud (plants and animals based) developed over many years at the mangrove substrate. Nitrogen (N) is an essential chemical parameter for plant growth and is taken up primarily.

Another important key element for mangrove growth is phosphorus. Phosphorus (P) plays a key role in different plant functions, such as photosynthesis and the transfer of energy. Phosphorus is also essential in stimulating early root formation and growth, which helps the plants to hasten maturity rates as well as seed production. Compared to total nitrate contents, available phosphorus is significantly high in percentage in the study area and recorded at the range of 0.15% to 0.42%, with an average of 0.28% (Fig. 10). However, the amount of available P decreases with depth on most sites.

Potassium (K), taken up by plants as potassium ion (K+), is vital in different plants' processes and functions. It also reduces respiration, prevents energy loss, improves the water regime of the plant, and increases its tolerance to salinity and drought. The plants are less affected by diseases if they are well supplied with potassium. The laboratory result for the soil test reveals that the soil of the study area was in the range of 0.06 to 0.21%. An average Potassium in the study area was recorded as
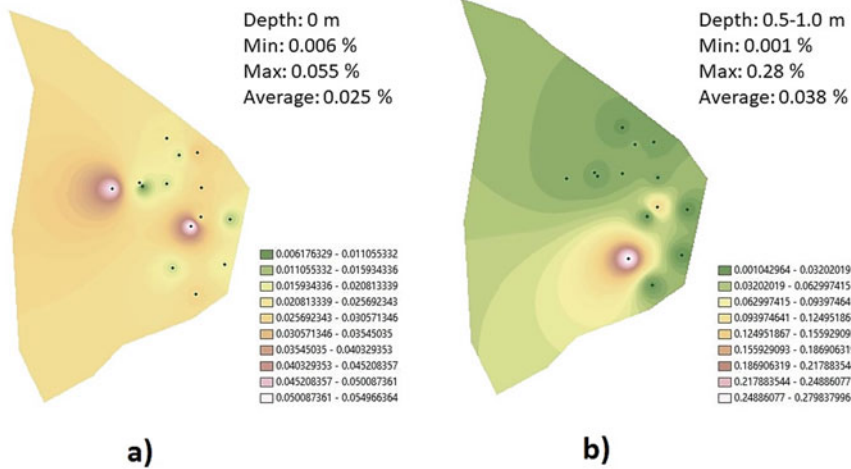
Fig. 9 IDW spatial analysis on nitrate from 14 points. **a** for sediment surface, **b** for 50 to 100 cm depth
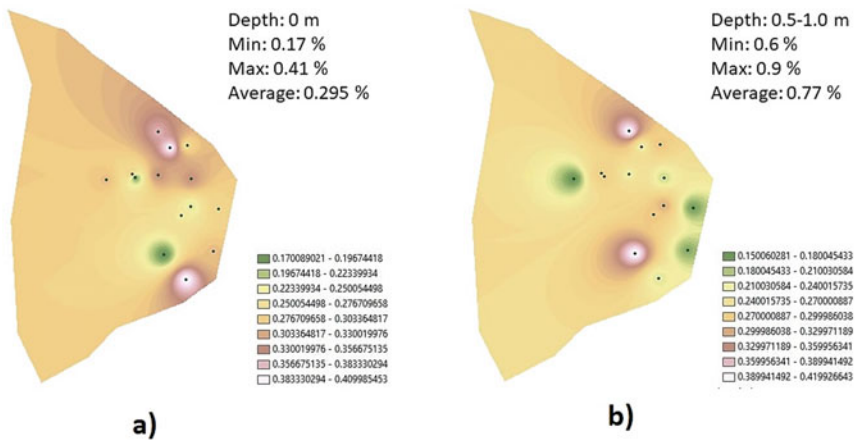
Fig. 10 IDW spatial analysis on phosphorus from 14 points. **a** for sediment surface, **b** for 50 to 100 cm depth

0.14% (Fig. 11). The results also indicate that the amount of K varies, while some are constant with depth.

The data showed that *Brugueira cylindrica* is most dominant at point 33 with nutrients content at sediment surface is N: 0.027%, P: 0.4%, and K: 0.18% and at 50 to 100 cm depth is N: 0.21%, P: 0.21%, and K: 0.006%. While *Rhizophora mucronate* is dominant at point 13 with nutrient content at sediment surface is N: 0.028%, P: 0.34%, and K: 0.12% and at 50 to 100 cm depth is N: 0.017%, P:
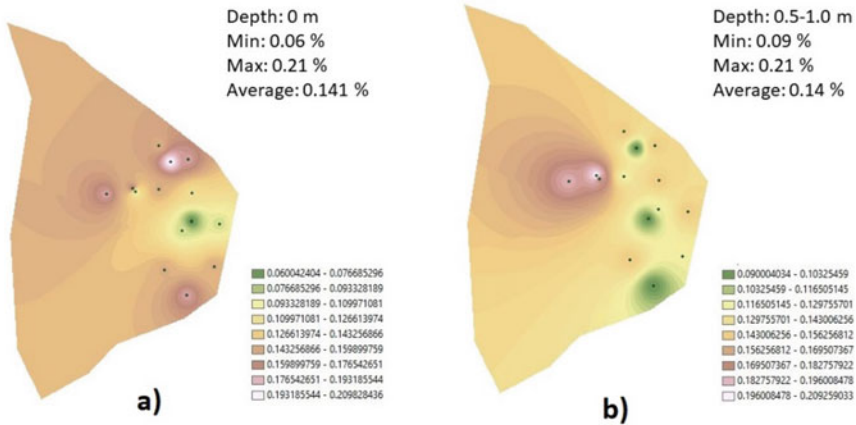
Fig. 11 IDW spatial analysis on potassium from 14 points. **a** for sediment surface, **b** for 50 to 100 cm depth

0.2%, K: 0.15%. However, this data does not show that these species are preferable to these values. It might vary geochemical processes, terrains, and waves. From the distribution perspective, *Brugueira cylindrica* mostly grow near the tide while *Rhizophora mucronate* mostly grow inner area of the island.

3.3 Particle Size Distribution

Particle size distribution is an index that shows what sizes (particle size) of particles are present in the sample particle group to be assessed in what proportions (relative particle amount as a percentage where the total quantity of particles is 100 percent). The majority of mangrove soils are mud, which is a mixture of silt and clay [8]. Record of the mangrove soils are identified as mud, which is the mixture of silt and clay which have the capability of soils to retain carbon, water and nutrient ions are strongly influenced by the soil texture but not all mangrove species favour the same type of soil [8]. The hydrometer method was used to determine the particle size distribution of mangrove soils passing 75 μ sieve. The hydrometer measures the specific gravity of the soil suspension. The specific gravity depends upon the mass of solids existing. The result shows that the soil sample consists of Gravel (larger than 2 mm), Sand (2.00–0.063 mm), Silt (0.063–0.002 mm), and Clay (smaller than 0.002 mm). The gravel contains ranges from zero (0) to 8%, with an average of 1.75%. Sand ranges from 2 to 26%, with an average of 10%. While for silt, its range was recorded from 61 to 95%, with an average of 83%. Finally, clay ranges from 0 to 23%, with an average of 5%. This result also shows that all the soil sample largely consists of silt which is it the number of percentages will increase with depth. Most of the soil determined in the study area was classified as silt loam soil. This type of

sediment characteristic is generally found at the mangrove substrate. [8] found that the Ramsar site, Johor which consist of Pulau Kukup, Tanjung Piai, and Sungai Pulai soil, is dominated by silty loam type.

4 Conclusion

The in-situ soil survey undertaken as part of the study supports the soil variable impacts on the geographic distribution of mangrove saplings. Soil maps were developed to determine the key properties of soils and their impact on the geographical distribution of mangrove saplings. This study indicates that the soils of Pulau Kukup are fine in texture at the surface layer as well as subsurface layer. All soils are categorized as very saline-sodic (very strongly saline and sodic). Mangroves, on the other hand, have a high salt tolerance and can absorb larger concentrations of salts and discharge them through the leaves, as well as tolerate high sodium levels. This is attributed to the nature of their habitat, which is constantly influenced by seawater. Meanwhile, the high availability of K and N, as well as the rich organic matter associated with soft mud deposits defined as fine silt and clay, enhance the health and development of mangrove forests. Tolerance of this characteristic is mostly suitable for *Brugueira cylindrica* and *Rhizophora mucronata* due to a high number of sapling species being found at each. However, inaccessibility to the whole Pulau Kukup had led to the lack of sample collected during the sampling process. This had compromised the interpolation output developed from the study. Therefore, it is suggested to use the data collected from the secondary and archive data while more extensive field data collection should be conducted to increase the data input, thus producing a more precise interpolation output map.

References

1. Azis SSA, Sipan I, Sapri M, Zafirah AM (2018) Creating an innocuous mangrove ecosystem: understanding the influence of ecotourism products from Malaysian and international perspectives. Ocean Coast Manag 165:416–427. https://doi.org/10.1016/j.ocecoaman.2018.09.014
2. Bouillon S, Borges AV, Castañeda-Moya E, Diele K, Dittmar T, Duke NC, Kristensen E, Lee SY, Marchand C, Middelburg JJ, Rivera-Monroy VH, Smith TJ, Twilley RR (2008) Mangrove production and carbon sinks: a revision ofglobal budget estimates. Global Biogeochem Cycles 22(2):1–12. https://doi.org/10.1029/2007GB003052
3. Irsadi A, Angggoro S, Soeprobowati TR (2019) Environmental factors supporting mangrove ecosystem in Semarang-demak coastal area. In: E3S web of conferences, vol 125, pp 0–4. https://doi.org/10.1051/e3sconf/201912501021

4. Mcivor A, Spencer T, Möller I, Spalding MD (2013) The response of mangrove soil surface elevation to sea level rise Natural Coastal Protection Series: Report 3. In: Natural coastal protection series. ISSN: Vol Report 3
5. Othman MA (1994) Value of mangroves in coastal protection. Hydrobiologia 285(1–3):277–282. https://doi.org/10.1007/BF00005674
6. Romañach SS, DeAngelis DL, Koh HL, Li Y, The SY, Raja Barizan RS, Zhai L (2018) Conservation and restoration of mangroves: global status, perspectives, and prognosis. Ocean Coast Manag 154:72–82. https://doi.org/10.1016/j.ocecoaman.2018.01.009
7. Singh G, Ramanathan AL, Prasad MBK (2005) Nutrient cycling in mangrove ecosystem: a brief overview. Int J Ecol Environ Sci 31(3):231–244
8. Sofawi AB, Nazri MN, Rozainah MZ (2017) Nutrient variability in mangrove soil: anthropogenic, seasonal and depth variation factors. Appl Ecol Environ Res 15(4):1983–1998. https://doi.org/10.15666/aeer/1504_19831998
9. Tan DD, Wan Juliana WA, Maimon A (2012) Community structure and productivity of mangrove forests in two national parks of West Malaysia. Malaysian Forest 75(2):165–176
10. Wells AG (2006) Distribution of mangrove species in Australia. Table 2:57–76. https://doi.org/10.1007/978-94-017-0914-9_6
11. Holmer M (2020) Mangroves of Southeast Asia. In: Biogeochemistry of marine systems, pp 1–39. Blackwell
12. Primavera JH, Friess DA, Van Lavieren H, Lee SY, (2019) The mangrove ecosystem. In: World seas: an environmental evaluation, pp 1–34
13. Primavera JH, (1995) Mangroves and brackishwater pond culture in the Philippines. In: Asia-Pacific symposium on mangrove ecosystems, pp 303–309. Springer, Dordrecht. https://doi.org/10.1007/978-94-011-0289-6_34
14. Memon JA, Chandio AA (2011) Critical appreciation of restoration and conservation of degraded mangroves in Thailand. Int J Environ Rural Dev 2(2)
15. Low JKY, Arshad A, KH L (1994) May. Mangroves as a habitat for endangered species and biodiversity conservation, 157-170. In: Wilkinson C, Sudara S Chou. LM Proc. Third ASEAN-Australia Symposium on Living Coastal Resources, pp 16–20

Potential Development of Coastal Reservoir in Malaysia

M. R. Razali, A. F. Hamzah, I. K. Othman, H. L. Lee, N. S. Rosli, W. A. H. W. M. Azhary, A. Ahmad, S. B. Hamzah, and M. H. Jamal

Abstract Malaysia is a tropical Southeast Asian country with a steady annual rainfall and river flow pattern. The enormous river networks provide enough supply to build a coastal reservoir study, which would coincide with the government's goal of exploring new raw water storage and delivery options. This study examines the present state of knowledge, technical features, and studies concerning coastal reservoirs around the world. Despite the possibility of high costs on the reservoir

M. R. Razali (✉) · H. L. Lee · W. A. H. W. M. Azhary · A. Ahmad · S. B. Hamzah
Coastal and Oceanography Research Centre, National Water Research Institute of Malaysia
(NAHRIM), Seri Kembangan, Selangor, Malaysia
e-mail: mrizal@nahrim.gov.my

H. L. Lee
e-mail: hllee@nahrim.gov.my

W. A. H. W. M. Azhary
e-mail: wanhafiz@nahrim.gov.my

A. Ahmad
e-mail: anizawati@nahrim.gov.my

S. B. Hamzah
e-mail: saifulbahri@nahrim.gov.my

A. F. Hamzah
Hydraulic and Instrumentation Laboratory, National Water Research Institute of Malaysia
(NAHRIM), Seri Kembangan, Selangor, Malaysia
e-mail: ahmadfarhan@nahrim.gov.my

I. K. Othman · M. H. Jamal
Center for Coastal and Offshore Engineering (COEI), School of Civil Engineering, Faculty of
Engineering, Universiti Teknologi Malaysia (UTM), Skudai, Johor, Malaysia
e-mail: ilya@utm.my

M. H. Jamal
e-mail: mhidayat@utm.my

N. S. Rosli
Corporate Planning Division, National Water Research Institute of Malaysia (NAHRIM),
Seri Kembangan, Selangor, Malaysia
e-mail: shahida@nahrim.gov.my

embankment and water delivery, feasibility studies are proceeding and yielding good results. According to this research, embankment design and reservoir operation must account for climate change implications such as rising groundwater level, changing streamflow discharge during intense and extended droughts, floods, and water quality issues. Although various technical aspects require further research current state of knowledge and technology are sufficient.

1 Introduction

The present water resources situation is already experiencing stress in terms of both quantity and quality. Thus, water resources planning is one of the main concerns of the Malaysia Government. A sustainable solution to water resources development is critical to support the increasing water demand due to the population growth and needs demand for local agricultural activities. As stated by Yang et al. (2015), the concept of the coastal reservoir has been adopted and successfully implemented in many countries such as India, China, Singapore, North/South Korea, Netherlands and United Kingdom, as shown in Table 1. This concept can be similarly implemented in Malaysia, which has an abundance of rainwater but faces a water supply shortage [8].

The coastal freshwater reservoir is a new emerging concept of storing floodwater in the sea close to the shoreline. A coastal reservoir is defined as any structure designed to capture fresh river flow before it enters the sea and mixes with saltwater. These water retention structures, by the very nature of their design, have to be placed at the tail end of the catchment; hence they will be naturally affected by the various

Table 1 Existing sea-based reservoirs around the world with their usage (Yang et al. 2015)

Country	Locality	Purpose
Netherlands	Afsluitdijk in the Ijsselmeer, 1932	Flood control
India	Thanneermukkom Bund, 1974	Agriculture
South Korea	Sihwa, 1994 Saemanguem, 2010	Tidal energy Land reclamation and freshwater
Hong Kong	Shek Pik, 1968 Plover Cove High land	Freshwater Freshwater Freshwater
China	Qingcaosha, 2011 Chenhang, 1992 Baogang, 1985	Freshwater Freshwater Freshwater
Singapore	Marina Barrage, 2008	Freshwater
United Kingdom	Cardiff Bay Barrage, 1987	Freshwater lake

hydrologic, hydraulic, hydrodynamic, tidal and other environmental processes that occur upstream of a coastal reservoir [22, 28–30]. Hence, it is vital that a deep understanding of these processes is essential so that coastal reservoirs can be designed, constructed and operated in a sustainable manner.

Coastal reservoirs can be constructed in shallow waters at appropriate locations close to the river's mouth, along with a barrage at one or two ends [17, 26]. River/tidal gates and barrages, preferably at the watershed's lower boundary, especially near the coastal region [7]. Cut-off walls are commonly used as an alternative to the desalination of coastal aquifers in many coastal regions. Current research suggested that the high-velocity freshwater flow at the bottom cut-off wall opening was critical to prevent seawater intrusion [4]. These are barriers between saline and freshwater environments in the coastal or river mouth. The water in the coastal reservoir can be used for drinking, irrigation or industrial usage compared with water from seawater desalination processes. The water quality is similar to stormwater or dam water in the inland reservoir, which saves costs by using natural resources. There is a severe demand–supply mismatch. Though there has been no significant change in Malaysia's rainfall pattern, the number of areas under the dry season most probably is increasing due to climate change [18]. An increase in population is one of the reasons for water scarcity, but the inefficient management of the received precipitation stands as the major cause [7, 15]. Though extreme rainfall events are significantly increasing, there is a spatial non-uniformity in the rainfall events. This makes it difficult to pre-plan large-scale water storage at different locations.

Demand for water keeps on increasing day by day. However, average rainfall has remained constant, and it is plentiful. Based on the National Water Resources Study (2000–2050) and the Formulation of National Water Resources Policy (2011) [6], the wet season in Malaysia falls on over three months, starting from November to January and a dry season from February to July, with some regions facing water shortage. According to the [13], Malaysia requires some preparation to manage freshwater from rainfall during the rainy season in the existing circumstances (Fig. 1).

The currently available solutions are unable to satisfy people's increasing need for water. As far as rainwater is concerned, one area receives too much rain in the wet seasons, causing floods and excess rainwater to discharge into the sea while receiving a shortage of rainfall in dry seasons. Hence, the solution lies in utilizing or conserving the abundant monsoon water that runs off the ocean. There is a need for a method for developing a sustainable water source for managing rainwater. There is further a need to store floodwater in sea-based reservoirs by building impermeable sea walls and interlinking these reservoirs to transfer water from one place to another. The primary objective of the present paper is to highlight the potential of coastal reservoirs for storing runoff and floodwater.
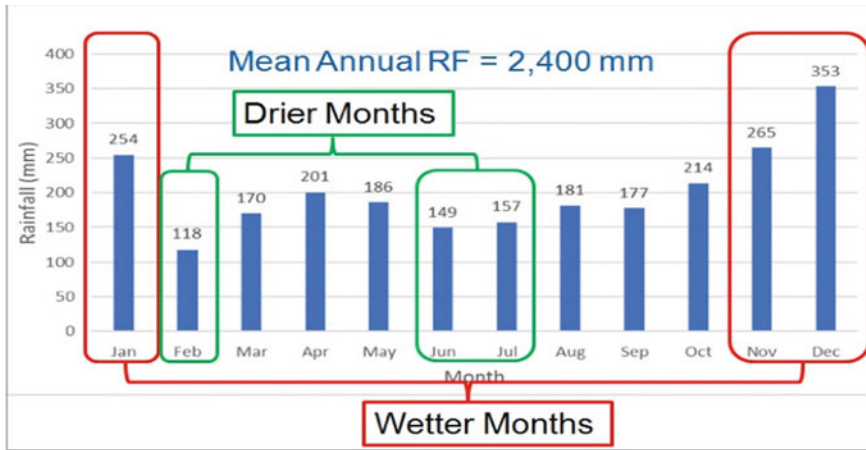
Fig. 1 Typical monthly rainfall distribution of Malaysia, [13]

2 Application and Function

The increasing demand for a clean and safe drinking water supply has become one of the key challenges facing sustainable coastal socio-economic development because most urbanized coastal cities lack freshwater resources [5]. The coastal freshwater reservoir is a new emerging concept of storing floodwater in the sea close to the shoreline. Coastal reservoirs can be constructed in shallow waters at appropriate locations close to the river's mouth, along with a barrage at one or two ends [17]. A coastal reservoir with freshwater has been created by constructing the saltwater barrier to increase agricultural activities and facilitate land development [20]. A coastal reservoir is a unique structure constructed at an estuary or gulf, bay or in the sea (the point where a river meets a sea) to store the portion of excess water at flood time. This sea wall or dike structure may run for kilometres together on the coastline. A coastal reservoir means building a storage structure near the mouth of a river. In this way, the amount of water that is wasted as runoff can be stored.

Coastal reservoirs do not require land acquisition and do not cause land submergence like inland reservoirs. The construction of a coastal reservoir does not involve many risk factors and disadvantages like relocation in an inland dam construction. Land-based reservoirs like dams have various advantages. They also have their disadvantages. Land acquisition, clearing of forest areas, loss of biodiversity, submergence of lands and forests, diversion works during construction. Tables 1 and 2 provide a comparison of land-based reservoirs and sea-based reservoirs, as well as the advantages of coastal reservoirs over traditional dams.

With considerations from the benefits of sea-based reservoirs in Table 3, the solution is to store floodwater in sea-based reservoirs, which are extremely valuable because they do not submerge land.

Table 2 Comparison of sea-based reservoir vs land-based reservoir [19, 23, 24]

Criteria	Sea based reservoir	On land reservoir
Dam site	Sea (Inside/outside river mouth)	Valley (limited area)
Water level	At sea level	Above sea level
Pressure	Low pressure along with wave surges	High water pressures
Catchment area	Entire Catchment of the river course	Partial catchment
Seepage	By density difference (Slow)	By head difference (fast)
Pollutant	Land based and sea water	Land based
Land acquisition	Nil	High
Environmental damage	Nil (no forest damage, no displacement of people, etc.)	Very high (difficult to build dams nowadays)
Water supply	By pumping	Mainly by gravity
Construction cost	Low	High

Table 3 The advantages of coastal reservoirs against conventional dams [23]

Comparison	Dam	Coastal reservoir
Land acquisition	• A large land area is required to be inundated • Loss of productive land	• Minimum land acquisition, utilizing river reserves, buffers, waterways, shore area etc • Potentially creates new land area and enhances surrounding property value with a significant water body
Environmental impact	• Loss of fauna and flora • Loss of green area and thus carbon absorption	• Minimum or no impact
Social impact	• Creates social issues and faces strong objection from locals and public	• Less social issues as site selection can be very flexible
Heritage/historical site	• Sometimes may inundate heritage or historical site • Very far, up to hundreds of km	• Unlikely and can be avoided as site selection is flexible • Very near to demand points
Distance to demand point	• High energy cost as it involves booster pumping from source to demand points • More losses due to longer pipe length	• Low energy • Fewer losses due to much shorter pipe length
Catchment area	• Often site at upstream, thus having a smaller catchment area • During drought, the reservoir gathers no rainfall	• Sited downstream, thus having a much larger catchment area • Gathers flow potentially throughout the year

Table 3 (continued)

Comparison	Dam	Coastal reservoir
Expandability	• Limited and difficult	• Can be easily expanded
Risk	• Create dam break risk to downstream population and properties	• Minimal or no risk
Maintenance cost	• Higher	• Lower
construction	• Slower	• Faster

3 Design Concept and Issues on Coastal Reservoir

Currently, the main source of water is river runoff. Surface water is the most extensively developed resource due to the abundance of rainfall in Malaysia, as shown in Fig. 2.

Based on the rainfall depths and recipient land surface areas, there is an annual rainfall volume of roughly 990 billion m^3 [14]. We can retain and store the surface or river runoff at the downstream or nearshore by utilizing a river reservoir or by constructing the reservoir at the nearshore, as shown in Fig. 3. Locating the reservoir close to the demand centre downstream captures a more significant portion of catchment runoff. It alleviates the need for regulating environmental flow from a dam or to other river intakes. In contrast to conventional downstream river intakes, a
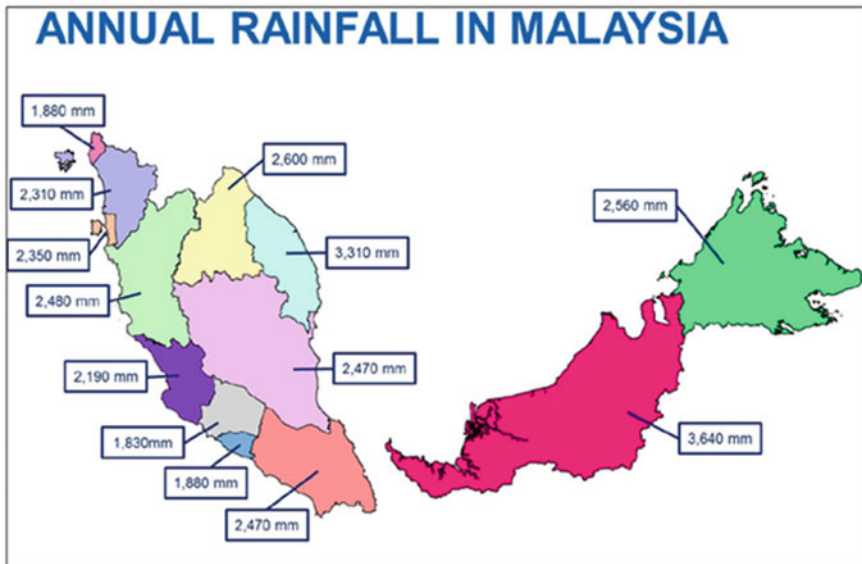
Fig. 2 Annual rainfall distribution in Malaysia (The Malaysian National Water Resources study 2010)
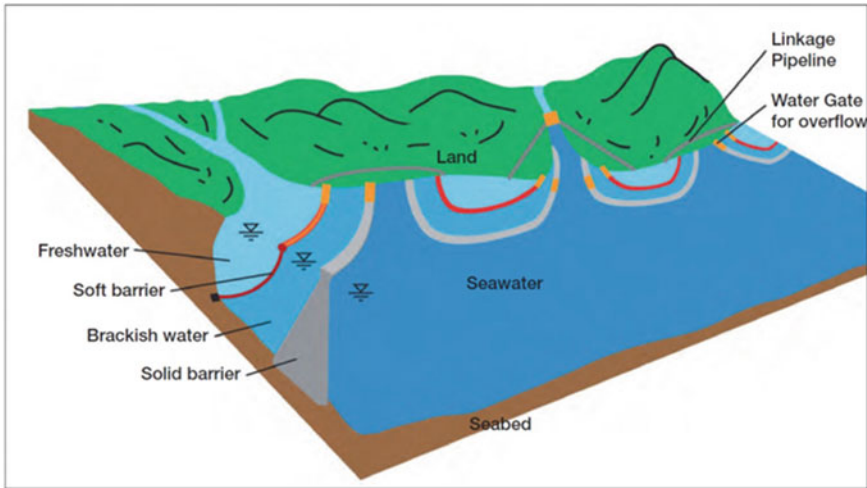
Fig. 3 Coastal reservoir concept [16]

downstream or coastal reservoir is also protected from salinity intrusion by virtue of its containing structure and can be selective about receiving a flow of suitable water quality [16].

The coastal reservoir also takes advantage of the monsoon pattern in Malaysia, which dominates rainfall patterns and monthly distribution. Storage of excess flood water during wet seasons allows for distribution during the next dry spell. Sizing of the storage required can be estimated by assuming zero inflow into the reservoir during drought [16], and the actual storage requirements may require detailed design and reservoir storage simulations (Yang 2016) [23, 25]. Coastal reservoirs can be designed to absorb the flood water shocks and release water out to sea only during low tides. Even the sand, silts and salts can join the ocean partly through the sea-based reservoir. The sea-based reservoir can be constructed in shallow waters at appropriate locations close to the mouth of the river, along with a barrage at one or two ends. They are designed with gates so that the excess flood water that is more than the reservoir's capacity can be discharged into the sea. Even inlets and outlets are controlled so that only good-quality water enters the reservoir with very little water stagnation. One can adopt very innovative designs with smart sensor networks to operate the coastal reservoirs efficiently [21, 26]. Hydraulic and physical barriers are the main measures to prevent seawater intrusion. Implementation of hydraulic barriers may be limited by the requirement of freshwater recharge, where coastal aquifers face water shortages [4]. A detailed study is needed, even considering saltwater intrusion through estuaries, bays and gulfs.

The coastal reservoir can be constructed of concrete, earth or other materials depending on the soil condition and consists of a primary and secondary barrier. The primary barrier should be high enough to avoid tidal flux and significant wave height and withstand the forces imparted on the wall by wave and tidal actions. The
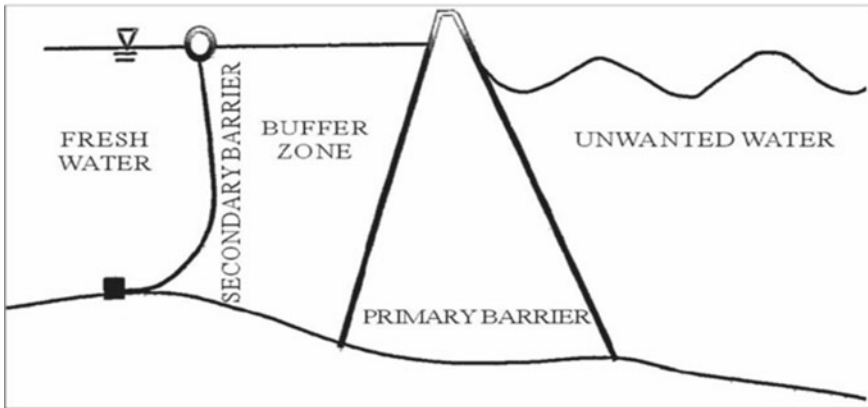
Fig. 4 Illustration of buffer zone created by primary and secondary barriers (Yang et al. 2005)

secondary barrier is typically a floating barrier with a suspended skirting that extends to the reservoir floor and can be weighted with ballast to fix it in place. This allows a buffer zone that can be varied in volume to maintain and separate contaminated water from uncontaminated freshwater, as shown in Fig. 4 [10, 11].

The sidewalls consist of impermeable sea dikes at one side and the coast bound on the other side [27]. These sea dikes with suitable modifications can create coastal reservoirs within the shallow waters of the coast. Sea dikes are classified as a hard engineering shore-based structure used to provide protection and lessen coastal erosion. Sea dikes may also be constructed from various materials, most commonly: geosynthetic tubes, geo-cells, reinforced concrete, boulders, steel, or gabions. Sea dikes are primarily used at exposed coasts, but they are also used at moderately exposed coasts. Commonly, the use of sea dikes is presented for the separation of ocean saltwater from the floodwater from rivers stored in coastal reservoirs [17, 21]. A sea dike is an embankment widely used to protect low-lying areas against inundation and acts as a backwater to prevent erosion of the coast and encroachment of the sea. The purpose of a sea dike is to protect areas of human habitation like towns and villages and conservation and leisure activities from the action of tides and waves [9, 12, 17] (Fig. 5).

Further, it prevents coastline erosion and creates calm water in the coastal reservoir area for many activities. The most important function of the dike, in this case, is to separate saltwater and freshwater in the coastal reservoir. The dock also allows freshwater fishing and other activities in calm water conditions, and it can also provide dock or quay facilities along with the support of floating solar panels for energy production [17] (Fig. 6).

A review of the available geotechnical information helped in deriving a generalized geological model as a useful preliminary design profile for a quick check on stability and settlement of the proposed coastal reservoir, which is good enough for the feasibility study stage. However, a site-specific detailed integrated site survey is
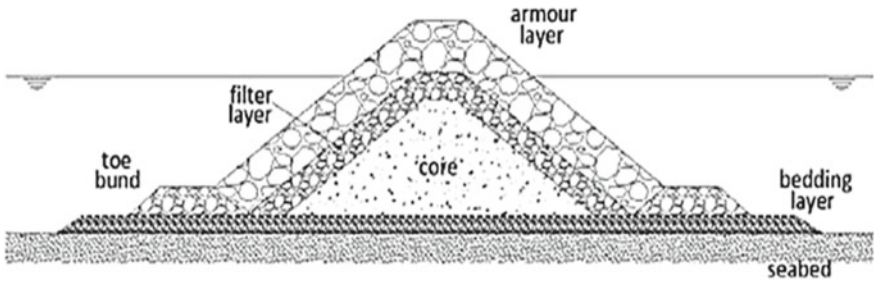
Fig. 5 Typical features of sea dike [17]
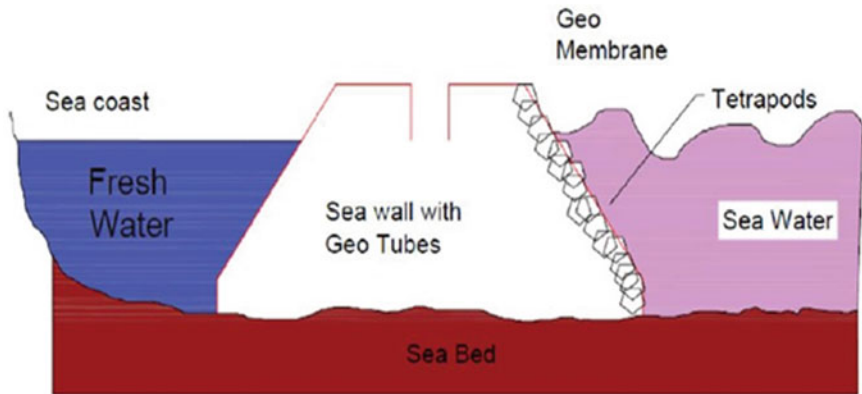
Fig. 6 A typical impermeable sea dike for the coastal reservoir [17]

warranted during the detailed project report stage. A detailed integrated site survey comprising of geophysical investigation (bathymetry, side-scan sonar and sub-bottom profile) and geotechnical investigation (boring, in situ testing and laboratory testing) shall be planned to be undertaken to derive the geological model appropriate for the location demarked for the coastal reservoir [1–3].

4 Conclusion

The increasing demand for clean and safe drinking water supply has become one of the key challenges facing sustainable coastal socio-economic development because most urbanized coastal cities lack freshwater resources. The continuous expansion of urban areas and growing populations are associated with increasing water demand, both for domestic and non-domestic uses. Improving water resources management by adopting the new and innovative approach of a coastal reservoir can potentially

increase the utilization of raw water resources. This potentially resolves the water shortage problem during drought by storing the excess water during wet seasons. The paper explored the application of coastal reservoirs. The coastal reservoir can be located away from environmentally sensitive areas, which is beneficial in protecting the environment. Overall, the coastal reservoir is a cost-effective, environmentally friendly, green and sustainable solution for raw water resources development in Malaysia. For more rational use of water, coastal reservoirs might be the future in planning a cheaper and more sustainable way. In a further study, more coastal reservoir applications will be more deeply discussed.

References

1. Armandei M, Linhoss AC, Camacho RA (2021) Hydrodynamic modelling of the Western Mississippi Sound using a linked model system. Reg Stud Marine Sci 44:101685. https://doi.org/10.1016/j.rsma.2021.101685

2. Abd-Elaty I, Abd-Elhamid HF, Nezhad MM (2019) Numerical analysis of physical barriers systems efficiency in controlling saltwater intrusion in coastal aquifers. Environ Sci Pollut Res 26(35):35882–35899. https://doi.org/10.1007/s11356-019-06725-3

3. Bortolin EC, Weschenfelder J, Fernandes EH, Bitencourt LP, Möller OO, García-Rodríguez F, Toldo E (2020) Reviewing sedimentological and hydrodynamic data of large shallow coastal lagoons for defining mud depocenters as environmental monitoring sites. Sed Geol 410:105782. https://doi.org/10.1016/j.sedgeo.2020.105782

4. Chang Q, Zheng T, Chen Y, Zheng X, Walther M (2021) Influence of inland freshwater influx on the natural desalination of coastal aquifers with a cut-off wall. Desalination 499:114863

5. Chen N, Hong H, Gao X (2021) Securing drinking water resources for a coastal city under global change: Scientific and institutional perspectives. Ocean Coast Manag 207:104427. https://doi.org/10.1016/j.ocecoaman.2018.02.023

6. Department of Irrigation and Drainage (DID) (2010) Review of the National Water Resources Study (2000–2050) and formulation of National Water Resources Policy, Ministry of Natural Resources and Environment, Malaysia

7. Heng HH, Pan WF, Siaw FL, Hii CP (2017) Coastal and estuary reservoir: case studies for Johor River Basin. J Civil Eng Sci Technol 8(1):25–40

8. Lim SP, Teo FY, Tan YC, Mohd Noh MN (2020) A paradigm shift of water resource management from upstream reservoirs to downstream/coastal reservoirs in Malaysia. Sustain Water Res Dev Using Coast Res, 231–246. https://doi.org/10.1016/b978-0-12-818002-0.00012-5

9. Liu J, Sivakumar M, Yang S, Jones BG (2018) Salinity modelling and management of the lower lakes of the Murraye Darling basin. Australia. WIT Trans Ecol Environ 228:257–268

10. Liu J, Yang S, Jiang C (2013) Coastal reservoirs strategy for water resource development—a review of future trend. J Water Res Prot 5:336–342

11. Liu X, Wang X, Guan X, Kong L, Su A (2009) Study on storage capacity and characteristic water level for qingcaosha reservoir. Water Res Hydropower Eng 7(002)

12. Miao T, Lu W, Lin J, Guo JY, Fan Y (2019) Simulation of seawater intrusion and optimization of cut-off wall schemes based on surrogate model. Hum Ecol Risk Assess 25(1–2):297–313. https://doi.org/10.1080/10807039.2018.1553611

13. National Integrated Water Resources Management Plan (2016) Academy of Sciences Malaysia (ASM), Malaysia Ministry of Environments and Water. https://www.kasa.gov.my/resources/air/national-water-innovation-roadmap-vol2.pdf. Accessed 1 Mar 2022

14. National Water Resources Study (2000–2050) and the Formulation of National Water Resources Policy (2011) Jabatan Pengairan dan Saliran (JPS) Malaysia. https://www.water.gov.my/jps/resources/PDF/Hydrology%20Publication/Vol2WaterGovernance.pdf. Accessed 1 Mar 2022

15. Tan ML, Liang J, Hawcroft M, Haywood JM, Zhang F, Rainis R, Ismail WR (2021) Resolution dependence of regional hydro-climatic projection: a case-study for the Johor River Basin, Malaysia. Water 13:3158. https://doi.org/10.3390/w13223158

16. Teh MJC, Lim SP (2017) Coastal reservoir as an innovative and sustainable solution to raw water resources development in Malaysia. In: G&P Water & Maritime Sdn. Bhd. Proceedings of the 37th IAHR World Congress, Kuala Lumpur, Malaysia

17. Parthasarathy CR, Sitharam TG, Kolathayar S (2018) Geotechnical considerations for the concept of coastal reservoir at Mangalum to impound the flood waters of Netravati River. Marine Geores Geotechnol 37:236–244. https://doi.org/10.1080/1064119X.2018.1430194

18. Razi MAM, Daud HZBH, Mokhtar A, Mahamud M, Rahmat SN, Al-Gheethi AA (2022) Climate change, tsunami and biodiversity endangered at the South China Sea, past, current and prediction models for the future: a comprehensive study. Mar Pollut Bull 175:113255. https://doi.org/10.1016/j.marpolbul.2021.113255

19. Yang SQ, Ferguson S (2010) Coastal Reservoirs Can Harness Stormwater. Water Engineering Australia, pp 25–27

20. Sitharam TG, Kolathayar S (2018) Thaneermukkom saltwater barrier to prevent saltwater intrusion: an overview of kuttanad low land development. Hydrolink IAHR 1(2018):14–15

21. Sitharam TG (2017) Efficacy of coastal reservoirs to address India's water shortage by impounding excess river flood waters near the coast. J Sustain Urban Plan Prog 2(2):50–55

22. Sivakumar M, Jones BG, Yang SQ (2020) Water quality considerations: from catchment to coastal reservoir. Sustain Water Res Dev Using Coast Res 3:33–59

23. Yang, S, Liu J, Lin P, Jiang C (2013) Coastal reservoir strategy and its applications. In: Wurbs R (ed) Water resources planning, development and management. Intech, United States, pp 95–115

24. Yang S (2010) Coastal reservoir in Murray-Darling River and its useful experience for Yellow River. In: Proceedings of the 4th international yellow river forum on ecological civilization and river ethics, vol 11, pp 65–79

25. Yang S, Lin P (2011) Coastal reservoir by soft-dam and its possible applications. Recent Patents Eng 5:45–56

26. Yang S (2005) Coastal reservoir. Singapore Patent no. 200504653–7

27. Yang S (2015) Coastal reservoir: a technology that may dominate future water supply. J Water Res Hydraul Eng 4:388–397

28. Yang S, Liu J, Lin P, Jiang C (2013) Coastal reservoir strategy and its applications. In: INTECH Open Science|Open Mind, vol 5, pp 95–115

29. Yang S, Ferguson S (2010) Coastal reservoirs can harness stormwater. Water Eng. Aust 5(2010):25–27

30. Xu Z, Ma J, Wang H, Hu Y, Yang G, Deng W (2018) River discharge and saltwater intrusion level study of Yangtze River estuary, China. Water 10(6):683

Numerical Study of Wave Groups in Wind-Swell Seas

A. M. Mansoor and M. Latheef

Abstract This paper concerns the study of focused wave groups in mixed sea states. These focused wave events are considered representative of the largest events that occur in a random sea state. A fully non-linear Higher-Order Spectral (HOS) solver was adopted to simulate the wave groups and investigate the physical mechanisms that govern the evolution of these events. For the near breaking uni-directional wave groups in deep-water conditions considered, it was seen that irrespective of the relative strength of the swell and wind component, the maximum crests obtained were much larger than those predicted by the commonly adopted linear and second-order solutions. Further analysis revealed that the third-order resonant interactions that alter the underlying free wave components are responsible for these larger crests. However, the most important parameter that determines the amplification was found to be bandwidth; the smaller the bandwidth, the larger the resonant interactions and hence the larger the crest elevation obtained. More importantly, it was found that for the mixed seas, once steepness and bandwidth are taken into consideration, the level of nonlinear amplification of the crests was independent of the shape of the underlying wave spectrum.

Keywords Focused waves · Non-linear waves · Unidirectional waves · Resonant interactions · Wave spectrum · Double-peaked spectra · Numerical wave modelling · Extreme ocean waves

1 Introduction

From an offshore engineer's perspective, random sea states that occur in the open ocean can be broadly categorised into wind sea states and swell sea states; as implied by the name, the former arises due to storm winds directly forcing the sea surface

A. M. Mansoor (✉) · M. Latheef
Civil and Environmental Engineering, Universiti Teknologi PETRONAS, Bandar Seri Iskandar, Malaysia
e-mail: mohamed_25561@utp.edu.my

M. Latheef
e-mail: mohamed.latheef@utp.edu.my

while the latter is the result of these wind seas propagating large distances away from the region where they are generated. Due to the differences in the origin of these two types of sea states, how the energy in these sea states is distributed across frequencies – known as a wave spectrum- have large differences. Typically, wind seas have a broader spectrum with significant energy across all frequencies, while swell seas are narrow-banded and have energy concentrated around a small range of frequencies. Figure 1 provides an illustration of a pure wind and pure swell wave. While the classification adopted so far is binary, wind seas may be generated at a location with significant swell energy, while a swell sea state may propagate onto a region where a wind sea is being generated. In these two situations, the sea resulting sea state is known as a mixed sea state with significant wind and swell energy.

Owing to the fact that wind seas are more severe compared to swell seas and also due to the fact that in regions such as the Gulf of Mexico and the North Sea, the most extreme sea states are wind seas, wind seas have received the most attention from researchers. A recent occurrence of these extreme seas states is the Tropical Storms (TS) in the Northwest Pacific, which includes the SCS. This region is known to have the most TS occurrences globally, with an annual average occurrence of 44, of which 40% of them exceed the typhoon intensity. The most recent TS was Typhoon Pabuk in 2018–2019, where the waves observed during the storm exceeded the wave conditions associated with a 100-year Return Period and were much larger and steeper than waves recorded in the previous 59 years. However, when the produced waves were compared to the local wind field, it was discovered that swell was responsible for the peaks in the wave conditions [5].

Limited experimental studies have proven to be complex, and some numerical studies are also limited because they investigate the statistical properties of the seas. Existing studies that understand extreme wave occurrences have been limited in mixed seas and is further limited when focused on the South China Sea (SCS); due to the lack of such sea states in other seas, like the North Sea, which usually contains mainly wind seas. Two important things that stand out from the existing studies
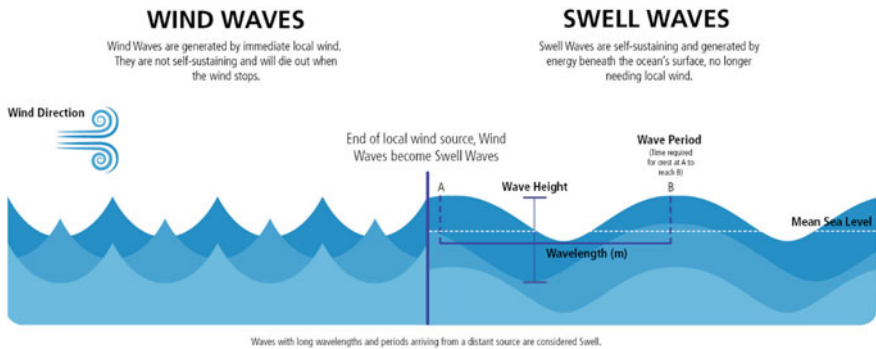
Fig. 1 Illustration of a pure wind and pure swell wave (Why Douglas Sea State 3 Should Be Eliminated from Good Weather Clauses, 2021) [8]

are how mixed seas have changes in nonlinear amplification of crests in deep and shallow water, looked at from statistical averages. This further brings into question the behaviour of individual wave events and why they undergo these changes. Furthermore, understanding these occurrences and isolating large events in such sea states and studying their individual evolution have yet to be investigated. These sea states need to be looked into in terms of the pure components and the mixed components in deep and shallow water conditions.

Therefore, the main aim of the present work is to investigate the physics underpinning the nonlinear amplification of wave groups occurring in mixed sea states. The paper continues in Sect. 2 with a background of mixed seas, a brief summary of previous studies on mixed sea states and the numerical model adopted in the present study. Section 3 introduces the deepwater cases considered in the present study, while Sect. 4 provides the main results before concluding in Sect. 5.

2 Background

Wind and swell seas are usually characterised as a mix when studying the behaviour of waves, known as a wind-swell mix. The contribution of either of these mixed seas depends on the region being looked at. The North Sea, for instance, has a larger wind component, while the South China Sea has a larger swell component for the extreme events occurring within the region. The most important aspect of studying wind and swell seas is to be able to represent them. To accurately represent the wave models, wind and swell seas are best represented using spectrum models. According to [4], the best models to represent wind seas are JONSWAP and Brettschneider spectra and the best models to represent swell seas are gaussian shape spectra. Figure 2 provides a detailed understanding of the best spectrum model representations used for wind and swell sea states.

Recent experimental studies have been able to investigate how the extreme wave statistics of a combined wind sea and swell differ from the extreme wave statistics of the corresponding wind sea and swell partitions in order to better understand these sea states. One paper, in particular, investigated why the following swell has no effect on the extreme wave statistics of a long-crested wind sea, but the extreme wave statistics of the combined long-crested wind sea and swell are more Gaussian and thus less extreme [6]. It also shows how analysing partitioned wave systems can expose non-linear interactions between them and suggests that one of the systems be studied separately. This reflects one of the study's aims, which will be focused on the examination of non-linearities in wind-only, swell-only, and mixed-state sea states. It is worth noting that experimental studies have proven to be difficult, time-consuming, and limited in scope, so numerical studies should be pursued for a more efficient and accurate investigation.

Another method of accurately and efficiently analysing sea states can be through numerical studies. [7] used numerical analysis to determine the statistical properties of uni-directional wave trains with a single peak and bimodal spectra, concluding
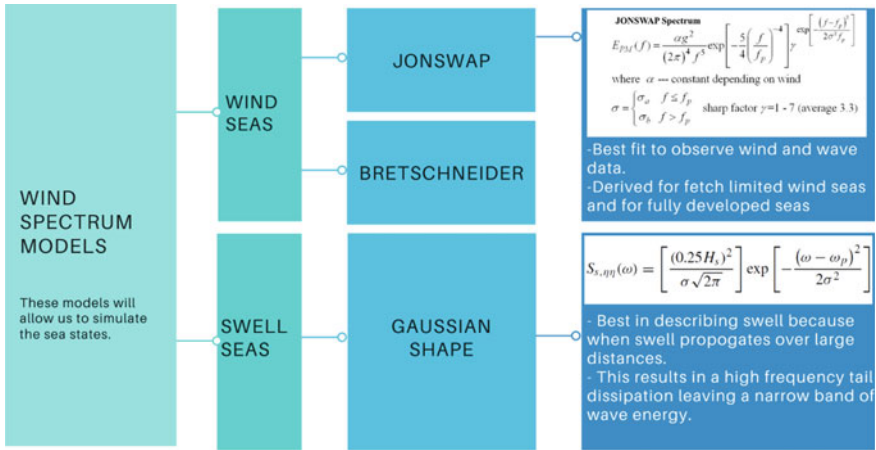
Fig. 2 Spectrum model representations for wind and swell sea states

that the non-linear evolution is not as intense as in swell and wind only sea states. According to the analysis, when a wind sea state exhibits strong non-linear behaviour and mixes with a moderately non-linear swell function, it behaves in a weakly non-linear manner. Another important finding is the validation of numerical data in relation to experimental data, which was also highlighted in the study, which included a comparison of free-surface elevations between experimental data and numerical results along with a wave tank.

The model to be adopted for the study of mixed seas in SCS is known as the pseudo spectral model, which is able to produce the wind data because the numerical scheme is validated against available analytical theories and high-quality experimental data. It is effective and reliable, and the model is suitable for waves propagating in constant depth water [1]. Because of its ability to integrate all non-linear wave interactions of irregular waves, this model is also known as a non-linear solver. It is computer-based and reliable enough to predict the evolution of near-breaking waves. [1] showed that this model is capable of numerically simulating directionally dispersed surface water waves. Plots extracted from the study by [2] shows the comparison of water surface elevation of linear, 2nd order, numerical and experimental outputs produced, as shown in Fig. 3. It can be seen that the numerical model replicates the same water surface elevation as compared to 2nd order stokes and experimental data. This not only allows for numerical simulation waves but also replaces the need for physical experiments. Hence, confirming the validation of the model that can be used in the study.
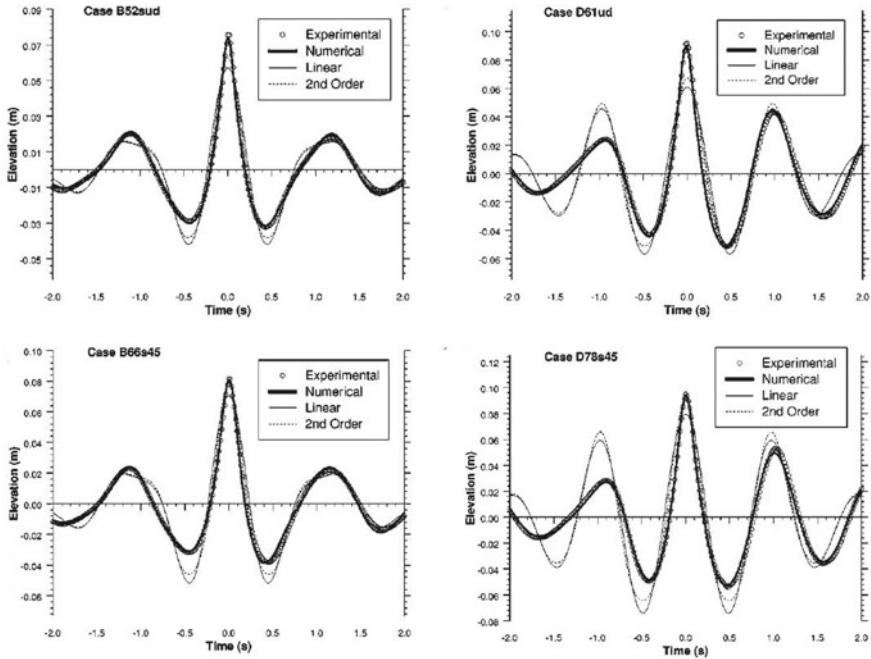
Fig. 3 Comparison of surface elevation between numerical and experimental data (Batemen et al. 2003)

3 The Deep Water Cases

To effectively validate the numerical models used, a second-order case was produced from the HOS model to reinforce the validity of the numerical models. The model was used to check if the second-order contributions extracted are identical to the second-order case profiles produced by the HOS model. Comparison of the second-order case produced by the HOS model and the extracted second-order contributions were analysed. Figure 4 shows a magnified plot of the maximum crest elevation and the adjacent troughs and Fig. 5 shows the corresponding amplitude wavenumber spectrum. The plots show that the extracted second-order contributions agree with the second-order case produced by the HOS model because they are identical. Once the outcome of the models has been validated, the extremely focused individual wave groups can now be simulated.

A total of 5 Deepwater cases were simulated and analysed, including a pure wind, a pure swell and three mixed wind-swell cases shown in Table 1. The spatial profiles and amplitude wavenumber spectrums of the waves were identified from the cases mentioned in Table 1. These cases are from a large, focused wave group in a unidirectional sea state. The ratios shown in the table are the representative value of the wind-swell mix. This means that the swell amplitude is divided by the total input

Fig. 4 Comparison of the spatial profiles of the case V1 produced by the HOS model (black solid line) with the second-order contributions extracted using second-order random wave theory (grey stars)
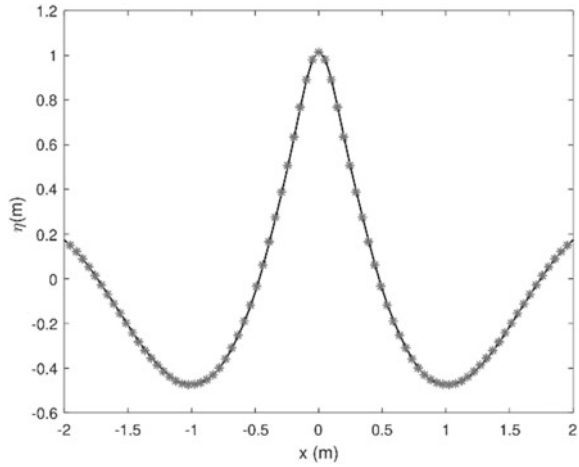
Fig. 5 Comparison of the amplitude wavenumber spectrums of the Second Order case produced by the HOS model (black solid line) with the second-order contributions extracted using second-order random wave theory (grey stars)
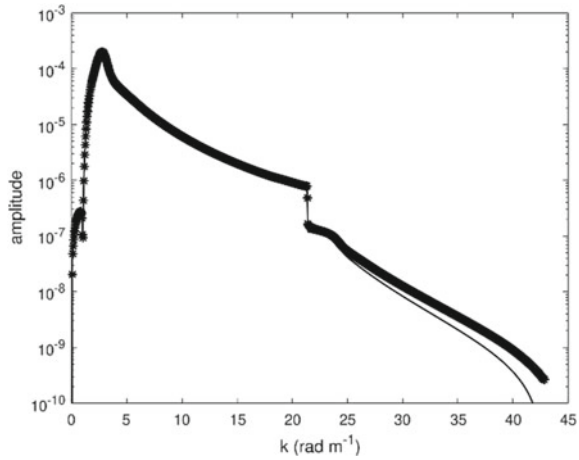
amplitude of 6.3 m. Therefore, a wind-swell ratio of 0.5 has half of the input wave height of 6.3 m from a swell component and the other half from a wind component. The model simulates the focused wave groups in such a way that all energies are focused up at the time, $t = 0$, and this is the point where the crests of the waves come in phase and are amplified. Mixing a wind and swell case together results in two-peak spectra, which is the wind-swell spectra, also known as a double-peaked spectrum. The double-peaked spectra of a mixed sea state are presented in Fig. 6 and are what a mixed sea state is represented as.

Table 1 Details of wave spectra investigated for deep-water cases and a maximum linear input amplitude of 6.3 m

Case	Depth	Type	Ratio
DW0	Infinity	Pure Wind	0
DM.67	Infinity	Mixed	0.67
DM.5	Infinity	Mixed	0.5
DM.33	Infinity	Mixed	0.33
DS1	Infinity	Pure Swell	1

Fig. 6 Mixed Sea, double-peaked spectra (black solid line) consisting of the wind component (black dotted line) and the swell component (black dashed line)
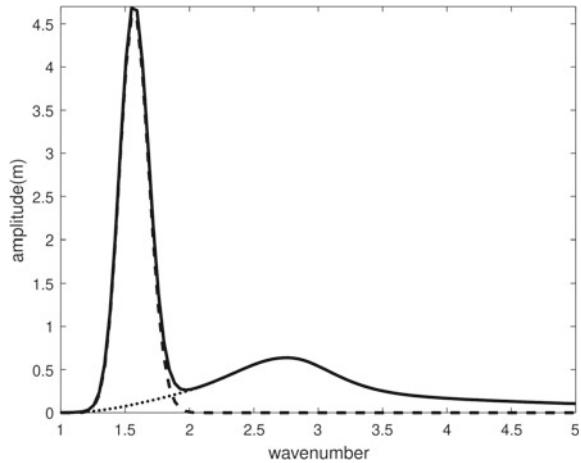
4 Results and Discussion

When the deep-water cases were simulated, an apparent observation was that all the cases showed a maximum crest elevation larger than the values obtained using linear or second-order theory. The linear input value of the maximum crest elevation was 6.5 m. Furthermore, the large, focused wave crests in the focused wave groups were proven to be transient because of energy transfers seen in the amplitude wave number spectra shown in Fig. 7. These wave profiles also showed significant crest–trough asymmetry shown in Fig. 8, where significant and rapid nonlinear interactions can occur during its formation, increasing both the crest elevation of the wave and the steepness of the wave. This increase in crest elevation was more than the linear and second-order values obtained. Analysis was then done to observe a trend that can explain the underlying mechanisms behind the non-linear amplification of the waves.

Different mechanisms that contribute to the evolution of the waves were analysed. When the amplification vs the wind-swell ratio and amplification vs steepness plots was observed, they did not correspond to any trend. Logically, a higher steepness should correspond to a higher elevation, which was not the case in the plots where at low values of steepness, larger crest elevations are observed and again did not correspond to a trend. Further analysis was then done to see the effect of bandwidth with

Fig. 7 Comparison of a focused wave group's wave propagation in a unidirectional sea state with infinite depth; comparison of the amplitude wavenumber spectrum at its maximum elevation (black solid line) and at its beginning (grey solid line)
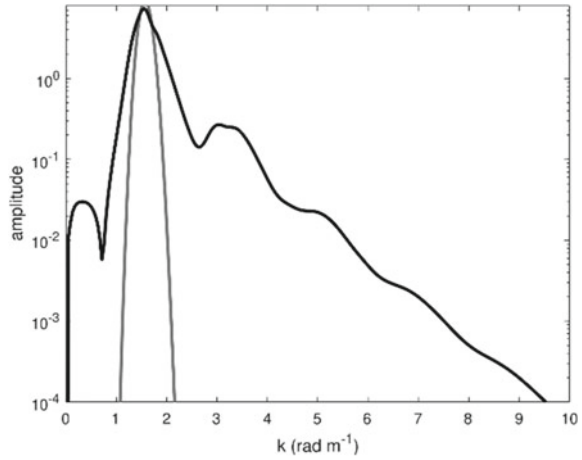
Fig. 8 Amplification in the space of all deep-water cases plotted and overlapped on top of each other for case DW0 (black solid line), case DM.67 (black dashed line), case DM.5 (black dotted line), case DM.33 (grey solid line), case DS1 (grey dashed line)
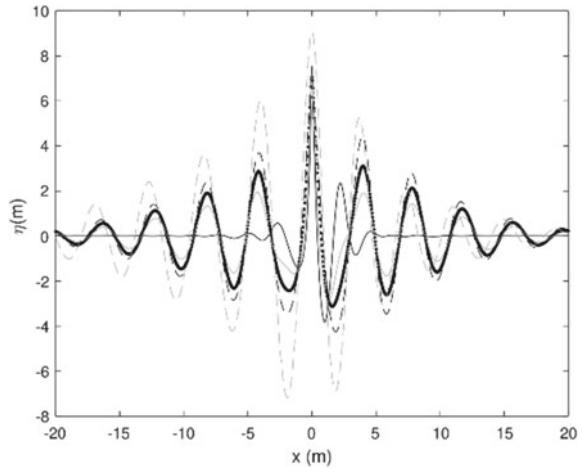
respect to the wind-swell ratio. The bandwidth was computed using spectral moments and computing the area under the amplitude spectrum of the cases. The nth moment of the spectrum is defined as:

$$m_n = \int_0^\infty \omega^n S_{\eta\eta}(\omega)d\omega \tag{1}$$

A plot of the bandwidth vs the wind-swell ratio was observed and did not correspond to a specific trend. Subsequently, a plot of the steepness vs the wind-swell ratio was analysed and showed a linear co-relation but only explained that steepness played a role in the overall contribution, as shown in Fig. 9. Additionally, a plot of the amplification vs the bandwidth was then plotted and showed a trend. Figure 10

shows that as the amplification decreases, the bandwidth increases, proving that more energy transfers and resonant interactions are observed in narrow banded cases.

It is known that there are contributions other than second-order terms that are involved in the non-linear amplification of waves. This includes the third order and above resonant interactions. Further spectral analysis was conducted to explain the importance of resonant interactions and subsequent evolution of the spectra and the relations with bandwidth. The Fourier transform applied to the profile when it reaches its maximum values, according to [3], assumes that the wave profile is the linear sum of various wave components, including both bound and free wave components. According to Johannessen and Swan (2003), separating a wave spectrum into its odd- and even-order wave components is a method for extracting resonant interactions and freely propagating wave contributions.

Fig. 9 Steepness vs wind-swell ratio of the 5 deep-water cases
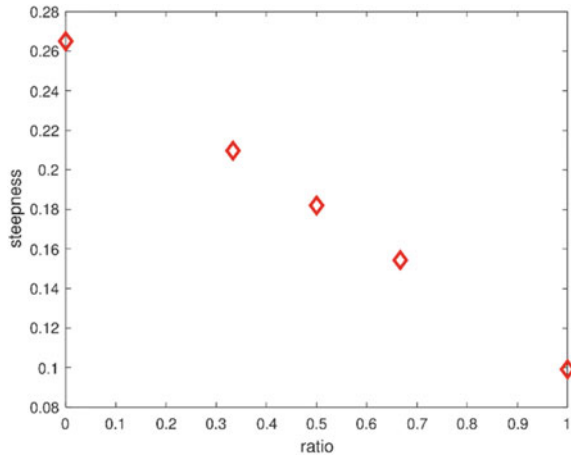
Fig. 10 Amplification vs the bandwidth of the 5 deep-water cases
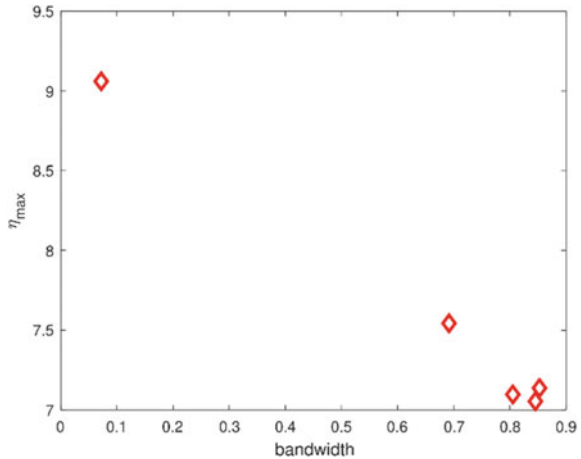
In Figs. 11 and 12, the grey dashed line is the second-order bound term which includes the second-order sum and difference terms computed from the free waves. However, since the input spectrum has been altered, as seen in the figures below, the second-order terms were observed to be altered too. It can be clearly seen that the swell only case has the largest transfer of energy and the freewave has altered the most, explaining its largest maximum amplification compared to other cases and a large shift in energies seen between the input wave and the resonant interactions. In comparison to the other cases, it can be seen that the input spectrum is limited to a smaller range of wavenumbers. This is in contrast to the odd-order contributions, which show a transfer of energies to a wider range of wavenumbers as a result of the creation of free wave components as a result of third-order and above resonant interactions.

Fig. 11 Surface profile of linear input amplitude (solid black line), inverted wave profile (black dashed line), odd-order contributions (solid grey line), even order contributions (grey dashed line)
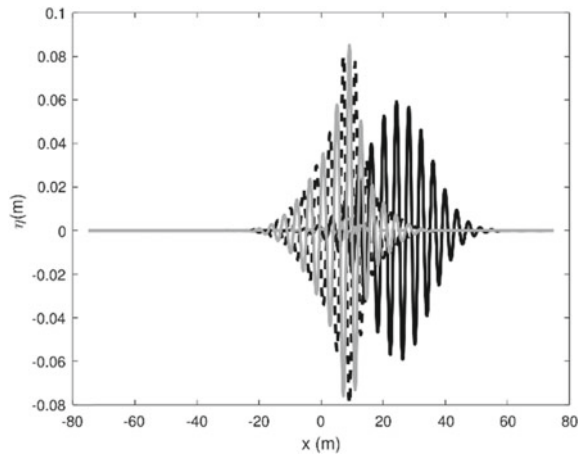
Fig. 12 Amplitude-wavenumber spectra of linear input amplitude (solid black line), inverted wave profile (black dashed line), odd-order contributions (solid grey line), even order contributions (grey dashed line)
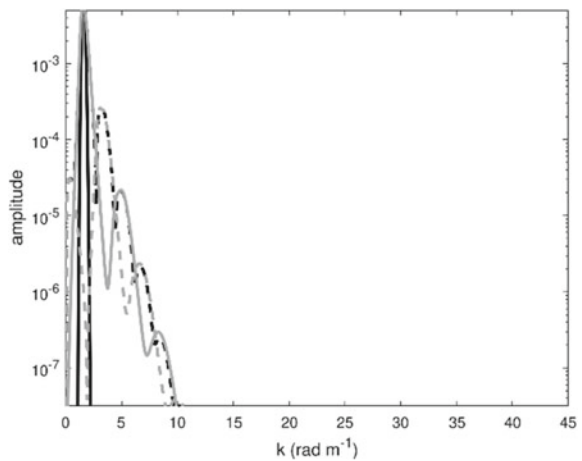
5 Conclusion

In the vicinity of an extreme wave event, the underlying or freely propagating wave spectrum undergoes significant and rapid changes. As a result, a linear solution based on a constant underlying spectrum is not the best representation for an extreme wave event propagating in space and time, which prompted further investigation into other factors at work. Particular emphasis was placed on bound interactions of second-order and higher, as well as resonant interactions of third-order and higher. Resonant interactions cause the formation of new freely propagating wave components. These were interactions in which three freely propagating wave components interacted to create a fourth freely propagating wave component that grew in size. As a result, the resonant interactions redistribute energy within the linear wave spectrum, affecting both the amplitude and phase of the underlying linear wave components. As a result, in a deep water focused wave group, where the surface profile is thought to represent an extreme wave event, third-order resonant interactions can be responsible for highly localised and very rapid energy transfers. Further investigation of these resonant interactions revealed that the steepness of the underlying wave group has a positive correlation with the highest crest elevation obtained. However, bandwidth was discovered to be the most important parameter determining amplification; the smaller the bandwidth, the larger the resonant interactions and thus, the larger the crest elevation obtained. More importantly, once steepness and bandwidth were considered, the level of nonlinear amplification of crests in mixed seas was found to be independent of the shape of the underlying wave spectrum.

References

1. Bateman WJ, Swan C, Taylor PH (2001) On the efficient numerical simulation of directionally spread surface water waves. J Comput Phys 174(1):277–305
2. Bateman WJ, Swan C, Taylor PH (2003) On the calculation of the water particle kinematics arising in a directionally spread wavefield. J Comput Phys 186(1):70–92
3. Gibson RS, Swan C (2007) The evolution of large ocean waves: the role of local and rapid spectral changes. Proc R Soc A Math Phys Eng Sci 463(2077):21–48
4. Latheef M, Abdullah MN, Jupri MFM (2020) Observed spectrum in the South China Sea during storms. Ocean Dyn 70(3):353–364
5. Shamsudin MA, Latheef M, Abdullah MN, A Rahman A, Rashid RM (2020) Characteristic of tropical storm Pabuk based on field measurement. In: Offshore Technology Conference Asia. OnePetro, October 2020
6. Støle-Hentschel S, Trulsen K, Nieto Borge JC, Olluri S (2020) Extreme wave statistics in combined and partitioned windsea and swell. Water Waves 2(1):169–184
7. Wang L, Li J, Liu S, Ducrozet G (2021) Statistics of long-crested extreme waves in single and mixed sea states. Ocean Dyn 71(1):21–42
8. StormGeo. https://www.stormgeo.com/products/s-suite/s-routing/articles/why-douglas-sea-state-3-should-be-eliminated-from-good-weather-clauses/

Numerical Simulations of Wave Diffraction Around a Low-Crested Semicircular Breakwater

Muhammad Nur Aiman Bin Roslan, Hee Min Teh, and Faris Ali Hamood Al-Towayti

Abstract Wave diffraction is a phenomenon of lateral energy transferring along the wave crest. This phenomenon could be seen as the waves being disrupted by a barrier (breakwater). In past decades, semi-circular breakwater (SCB) has been used to protect the coastal areas and has a semi-circular shaped hollow caisson founded on top of a rubble mound. Analysis method utilizing 1-Dimensional (1D) study is common in past research, yet the method dampened to provide vital phenomenon data likewise the diffracted wave height. 2-Dimensional (2D) study approach is viable to provide such data. Thus, it was employed for this study. Besides, previous research only focused on large-scale structures, and this study will focus on a small-scale structure since muddy coast is available in Malaysia. Hence, this paper aims to evaluate wave diffraction within submerged and emerged SCB vicinity subjected to regular waves using numerical modelling (FLOW 3D). Flow 3D is capable of handling coastal issues, especially for evaluating 3-Dimensional (3D) problems, i.e., wave diffraction. This paper focused on regular waves using wave period, 0.8 s, water depth, 0.4 m and wave steepness, 0.02. As a result, the wave diffraction coefficient, Kd value, showed a decreasing trend as the relative breakwater width, B/L value, increased.

Keywords Wave diffraction · Semicircular breakwater · FLOW 3D · Simulation · Numerical modelling

M. N. A. B. Roslan · H. M. Teh (✉) · F. A. H. Al-Towayti
Civil and Environmental Engineering Department, Universiti Teknologi PETRONAS, Bandar Seri Iskandar, 32160 Seri Iskandar, Perak, Malaysia
e-mail: heemin.teh@utp.edu.my

M. N. A. B. Roslan
e-mail: muhammad_20001481@utp.edu.my

F. A. H. Al-Towayti
e-mail: faris_18000464@utp.edu.my

1 Introduction

Nowadays, coastal engineers need to protect the coastal areas from wave activity due to various reasons, which is to protect the infrastructures, amenities as well as communities that live near the coastal areas. Due to this reason, coastal structures, i.e., harbours, need certain tranquillity conditions for the ships to get safe navigation and a place to berth. Other than that, due to the harsh conditions of the waves, our coastal areas had been attacked by severe erosion problems. Erosion is one of the main problems that threaten coastal areas around the world. According to Hashim et al. [10] and [9], coastline retreat could result in very serious social, economic and environmental impacts subjected to the eroded area. The consequences of the coastal erosion may lead to habitat loss, especially for marine species diversity that lived near the coastal areas and intertidal zone ecosystem. Thus, coastal structures were built to prevent further erosion of the shorelines and restoring the eroded coastal areas to their initial phase.

Kudumula and Mutukuru [14] said that the development of various coastal defence structures is very important to coastline protection and breakwater is one of the coastal protections that have been introduced to cater to this problem. Due to the fast growth in design and construction techniques, a new type of breakwater was introduced in the early 90 s, which is semi-circular breakwater. Semi-circular breakwater has a semi-circular shape with a hollow caisson laying on top of a rubble mound. Scholars nowadays are focusing on this type of breakwater, and most of the topic that has been selected is 1-Dimensional (1D) study.

Most of the researchers only focused on the 1D study, either physical modelling, numerical modelling or computational modelling. Gomes et al. [7] focused on computational modelling by using the Computational Fluid Dynamic (CFD) method, and Xu and Tao [26] used Artificial Neural Network (ANN) method to evaluate perforated semi-circular breakwater. Lyu et al. [17] and Fathi and Ketabdari [6] used numerical modelling to evaluate hydrodynamic characteristics of the semi-circular breakwater. Not only that but physical modelling has also been used to evaluate the performance of semi-circular breakwater [12, 24].

The studies mentioned earlier were done by using a 1D study, which includes wave transmission and wave reflection subjected only towards unidirectional waves. The previous literature portrayed a gap that 1D study is insufficient to provide vital data of wave diffraction data and made the wave diffraction near semi-circular breakwater has not been explored extensively by other researchers. Wave diffraction provides a variation of the wave height behind the structure (semi-circular breakwater), and this only can be obtained through 2-Dimensional (2D) study. By using a 2D study, a detailed evaluation of semi-circular breakwater can be done as wave diffraction is included in the study.

This research will develop a good understanding of a semi-circular breakwater, particularly on wave diffraction around the semi-circular breakwater, with the objective to evaluate wave diffraction in the vicinity of a submerged and emerged semi-circular breakwater subjected to head-on regular waves using numerical modelling (Flow 3D software).

2 Literature Review

A gravity-type breakwater is the favourite type of breakwater being used to protect the coastal areas. Due to the massive size and heavy, gravity-type breakwater can provide structural strength and stability against the waves. According to Teh [23] and Allsop et al. [2], gravity-type breakwater can be divided into three categories which are composite breakwater, vertical breakwater and rubble mound breakwater.

In past decades, the semi-circular structure has been used as a vertical breakwater and can be found on a rubble mound breakwater. The first prototype of semi-circular caisson breakwater was installed at Miyazaki Port in Kyushu Island, Japan, from 1992 to 1993. Semi-circular caisson breakwater at Miyazaki Port is made from prestressed concrete for semi-cylindrical caisson and a bottom slab laid onto a low crested rubble mound foundation. After the successful installation of the breakwater in Japan, China also adopted the semi-circular breakwater to protect the south harbour area at Tianjin Port in 1997. Later in 2000, another 18 km long semi-circular breakwater was installed at Yangtze Estuary, China, for the first phase of works of Deep Channel Improvement Project.

There are a few advantages of the semi-circular breakwater, such as good scenery enhancement, easy to relocate and reuse, easy to construct, low cost, suitable for poor soil condition, high stability against the wave action and high structural stability. Semi-circular breakwater also can be used in poor soil conditions. Tanimoto and Goda [22] commented that uniform distribution of subgrade reaction across the bottom slab is due to the wave forces exerted on the curved surface, which always been directed to the centre of the semicircle and resulted in smaller subgrade reaction per unit area. Aburatani et al. [1] mentioned that semi-circular breakwater has greater sliding stability against the wave compared to the vertical breakwater. This is because the wave force (vertical component) is applied downward along the curved wall and eventually been transferred to the foundation soil. Thus, the breakwater can withstand the waves. Lastly, the arch feature of the semi-circular breakwater can reduce the risk of overturning [8].

As reported by Shore Protection Manual [20], diffraction is a phenomenon where energy is transferred laterally along a wave crest. It is not noticeable when it occurs, but when the regular train of waves is interrupted by a barrier like a breakwater or an island, it can be seen. U.S. Army Corps of Engineers [25] stated that diffraction is a long-crested wave that has various heights along the crest. As the wave moves forward, the wave energy will laterally transfer along the crest, and the energy will be from the point of greater wave height to lesser wave height. A diffraction coefficient

can be described as below:

$$K' = Hd/Hi \tag{1}$$

where K' is the diffraction coefficient with the function of θ, β and r/L, H_d is the diffracted wave height, Hi is the incident wave height, θ is the incident wave direction from the breakwater, β is the angle between the breakwater and the radial, r is the radial distance from the breakwater tip to the point of interest and L is the wavelength.

Few physical processes involved in wave transformation around detached breakwater are spectral evolution due to wave-wave interaction, wave transmission through and over permeable structures, wave reflections from structures and beaches, the interaction of waves and currents, energy dissipation due to seabed friction and wave breaking, shoaling, refraction, and diffraction. Carmo [5] listed a few advantages of using numerical modelling: (1) numerical modelling is useful because they represent the real problem, (2) numerical model can validate data acquisition and analysis systems, fast processing and increase data storage capabilities; and (3) numerical modelling can reduce the time-consuming and expenses used for the physical model as they can help to interpret the experimental results in short of time and reduce the number of tests to be performed.

The diffraction of water waves by porous breakwaters is studied based on the linear potential wave theory by Sasmal and De [19], Yu [27]. The formulation of the problem includes a newly derived relation for the fluid motion through the porous structures in addition to the conventional governing equation and boundary conditions for small amplitude waves in ideal fluids. It is demonstrated that neglect of the inertial effect of the porous medium leads to an underestimate of the functional performance of a porous breakwater. Detached breakwaters have been widely constructed for the purpose of shore protection in coastal engineering practice. For this reason, a good understanding of the interaction between waves and porous structures has long been demanded by practising engineers. Despite such a background of extensive applications and practical interest, rigorous treatment of the wave field around a porous structure in full dimensions does not seem to have received the appropriate attention. Diffraction of water waves by a vertical wall with zero thickness has been studied as a mathematically analogous problem to that of the diffraction of light. Practical problems of wave diffraction are usually related to the complex geometry of the structures and the combination of the diffraction with other wave transformation processes, including the refraction due to topography variation.

According to Lynett et al. [16], many researchers have been focused on reflection and transmission characteristics of porous rubble mound breakwater but least focus on diffraction associated with a detached porous breakwater. In the study, they used numerical modelling to see wave interaction with porous structures in the horizontal plane. From the study, the wavefield in the shadow zone differs from each other due to the different diffraction mechanism that occurs. In the shadow zone of the porous breakwater, when the oblique waves hit the breakwater, the diffraction occurs in two ways, (1) diffraction of the wave energy occurs behind the transmitted wave same observation been made for the solid breakwater, and (2) diffraction of the wave

energy occurs at the transmitted wavefront from the incident wavefront because of the discontinuity of wave amplitude. In the shadow zone, the average difference in the maximum wave height between the numerical model and experimental results is in the range of 0–3% of the incident wave height. From their experiment, the empirical coefficients, α and β, as well as the formulation for the hydraulic conductivity of the breakwater, K, need to be reinvestigated for the betterment of the results in future.

The linearized theory of water waves is used to study the diffraction of an incident wave by a gap in a permeable breakwater [4]. Under the assumption that the wavelength is much greater than the thickness, the breakwater is replaced by a thin barrier and a suitable boundary condition is applied on the barrier to model the permeability. Thus, an approximate solution valid for large gaps is also given. This study is concerned with the diffraction of monochromatic water waves by a permeable breakwater standing in a fluid of constant depth. When the wavelength of the incident wave is much greater than the thickness of the breakwater, then the breakwater may be modelled as a thin vertical barrier, which is a geometry more amenable to theoretical investigation. The two-dimensional problem of diffraction waves by solid (nonpermeable) thin barriers has interpretations in acoustics and electromagnetic waves and has attracted considerable attention in the literature. A detailed examination of the problem of wave diffraction by a gap in a solid breakwater is given by Linton and McIver [15]. Recently, attention has turned to the problem of wave diffraction by a permeable breakwater. Yu [27] used an approximate procedure to solve the problem of diffraction of a normally incident wave by a semi-infinite permeable breakwater using a boundary condition based on the formulation of Sollitt and Cross [21] for time-harmonic motion within a porous medium. Yu and Togashi [28] considered the diffraction of waves by a permeable breakwater with a gap. Unfortunately, their solution is in error, as they effectively assume that the asymptotic form of the solution at large distances along the barrier applies along the whole length of the barrier.

Ilic et al. [11] recorded that few studies have been made to take field measurements of waves around the detached breakwaters which lead to little information of the spectra transformation due to the structures. The main objective for computational modelling was to evaluate the new function of SWAN (phase-decoupled refraction-diffraction spectral wave model) in the prediction of frequency and directional spectra around the shore-parallel breakwater. The advantages of using SWAN were the prediction of wave transformation of the directional wave spectra, dissipation and wave-wave interactions processes and feasibility of computation over large areas. The validation of the test result with the laboratory data received showed that there was an improvement in the inclusion of diffraction in the model for the estimation of the wave heights in the shadow area behind the breakwater. Diffraction was less pronounced as well as fewer instabilities were introduced when the directional spectrum of broad frequency and directional distribution were observed.

Kang et al. [13] carried out a numerical model study on the effect of waves around a single breakwater by using the SWAN model. From their test, a SWAN model version 40.51 was used to simulate the effect of wave diffraction, and they were using Wu's spectrum and JONSWAP spectrum to compare the difference in the result. As a result, they conclude that the SWAN model used with the JONSWAP spectrum provide a

better result than the SWAN model used with Wu's spectrum. The SWAN model used with the JONSWAP spectrum gave the result which closely approximated the measured data compared to the other one. Thus, this would make the SWAN model with JONSWAP spectrum is better when it comes to the investigation of numerical modelling for wave diffraction.

Masoudi and Gan [18] studied an analytical and numerical approach for wave diffraction on large aspect ratio rectangular submerged breakwaters. The diffraction problems were solved by using linear wave theory, and the results were compared by using the numerical method of the boundary element method. From their study, they concluded that the vertical flat submerged breakwater produces almost no diffraction wave and transmit a lot of the incident wave energy while the horizontal flat submerged breakwater gives relatively low transmission ability, and it has been required for many practical applications nowadays. The diffraction wave formation with two dimensional rectangular submerged breakwater is a decaying/growing function of *x, exp($\pm jx$)*, which maximum value had been reached at the free surface and on one of the breakwater edges; depending on the wave incident direction. Besides, larger breakwater produces a smaller diffraction wavelength for a given wave frequency. Besides, diffraction wave amplitude is prone to converge to a certain value at small submergence depth to total width ratio and the maximum amplitude corresponds to zero transmission coefficient resulting that submerged breakwater at better circumstances can reflect all incident wave energy.

3   Methodology

In this study, a solid-type semi-circular breakwater (SCB) was simulated using FLOW 3D software. The model has a radius of 0.6 m (to the external wall) and a length (normal to the wave approaching direction) of 2.4 m. The thickness of the test model is 0.20 m. Figure 1 presents the dimensions of the SCB model.

Figure 2 shows the set-up for the experiment in the wave tank with the model located at the right side of the wave tank. The dimension of the tank is 20 × 5 × 1.5 m. Two wave probes were in front of the SCB to capture the incident wave height, while twelve wave probes were arranged in a grid form behind the SCB to get the diffracted wave height. The distances of the wave probes were 1 m apart from each other horizontally and vertically. This numerical study aimed to investigate the wave diffraction near the semi-circular breakwater with the condition of submerged and emerged condition subjected to regular waves. The wave probes were in the arrangement of grid form to obtain the wave diffraction contour in the vicinity of a submerged and emerged SCB and to enhance the visual hierarchy of the test model. Not only that, this form also would ease the collection of the diffracted wave height behind the breakwater.

The input for this numerical simulation was the wave period, wave steepness H_i/L and water depth, d. H_i is the wave height, and L is the wavelength. For this experiment, the model had been exposed to a regular wave. The wave period for
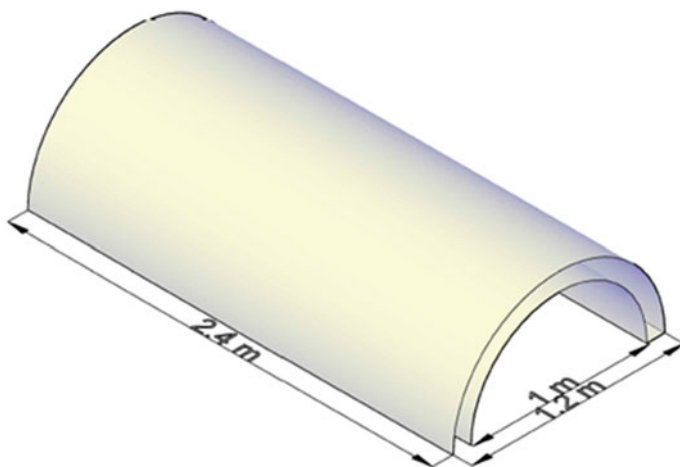
Fig. 1 Semicircular breakwater model
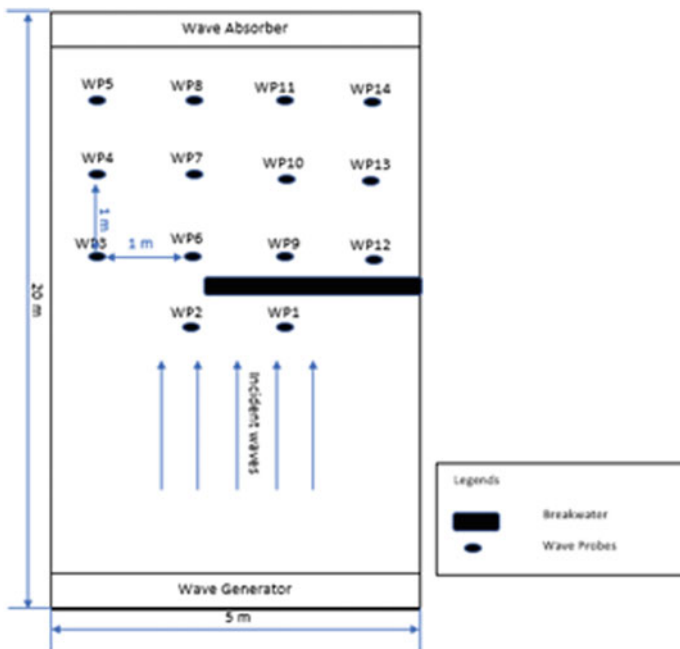
Fig. 2 Setup of the model in the simulation

Table 1 Test matrix

Wave type	Test conditions			Number of test run
	Wave period, T (s)	Wave steepness (Hi/L)	Water depth, d (m)	
Regular	0.8	0.02	0.4	1

regular waves (T) was 0.8 s, water depth of 0.4 m, and the wave steepness would be 0.02. The detailed test matrix is presented in Table 1.

Flow 3D is a software that can optimize the product design and can reduce the time to market the design. It is also a high accuracy CFD software that specializes in solving transient, free-surface problems. Flow-3D can provide a complete and versatile CFD simulation platform for engineers to investigate the dynamic behaviour of liquids and gas in a wide range of industrial applications and physical processes, including in civil water infrastructure. According to Bayon et al. [3], Flow 3D software is a commercial software package based on the Finite Volume Method (FVM), which can be used without being to deal with the complex mathematical background. The results being generated by the software will be validated by using physical modelling results with a percentage error of less than 30%. The boundary conditions for this model are: (1) specified wave period on the inlet, (2) outflow boundary that minimizes the wave reflections; (3) breakwater surface will be a rough surface; (4) symmetry plane, side, bottom, and top side of the domain is a free slip wall; and (5) atmospheric pressure will be imposed at the top of the plane.

The study was started with finding a suitable personal computer (PC) as FLOW 3D need higher specification in term of central processing unit (CPU), processor, random-access memory (RAM), windows, graphic card, and storage size. After getting the suitable PC, tutorials provided by the software were done. This is to ensure that all commands in the software can be familiarised before doing the actual simulation. By following the tutorials, the 1D study also had been done as part of practices. Later, the 2D study was done by using the test matrix shown in Table 1. Following the 2D study, the data analysis was done by using WaveLab software to derive the relevant output from the raw simulation data. WaveLab software is a user-friendly software for data acquisition and data analysis, mainly for waves graphical interface. The software has the advantages of providing wave analysis with high accuracy and reliability in short computation time was made by the Department of Civil Engineering, Aalborg University, Denmark. The software is also capable of performing time and frequency domain analysis of wave signals, reflection separation and 3D wave analysis.

4 Results and Discussion

Table 2 shows the mean wave height and the mean wave period for the preliminary result using the condition of 0.8 s wave period, 0.02 wave steepness and 0.4 m of water depth. This test was also on the condition of regular waves. Wave probe 1 and 2 was in front of the semicircular breakwater inside the wave tank to measure the incident wave height, while the rest were behind the semicircular breakwater to measure the diffracted wave height. From the table, wave probes 1 and 2 would have nearly the same mean wave period, which is 1.1770 s and 1.1710 s, respectively, while for mean wave height are 0.0658 m and 0.0627 m, respectively.

The highest mean wave height is at wave probe 5 with the value of 0.0782 m. This is because wave probe 5 is located at the left end of the wave tank, which is far from the barrier, i.e., semicircular breakwater. The wave energy can be transferred along the wave crest without any obstruction making the mean wave height at wave probe 5 highest among the others. The lowest mean wave height is a wave probe 11, which is 0.0367 m. This is because the wave probe is located behind the structure, and the energy has already been transferred laterally along the wave crest. The highest mean wave period is at wave probe 12 (3.8020 s), and the lowest mean wave period is at wave probe 11 (1.2240 s).

Table 2 shows the mean wave height and the mean wave period for the preliminary result using the condition of 0.8 s wave period, 0.02 wave steepness and 0.4 m of water depth. This test was also on the condition of regular waves. Wave probe 1 and 2 was in front of the semicircular breakwater inside the wave tank to measure the incident wave height, while the rest were behind the semicircular breakwater to measure the diffracted wave height. From the table, wave probes 1 and 2 would have nearly the same mean wave period, which is 1.1770 s and 1.1710 s, respectively, while for mean wave height are 0.0658 m and 0.0627 m, respectively.

The highest mean wave height is at wave probe 5 with the value of 0.0782 m. This is because wave probe 5 is located at the left end of the wave tank, which is far from the barrier, i.e., semicircular breakwater. The wave energy can be transferred along the wave crest without any obstruction making the mean wave height at wave probe 5 highest among the others. The lowest mean wave height is a wave probe 11, which

Table 2 Mean wave height and mean wave period

Wave probe	Hm	Tm	Wave probe	Hm	Tm
1	0.0658	1.1770	8	0.0575	2.8950
2	0.0627	1.1710	9	0.0541	2.9960
3	0.0707	2.5730	10	0.0536	3.3540
4	0.0708	2.4140	11	0.0367	1.2240
5	0.0782	2.8830	12	0.0516	3.8020
6	0.0639	2.1920	13	0.0519	2.8910
7	0.0536	2.2530	14	0.0556	3.4860
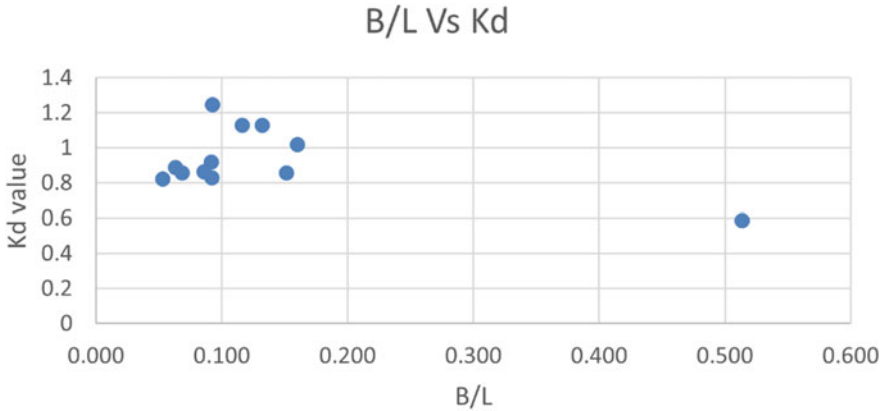
Fig. 3 Graph B/L against Kd value

is 0.0367 m. This is because the wave probe is located behind the structure and the energy is already transferred laterally along the wave crest. The highest mean wave period is at wave probe 12 (3.8020 s), and the lowest mean wave period is at wave probe 11 (1.2240 s).

The relative breakwater width (B/L) value is the dimensionless parameter that most researchers used for comparison purposes. In this case, the B represents the breakwater width (1.2 m) and L is the wavelength. From Fig. 3, the diffracted coefficient (Kd) value is scattered with a varying values of 0.59–1.25. The Kd value also shows a decreasing trend with the increase of B/L. This indicates that a lot of energy is being transferred laterally along the wave crest when subjected to smaller wave periods.

Figure 4 shows the illustration of wave contour for the test case using a 0.8 s wave period, 0.02 wave steepness and 0.4 m of water depth. This wave contour had been adapted from the Shore Protection Manual [20]. This wave diffraction contour is the expected result for this research and for future use, engineers may use this contour to design a small structure near the coastal area. From Fig. 4, the Kd value is higher when it is far from the SCB, while at the lee side of the SCB, the Kd value is varied from 0.82 to 0.89.
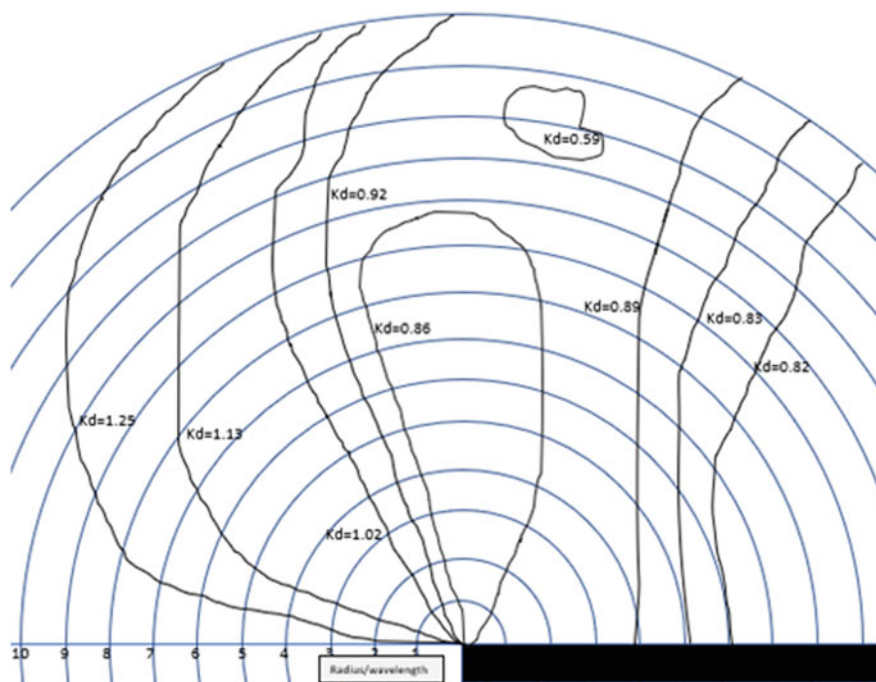
Fig. 4 Wave diffraction contour

5 Conclusion

From this research, the wave diffraction contour can be generated and used for designing a small-scale structure near the coastal area. The Kd value is varied from 0.59–1.25 with the B/L value of 0.053–0.561. The limitation of this study is it only caters for one wave direction only (90° wave approaching angle). It is better to provide a range of 0°–180° wave approaching angle for the wave contour so that engineers can have better guidelines in designing the structure. This preliminary result also shows that a lot of modifications or changes need to be made, especially regarding the size of the model. A lot of wave probes need to be put inside the wave tank to get a better understanding of wave diffraction. For future work, it is recommended that the wave tank needs to be upgraded to 50 × 50 × 1.5 m and about 1300 wave probes need to be used.

References

1. Aburatani S, Koizuka T, Sasayama H, Tanimoto K, Namerikawa N (1996) Field test on a semi-circular caisson breakwater. Coast Eng Japan 39(1):59–78
2. Allsop NWH, Vicinanza D, McKenna JE (1996) Wave forces on vertical and composite breakwaters. Report SR 443
3. Bayon A, Valero D, Garcia-Bartual R, Valles-Moran FJ, Lopez-Jimenez PA (2016) Performance assessment of OpenFOAM and FLOW-3D in The numerical modelling of a low Reynolds number hydraulic jump. Environ Model Softw 80:322–335
4. Bowen MK, McIver P (2002) Diffraction by a gap in an infinite permeable breakwater. J Water Port Coast Ocean Eng 128:2–9
5. Carmo JSA (2020). Physical modelling vs numerical modelling: complementarity and learning. https://doi.org/10.20944/preprints202007.0753.v1
6. Fathi A, Ketabdari MJ (2018) Modelling of emerged semi-circular breakwater performance against solitary waves using SPH method. J Braz Soc Mech Sci Eng 40
7. Gomes A, Pinho JLS, Valente T, Carmo JSA, Hegde AV (2020) Performance assessment of a semi-circular breakwater through CFD modelling. J Marine Sci Eng 8
8. Graw KU, Knapp S, Sundar V, Sundaravadivelu R (1998) Dynamic pressure exerted on semicircular breakwater. Retrieved from Leipzig annual civil engineering report
9. Hashim R, Kamali B, Hashim AM, Ismail Z (2010) Morphological changes in the vicinity of detached breakwater at Sungai Haji Dorani, Peninsular Malaysia. Paper presented at the international MIKE by DHI conference 2010
10. Hashim R, Kamali B, Tamin NM, Zakaria R (2010) An integrated approach to coastal rehabilitation: mangrove restoration in Sungai Haji Dorani, Malaysia. Estuar Coast Shelf Sci 86:118–124. https://doi.org/10.1016/j.ecss.2009.10.021
11. Ilic S, Westhuysen AJ, Roelvink DJA, Chadwick AJ (2007) Multidirectional wave transformation around detached breakwaters. Coast Eng 54(10):775–789
12. Jiang XL, Zou QP, Zhang N (2017) Wave load on submerged quarter-circular and semicircular breakwaters under irregular waves. Coast Eng 121:265–277
13. Kang HG, Zhang HW, Qu XT (2009) Numerical study of effect of wave around single breakwater with the SWAN model. J Hydrodyn 1(21):136–141. https://doi.org/10.1016/S1001-6058(08)60129-8
14. Kudumula SR, Mutukuru MRG (2013) Experimental studies on low crested rubble mound, semicircular breakwaters and vertical wall system. Int J Ocean and Clim Syst 3(4):213–226
15. Linton CM, McIver P (2001) Handbook of mathematical techniques for wave/structure interactions. Chapman and Hall/CRC, Boca Raton
16. Lynett PJ, Liu PLF, Losada IJ, Vidal C (2000) Solitary wave interaction with porous breakwaters. J Water Port Coast Ocean Eng 126(6):314–322
17. Lyu Z, Liu Y, Li H, Mori N (2020) Iterative multiple solution for wave interaction with submerged partially perforated semi-circular breakwater. Appl Ocean Res 97
18. Masoudi E, Gan L (2020) Diffraction waves on large aspect ratio rectangular submerged breakwaters. Ocean Eng. https://doi.org/10.1016/j.oceaneng.2020.107474
19. Sasmal A, De S (2020) Energy dissipation and oblique wave diffraction by three asymmetrically arranged porous barriers. Ships Offshore Struct. https://doi.org/10.1080/17445302.2020.1816783
20. Shore Protection Manual, t. e., 2 Vols (1984) U.S. Army Corps of Engrs. (USACE) Waterway
21. Sollitt CK, Cross RH (1972) Wave transmission through permeable breakwaters. In: Proc. 13th conf. on coastal engineering, ASCE, New York, pp 1827–1846
22. Tanimoto K, Goda Y (1992) Historical development of breakwater structures in the world. Paper presented at the proceeding of the conference on coastal structures and breakwaters, Thomas Telford, London
23. Teh HM (2012) Hydrodynamic performance of free surface semicircular breakwaters (Doctoral) University of Edinburgh

24. Teh HM, Venugopal V (2015) Optimization of hydraulic efficiency of a free surface semicircular breakwater using wave screens. Paper presented at the international conference on ocean, offshore and arctic engineering. http://proceedings.asmedigitalcollection.asme.org/
25. U.S. Army Corps of Engineers (2008) Coastal engineering manual
26. Xu J, Tao J (2003) Simulation of wave forces on a semi-circular breakwater using multilayer feed forward network. China Ocean Eng 17(2):227–238
27. Yu X (1995) Diffraction of water waves by porous breakwaters. J Water Port Coast Ocean Eng 6(121):275–282
28. Yu X, Togashi H (1997) Combined diffraction and transmission of water waves around a porous breakwater gap. In: Proc. 25th conf. on coastal engineering, ASCE, New York, pp 2063–2076

Modelling of Wave Runup and Overtopping Over Accropode II Breakwater

V. K. Krishnasamy, M. H. Jamal, and M. R. Haniffah

Abstract   This paper discusses a numerical model in a study of wave overtopping on a single layer amour unit (Accropode II) breakwater in order to understand the efficiency of the breakwater design by analyzing the wave overtopping and comparing with the physical model results and additional simulation in different crest heights of the breakwater and numerical wave run up analysis. The numerical model used is FLOW 3D. The prototype was physically modelled and tested in the HR Wallingford laboratory in 2012. In the current research, FLOW 3D is used to provide approximate wave runup and overtopping over the breakwater structure. There are three breakwaters of different heights (1.2 m, 1.3 m, and 1.4 m) were made in order to achieve the objective of the project. Hence, the numerical simulations were carried out and compared with the experimental results. Based on the observation of the preliminary simulation, the results show a decrease in overtopping in the numerical study, and the main idea is to understand the FLOW 3D simulation processes.

Keywords   Numerical model · Computational Fluid Dynamic (CFD) · Breakwater · Physical model · Wave runup

1   Introduction

Coastal defence and shoreline protection methods have been implemented worldwide, aiming to protect wave action and beach stability. The marine structures are constructed in various types and sizes to dissipate and disperse wave energy. Erosion

V. K. Krishnasamy (✉) · M. H. Jamal (✉) · M. R. Haniffah (✉)
School of Civil Engineering, Universiti Teknologi Malaysia, Johor Bahru, Malaysia
e-mail: viknesvaran1977@graduate.utm.my

M. H. Jamal
e-mail: mhidayat@utm.my

M. R. Haniffah
e-mail: mridza@utm.my

of many coastal beaches globally occurred due to waves characteristics and population threats. Therefore, mitigation measures against groynes detached breakwaters and rubble mound breakwaters [4].

The rubble mound breakwaters are generally built along the coast to eliminate or minimise the waves' attack and are environmentally friendly and also least optical interference [5].

Wave overtopping over the breakwater is considered an important aspect to determine the effectiveness of breakwater structures. Along with that, many researchers have conducted numerous investigations physically and theoretically on overtopping models. Amongst them is the wave overtopping prediction model from an experimental result of impermeable, smooth, rough, and beam slope breakwater [7]. Meanwhile, in armoured breakwater designs, the overtopping discharge estimation will be done reasonably to determine the top elevation of the breakwater [6]. Several ways are available to estimate the wave overtopping discharge. One of the most common ways is the physical model test [10]. Also, the phenomena of wave run-up and overtopping are influenced by the geometry's parameters and hydraulic parameters [9].

Now, numerical simulation is known as the most effective technique or method to estimate the wave overtopping rate because of computer technology and computational methods. The present studies of the numerical simulation focus on hydraulic performance for wave overtopping on the single layer of Accropode™ II breakwater. Moreover, the wave overtopping analysis has previously been solved by the use of physical models. However, physical models are too costly and time-consuming compared to CFD modelling.

The overall aim of the present study is to calibrate and validate the hydraulic performance of the numerical model against the experiments of wave overtopping. This paper discusses the preliminary results of a numerical investigation conducted with the aim to have some understanding of wave runup and overtopping characteristics.

2   Experimental Data

The 2D model of the Accropode™ II was modelled by using a scale of 1:30.8 and was tested at HR Wallingford, UK. The flume is 40 m long, 1.2 m wide and had a maximum working depth of 1.2 m in 2012 in Fig. 1. The experimental data were obtained from ECERDC (East Coast Economic Region Development Council), which have carried out the model testing in order to construct a breakwater in Kuantan, Pahang.

Basically, five (5) test series was carried out in various wave heights in the laboratory in Table 1. The design conditions of the breakwater have a return period of 100 years, a significant wave height of $H_s = 4.5$ m, a peak wave period of 12.1 s and still water of $+ 4.0$ m LAT. The crest design was stable in all test conditions.

The effect of a possible Typhoon Vamei is quite unclear and may be significantly worse than the 100 years condition based on monsoon winds. It is for this reason that at least an overload of 120% is used with respect to the 100 years and H_s

Fig. 1 2D Flume physical model test

Table 1 Mean overtopping discharges recorded

Test series	T_r (years)	Sea state H_s (m)	q (l/s/m) - Overtopping discharges
1	10	3.5	No overtopping
2	50	4.2	Splash
3	100 (High water)	4.5	Splash
4	100 (Low water)	4.5	Splash
5	Overload	5.4	3.1

= 5.4 which is a value between 500 and 1000 years return period on monsoon winds. The significant wave height for the overload return period was tested in the physical model, and 3.1 l/s/m was captured. Therefore, this study was adopted the test series five output data for numerical simulation. The numerical model hydraulics parameters have been scaled down in order to run the simulation.

Based on the lab performance results, the rocks layer has some damage from overtopping in the overload test but protected the harbour side of the structure and provided a stable interference with the concrete armour layer on the crest.

The water overtopping was collected in a chute, from which it flowed into a tank. The volume of water collected during each test and was used to determine the mean overtopping discharge per unit length of the breakwater (l/s/m). Overtopping criteria

was specified during the test where mean overtopping discharges is q < 1.0 l/s/m in the 1:100-year sea state and is q < 10 l/s/m is in the overload sea state [8].

The discharge was recorded as a light splash at volumes too small to be accurately measured and scaled. The 1:100-year discharge limit of < 1.0 l/s/m was therefore satisfied. The overload criteria of q < 10 l/s/m were also satisfied, as a discharge of 3.1 l/s/m was measured in the overload sea state.

3   Numerical Modelling

FLOW-3D is a Computer Fluid Dynamic code developed by *Flow Science Inc.* (USA). The fluid motion for the model based on the Navier–Stokes equation will control by one principal technique, the Volume of Fluid (VOF) method illustrated by [3]. Subsequently, a volume of fluid (VOF) technique can be included to track the free surface, and it can handle the large reformations of the free surface.

This method also has been used to study the reliability of 3D numerical simulation over the structure and wave overtopping over rubble mound breakwater [1]. The workflow chart for this CFD study is given in Fig. 2.

The benefits of this FLOW 3D are faster solution and quite cheaper compared to the experiment model test in Laboratory. The hydrodynamics behaviours and structural design performance were investigated by using this method to determine the wave overtopping discharges parameter [2].

Under the simulation setup for geometry, there are two main components that had been defined in the simulation, which are Breakwater and Seabed. This set-up was created as per physical hydraulic modelling test in the Laboratory.

The 3D model of the breakwater had been constructed using CAD software in Fig. 3, which later had been exported in format stereolithography (.STL), so that it could be imported and used in FLOW-3D. There are three breakwaters of different heights (1.2 m, 1.3 m, and 1.4 m) were made in order to achieve the objective of the project.

The dimension of the physical and numerical models is 1.2 m (H) × 1.6 m (B) × 1.2 m (L), is similar in size. In addition, two geometries were modelled and have increased their heights to evaluate the overtopping discharge rate shown in Table 2.

In order to simulate the fluid flow and its interaction with surroundings, several physics models were activated. The Reynold Average Navier Stokes (RANS) Renormalized Group (RNG) k-Epsilon model was used in order to capture the turbulence flow. The Volume of Fluid (VOF) model also had been activated in order to locate and simulate proper dynamic boundaries on the fee surface of the fluid.

Five mesh blocks were created; four of them were used in order to define the computational domain, while one mesh block was defined as a Conforming Mesh Block in order to adequately capture the complex geometry of the breakwater, as shown in Fig. 4. The conforming mesh that had been defined with a smaller Cell Size is added in order to resolve the geometrical complexity that the breakwater has.
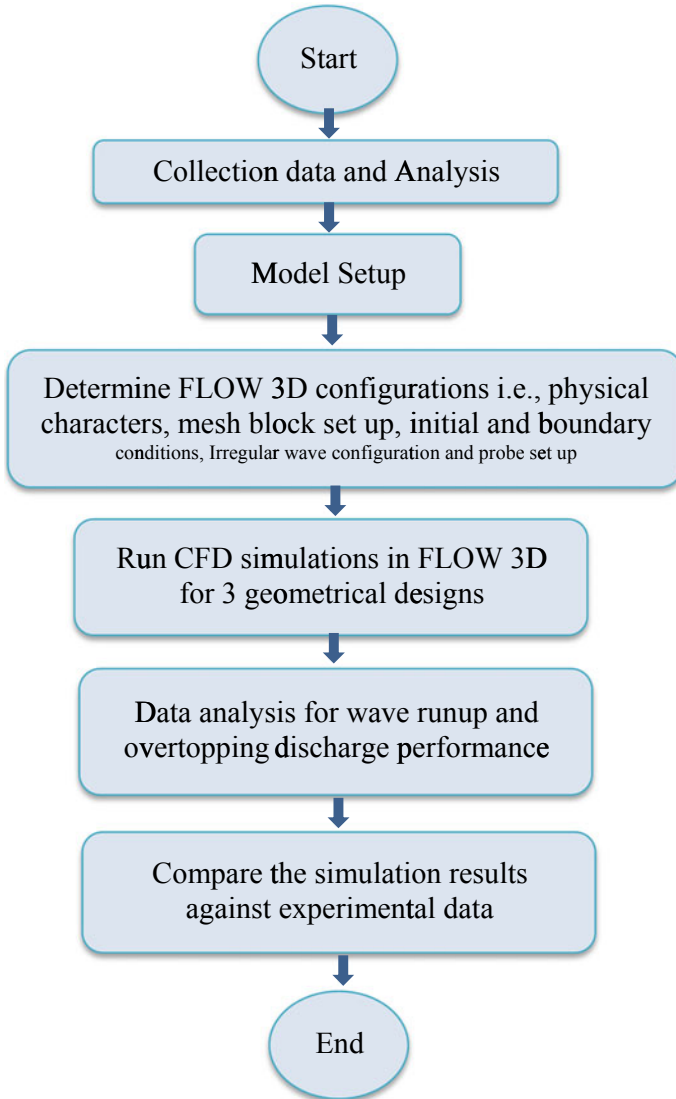
Fig. 2 Workflow chart

This method will create a mesh that will conform only to the breakwater, which will avoid a large number of cells. As a result, this will reduce the total run time of the simulations.

The dimension of the mesh block had been defined based on the length of the physical flume that had been used in the physical experiment. In order to optimize the simulation runtime, three different cells size were utilized for each mesh block (Flow Science, 2012).
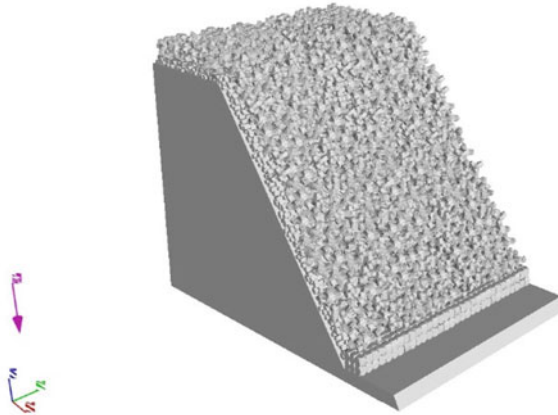
Fig. 3 3D rubble mound breakwater

Table 2 Numerical model mean overtopping discharges

Test Series 5 (Hs)	Time (s)	Experiment		Model 1.2 m height		Model 1.3 m height		Model 1.4 m height	
		Mean (m^3/s)	Max (m^3)	Mean (m^3/s)	Max (m^3)	Mean (m^3/s)	Max (m^3)	Mean (m^3/s)	Max (m^3)
5.4 m (0.175 m)	60	3.10E-03	2.30E-01	2.32E-04	9.19E-03	1.94E-05	1.86E-03	1.01E-05	6.09E-05

Table 3 Test series 1 to 4 results

Test Series	(Hs) (m)	Overtopping discharges result
1	3.5	Light splash reached the crest front but did not pass through the crest and the collection chute. Zero collection
2	4.2	Overtopping was very similar to that observed during test series 1, and no discharge reached the collection chute. Zero collection
3	4.5	There was little quantity of splash to the crest but no collection. (Tested in High water)
4	4.5	There was little quantity of splash to the crest but no collection. (Tested in Low water)

Mesh Block 1 had been built with the coarsest cell size of 0.04 m, which made the total number of cells in Mesh Block 1 is 436500. On the other hand, the size of the cell used in Mesh Blocks 2, 4 and 5 is 0.02 m. This makes the total number of cells in Mesh Block 2 is 241500, while the total number of cells in Mesh Block 4 and 5 is 16500 each. Mesh Block 3, which is the Conforming Mesh Block, contains cells of 0.01 m.

The computational burden is very heavy; the simulation runtime is around 14 days for a simulation of 60 s which is the reason why the mesh dependency study was not carried out.
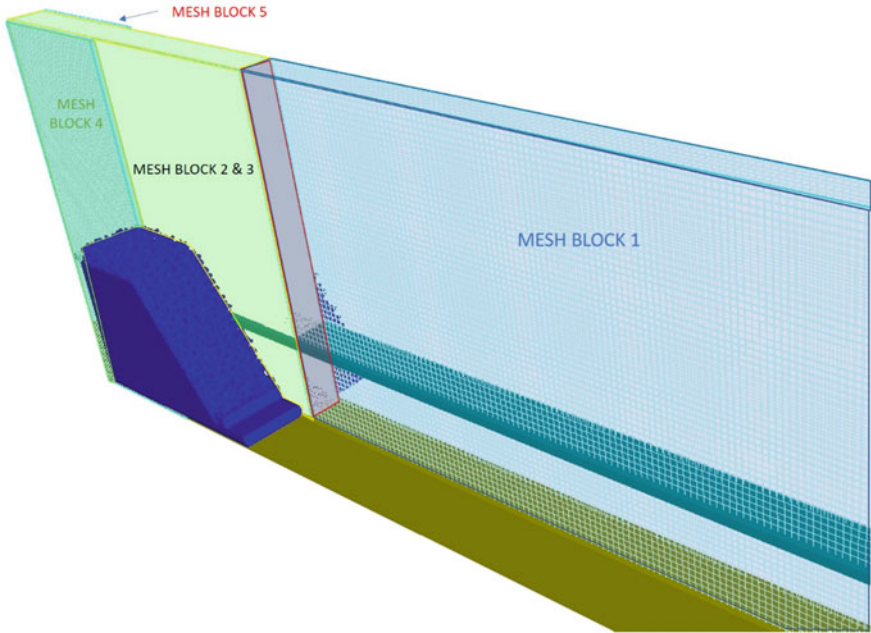
Fig. 4 Five (5) mesh blocks
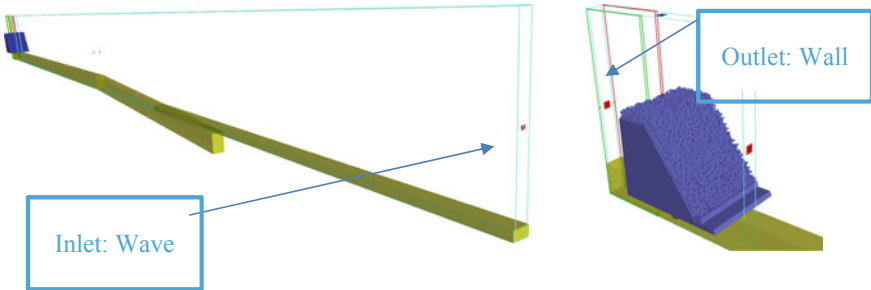
Fig. 5 Boundary conditions and initial conditions

Each face of the mesh blocks had been defined with a boundary condition. The non-inflow and non-outflow boundaries had been set Symmetry by default. The boundary between the fluid and the solid had been defined as no-slip or partial slip Wall Shear boundary condition. The boundary between mesh blocks had been automatically defined as Symmetry.

The inlet of the domain had been set with a wave boundary condition. The wave model that had been used for the boundary is the Random Wave model. The random wave model is treated as a superposition of many linear component waves with different wave periods, amplitudes and initial phases.

In FLOW-3D, the code automatically generates 1000 linear component waves at the wave boundary for a random wave simulation. The periods are evenly distributed from 0.2 s to 2 s. The initial phases are randomly selected between 0 to 2\pi. The wave amplitudes are calculated using the wave energy spectrum. The energy spectra used was the JONSWAP Spectrum. To use the JONSWAP spectrum, the parameters that had been defined are the fetch length of the wave:180,000 m, peak enhancement factor: 0.03, and wind speed: 2.5 m/s.

4 Results and Discussion

Numerical modelling is used to support the validation exercise against experimental results. This paper presents the validation results for overtopping discharges of the various heights breakwaters. Also, the evaluation of the wave motion along the external of the wave run-up breakwater is basically important in this study. This phenomenon extremely influenced the choice of the breakwater height. The initial values were evaluated by processing the time series. (Fig. 6) captured by the wave run-up over the breakwater slope.

The outcomes of the CFD simulation showed initial discharge rate and volume prediction results only where these results have huge variances to provide accurate validation data, as given in Table 2.
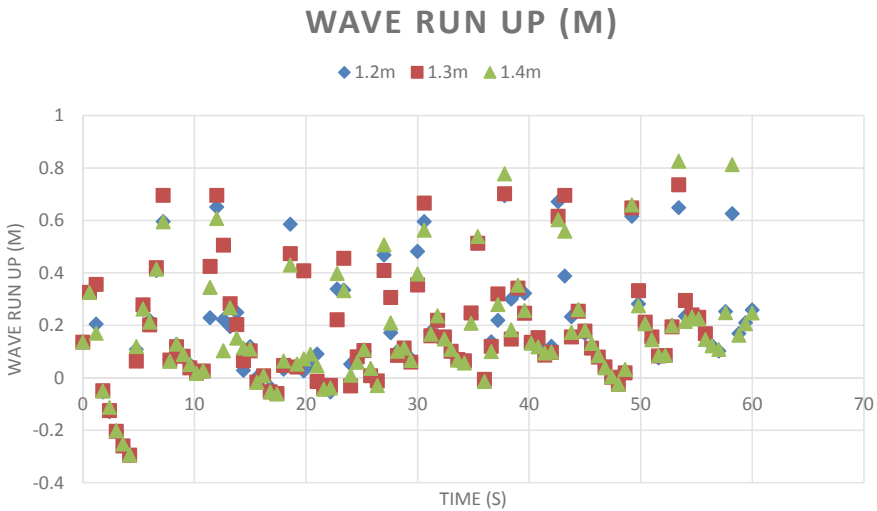
Fig. 6 Wave run-up results
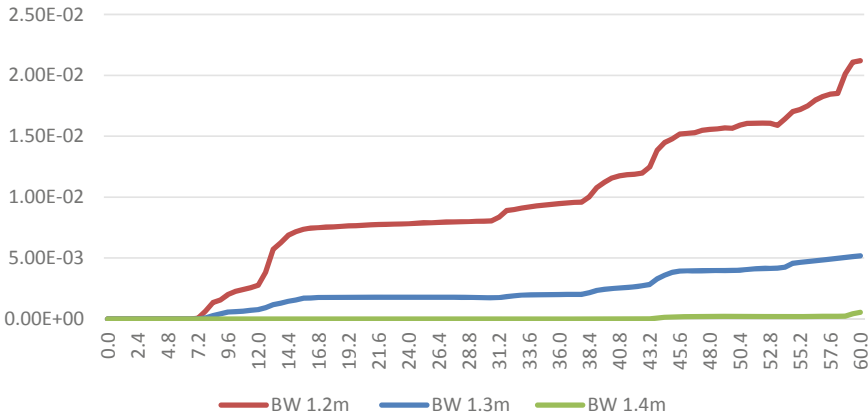
Fig. 7 Individual overtopping discharge (Hs = 5.4 m)

5 Conclusion

Based on the results shown in the previous section, there is a significant difference in the result of overtopping mean flow rate and volume. The difference between the two results occurs might be due to the factors below. Future improvement can be made on the factors in order to ameliorate the findings of this study:

a. **Geometry**: Even though the same dimension of the breakwater has been used for the physical and the numerical model, however, the arrangement of the Accropodes used in both models might not be similar. The difference causes different flow resistance, which as a result, different overtopping conditions can be observed in the physical and the numerical model.

b. **Wave Boundary Condition:** The physical and the numerical model has used JONSWAP energy spectra (defined with the same parameters as explained in the previous section) to define the wave energy spectrum of the Random Wave Model. However, it is difficult to verify that the same form of waves had been applied in both models. The uncertainty might be contributing to the difference in the results.

c. **Finish time**: Due to computational resources limitation, the simulation finish time had been scaled down and reduced to 60 s. The scaled-down finish time might have affected the accuracy of the simulation results.

d. **Mesh**: Due to the same reason above (limited computational resources), the mesh sensitivity analysis was not carried out. Executing the analysis will allow us to understand if the results difference that we obtained was due to the mesh settings that had been implemented.

2) The result of Overtopping Volume for different heights of breakwater shows that the overtopping volume can be reduced by increasing the height of the breakwater's crest. As explained in the previous section, a significant difference

can be observed when especially the crest of the breakwater is increased from 1.2 to 1.3 m. However, the result of Wave Run-up shows that the maximum wave run-up also increases when the crest of the breakwater is higher, which can affect the safety of sea dikes or coastal settlements.

3) The test series 1 to 4 was carried out as an initial simulation and resulted as follows:

A few simulations are encouraged to be carried out to improve the overtopping performance for the test series 1,2,3, and 4. Therefore, there is an urgent to work in this area. On the other hand, to increase the numerical modelling part of this study, further studies need to be carried out for the sensitivity analysis.

References

1. Cavallaro L, Dentale F, Donnarumma G, Foti E, Musumeci RE, Pugliese Carratelli E (2012) Rubble mound breakwater overtopping estimation of the reliability of a 3D numerical simulation. In: 33rd international conference on coastal engineering, pp 1–9
2. Dentale F, Donnarumma EP, Caratelli, Giovanni V, Li P, Sa F (2014) A new numerical approach to the study of the interaction between wave action and rubble monund breakwater. Latest trends environmental, mechanical. Structure Engineering. Geology A, pp 45–52
3. Hirt N (1981) Volume of fluid (VOF) method for the dynamics of free boundaries. J Comput Phys 39(1):201–225
4. Komar PD (2003) Beach processes and sedimentation, second, prentice hall, new Jersey, USA (1998). Measurement of seas and coastal regions. Coast Eng VI, Cadiz, Spain, pp 429–438
5. Kuriyama Y, Banno M (2016) Shoreline change used caused by the increase in wave transmission over submerged breakwater due to sea level rise and land subsidence. Coast Eng
6. Losada IJ, Lara JL, Guanche R, Gonzalez Ondina JM (2008) Numerical analysis of wave overtopping of rubble mound breakwaters. Coast Eng 55:47–62
7. Owen MW (1980) Design of seawalls allowing for wave overtopping. Report Ex 924:39
8. Pullen T et al (2007) EurOtop, wave overtopping of sea defences and related structures, assessment manual
9. Shankar NJ, Jayaratne MPR (2003) Wave run-up and overtopping on smooth and rough slopes of coastal structures. Ocean Eng 30:221–238
10. Van der Meer JW, Verhaege H, Steendam GJ (2009) The new wave overtopping database for coastal structures. Coast Eng 56:108–120

Marine Debris Assessment and Clean Coast Index of Pantai Navy Labuan, Wilayah Persekutuan Labuan, Malaysia

Diyana Hazierah Abdullah, Norasikin Saman, Nurfarhain Mohamed Rusli, Mohd Rizalman Mohd Ali, and Shazwin Mat Taib

Abstract Marine debris is described as any solid materials that are directly discharged into the marine and coastal ecosystems. Marine debris issues are recognized as a major stressor on the marine and coastal ecosystem around the world, including Malaysia. In this study, the coast cleanliness of Navi Beach, Labuan (coordinates of 5.2759, 115.2587) was assessed using Clean-Coast Index (CCI). The marine debris was collected for two days during northeast monsoon season at the same coastal area around using the transect survey method. Marine Debris Tracker application was used to record the type of debris found and categorized by type of material. The number of debris collected for Day 1 and Day 2 were 73 items and 288 items, respectively. 61.6% of the total debris found on Day 1 of the survey was categorized as plastic items. While for Day 2, 56.6% of the debris was categorized as lumber types, 24% was plastic and 18.8% was other items. The average value of CCI at the coastal area of Navi Beach, Labuan, was 0.64, considered as 'very clean according to the CCI index value.

Keywords Marine debris · Debris composition · Malaysia's beach · Navy beach · Clean-coastal index · Transect survey

---

D. H. Abdullah · N. Saman · N. Mohamed Rusli · S. Mat Taib (✉)
School of Civil Engineering, Faculty of Engineering, Universiti Teknologi Malaysia, Johor Bahru, Johor, Malaysia
e-mail: shazwin@utm.my

N. Mohamed Rusli
e-mail: nurfarhain@utm.my

N. Mohamed Rusli
Centre of Lipid Engineering and Applied Research (CLEAR), Universiti Teknologi Malaysia, Johor Bahru, Johor, Malaysia

M. R. Mohd Ali
Spritzer Berhad, No.1, Jalan Sitar 33/6, Seksyen 33, 40400 Shah Alam, Selangor, Malaysia
e-mail: rizalman@spritzer.com.my

S. Mat Taib
UTM Campus Sustainability (UTMCS), Block M38, Universiti Teknologi Malaysia, Johor Bahru, Johor, Malaysia

1   Introduction

Marine debris is described as any solid material that is manufactured or processed and directly or indirectly, intentionally or unintentionally, disposed of or abandoned into the marine environment. It is primarily the result of human activity due to poor or improper waste management, dumping and littering, or stormwater runoff [16]. Marine debris is known as a major stressor on the marine and coastal ecosystem around the world, with documented implications on marine biodiversity as well as negative social consequences, as debris can pose a health and safety risk, as well as wreak havoc on commercially valuable resources [8].

The marine debris can be broadly categorized as land-based (originating on land) or marine-based (originating at sea) sources [4]. The land-based source included recreational activity at the coast, public wastes, industrial wastes, and unregulated landfills areas (e.g., landfills near the shore). The ocean-based source comprises commercial shipping, ferries and liners, fishing vessels (recreational and commercial), leisure boats and offshore structures such as platforms, rigs and aquaculture sites. Previous studies found that land-based sources contributed a larger portion of the debris in the marine environment [9, 15, 17]. Plastic objects included plastic bags, cups and plates made from Styrofoam, food wrappers, plastic packaging products, plastic bottle caps, clear plastic bottles and coloured plastic bottles, contributing the largest portion of the total debris items. Plastic-based marine debris also makes up most of the marine litter worldwide. Approximately 80 per cent of debris is washed off from the land, blown by winds, or intentionally dumped from shore.

Beaches are one of the mainland-based sources of litter entering the marine environment due to poor waste management. Beaches in Malaysia are also experiencing threats from this solid pollution due to increasing population and rapid development. Marine debris Malaysia has been placed under the purview of local authorities. Solid trash management, on the other hand, was privatised in September 2011 under the Solid Waste and Public Cleansing Management Act 672 [5]. Various initiatives have been taken to keep Malaysian beaches clean and pristine.

Previous studies have also documented the presence of marine debris in Malaysian beaches. Abdul Kadir et al. [1] studied the presence of debris at two beaches, namely Sungai Lurus and Minyak Beku, in Batu Pahat district. Agamuthu et al. [2] studied the composition and abundance of marine debris at beaches in Peninsular Malaysia, namely Teluk Kemang, Pasir Panjang, Batu Burok, and Seberang Takir. Mobilik and coworkers studied the abundance of marine debris at Sarawak's beaches, namely Pandan beach, Pasir Pandak beach, Temasyah beach, and Tg. Lobang beach [7, 14]. Assessment of marine debris at Sabah beaches was conducted previously at Tg. Aru and Kosuhoi beaches [13]. They found the density of debris on these beaches were found to be comparable to other beaches worldwide in the range of 0.142–0.884 items/m.

Although these studies give an overview of debris pollution levels in Malaysia beaches, however, the data is still limited. This study was conducted to (i) assess the presence of marine debris and (2) evaluate the cleanness by using the Clean-Coast

Index (CCI) value of Navy Beach, Labuan, Sabah. The assessment of the type of marine debris in Malaysia is well discussed by the previous studies [1, 2, 7, 13, 14]. Maritime Institute of Malaysia (MIMA) conducted Clean Coast Index (CCI) for cleanliness assessment of coastal areas in Malaysia in 2010, and the results indicated plastic waste had been proven to be the major contributor of coastal litter in Malaysia beaches, with 66% of the overall litter collected (Hagir et al. 2013).

2 Materials and Methods

### 2.1 Study Area and Debris Sampling Method

In this study, the assessment of marine debris and cleanness index was carried out at Navy beach of Labuan Island. Labuan Island is located on the northwest coast of Borneo, north of Brunei and south of Kota Kinabalu, the capital of the state of Sabah. The Navy beach is located in the Southern part of Labuan Island, 5.2 km from Labuan town. The beach is not the main attraction for recreational activities; nevertheless, there are also people who visit the beach. There are two restaurants and a marine museum in the area of the beach.

The transect survey method is used for the debris collection. The sampling station is determined using a 100 m × 20 m transect. The Measure App that used the augmented reality (AR) technologies to show the length or measurement walking was used to determine the transect survey area (coordinates of 5.2759, 115.2587). Figure 1 shows the transection walking pattern for the transect area.

After the transect area was determined, all the visible debris was collected by walking within the transect area. In order to maximize the collection of the samples, the sampling process was conducted two times. The first survey was done on a weekday (March 19, 2021), and the second survey was conducted on the weekend (April 3, 2021). It must be noted that only debris that has a size larger than 2.5 cm were collected.

2.2 Classification of Debris Composition

The collected debris was then sorted and separated according to the material types. The number and type of material for each collected debris were recorded using the Marine Debris Tracker mobile application. From this application, the marine debris was categorized into nine types, namely plastic, metal, glass, rubber, cloth, paper and lumber, fishing gear, other items, and the amount of beach debris type was counted. After that, the debris was classified into various sub-categories listed as listed in the application. After separation and categorization, the amount of each type of debris
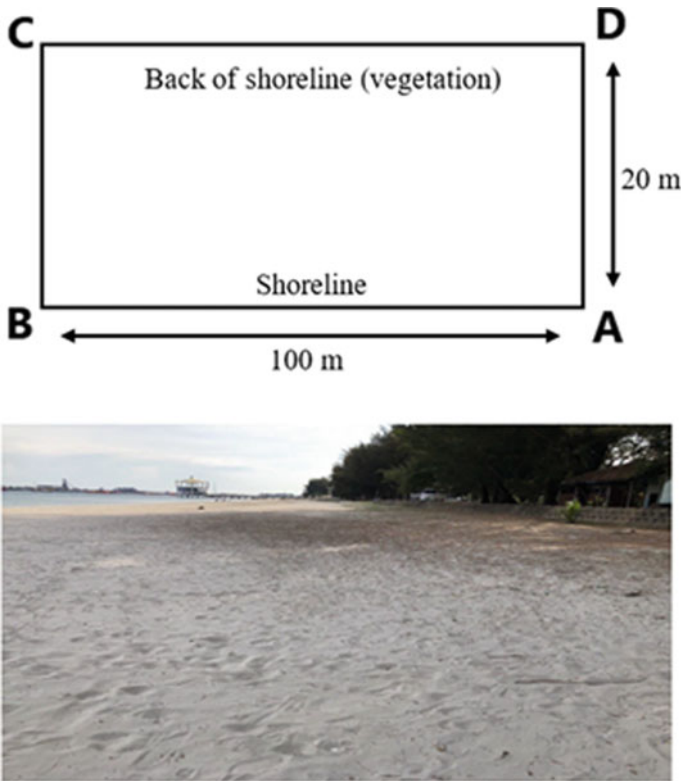
Fig. 1 Transect survey area for debris collection in navy beach, Labuan

was expressed as the number of items. The debris composition was counted and recorded in the Table in the worksheet classification of debris composition.

2.3 Clean-Coast Index (CCI)

The cleanness of the beach was measured by determining the clean-coast index (CCI) value. The index indicates how many plastics trash objects (man-made debris) were counted per square metre of the transect region, which is the product of the length and depth of the transect. The CCI uses a ranking system that ranges from "Very clean" to "Extremely Dirty" (see the range (from 0 to 20 +) mentioned in Table 1). The index is calculated as follows:

$$CCI = K\left(\frac{Total\ debris\ in\ transect}{Total\ area\ of\ transect}\right)$$

Table 1 CCI index categories

Numeric index	Coast index
0–2	Very clean
2–5	Clean
5–10	Moderate
10–20	Dirty
20+	Extremely dirty

where coefficient K = 20 was used as a multiplier to ensure that the value of the resulting index would not fall between 0 and 1.

3   Result and Discussions

### 3.1   Types of Debris Collected at Navy Beach

The number of debris collected from Day 1 was 73 debris while 288 of debris was collected on the second day. The debris was categorized into nine categories, namely plastic, metal, glass, rubber, cloth, paper and lumber, fishing gear and other items. Figure 2 shows some of the debris collected at Navy beach. Plastic and lumbar were the most abundant types of debris collected at the beach. There is only one item found for each type of debris, namely metals, glass, rubber and fishing gear. Figure 3 and Table 2 shows the number, percentage and categories of debris collected at the Navy beach for two days of sampling.

The total number of plastic debris from two days' collection was 114 items ranging from food wrappers, beverage bottles, other jugs or containers, plastic bags, hard plastic fragments, foam fragments, and film fragments. Table 3 shows specific plastic-type sub-categories as classified from the 'Marine Debris Tracker' application and the number of samples found during sampling activity. The number of foam and plastic fragments contributed a relatively larger portion as compared with other plastic sub-categories. Relatively big size plastic-based materials would transform into plastic fragments through the degradation process (O'Brine and Thompson, 2010) and remain to contaminate the beach environment. The polystyrene fragment, plastic bags, and beverage bottles debris might be contributed from the beachgoers, fishing, and picnic activities. Plastic debris is known as a major contributor to marine litter in Malaysia (Hagir et al. 2011b; [1]. By minimizing plastic intake, there will be lesser plastic waste produced.

Besides plastics materials, lumber in the form of wood sticks was also found in a large number. This lumber mainly contributed from the broken tree branches around the beach and was swiped to the transect area. Other items collected in this study shows the variety of organic debris types, such as fruit tree, seaweeds, plant stem

Fig. 2 Example of debris collected at navy beach, Labuan
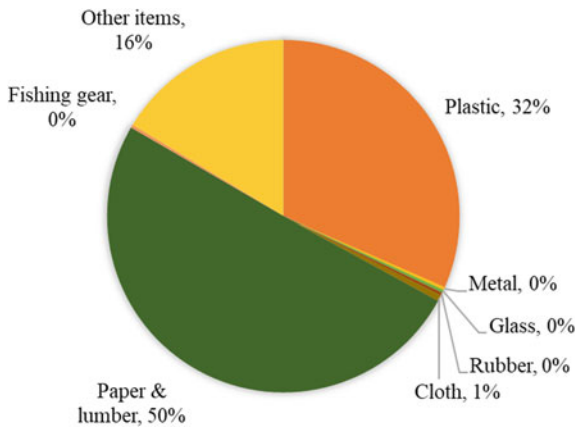
Fig. 3 Percentage of debris items collected from survey sites according to categories for two days of collection

with leaves, shell, birds' feather, stone, peanut shell, concrete piece, leaves, marine life and others. Rare items such as mop and washing machine parts were found on Day 1 of sampling. These items are believed to come from nearby restaurants. Types of other man-made debris collected during the survey are listed in Table 4.

The number of debris collected for the second day of the survey was 3.9 times higher than the first day. 56.6% of the debris was categorized as lumber types, 24.0% was plastic, and 18.8% was categorized as other items. Most of the lumber types were found in the form of wood sticks, and one item in the form of a wooden board was

Table 2 Types and number of marine debris collected at navy beach, Labuan

Categories	Day 1 (19 March 2021)		Day 2 (3 April 2021)	
	Number of items	Percentage (%)	Number of items	Percentage (%)
Plastic	45	61.6	69	24.0
Metal	1	1.4	0	0.0
Glass	1	1.4	0	0.0
Rubber	1	1.4	0	0.0
Cloth	1	1.4	1	0.3
Paper & lumber	19	26.0	163	56.6
Fishing gear	0	0.0	1	0.3
Other items	5	6.8	54	18.8
TOTAL	**73**	**100**	**288**	**100**

Table 3 Sub-categories of plastic debris collected at navy beach

Plastic item sub-categories	Day 1 (19 March 2021)		Day 2 (3 April 2021)	
	Amount	Specific items	Amount	Specific items
Food wrapper	1	Apple wrapper	6	
Beverage bottles	10		-	
Jugs or container	1	Bleach bottle	-	
Bottle/ container caps	-	-	7	
Cigar tips	-	-		
Cigarettes	-	-	6	
Disposable cigarette lighters	-	-	-	
Six-pack rings	-	-	-	
Plastic Bags	10		5	
Foam/ Plastic cups	-	-	2	
Plastic utensils	-	-	7	Lollipop stick
Straws	-	-	5	
Balloons-Mylar	-	-	-	
Personal care products	-	-	-	
Hard plastic fragments	7	Pail holders, pen, and plastic	10	Box tiers
Foam fragments	11	Polystyrene	6	Polystyrene
Film fragments	5	Plastic	15	Plastic
Other (Shotgun shells/wads)	-	-	-	-
Other (aquaculture debris)	-	-	-	-
Other plastics	-	-	-	-

Table 4 Other man-made debris collected at navy beach

Categories	Sub-categories	Day 1	Day 2
Metal	Metal Bottle Caps	1	
Glass	Glass fragments	1	
Rubber	Rubber fragments	1	
Cloth	Fabric pieces	1	1
Paper and lumber	Lumber	18	162
	Paper and Cardboard	1	
	Pallets		1
fishing gear	Fishing lures and lines		1
Others	Mop/ Washing Machine part and others	4	3

also found. These items are believed to be stranded at the area of the transect due to the rain and strong winds a day before the sampling was done. The number of plastic debris slightly increased as compared with the first day of collection. Most of the plastic debris was used for food packagings, such as food bottles or container caps, cigarettes, plastic bags, foam or plastic cups, plastic utensils, straws, hard plastic fragments, foam fragments, and film fragments. Since the time of collection was carried out on the weekend (Saturday), the high amount of food packaging is related to recreational activities such as picnic beachgoers who visited the beach after the working day of Friday.

Since the beach is not the main attraction for tourism industries, the main source of the debris is mainly associated with socio-economic activities from local people who live near the beach.

3.2 Clean Coast Index (CCI) for Cleanliness Assessment of Coastal Areas in Malaysia

The CCI is a metric used by the "Clean Coast" programme, which is a novel, long-term strategy to cleaner beaches involving a variety of activities such as increased public awareness and motivating the authorities to clean their beaches. The method is a simple, useful instrument for tracking progress and evaluating the effectiveness of operations such as public awareness campaigns, media coverage, and enforcement actions. The visual assessments appeared to have a high correlation with the index outcome.

In our study, we only considered man-made debris for the CCI calculation. As previously discussed, the CCI measures plastic debris or artificial waste made as a beach cleanliness indicator (Alkalay et al. 2006; [11]). Organic materials such as timber, lumbar, seaweeds, leaves, shells and other living organisms that can be counted were not included in the CCI calculation. Made-made organic materials such

Table 5 Value of parameters used for CCI calculation

Parameters		Values
Debris counts		
Day 1	:	54 items
Day 2	:	72 items
Width of sampling area, *w*	:	20 m
Length of sampling area, *l*	:	100 m
Total area surveyed	:	2000 m^2
Constant K	:	20
CCI values		
Day 1	:	0.54
Day 2	:	0.73
Average	:	0.64

as paper cups, board fragments and pallets are also not considered in the calculation. This method is in accordance with the procedure described by Hagir et al. [6] and MIMA [12], which only considered plastic pieces for the CCI calculation.

Out of 73 debris found on Day 1 of the survey, 54 items were considered as artificial debris, while only 72 items were found on Day 2 of the survey. The value of parameters used in this study and the calculated CCI are listed in Table 5. The average CCI value of Navy beach was 0.64, meaning that the Navy beach can be considered 'very clean' according to the scale presented in Table 1.

The CCI is seen to be an easy tool to help enforcement bodies and authorities in assessing and managing the cleanliness level of coastal areas in Malaysia. In 2010, the Malaysian Maritime Institute (MIMA) published a report on "Coastal Litter Management," using CCI values for assessing the cleanliness of Malaysian coastal areas. Malaysian coastal locations namely Pantai Morib and Kelanang (Selangor), Pantai Desaru (Johor), Pantai Cenang (Langkawi), Pantai Balok (Pahang), Pantai Puteri (Malacca), Tanjung Tuan and Pantai Cermin (Port Dickson), Pantai Puteri (Sarawak), Tanjung Aru (Sabah) were chosen for the sampling area. These locations are known as famous recreation areas in Malaysia. Pantai Cenang in Langkawi has the lowest score of 1.08 based on the defined baseline CCI for the sampled recreational areas, showing that the beach is very clean from plastic trash in the coastal area. Meanwhile, the highest index is 7.11 at Pantai Desaru, Johor. In 2017, another series of CCI assessments were carried out by MIMA presented the CCI values at Bagan Lalang, Pantai Remis, Pantai Morib, and Tanjung Harapan. It found that the CCI index for all the beaches was categorized as very clean. Table 6 shows the CCI values and status of Malaysian beaches from the survey [6, 12].

According to the previous research, there is no specific total area and no specific frequency for debris collection in CCI calculation. All the researchers used different total areas of sampling [9, 12], Munari et al. 2015; [3, 10]. According to MIMA [12], the larger the transect area or more transect are, the better the result. However, due to the technical difficulties with regard to the different beach types, the coverage area

Table 6 Clean Coast Index (CCI) and status of Malaysian beaches

Study site	CCI	Beach status	References
Pantai Morib and Kelanang (Selangor)	5.68	Moderate	Hagir et al. [6]
Pantai Desaru (Johor)	7.11	Moderate	Hagir et al. [6]
Pantai Cenang (Langkawi)	1.08	Very clean	Hagir et al. [6]
Pantai Balok (Pahang)	4.82	Clean	Hagir et al. [6]
Pantai Puteri (Malacca)	6.57	Moderate	Hagir et al. [6]
Tanjung Tuan and Pantai Cermin (Port Dickson)	4.62	Clean	Hagir et al. [6]
Pantai Puteri (Sarawak)	2.95	Clean	Hagir et al. [6]
Tanjung Aru (Sabah)	3.8	Clean	Hagir et al. [6]
Pantai Remis (Selangor)	0.5	Very clean	MIMA, [12]
Pantai Bagan Lalang (Selangor)	0.1	Very clean	MIMA, [12]
Pantai Tanjung Harapan	0.3	Very clean	MIMA, [12]
Pantai Morib	1	Very clean	MIMA, [12]
Pantai Navy, Labuan	0.64	Very clean	This study

differs. In addition, there is no limitation on how frequent the sampling is needed to show the level of cleanliness. For the Malaysia scenario, the CCI value was compared using a single day of sampling. Studies by Akalay et al. [3] show that there is no specific trend is recorded when comparing the CCI value measured every four weeks for six months. They found that drastic CCI value changes from not clean to clean basically due to the enforcement activities and cleaning activities conducted by local authorities. MIMA monitored the CCI value of Pantai Morib, where the CCI value in the years 2010 and 2017 were 5.68 and 1.0, respectively. The changing of level of cleanliness after seven years at Pantai Morib might be due to the awareness campaign and improvement provided by local authorities to maintain the cleanness of the beach, thus the motivate the general public for keeping the coast clean.

4 Conclusions

The CCI values of Navy beach indicate that the beach was categorized as 'very clean. Made-made debris such as plastic materials contributes significant effect towards the cleanness index of the Navy beach. Plastic debris was the most abundant item found on the beach, among other man-made debris. This type of debris is mainly connected to the socio-economic activities done by local people near the beach. Besides plastic debris, a huge number of organic-type debris such as lumber, tree branches, and leaves are also present at the beach. These types of debris were mainly related to the weather before the debris was collected. In general, our results add up to increased evidence indicating that man-made plastic pollution is a significant problem for the marine environment in Malaysia beaches.

References

1. Abdul Kadir A, Hasni AF, Sarani NA (2015) Marine debris composition in Batu Pahat, Johor: a comparison between Sungai Lurus and Minyak Beku beaches. ARPN J Eng Appl Sci 10(15):6553–6557
2. Agamuthu P, Fauziah SH, Khairunnisa AK (2012) Marine debris on selected Malaysian beaches: impacts of human ignorance. In: Proceedings of the 10th expert meeting on solid waste management in Asia and Pacific Islands (SWAPI) Feb 20–22, pp 1–8
3. Alkalay R, Pasternak G, Zask A (2007) Clean-coast index-a new approach for beach cleanliness assessment. Ocean Coast Manag 50(5–6):352–362
4. Galgani F, Hanke G, Maes T (2015) Marine anthropogenic litter. Springer, Cham, pp 1–447. https://doi.org/10.1007/978-3-319-16510-3
5. Hagir R., Mahmudah AL, Eric C (2012a) Application of the clean coast index for cleanliness assessment of coastal areas in Malaysia. In: Clean cost index report 2011-part 1. https://mns marine.wordpress.com/2012/07/09/clean-coast-index-report-2011-part-1/
6. Hagir R., Mahmudah AL, Eric C (2012b) Application of the clean coast index for cleanliness assessment of coastal areas in Malaysia. In: clean cost index report 2011-part 2. https://mns marine.wordpress.com/2012/07/16/clean-coast-index-report-2011-part-2/
7. Hassan R, Mobilik JM (2012) Debris Marin: punca dan penyelesaian. Universiti Malaysia Sarawak, Malaysia, Penerbit Unimas
8. Kühn S, Bravo Rebolledo EL, van Franeker JA (2015) Deleterious effects of litter on marine life. In: Bergmann M, Gutow L, Klages M (eds) Marine anthropogenic litter. Springer, Berlin, pp 75–116. https://doi.org/10.1007/978-3-319-16510-3_4
9. Laglbauer BJL et al (2014) Macrodebris and microplastics from beaches in Slovenia. Mar Pollut Bull 89:356–366
10. Loizia P, Voukkali I, Chatziparaskeva G, Navarro-Pedreño J, Zorpas AA (2021) Measuring the level of environmental performance on coastal environment before and during the COVID-19 pandemic: a case study from Cyprus. Sustainability 13(5):2485
11. Marin CM, Niero H, Zinnke I, Pellizzetti MA, Santos PH, Rudolf AC, Beltrao M, Waltrick de Souza D, Polette M(2019) Marine debris and pollution indexes on the beaches of Santa Catarina State, Brazil. Regional Stud Mar Sci 31:100771
12. Maritim Institute of Malaysia (MIMA) (2019) Monitoring and assessment methodologies using practical examples application of the clean coast index (CCI) – the Selangor State level case study, national stakeholders consultation on Marine Litter – solving plastic pollution at source port dickson, 5 – 6 November
13. Mobilik JM, Ling TY, Hassan R (2017) Type and quantity of marine debris at selected public beaches in Sabah (Tg. Aru and Kosuhoi) during different monsoon seasons. Borneo Sci 38(1):13–27
14. Mobilik JM, Ling TY, Hassan R, Husain ML (2014) Type and abundance of marine debris at selected public beaches in Sarawak, east Malaysia, during the northeast monsoon. J Sustain Sci Manag 9(2):43–52
15. Munari C, Corbau C, Simeoni U, Mistri M (2016) Marine litter on mediterranean shores: analysis of composition, spatial distribution and sources in north- western Adriatic beaches. Waste Manage 49:483–490

16. National oceanic and atmospheric administration, NOAA (2021) FY2021 marine debris removal. https://marinedebris.noaa.gov/sites/default/files/NOAA-NOS-ORR-2021-200 6620%20NOFO%20Report_0.pdf

17. Thiel M, Hinojosa IA, Miranda L, Pantoja JF, Rivadeneira MM, Vásquez N (2013) Anthropogenic marine debris in the coastal environment: a multi-year comparison between coastal waters and local shores. Mar Pollut Bull 71:307–316